DOE/ER/40150--79

DE89 014424

Proceedings

CEBAF/SURA

1984 SUMMER WORKSHOP

Continuous Electron Beam Accelerator Facility

Newport News, Virginia

June 25-29, 1984

Edited by: Franz Gross and R. Roy Whitney

Sponsored by: CEBAF and SURA

Endorsed by: The Department of Energy
and
The National Science Foundation

Continuous Electron Beam Accelerator Facility

12070 Jefferson Avenue

Newport News, VA 23606

November, 1984

Printed in the United States of America

To order a copy of the Proceedings,
send $25 ($35 for overseas air mail) to:

CEBAF 1984 Summer Workshop
12070 Jefferson Avenue
Newport News, VA 23606

PREFACE

Discussion of the scientific need for a high energy, high duty factor electron accelerator has been underway since the mid 1970's. In January of 1979, a conference on "Future Possibilities for Electron Accelerators" was held at the University of Virginia in Charlottesville to focus on creating the appropriate tools. After the 1979 NSAC long range plan was released, in January 1980, the Bates User's Group hosted the first of a series of meetings at MIT which eventually led to publication of the "Blue Book" in 1982. Specific planning for CEBAF (then called NEAL) by physicists in the Southeast began in May, 1980, with the first organizational meeting of SURA physicists at Williamsburg. Over 40 physicists from the Southeast met 6 times during 1980-82 to discuss and prepare the scientific justification for the SURA 1980 and 1982 NEAL proposals. In April of 1982, the conference on "New Horizons in Electromagnetic Physics" was held at Charlottesville. After the SURA proposal was accepted by NSAC and DOE, a new round of discussions began with a two week meeting of theorists in Blacksburg in August 1983, and the Spectrometer Workshop held in Williamsburg, Oct. 10-12, 1983, at which three national working groups were organized. Each of these working groups met several times during the Fall of 1983 and the Spring of 1984.

The CEBAF 1984 Summer Workshop was held at the CEBAF site in Newport News from June 25 to June 29, 1984. The program consisted of invited talks on both theoretical and experimental topics, and continuation of the working group meetings.

This Proceedings is divided into four parts. The first part contains the reports of the three working groups which had been active before the workshop convened, questions for the theory working group, and a status report on the CEBAF project. During the workshop, the original groups on Tagged Photon Production and Internal Targets (D. Jenkins, Chairman) and Large Acceptance Detectors (R. Whitney, Chairman) were organized into groups on Large Acceptance Detectors and Tagged Photons (with R. Whitney as chairman) and Internal Targets (with R. Holt as chairman), and a new working group on Positrons was organized by B. Berman. The magnetic spectrometer and theory groups, headed by J. Lightbody and F. Gross respectively, continued as currently organized.

These groups met during the week, and reports of this discussion are included in Part III of these proceedings. Part II contains the invited talks, presented in the order in which they were given during the week, and Part IV contains short papers contributed to the workshop.

The first formal meeting of the CEBAF User's Group was held on Wednesday, June 27, with newly elected chairman Hall Crannell presiding. The next User's meeting is promised for sometime in May, 1985.

We wish to thank all the physicists who attended and contributed their ideas so freely, and look forward to seeing you again in May. Special thanks go to the staff at VARC (now CEBAF), particularly Penny Champine, Frank Heidt, Sylvia Smith and Anne Stewart who took the major responsibility for organizing the local arrangements, and to Gail Wilson for assuming responsibility for producing these proceedings.

Franz Gross
R. Roy Whitney

CEBAF
12070 Jefferson Avenue
Newport News, VA 23606

TABLE OF CONTENTS

Summary: Magnetic Spectrometer Working Group

J. W. Lightbody, Jr.
National Bureau of Standards
Gaithersburg, MD 20899

INTRODUCTION

The magnetic spectrometer working group goals are (i) to define the magnetic spectrometer requirements for CEBAF and (ii) to make recommendations to the management on related R&D work. In an earlier meeting we have identified the major physics programs and the spectrometer requirements. These are shown in Figs. 1, 2, and 3. We wish to find the common, minimum set of spectrometers that will serve most if not all of the planned experiments. Care must be taken in this choice so as not to preclude experiments which will be done of order six years from now when we hope CEBAF will be completed. Clearly some of the top priority experiments such as the neutron form factor and deuteron tensor polarization measurements may be completed. We must look to what may be required beyond these experiments. In designing the spectrometers we do not want to repeat low energy designs at 4 GeV. That is simply too expensive. We also don't want to repeat the existing high energy spectrometer designs. They are not good enough - with small solid angles and low resolution. Modular spectrometer components may be the answer - using building block magnetic elements to cover some of the more exotic applications, and relying heavily on software rather than true magnetic focusing devices to achieve the high resolution.

In arriving at the spectrometer specifications, the maximum beam energy, beam current, beam emittance, and available polarization state are fixed parameters. The spectrometer solid angle, momentum acceptance, maximum momentum, resolvingpower, and angular range (in both the azimuthal and polar

directions) are degrees of freedom that must be varied within the reasonable constraints of building size and total experimental equipment budget of 37M$ (50M$ inflated over the project construction period).

One of our goals is to identify those areas in which R&D will be required. One example of such work is superconducting technology. Because of the large solid angles being discussed and because of the high energies, it is clear that quadrupole pole tip fields in excess of 3 Tesla will be required. In addition, higher multipole components must also be available to achieve the good magneto-optical characteristics necessary for high resolving power. Quadrupoles with of order 30 cm bore are required, yet to date no such large bore devices have been built. A serious R&D program in this area should begin as soon as possible. In order to better focus this effort, we might consider using this quadrupole or quadrupole pair together with a superconducting dipole as a prototype light weight spectrometer, maximally software corrected to push the resolving power limits. Such a device could for example be used as an out-of-plane spectrometer (discussed later). Questions that must be addressed include where such work can be done - MSU, Fermi lab, or should it be started at the CEBAF site itself? Who should do the work and how much money should be committed to the R&D? The scale of applications of superconducting technology at CEBAF must be examined carefully before answering these questions. Power consumption may dictate that superconducting coils be used in the beam transport and spectrometer dipoles. The amount of money spent on this R&D is related to the extent of application and is also the time scale.

In our February 1984 meeting we discussed in some detail the various experiments listed in Figs. 1 and 2. A master list of spectrometer requirements was generated and is shown in Fig. 3. We attached priorities to these experiments: (1) being highest, (2) indicating that this work might be done using the new SLAC injector (NPAS), and (3) indicating that such work might be

done at the Bates facility. Experiments were classified in terms of the number of reaction products - single arm, double arm, and triple arm set-ups. No experiment with more than three reaction products was considered as it appears that such experiments are best done using the large solid angle devices considered by another working group.

During the February 1984 meeting, it was also suggested that the experiment list discussed above be reduced in scope to a more realistic core group of experiments. This core group is shown in Fig. 4 and the names listed include people interested in working in these areas. Serious effort is to be given to these experiments in terms of design in order that the spectrometer requirements can be firmed up. Theoretical background work needs to be done and detailed experiment design begun in the form of documented proposals for each of the above experiments.

FIRST APPROXIMATION SPECTROMETERS

Figure 5 shows what we consider to be the first approximation to the spectrometers required for a single pivot set-up. One spectrometer will operate up to the maximum machine energy of 4 GeV with energy resolution on the order of 1 MeV, a scale set by the binding energy and threshold differences in the 2- and 3- body systems. The already large solid angle 20-50 msr should be expandable to of order 100 msr at reduced resolving power (10^3). The momentum acceptance is large, 20-30%, in order to maximize data rates in the continuum region. The 0.5 mrad angular resolution is required in order to reduce the effects of kinematic broadening on the resolution to a level commensurate with the figure 2×10^{-4}. An angular range of 5-160° is required to satisfy the needs of all the experiments considered although clearly the small angle region is going to require some additional magnetic elements to permit passage of the primary beam past the spectrometer yoke.

Possibly use can be made of a superconducting Danby type quad with open sides for passing the direct beam. Finally the usual long target is a necessity for the study of few nuclear systems. The 10 cm figure was somewhat arbitrary; 30 cm would be more realistic for a cryogemic or high pressure gas target.

The second spectrometer with maximum momentum of 2 GeV/c has resolution commensurate with the above spectrometer and will be used in double-arm coincidence studies. The higher resolution capability of $5\text{-}10^{-5}$ at reduced solid angle is to allow high resolution studies of hypernuclei via the (e,e^2K) or (γ,K) reactions. Larger solid angle (50 msr) should be obtainable at the expense of momentum acceptance and resolution.

The third spectrometer is to be used in low resolution, triple-arm coincidence studies such as (e,e'NN) or (e,e'πN). The maximum momentum of 1 GeV/c permits detection of protons with more than 400 MeV kinetic energy. This spans the minimum in the p-p total cross section where we can hope that distortion effects may be minimized. Resolution requirements are very modest (5×10^{-3}) for this device because of the continuum nature of the planned studies. A large solid angle is required because of the fact that it will be used in triple coincidence measurements where the rates are proportional to the product of three relatively small solid angles. A 100 msr solid angle at 20% momentum acceptance would be desirable for this device.

We felt later that the specifications on these three spectrometers were rather stringent if not impossible to meet. It was suggested, therefore, that we examine in detail what could be done with the three spectrometers shown in Fig. 6. The only understatement in this list is the target length - 5 and 10 cm targets may not be long enough as mentioned earlier. The SLAC cryogenic targets for example approach 30 cm in length. Since few nucleon studies will be a large part of the program at CEBAF, provisions must be given for larger targets.

DISCUSSIONS

In the following section, highlights and discussions of the experiment presentation (Fig. 1) are given.

It appears that one of the high priority activities at CEBAF will be (e,e'p) experiments. There is exciting new data from Bates (Finn, Bertozzi, et al.) which gives some indications that this reaction may help in separating one- and two-body effects in the nucleon momentum distribution or spectral function. Figure 7 shows a few details of this class of experiment as presented by Finn and Bertozzi. The design goals have been merged into the lists previously given. What we should focus on are details of the spectrometer configurations. Dispersion matching is naturally discussed in this connection because the primary beam spread from the stretcher ring can have a substantial energy spread ($\leq$0.2%). Double dispersion matching (two-spectrometers) can also be achieved which minimizes the missing mass energy resolution. It is clear from all designs being considered that the initial magnetic element of the spectrometers will have to be either a quadrupole singlet or doublet, with one or both quads having substantial higher multipole content to compensate for later magnetic aberrations in the system. This configuration seems essential for large solid angle devices in order to keep the dipole gaps to a minimum. Parallel-to-point transverse optics ($Y_{out} = (Y|\phi)\phi_{in}$) may be desirable from the standpoint of measuring the angle at which particles leave the target (scattering angle) by a position measurement at the focal plane. A secondary focus in one arm to define the object point on target, such as with the EPICS spectrometer at LAMPF and as discussed in the Argonne G.E.M. proposal, may be important with the distributed and dispersed beams from the ring. It should also be pointed out that dispersion matching is a special case of dispersed beam operation and is not the only technique available for achieving high missing mass resolution. Other details for the interested are

shown in Figs. 8 and 9.

In the discussion of coincidence spectrometers and experiment design one very critical element is missing mass resolution. Figure 10 taken from Zeidman's presentation shows the relation between missing mass and different kinematic inputs - particle energies and scattering or production angles. Missing mass resolution can be obtained by combining the various contributions following ΔM. The limits on angular resolution are clearly spelled out. If one desires 100 keV missing mass resolution the scattering and production angles must be defind to better than 0.5 m radian. Also the measured cross sections are strong functions of recoil momentum (P_r) and therefore consideration must be given to the resolution in recoil momentum and its connection with the scattering and production angles.

The entire subject of coincidence measurements relates to measuring new electromagnetic structure functions. Figure 11 shows the general expression where the f's are the new structure functions relating to the nuclear four-currents, and the ρ's are the kinematic factors relating to the electron current. The variable ϕ represents the angle which the reaction product plane (containing the momentum transfer and the reaction product momentum) makes with the scatteringplane (which contains the initial and final electron momentum). The f_{l-l} and f_{hel} amplitudes can only be measured by out-of-plane measurements ($\phi \neq 0, \pi$). In addition f_{hel} can only be measured using polarized electron beams. The three interference amplitudes contain a great deal of sensitivity to nucleon-nucleon interaction effects and are important quantities to measure. Figure 12 indicates some of the interest in out-of-plane measurements and Figure 13 indicates some of the methods for achieving such measurements and kinematical consideration. Both issues were discussed in the 1983 workshop. Basically there are three methods being considered - moving one or both of the spectrometers out-of-plane (possibly light weight

superconducting dipoles), changing the arrival direction of the primary beam on target, or employing a large solid angle electron spectrometer at small scattering angle and using software cuts to define the out-of-plane angle. One critical question must be answered before a sensible decision can be made regarding these options - how far out-of-plane must we go with our measurements. The third option above is limited to relatively low momentum transfers, while the second option is limited by constraints on the beam transport system. In this latter connection, when employing polarized beam one must consider the effect which the additional angular deflection of the primary beam has on the polarization state and compensate for it in the superconducting spin precessor system (up to 270 kg-m). This has been checked for 4 GeV beam deflections up to an additional 45° and remains practical. What is beginning to appear impractical with the beam swinger technique is the large vertical excursions (up to 4 m.) that the beam must make while in the beam transport system, the complexity of the pretarget dipole system and the large post target dipoles for returning the transmited beam to the remote dump area. It is however becoming clear that some of the most interesting physics at CEBAF could be related to spin physics and we must be prepared with out-of-plane measurements as required and with polarized beams.

The subject of large target spectrometers was discussed by York and Minehart (See Fig. 14). It apepars from preliminary work that one can only open up the target acceptance at the expense of reduced solid angle. It is clear that this subject needs further study because such large targets are an absolutely essential aspect of the core program for CEBAF. With large targets it may be necessary to employ immediate focus detectors such as with EPICS at LAMPF. During this workshop, Blomqvist will give a few examples of how one might proceed towards the goal of using ∿30 cm long targets.

Another area of major theoretical interest which can be addressed at CEBAF is the process of two-nucleon interactions within nuclear matter and characterization of the pp and np correlation functions. In order to probe this process experiments which look at ejected nucleon pairs have been examined. Figure 15 describes the kinematics of two-nucleon emission and the spectrometer requirements. The important points regarding the process itself are shown in Fig. 16. One can take advantage of kinematic focussing by employing large momentum transfers. The reaction products which share this transferred momentum travel largely within a core of base radium $2k_F$ and height q. At a momentum transfer of $4k_F$ to each nucleon, most are containd within 750 msr which means that a nucleon spectrometers with 100 msr will accept a substantial fraction of the particles. In addition by looking at ejected nucleon with momenta near $4k_F$ we are at a minimum in the total nuclear-nucleon cross section thereby minimizing final state interactions. Simple multiple scattering can be estimated to be small as well. Finally, it should be noted in the fundamental (e,e'2N) process that the pair correlation function is a function of the relative two-nucleon momentum and is probed to a relative momentum of 0.5 q_{max}.

The study of hypernuclear states populated by the reaction (γ,K) and (e,e^2K^+) is of major importance, and has demanding requirements on energy resolution. Electromagnetic probes can produce kaons over the nuclear volume, not just near the nuclear surface as with strongly interacting probes. Therefore, it is possible to preferentially populate deep-hole states, as noted at the bottom of Figure 17. Figure 17 also indicates details of the spectrometer requirements and counting rates. The major criterion for these experiments is that the nuclear recoil momentum be kept small so that the Λ's or Σ's can form well defined nuclear states. This implies operating the kaon spectrometer near 0° for the (γ,K^+) reactions. Also, because of the short

lifetime of the kaon, the spectrometer dimensions must be kept small and the kaon energy relatively high. A kaon spectrometer with 2% momentum acceptance would serve the production of Λ-hypernuclei very well, while a 10% acceptance would permit the simultaneous study of Λ and Σ hypernuclei. Given the above specifications Bernstein estimates count rates of order 30 counts/hour, and acceptable rate in this type of work. The resolution requirements of 10^{-4} would advance the field, however 10^{-5} would permit of order 10 keV resolution. Considering what future advances may bring we do not want to preclude such resolution if possible. Figure 18 shows survival factors for different kaon momenta and relevant kinematic factors such as the relation of angular resolution to energy resolution. Figure 19 shows the various experimental set-ups required to do such hypernuclei experiments. In February O'Connell pointed out a possible problem in these studies due to positron contamination. Operating near 0° one risks intercepting the pair production and multiple scattering cones with the spectrometer acceptance. As shown in Fig. 20 one must back the spectrometers off to near 3° before the positron production cross section is small enough to permit use of a Cerenkov detector veto. This is because of the 10^9 factor between e^+ and κ^+ production cross section within the e^+ production cone. In any case there appear to be reasonable count rate even at the larger angles in order to make this type of experiment very interesting.

Finally, something should be said about beam preparation. Given the extracted beam emittance shown in Fig. 21 we must examine how to best prepare the beam on target. For conventional spectrometers one considers the mono-energetic beam spot as limiting the resolution. The smaller this spot for a given resolving power the size of the spectrometer (bend radius) varies directly with the monoenergetic spot size (in the bend plane). We transport

the beam in a conventional fashion from the ring - a telescope to make the beam round, followed by a series of unit cell transport systems, a second telescope to squeeze the beam vertically, and finally a quad doublet to make as small a spot as possible on target. We choose this point to be a waist and find we can achieve a 0.25 mm vertical spot size. Given, for example, the high resolution spectrometer in the SURA proposal with 18.27 cm/% dispersion and a magnification of 1.19, one can achieve a resolution (1st order) of 1.6×10^{-5}. Using this same simple focusing system and having put the horizontal waist at the same location as the vertical waist we achieve a 1.7 mm horizontal spot size. However, we see that the spread in horizontal angles has become 0.7 mm. This angular spread is close to being unacceptably large given the relation between scattering angle resolution and energy resolutions (See Fig. 22). We may in fact want to rotate the emittance phase ellipses 90°, interchanging x and y with an emittance matching section. In this way the larger angle spread will come in the very weak ϕ-dependence of the scattering angle. For polarized beams, however, we may not have this freedom because of solenoids in the system mixing x and y phase spaces. We may have to settle for (0.3π mm-mrad) x (0.3π mm-mrad) transverse emittance, and a somewhat reduced resolution.

Another way around the problem of large angular spread in the primary beam would be to rotate or shear the horizontal phase ellipse which inroduces an x/θ correlation at the target. One could imagine using an intermediate focusing system in the spectrometer, identifying where on the target the particle came from and thereby eliminating this angle uncertainty from the scattering angle resolution. In this same connection, one can use an intermediate focusing system with a drift chamber system to define where on the target the particle left from in the vertical plane. With this scheme the

ultimate momentum resolution obtainable from the system is limited not by the mononenergetic beam spot size, but rather by the drift chamber spatial resolution which can be made of order 0.1 mm. Clearly there are many options to be looked at in the spectrometer design and we must begin to look seriously at details such as beam preparation because of the ultimate payoff in resolution versus cost.

CONCLUSION

Work must begin as soon as possible on serious designs of experiments and on optimizing spectrometer designs. What has taken place so far in many experiment justifications is soft count rate estimation. More details are required including theoretical work as final state interaction effects, MEC effects, the need for out-of-plane measurements, to name a few. Experimentally we need a few hard magnet designs to see what is even possible and where the R&D should be concentrated. Hopefully, the efforts of this working group will be greatly expanded in achieving the final experiment and spectrometer design for CEBAF. Figure 23 reiterates goals of the working group.

POSSIBLE PHYSICS EXPERIMENTS

MEDIUM AND HIGH RESOLUTION
WORKING GROUP

I.	Single Arm Experiments	
1.	(e,e') Nuclear elastic and inelastic $A > 4$ Heavy nuclei $E_e \leq$ 1GeV?	Bertozzi Lindgren Finn
2.	(e,e') Nuclear elastic $A \leq$ $E_e >$ IGeV neutron, deuteron charge form factor	Chang Blomqvist
3.	Deep inelastic, heavier nuclei	Blomqvist Finn
4.	Far forward angles	Lightbody
II.	DOUBLE ARM EXPERIMENTS	
5.	(e,e'X) Elastic coincidence measure polarization of recoil X	___
6.	(e,e'X) Giant resonances	Chang
7.	(e,e'p) Low resolution + neutrons also	Finn
8.	(e,e'p) High resolution + neutrons also	Zeidman Finn
9.	Out of plane (e,e'p) Look into feasibility of an out-of-plane arm	Lightbody
10.	(e,e'π), (e,e'κ) form factors	Funsten
11.	(e,e' neutral)	Arnold
12.	Long target (e.g. long liquid deuterium target)	Minehart
13.	(e,e'd), (e,e'He^3) etc.	Minehart Bosted Arnold
14.	Λ Hypernuclei	Pile Kowalski Bernstein Zeidman Funsten

Fig. 1

15. Fission — Lindgren, Maruyama

III. TRIPLE ARM EXPERIMENTS

16. (e,e'2N) — Lightbody

17. (e,e'2neutrals) neutrals= γ, π^0, κ^0 — Sober

18. (γ,γ)
pair spectrometer - large solid angle spectrometers ---

19. (e,e'πN) — Finn, Funsten

Fig. 2

Exp.	1 (e,e')	2 (e,e')	3 (e,e')	4	5	6	7	8	9	10 (e,eπ) (e,e'κ)	13 (e,e'd)	14 hyper nuclei	16 (e,e'2N)	19 (e,e'πN)
Priority	3(Bates)	2(SLAC)	2(SLAC)	1	1	3(Bates)	1	1½	1(?)	1	1	1	1	1
N_{spec}	1	1	1	1	2	1	2	2		2	2	2	3	3
$p_{max}^{(1)}$	1 GeV	4	4	1	4	1	4	1.5-2		3	4	2	4	2
$\Delta\Omega^{(1)}$	20-50	50	20	1	20-50	30	20-30	>25		20	20	10(3°x10°)	30-100	10-20
$\frac{\Delta p^{(1)}}{p}$	10^{-5}	$2\cdot10^{-4}$	$2\cdot10^{-4}$	$2\cdot10^{-4}$	$2\cdot10^{-4}$	$5\cdot10^{-4}$	$2\cdot10^{-4}$	$2\cdot10^{-5}$		1%	10^{-3}	10^{-5}	$s\cdot10^{-3}$	$5\cdot10^{-3}$
$\delta p^{(1)}$	5%	1%	20%	3%	5%	10%	20-30%	2%		20%	3%	2%	20%	20%
$\Delta\Theta^{(1)}$	.5mr	.5mr	.5mr	.1mr	10mr	1mr	.5mr	.5mr		2mr		.5mr	1mr	2mr
$\Delta\Theta^{(1)}$	20-160°	15-160°	20-160°	5-30°	5-90°	15-60°	20-160°	10-140°	NEEDS FURTHER STUDY	10-75°	10-60°	0-30°	5-30°	20-90°
$p_{max}^{(2)}$					1.5		2.5	1.2		2	1.5	2	1.5,1.5	1,1
$\Delta\Omega^{(2)}$					50-100		20-30	50		35		15(5°x10°)	100,100	20-30
$\frac{\Delta p^{(2)}}{p}$					1%		$5\cdot10^{-4}$	$5\cdot10^{-5}$		3%	10^{-3}	10^{-5}	$5x10^{-3}$	$5\cdot10^{-3}$
$\delta p^{(2)}$					10%		20-30%	20%		40%	30%	10%	20%	20%
$\Delta\Theta^{(2)}$					10mr		.5mr	1m5		2m5		.5mr	1m5	2mr
(1)							10-160°	10-140°		-30°+30° out of plane requir-ed	40 -80°	0-30° Flight path <20m	30-120°	20-160°

Fig 3

Assignments for April Meeting

(e,e'x) polarization transfer - F. Gross, G. Chang, Bill Dodge, R. Minehart

(e,e'p) low resolution - M. Finn, C. Perdrisat, S. Thornton

hypernuclei - A. Bernstein, P. Pile,

(e,e'2N) - R. Minehart, J. Lightbody

π,K Form Factors - H. Funsten, X. Maruyama, F. Gross

(e,e'πN) - P. Stoler, J. Winbold, M. Finn

Fig. 4

Summary of Spectrometers Presently Suggested

	#1	#2	#3
P_{max}	4 GeV	2 GeV	1 GeV
$\Delta p/p$	$2 \cdot 10^{-4}$ (10^{-4} @ 9 msr)	4×10^{-4}	$5 \cdot 10^{-3}$
		5×10^{-5} (@ 15 MSR)	
$\Delta\Omega$	20-50 msr	20 - 30 msr	30 - 100 msr
	(30 - 100 with $\frac{\Delta P}{p} = 10^{-3}$)		
δp	20-30%	20-30%	20%
		(10% @ 50 msr and 1% $\frac{\delta p}{p}$)	
$\Delta\Theta$	.5 mr	.5 mr	1 mr
$\delta\Theta$	5° - 160°	10° - 160°	20° - 160°
L	10 cm	?	?

Fig. 5

What Could Be Done With Following Spectrometers?

	#1	#2	#3
P_{max}	4 GeV	2 GeV	1 GeV
$\frac{\Delta p}{p}$	10^{-4}	5×10^{-5}	$5 \cdot 10^{-3}$
$\Delta\Omega$	20 msr (40 msr @ $\frac{\Delta p}{p} = 10^{-3}$)	20 msr (40 msr @ $\frac{\Delta p}{p} = 1\%$	40 msr
δp	20%	15%	30%
$\Delta\Theta$	.5 mr	.5 mr	1 mr
L	10 cm	5 cm	10 cm

Fig. 6

Design Goals for (e,e') and (e,e'p) Spectrometers

Finn
#1,7,8

	High Resolution	Low Resolution
Electron Arm		
MAXIMUM MOMENTUM	1 GeV	4 GeV
SOLID ANGLE	20 mstr	20-30 mstr
MOMENTUM ACCEPTANCE	20%	20-30%
MOMENTUM RESOLUTION	$1/2 \times 10^{-4}$	$1/2 \times 10^{-3}$
ANGULAR RESOLUTION	2/3 mr	2 mr
TIMING RESOLUTION	1/4ns/β	1/4ns/β
ANGULAR RANGE	20-160 °	20-160°
Proton Arm		
MAXIMUM MOMENTUM	1 GeV	4-5 GeV
SOLID ANGLE	20 mstr	20-30 mstr
MOMENTUM ACCEPTANCE	20%	20-30%
MOMENTUM RESOLUTION	1×10^{-4}	1×10^{03}
ANGULAR RESOLUTION	1 mr	2 mr
TIMING RESOLUTION	1/4ns/β	1/4ns/β
ANGULAR RANGE	<15°-160°	<15°-160°

Criteria: high resolution pair: $\sim$100 keV in mass-16 system @ 1$\sim$1.4 GeV

low resolution pair: $\sim$5 MeV @ 4 GeV

Probable Spectrometer Configurations

- Dispersion matching
- Initial quads for large solid angles
- Parallel to point transverse focusing
- Secondary focus in one arm to define object point on target

W. Bertozzi and J.M. Finn
2 February 1984

Fig. 7

Comments on Specific Reactions

I. (e,e'p) Coincidence Reactions

- High resolution requires that optics of spectrometers and beam transport system be considered as an integral design.

- Alignment geometry of spectrometer components and beam line relative to pivot point should be reproducible $\sim$1/2 mr. Software solid angle and momentum acceptances must be known and reproducible, implying stability of ofringe fields and aberrations.

- 3 to 5% absolute accuracy. Less than 2% error in relative measurements are needed for comparative studies such as R_L and R_T separations. Wire chambers must be uniform in response for high resolution work.

- Spectrometers must be well baffled and shielded and must be easy to move.

- Provisions for out-of-plane measurements and proton polarimetry are desirable.

II. (e,e') Inclusive Measurements

It is assumed that the electron arm of the (e,e'p) coincidence spectrometers would be used for these measurements.

A. High resolution spectroscopy

Only 2% momentum acceptance is required at 1 GeV. Design gives 50 keV resolution on a heavy nucleus at the full momentum acceptance and maximum solid angle. One should attempt to further optimize resolution over a restricted momentum bite and solid angle (5 mstr) with a goal of 10 keV if possible.

B. Low resolution deep inelastic measurements

Requires full acceptances but only 5 to 10 MeV resolution.

Data acquisition facilities will encounter rates on the order of 10^5 events/sec.

Fig. 8

High discrimination of particle I.D. essential.

C. Elastic scattering from the few body system at high momentum transfers.

The low resolution (e,e'p) pair can be used to reduce background and resolution requirements via the constraind D(e,e'D) reaction, for example.

Measurements of the polarization of the outgoing nucleus system can also be made such as in D(e,e'D) measurements.

III. (e,e'n) Experiments

In general the resolution possible with neutron detectors is much worse than for protons detected with magnetic spectrometers. Therefore the electron spectrometer designs for the (e,e'p) experiments will be suitable for future (e,e'n) measurements. The neutron detector would vary according to application.

Possible neutron detection schemes include:

- Large scintillator hodoscopes with $\sim 1°$ resolution per cell (suitable for interference amplitude measurements of the D(e,e'n)p reaction or for the ^{3}H(e,e'2n) experiments).

- A 'piggy-back' detector riding on the back of the low resolution proton spectrometer for simultaneous D(e,e'n) and D(e,e'p) measurements to determine the G_{En} form factor. This would require a large viewing port to the rear of the proton spectrometer for simultaneous measurements to reduce systematic problems.

- A 'stand-alone' neutron detector based on detecting protons from the H(n,p) and other (n,p) reactions. This may make (e,e'n) polarization measurements possible.

IV. (e,e'pπ) Measurements

For such reaction studies the low resolution (e,e'p) spectrometer pair could be used with a similar low resolution large pion spectrometer. Interest in this reaction could extend to 3 to 4 GeV.

A major problem is the large physical sizes of the spectrometers which make many interesting kinematical regions inaccessible to a three-spectrometer system. Alternate schemes of detecting at least one of the particles should be considered.

Fig. 9

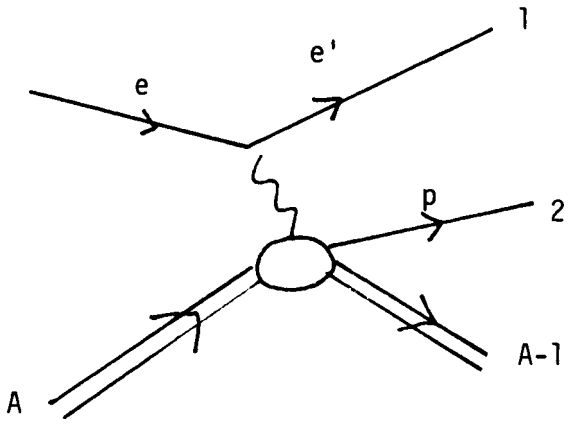

·Missing Mass Resolution Kinematics

$$\frac{\delta M}{\delta E_1} = 1; \quad \frac{\delta M}{\delta E_2} = 1 + \frac{3(E_B - E_1)}{M_T}$$

$$\frac{\delta M}{\delta \Theta_1} = \frac{P_1 P_B}{M_T} \left(\sin \Theta_1 + \frac{E_2}{E_B} \sin \Theta_{12}\right); \quad \frac{\delta M}{\delta \Theta_2} = \frac{P_2 E_B}{M_T} \left(\sin \Theta_2 + \frac{E_1}{E_B} \sin \Theta_{12}\right)$$

Ex $E_B = 2$ GeV, $E_1 = 1.5$ GeV, $T_2 = 300$ MeV, $P_2 = 0.8$ GeV, $\Theta_1 = 30°$, $\Theta_2 = 68°$

$$\Delta M \lesssim 1.25\ \Delta E_2,\ \Delta E_1,\ 200\ \frac{\text{keV}}{\text{mr}}\ \Delta\Theta_2,\ 110\ \frac{\text{keV}}{\text{mr}}\ \Delta\Theta.$$

$$\Delta P_r \lesssim 10\ \frac{\text{MeV/c}}{\text{mr}}\ \Delta\Theta_1,\ 10\ \frac{\text{MeV/c}}{\text{mr}}\ \Delta\Theta_2$$

·Dynamical Range $E_e \lesssim 2$ GeV, $P_p \lesssim 1.3$ GeV

$\delta P_1 \pm 5\%$ $\delta P_2 \pm 10\%$

$\Omega_1 \gtrsim 20$ msr $\Omega_2 \gtrsim 40$ msr

Fig. 10

Out-of-Plane Coincidence Measurements

$$d^3\sigma \sim \sigma_0 \left[f_{oo} + \left(\frac{\rho_{11}}{\rho_{oo}}\right) f_{11} + \left(\frac{\rho_{o1}}{\rho_{oo}}\right) f_{o1} \cos\phi + \left(\frac{\rho_{1-1}}{\rho_{oo}}\right) f_{1-1} \cos 2\phi \left(\frac{\rho_{hel}}{\rho_{oo}}\right) f_{hel} \sin\phi \right]$$

where $\frac{\rho_{11}}{\rho_{oo}} = \left(\frac{q^2}{q_\mu^2}\right)^2 \left[\frac{q_\mu^2}{2q^2} + \tan^2\frac{\theta}{2}\right]$

$$\frac{\rho_{o1}}{\rho_{oo}} = \left(\frac{q^2}{q_\mu^2}\right) \sqrt{1/2\left(\frac{q_\mu^2}{q^2} + \tan^2\frac{\theta}{2}\right)} \qquad \text{LT interference}$$

$$\frac{\rho_{1-1}}{\rho_{00}} = \frac{q^2}{2q_\mu^2} \qquad \text{TT interference}$$

$$\frac{\rho_{helicity}}{\rho_{00}} = \frac{1}{\sqrt{2}} \frac{q^2}{q_\mu^2} \tan\frac{\theta}{2} \qquad \text{LT interference}$$

Fig. 11

Experiments

- Details of reaction mechanism (transition amplitudes)
- In region of Δ have interesting test of theory for (e,e'p) reaction (MEC).
- (e,e'n) may display effect of Gen
- Polarized beams important
- At very high energy calculations are needed to see if new structure functions clean up reaction details
- Large acceptance spectrometers in the scattering plane integrate over a substantial ϕ-range therefore the behavior of the out-of-plane structure functions should be understood or at least measured.

Fig. 12

EXPERIMENTAL REALIZATION AND KINEMATICS

1. Move spectrometers out-of-plane. Practicality??

2. Beam swinger (10°)

   Small $\Delta\Omega$ spectrometer for electrons (10° clearance), resolution $\sim 10^{-4}$ (better than 1 MeV at 4 GeV incident energy).

   Auxilliary magnets required - two pre-target, one moveable vertically, two post target, one moveable vertically; relatively small gaps with 1.5 T-m pole regions.

   No trench required for 10° motion, however, larger deflections required for lower energy primary beam and hence, larger trench and auxilliary magnets.

   Possible to combine auxilliary magnet function with photon tagging magnet, as discussed for Saskatchewan accelerator.

3. Large solid angle spectrometer operation @Θ_e = 10°

   $\Delta\Omega$ = 50 msr., $\Delta\phi = 4\ \Delta\Theta$, $\Delta\phi = \pm$ 12.8°

   No beam swinger necessary. Use software cuts.

   i. Septum devices
   ii. Specialized ports for 10° operation
   iii. Open-sided quadrupoles in QQDD designs

4. Electron spectrometer requirements

   $P_{max} > 2$ GeV/c

   $\Delta P/P \sim 10^{-4}$

   $\Theta_e > 10°$

Fig. 13

LARGE TARGET SPECTROMETERS

Ref: York & Minehart, Workshop on High Resolution Large Acceptance Spectrometers, Argonne National Laboratory (1981), ANL/PHY-81-21, PV-G:

Experiments: Low cross section measurements on ^{2}H, ^{3}H, ^{3}He, etc.

Need:

1. Large acceptance
2. Long target
3. Moderate resolution $\sim 10^{-3}$

Difficulty: Opening up target acceptance reduces $\Delta\Omega$ of spectrometer.

They essentially cancel each other.

Is this a conservation law?

Need special purpose spectrometer - perhaps making generous use of intermediate detectors.

Fig. 14

(e,e'2N) Coincidence Studies (Ref. Blue Book)

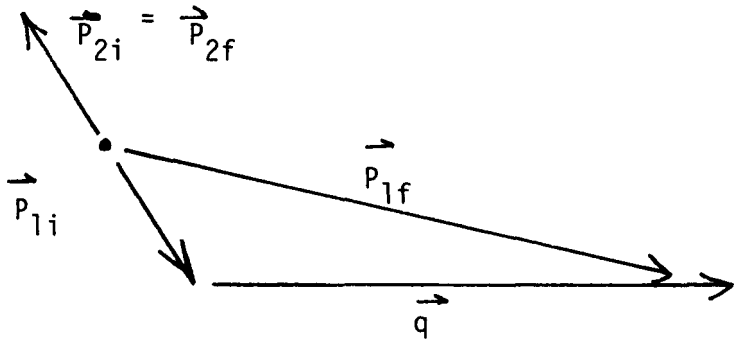

Experiments (e,e'pp), (e,e'np) for the pp, np correlation function

Resolution not important $\simeq$ 10 MeV

Electron arm:

$P_{max} \simeq$ 4 GeV (2 GeV)

$\Delta P/P \simeq 2 \cdot 10^{-3}$

$\Delta \Omega \simeq$ 30-100 msr

$\Delta P \simeq$ 20% (substantial fraction QF)

$\Theta_e \simeq 5°\text{-}30°$ (60°)

Proton arm:

$P_{max} \simeq$ 1 GeV ($\simeq$ 1/2 q_{max})

$\Delta P/P \simeq 5\ 10^{-3}$ (commensurate with e^- arm)

$\Delta \Omega \simeq$ 100 msr

$\Delta P \simeq$ 20% (substantial fraction QFP)

$\Theta_e \simeq 30°\text{-}120°$

Fig. 15

Kinematic focus

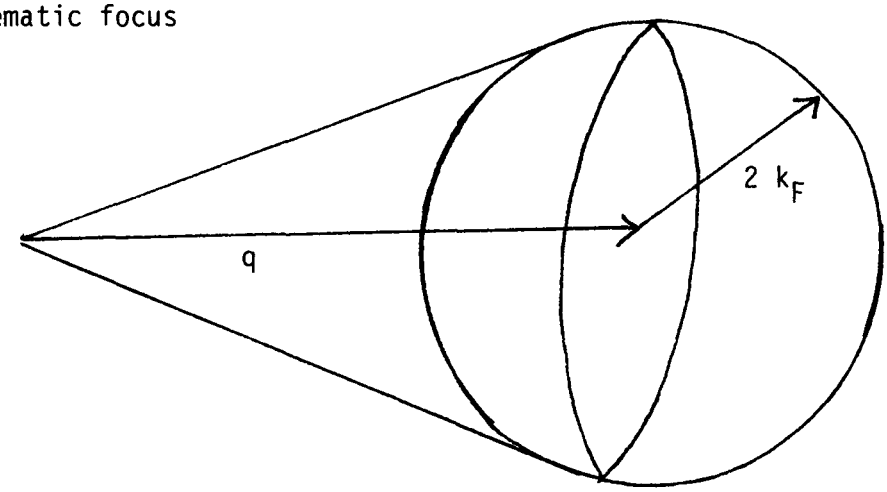

$P_i \sim 2k_F$

$q_{1,2} \sim 4\ k_F$

$\Delta\Omega \sim 750$msr

Multiple scattering, FSI

$$@\ P_p = 4\ k_F \qquad \Delta\theta_{ms} \simeq \frac{1/8\ k_p}{P_p} \simeq .03$$

Minimum in σ^{PP}_{total} @ $P_p \sim 0.7$-1.0 GeV/c

Pair correlation functions probed is function of P_{rel} and is probed to 1/2 q_{max}

How is momentum shared between two nucleons?

Fig. 16

Hyper-nuclear studies — Pile, Bernstein, Funsten, O'Connell

(γ,K^+), $(e,e'K^+)$ — 5-30 cts/hr ($^{12}C \rightarrow {}^{12}_{\Lambda}B$)

Spectrometers

Near 0° to limit $\mathcal{P}_{\Lambda,\Sigma}$ — P_{max} = 3 GeV(e^-), 2.5 (K^+)

Resolution to $10^{-4.5}$ (e, K) — Ω_c = 9 msr, Ω_k = 15 msr

ΔP_e = 2%, ΔP = 2-10% — Kaon flight path short

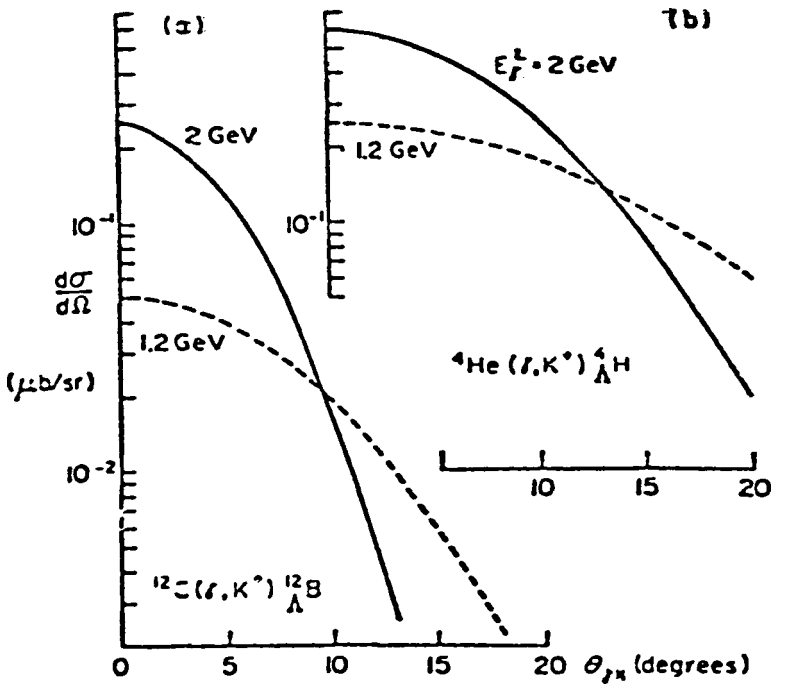

Differential cross sections versus C.M. angle $\theta_{\gamma K}$ for two laboratory photon energies (a) for the reaction $^{12}C(\gamma,K^+)^{12}_{\Lambda}B(1s_{\frac{1}{2}})(1s_{\frac{1}{2}}^{-1})_1$ and (b) for the reaction $^4He(\gamma,K^{+4}_{\Lambda}H$.

deep hole states

Fig. 17

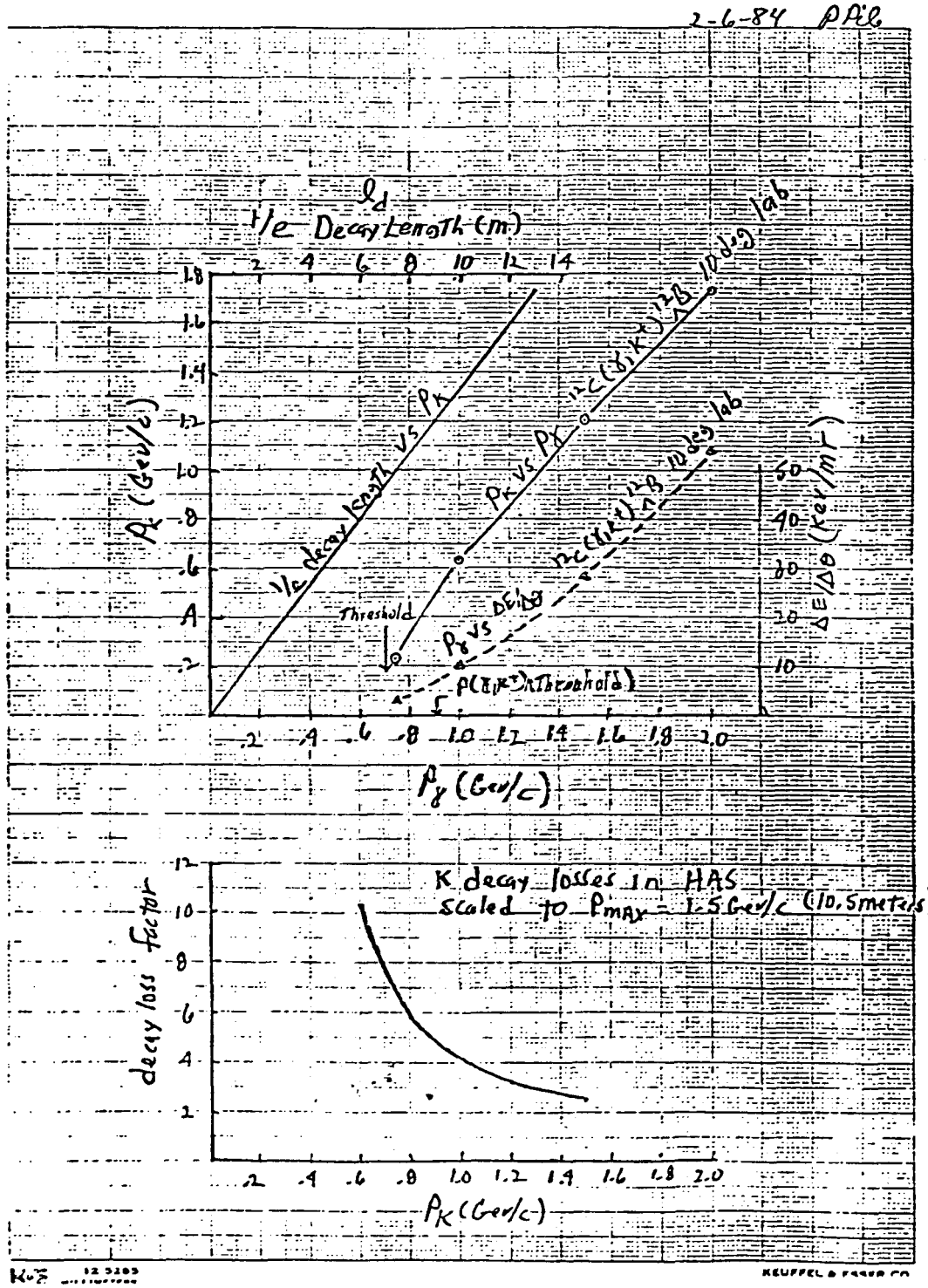
2-6-84 PAL
1/e Decay Length (m)
l_d
P_K (Gev/c)
1/e decay length vs P_K
P_K vs P_K
$\pi\mu(\nu_K)$ 10 deg lab
$\pi e(\nu_K)$ 10 deg lab
P_K vs $\Delta\theta$
Threshold
$P(\pi\mu\nu_K)$ Threshold
$\Delta E/\Delta\theta$ (Kev/mr)
P_γ (Gev/c)
decay loss factor
K decay losses in HAS
scaled to P_{max} = 1.5 Gev/c (10.5 meters)
P_K (Gev/c)
KEUFFEL & ESSER CO

Fig. 18

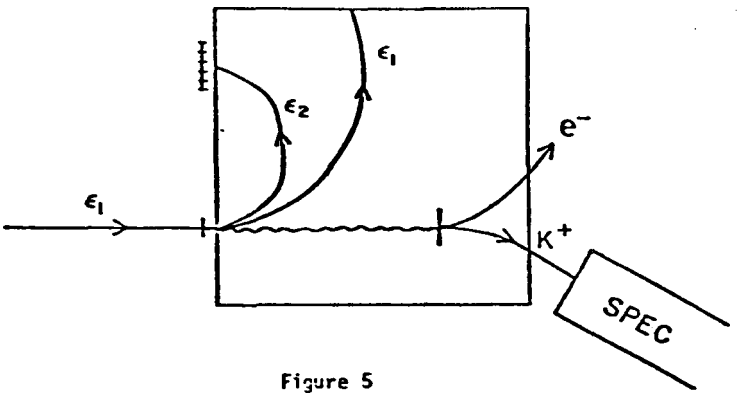

Figure 5
Schematic diagram for a tagged photon experiment

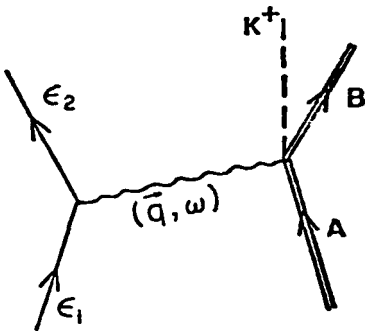

Figure 6
Feynman diagram for the $(e,e'K^+)$ reaction

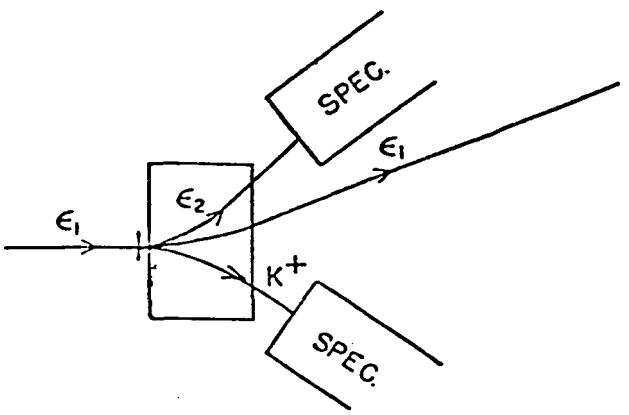

Figure 7
Schematic diagram for a $(e,e'K^+)$ experiment

Fig. 19

- Spectrometers must not intercept the pair production and multiple scattering cones
- Operating at $\bar{\theta}$ of 3°, most e^+ can be rejected using gas $\hat{C}$ counters
- Count rates fall ~ 50%

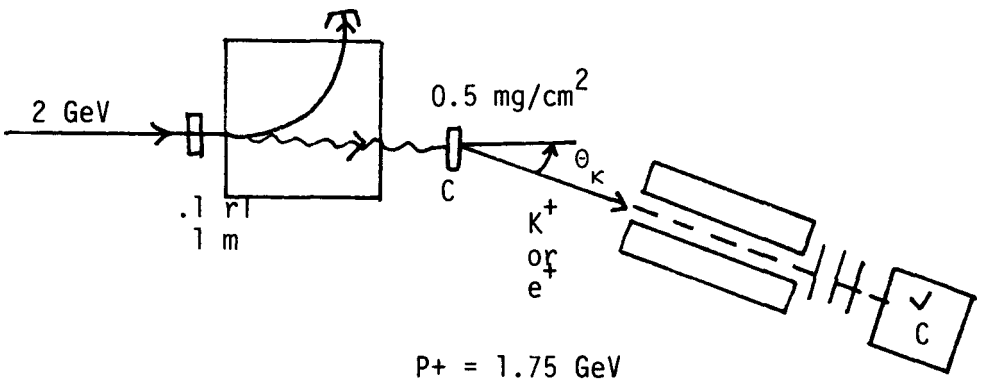

$$\theta_{pair} = \frac{M_e}{E_e} = 0.29 \text{ mr} - 0.02°$$

$$\theta_{ms} = \frac{20}{E_e} t_{re} = 1 \text{ mr} = 0.06°$$

$$d^2\sigma(\gamma,e^+) = 1.5 \times 10^{-22} \text{ cm}^2/\text{MeV-sr}$$

$$d^2\sigma(\gamma,\kappa^+) = 1.0 \times 10^{-31} \text{ cm}^2/\text{MeV-sr}$$

Fig. 20

BEAM CHARACTERISTICS

EXTRACTION

Vertical Emittance	0.1 π mm-mrad
Horizontal "	0.3 π mm-mrad
Vertical spot size	1.5 mm (FW)
Horizontal " "	6.0 mm "
Phase ellipse x_o, θ_o	= 3mm, 0.1 mrad (HW)
y_o, ϕ_o	= 0.75 mm, 0.133 mrad (HW)

TRANSPORT LINE (ILLUSTRATIVE)

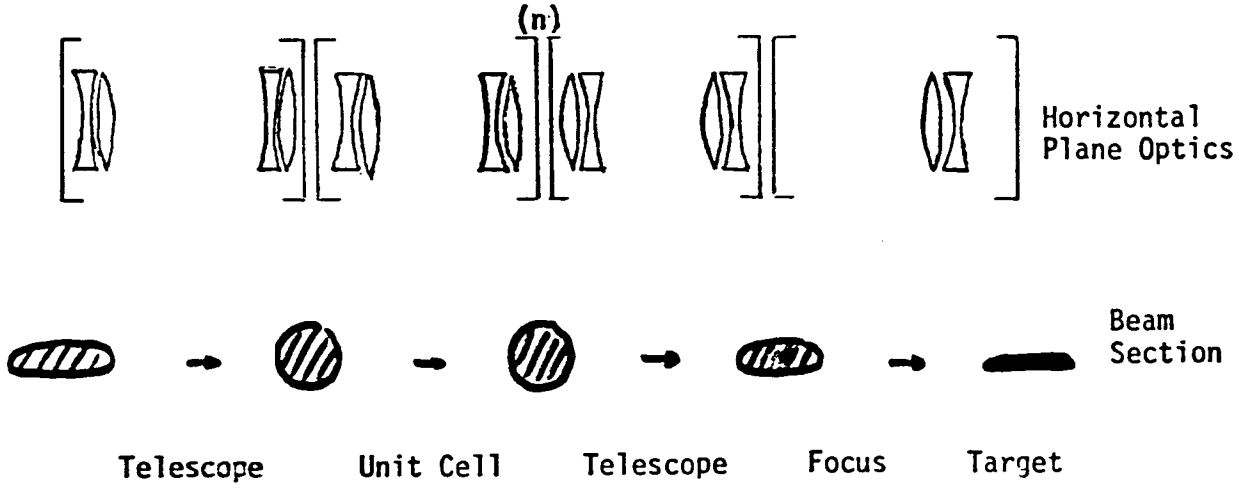

BEAM PREPARATION

Why a small beam spot ? Energy resolution limit $\Delta y \cdot m/(\text{dispersion})$

Final focus - simple waists ? x_o, θ_o = 0.864 mm, 0.347 mrad
y_o, ϕ_o = 0.122 mm, 0.816 mrad

x/θ correlation at target ? Eliminate $\Delta\theta_o$ contribution to ΔE

Other methods of achieving small beam spots ? Target re-imaging systems, wire chambers, etc.

Fig. 21

Kinematic Effects Related to Beam Preparation

$$\frac{\Delta E_f}{E_f} = \left(\frac{E_f}{M} \sin\Theta\right) \Delta\Theta_e \; ; \; \text{Ex.} \quad \Delta\Theta_e = 0.7 \text{ mrad.}$$

@ 2GeV	^2H	^{12}C	^{208}Pb
$\Theta_e = 10°$	E_f = 2.0 GeV	2.0 GeV	2.0 GeV
	$\frac{\Delta E_f}{E_f} = 1 \cdot 10^{-4}$	$2 \cdot 10^{-5}$	$1 \cdot 10^{-6}$
$\Theta_e = 90°$	E_f = 1.0 GeV	1.7 GeV	2.0 GeV
	$\frac{\Delta E_f}{E_f} = 4 \cdot 10^{-4}$	$1 \cdot 10^{-4}$	$1 \cdot 10^{-5}$

@ 4 GeV		
$\Theta_e = 10°$	E_f = 3.9 GeV	4.0 GeV
	$\frac{\Delta E_f}{E_f} = 3 \cdot 10^{-4}$	$4 \cdot 10^{-5}$
$\Theta_c = 90°$	E_f = 1.3 GeV	3.0 GeV
	$\frac{\Delta E_f}{E_f} = 5 \cdot 10^{-4}$	$2 \cdot 10^{-4}$

Fig. 22

MAGNETIC SPECTROMETER WORKING GROUP

1. DEFINE THE MAGNETIC SPECTROMETER REQUIREMENTS FOR CEBAF

- Working from the physics standpoint, what spectrometers are required to perform each planned experimental study?
- Find the common, minimum set of spectrometers. (Try to use vision!)
- What we are given are beam emittance, beam current, maximum beam energy, and available polarization state.
- What we have to adjust are:

$$\Delta\Omega,\ \Delta\ ,\ P_{max},\ \frac{\Delta P}{P}\ (R^{-1}),\ \theta_{max,\ min},\ \phi_{max,\ min}$$

within reasonable constraints of building size and total experimental equipment budget of 37 M$ (50 M$ inflated over project).

2. RECOMMENDATIONS TO THE MANAGEMENT ON RELATED R&D WORK

- What work needs to be done? Superconducting technology? What scale? Other?
- Where can and should the work be done? By whom?
- How much money needs to be spent in these efforts in view of the time sscale and extent of application?

Fig. 23

WORKSHOP REPORT

INTERNAL TARGETS AND TAGGED PHOTONS

June 18, 1984

TABLE OF CONTENTS

1. INTRODUCTION

The working group on internal target and tagged photons was organized to consider the experimental facilities which will be necessary to perform experiments with photons and internal targets. The group has reviewed the proposed experiments in both of these areas and looked at the facilities that would be necessary to perform them. The working group has held three meetings--an organizational meeting in Williamsburg, and two meetings at the George Mason campus in January and March.

Committee Membership

Jurgen Arends
Catholic University

Edward C. Booth
Boston University

Carl Carlson
William and Mary

Hall Crannell
Catholic University

William R. Dodge
Center for Radiation Research

Bill Donnelly
Mass. Institute of Technology

Ronald D. Edge
University of South Carolina

H. Funsten
William & Mary

Phillippe Gouffon

Evans Hayward
National Bureau of Standards

William Hesse
Randolph-Macon College

Roy Holt
Argonne National Lab

Harold J. Jackson
Argonne National Laboratory

David Jenkins (Chairman)
Virginia Tech

Marcos N. Martins

Bernhard Mecking
Physics Institute, Bonn

Blaine Norum (Secretary)
University of Virginia

C. N. Papanicolas
University of Illinois at Urbana

G. A. Peterson
University of Massachusetts

Janice Button-Shafer
University of Massachusetts

R. Roy Whitney
University of Virginia

2. PHYSICS PROGRAM

2.1 *ELECTRON SCATTERING WITH INTERNAL TARGETS*

2.1.1 *Few Body Experiments*

The use of internal targets in circulating beams of electron storage and stretcher rings has been widely discussed[1] as a method of achieving high luminosity under conditions of low background, superior energy resolution, negligible multiple scattering with minimal demands for beam from the primary accelerator. This approach represents an attractive option for pursuing some of the experiments of highest priority in the prospective research program at CEBAF. For polarization physics of the nucleon and few body nuclei, it may be the optimum experimental technique. In this section we will assess the comparative merit of internal target rings and the role a dedicated electron ring for internal targets could play at CEBAF in experiments with low Z nuclei.

In its simplest realization the internal target configuration consists of a thin gaseous target of thickness in the range of 1 - 100 nanograms located to intercept the beam at a point in the lattice of a conventional stretcher ring where the circulating electrons are highly focused. The high luminosity is achieved by recirculating the same electrons through the target many times per second. The stored energy in the circulating beam is small compared to that dissipated in burying an external beam of comparable luminosity. Consequently, backgrounds and shielding requirements for an internal target facility are modest compared to those for a conventional external beam installation. The

requirements of the ring place very limited demands on the performance of the injecting linear accelerator. Only one pulse per second for circulating currents of 100 to 1000 mamp is needed. From the point of view of the remainder of the accelerator complex, the operation of the ring is essentially parasitic.

Comparison of Internal and External Target Experiments

In discussing the role of an internal target facility, we will examine its application to the study of hadronic structure and the physics of the few nucleon system. Experiments using polarized targets and/or polarized electron beams are expected to play a major role. One of the most fundamental experiments to be done will be determination of the electric form factors of the proton and neutron. Polarization transfer from polarized electrons to an unpolarized target,[2] or alternatively, measurement of the asymmetry (analyzing power) in scattering of polarized electrons by a polarized target[3] have been proposed as techniques for such measurements. We will assume that the measurement of the analyzing power is representative of the internal target technique and compare a figure of merit for the polarization transfer measurement as it has been proposed using an external beam with the corresponding figure for the measurement of the analyzing power. Specifically, we will consider the measurement of the electric form factor of the neutron in the reaction ^{2}H(e,e'n)p.

Both experiments use the fact that the polarization transfer from polarized electrons is directly proportional to the nucleon electric form factor:

$$p_x = -2\sqrt{\tau(\tau+1)}G_E G_M \tan\tfrac{1}{2}\theta / \{G_E^2 + \tau G_M^2 \{1+2(1+\tau)\tan^2\tfrac{1}{2}\theta\}\}$$

where $\tau = Q^2/4M^2$. In the measurement of polarization transfer to unpolarized protons the asymmetry, detected in a second scattering by an analyzer (see Fig. 1), is equal to the product

$$A = a\, p_x\, A_y$$

where a is the polarization of the incident beam and A_y is the analyzing power of the second scattering. The neutron detection efficiency will be a product of the polarimeter efficiency, $\varepsilon_p \sim 0.01$, and the neutron detection efficiency, $\varepsilon_n \sim 0.1$. A reasonable value for the analyzing power of the polarimeter is $A_y = 0.3$.[4] In the measurement of the analyzing power, the asymmetry will be:

$$A = a p_T p_x' = a\, p_T p_x$$

where we have used the fact that $p_x' = p_x$ which follows from time reversal. p_T is the target polarization which we take to be 1.0.

A valid figure of merit for the two methods is

$$F = A^2 \varepsilon L / a^2 p_x^2$$

where ε is the effective total neutron detection efficiency and L is the luminosity. For the external beam experiment, the luminosity will be limited by the beam power dissipation in the liquid deuterium target. Current experience suggests that 100 watts is a reasonable limit. This corresponds to a luminosity of 10^{38}. For the ring experiment we assume a circulating current of 500 mamp, a number suggested by present electron ring operating experience. We use a deuterium target thickness of 20 nanograms which appears to be a reasonable design objective for target development over the near future. The resulting luminosity is 2×10^{34}. The figure of merit is tabulated in Table 1 together with the values assumed for the pertinent parameters. The

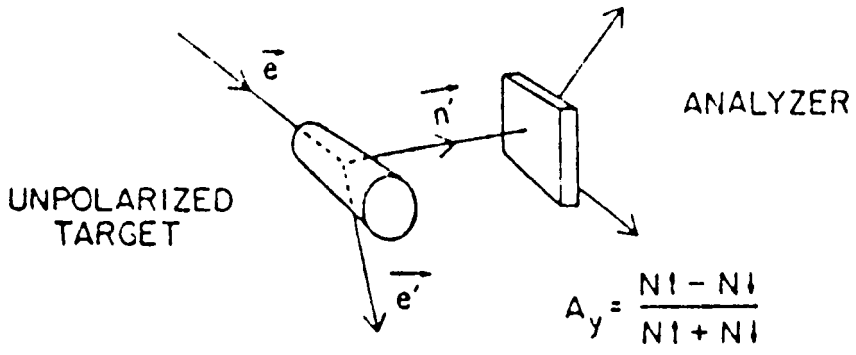

a) POLARIZATION TRANSFER MEASUREMENT

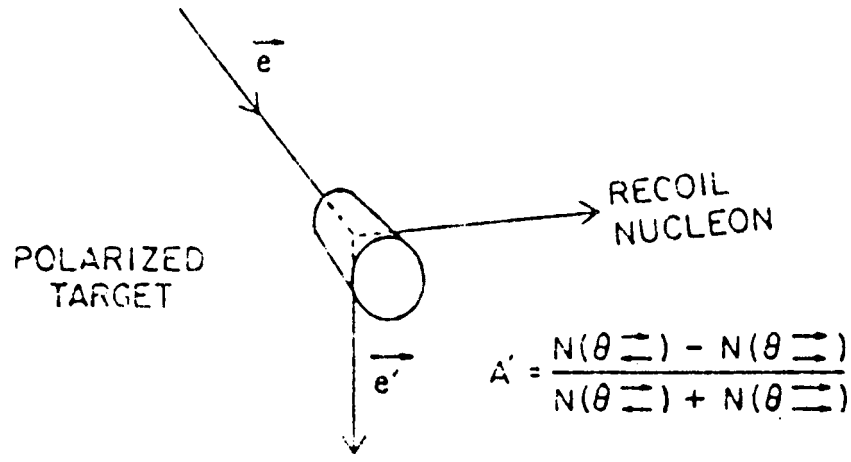

b) MEASUREMENT OF ANALYZING POWER

Figure 1. Possible experimental configurations for measurement of the polarization transfer to the nucleon in the elastic scattering of polarized electrons.

internal target method is clearly superior. However, the internal target ring has the additional advantage of what is essentially parasitic operation with respect to the main accelerator complex. In addition, the much lower luminosity of the internal target configuration raises other possibilities. The total interaction rate in the target will only be in the range of 10^4 - 10^5 counts/sec. One can consider the use of large solid angle systems for experiments on this facility. Much lower backgrounds resulting from the small loss of electron beam per second will minimize the need for experimental and structural shielding.

TABLE 1

Parameters for Experiments on Neutron Form Factors*

	External Beam Experiment	Internal Target Experiment
$L\ (b\text{-}sec)^{-1}$	10^{38}	2×10^{34}
A_y	0.3	-
Polarimeter Efficiency	0.01	-
Neutron counting efficiency	0.1	1.0**
Incident beam polarization	1.0	1.0
$d\Omega_{electron}$ (msr)	5	25
F (msr/b - sec)	4.5×10^{34}	5×10^{35}

*Parameters are defined in text
**Assuming the proton is counted in place of the neutron in a kinematically complete measurement.

Typical Experimental Rates

An estimate of the time required for a measurement of the electric form factor of the neutron using an internal deuteron target and the reaction $^2H(e,e'n)p$ with 2 GeV electrons can be made using the cross sections estimated by Cheung and Woloshyn.[3] We consider a momentum transfer $Q^2 = 10$ fm^{-2} where the experimental sensitivity is greatest. Using the cross sections calculated for 1 GeV electrons and assuming that they scale with electron energy like the Mott cross section, we find at 2 GeV for $Q^2 = 10$ fm^{-2}

$$d\sigma^3/d\Omega_e dk d\Omega_p \sim 4 \times 10^{-2} \ \mu b/sr\text{-}MeV$$

If we assume $\Delta\Omega_e = 25$ msr, $\Delta\Omega_p = 50$ msr, and a quasifree peak with a 30 MeV width, the parameter of the accelerator and target cited earlier give an event rate of 50 events/sec. To measure a 10% asymmetry with an accuracy of 0.5% will require 4×10^4 events, or about 800 seconds (15 minutes).

Conclusions

Several important conclusions can be drawn. First, internal target technology provides an extremely powerful means of studying the nucleon and light nuclei. Second, the method is superior to polarization experiments using external beams in which the nucleon polarization is measured. If allowances are made for the essentially parasitic character of a dedicated internal target stretcher ring and the possibility of use of large acceptance or 4π detector systems, the method is probably the optimum. For measurements of deuteron tensor polarization, the comparison with external beam methods is even more dramatic. Third the estimates used here for various operating

parameters are deliberately conservative. Previous discussions of internal target systems have been based on much larger internal target densities. Design objectives range as high as $10^{17}/cm^2$ for internal polarized hydrogen targets.[5] There is a substantial probability that ultimate luminosities will be much greater than we have assumed here.

2.1.2 *Physics with Polarized Electrons*

We summarize the nuclear structure information which may be extracted from analyses of inclusive electron scattering from polarized nuclei in the situation where the incident electron is longitudinally polarized. A more detailed analysis is given in reference 6.

General Form of the Cross Section

We begin by discussing the problem of scattering polarized electrons which may be polarized in the most general way both before and after the scattering. We shall assume that a single virtual photon is emitted in the process (see Fig. 2), to be absorbed by a nucleus which proceeds from the initial state i to the final state f. The three-momenta of the electrons are labelled k and k' and their energies are ε and ε'. The three-momentum transfer is $q = k - k'$; the energy transfer is $\omega = \varepsilon - \varepsilon'$. Furthermore, unit vectors have been defined with u_L = unit vector along k, u_N = unit vector normal to the scattering plane and $u_S = u_N \times u_L$ = "sideways" unit vector. Similarly unit vectors $u_{L'}$, $u_{N'}$ and $u_{S'}$ are defined with reference to k'. The general spin vectors for the incident and scattered electrons may be written in the laboratory system

$$S = h(\gamma S_L u_L + S_N u_N + S_S u_S)$$

$$S' = h'(\gamma' S_{L'} u_{L'} + S_{N'} u_{N'} + S_{S'} u_{S'}),$$

respectively, where $h = \pm 1$ and $h' = \pm 1$. The relativistic γ-factor is defined in the usual fashion, $\gamma = \varepsilon/m_e$ and $\gamma' = \varepsilon'/m_e$, where m_e is the electron mass. The S's involve sines and cosines of angles specifying the orientations of the electron spins and so lie between -1 and +1 in magnitude.

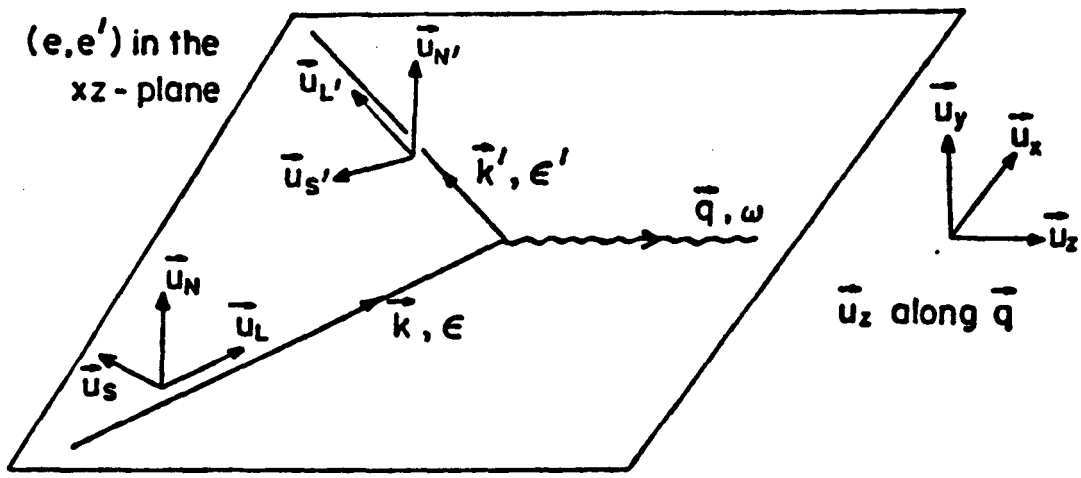

Figure 2. Kinematics for scattering of polarized electrons.

The general cross section for scattering of electrons with arbitrary polarizations contain terms of the following kinds:

1. terms with no h, h' or S's--these occur even if no electron polarizations are involved
2. terms with h, but not h'--these occur when the incident electron beam is polarized
3. terms with h', but not h--these occur when the scattered electron's polarization is measured, and
4. terms with the product hh'--these occur only if the incident electron beam is polarized and the scattered electron's polarization is measured.

As it is considerably more difficult to measure the scattered electron's polarization than it is to prepare a polarized electron beam we consider only that situation in all that follows. Then terms of classes 3 and 4 above are absent. The remaining terms of classes 1 and 2 yield an electron scattering cross section of the form

$$(d\sigma/d\Omega)^{h}_{fi} = \Sigma_{fi} + h\Delta_{fi},$$

where fi refers to a transition from initial state i to final state f. Σ_{fi} contains the dependence of class 1, i.e. occurs whether or not the incident electron is polarized. Δ_{fi} refers to the class 2 dependence and can only be probed with polarized electrons. In fact Σ_{fi} is the electron-spin-averaged cross section

$$\Sigma_{fi} = \tfrac{1}{2}\{(d\sigma/d\Omega)^{+1}_{fi} + (d\sigma/d\Omega)^{-1}_{fi}\}$$

and Δ_{fi} is the electron polarization cross section

$$\Delta_{fi} = \tfrac{1}{2}\{(d\sigma/d\Omega)^{+1}_{fi} - (d\sigma/d\Omega)^{-1}_{fi}\}.$$

Looking more carefully at the detailed nature of the electron polarization cross section Δ_{fi}, it may be shown to have the form

$$\Delta_{fi} = S_L \Delta_{fi}^{0} + \Delta_{fi}'$$

Here $S_L = 1$ for longitudinal electron polarization and $S_L = 0$ for normal or sideways (i.e. for transverse) electron polarizations. The term labelled Δ_{fi}' is of order γ^{-1} compared to Δ_{fi}^{0} and so may safely be dropped at electron energies of interest in most nuclear physics experiments. Thus one arrives at the conclusion that only longitudinally polarized electrons are of practical interest here.

Nuclear States having Specific Angular Momentum

We now examine nuclear details by focussing on a transition from state i to state f where both states are presumed to have good angular momenta, J_i and J_f respectively, as well as parities π_i and π_f respectively. Furthermore, let us assume that the initial state is polarized (i.e. the nuclear target is polarized whether or not the electron is polarized.).

The introduction of the nuclear coordinates is best illustrated by specific examples.

(i) Elastic Scattering: $J_i = J_f = 1/2$.

Only the charge monopole (CO) and the magnetic dipole (M1) can occur. With a polarized target and no electron polarization one does not learn anything beyond the usual unpolarized (e,e') cross section. In cases where $|F_L(q)| << |F_T(q)|$ or $|F_L(q)| >> |F_T(q)|$ the small form factor is hard to separate from the large one using the usual Rosenbluth separation method as they occur as their squares. On the other hand for polarized targets and polarized electrons one may

determine Δ_{fi} which involves the interference between the longitudinal and transverse form factors and hence is a much more sensitive probe of the small piece.

(ii) Elastic Scattering: $J_i = J_f = 1$

In this case C0, M1 and the charge quadrupole (C2) contribute. With unpolarized scattering only the sum of the squares of the C0 and C2 contributions may be determined, not the C0 and C2 separately. With polarized targets, however, the C0 and C2 contributions can be determined separately.

(iii) Elastic Scattering: $J_i = J_f = 3/2$.

In this case, the C0, M1, C2 and M3 (magnetic octupole) can contribute. As a specific example of such a case, we consider the $3/2^-$ ground state of ^{7}Li. The form factors were calculated using Cohen and Kurath wave functions. Some of the results are displayed below. In particular we show curves for the situations when the target nucleus ^{7}Li is polarized along the directions L, N, and S in Fig. 2.

Fig. 3 shows the cross section Σ_L obtained by polarizing ^{7}Li along the direction of the incident electron beam (L), but not requiring polarized electrons. Assuming that a practical minimum cross section is on the order of 10^{-33} cm^2/sr, electron energies of the order of 500 MeV cannot reach far beyond q = 400-500 MeV/c. The interesting high-q region ($q > 3$ fm^{-1}) may be inaccessible in such experiments.

To illustrate the polarization sensitivities we show in Figs. 4 various asymmetries, for example $(\Sigma_L - \Sigma_N)/\Sigma_0$, where Σ_0 is the unpolarized cross section. Clearly large asymmetries are present in regions where the cross sections are greater than 10^{-33} cm^2/sr. The asymmetries are

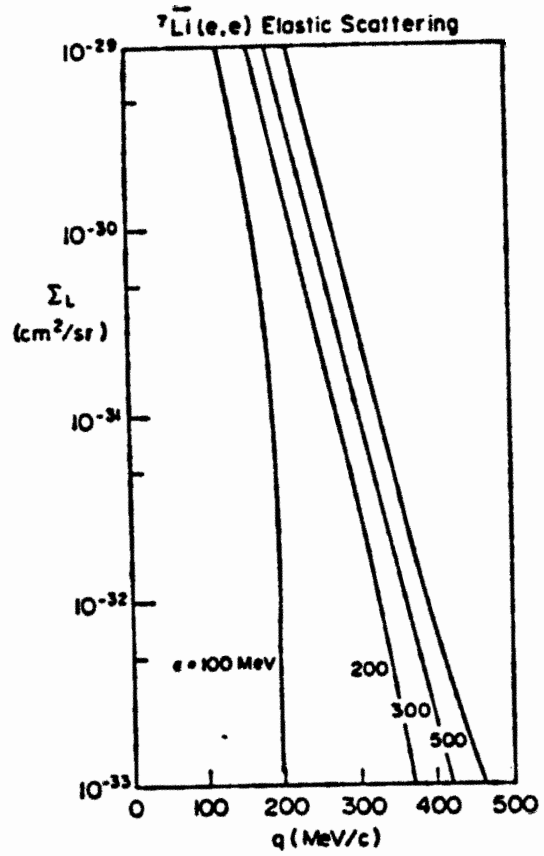

Figure 3. Elastic scattering from polarized ^{7}Li with unpolarized electrons. The target is assumed to be polarized along the along the directions of the incident electron (u_L).

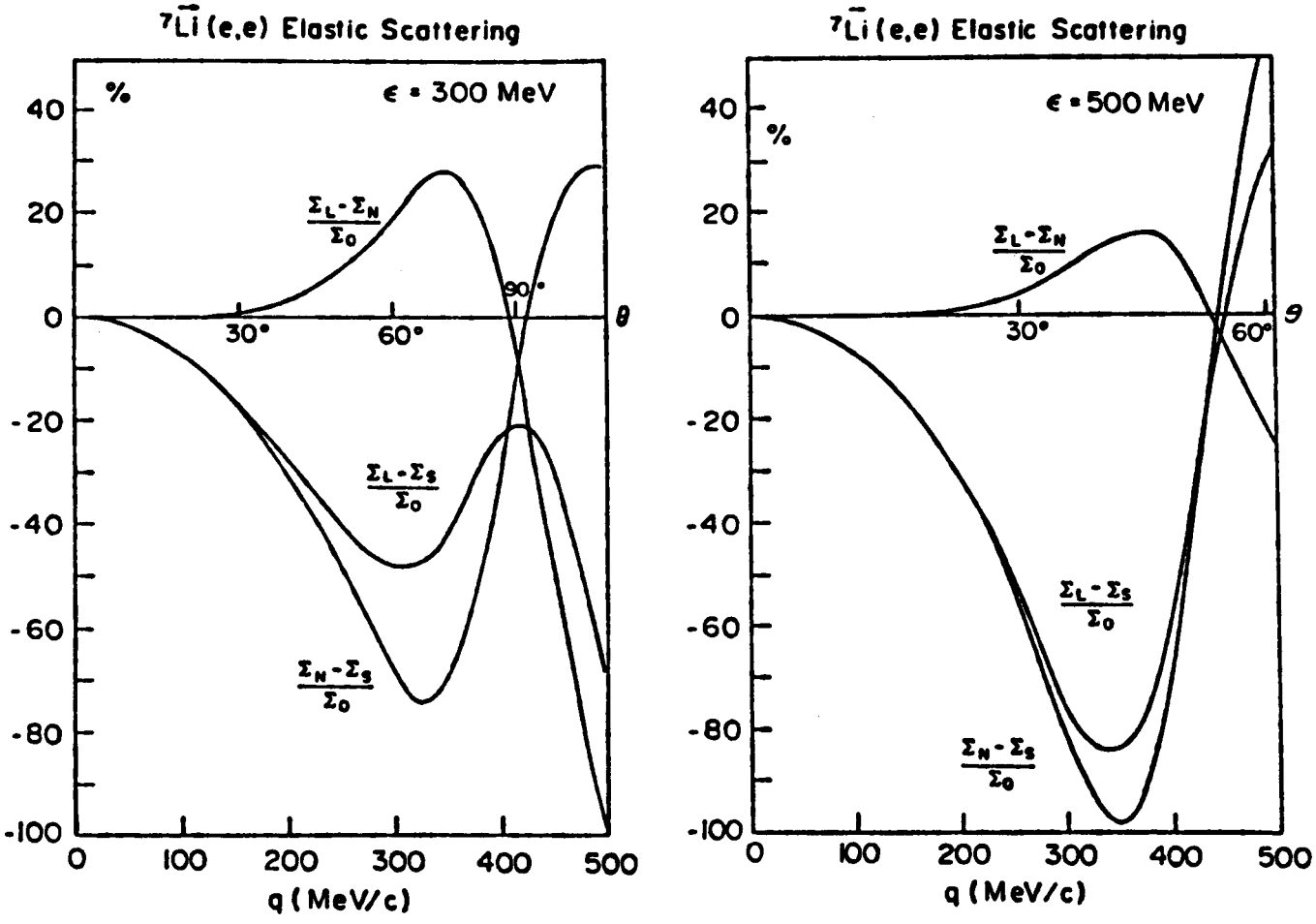

Figure 4. Unpolarized elastic electron scattering from polarized ^{7}Li at incident electron energies of 300 and 500 MeV.

large over a significant range of momentum transfer and all of the various pieces play sufficiently important roles in arriving at the overall asymmetry to suggest that the entire set of elastic form factors may be separately determined even without resorting to experiments with polarized electrons.

For completeness, in Fig. 5 we show the asymmetry Δ/Σ obtained when polarized electrons are considered along with the ^{7}Li target polarized in the L or S directions (the N direction polarization yields zero for Δ). Again quite large asymmetries are found in regions where the cross sections exceed 10^{-33} cm^2/sr. Both purely magnetic and Coulomb-magnetic interference terms contribute significantly when the asymmetry is large, with the former generally dominating at high q. From similar analyses still different combinations of the four basic form factors can be obtained.

(iv) Inelastic Scattering: $J_i = 1/2$, $J_f = 3/2$, $\Delta\pi$ = no.

In this case we may have M1, C2 and E2 multipoles. With polarized targets, but not polarized electrons, only the usual unpolarized cross section may be measured. On the other hand, with polarized targets and polarized electrons, it may be possible to observe the C2/M1 interference providing greater sensitivity to the small (and interesting) quadrupole form factors.

(v) Inelastic Scattering: $J_i = 3/2$, $J_f = 1/2$, $\Delta\pi$ = no

As a final example consider a $3/2^{\pm} \rightarrow 1/2^{\pm}$ transition again with M1, C2 and E2 multipoles. As a specific example we consider the transition from the $3/2^-$ ground state of ^{7}Li to its $1/2^-$ (0.478 MeV) first excited state. One again Cohen and Kurath wave functions were employed.

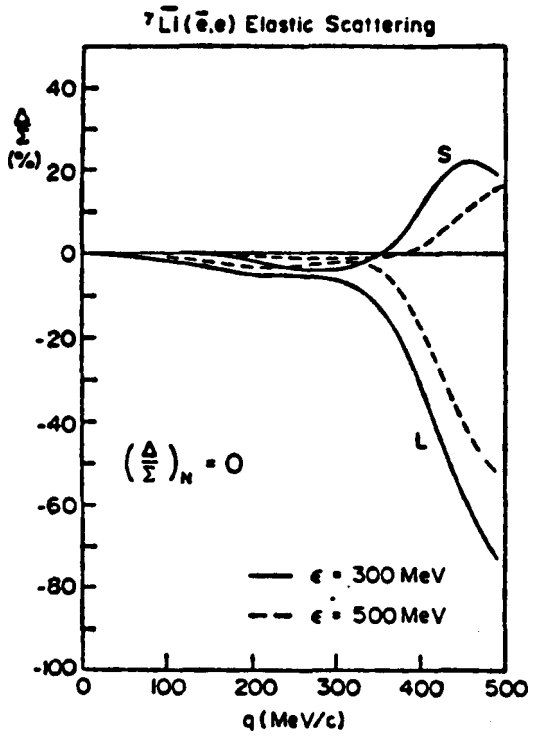

Figure 5. Scattering of polarized electrons from polarized ^{7}Li.

Beginning first with the situation where the ground state of ^{7}Li is polarized as in the elastic scattering case above (iii), but where the incident electron is not polarized, we have the results shown in Fig. 6. The cross sections remain above the 10^{-33} cm^2/sr level out to beyond 400 MeV/c momentum transfer for this case where ε = 300 MeV. In contrast to the elastic scattering situation where the asymmetries became small at low q (see Fig. 4), here they may remain large down to the lowest momentum transfers. The reason is that in the elastic case the low-q behaviour is dominated by the elastic monopole charge form factor and at low-q this piece has no interesting polarization dependence by itself and so diminishes the overall effect at low momentum transfer.

In Fig. 7 we show a more complete representation of the cross section Σ as a function of θ^* and ϕ^* for fixed electron energy and angle. The curve labelled $\phi^* = 0^\circ$ corresponds to sweeping the ^{7}Li polarization around from the direction of q ($\theta^* = 0^\circ$) to the direction opposite to q ($\theta^* = 180^\circ$) in the electron scattering plane. In the process one encounters the direction of the incident electron (labelled L) and the sideways direction (labelled S). A similar sweep, but reflected in the plane defined by the normal direction and the direction q, is obtained when $\phi^* = 180^\circ$. The remaining curve has $\phi^* = 90^\circ$ and so sweeps out directions in polarization space from q up through the normal direction (labelled N) and back to -q. Clearly these cross sections are large enough to make such experiments interesting (using our criterion of 10^{-33} cm^2/sr, the units used here). By looking at the dependence on the three form factors we wish to have separated, M1, C2 and E2, it is clear that a decomposition can be accomplished.

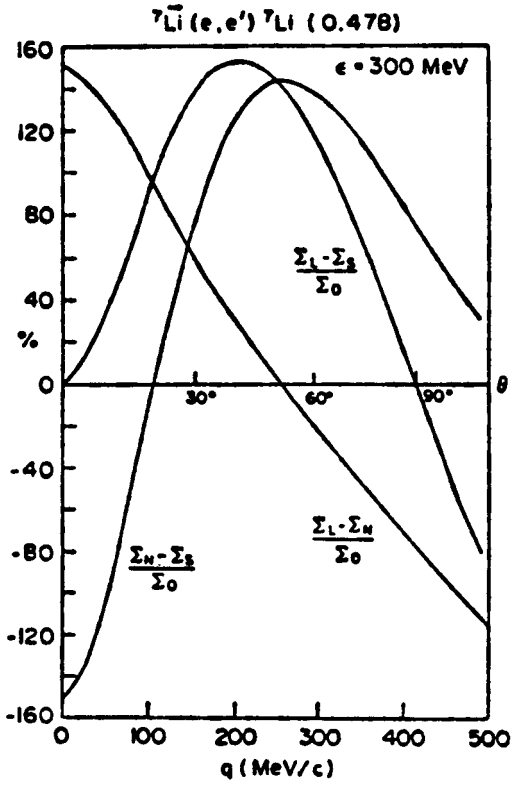

Figure 6. Inelastic scattering of unpolarized electrons from polarized ^{7}Li.

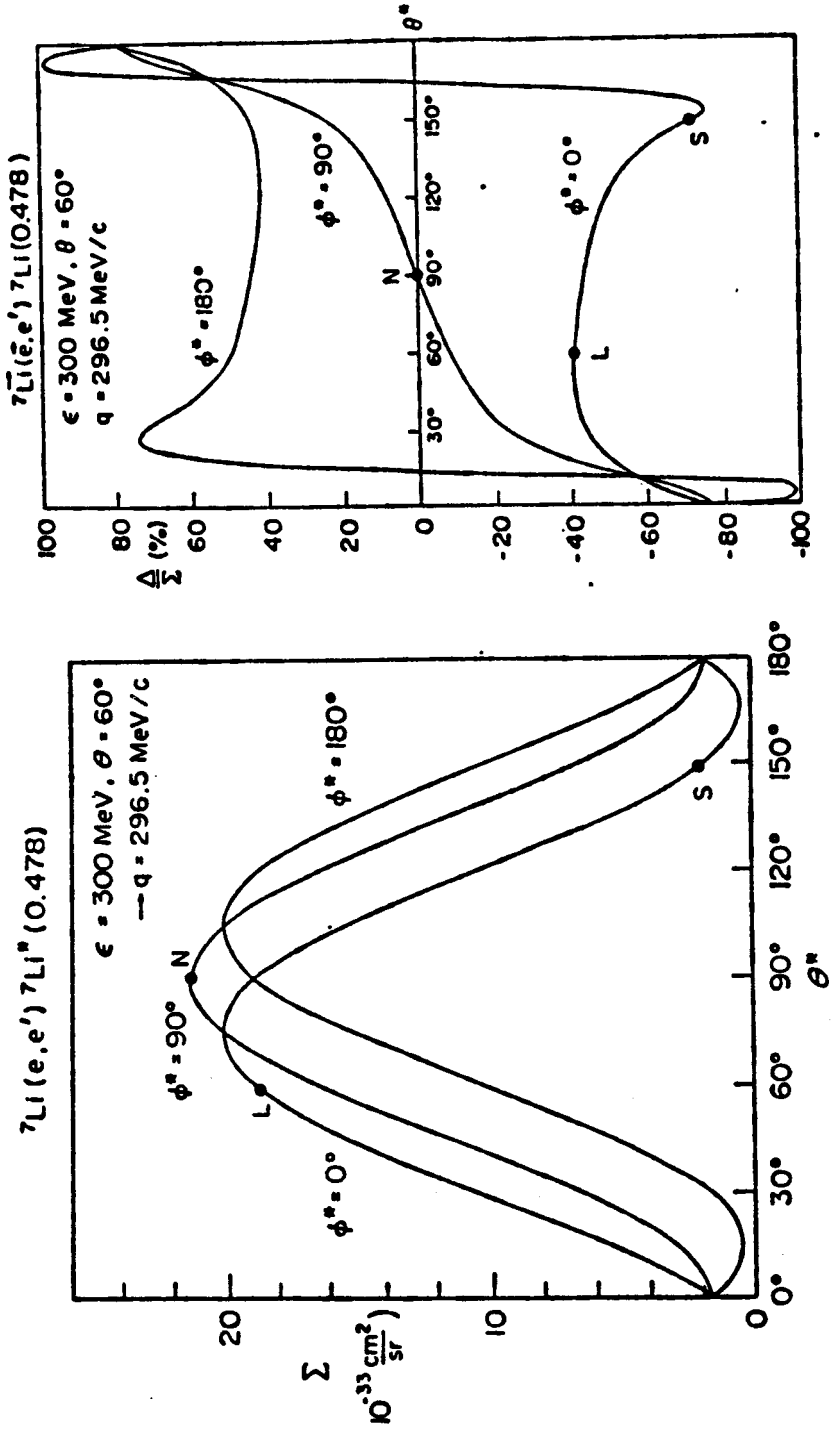

Figure 7. Inelastic electron scattering from polarized ^7Li at ε = 300 MeV and θ = 60°. Results are given as functions of the target polarization direction specified by (θ^*,ϕ^*). The special directions corresponding to L, N and S (see Fig. 2) are indicated. The top figure assumes no electron polarization, whereas the lower does not assume an electron polarization.

Finally in Fig. 7 we show the asymmetry Δ/Σ as could be obtained if polarized targets and polarized electrons were available. This is perhaps a good point to mention that, while we have been stressing the variation of the cross sections as functions of (θ^*, ϕ^*), of course one may reach other values of these angles by changing the populations in the magnetic substates of the polarized nucleus.

Another example of a $3/2 \rightarrow 1/2$ transition is shown in Fig. 8. Here we take the $3/2^+$ ground state of ^{39}K to be a $1d_{3/2}$ proton hole in ^{40}Ca and $1/2^+$ excited state at 2.53 MeV to be a $2s_{1/2}$ proton hole in ^{40}Ca. Results are shown for the asymmetries $(\Sigma_N - \Sigma_S)/\Sigma_0$ and $(\Sigma_L - \Sigma_N)/\Sigma_0$ for a variety of electron energies ε and scattering angles θ. Near each point is a number indicating the value of Σ_0 in units of 10^{-33} cm^2/sr. Clearly once again the asymmetries are large over a wide kinematic region, although, if cross sections must remain above the 10^{-33} cm^2/sr level, the high-q region will be inaccessible.

Conclusion and Discussion

We summarize here some of the basic conclusions reached in this discussion of polarization in electron scattering from discrete states:

1. Practically speaking only longitudinally polarized electrons appear to be of interest for nuclear physics studies. They may prove difficult to obtain under conditions where such experiments are likely to be most practical, viz. internal targets in electron stretcher rings. In such a case, when electrons are constrained to closed orbits, the spins will precess and so one will not in general have a beam of longitudinally polarized electrons.

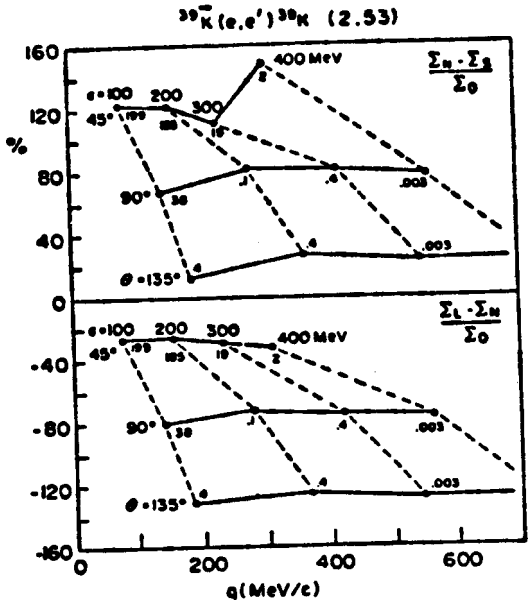

Figure 8. Inelastic scattering of unpolarized electrons from polarized ^{39}K.

2. For inclusive scattering with polarized electrons, the cross section Δ_{fi} will vanish unless a nuclear polarization is also known (that is, ignoring parity-violating effects from the weak interaction).

3. With polarized targets, but without having polarized electrons, there is new information in the cross sections Σ_{fi}. These contain CJ/CJ', EJ/EJ', MJ/MJ', EJ'/MJ', CJ/EJ' and CJ/MJ' interferences in general, in addition to the usual unpolarized cross sections which depend only on $(CJ)^2$ and $(EJ)^2 + (MJ)^2$, where the electric and magnetic form factors cannot be separated from one another. By varying the direction of polarization of the target, it is possible in principle to determine separately each of the multipole matrix elements for a given transition.

4. Over a significant range of electron energies and scattering angles the typical cross sections remain above 10^{-33} cm^2/sr and so, from the criteria established in discussions of internal target physics with an electron stretcher ring, appear to yield practical counting rates.

5. Elastic scattering has a feature which differs from inelastic scattering: the coherent elastic monopole charge form factor, F_{CO}^2, involves a factor Z^2 and so may be very large at low q. On the other hand, this piece contains no interesting polarization dependence. Thus at low q the typical asymmetries are small for elastic scattering. Such is not the case for inelastic scattering where in general the asymmetries may remain large even at very low q.

6. With polarized electrons and polarized targets the cross section Δ_{fi} will be accessible. This contains EJ/EJ', MJ/MJ', EJ/MJ',CJ/EJ' and CJ/MJ' interferences in general which may be separated from one another by varying the direction of polarization as in case (3) above. Note, however, that the problem of the large coherent F_{CO}^2 form factor (discussed above) does not occur for Δ_{fi}. Of course Σ_{fi} and Δ_{fi} may be separated by taking sums and differences of the overall cross section with electron helicities $\pm$ 1.

The ability to separate all of the various electromagnetic multipole matrix elements as functions of q in a mixed multipole situation is highly desirable and yet is not possible with inclusive electron scattering lacking information about nuclear polarizations.

2.1.3 *Polarization Measurements*

The high circulating currents (0.1 to 1.0 A) which can be achieved in storage rings should permit one to perform studies of electron scattering from rare or specially prepared targets which are not accessible by conventional methods. In addition, background levels typically are low at electron storage rings and this should allow one to use large solid angle detectors.

Recently, it has become apparent that polarization phenomena in electron scattering will play an increasingly important part in the study of nuclei. For example, polarization studies are essential in isolating the charge form factors of nuclei with spin >1. Work has begun already at the MIT-Bates Linear Accelerator Center to measure the tensor polarization in electron-deuteron elastic scattering in order to determine the charge F_C and quadrupole F_Q form factors of the deuteron.[7] Polarization experiments are expected to have a central role in studies of the electric form factors of the nucleons.

As an example of the possibilities of polarized targets, we will describe a proposed experiment at the Aladdin storage ring with the objective of measuring electron scattering from a tensor polarized deuterium target. The expression for the tensor polarization t_{20} in terms of the elastic form factors (F_C, F_Q and F_M) of a spin-one target, say, the deuteron is given by

$$t_{20} = -\sqrt{2}\{(X(X + 2) + Y/2\}/\{1 + 2(X^2 + Y)\}$$

where

$$X = 2/3\eta F_Q/F_C$$

$$Y = 2/3\eta f(\theta)F_M^2/F_C^2$$

$$\eta = q^2/4M_d^2$$

$$f(\theta) = \tfrac{1}{2} + (1 + \eta)\tan^2(\theta/2)$$

Here, q is the four-momentum transfer, M_d is the rest mass of the deuteron and θ is the angle of the scattered deuterons. Since F_M is small for $q \leq 5$ fm^{-1}, a measurement of t_{20} essentially yields the ratio: F_Q/F_C.

As a comparison of the merit of the polarized internal target experiment with an external beam experiment, the expected counting rates as well as the actual counting rates in a recent experiment at Bates are given in Table 2. The expected rates in the Aladdin experiment are more than a factor of 100 greater than the external beam experiment at Bates. The assumptions which were used in determining this rate estimate are: (i) an electron current of 100 mA (ii) a target thickness of 10^{14} atoms/cm^2 (iii) a solid angle of 75 msr and (iv) a beam energy of 1.0 GeV. In a ring devoted to nuclear studies, one could consider developing thicker polarized targets and higher circulating currents.

Thus a tensor polarized target even in an *existing* storage ring could give a remarkable improvement over the conventional external beam experiment. Table 2 also compares the rates to those expected at CEBAF. The assumptions in the estimate for a ring at CEBAF are that one gains a factor of 16 over Aladdin from the 4.0 GeV electron energy instead of 1.0 GeV, a polarized target of 10^{15} atoms/cm^2 in thickness could be used and a circulating electron current of 0.5 A should be

TABLE 2

Counting rates for a t_{20} measurement

q (fm^{-1})	Count Rates (hr^{-1}) MIT/Bates (actual)	Aladdin (expected)	CEBAF (expected)
1.74	40	5×10^3	4×10^6
2.03	12	1×10^3	8×10^5
3.0	-	45	4×10^3
4.0	-	2	1.6×10^3
5.0	-		90
6.0	-		13

The rates for Aladdin assume: I_{circ} = 100 mA, E_e = 1.0 GeV, n_d = 10^{14} atoms/cm² and $\Delta\Omega$ = 75 msr. Note that all values of t_{20} in this momentum transfer range can be measured simultaneously; whereas, in the experiment at MIT/Bates, which involved the use of a polarimeter, only one value of $t_{20}(q)$ could be measured at a time.

The assumptions in the estimate for CEBAF are an electron energy of 4.0 GeV, a current of 0.5 A and a target thickness of 10^{15} atoms/cm².

feasible for short storage periods, say 1 sec. The expected advantage in count rate of this experiment at CEBAF as compared with that expected at Aladdin would be a factor of 800 or a factor of ≥80,000 as compared with the external beam experiment performed at MIT/Bates. Then, a momentum transfer range in excess of 4 fm^{-1} would become accessible. Thus, an internal target facility at CEBAF could contribute significantly to the research capability.

2.2 *PHOTON INTERACTIONS WITH TAGGED PHOTONS AND BACKSCATTER LASER*

2.2.1 (γ,*K*) *Reactions*

Hypernuclei can be produced through both photo and electroproduction. One of the recent results of hypernuclear physics has been the discovery of narrow Σ hypernuclear states and raises the prospect of Σ as well as Λ hypernuclei. At present most of the information on hypernuclei has been extracted from (K^-,π^-) reactions. Such reactions excite strongly only the natural parity hypernuclear states, and, because the K^- and π^- are strongly absorbed, they occur near the nuclear surface with a reaction mechanism which may not be a simple one-step process. In contrast (γ,K^+) and (γ,K^0) excite both natural and unnatural parity hypernuclear states with comparable strength, and γ and K^+ and K^0 particles are only weakly absorbed so that the reaction is not confined to the nuclear surface and is predominantly a simple one-step process.

An exciting prospect for (γ,K^+) and (γ,K^0) experiments is that they may be a unique probe for studying deeply bound Λ and Σ hypernuclear states. It appears that the K^+ and K^0 are sufficiently weakly absorbed in the final state that it should be possible to deposit a Λ in its lowest shells even in a very heavy nucleus.

Two experiments which propose to examine photoproduction of hypernuclei are included in the appendix.

2.2.2 *Pion Photoproduction*

Pi meson photoproduction experiments on light nuclei are very interesting for two reasons: they can be used as laboratories to study details of mesonic propagation in the few-nucleon environment, and they can be used to search for new and exotic effects which test our current theories about nucleon and elementary particle interactions.

The use of monochromatic photons adds an extra dimension of flexibility in choosing experiments, especially on nuclei with $A > 2$. The use of the photon as a probe makes the interpretation more tractable than with a hadron probe since the initial state interaction is well know, and the relative weakness of the electromagnetic interaction minimizes disruptive nuclear effects preceding the processes of interest. On the other hand, the basic cross sections are small, especially since momentum transfers are required to be high in comparison to those of the less interesting quasifree processes.

The photoproduction of pions from light nuclei is discussed in in the appendix.

2.2.3 *Photoproduction of Vector Mesons*

The properties of the vector mesons are extremely important to any fundamental theory of hadronic matter. In terms of the meson theory of nuclear forces, the coupling constants of the vector mesons to nucleons are among the most basic parameters of the theory, and the electromagnetic couplings are needed to understand meson exchange currents (MEC). More generally, the magnetic moments, masses, and strong coupling constants of the vector mesons can be predicted from

bag models, and their measurement provides an important test of such models.

A program of measurements designed to considerably extend current knowledge of vector meson is outlined in the appendix . It makes use of the proposed tagged-photon facility and would need 2 GeV energy to study the ω, ρ and ϕ meson. Study of higher lying states would require more energy. The polarized beam (and polarized targets) would allow the measurement of the three polarization parameters, Σ, T and P, which would significantly improve present knowledge of these important particles.

2.2.4 *Photoexcitation of Baryon Resonances*

The analysis of elastic πN scattering data has given detailed information on higher excitation modes of the nucleon. The mass, width, spin and parity for approximately 30 3-quark systems with zero strangeness have been determined.[8] This experimental information has to be explained by microscopic models for the structure of 3-quark systems. While models such as the non-relativistic quark model with QCD-inspired additions have only a phenomenological basis, calculations on the basis of pure QCD will improve in the near future. These theoretical models are required to predict not only the static properties of 3-quark systems but also their decay modes. In contrast to hadronic decays the electromagnetic decay $N^* \rightarrow N\gamma$ can easily be calculated once the spatial distribution of the quarks in the initial and the final state is given. Therefore, the measurement of the electromagnetic coupling at the γNN^* vertex for real and virtual photons provides the best way to

test the dynamical features of microscopic models for the structure of 3-quark objects.

Single Pion Photoproduction with Real Photons

Most of the information on the electromagnetic properties of nucleon resonances has been obtained by exciting a nucleon to a resonance N* using real photons and observing the subsequent πN decay. By comparing the $\gamma N \to N^* \to \pi N$ process with $\pi N \to N^* \to \pi N$ as shown in Fig. 9, one obtains directly, in principle, the coupling constant at the γNN^* vertex. In practice the situation is complicated because

1. The resonances are broad and overlapping (see Fig. 10)
2. There is background from nonresonant π-production (Born terms) as shown in Fig. 11.
3. The experimental information on $\gamma N \to \pi N$ is far from being complete.

Even in this situation the photocouplings of many nucleon resonances have been determined with some accuracy using the π photoproduction data that have been accumulated in the last two decades.[9] However, due to the limited amount of experimental information the photocouplings of those resonances that are only weakly excited in γN reactions could not be determined. This is entirely an experimental problem that can be solved by measuring accurate data sets for all necessary observables over a complete range of kinematical variables.

A tabulation of the three most recent analyses of the photoproduction data is given in Table 3[10]. The Nagoya analysis[11] provides results using data from a proton target, but does not analyze

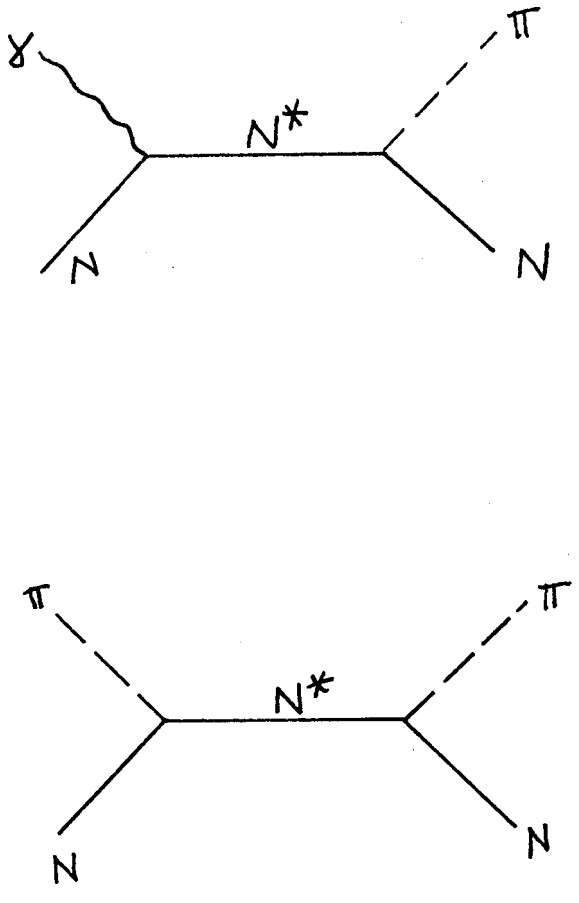

Figure 9. Comparison of γN and πN Reactions

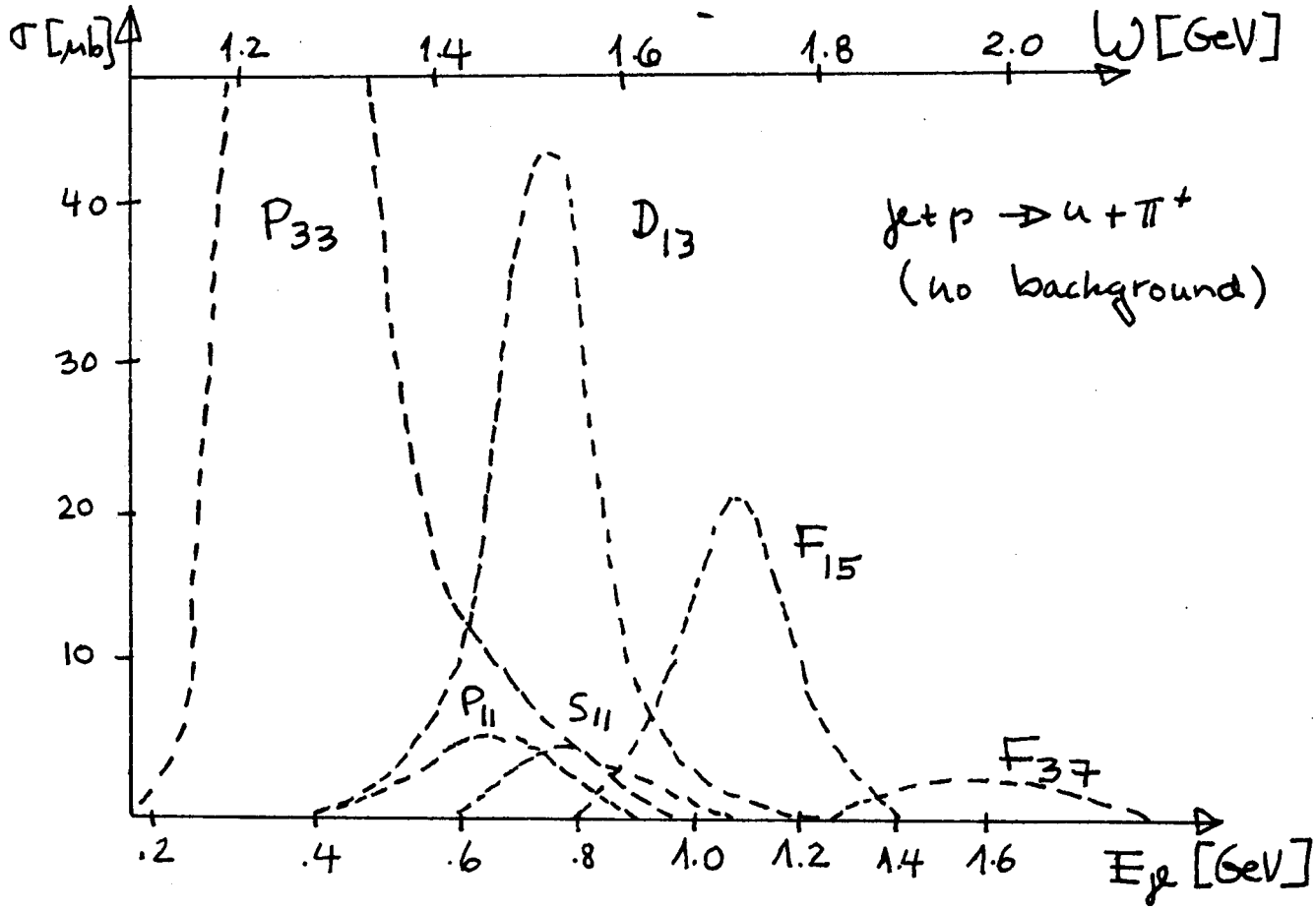

Figure 10. Photoexcitation of Nucleon Resonances

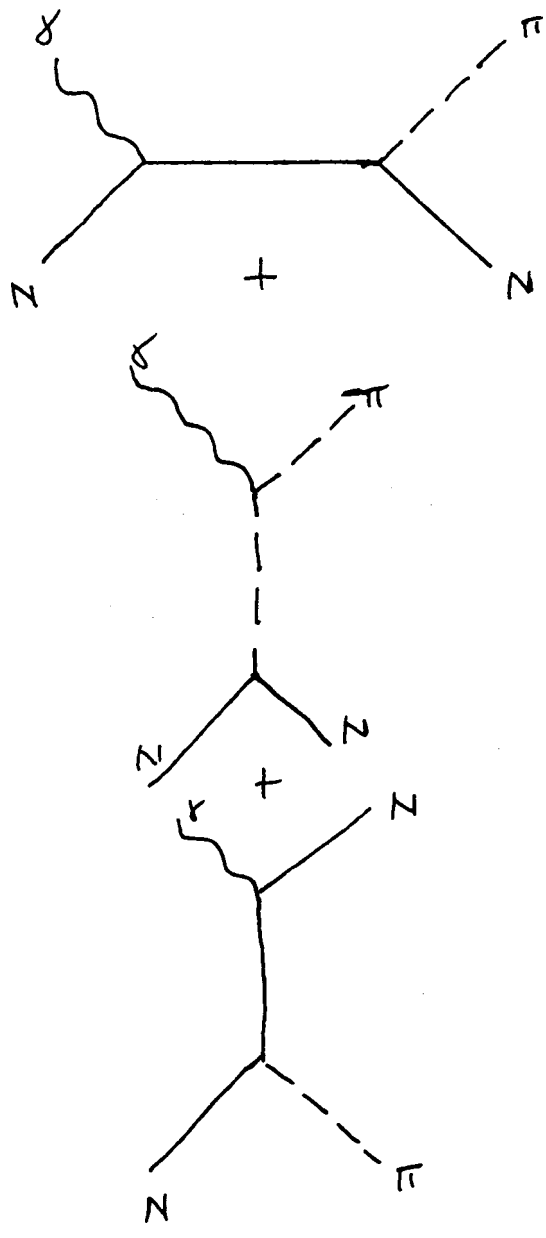

Figure 11. Non-resonant π production.

any neutron target data. The Tokyo analysis[12] includes both proton and neutron target data, but no attempt was made to include systematics in the quoted errors; the errors are purely statistical. The Glasgow analysis[13] provides preliminary results for many new resonances as well as for older ones. The errors quoted by the Glasgow analysis include an estimate of systematic effects. In many cases the different analyses do not agree with each other within their quoted errors. On occasion, even the signs of the coupling are in doubt.

The $\gamma N \to \pi N$ reaction is completely determined once four complex helicity amplitudes are known as a function of two kinematical variables, usually the photon energy and the π center-of-mass angle. Since only the phase is arbitrary, the experimental determination requires seven different measurements for each kinematical setting. The best combination of experiments involves single and double polarization measurements as shown in Table 4.

For most reactions only the single polarization data are presently available although some double polarization information for G and H exists from Daresbury experiments.

To reduce the influence of experimental errors and to get rid of discrete ambiguities, it will be useful to complement these measurements by additional double polarization experiments--especially using circularly polarized photons from the bremsstrahlung of longitudinally polarized e^- in combination with a polarized target.

To disentangle the isospin structure of the π photoproduction these measurements have to be made for three of the four possible reaction channels:

TABLE 3

Experimental Photo Couplings

Helicity Amplitudes in $GeV^{1/2} \times 10^3$

State		Nagoya	Tokyo	Glasgow
P11 (1440)	P1/2	-87 ± 6	-69 ± 4	-68 ± 15
	N1/2		23 ± 9	56 ± 15
F15 (1680)		121 ± 10	115 ± 3	141 ± 14
	P1/2	-9 ± 2	-28 ± 3	-18 ± 14
	N3/2		-24 ± 9	-33 ± 15
	N1/2		26 ±	44 ± 12
P33 (1232)	P3/2	-256 ± 3	-264 ± 2	-247 ± 10
	P1/2	-141 ± 4	-147 ± 1	-136 ± 6
F35 (1910)	P3/2		-29 ± 7	-72 ± 35
	P1/2		-22 ± 10	24 ± 14
F37 (1950)	P3/2		-101 ± 5	-82 ± 17
	P1/2		-91 ± 5	-67 ± 14
S11 (1550)	P1/2	70 ± 4	83 ± 7	65 ± 16
	N1/2		-75 ± 19	-98 ± 26
D13 (1525)	P3/2	164 ± 8	178 ± 3	167 ± 10
	P1/2	-5 ± 5	-32 ± 5	-19 ± 7
	N3/2		-147 ± 8	-147 ± 15
	N1/2		-76 ± 6	-56 ± 11
D15 (1675)	P3/2	19 ± 9	30 ± 4	3 ± 12
	P1/2	34 ± 4	6 ± 5	23 ± 15
	N3/2		-66 ± 26	-59 ± 20
	N1/2		-39 ± 17	-59 ± 15
D33 (1710	P3/2	87 ± 23	47 ± 7	102 ± 22
	P1/2	72 ± 33	112 ± 6	123 ± 22
D35 (1940)	P3/2			-23 ± 80
	P1/2			-38 ± 47

TABLE 4

Measurements Needed for Determination of Amplitudes

Observable	linearly polarized photons	polarized target	measurement of recoil nucleon polarization
Single Polarization:			
1. $d\sigma/d\Omega$ (differential cross section)	-	-	-
2. T (target asymmetry)	-	✓	-
3. Σ (beam asymmetry)	✓	-	-
4. P (recoil nucleon polarization)	-	-	✓
Double polarization:			
5. G	✓	✓	-
6. H	✓	✓	-
7. T_x	-	✓	✓

Note that only one time consuming double scattering experiment to determine the transverse recoil nucleon polarization will be necessary.

$$\gamma + p \rightarrow \pi^+ + n$$

$$\gamma + p \rightarrow \pi^0 + p$$

$$\gamma + n \rightarrow \pi^- + p$$

$$\gamma + n \rightarrow \pi^0 + n$$

Usually the π^0, n channel is omitted.

Multiple π Photoproduction

With increasing mass of the nucleon resonance, the decay mode $N^* \rightarrow \pi N$ is suppressed in favor of decay modes like $N^* \rightarrow \pi\Delta$ or $N^* \rightarrow \rho N$. Therefore, these resonances are only weakly excited in πN reactions and are very difficult to observe in elastic πN scattering. This offers an explanation for the fact that theoretical models predict

many more nucleon resonances than have been observed in πN scattering. On the other hand the coupling to the γN channel can still be reasonably strong. This offers the unique possibility to search for those resonances in $\gamma N \to N\pi\pi$ reactions since this is the only decay channel that is accessible in a formation experiment.

The background in the $N\pi\pi$ channel consists mainly of nonresonant $\pi\pi$ or $\pi\Delta$ production and the production of vector mesons. Disentangling the isospin structure of dipion production is more difficult than for single pion production since more charge channels are available. An isobar-model partial-wave analysis would be necessary to determine the experimental photoproduction amplitudes: $\gamma N \to \pi\Delta$, $\gamma N \to \rho N$, $\gamma N \to \varepsilon N$, $\gamma N \to \pi N^*$ such as is now done for the $\pi N \to \pi\pi N$ data.[15]

The experimental information is very scarce compared to single π photoproduction. This is essentially due to difficulties in measuring multiple particle final states with high efficiency.

Experimental Setup

Practically all experiments in single π photoproduction have been made using a bremsstrahlung photon beam and detecting the pion or the nucleon (sometimes both) in the final state. The primary photon energy has to be determined by measuring the energy and angle of one of the outgoing particles precisely. This leads to experimental setups that are capable of determining only one observable at one kinematical setting at a time. This results not only in unacceptably long running times, but also introduces additional systematic errors due to changes in efficiencies, polarization etc. from one kinematical point to the next.

These difficulties can be avoided by using a broad band bremsstrahlung tagging system to determine the energy of the primary photon. Since now high resolution for the final state particles is no longer required it is possible to use a large solid angle detector (close to 4π) and measure one observable over the whole kinematical range of interest simultaneously.

A bremsstrahlung tagging system also provides precise photon flux determination by counting the recoil electrons one by one. It also provides kinematical overdetermination for the suppression of unwanted backgrounds such as events from nuclear processes in the case of polarized proton or deuteron targets or events from the unpolarized part of the bremsstrahlung spectrum in the case of coherent bremsstrahlung from a crystal radiator. Using an electron beam with a duty-cycle close to one, tagged photon rates, limited by accidental coincidences between the tagging counters and the hadron detector, of 10^7/sec can be obtained. At this rate the operation of large solid angle detectors does not present any difficulties. Also polarized proton or deuterium targets do not suffer from radiation damage.

A large solid angle detector will not only give high counting rates for single π production but will also have high efficiency for the detection of multiple particle final states. A suitable detector should have good momentum resolution and particle identification for charged particles as well as high efficiency and energy resolution for photons over a wide kinematical range. Detectors of even greater complexity are presently at use at high energy e^+e^- and p-pbar colliders.

Conclusions

Single pion photoproduction can be used to determine the photocoupling of the nucleon resonances. This information provides one of the most important tests of microscopic models for the structure of 3-quark systems. Understanding the properties of the nucleon and its excited states on the basis of the fundamental theory of hadronic interactions can provide the foundation for a better understanding of NN-interaction and nuclear physics in general.

Experimental investigation of pion photoproduction will be considerably facilitated by the use of monochromatic photon beams and large solid angle detectors for the outgoing hadrons. Polarized photons and polarized proton or deuterium (as a source of polarized quasifree neutrons) targets will have to be combined for double polarization experiments. The detection of multiple π final states will serve to look for the resonances predicted by theoretical models that couple only weakly to the πN-channel.

A 4 GeV high duty-cycle e^- accelerator combined with general purpose detectors is well suited to solve the experimental problem.

2.2.5 *Photodisintegration of the Deuteron*

The photodisintegration of the deuteron is one of the most fundamental processes in photonuclear physics. Therefore, careful experimental investigations and a detailed theoretical understanding of the process are of great importance for all photonuclear reactions.

Below the pion production threshold where the process is dominated by the diagram (a), the deuteron wave function and details of the NN-interaction can be studied. Above the pion threshold the cross section is enhanced by the production and reabsorption of nearly real pions (diagram (b)). In the region of the nucleon resonances the interaction between a nucleon and its excited partner can be studied (diagram (c)).

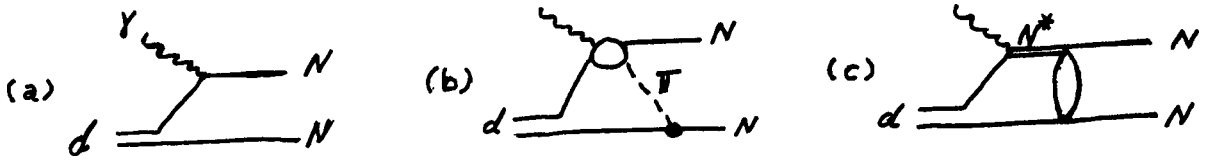

Despite these interesting aspects both the theoretical and the experimental situation in deuteron photodisintegration is unsatisfactory. The theoretical treatment of the process requires a good knowledge of the deuteron wave function (including the eventual admixtures of nucleon resonances and 6-quark configurations) and a reliable description of nonresonant pion photoproduction and of the photoexcitation of the nucleon resonances and their interaction with nucleons (see e. g. ref. 16). In the framework of perturbative QCD a prediction for the asymptotic behavior of the cross section has been made.[17]

The experimental situation (above k ~ 100 MeV) is characterized by large discrepancies between different data sets for the differential cross sections (see Fig. 12). The data stop at k ~ 800 MeV. Only few experiments have been performed to investigate single polarization quantities like target asymmetry (using a vector polarized deuterium target), beam asymmetry (using linearly polarized photons) and recoil nucleon polarization. No data exist for double polarization quantities.

Deuteron photodisintegration has a complicated spin structure. A completely model independent determination of the 12 complex helicity amplitudes will require 23 different observables to be measured as a function of the photon energy and the proton c.m.s. angle. Most of the experiments require the combined use of a (linearly or circularly) polarized photon beam and a (vector or tensor) polarized deuterium target.

In conclusion, a detailed study of the deuteron photodisintegration process is both important and experimentally feasible. The experimental equipment will be similar to the apparatus needed for the investigation of vector meson production or the excitation of baryon resonances.

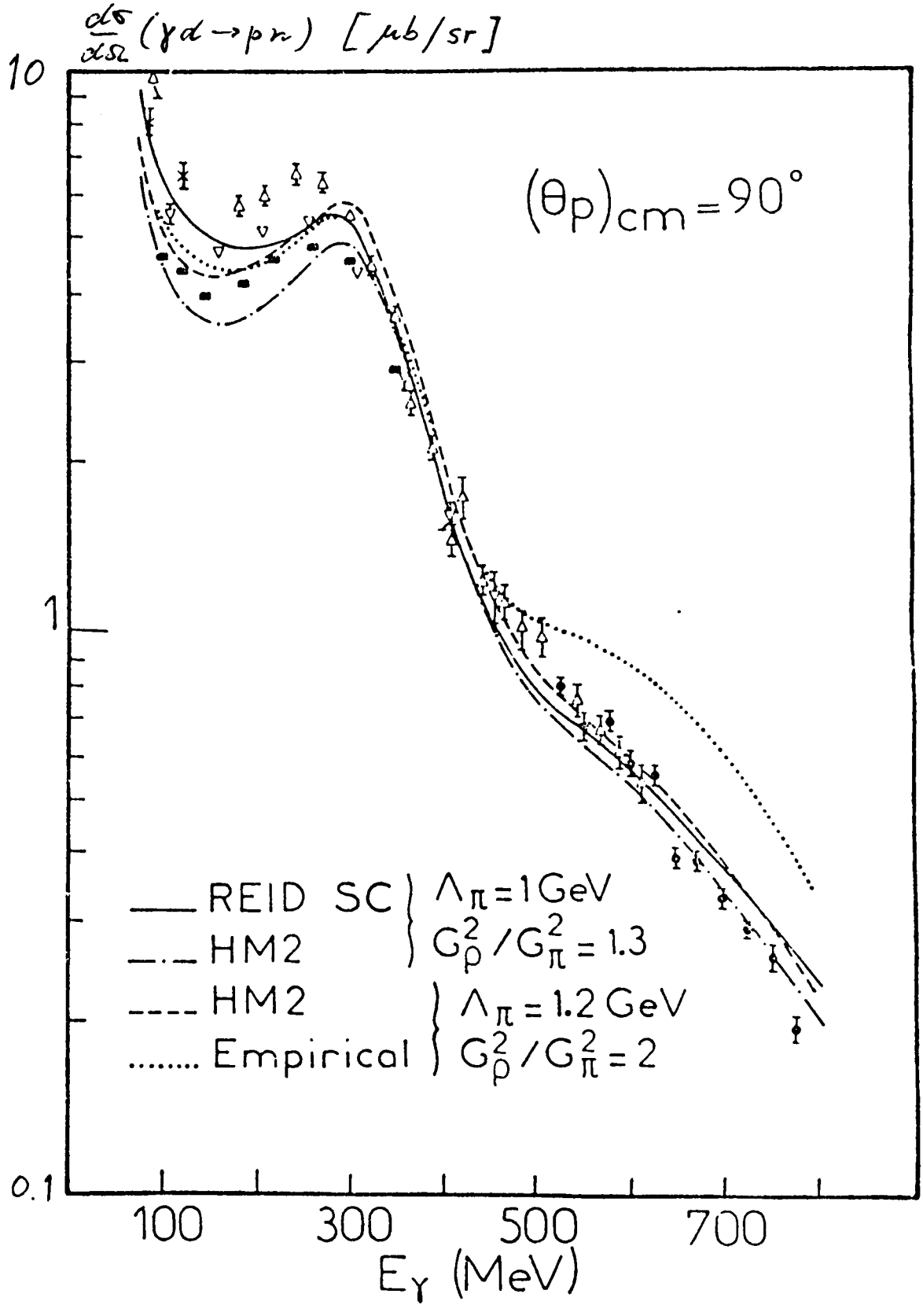

Figure 12. Differential cross section for the deuteron photodisintegration at 90° (from ref. 16).

2.2.6 *Photon Scattering*

Photon scattering is a very fundamental electromagnetic process in its own right. It is also of interest because of its relation to the total absorption cross section though the optical theorem and the dispersion relation.

$$\sigma_a(E) = 2\lambda \mathrm{Im}\ R(E,0^\circ) \tag{1}$$

$$\mathrm{Re}\ R(E,0^\circ) = (E^2/\pi hc\ P\int \sigma_a(E')dE'/(E'^2-E^2) \tag{2}$$

These rules result because the coherent scattering cross section and the total absorption cross section stem from the same complex scattering amplitude. This amplitude refers only to those transitions that leave the nucleus in its initial state of energy and angular momentum, i.e. the same m state. Thus nuclei having spins different from zero can have elastic scattering which is incoherent and not described by the above equations.

As Moniz and Koch[18] have emphasized the amplitudes for elastic (π,π) scattering and coherent π^0 production and photon scattering are matrix elements of the same Δ-hole propagator. These are all coherent reactions in which the nucleus is left in its initial state.

This discussion is divided into two parts: first, the photon scattering data above ~ 200 MeV will be summarized and second, the problems connected with performing such experiments at CEBAF will be identified.

Photon Scattering Results

Fig. 13 shows the total absorption cross sections[19] for the proton and the deuteron. The region below 2 GeV is dominated by four bumps and is called the resonance region. At higher energies the cross section is fairly flat.

The photon scattering cross sections for the proton have been measured extensively in the resonance region. A few measurements for the deuteron have also been made. In both cases the photon scattering angle is large and the important background, photons from π^0 annihilation, was circumvented by requiring a coincidence between the photon and the recoil proton or deuteron. In Fig. 14 and Fig. 15 are shown[20] the forward scattering cross sections calculated from the optical theorem and dispersion relation, Eq. 1 and 2. The pronounced dip in the scattering cross sections near the pion threshold is produced by the cancellation of the real part of the scattering amplitude by the negative Thomson amplitude. The data were obtained from the back-angle measurements[21] using the Ansatz:

$$d\sigma(\theta)/d\Omega = d\sigma(0)/d\Omega \; F^2(\theta)(1 + \cos^2\theta)/2 \qquad (3)$$

where $F^2(\theta)$ is the form factor for elastic electron scattering. In both cases it can be seen that the measured cross sections are larger than those obtained from this formula. There are two possible explanations: 1) the elastic electron scattering form factor does not describe coherent photon scattering or 2) there is incoherent elastic scattering not described by the optical theorem and dispersion relation but which does contribute to the measurement. This scattering can result from the finite spins of the proton and deuteron.

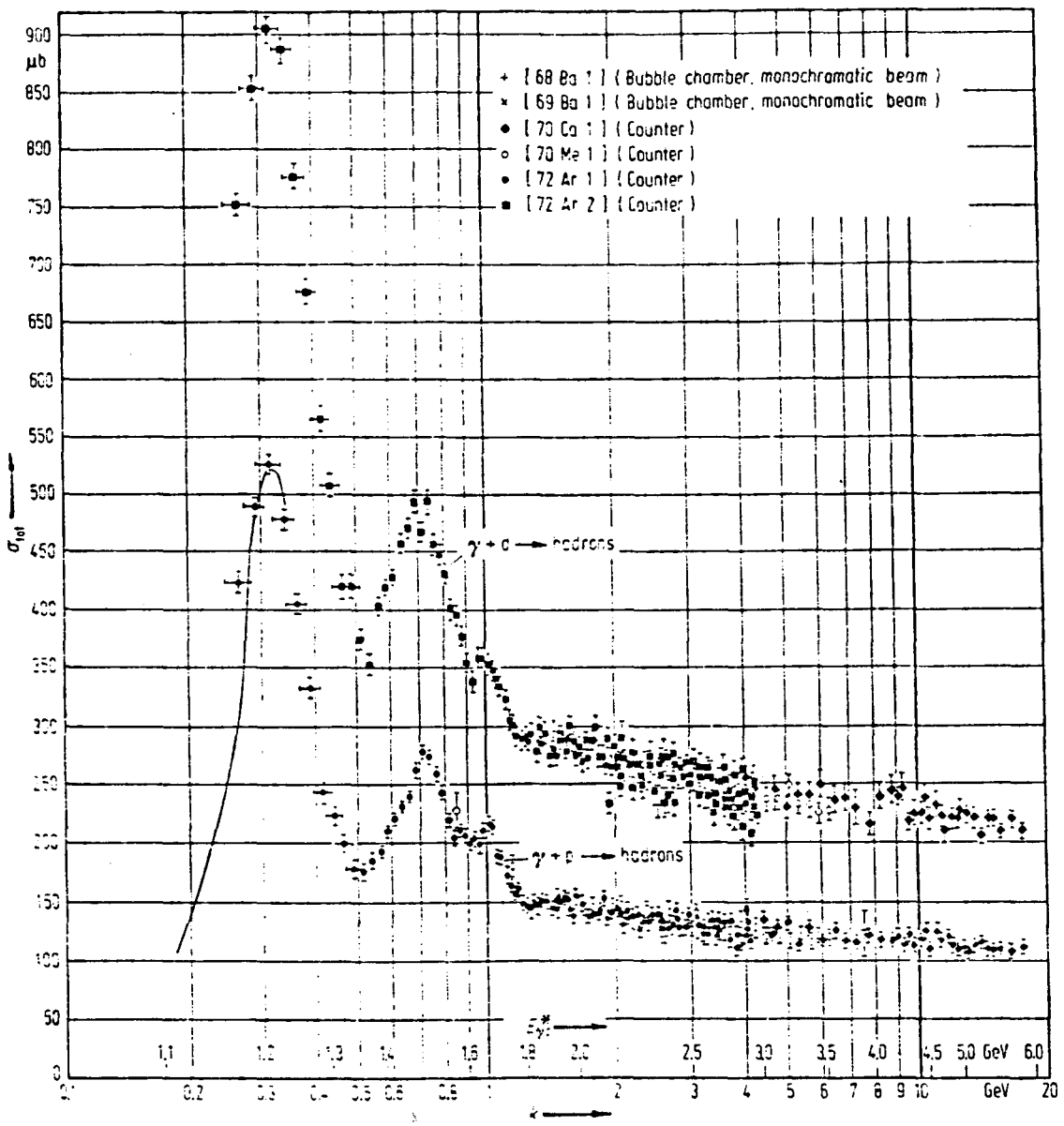

Figure 13. The total photon absorption cross section for the proton and the deuteron.

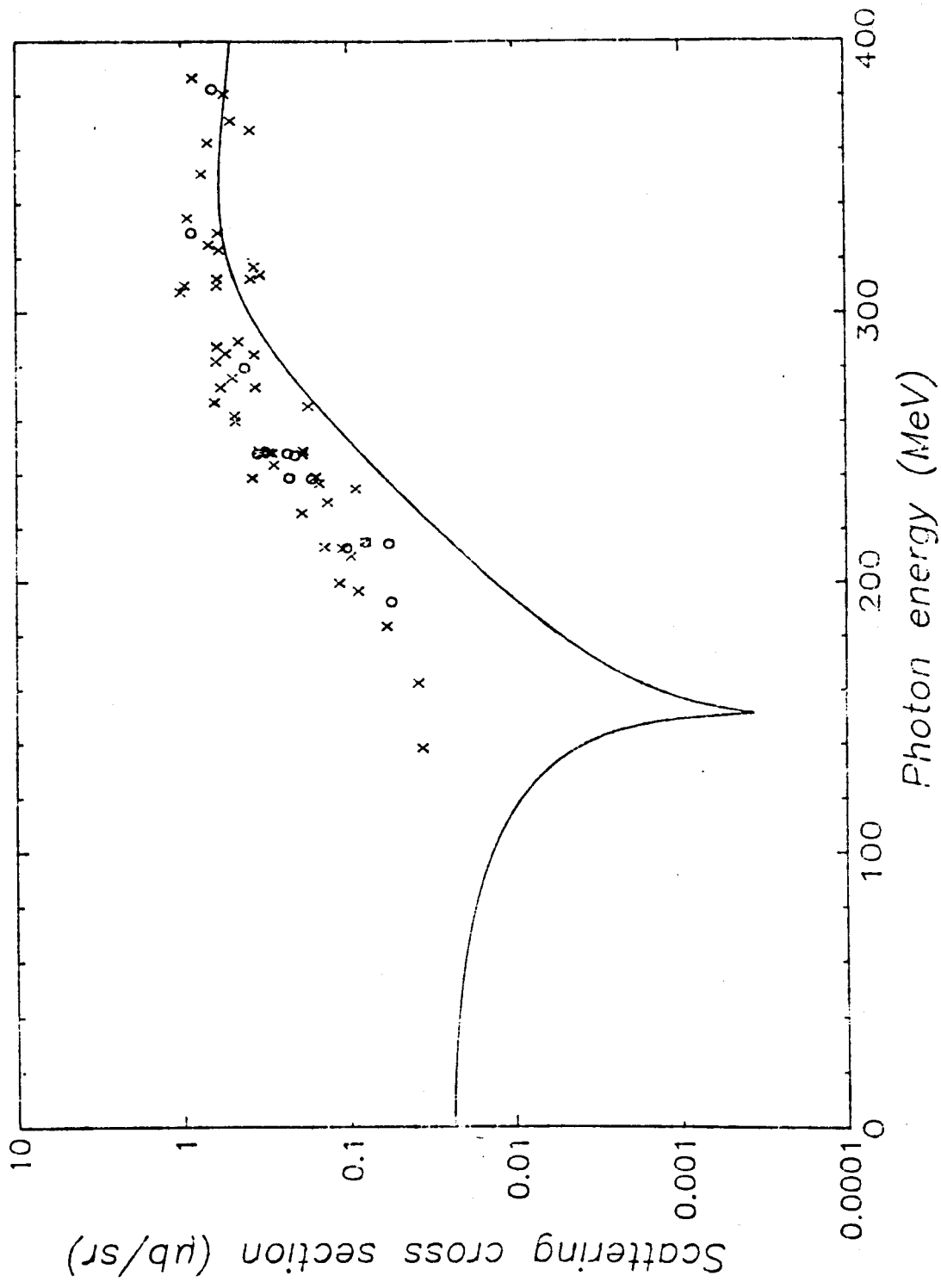

Figure 14. The forward scattering cross section for the proton calculated using Eq. 1 and 2. the very sharp minimum results from the cancellation of the real part of the forward scattering amplitude by the Thomson scattering amplitude. The data have been adjusted to the forward direction using Eq. 3.

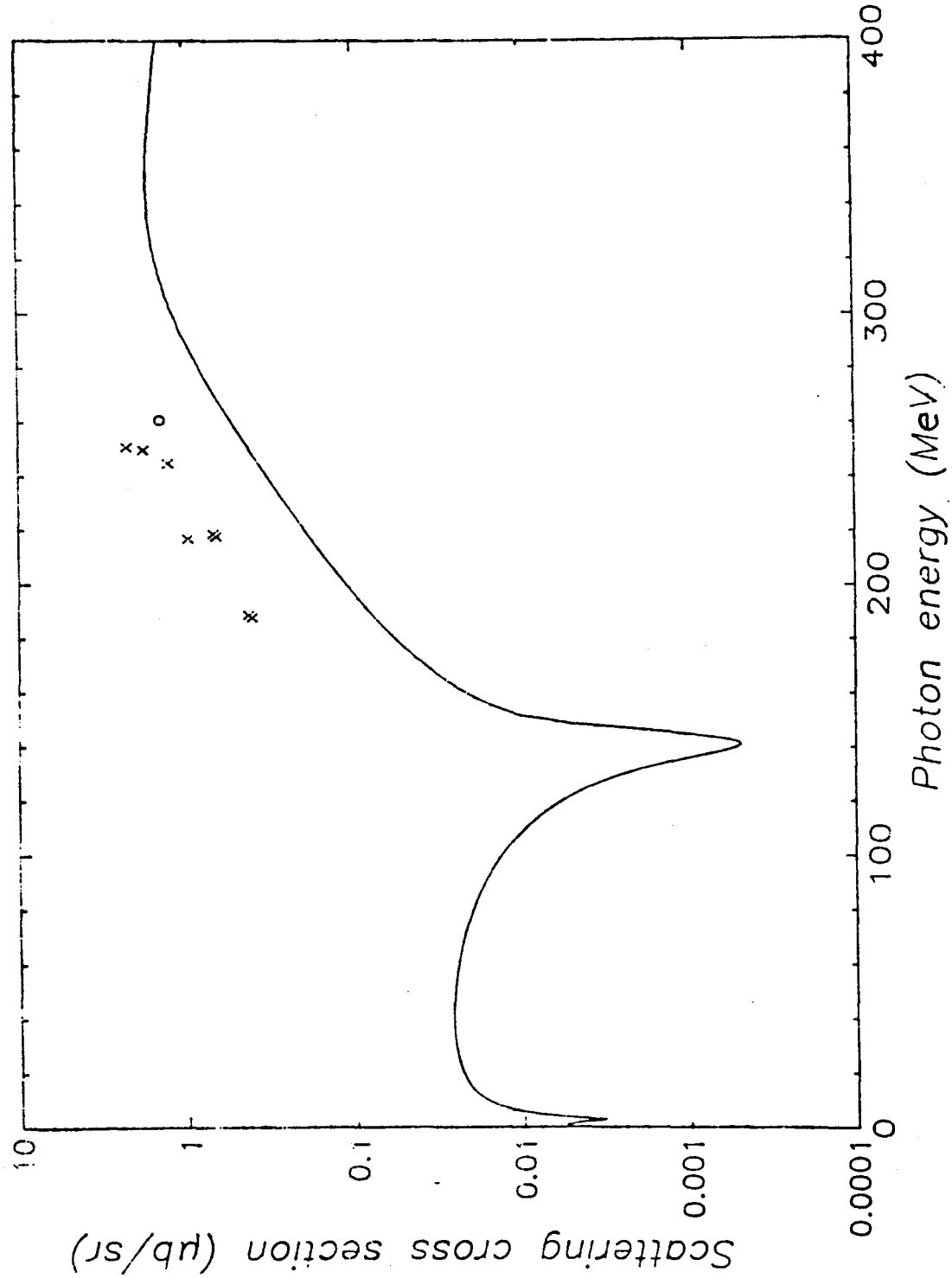

Figure 15. The forward scattering cross section for the deuteron. See the caption for Fig. 14

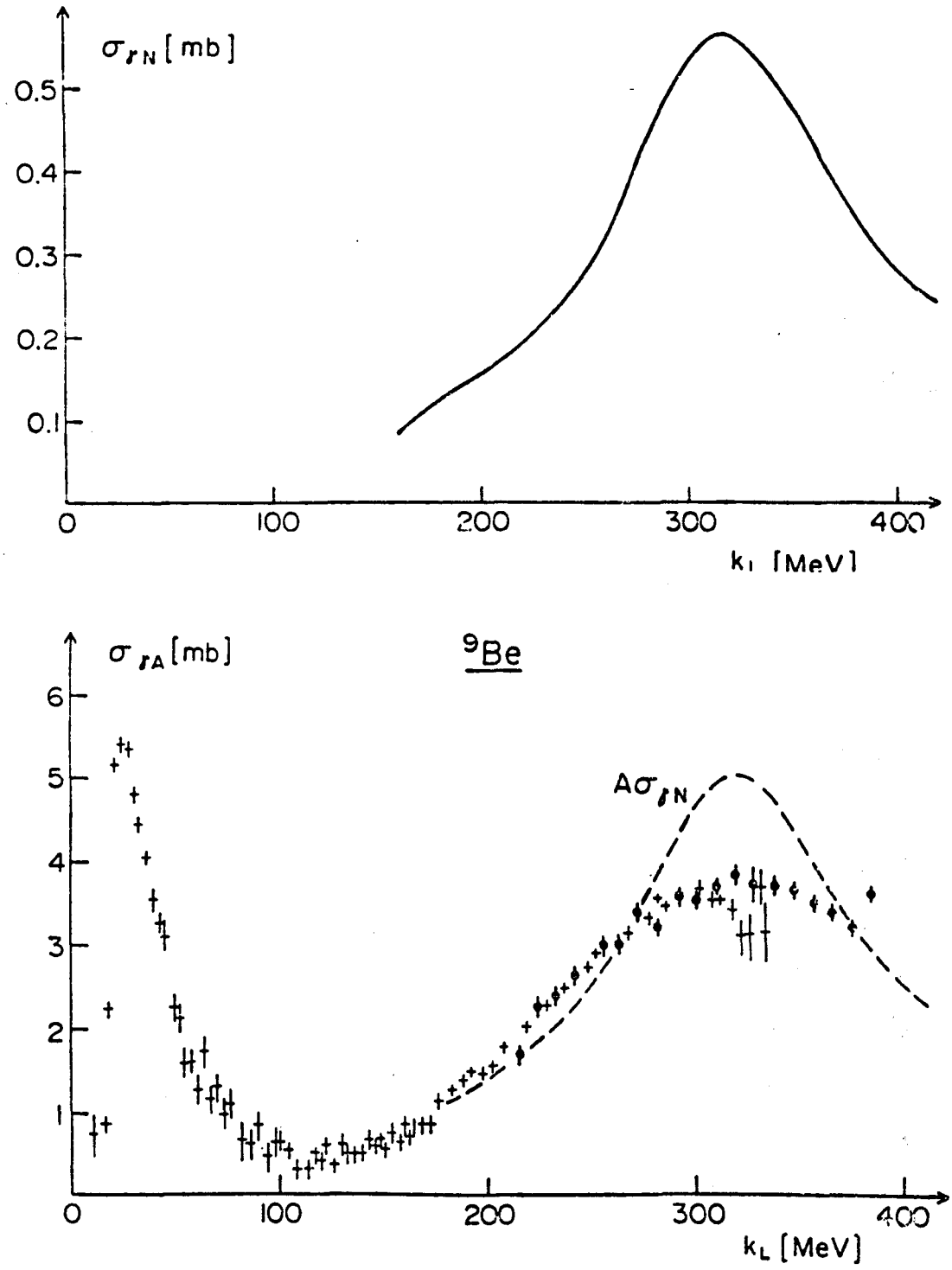

Figure 16 a) the total photon absorption cross section on the nucleon in the Δ-region. b) The experimental data on the total photonuclear cross section for Be. The dashed line is the incoherent sum, A $\sigma_{\gamma N}$.

Fig. 16 shows the total absorption cross section on the nucleon, $\sigma_{\gamma N}$, in the Δ-region. The lower graph compares A $\sigma_{\gamma N}$ with the absorption cross section for a real nucleus, Be. As far as the total area is concerned, the Δ resonance is even more important that the giant dipole resonance. The Δ in real nuclei is broadened by several different effects including the Fermi motion of the nucleons. We have learned[22] [23] [24] in the last year that the cross sections in the Δ-region for real nuclei are proportional to A.

In a recent experiment[25] the "elastic" scattering cross sections for ^{12}C and ^{208}Pb were measured at a back angle over the Δ resonance. Fig. 17 shows a linear plot of the data for ^{12}C and Figs. 18 and Fig 19 show the data for both targets compared with the prediction of Eq. 3. For both targets the measured cross sections exceed this prediction. These nuclei both have spin zero so there can be no incoherent elastic scattering. On the other hand, the experimental energy resolution is only 10% so that the data can include inelastic scattering. All of these results point out the importance of measuring the scattering cross section for helium in the Δ-region as has been proposed by Booth and Miller. This nucleus has spin zero and no low-lying excited states.

Fig. 20 is a second plot of the Pb data (150 - 400 MeV) from Ref. 25 along with the previous lower energy results obtained[26] using positron annihilation radiation.

The situation in the Δ-region is in contrast to that at higher energies, 2 - 7 GeV. Here the scattering cross section from the proton has been measured[21] at photon angles as small as 4°, not far from 0°. The dependence on four-momentum transfer, t, is $d\sigma/dt = Ae^{-Bt}$ which

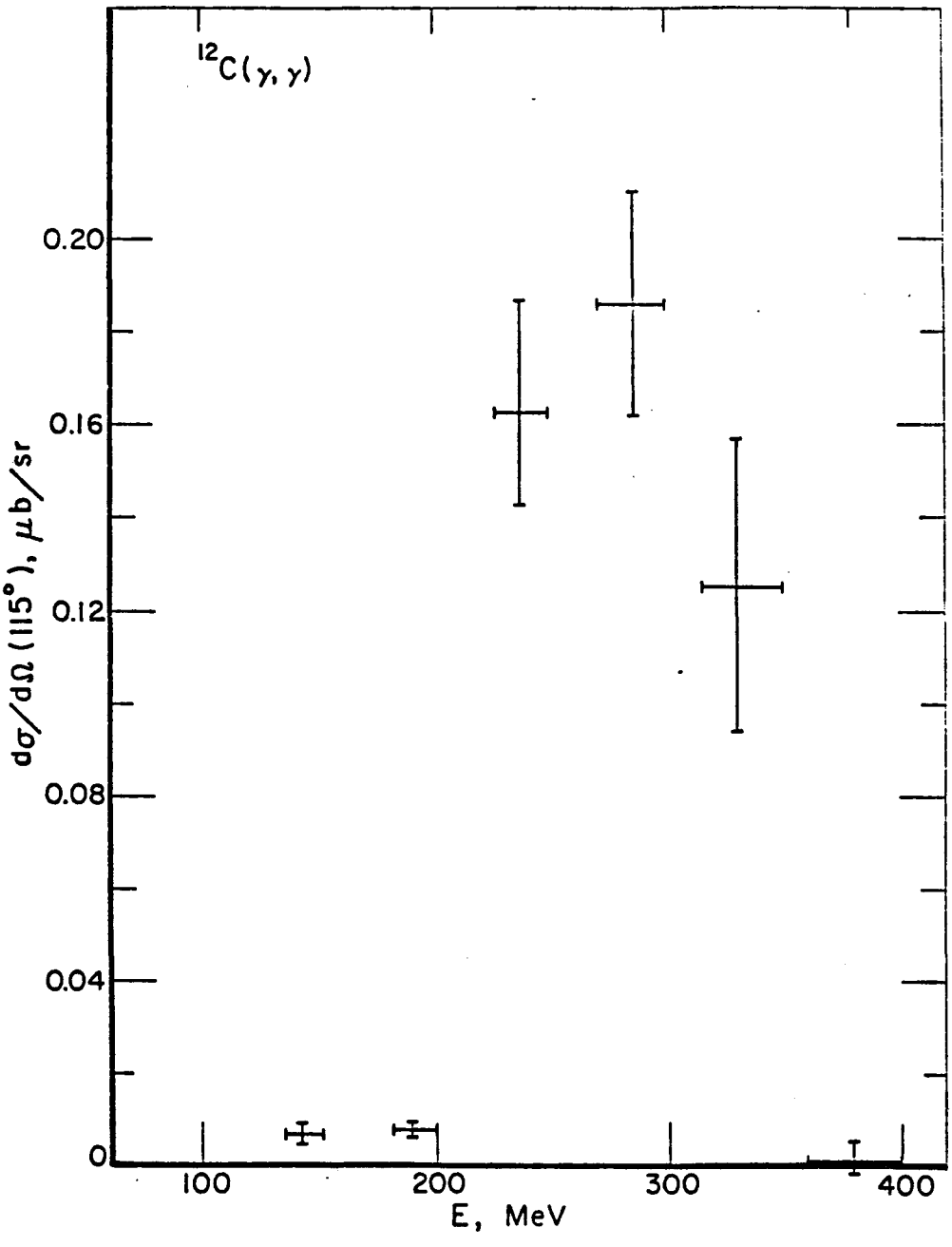

Figure 17. The measured photon scattering cross section for ^{12}C.

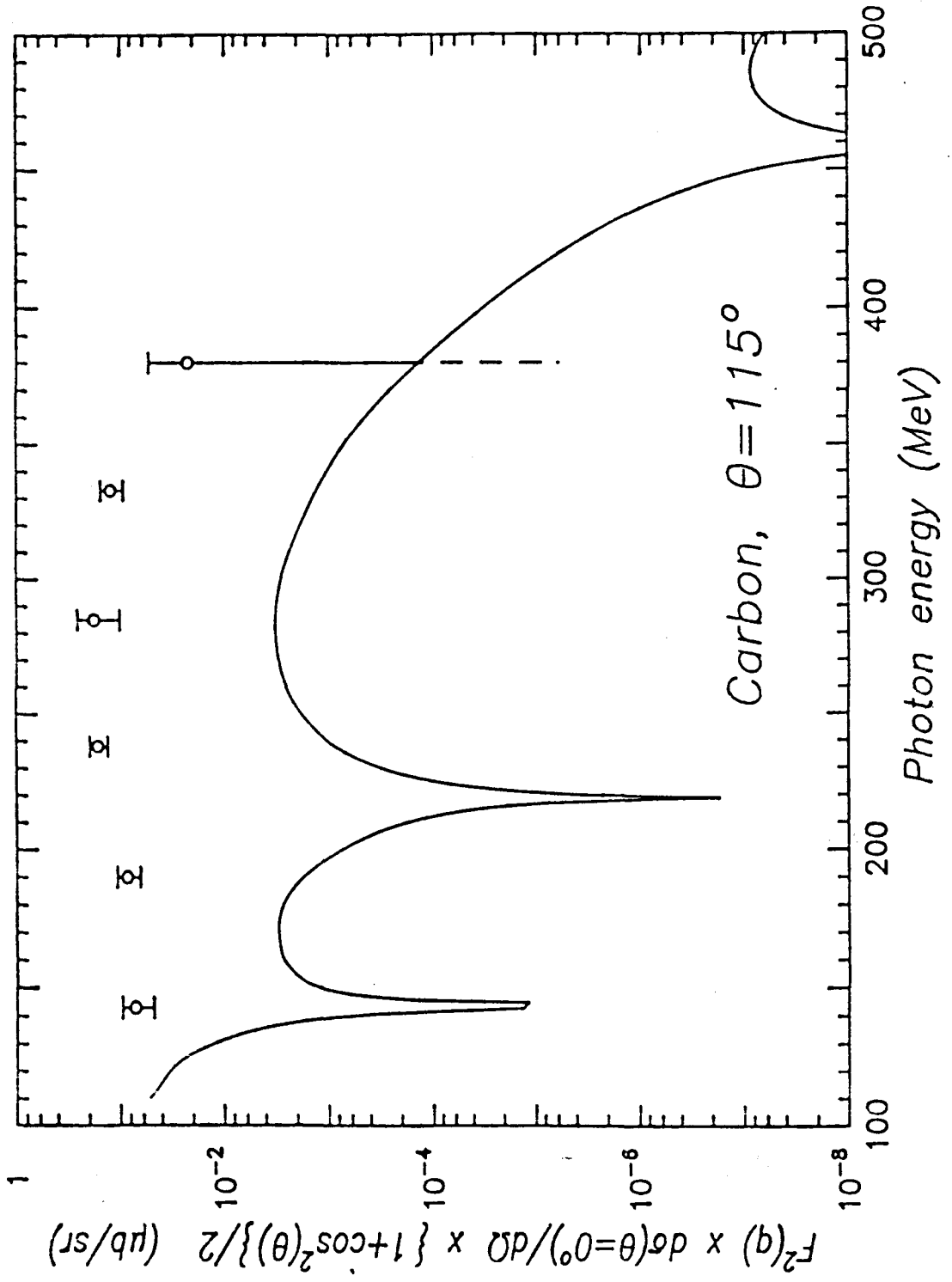

Figure 18. The measured photon scattering cross section for ^{12}C compared with the prediction of Eq. 3.

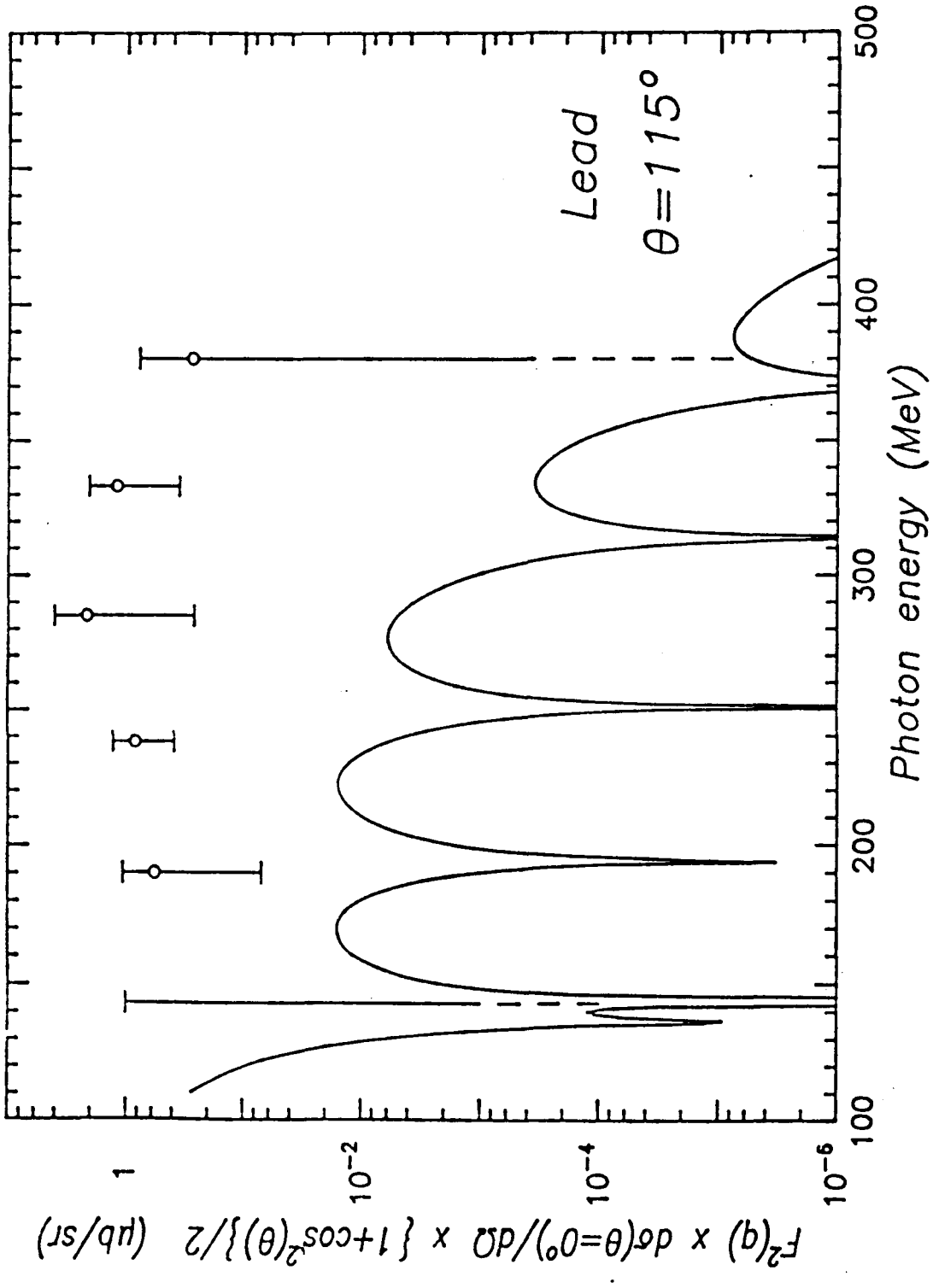

Figure 19. The measured scattering cross section for ^{208}Pb compared with the prediction of Eq. 3.

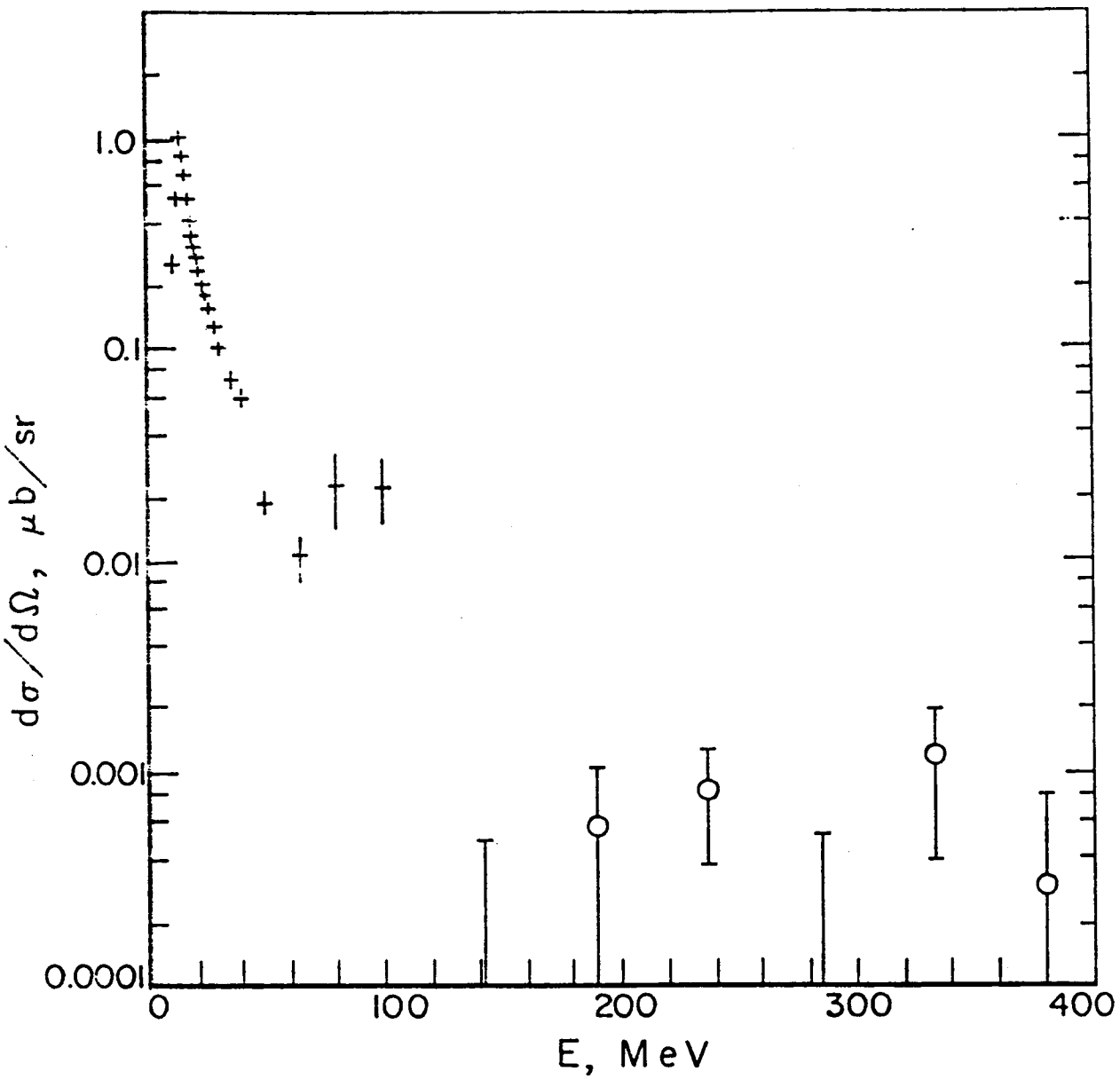

Figure 20. The ^{208}Pb scattering cross section in the Δ-region compared with that obtained at lower energies.

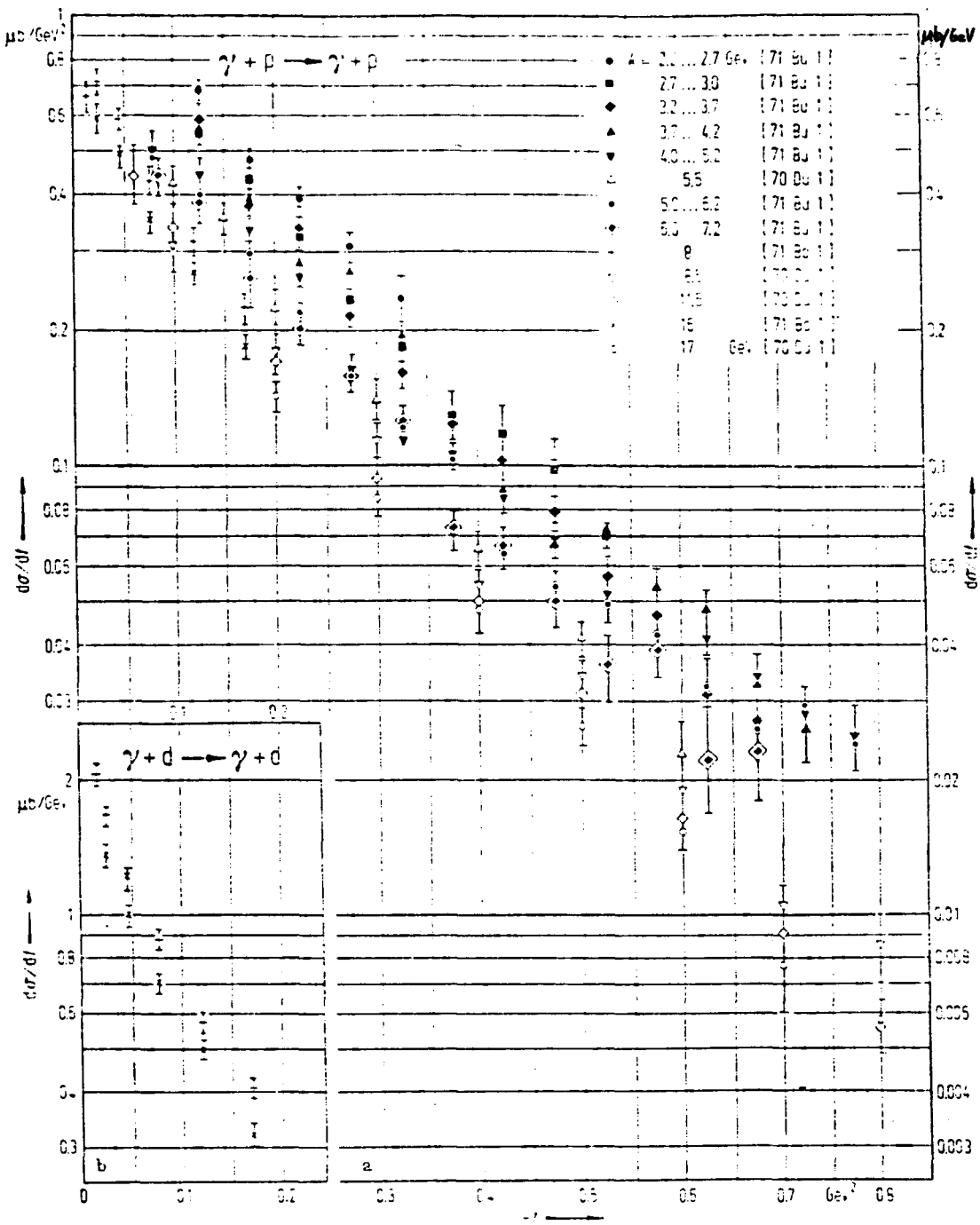

Figure 21. The photon scattering cross sections for the proton and the deuteron for energies between 2 and 20 GeV.

can easily be extrapolated to 0° as is shown in Fig. 21. The results are in fair agreement with those obtained using the optical theorem and dispersion relations. This result in itself says that the physics in this realm is vastly different from that in the Δ region.

Practical Matters

Now we need to consider some realities; i.e. practical matters. The photon scattering cross sections in the backward hemisphere are ~ 0.1 μb/sr. The forward scattering cross sections are much larger; they can be millibarns.

First let us consider doing a photon scattering experiment using a tagging system.

counts/sec = $d\sigma/d\Omega\ \varepsilon\ \Delta\Omega$ photons/sec atoms/cm^2

$d\sigma/d\Omega$ (large angle) = 10^{-31} cm^2/sr

$\varepsilon\ \Delta\Omega = 3\ 10^{-5}$ sr (SIN spectrometer)

10^7 photons/sec

10^{23} atoms/cm^2

counts/sec = $3\ 10^{-6}$

counts/hr = $3600 \times 3\ 10^{-6}$

counts/hr = $3600 \times 3\ 10^{-6} = 0.01$/hr

Possible solutions

1. Make $\varepsilon\Delta\Omega$ bigger
2. Work at a small angle

We cannot underestimate the importance of designing and building a pair spectrometer with energy resolution better than 1 MeV and with a large $\varepsilon\Delta\Omega$.

An important background in photon scattering experiments above the π^0 threshold is that produced by π^0 annihilation. These photons have an intensity about 100 times that of the scattered photons and can be expected to be an important source of accidentals when using the tagger and, in fact, in any coincidence experiment that involves photon detection.

What are the maximum photon energies that can come from π^0 decay? Suppose a photon of energy, E, converts all of its energy into a π^0, E_π, then the energy of the decay photon is $E_\gamma = \frac{1}{2}E_\pi(1 + \beta\cos\delta)$, δ being the angle with respect to the π^0 velocity in the center of mass system. The maximum occurs for $\delta = 0$. $E_\gamma = E_\pi(1 + \beta)/\gamma$. $\gamma = E_\pi/M_\pi$ $= E_\pi/135$ MeV.

Fig. 22 is a plot of the energy of the photon elastically scattered from ^{12}C at 115°, including the recoil of the C nucleus, the conditions of the experiment described in Ref. 25. Also shown is the energy of the highest energy photon from π^0 decay with recoil included. One might think of eliminating the π^0 photons by having a second detector viewing the target from the opposite side and placed in anticoincidence with the first one. Fig. 23 shows a plot of the energy of the backward-going photon; they range between 10 and 40 MeV for incident photons in the Δ-region.

The photon scattering cross sections for C and Pb, shown in Figs. 18 and 19 were measured using the Mainz linear acceleration which has a duty cycle of a few $\times 10^{-4}$. The bremsstrahlung end point was used and photons having energies above 0.9 E_0 were accepted. The experimental arrangement is shown in Fig. 24. Because of the low duty

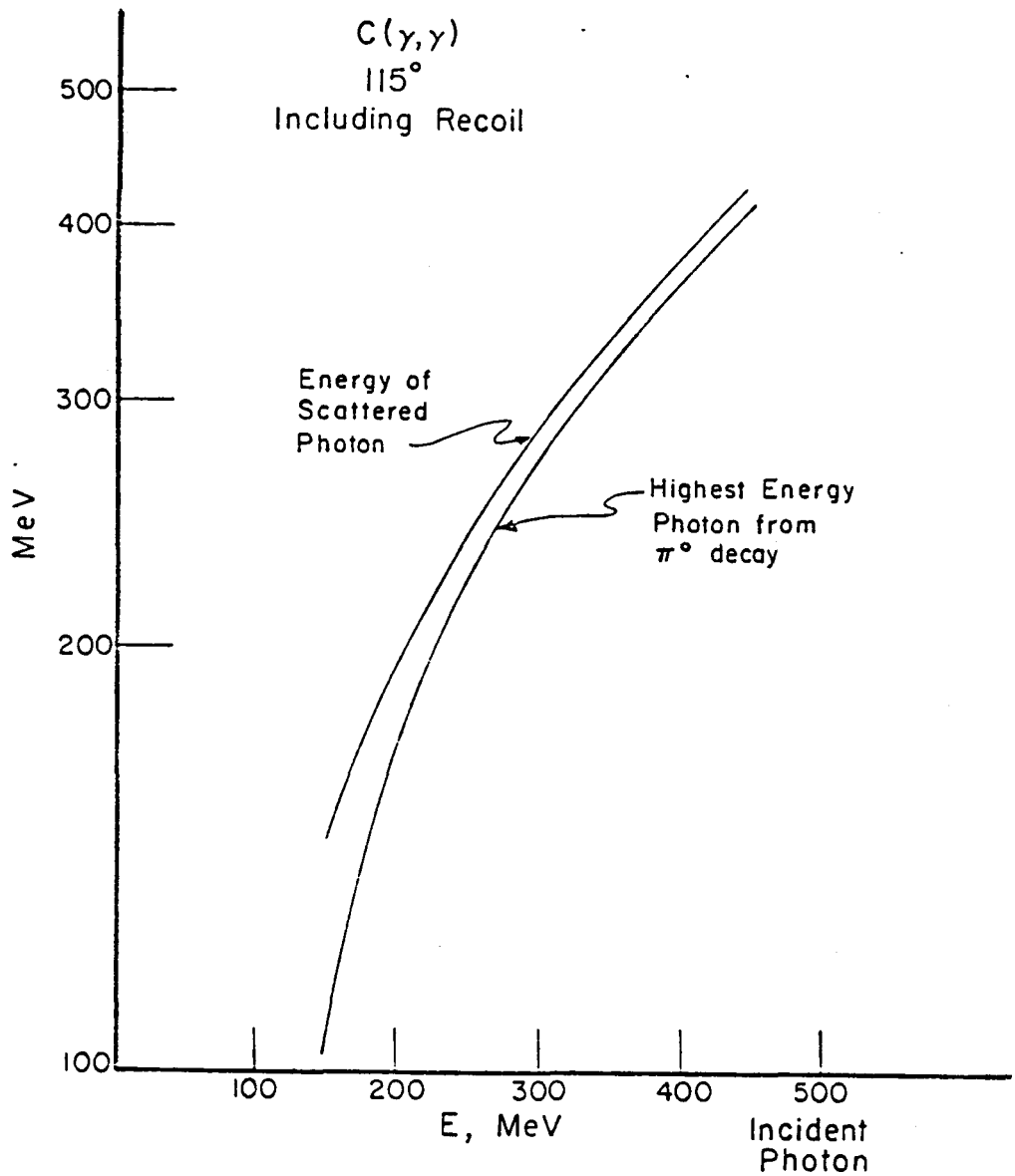

Figure 22. The energy of the elastically scattered photon from carbon at 115° including the recoil of the carbon nucleus. Also shown is the energy of the highest energy photon from π^0 decay with recoil included.

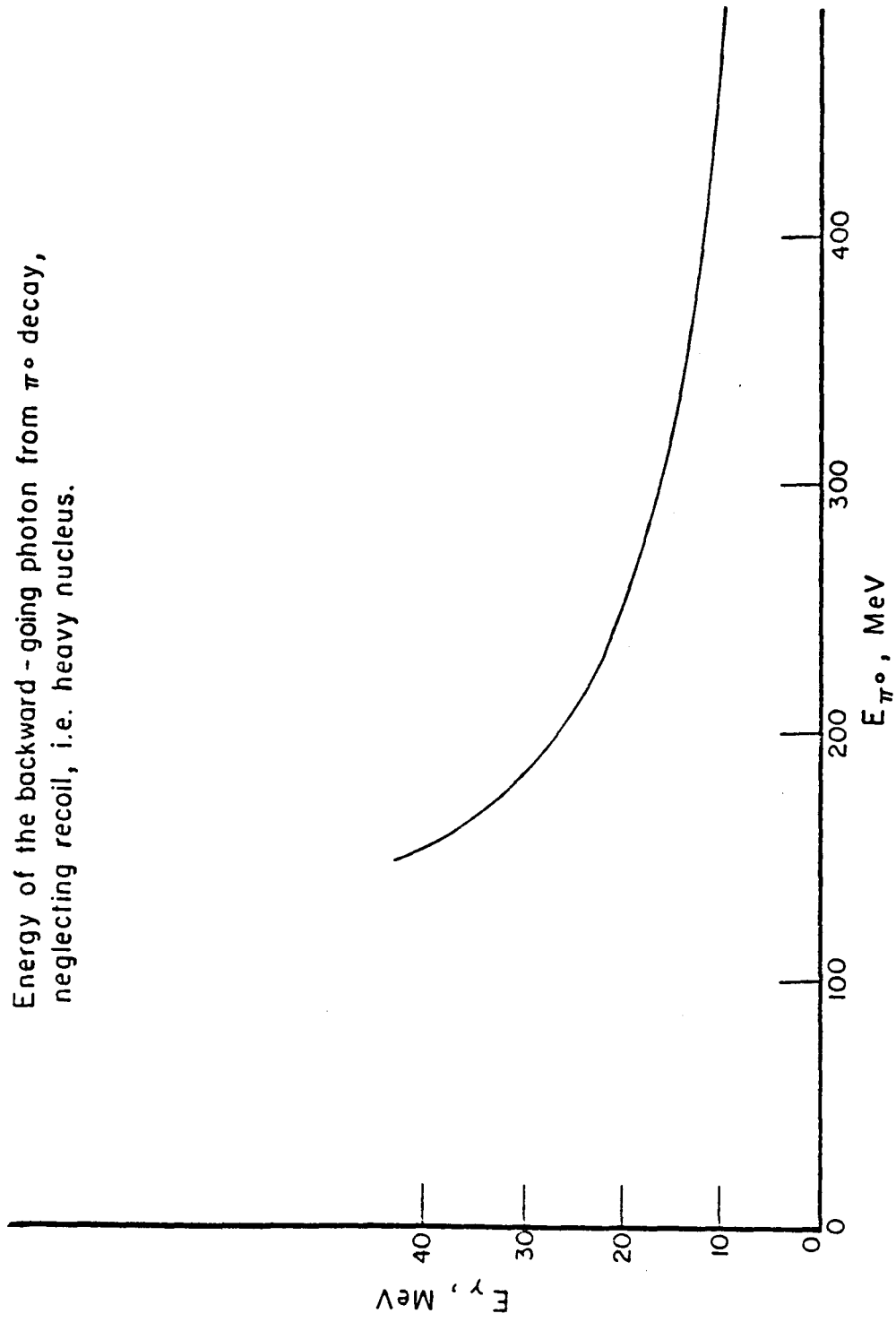

Figure 23. The energy of the backward-going photon.

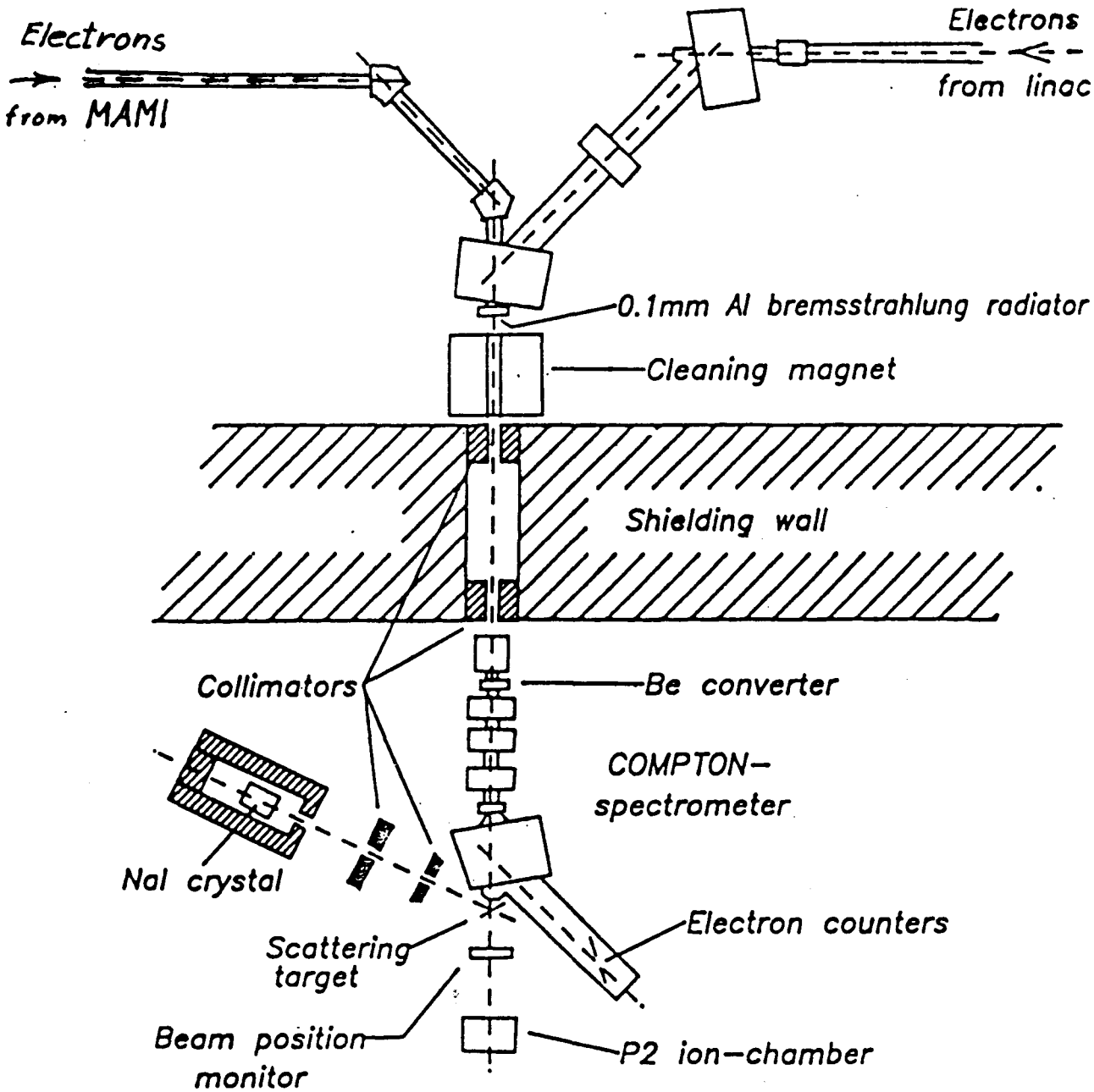

Figure 24. The experimental arrangement used in Ref. 23.

factor this experiment was counting-rate limited. Neither a radiator thicker than the 0.1 mm Al window of the vacuum system nor a solid angle larger that 5.6 10^{-4} sr could have been used.

Fig. 25 has been prepared to illustrate how the situation is improved when a CW beam is available. The upper graph is the pulse height distribution produced by the photons scattered from a C target irradiated by 150 MeV bremsstrahlung from the linear accelerator. The peak comes from the resonance fluorescence of the 15.1 MeV state in ^{12}C, and the rise of the distribution toward low pulse heights results very largely from pulse pile-up. The lower distribution was obtained using the 180 MeV bremsstrahlung spectrum from the CW microtron, all other parts of the experiment remaining unchanged. There is an incredible improvement in the CW situation.

Another practical matter that is worth mentioning is that the target-out background from neutrons increases enormously as the end energy is increased from 150 to 200 MeV. The assumption made in Ref. 25, that at least two neutrons are emitted following the production of every pion in a heavy target, is probably true.

One final result obtained with the CW beam is of interest. The pulse height distribution produced by 180 MeV bremsstrahlung scattered by the carbon target was measured. It was assumed that all of the scattered photons were elastic. i.e. populated the ground state, and the bremsstrahlung cross section was divided out. The result is plotted in Fig. 26 We see clearly a peak produced by the resonance fluorescence of the 15.1 MeV line, the scattering off the giant resonance, and a huge bump extending from ~ 40 to ~ 140 MeV. That

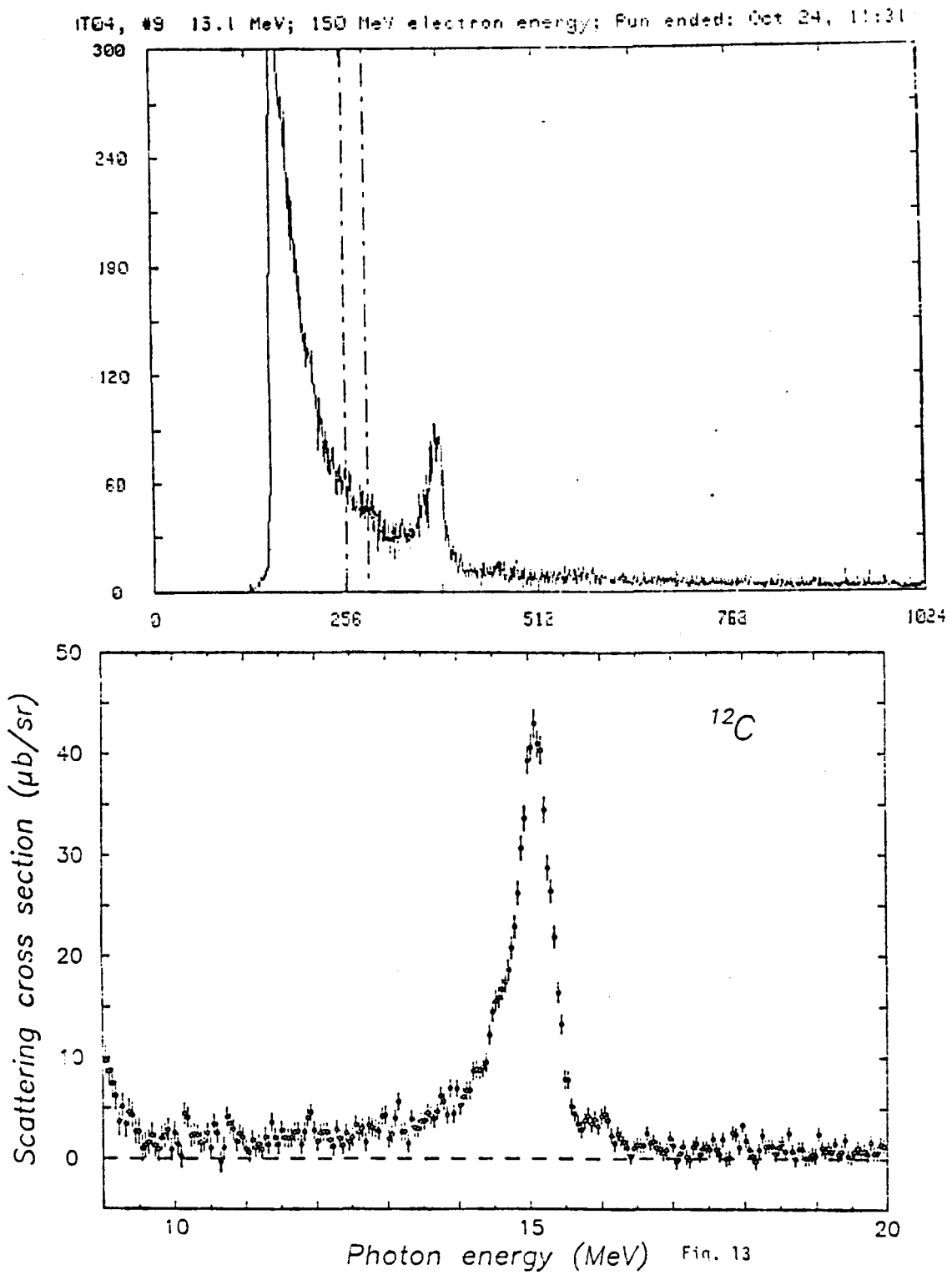

Figure 25. a) The pulse height distribution produced by photons scattered by ^{12}C when irradiated by 150 MeV bremsstrahlung from the linear accelerator having a low duty cycle. b) The pulse height distribution produced when 180 MeV bremsstrahlung from the CW microtron is used.

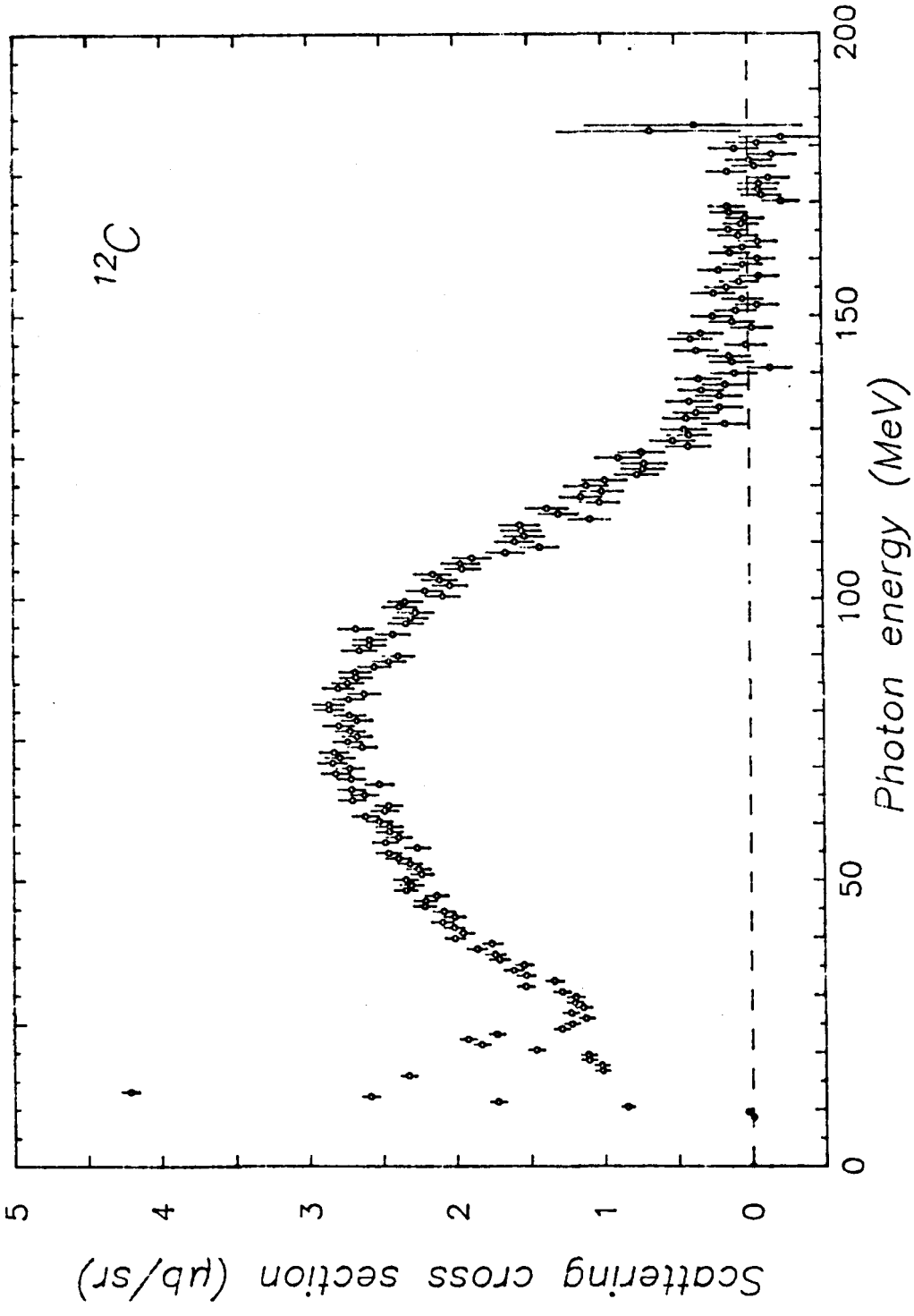

Figure 26. This "Cross Section" has been obtained from the pulse height distribution by dividing out the bremsstrahlung which assumes all ground-state transitions. The broad peak extending from 40 - 140 MeV is produced by the photons from π^0 decay and certainly shouldn't be treated this way.

bump comes from the π^0 decay photons. The data analysis is certainly wrong for these pulses but its intensity is so great as to make it a major background for a photons scattering experiment. This bump disappears when 140 MeV bremsstrahlung is used. In the experiment described in Ref. 25, the photons in the top 18 MeV of this spectrum would have been used to calculate the cross section. It is 0 on this scale and may be seen to be ~ 0.01 μb/sr in Fig. 17.

The conclusion from all this is that photon scattering experiments are very important but difficult to perform.

3.1 *Polarized Targets*

A feasibility study is underway at the Argonne National Laboratory in order to determine the usefulness of polarized internal targets at an electron storage ring. There has been considerable development already of polarized internal targets for high energy physics experiments. A target thickness of polarized hydrogen of 5×10^{11} atoms/cm^2 has been achieved[27] from a room-temperature, conventional atomic beam source at CERN. Development of a cryogenically-cooled source is expected to improve the target thickness by a factor of 10 to 100. Another polarized internal target development is underway at Brookhaven for the AGS ring.[28] This target is expected to use a new procedure reported by Cline et al. in which polarized hydrogen nuclei of density 10^{17} atom/cm^3 can be stored in a high magnetic field.[29] If the spins of the atoms are suddenly reversed by microwave radiation, then the polarized atoms are ejected by the field. This could result in a pulsed target which is suitable for the AGS operation. A third method, which will be discussed in more detail here, is based on atomic spin-exchange scattering from polarized alkali atoms.[30] These methods are summarized in Table 5.

A major disadvantage of the first two methods is that they are specific to hydrogen and deuterium; whereas, the latter method can be used with a large variety of nuclei, i. e. atoms which have a large spin-exchange cross section (atoms which have an unpaired electron). An additional disadvantage to the conventional method is that large vacuum pumping speeds are necessary to remove approximately 99% of the atoms which are not accepted by the hexapole magnet.

TABLE 5

Polarized Internal Targets in Development

Type of Target	Nuclei	Facility	Target thickness expected (atoms/cm^2)
Conventional atomic beam (cryogenically cooled)	H,D	CERN (SPS)	5×10^{12}-5×10^{13}
Low temperature recombination of polarized atoms	H,D	BNL-MIT (AGS)	10^{17} (pulsed)
Spin-exchange scattering from polarized alkali atoms	H,D,^{6}Li,^{7}Li N,...etc. (Nuclei with unpaired e)	ANL (Aladdin)	10^{14}

In order to estimate the target density and polarization that one could achieve with the spin-exchange method (SEM), we will consider the geometry shown schematically in Fig. 27. The primary electron beam should enter and leave a spherical target cell through holes of diameter r. A circularly polarized photon beam would be used to optically pump Na atoms in a tube of length *l* and diameter a. The deuterium atoms enter the optical pumping region after passing from the dissociator and become polarized through spin-exchange scattering. It is straightforward to show that the density of deuterium in the target cell is given by

$$n_d = R_p(a/r)^2/\{2\sigma_{se}v_d(1+3l/4a)\}$$

where R_p is the optical pumping speed, σ_{se} is the spin-exchange cross section for the N a($\uparrow$) + D($\downarrow$) $\rightarrow$ Na ($\downarrow$) + D($\uparrow$) process and v_d is the mean speed of the deuterium atoms. Here, for optimum target density,

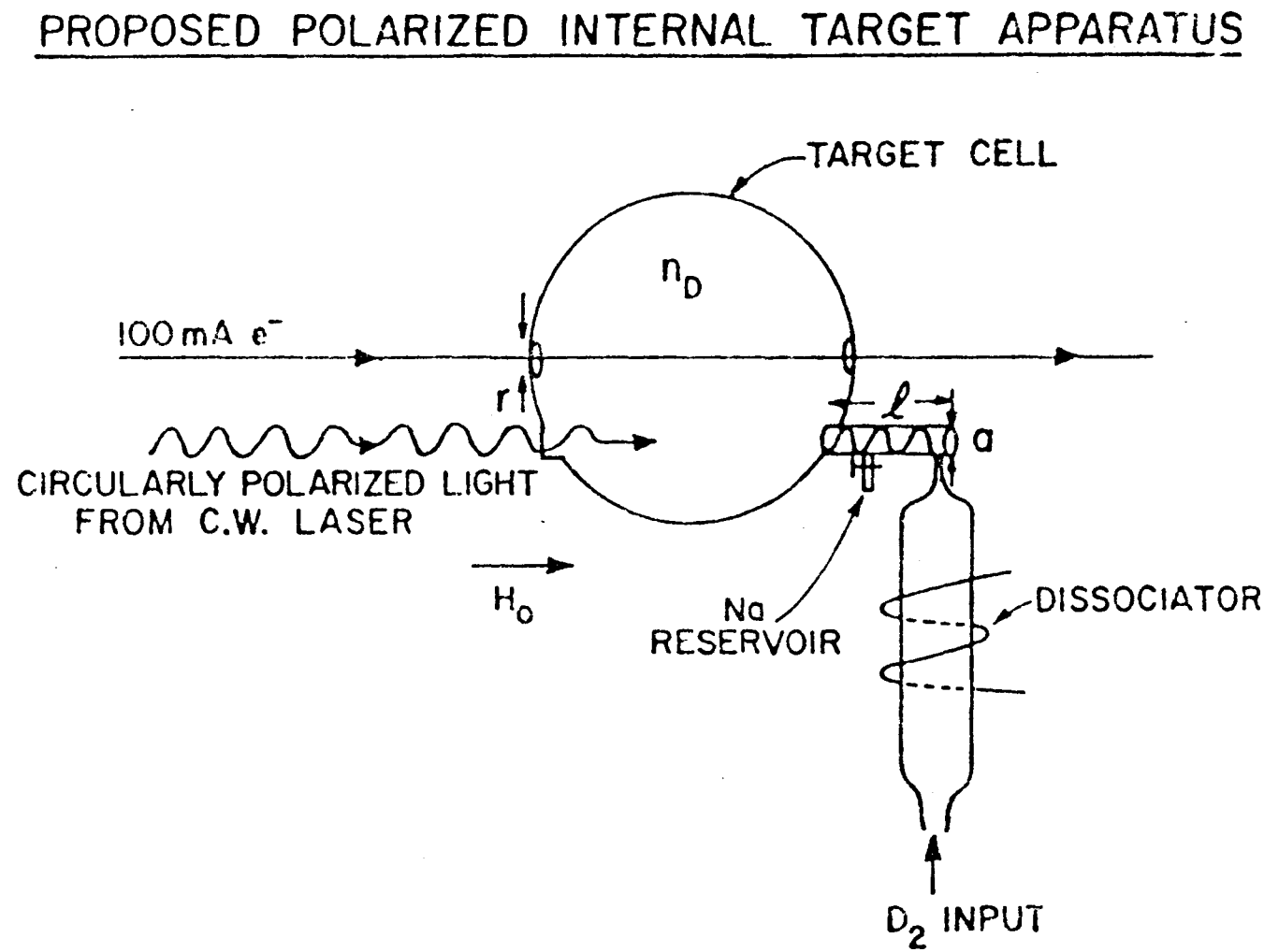

Figure 27. Polarized Target Apparatus

it has been assumed that the optical pumping speed is equal to the spin-exchange rate. The density of polarized deuterium nuclei depends directly on the optical pumping rate; and thus, it is necessary to achieve as high a pumping speed as possible. A reasonable value of $R_p = 10^6\ s^{-1}$ was chosen for the present discussion. The details of optical pumping will not be presented here. Geometrical factors enter the problem since the main loss mechanism of the polarization is due to the atoms leaking from the holes in target cell. Of course, these holes are necessary to allow the electron beam to pass through the target region. The hole diameter r was chosen to be 7 mm in this case. It is important for the design to determine just how small one can make these holes and this represents a major component of the feasibility study. A test facility has been constructed to determine the background and beam losses associated with apertures in the storage ring. This assembly will be installed as soon as Aladdin becomes operational. Another way to increase the density is to reduce the speed of the deuterons, by perhaps, cooling the target cell. However, in the present example, we will assume that T = 400° K. The spin exchange cross section for Na $^+$D scattering is expected to be 10^{-14} cm^2.[31] With these considerations one can readily see that the expected target density is $n_d \sim 3 \times 10^{13}$ atom/cm^3. Thus, a target cell of only several cm in length will be necessary to achieve the target thickness of 10^{14} atoms/cm^2 which is permitted at Aladdin. Although it is not necessary for the Aladdin experiment, it is clear that the target thickness could be increased by applying more laser power, reducing the hole size at the electron beam axis or cooling the target cell.

In order to estimate the amount of Na that is necessary to polarize the deuterium, we will assume that N_s spin exchange collisions are necessary to polarize the deuterium. (The polarization as a function of the number of collisions will be discussed later.) Then, it is straightforward to show that the density of Na atoms in the target cell is given by

$$n_{Na} = N_s(a/r)^2/\{\sigma_{se} l(1+3l/4a)^2\}$$

for $N_s = 10$, this yields a density of 6×10^{11} or 50 times smaller than the deuterium density. Thus, the presence of Na atoms should not represent a large background effect. In order to estimate the polarization of Na atoms, it is straightforward to take the steady state solution of the rate equation for producing spin-up atoms, say. Here, we assume that the largest relaxation of the polarization of Na is due to spin-exchange with the deuterium, then the polarization is given by

$$p_{na} \sim R_p/(R_p + 2R_{se})$$

where R_{se} is the spin-exchange rate. For $R_{se}/R_p = 1/3$ the steady state polarization of the Na atoms would be 60%.

The polarization of the deuterium nuclei can be determined by considering the eigenvectors in the basis of m_d and m_e for the six hyperfine states of deuterium. The key to this method is to perform the spin-exchange scattering at low field (≤5.0 gauss) so that the nuclear spin is not decoupled from the electron spin. This is contrary to the conventional atomic beam source method. Then, the six wave functions in the total spin quantum numbers $|F,m_F\rangle$ can be written in terms of the magnetic quantum numbers of the deuteron and electron $|m_d\ m_e\rangle$ as follows:

$$|\ 3/2\ 3/2\rangle = |\ 1\ 1/2\rangle \qquad a$$

$$|\ 3/2\ 1/2\rangle = (\sqrt{2}|\ 0\ 1/2\rangle + |\ 1\ -1/2\rangle)/\sqrt{3} \qquad b$$

$$|\ 3/2\ -1/2\rangle = (|-1\ 1/2\rangle + \sqrt{2}|0\ -1/2\rangle)/\sqrt{3} \qquad c$$

$$|\ 3/2\ -3/2\rangle = |-1\ -1/2\rangle \qquad d$$

$$|\ 1/2\ -1/2\rangle = (|\ 0\ -1/2\rangle - \sqrt{2}|-1\ 1/2\rangle)/\sqrt{3} \qquad e$$

$$|\ 1/2\ 1/2\rangle = (\sqrt{2}|1\ -1/2\rangle - |\ 0\ 1/2\rangle)/\sqrt{3} \qquad f$$

These states may be labeled a through f so that the probabilities p_{if} for transition from state i to f upon spin exchange collision are given by

$$p_{fa} = p_{de} = 2/3,\ p_{dc} = p_{ba} = 1/3,$$

$$p_{eb} = p_{cf} = 2/9,\ p_{ef} = 1/9,\ p_{cb} = 4/9.$$

A study of these transition probabilities would show that eventually all the atoms would end up in state a after enough spin-exchange scatterings from a 100% polarized Na reservoir. This would mean that the deuterium nuclei would have pure vector and tensor polarization. For example, atoms in state b which start out as mixture of $m_d = 0$ and 1 can be transferred by spin-exchange scattering to the pure state, $|1,\frac{1}{2}\rangle$, through the $|1,-\frac{1}{2}\rangle$ part of state b. The non-equilibrium distribution of atoms left in state b then undergo a recoupling between the nucleus and the electron via the hyperfine interactions to produce the mixed state b again. The time between collisions is ~10 μs; whereas the hyperfine recoupling time is ~ 1 ns, and thus, there is ample time for rearrangement of the nuclear spin between atomic collisions. A physical limit on the target density would be given by comparing these time scales. However, other factors, such as laser power, provide present-day limitations on the target density. When all possible

spin-exchanges are considered, the polarizations t_{10} and t_{20} can then be determined according to the expressions

$$t_{10} = \sqrt{3}/2 \ (N_{+1} - N_{-1})$$

$$t_{20} = \sqrt{1}/2 \ (1 - 3 \ N_0)$$

where $N_{+1} + N_{-1} + N_0 = 1$ are the populations of the three magnetic substates of the deuteron. These polarizations were computed as a function of the number of spin-exchange scatterings from a collection of Na atoms of 50%, 75% and 95% polarization. These results are shown in Fig. 28. The polarizations which can be achieved are quite reasonable for the design goal of 10 scatterings denoted by the arrows in the figure.

The polarization of the target will be determined in a separate feasibility study at ANL. The polarization will be measured with the use of the $^3He(d,p)^4He$ reaction and the ^3He beam from the dynamitron. Of course, a variety of surface coatings will be tested in the target cell in order to minimize relaxation of polarization on the vessel walls.

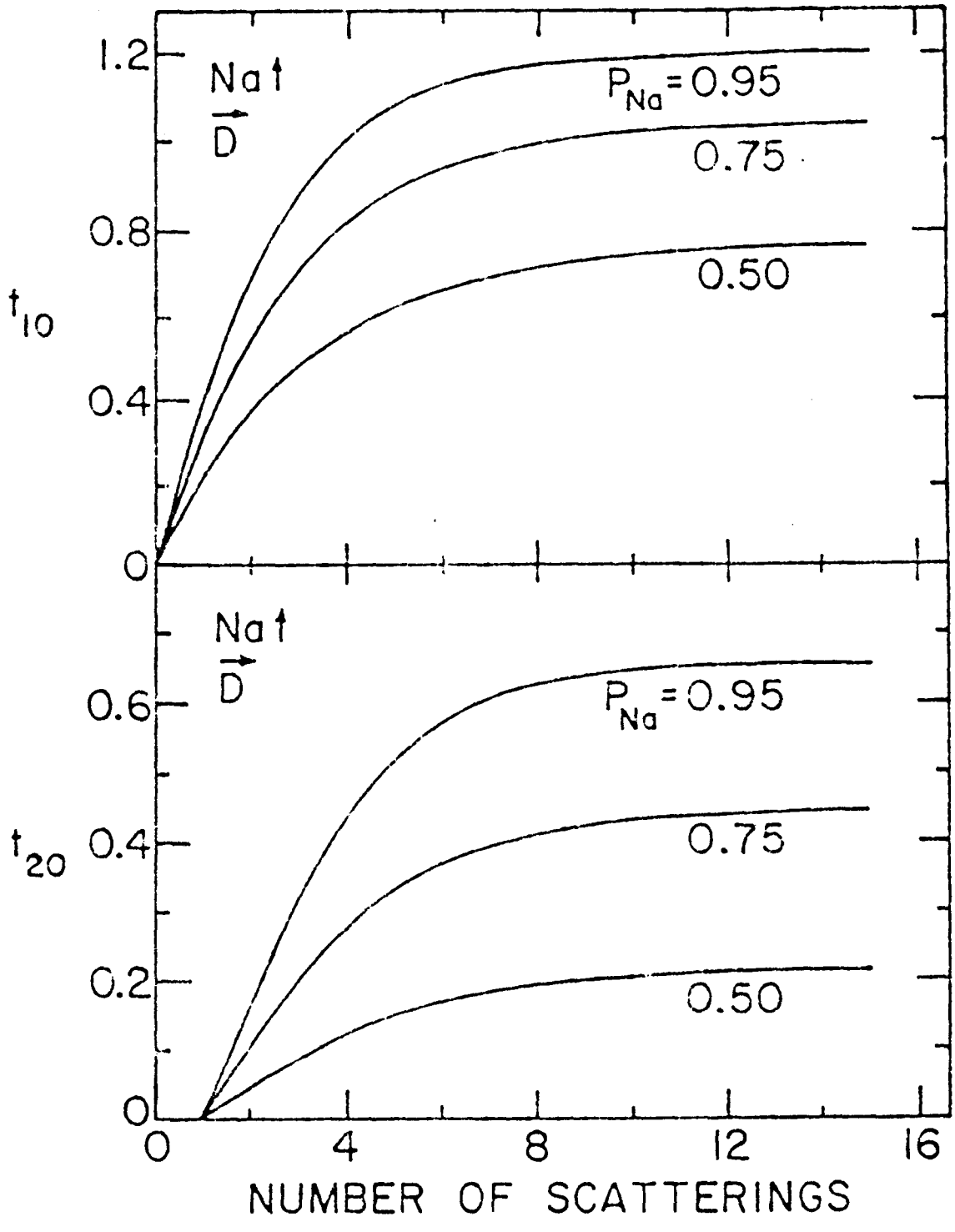

Figure 28. Expected polarizations for the deuterium nuclei as a function of the number of spin-exchange scatterings with polarized Na.

3.2 *TAGGED PHOTONS AND LOW CURRENT ELECTRONS*

3.2.1 *Electron Beams for Photon Tagging*

3.2.1.1 Photon Tagging in the Pulse Stretcher Ring

The original proposal for the CEBAF accelerator called for producing photons by inserting a radiator in the pulse stretcher ring. Several problems are anticipated with this design:

1. The halo of the primary electron beam, caused by inefficient extraction, might ruin the direct relationship between electrons detected in the tagging counters and the photons in the beam. The intensity of the primary beam is of the order of 10^5 times larger than necessary.

   The distance between the radiator and the production target determining the beam size will be unnecessarily large due to the shielding requirements of the main ring. Small spots size is important for small dE/dx, low probability for double processes, etc.

2. The energy of the main ring will be determined by the main use. Since tagging experiments, even at 100 duty cycle, will still take running times of the order of weeks it is likely that the main user will change the energy several times during the tagging experiment. This will greatly complicate the analysis of the tagging experiment. Some portions of the data may not be useful at all because they cover an uninteresting energy range.

3. There should be no background source close to the detector for outgoing hadrons. Large solid angle detectors are nearly impossible to shield against background produced by the main ring.

3.2.1.2 Extracted Beam from the Pulse Stretcher Ring

Since a beam intensity of 10 na is the maximum which can be used for photon tagging, the problem in working with the extracted beam from the pulse stretcher ring is to reduce the intensity from 100 μa to the level which can be accepted by the photon tagging spectrometer while minimizing interference with the primary beam. It is anticipated that the photon tagging experiments would work in a secondary mode with a prime user taking the full beam intensity.

There are two techniques which could be used to reduce the beam. One method, now used at Fermilab, would split off a part of the beam halo to derive a secondary beam. However, the beam halo may have a time dependence which would reduce the duty factor of the beam for photon tagging. Since photon tagging requires a coincidence which would be limited by a poor duty factor, it is essential that a beam with a good duty factor be made available to the photon tagging spectrometer. Therefore, a second method, which places a very thin foil in the center of the beam, is being considered. The objective of this method is to reduce a small fraction of the beam in energy so that this fraction can be separated by magnetic analysis. A thin foil in the center of beam would give optimum time structure for the extracted beam, while not interfering with the beam delivered to the primary user.

A procedure for achieving beam separation would be to disperse the beam to get a $\Delta p/p$ of 10^{-4}, then insert a foil of 0.2 gm/cm^2 thickness in the beam direction to produce an energy loss of about 0.4 MeV in a segment of the beam. This segment could then be separated from the main beam by magnetic analysis. To get an intensity reduction of 10^{-4}, the foil thickness would be about 1 micron. If this thickness is not practical, a thicker foil could be used with downstream slits to further reduce the beam intensity. If successful, this technique could be used to produce several secondary beams without a significant affect upon the primary beam.

The difficulty with using this secondary beam is that the tagged photon experiments will have to accommodate changes in the beam as the primary beam is adjusted . The primary beam could be changed in energy, intensity and beam structure as the primary users change their requirements. Since many of the photon experiments are of a long term nature and require a careful tuning of the tagging spectrometer to the energy and intensity of the electron beam, this mode of operation may not be compatible with may of the proposed photon experiments.

3.2.1.3 Positrons for Tagging Photons

In the late '60's the external C-beam line at SLAC was used to produce positrons at 95% of the extracted electron beam energy, typically 20 GeV. The positrons were used to produce tagged photons which ranged between 3.7 and 18.3 GeV, depending upon the positron momentum selected thorough beam optics by the experimenters. The experiments done with that photon beam did not require high

resolution[32]. In addition to some independence from other users the positron beam allowed the tagging spectrometer polarity to significantly reduce the troublesome atomic electrons. The purpose of this discussion is to see if such a facility might be useful for the tagged beam line at CEBAF.

Beam Line Overview

Figure 29 presents the projected layout of CEBAF with the area of the tagged beam line in the dotted curve expanded in Fig. 29b. Once the electron beam is injected into the beam line it would go through a thick foil converter which will electroproduce pairs by the processes shown in Fig. 30. The thickness of the converter will be set by limiting emittance of positron beam due to multiple scattering and average production angles. Parallel focussing at the converter is not difficult and the incident electron beam divergence can be neglected.

The positron beam then goes through collimators and momentum defining optics to a thin foil radiator, whose thickness depends upon the energy resolution needed in the tagging spectrometer vs. the photon flux desired.

Such a configuration would of course require the placement of the electron beam dump in the switchyard rather than at the back of the experimental hall.

The Converter

Assuming a divergence of less than 2 mrad as acceptable to the positron beam transport, an estimate is now made of the converter thickness so that the combination of multiple scattering and the average production angles of the photon and the pair stay under this limit.

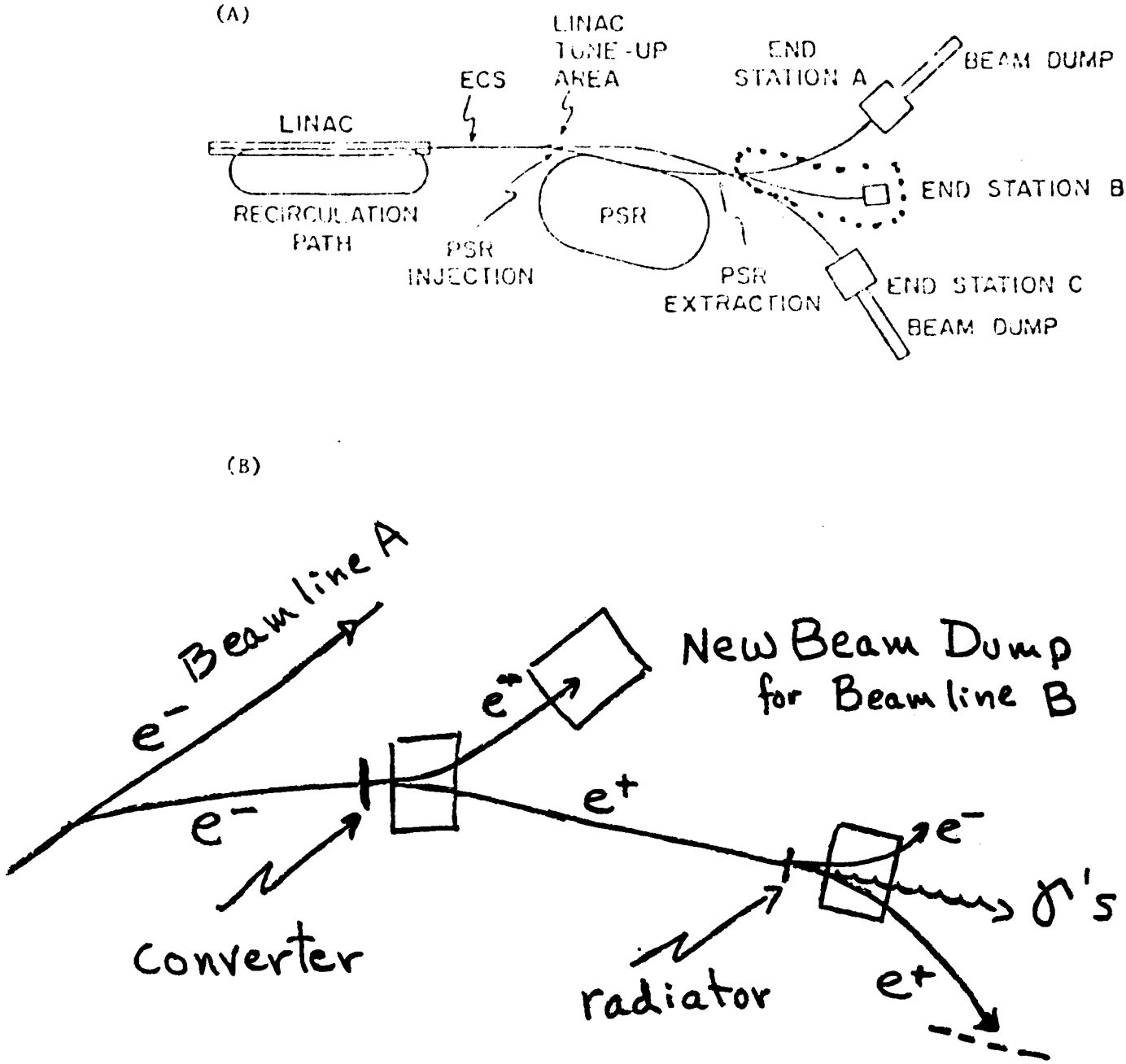

Figure 29. Proposed beamline.

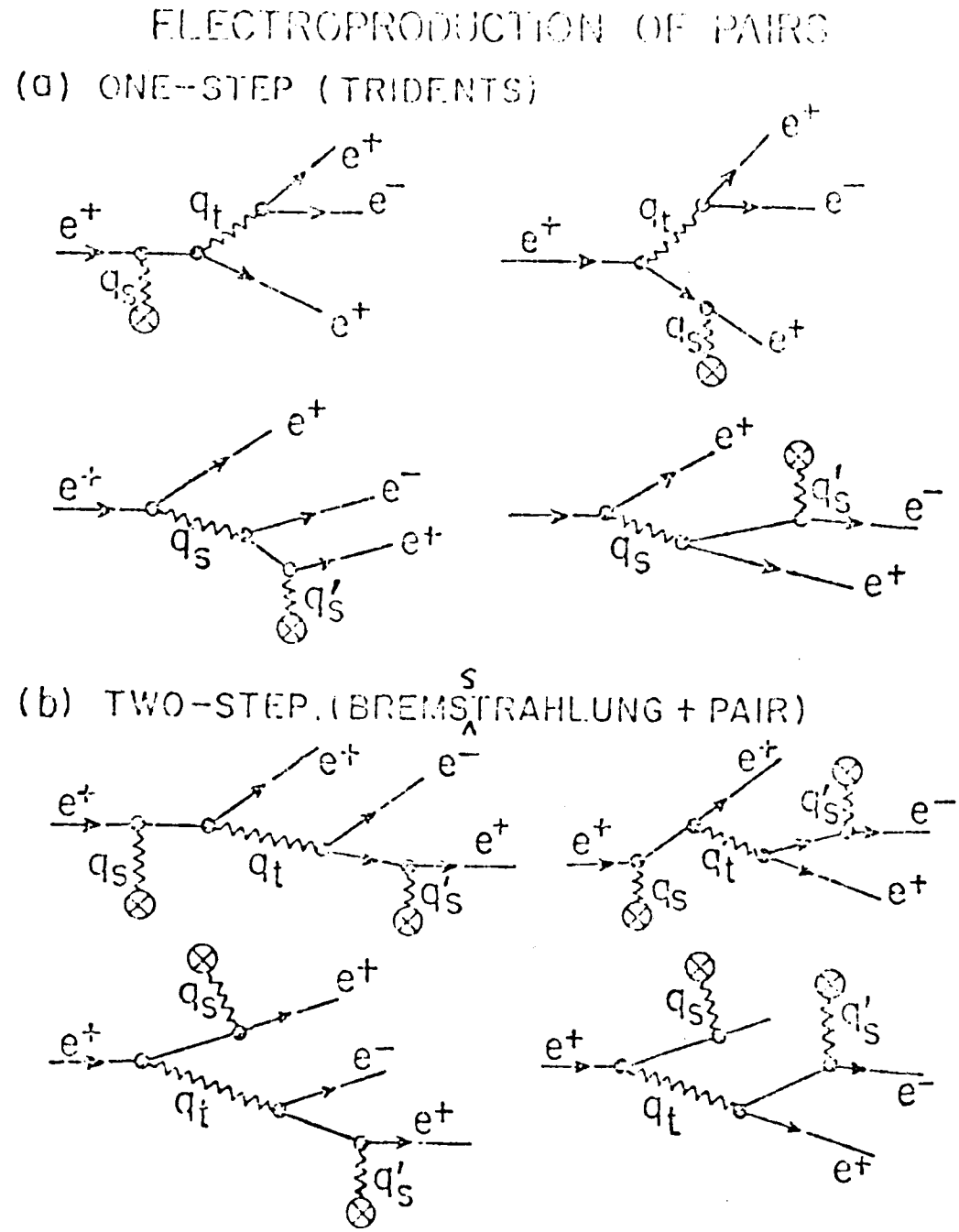

Figure 30. Diagrams contributing in lowest order in α to the electroproduction of pairs (a) on a single nucleon, tridents, and (b) on two different nuclei, bremsstrahlung plus pair production.

The standard value for the rms multiple scattering angle of an electron of energy E passing through a material of thickness t in units of radiation lengths (X_0) is:

$$\theta_{rms} = 21 \text{ Mev}\sqrt{t/E} \qquad \text{(Rossi}^{33}\text{ 2.16.7)}$$

This will slightly over estimate the multiple scattering for both the incident electron before it radiates and the energetic positron after production.

The characteristic opening angle for bremsstrahlung θ_{bs} produced by an electron of energy E, and for pair production, θ_{pp}, by a photon of energy k, are often quoted as $\theta_{bs} \sim m/E$ and $\theta_{pp} \sim m/k$, which is fine at lower energies, but above a GeV it is useful to remember:

$$\theta_{bs} \sim 2/3 \times m/E \times \ln (E/m) \qquad \text{(Rossi 2.11.19)}$$

and

$$\theta_{pp} \sim 0.6 \times m/k \times \ln(k/m) \qquad \text{(Rossi 2.19.16)}$$

Note that at 4 GeV, $2/3 \ln(E/m) = 6$.

Adding the above three sources of positron divergence in quadrature and setting them equal to the divergence, D, gives us a reasonable way to estimate a converter thickness, namely

$$D^2=\{2/3 \times m/E \ln(m/E)\}^2 + \{0.6 \times m/k \ln(k/m)\}^2 + t \times (21/E)^2$$

The divergence for different radiator thicknesses is given in Table 6.

As a point of interest Stahelin[34] has shown that the converter thickness where the one-nucleon (trident) and two-nucleon (triplet) processes are equally likely is given by

$$t = -4\alpha/\pi \times \{1 + 0.5 \ln^2(m/E)/\{1 \ln(m/E)\}\}$$

Evaluating at 4 GeV yields $t = 0.038 X_0$.

TABLE 6

Divergence of positron leaving converter for various thicknesses, assuming incident, divergent-free electrons at 4 GeV and photons of average energy 3.9 GeV producing the pair with a 3.8 GeV positron.

Divergence (mrad)	Thickness (X_0)
1.04	0
1.2	0.013
1.5	0.043
1.5	0.043
2.0	0.106

Probability of Electoproduction of High Energy Positrons

Neglecting recoil effects, Rossi has given us a differential probablility than an electron of total energy E on a foil of thickness $t(X_0)$ will produce a pair with kinetic energy T' for various ratios of electron and positron energies parameterized as u, namely

$$dProb = 2/3 - t\ \ln(1/v)/v\ (1+u^2/2)dT'du \qquad \text{(Rossi 2.20.4b)}$$

where the total energy of the pair electron and pair positron are E'_- and E'_+; total pair energy $E' = E'_- + E'_+ = vE$; pair energy division $u = (E'_- - E'_+)/E'$. By definition $E' = T' + m$ and thus $dT' = E\ dv$.

The absolute normalization is given by integrating over the entire range, namely, $-1 + 2\delta < u < 1 - 2\delta$ and $2\delta < v < 1 - 2\delta$, where $\delta = m/E$. The total probability of electroproduction of a positron is given in Table 7.

Of real interest is the probability of producing a positron of energy greater than some fraction of the total incident energy, say f. The limits of integration than reduce to $\delta + f < v < 1 - 2\delta$ and $-1 + 2\delta < u < 1 - (2f/v)$. Some of these probabilities are tabulated in Table 8.

TABLE 7

Total probability of electroproduction of a positron

Incident Electron Energy (MeV)	Total Prob. $(1/e^-/X_0)$	Total Prob. $(1/\mu a/X_0)$
4000	0.109	$6.82\ 10^{11}$
3000	0.101	$6.32\ 10^{11}$
2000	0.091	$5.66\ 10^{11}$
1000	0.074	$4.62\ 10^{11}$

A positron flux on the radiator can be estimated 1) assuming 100% transmission from converter to radiator and 2) assuming 0.03 X_0 to be a reasonable thickness for the converter. Selecting 3800 ± 20 MeV positrons because they are at 95% of the incident electron's energy, the probability is $1.22 \times 10^7/\mu a\text{-}X_0$ so the number of positrons per μa of incident beam current is given by:

$$N^+(3800 \pm 20\ MeV)/\mu a = Prob^+ \times t_c = 1.22 \times 10^7 \times 0.03$$

$$\text{or } N^+ = 3.66 \times 10^5/\mu a$$

TABLE 8

Partial probabilities for positron production

Amin [MeV]	Production [1/mA/X_o]	Probability [1/e^-/X_o]
3960	1.11E+06	1.78E-07
3880	1.04E+07	1.66E-06
3800	2.95E+07	4.73E-06
3720	5.92E+07	9.47E-06
3640	1.00E+08	1.60E-05
3560	1.53E+08	2.45E-05
3480	2.18E+08	3.49E-05
3400	2.98E+08	4.76E-05
3320	3.91E+08	6.26E-05
3240	5.00E+08	8.01E-05
3160	6.26E+08	1.00E-04
3080	7.70E+08	1.23E-04
3000	9.33E+08	1.49E-04
2920	1.12E+09	1.79E-04
2840	1.32E+09	2.12E-04
2760	1.55E+09	2.48E-04
2680	1.81E+09	2.89E-04
2600	2.09E+09	3.35E-04
2520	2.41E+-0	3.85E-04
2440	2.76E+09	4.41E-04
2360	3.14E+09	5.02E-04
2280	3.56E+09	5.70E-04
2200	4.03E+09	6.45E-04
2120	4.55E+09	7.27E-04
2040	5.11E+09	8.18E-04

Part b of table

ΔE [MeV]	Production [1/mA/X_o]	Probability [1/e^-/X_o]
3999-3960	1.11E+06	1.78E-07
3920-3880	5.83E+06	9.33E-07
3840-3880	1.09E+07	1.74E-06
3760-3720	1.62E+07	2.59E-06
3680-3640	2.19E+-7	3.50E-06
3600-3560	2.79E+07	4.47E-06
3520-3480	3.44E+07	5.51E-06
3440-3400	4.13E+07	6.61E-06
3360-3320	4.87E+07	7.79E-06
3280-3240	5.66E+07	9.06E-06
3200-3160	6.51E+07	1.04E-05
3120-3080	7.42E+07	1.19E-05
3040-3000	8.40E+07	1.34E-05
2960-2920	9.45E+07	1.51E-05

Fig. 3

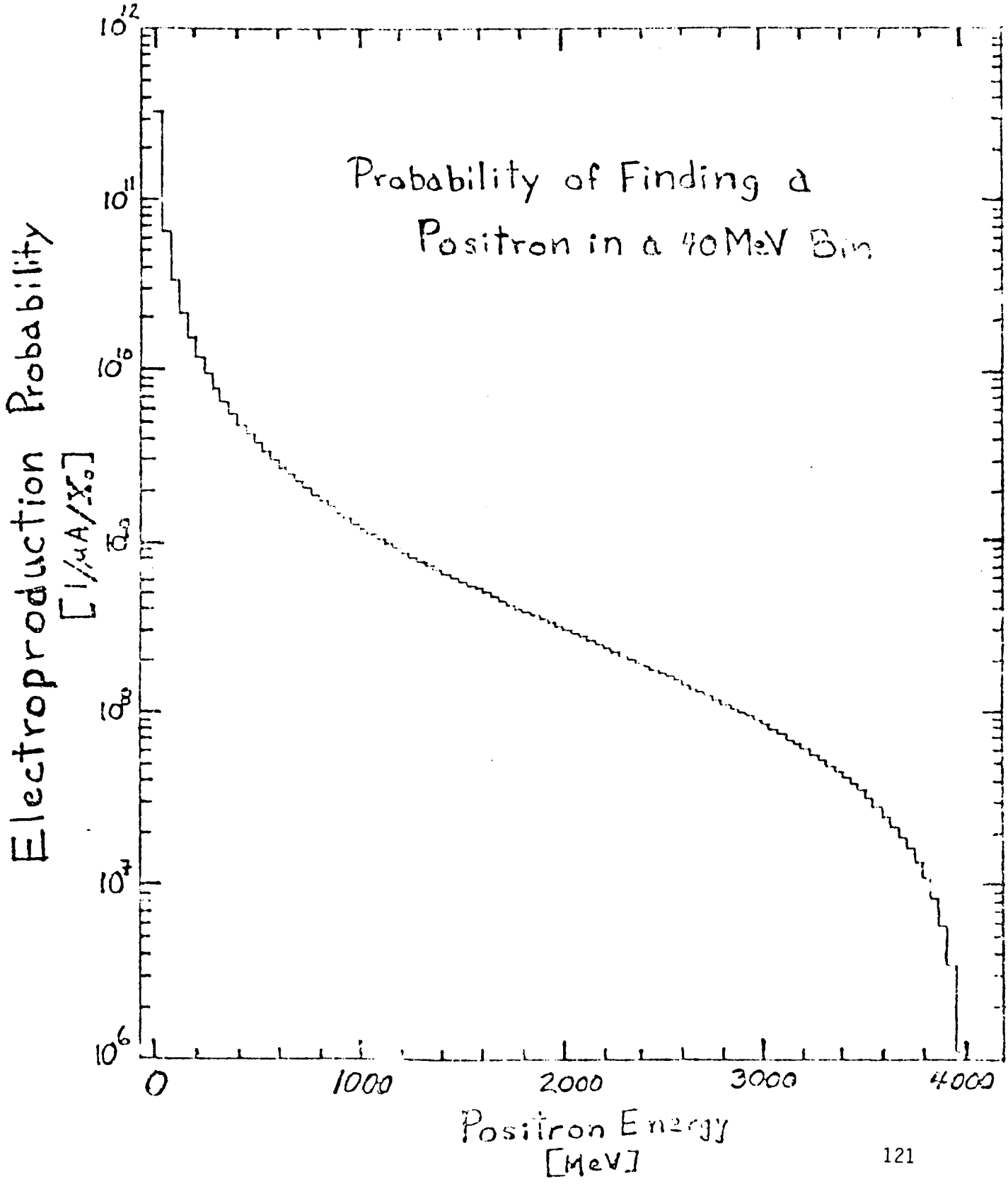
Probability of Finding a
Positron in a 40MeV Bin
Electroproduction Probability
[1/μA/X₀]
10¹²
10¹¹
10¹⁰
10⁹
10⁸
10⁷
10⁶
0
1000
2000
3000
4000
Positron Energy
[MeV]

2880-2840	1.06E+08	1.69E-05
2800-2760	1.18E+08	1.98E-05
2720-2680	1.31E+08	2.10E-05
2640-2600	1.46E+08	2.33E-05
2560-2520	1.61E+08	2.58E-05
2480-2440	1.78E+08	2.85E-05
2400-2360	1.97E+08	3.15E-95
2320-2280	2.17E+08	3.47E-05
2240-2200	2.39E+08	3.83E-05
2160-2120	2.64E+08	4.22E-05
2080-2040	2.91E+08	4.65E-05

Photon Beam

Again following Rossi (Fig. 2.11.2-3) it is clear that a copper radiator will have a differential probability per incident positron per radiation length of producing a photon in the energy range k to k + dk given by

$$dProb_{\gamma} = 0.9 \times N^{+} \times dk/k$$

If we assume, as most of the CEBAF tagging proposals have, that we tag the 0.5 to 0.95 fraction of the photons, then the number of tagged photons is

$$N_{\gamma}(0.5\text{-}0.95) = 0.576 \times N^{+} \times t_{r}.$$

Assuming a standard $t_r = 0.001\ X_0$, then the number of photons tagged between 1900 - 3600 MeV would be only 2100/μa.

The only thing we can do to improve this is to turn the few knobs we have available to us and plug them into the summary formula

$$N_{\gamma}(0.5 - 0.95) = 0.576 \times Prob^{+}(40\ MeV) \times I \times t_{c} \times t_{r},$$

where $Prob^{+}$ assumes you can stand 40 MeV resolution (see Table 8b), I is the machine beam current, and the t's are the converter and radiator thicknesses. Assume a beam current of 100 μa, a converter with $T_c = 0.1\ X_0$, and a radiator with $T_r = 0.005\ X_0$, then the results for different positron (tagging) energies are still below the generally

considered canonical value of 10^7/second. The results are given in Table 9.

TABLE 9

Tagging Fluxes

Positron (MeV)	Tagging Range (MeV)	Tagging Flux (Hz)
3800±20	1900 - 3610	$3.5\ 10^5$
3000±20	1500 - 2850	$2.5\ 10^6$

Conclusion

It appears that tagged photon fluxes produced by an externally produced positron beam would be too low by several orders of magnitude to be of use in first round experiments.

3.2.2 *Tagging of Bremsstrahlung Photons*

The bremsstrahlung of high energy electrons that are decelerated in the Coulomb field of a nucleus A ($eA \rightarrow e'A\gamma$) is the common source of photons for the investigation of photonuclear reactions. The main disadvantage is the continuous energy spectrum characterized by an energy flow that is nearly independent of the photon energy k:

$$k \times N(k) \sim \text{const for } k < E_o,$$

where E_o is the energy of the primary electron. The continuous spectrum makes it

1. necessary to determine the photon energy from an analysis of the photoproduced hadronic events,

2. difficult to normalize the photon flux with high precision.

Both problems can be solved by detecting the final electron in coincidence with the hadronic event. The photon energy k is then determined by the energy difference between the initial and the final state electron; $k = E_0 - E'$ independent of the hadron detection. An appropriate scheme for "tagging" the bremsstrahlung photons is shown in Fig. 31. The decelerated electrons are magnetically analyzed and detected in a multi-channel hodoscope (tagging counters). The flux normalization of the hadronic cross section can now be obtained for each photon energy bin (corresponding to one electron detector) from

$$\sigma_{had} \sim N_c/N_e$$

where N_c is the coincidence rate between the hadron detector and the electron detector and N_e is the electron detector rate. The ratio is independent of the absolute detection efficiency of the electron detectors. Therefore, the effective photon flux can be determined with high precision (< 1%).

Intensity Limitations

The maximum photon beam intensity that can be handled by a photon tagging system is limited by accidental coincidences between the hadron detector and the tagging counters. It is important to make a clean distinction between two different types of accidental coincidences.

a) Two tagging counters fire simultaneously (one real and one accidental hit within the resolving time of the coincidence τ). These events can easily be eliminated by rejecting double hits in the tagging counters (eventually already in the trigger).

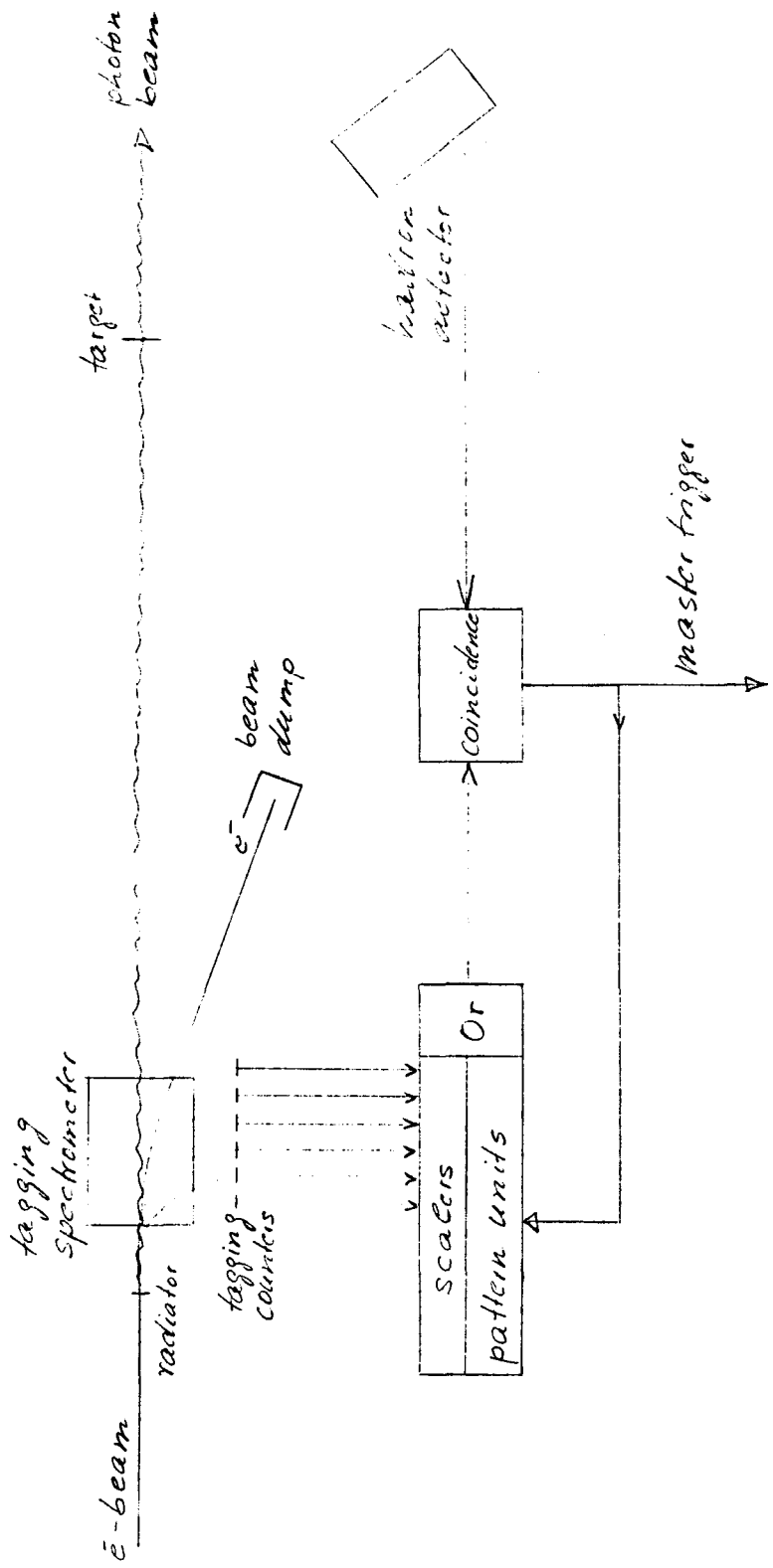

Figure 31. Photon tagging system

b) The hadronic event is not caused by the tagged part of the photon spectrum but by untagged part or by background. Ideally, there should be no hit at all in the tagging counters. Therefore, a single accidental hit has be treated as a real event. The corresponding correction can only be made by measuring and subtracting delayed coincidences. This requires additional data to be taken and analyzed; it also reduces the statistical accuracy.

Accidental contributions of the type (b) should therefore be kept small. This can be achieved by using

1. a high quality hadron detector that is not sensitive to background or the untagged part of the photon spectrum.
2. A wide energy range tagging system that leaves only a small fraction of the photon energy spectrum uncovered.

The total correction factor f_{corr} for the accidental contributions from both (a) and (b) determines the maximum photon rate N_γ^{max}

$$N_\gamma^{max} = f_{corr} \times d/ (\tau \times (1 + \varepsilon))$$

where τ is the coincidence resolving time, d the duty-cycle of the electron beam and ε the ratio of the untagged hadronic rate to the hadron rate from the tagged part of the photon spectrum. Using τ = 1.4 nsec (τ is limited by the CEBAF bunch separation), a duty-cycle of 90%, a total correction factor f_{corr} = 5% and ε = 2 yields N_γ^{max} = 10^7/sec. (This value should be treated as a soft number since it depends on the details of the process under investigation and on the size of the correction that the experimenter is willing to tolerate.) For the production of 10^7 photons/sec an electron current of 1 nA is sufficient (assuming a radiator thickness of ~ 10^{-3} X_o).

Tagging Spectrometer

The magnetic spectrometer for the analysis of the decelerated electrons should have the following properties:

1. Broad energy range. With a general purpose system it should be possible to cover the photon energy range $k \sim (0.2 - 0.95) \times E_0$. This offers the following advantages:
   a) Reduction of systematic errors and run time (if the whole range of interest can be covered simultaneously)
   b) Reduction of the type (b) accidentals
   c) Tagging of linearly polarized photons produced by coherent bremsstrahlung on a crystal radiator becomes possible (high photon polarization occurs only in the range $k \sim (0.2 - 0.5) \times E_0$). The count rate distribution in the tagging counters gives a high speed measurement of the photon spectrum that is needed to derive the photon polarization.
   d) Measurement of the polarization of incident electrons (needed for the production of circularly polarized photons). With a magnetized iron foil as a radiator the analyzing power of Moller scattering ($e^- e^- \rightarrow e^- e^-$) can be used. The two final state electrons both with $E_o/2$ have to be detected in the tagging spectrometer.
2. Point-to-point (between the radiator and the tagging counters) focussing in the deflecting plane. (This is necessary to achieve high photon energy resolution independent of the angular divergence of the outgoing electrons.)

3. Solid angle acceptance matching the angular divergence of the outgoing electrons (the divergence increases roughly with 1/E).
4. Short overall distance between the radiator and the production target to keep the beam spot size on the target small.
5. Sufficient deflection angle for the primary electron beam to avoid interference with the hadron detector.

A possible design for a tagging spectrometer is given in Fig. 32. The spectrometer uses a single synchrotron type magnet with a strong radial gradient to provide focussing over an electron energy range E' = (0.1 - 0.3) GeV. The primary beam with E_0 = 4 GeV is deflected by 35°. The average dispersion in the detector plane is 2 mm/MeV.

Experimental Setup for Tagged Photon Beams

At a photon beam intensity of 10^7 photons/sec the total counting rate from hadronic reactions is of the order of 10^3/sec. This low rate makes large acceptance detectors both necessary and feasible. Detectors with close to 4π solid angle and a wide energy range have the additional advantage of a high detection efficiency for processes that lead to multiple particle final states. The low intensity also offers interesting possibilities for the use of novel experimental techniques, e.g. the detection of low energy decay products of the final nucleus or the detection of heavy recoil nuclei in active targets (e.g. scintillating gasses, high pressure drift chambers, etc.)

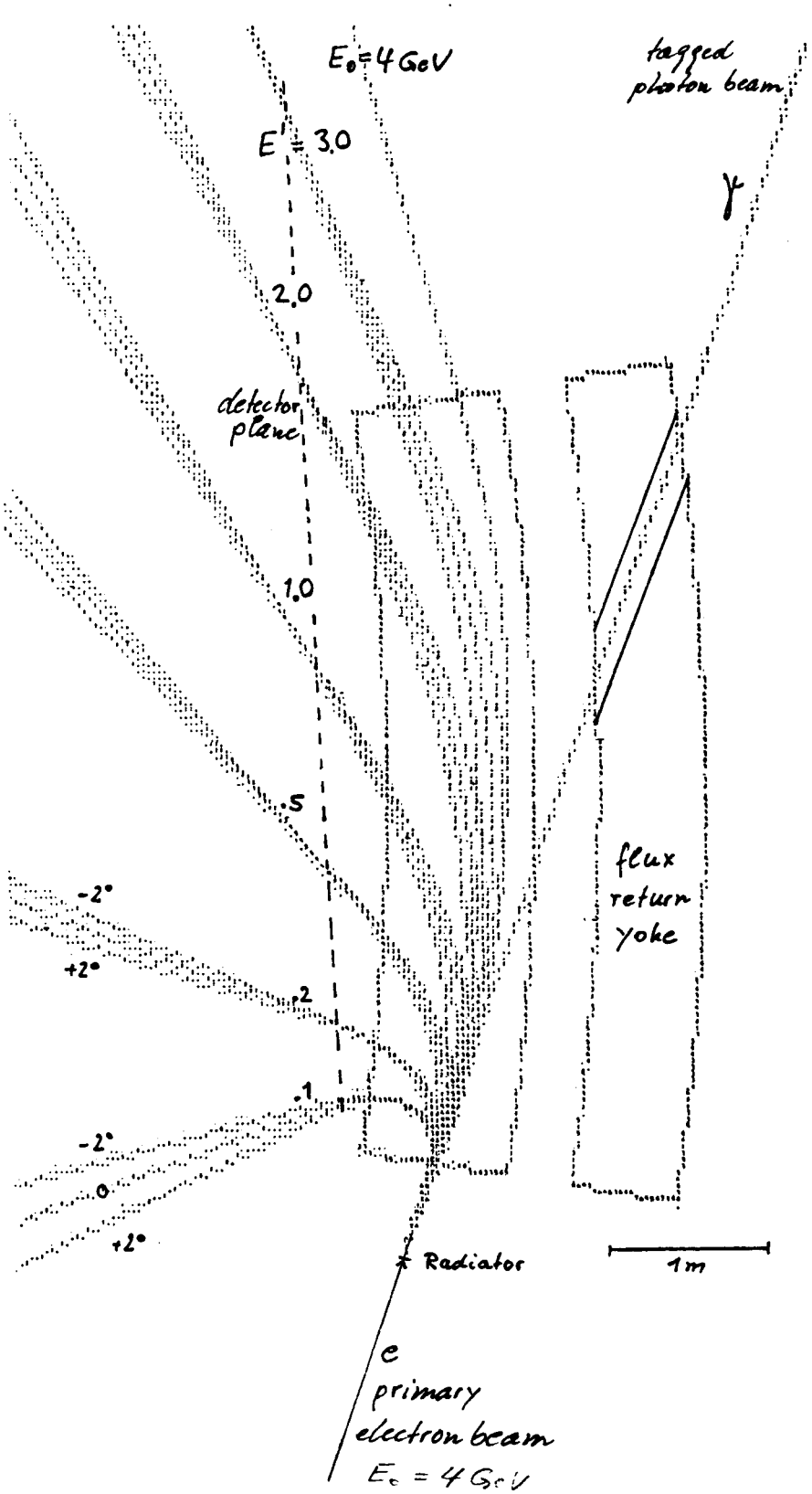

Figure 32. Photon tagging spectrometer.

3.2.3 *Large Solid Angle Detectors*

3.2.3.1 Very Large Aperture Detectors

Abstract

Very Large Aperture Detectors, VLADs, are envisioned for several classes of photo- and electroproduction experiments to be carried out at CEBAF. This section: 1) explains why VLADs rather than focusing magnetic spectrometers are being considered for many experiments, 2) summarizes the physics of many of these experiments and 3) describes the VLADs that are being considered for use as of the spring of 1984. Some information on photon tagging is also included. Many members of both CEBAF Photoproduction and VLAD workshops have contributed to the information contained in this report.

Introduction

Very Large Aperture Detectors, VLADs, are envisioned for several classes of photo- and electroproduction experiments to be carried out at CEBAF. This report summarizes the physics of many of these experiments and describes the VLADS that are being considered for use as of the spring of 1984.

Most VLAD concepts involve the use of nonfocusing large magnetic volumes filled with wire chamber, Cherenkov, dE/dx and total absorption detectors. Momentum resolutions on the order of dp/p=1% can be achieved with this technique for most charged particles. This resolution is adequate for many experiments looking at the production of nucleon resonances, mesons and/or strange particles and quasifree

processes. Focusing magnetic spectrometers with their higher resolutions are usually required when the scattering or reaction products involve discrete nuclear states. Many experiments proposed for CEBAF can make use of VLADS.

Photoproduction

Photoproduction experiments performed to date have frequently used VLADs because the incident photon flux was too low to achieve a reasonable counting rate using the small solid angles of focusing magnetic spectrometers. The large solid angle of the VLADS brought the counting rate up to more reasonable numbers. Extrapolating to the nearly CW beam conditions planned for CEBAF, photon fluxes on the order of 10^8 photons per second are viable for use in combination with VLAD detectors.

Electroproduction

Before discussing the physics experiments to be carried out using VLADs at CEBAF, it is important to realize why electroproduction as well as photoproduction experiments are being considered for VLADs. Electroproduction experiments involve an electron and one or more nucleons or mesons in the final state. Frequently, all but one of the observed particles are out of the scattering plane. If focusing magnetic spectrometers are used to carry out these experiments then complex geometries having the incident beam pass through the scattering chamber at varying angles to the horizontal, or geometries having a

huge magnetic spectrometer moving in the vertical as well as the horizontal direction are required. So the question is: can VLADs replace all or all but one of these magnetic spectrometers?

The answer to the question posed is determined by investigating to equation for the experimental event rate:

$$\text{Event Rate} = E*I*T*S*O_1*---*O_N*P_1*---*P_n$$

where: N is the number of independent particles detected

E is the net efficiency factor

I is the incident particle flux

S is the cross section

O_i is the solid angle for the ith particle

P_i is the momentum bite for the ith particle

$0 < P_i < 1$

Care must be taken to only include those 0_i and P_i which are independent.

VLADs make the 0_i large and usually they will also make the P_i large. VLADs will be useful whenever the product of E, I, T and S are small and whenever the number of observed particles is large. The following example using electrons as the incident particles will demonstrate the relevant points. A VLAD is compared to and assembly of focusing magnetic spectrometers, AFMS. The assumptions made are that E, T and S are the same for both systems. The values taken by the other variables are:

I(VLAD) = 10^8 electrons per second. This is the

number of photons per second that VLADS can currently handle. As long as the very forward (i.e. scattering angles less than several degrees) electrons are seen by the detector, this rate is reasonable for electrons also.

I(AFMS) = 160 micro amps = 10^{15} electron per second. This is approximately two thirds of the anticipated beam current of CEBAF.

O_1 (VLAD) = 10, four pi is almost possible but ten is a reasonable number to work with for estimates.

O_1 (AFMS) = 0.05, optimistic
0.03, more realistic

P_1 (VLAD) = 0.9

P_1 (AFMS) = 0.5, optimistic
0.2, more realistic

The ratio of the VLAD to AFMS event rates can now be calculated for different values of N:

N	Fvent Rates: VLAD/AFMS	
	Optimistic	More Realistic
2	0.01	0.2
3	5	300
4	$2x10^3$	$5x10^5$

Even for the N = 2, a VLAD may be nearly as good as an AFMS. For N = 3 and higher, the VLAD is unquestionably superior.

The answer to the question posed above is that, if there are two or more uncorrelated particles to be detected in the scattering or reaction process and a one percent momentum resolution is adequate, then a

VLAD should be considered. If the number of particles is three or more then the VLAD is the detector of choice.

Electron beam currents significantly above 10^9 electrons per second may also be appropriate for the VLADs. The 10^9 number allows for targets approaching a gram per square centimeter in thickness. By reducing the target thickness the beam current can be increased. Also, as the technology evolves for VLADs, it is likely that the usable event rates can be increased. This is particularly true for situations where only selected cross sections having online decidable features are considered.

Physics Experiments Using VLADs

The numerous experiments appropriate for VLADS can be grouped into several categories. The numbers following the categories listed below refer to the experiment number in the Review of Specific Experiments Section of the 1982 SURA proposal for CEBAF where additional information may be obtained on particular experiments, all or some portions of which may be appropriate for VLADs:

1)	Nucleon Resonances and Pions	#3, #13, #14
2)	Vectors Mesons	#2, #18
3)	Continuum Inelastic	#9, #10, #11, #12
	Scattering	#15, #16, #17,
	Strange Particles	#4, #21a

Examples follow for each of these four area of physics. Note that in each example there tends to be one particle carrying most of the

momentum off in a forward direction. One or more particles come off in other directions.

1) Nucleon Resonances and Pions

(e,e',p,π^+) and (e,e',p,π^-)

This reaction will investigate pion production and the character of certain classes of nucleon resonances in nuclei. Most often the final electron will go off at a forward angle. To effect longitudinal and transverse separations, electrons would also need to be detected at backward angles. In this case the proton and, or the pion would take the forward going momentum.

If the dominant case of the electron going forward is considered, it needs to be noted that there is typically a large opening angle between the final proton and pion. This means that while the direction of their center of mass is correlated with the scattering angle of the electron, the proton and pion are much less so correlated. A VLAD is needed for the proton and pion and possibly even for the electron.

(e,e',p,π^0)

This case is the same as the previous one except that the pion in the final state is neutral and neutral pions decay into two photons with typically a large opening angle at the kinematics under consideration. This means that there are at least three particles to be detected by VLAD, and further the VLAD must have total absorption counters to detect the photons.

(γ, p, π)

Using the incident photon rather than an electron only means that the proton and pion must share the forward momentum. There are still two

or more particles to detect.

It is important to consider that all of these reactions also have multi particle background processes that need to be determined. If a nucleus is used there are additional nucleons or nuclear fragments to be considered.

2) Vector Mesons

Vector mesons in and of themselves require a multi particle detector. This can be seen from the table below where several of their properties are listed:

Vector Meson	I	J^{π}	Mass MeV	Width MeV	Principal Decay Modes	%
ρ	1	1^-	769	150	π, π	100
ω	0	1^-	783	9.9	π^+, π^-, π^0	90
					π^0, γ	
					π^+, π^-	
ϕ	0	1^-	1020	4.2	K^+, K^-	49
					K_L, K_S	35
					π^+, π^-, π^0	15

Clearly to see any of these mesons in a reaction, at least three and more realistically four or more particles will need to be detected in the final state. This is because in electroproduction there will be the electron to detect and in both electro- and photoproduction at least one

hadron is also in the final state. These numbers of particles in the final state mean that only a VLAD is a realistic detector to consider for carrying out any experiment involving vector mesons. As the physics of vector mesons is very important for understanding how nucleons join to form nuclei, CEBAF is expected to preform numerous experiments studying their properties.

3) Continuum Inelastic Scattering

Single arm (e,e') measurements made to date come up with too much transverse strength in the region between the quasifree peak and the delta peak and too little or unusually distributed strength in the longitudinal component of the quasiefree peak. Two arm (e,e',p) measurements have largely only looked in the scattering plane at protons at the conjugate scattering angles to be scattered electrons. To fully understand the physics of these regions as well as the scaling behavior in the threshold breakup region at high momentum transfer, the complete final states needs to be measured. This includes the photons radiated in the scattering process, especially for the higher Z nuclei. Ambiguities coming from the radiative process would be removed. A VLAD is ideal for these experiments.

Final states involving multiple nucleons and, or deuterons etc. can then be investigated. By appropriate kinematic reconstruction, the difficult to be detected neutrons can be dealt with because all of the other particles would be observed. Questions of bound deltas and delta production in nuclei could be investigated. For example, at many kinematics the pion from the decay of the delta in delta production is strongly absorbed by the spectator nucleons. A signature of this is to

observe two protons back to back in the final state rather then the pion.

4) Strange Particles

Such basic measurements as the determination of the electromagnetic form factor of the kaon have not been done to date.

(e,e',K^+,L)

$L\text{-}p,\pi^-$ (64%)

$L\text{-}n,\pi^0$ (36%)

A VLAD would see the K^+, p and π^- easily and possibly the e' as well. Such a complete determination of the final state would mean that the measurement would have a very clean signature.

The same reaction can of course be carried out for incident photons and for the production of negative kaons. Also, the process can be investigated in the quasifree region for nuclei. VLADs would not likely have the resolution to detect the process when discrete nuclear states were involved unless the VLADs photon detection system was used to detect the nuclear decay photons or a focusing magnetic spectrometer was used to observe the kaons. A VLAD would still be needed for the protons and pions.

VLADs - The Hardware

The VLADS to be used at CEBAF will probably be in two sections: 1) a detector around the target to detect particles having momenta from 0.1 to 2 GeV/c and having a solid angle greater than 3π. 2) a forward looking detector for particles having angles from approximately 3 to 25 degrees to the beam direction. The forward looking detector will

analyze particles from 0.5 to 4-5 GeV/c. Both detectors will be capable of handling multiple events.

A preliminary design for a VLAD is shown in for figure on the following page. The detector around the target has a superconducting solenoidal magnet with an iron return path. The magnetic volume will be approximately two meters in diameter and three to four meters long. The central magnetic field will be variable up to two or more tesla. At the higher field setting particles in the momentum region from 0.1 to 2 GeV/c can be analyzed. The inner region will have wire chambers. The next regions will consist of Cherenkov, dE/dX and total absorption detectors. This will allow particle identification and momentum determination for charged mesons and hadrons. The photons from the neutral pion decay will be detectable using the total absorption detectors.

In photon production experiments from large gas targets the wire chambers in the inner region of the solenoid are used to determine the vertex of the event. Because the current can be turned up in electroproduction experiments, small targets can be used even if the target is gaseous. The vertex is determined by the small beam on the small target and the inner region of wire chambers is not needed. They will be removed for electroproduction. This way the background of low energy electrons and protons created in the electron scattering processes will take unobstructed helical paths out of the solenoid. This VLAD can be used for both electro- and photoproduction.

The forward looking detector for the VLAD is a superconducting toroidal magnet possibly having eight segments. The electrons that

have only scattered a few degrees pass through the hollow core. This allows for a very large solid angle for the high momentum particles going forward.

In some electroproduction experiments it may be worth while to have a focusing magnetic spectrometer at the forward angle. This is because the cross section varies so rapidly for some reactions at the forward angles that the small solid angle of the focusing magnetic spectrometer would still see a significant fraction of the electrons of interest. With the toroidal magnet appropriate trigger counters can be used to select only narrow classes of events.

The solenoidal magnet may be replaced by a crystal ball or sphere of liquid argon or xenon for some experiments. However, the total absorption layer of detector in the solenoid will likely be able to perform the crystal ball function. The spheres of liquid noble gasses are yet to be developed.

Summary

This is a working report meaning that comments are welcome and that it will change and grow as we make progress. We plan to proceed in several directions. Models of the experiments will be made so as to make more accurate estimates of the event rates in the various components of the detectors. Models of the VLADs will be made so as to determine the geometry of the detectors, i. e. everything need to fit in the space available.

Studies of existing VLADs are underway. It may be possible to acquire the solenoidal portion of the LASS detector at SLAC if we show adequate justification. The magnetic field is almost two meters in

diameter and three and one half meters long. This is the size we plan for CEBAF. The toroidal magnet described above will be investigated in more detail. Models of its fields and detectors will be created.

3.2.3.2 Liquid Counters

Many experiments in high energy physics now use liquid argon as a calorimeter and liquid argon is also being considered for the medium in a time projection chamber.[35] [36] Energy and position can be measured by monitoring the electrons produced by ionization in the liquid argon. To minimize electron capture, oxygen impurities must be maintained at the part per million level for a calorimeter. However in a time projection chamber the electrons must drift over large distances and even low concentrations of impurities which can capture electrons will impair its operation. In this case the oxygen impurity level must be maintained at the part per billion level.

In order to be considered as a candidate for a liquid TPC medium, a liquid must have free ionization electrons. Examples of suitable liquids are the noble liquids, argon, krypton and xenon, and highly symmetric liquid hydrocarbons, such as CH_4, CD_4 and $Si(CH_3)_4$. Argon has the advantage of being inert and available at low cost while xenon has a short radiation length. $Si(CH_3)_4$ has a boiling point near room temperature.

The properties of several liquids of interest for a large solid angle detector at CEBAF are listed in Table 10.

There are several differences between the gas and liquid counters which should be noted.

TABLE 10

Properties of Several Liquid Counter Media

	Ar	Xe	CH_4
Boiling Point at 1 atm (°K)	87.5	166.1	109
Density at b. p. (gm/cm^3)	1.4	3.5	0.47
$(dE/dx)_{min}$ (MeV/cm)	2.1	4.4	1.2
Radiation length (cm)	14.0	2.6	99
Average Ionization Energy (eV)	23.6	15.6	27
Recombination at 1 kV/cm (%)	30	16	65

1. Recombination in the liquid is significant at fields of order 1 kV/cm.
2. Because of high density, attachment of electrons to impurities can be serious. Therefore impurities must be kept to the level of a few parts per billion oxygen equivalent in order to drift electrons up to a meter.
3. The electron drift velocity is slower in liquids than in gases by about an order of magnitude. Therefore the electronics will be less expensive, especially in analog to digital conversion.
4. Charge multiplication in liquid argon is difficult requiring the operation of the detector in the ionization mode with low noise preamps. However charge multiplication does occur in liquid xenon.

The lower drift velocity of ionization electrons in liquids as compared to gases restricts their applications to experiments with low event rates such as are anticipated in the photoreactions at CEBAF. Liquid xenon may be useful as a detector for photoelastic scattering experiments.

The liquid counters are also able to measure the energy deposited to a high precision. A spectrum of ^{207}Bi taken with a liquid argon counter is shown in Fig. 33. [37] The width of the ^{207}Bi line at 976 KeV is 34 KeV which can be compared to the predicted electronic noise of 15 KeV and a Fano factor calculation of 4 KeV for the resolution of this peak. At this time the difference between the measured and predicted width is not understood. However, the Fano factor calculation suggests the possibility that a study of this detector could greatly improve its resolution.

The properties of liquid xenon are even more favorable for gamma detection because of its longer radiation length and a Fano factor calculation of 2 KeV for the limit to its energy resolution at 1 MeV.[37] A spectrum for ^{137}Cs in liquid Xe is shown in Fig. 34, at an electric field of 6.5 kV/cm.[38] [39] As the field is increased, the resolution improves as shown in Fig. 35. At energies above 1500 KeV, the resolution of liquid Xe surpasses NaI.

A major impediment to the use of liquid xenon is its cost. At the current price of about $6000/liter, a detector which is 20 radiation lengths thick in a spherical shape surrounding a target would cost about $2 million.

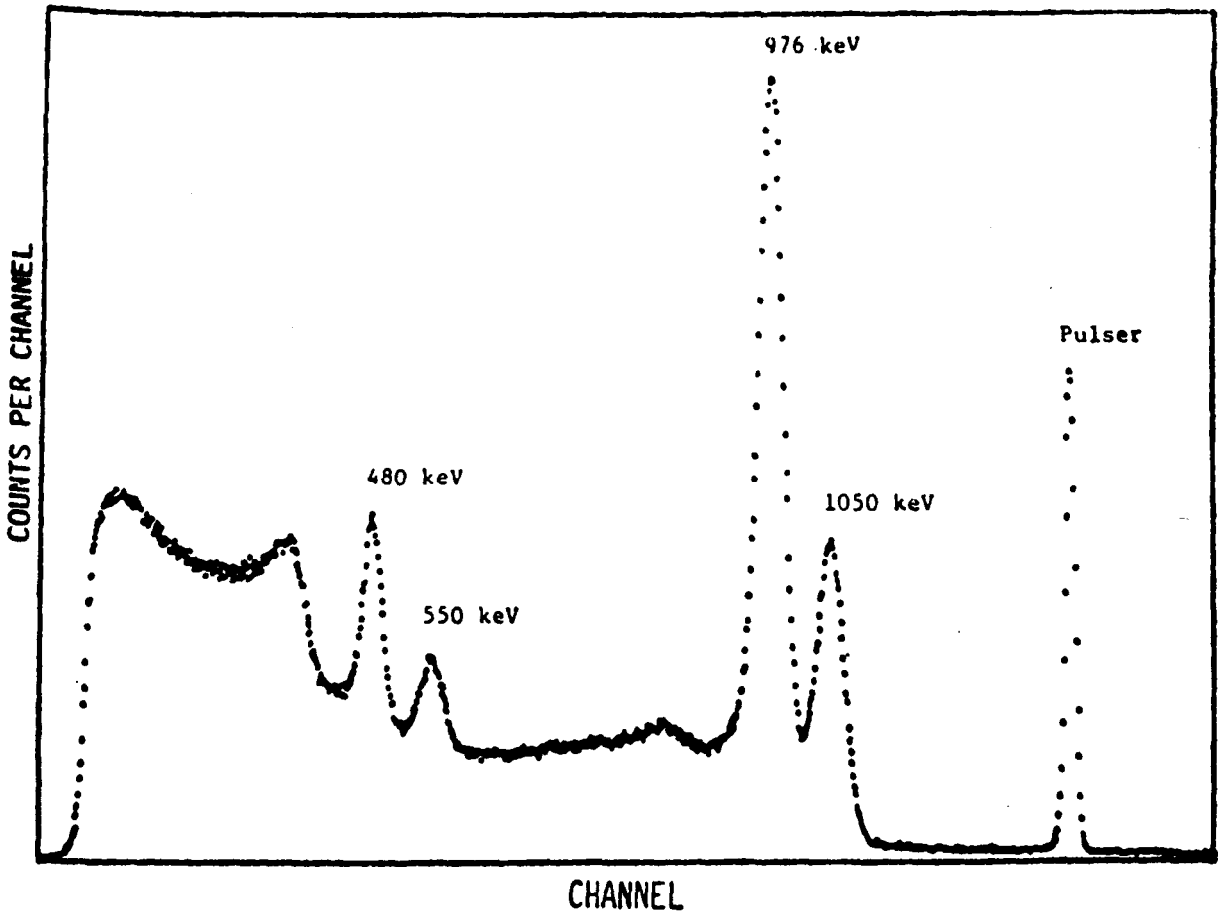

Figure 33. The spectrum of ^{207}Bi as detected in a liquid argon ionization chamber.

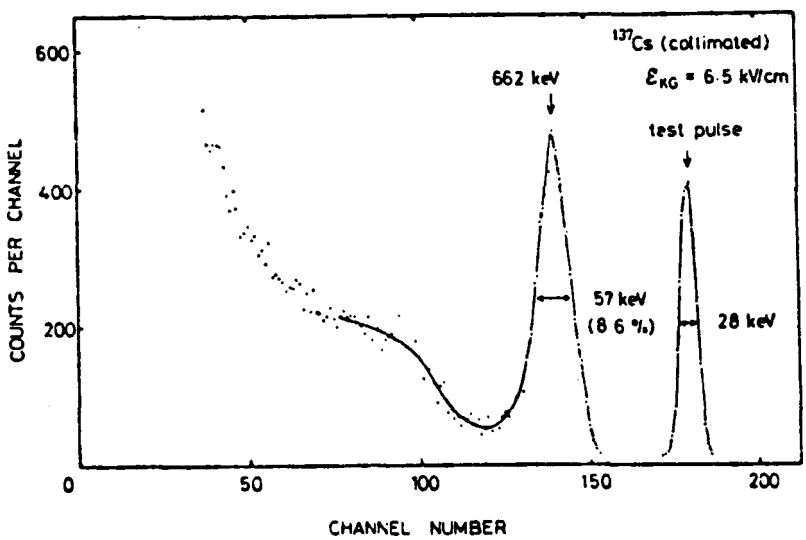

Figure 34. A typical pulse height spectrum of ^{137}Cs obtained for an electric field of 6.5 kV/cm.

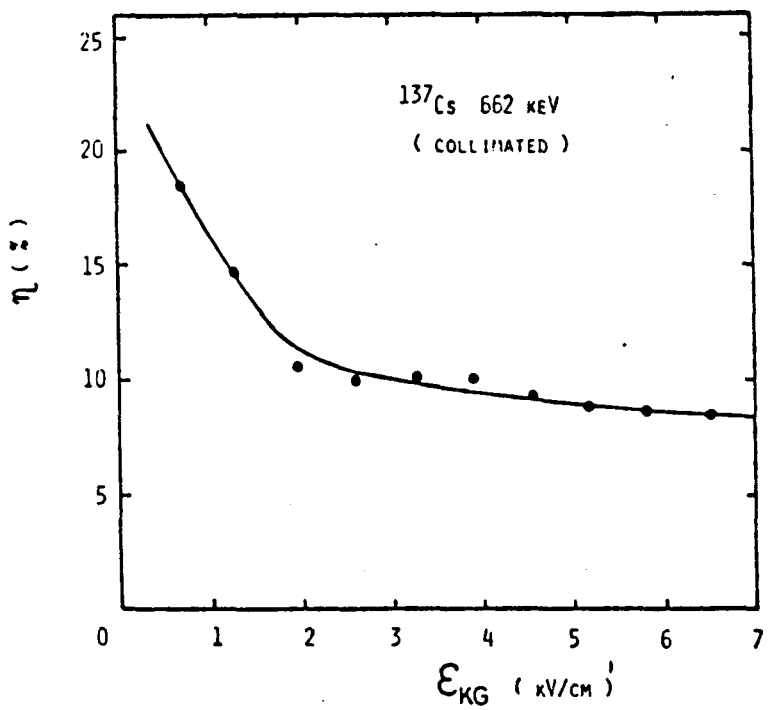

Figure 35. The variation of the energy resolution (fwhm) for liquid xenon with the electric field.

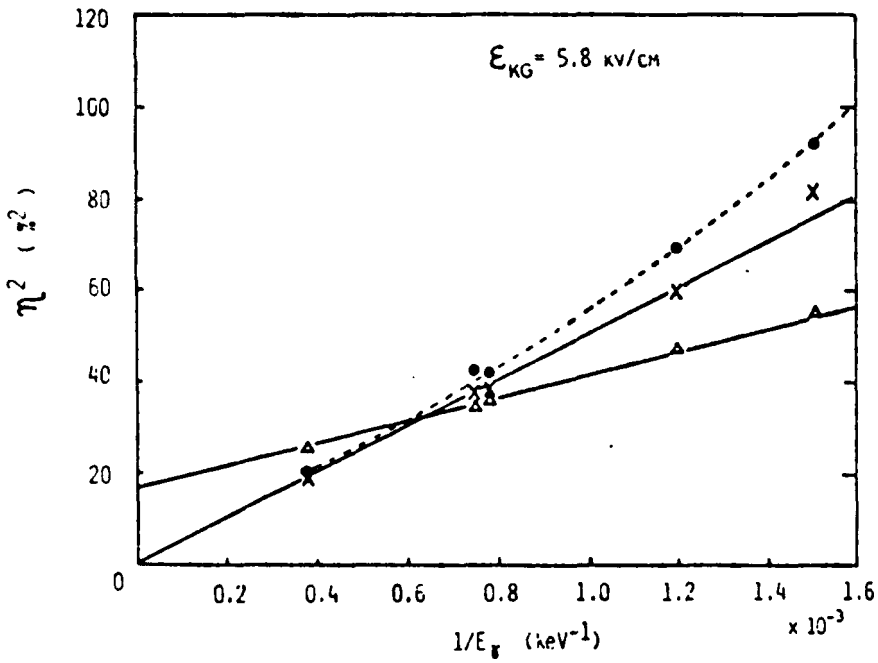

Figure 36. The square of the relative energy resolution for non-collimated gamma-rays versus the reciprocal of the gamma-ray energy $1/E_\gamma$. The full circles are for liquid xenon; crosses, after noise correction; and open triangles, for NaI(Tl).

4. RECOMMENDATION FOR A DEDICATED RING

After reviewing experiments with tagged photons and internal targets, the group has decided that the advantages of the second ring for photon tagging and the possibilities for internal target experiments justify the addition of a dedicated ring to the Continuous Electron Beam Accelerator Facility (CEBAF).

A second ring for the CEBAF facility will offer the following advantages:

1. The second ring can be used for internal target electron scattering experiments using gas jet targets. The possibility of polarized electron beams and polarized gas jet targets will open opportunities for important experiments which cannot be pursued with the present accelerator configuration. The low target density will allow novel detection techniques such detection of low range heavy nuclear recoils.
2. The ring will provide an independent electron beam with an energy and intensity which can be varied independently from the main ring. At intensities of only a few nanoamps, the ring would be useful for the operation of a tagged photon beam.
3. If the ring is capable of delivering high intensity beams, it could also be used to serve electron scattering experiments in the second end station.
4. The ring would provide the target for backscattering of laser light from high energy electrons. This is the only known process to give monochromatic photons with nearly 100% (linear or circular) polarization. Future developments in laser

technology may allow the operation of a high power light source with energies greater than 100 eV. The high energy of the initial photons will greatly increase the efficiency of the procedure since E_γ/E_e will be close to 1. Also the requirement for collimation will be reduced by using relatively high energy photons in the initial state.

5. REFERENCES

1. "Electron Rings for Nuclear Physics Research", Proceedings Lund, Oct. 5 - 7, 1982, University of Lund Internal Report.

2. R. G. Arnold, C. E. Carlson, and F. Gross, Phys. Rev. *C23*, 363 (1981)

3. C. Y. Cheung and R. M. Woloshyn, Phys. Lett. *127B*, 147 (1983).

4. R. Diebold et al., Physical Review Letters *35*, 632 (1975).

5. D. Kleppner and T. J. Greytak, High Energy Spin Physics - 1982, AIP conference Proceeding No. 95, American Institute of Physics, page 546 (1983).

6. T. W. Donnelly, "Considerations of Polarization in Electron Scattering", Talk given at the Workshop on Perspectives in Nuclear Physics at Intermediate Energies at the International Centre for Theoretical Physics, Miramare-Trieste, Italy, October 10-14, 1983.

7. M. E. Schulze et al., Tenth Int. Conf. on Few Body Problems in Physics, Karlsruhe, 1983.

8. G. Hohler et al, *Handbook of Pion-Nucleon Scattering* (Fachinformationszentrum Energie, Physik, Mathematik, Karlsruhe, 1979), Physik Daten Vol. 12-7.

9. R. Kajikawa, "Pion Photoproduction and Compton Scattering in the Resonance Region", Symposium on Lepton and Photon Interactions, Bonn (1981).

10. Forsyth, Charles Patterson, "A Quark Model of the Non-Strange Baryons", thesis submitted to the Department of Physics, Carnegie-Mellon University, May, 1981.

11. R. Kajikawa, in *Proceedings of the IV International conference on Baryon Resonances*, Toronto, 1980, page 43.

12. I. Arai, in *Proceedings of the IV International Conference of Baryon Resonances*, Toronto, 1980, page 93.

13. R. L. Crawford, in *Proceedings of the IV International Conference on Baryon Resonacnes*, Toronto, 1980, page 107.

14. Barker et al., Nuclear Physics *B95*, 347 (1975).

15. D. M. Manley, R. A. Arndt, Y. Goradia, and V. T. Teplitz, "An Isobar-Model Partial-Wave Analysis of $\pi N \to \pi\pi N$ in the c.m. Energy Range 1320 - 1930 MeV, submitted for publication, March 1984.

16. J. M. Laget, Nucl. Phys. *A312*, (1978) 265.

17. S. J. Brodsky and J. R. Hiller, SLAC-PUB-3047 (1983).

18. J. H. Koch, E. J. Moniz and N. Ohtusuka, Annals of Physics, to be published.

19. P. Joos, Landolt-Bornstein I/8, 303 (1973).

20. K. P. Schelhaas, B. Ziegler, and E. Hayward, Proceedings of the International Conference on Few Body Problems in Physics, Karlsruhe, W. Germany, August, 1983.

21. H. Genzel and W. Pfeil, Landolt-Bornstein I/8, 1 (1973).

22. C.I Choller, J. Arends, H. Beil, R. Bergere, P. Bourgeois, P. Carlos, F. L. Fallou, J. Fagot, P. Garganne, A. Legpretre, and A. Veyssiere, Phys. Lett. *127B*, 331 (1983).

23. J. Ahrens. H, Gimm, and B. Ziegler, Proceedings of the

International Conference on Nuclear Physics, Florence (Italy) August 29 - September 3, 1983).

24. J. Ahrens, J. Arends, P. Beurgeois, P. Carlos, J. L. Fallow, N. Floss, P. Garganne, S. Huthmacher, U. Kneissl, G. Mank, B. Mecking, H.Ries, R. Stenz, and A. Veyssiere, ibid.

25. E. Hayward and B. Ziegler, Nucl. Phys., to be published.

26. R. Leicht, M. Hammen, K. P. Schelhas, and B. Ziegler, Nucl. Phys. *A362*, 111 (1981).

27. J. Antille et al., "Proposal for the Study of e^+e^-, γ, π^0 and Hyperon Production in pp Reactions at $\sqrt{s}$ = 22.5 GeV Using an Internal Jet Target at the SPS", SPSC/80-63 CERN (1980).

28. D. Kleppner, private communication, 1983.

29. R. W. Cline et al., Phys. Rev. Lett. *47*, 1195 (1981).

30. N. D. Bhaskar et al., Phys. Rev. Lett. *49*, (1982) 25.

31. W. Happer, private communication, 1983.

32. D. O. Caldwell, et al, "Total Hadronic Photoabsorption Cross Sections on Hydrogen and Complex Nuclei from 4 to 18 GeV", Physical Review *D7*, 1392 (1973).

33. Bruno Rossi, High Energy Particles, Prentice-Hall, 1952.

34. Peter Stahelin, DESY Lecture Notes, 1966.

35. For an example of the use of liquid argon in a calorimeter, see J. Houston, "Measurement of the Radiative Decay Width of the Positive Rho Meson", Thesis submitted to Department of Physics and Astronomy, The University of Rochester, 1982.

36. H. H. Chen, "Search for Proton Decay and Solar Neutrinos with a Liquid TPC" in Proceedings of the 1982 Summer Workshop on Proton Decay Experiments, June, 1982, Report ANL-HEP-PR-82-84.

37. M. D. Edmiston and C. R. Gruhn, "Energy Resolution Considerations in Liquid Ionization Chambers", IEEE Trans. Nucl. Sci. NS- *25*, 352, (1978).

38. T. Doke, "Fundamental Properties of Liquid Argon, Krypton and Xenon as Radiation Detector Media", Portgal Phys, Vol 12, page 9 (1981).

39. T. Doke, "Recent Developments of Liquid Xenon Detectors", Nuclear Instruments and Methods *196*, (1982) page 87.

Appendix A

PROPOSALS FOR PHOTON INDUCED REACTIONS

The following proposals, which are given in the 1982 SURA proposal, are concerned with photon induced reactions:

1. Photoproduction Part I: Vector Mesons (Crannell, Noble and Whitney)
2. Photoproduction part II: Baryon Resonances (Crannell, Noble and Whitney)
3. Pion Photoproduction on Very Light Nuclei (Laget and Stoler)
4. (γ,πN) and (e,e'πN) Experiments At 1-2 GeV (Redwine and Jackson)
5. Production of Hypernuclei by the (γ,K) Reaction (Bernstein, Donnelly and Epstein)
6. Production of Nuclear Kaons with Tagged Photons (Whitney and Booth)
7. Photon Tagging (Hayward)

QCD studies with 4-Gev photon and electron beams

C. E. Carlson
College of William and Mary

Three topics will be dealt with in this report. The first is the possibility of finding glueballs in experiments with a photon beam; the second is tests of perturbative QCD involving photons; the third is high momentum transfer predictions for the deuteron electromagnetic form factors when the deuteron is treated as a six-quark object.

I. Glueballs

QCD [1] suggests the existence of states which have no valence quarks, only valence gluons. These states are variously called gluonic mesons, gluoniums, or glueballs. The cross sections for producing glueballs with a 4-Gev photon beam are not large, but since properties of known mesons are going to be studied by photoproducing them [2] one should be aware that glueballs could be found in the same apparatus. Also, one should be aware that one of the leading glueball candidates [3], now called the iota, was apparently first discovered [4] in an even lower energy situation than we are now discussing, namely in pp-bar annihilation at rest.

At first thought, prospects for photoproducing glueballs do not seem good. Photons couple to quarks and so produce ordinary mesons easily enough. But gluons are neutral, so it would seem that the procedure for discovering glueballs in photoproduction is the following: list all known glueball candidates; search for them via photoproduction; if sucessful strike them from the list. The unfindable rather than the findable candidates are the glueballs.

This unsatisfactory situation is not the final story. There are gluons inside the photon and their distribution is calculable. They come from the breakup of the photon into quark-antiquark pairs which in turn bremsstrahlung gluons. The number and distribution of these gluons and quarks can be calculated from the Altarelli-Parisi equations [5,6]. In contrast to the Altarelli-Parisi equations as applied to hadrons rather than photons, there is a driving term in the equations [6], which is not stongly coupled and which comes from the $\gamma \to q\bar{q}$ interaction that initiates the development of gluons and further quarks. And now we come to a remarkable fact. The gluon distribution within a photon is more singular as x approaches zero [7] (where x is the fraction of the parent particle's momentum carried by the gluon) than the corresponding distribution in a hadron. The gluon distribution in a hadron [8] goes like 1/x for small x (up to some logarithmic factors) while for a photon the power depends on the number of relevant quark flavors and for four flavors the gluon distribution in a photon [7] goes like 1/x**1.59 for small x. This means that there are in the kinematic region corresponding to small x a relativly large number of gluons in a photon beam and the photoproduction cross section for glueballs will not be hopelessly small.

Figure 1 shows the total cross section for $\gamma p \to G + \text{anything}$ calculated according to the gluon fusion process [9] shown in

Fig. 2, viz.,

$$(1)\quad \sigma = \frac{\pi^2}{8M_G^3}\,\Gamma(G\to gg)\,\tau \int_\tau^1 \frac{dx}{x} P_{g/\gamma}(x)\, P_{g/p}(\tau/x)$$

Here G is a glueball, which for definiteness we take to be a spin-parity pseudoscalar with the mass and width of the iota, 1440 Mev and 50 Mev, repectively. $P_{g/A}(x)$ is the probability distribution for finding a gluon in A with a momentum fraction x; $P_{g/\gamma}$ is calculable but not measured and $P_{g/p}$ is the reverse. Also, $\tau = M_G**2/s$ where s is the c.m. energy squared and we approximate the G -> gg width by the full width.

The γp c.m. energy for E_γ = 4 GeV is

$$(2)\quad \sqrt{s} = \sqrt{m_p(m_p + 2E_\gamma)} = 2.90\ \text{GeV}$$

The cross section at this s is about 2 nanobarns. This should be regarded as an estimate; eqn. (1) works best far above threshold and threshold for the present example is 2.38 GeV.

At energies under discussion here, the observed momentum distribution if produced glueballs will not be strikingly different from most ordinary mesons that will be produced. An exception may be photoproduced vector mesons which come out dominantly forward. The momentum distributuion of a glueball is given in terms of its longitudinal momentum $p_{\|}$, using $x_F = 2p_{\|}/\sqrt{s}$ by

$$(3)\quad \frac{d\sigma}{dx_F} = \frac{\pi^2}{8M_G^3}\,\Gamma(G\to gg)\,\frac{x_+ P_{g/\gamma}(x_+)\; x_- P_{g/p}(x_-)}{x_+ + x_-}$$

where

$$(4)\quad x_\pm = \tfrac{1}{2}\left(\sqrt{x_F^2 + 4\tau} \pm x_F\right)$$

One might have expected that the peaking at small $x = x_+$ for gluons in the photon would also show up as a peak in the momentum distribution, but for s $\cong$ 3 GeV, the minimum possible value of x_+ is 0.23. (Below this, the fusing gluons cannot have enough energy to produce a 1.44 GeV glueball.) Hence the peaking is not seen, and the momentum distribution of the glueballs is not so different from mesons produced by quark fusion.

Still the glueballs will be there, should be looked for, and will distinguish themselves from ordinary mesons via the standard tests [10] of decay democracy, overpopulation, and possibly their oddball quantum numbers. [Decay democracy has to do with the gluons coupling equally to all flavors of quarks. Modulo phase space and perhaps other considerations in special cases, a glueball should decay equally into final states containing strange or containing non-strange hadrons. Quarkic mesons tend to decay into final states which retain the original quarks, so

that a phi meson (an strange-antistrange bound state) decays mainly into K-mesons. Overpopulation has to do with counting. From u,d, and s quarks and their antiquarks we can make nine flavor states, two of which have zero charge and isospin and can mimic glueballs. Finding a third such state of given quantum numbers in a given mass range would give us a glueball candidate. Oddballs are states whose quantum numbers cannot be obtained from a quark-antiquark bound state. States with J^{PC} =(odd)$^{-+}$, (even)$^{+-}$ or 0^{--} are oddballs.]

II. Testing perturbative QCD

QCD may be the correct theory of strong interactions, and recently it has become known how to do perturbative calculations with it in exclusive (i.e., some or all of the final state measured) channels [11]. It may be that a several hundred GeV momentum scale is needed before perturbative QCD calculations are accurate [12]. But maybe not: it has been claimed in the literature [13] that perturbative QCD correctly gives the deuteron form factor A(Q) for Q**2 $\gtrsim$ 1(GeV)**2.

Brodsky and Lepage have given some QCD predictions for reactions involving real photons [14], specifically for $\gamma\gamma \to$ meson+meson. These can be modified to be more relevant to a machine with a single photon beam. We will, as an example, consider a Bethe-Heitler-like process $\gamma + A \to \gamma + (\pi^+) + A'$, shown in Fig. 3, with the kinematics arranged so we are close to the pion pole. We will make an order of magnitude estimate of the cross section and show its momentum dependence. (A similar order of magnitude estimate [15] of the usual Bethe-Heitler process is correct within a factor of 3.)

We begin with the Brodsky-Lepage result for $\gamma\gamma \to \pi\text{-}\pi$,

$$(5) \qquad \frac{d\sigma}{dt}(\gamma\gamma \to \pi^+\pi^-) = \frac{d\sigma}{dt}(\gamma\gamma \to \mu^+\mu^-)\,\frac{4F_\pi^2(s)}{1-\cos^4\theta_{cm}}$$

valid for high s and large angles. F_π is the pion electromagnetic form factor, predicted to fall like $F_\pi(s) \cong B/s$ and with the best fit to data got with B = 0.4 (GeV)**2. Using this for γ+A -> γ+(pi+)+A' gives

$$(6) \qquad \frac{d\sigma}{d\Omega} = \frac{A\alpha^2\alpha_\pi}{\hat{t}^2}\,|F_\pi(\hat{t})|^2\,\frac{d^3p_\pi}{E_\pi}$$

where A is the number of nucleons in the target nucleus, $\hat{t}$ is the momentum difference-squared, between the incoming and outgoing photons, and $\text{alpha}_\pi = g_{\pi NN}^2/4\pi \cong 10$. To ensure that QCD be valid, $\hat{t}$ should be large, so we require

$$(7) \qquad \hat{t} \gtrsim \tfrac{1}{2}s \simeq m_p E_\gamma$$

where s is the γ-nucleon c.m. energy squared. Then upon integrating we get

$$(8) \qquad \frac{d^3p_\pi}{E_\pi} \to m_p E_\gamma$$

and

$$\frac{d\sigma}{d\Omega} \simeq \frac{A\alpha^2\alpha_\pi^2\ (0.4\ GeV^2)}{m_p^3 E_\gamma^3} \qquad (9)$$

For E_γ =4 GeV,

$$\frac{d\sigma}{d\Omega} \simeq A \times 1\ mb/sr. \qquad (10)$$

The size and E_γ dependence given above is predicted by QCD, and more detailed calculations are easy enough to do on a computer for given kinematics.

III. Deuteron electromagnetic form factors.

It is important to compare the consequences of QCD with those of classical nuclear physics. The latter is a phenomenological theory written in terms of nucleons bound together by a finite number of different types of mesons and which is valid within certain limits. Often, the predictions of QCD can be matched by classical nuclear physics. It is important to search for situations where this cannot be the case, and to see for what parameter or what momentum transfers one theory begins to fail and the other to succeed.

Let us focus on high-Q^2 elastic electron-deuteron scattering. The QCD result [13] that the form factor A(Q) falls like Q**-10 can be got from classical nuclear physics, as may be seen below. However, upon examining the spin dependence of this process we find that the results of the two theories are not the same. In particular, QCD gives a unique relation between the charge and quadrupole form factors at high Q,

$$\lim_{Q\to\infty} G_C = \frac{2}{3}\eta G_Q \qquad (11)$$

where $\eta = Q^2/4M_d^2$.

To get the Q dependence of the form factors at high Q it suffices to consider the deuteron as a collection of parallel moving constituents [11,13], six quarks in QCD as in Fig. 1a. One of the quarks absorbs a virtual photon of momentum q, with $Q^2 = -q^2 > 0$. To rebind the deuteron the momentum must be shared equally among the six quarks. We deal with a Q high enough to be much greater than the mean fermi momentum of the quarks. The fermi momentum distribution will determine how much deviation from equal sharing of momentumis allowed and so sets the scale of normalization but does not determine the asymtotic dependence of the amplitude on Q. The analysis that leads to eqn. (11) is easy to work out [16], particularly in the overall Breit frame.

Treating the deuteron as two collinear nucleons, Fig. 2, can give the high Q limit of the form factor from classical nuclear physics. If we put a dipole form factor at the γNN vertex and a monopole form factor at each meson-N-N vertex, then a Q**-10

falloff for the leading deuteron form factor follows. However the exchanges can now be pseudoscalar and scalar as well as vector bosons and the tendencies to conserve or flip helicity at each vertex will not be the same. The ratio G_C/G_Q will depend on the relative size of the various coupling constants and on the asymptotic meson-N-N form factors

One of the methods that has been suggested [17] for separating the G and G form factors is measuring the polarization ratio of p_x/p_{xz}. The vector polarization p_x of the outgoing deuteron need not be zero if the initial electron is polarized, and p_{xz} is a tensor polarization. We have

$$I_0 p_x = -\frac{4}{3}\left[\eta(1+\eta)\right]^{1/2} G_M \left(G_C + \tfrac{1}{3}\eta G_Q\right) \tan\tfrac{1}{2}\theta$$

(12)

$$I_0 p_{xz} = -2\eta\left[\eta + \eta^2 \sin^2\tfrac{1}{2}\theta\right]^{1/2} G_M G_Q \sec\tfrac{1}{2}\theta$$

where $I_0 = A + B \tan^2 \theta/2$. Thus,

(13)

$$\lim_{Q^2\to\infty} \frac{p_x}{p_{xz}} = \frac{2}{3} \frac{G_C + \frac{1}{3}\eta G_Q}{\eta G_Q} = \frac{2}{3}$$

where the last equality used eqn. (11).

A plot of this polarization ratio for several classical nuclear physics models of the deuteron wave function is shown in Fig. 5. The Q's on this plot are not "asymtotic", but are in the range where agreement with QCD is claimed for A(Q) [13, but see also 12]. The classical nuclear physics predictions differ in both sign and magnitude from the asymtotic QCD prediction. If we suppose that the form factors G_C and G_Q have their asymtotic ratio and take account of the kinematic factors given in eqn. (12), the predictions from QCD are reduced for $\theta<180^\circ$ [Fig. 5] but the difference from classical nuclear physics is still dramatic.

REFERENCES

1. W. Marciano and H. Pagels, Phys. Rep. 36, 137 (1978).
2. B. Mecking and R. Whitney, this report.
3. D. L. Scharre et al, Phys. Lett. 97B, 329 (1980).
4. P. Baillon et al, N. Cimento 50A, 393 (1967).
5. G. Altarelli and G. Parisi, Nucl. Phys. B126, 298 (1977).
6. R. J. DeWitt et al, Phys. Rev. D 19, 2046 (1979).
7. E. Witten, Nucl. Phys. B120, 189 (1977).
8. Yu. L. Dokshitser, JETP 46, 641 (1977).
9. H. C. Liu, Phys. Rev. D 29, 36 (1984). We also include some VMD terms in the calculation, following this reference.
10. E.g., C. E. Carlson in Field Theory in Elementary Particles (Proceedings of Coral Gables Conference 1982, A. Perlmutter, editor), p. 263.
11. G. P. Lepage and S. Brodsky, Phys. Rev. D 22, 2157 (1980).
12. N. Isgur and C. Llewellyn Smith, Phys. Rev. Lett. 52, 1080 (1984).
13. S. Brodsky, C.-R. Ji, and G. P. Lepage, Phys. Rev. Lett. 51, 83 (1983).
14. S. Brodsky and G. P. Lepage, Phys. Rev. D 24, 1808 (1981).
15. T. D. Lee, Particle Physics and Introduction to Field Theory (Harwood Academic Publishers, New York, 1981), pp. 173ff.
16. C. E. Carlson and F. Gross, "Smoking gun" signatures for QCD in nuclear physics," Wm. and Mary preprint (1983),
17. R. G. Arnold, C. E. Carlson, and F. Gross, Phys. Rev. C 23, 363 (1981).

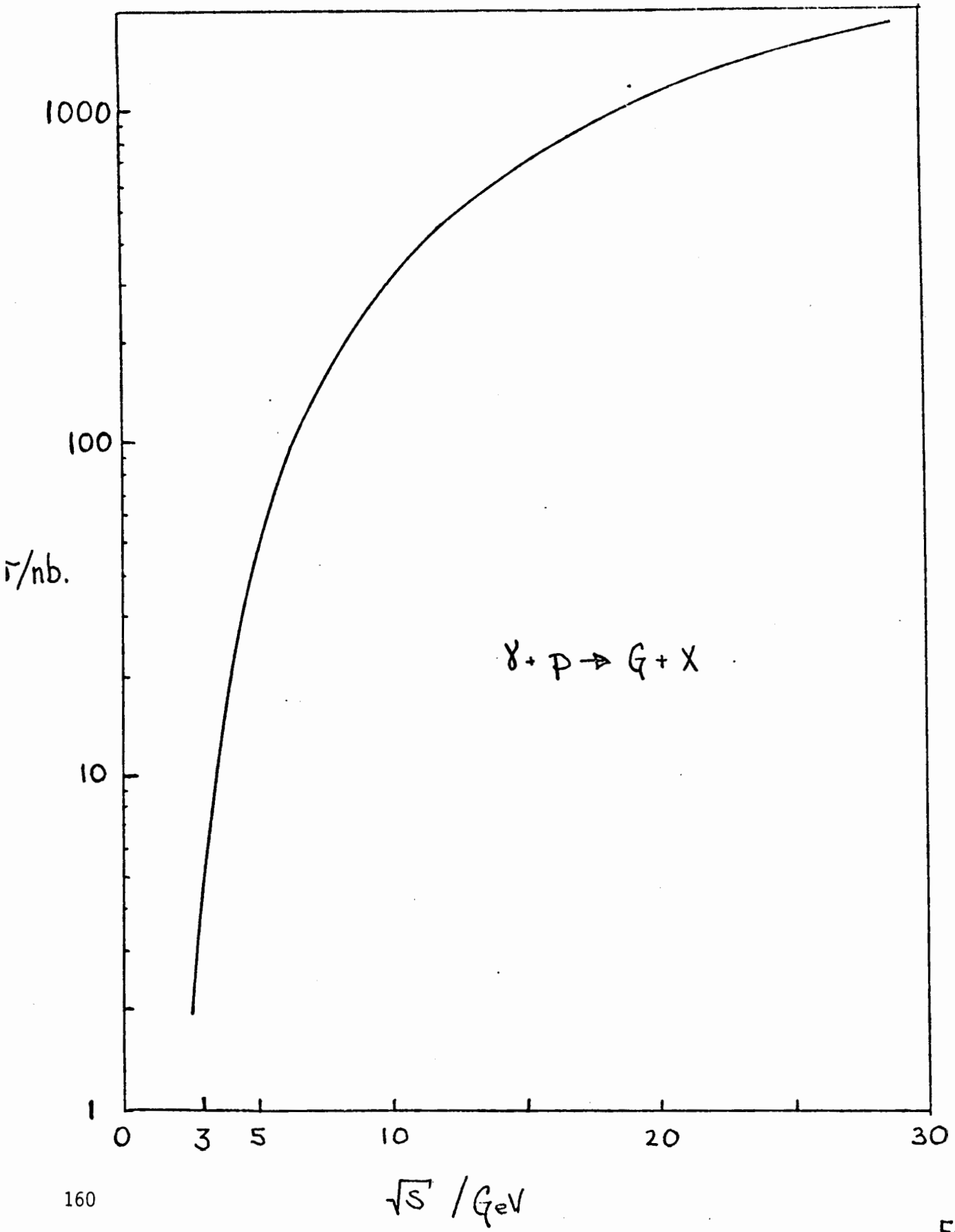

FIG.

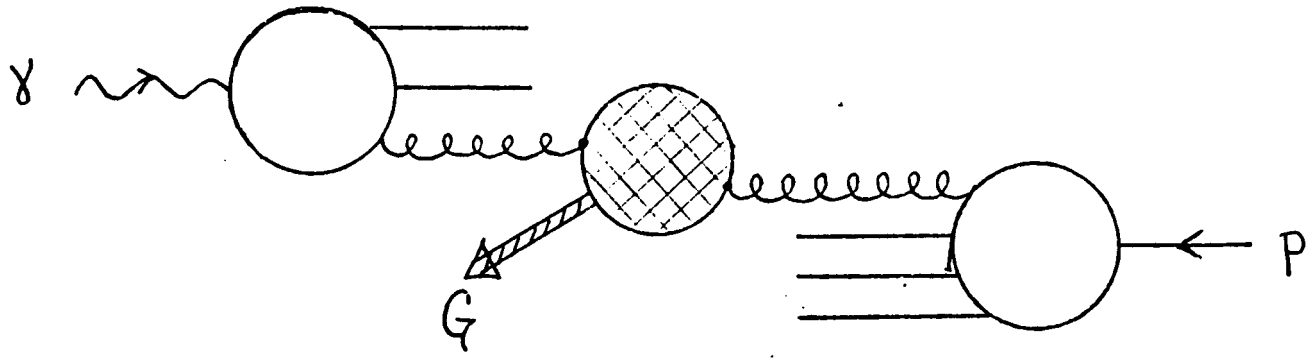

FIG. 2

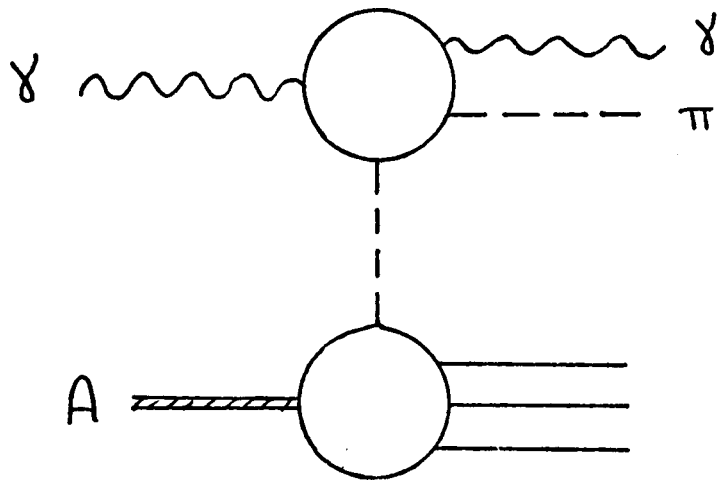

FIG. 3

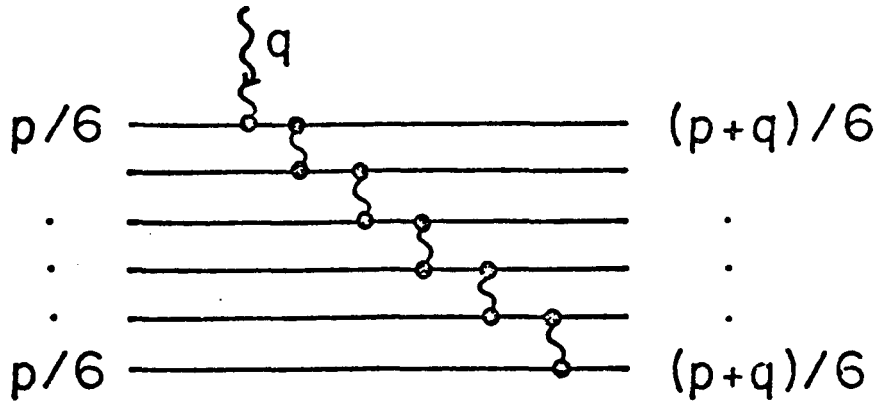

(a)

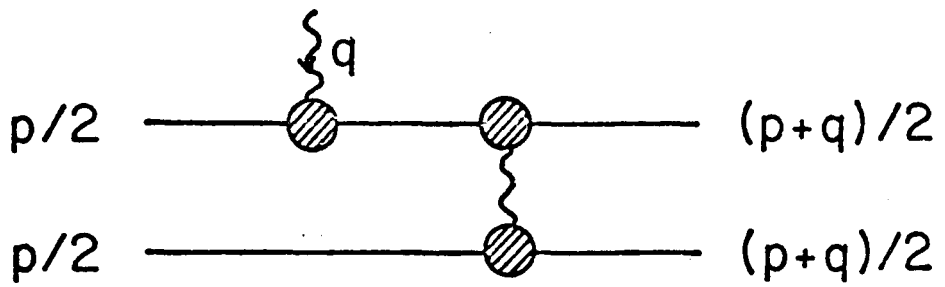

(b)

Fig. 4

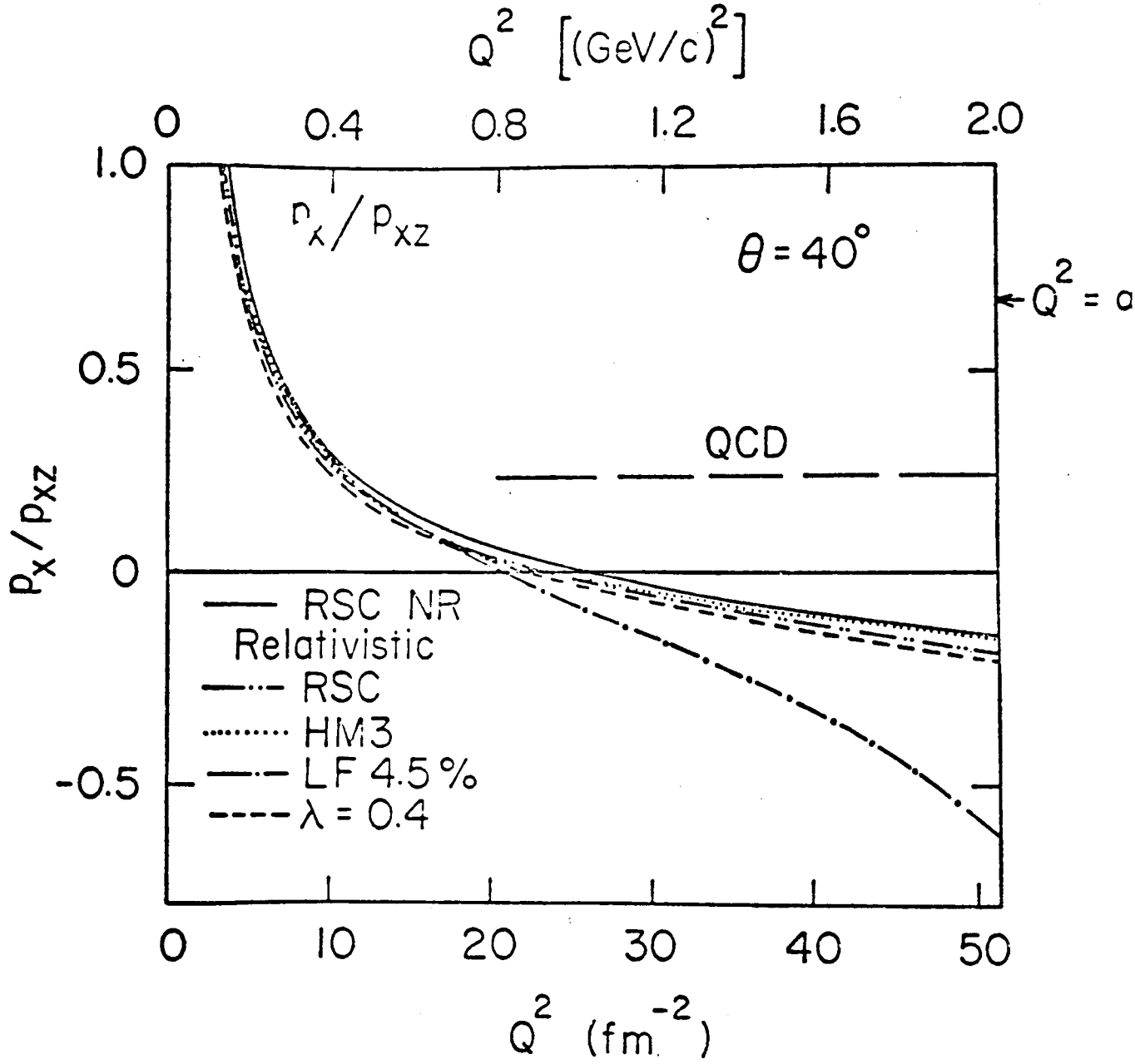
Q^2 $[(GeV/c)^2]$
0
0.4
0.8
1.2
1.6
2.0
1.0
0.5
0
-0.5
p_x/p_{xz}
$\theta = 40°$
$\leftarrow Q^2 = a$
QCD
RSC NR
Relativistic
RSC
HM3
LF 4.5%
$\lambda = 0.4$
p_x/p_{xz}
0
10
20
30
40
50
Q^2 (fm^{-2})

Fig. 5

APPENDIX C. LASER BACKSCATTER

Laser-Undulator Backscattered Photons

R. Roy Whitney

Laser photons have been backscattered from beams of high energy electrons to produce secondary beams of gamma rays in a variety of particle and nuclear physics experiments. The reason for using this technique is that gamma ray beams with state of polarization or helicity of nearly 100% can be achieved. Also, if a narrow enough angular acceptance is used, the gamma beam has a much narrower spread in energy than a typical bremstrahlung beam should have.

Figure 1 shows the angles and energies for a photon to backscatter from a highly relativistic electron. The equation below gives the kinematic relationships:

$$E = \frac{4\varepsilon\gamma^2}{1 + \frac{4\varepsilon\gamma}{mc^2} + \Theta^2 + \gamma^2}$$

where: E is the scattered photon's energy.

γmc^2 is the incident electron's energy.

ε is the incident photon's energy.

Θ is the angle between the direction of the incident electron and scattered photon. (Assumed small for this result).

φ is 180° minus the angle between the incident electron and incident photon. Note that the gamma ray energy does not depend on this angle except for angles very near 180°.

The easiest way to see the behavior of this equation is to graph a few examples. Shown in Figure 2 are the gamma ray values for incident photons of 10, 100, 1,000 and 10,000 eV as a function of scattering angle. The incident energy is 2 GeV, but from 1-4 GeV the main effect in changing the incident electron energy is not to change the relative shape of the curves but just to half or double respectively the photon energy scale.

The primary observation to be made from Figure 2 is that except at the highest incident photon energies, the scattered gamma ray energies vary significantly with scattering angle. Next, except at the highest incident photon energies, the gamma rays are at energies significantly below the incident electron energy.

There is currently a backscattered laser operation being set up at the National Synchrotron Light Source, NSLS.[1] Photons of 3.5 eV will be backscattered from 2.5 GeV electrons. To increase the energy resolution the recoiling electrons will be tagged. This will allow a large range of scattering angles to be accepted. Note from the curves shown in Figure 2, that the 3.5 eV photons will produce gamma rays with even more variation with scattering angle than the 10 eV ones. With lasers it is very difficult to impossible to achieve photons much higher in energy than the 3.5 eV level.

If only a very small range of scattering angles were accepted, the gamma rays could be made to have increased resolution. However the flux would drop significantly. The variation of the scattered gamma ray energy with the incident photon energy means that broad band incident photons with energies below 10,000 eV are not useful. The ideal incident beam would be narrow band, above 10,000 eV and have a high brightness.

This ideal incident photon beam can be produced by using an undulator in an appropriate electron ring operating in the region of 5-6 GeV.

For CEBAF, producing an undulator beam in its early years is highly unlikely. The facility needs to begin operation of its linac, pulse stretcher ring and experimental halls first. Early operation of a backscattered laser is a more likely possibility as it is much less expensive than the ring needed to produce a useful undulator beam. However, in the design and layout of the initial components of the facility, it is desirable that provision be made for the eventual installation of a ring to produce the requisite undulator beams and the backscattering interaction regions. The physics, the availability of funds and the interests of the facility will of course determine as to whether laser or undulator backscattering will eventually be set up at CEBAF.

---

1. NSLS Proposal: "The Fabrication of a Very High Energy Polarized Gamma Ray Beam Facility and Program of Medium Energy Physics Research at the National Synchrotron Light Source", September 1982.

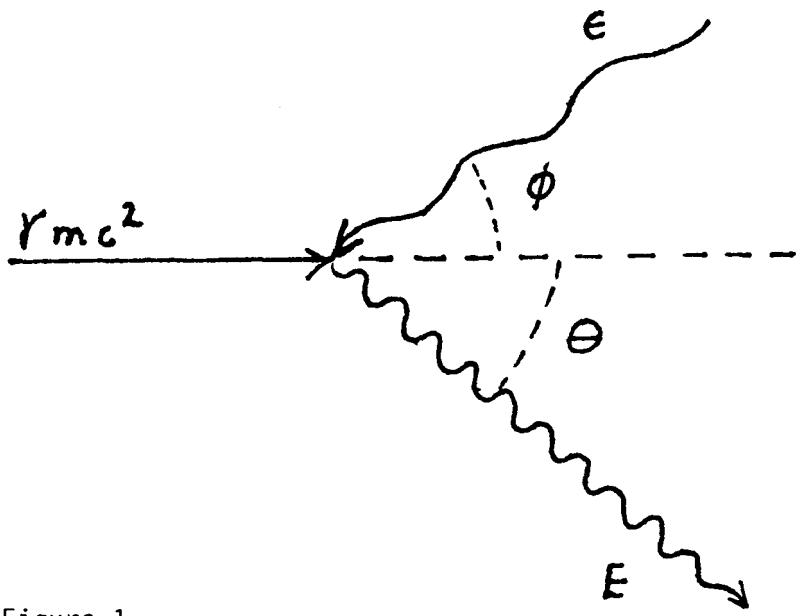

Figure 1

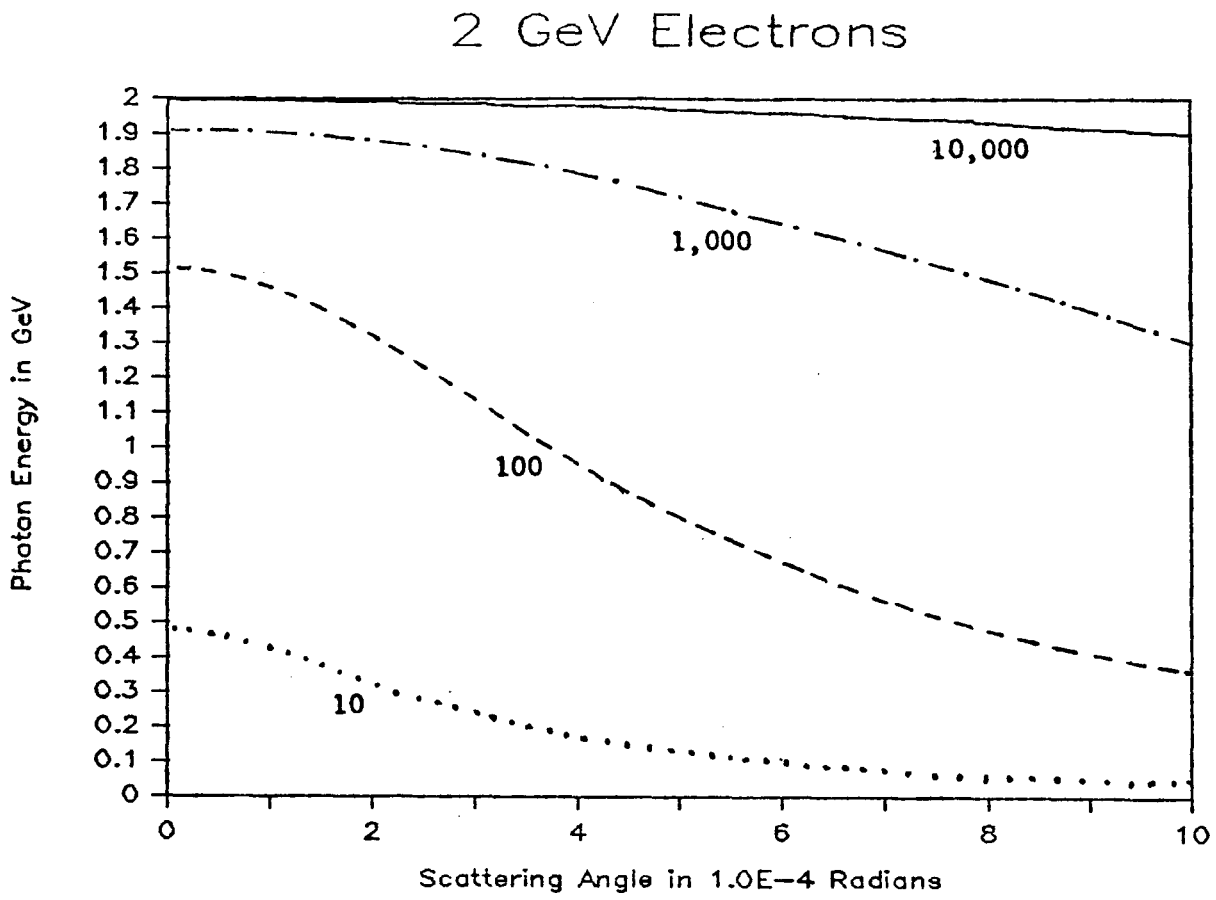

Figure 2

QUESTIONS FOR THE THEORY WORKING GROUP

Franz Gross

College of William and Mary, Williamsburg, VA 23185

Before I pose some specific questions which the theory working group might wish to discuss, it may be useful to first review broadly some of the theoretical areas of relevance to CEBAF. The proposal for a Theory Group for CEBAF [1] submitted to DOE in December, 1983, divided this subject into five areas. After a brief introductory section, the next four sections of this talk will review the first four of these five areas: Nuclear Chromodynamics, Models of Hadrons, Relativistic Few Body Problem, and Nuclear Structure and the Nuclear Medium. The fifth in the Theory Proposal, Electromagnetic (and Weak) Interactions, will be discussed by T. W. Donnelly and D. Walecka, and will not be reviewed here. Finally, the sixth and last section will pose the questions.

1. Introduction and Kinematics

For those unfamiliar with electron scattering, the basic kinematics are shown in Fig. 1.

For single arm scattering there are three variables: the energies of the incoming and outgoing electrons (E and E'), and the laboratory scattering angle θ. Only two combinations of these three variables are needed to describe the unknown strong vertex; the dependence on the third variable, θ, is given by the electromagnetic interaction with the point like electron, which is known exactly. One of these two hadronic variables is Q^2, the square of the 4 momentum

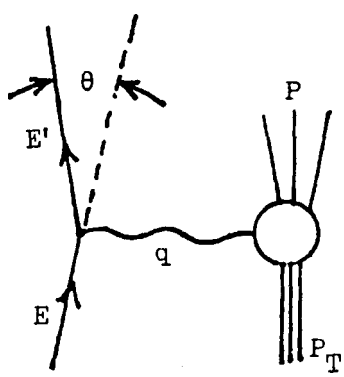

Fig. 1. Kinematics of single arm electron scattering

transferred by the electron,

$$Q^2 = -q^2 = 4EE'\sin^2\theta/2 \qquad (1)$$

and the other is either ν, the energy lost by the electron in the laboratory system, or W^2, the square of the invariant mass of the final hadronic state

$$\nu = \frac{q.P_T}{M_T} = E-E'$$

$$W^2 = p^2 = M_T^2 - Q^2 + 2M_T\nu \qquad (2)$$

where M_T is the target mass.

If the scattering is to a definite final state with a fixed mass $W^2=M^{*2}$, then the hadronic part of the cross section depends only on one variable, Q^2. Such measurements give elastic or transition form factors, which give precise information about charge and magnetic moment distributions of nuclear states. If the scattering is inclusive, then the single arm cross section can be written

$$\frac{d\sigma}{d\Omega} = \sigma_M \left\{ W_2\ (Q^2,\nu) + 2W(Q^2,\nu)\ \tan^2\theta/2 \right\} \qquad (3)$$

where the magnitude of the scattering is roughly determined by the Mott cross section

$$\sigma_M = \left(\frac{\alpha\ \cos\frac{\theta}{2}}{2E\ \sin^2\frac{\theta}{2}} \right)^2 , \qquad (4)$$

W_1 and W_2 are the structure functions which contain all the hadronic information, and α is the fine structure constant. Inclusive measurements have been made from both simple targets like the proton, and complex nuclei. As an example, the proton structure function νW_2 measured at SLAC in the early 1970's is shown in Fig. 2, taken from the

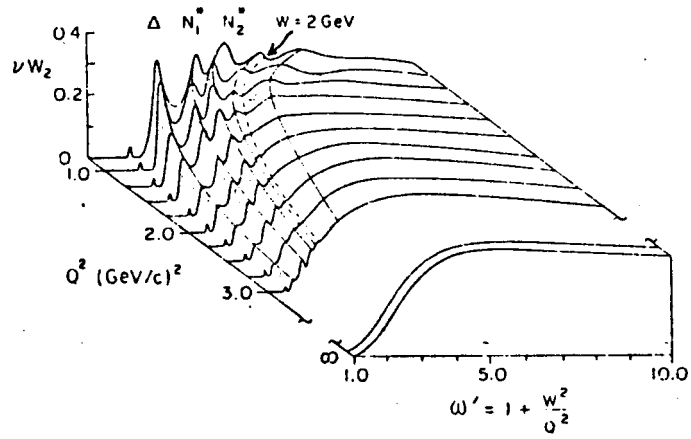

Fig. 2. The proton inelastic structure function νW_2 shown as a function of Q^2 and the scaling variable ω'.

Barnes' Committee report.[2] Here the second variable is a dimensionless scaling variable ω' obtained from the ratio of W^2 to Q^2. The figure clearly shows the electromagnetic excitation of three nucleon resonances: the Δ (1232), N_1^* ($\simeq$1500) and N_2^* ($\simeq$1650). The dashed line just above the N_2^* peak is the line with fixed W = 2 GeV. Above this boundary individual resonances begin to disappear and the structure function begins to assume a featureless shape which becomes a universal function of the scaling variable ω', independent of Q^2. It is now known that this scaling behavior is due to the incoherent scattering of the electrons from the point-like quark constituents, and it follows that the disappearance of the resonance peaks and the emergence of the smooth scaling behavior is a signal of the transition from a region where the physics is dominated by collective quark degrees of freedom (or excited baryons and meson clusters) to one where individual quark degrees of freedom emerge as the dominant effect. This scaling region is bounded roughly by

$$W \gtrsim 2 \text{ GeV}$$
$$Q^2 \gtrsim 1 (\text{GeV})^2 \qquad (5)$$

The primary mission of the CEBAF is to study this transition region in greater detail than has ever been possible. The continuous beam supplied by this Facility will make it possible to study the individual inelastic channels which make up the total inclusive cross section. Such a study will give insight into the role of quarks in nuclear matter.

A major program of theoretical physics is needed to support this effort. The kinds of theoretical work needed range from basic studies of multiquark systems, such as those described by N. Isgur and C. Carlson at this workshop, to detailed analyses of the kinematics of coincidence measurements, described by T. W. Donnelly. The following sections review some of the theoretical areas of relevance to CEBAF.

2. Nuclear Chromodynamics

The direct application of Quantum Chromodynamics (QCD) to nuclear

physics has been called Nuclear Chromodynamics.[3] Three lines of investigation can be singled out. These are (i) use of perturbative techniques, (ii) the development of models of hadronization; and (iii) lattice gauge calculations.

Perturbative Techniques - It is well known that the strong quark-gluon coupling constant becomes weak at high Q^2; the way in which this coupling constant varies with the four momentum Q transferred by the gluon is

$$\alpha_s = \frac{4\pi}{\left(11 - \frac{2}{3}n_f\right)\ell n\frac{Q^2}{\Lambda^2}} \simeq 0.70 \left[\ell n \frac{Q}{\Lambda}\right]^{-1} \quad (6)$$

where n_f is the number of flavors (3 in the above example) and Λ is a scale parameter believed now to be about 150 MeV. Eq. (6) shows that α_s is less than 0.5 for momentum transfers above one GeV, which suggests that perturbative QCD calculations might work in this region. In fact, we now know that inclusive scattering in the deep inelastic region defined by Eq. (5) and shown in Fig. 2 is due to incoherent scattering from individual quarks, and that this process can be described perturbatively. This means that the inclusive cross section can be calculated using the Feynman diagrams shown in Fig 3, and that the radiative gluonic contribution Fig. 3b is a small correction to the principal impulse contribution (3a). Note this calculation has a non-perturbative

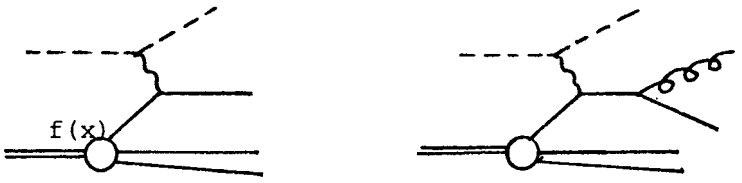

Fig. 3. First two perturbative contributions to inclusive scattering from the proton.

aspect to it; the result is given in terms of the quark distribution function f(x), which is related to the probability that the proton will have quarks with momentum fraction x, and which cannot itself be calculated perturbatively. Nevertheless the perturbative features of the calculation are sufficient to describe the scaling and magnitude of the cross section, and are universally recognized to be one of the

outstanding successes of perturbative QCD.

One of the interesting theoretical questions is whether the exclusive processes to be measured at CEBAF using coincidence experiments can also be studied using perturbative QCD. Brodsky and his collaborators[4] have shown that perturbative techniques give the observed power law behavior for many cross sections and form factors at high energy and momentum transfer, but the normalization of these asymptotic results cannot be calculated using perturbative techniques alone. Isgur and Llewellyn-Smith[5] have recently argued that no reasonable choice for the quark wave function of the proton can give a normalization of the Q^{-4} behavior of the proton magnetic form factor G_{Mp}, which comes anywhere near the observed result. (This is discussed in some length in Isgur's contribution to this workshop, and was also discussed by the Theory working group.) From this negative result they draw the conclusion that perturbative calculations of all exclusive processes are bound to fail. However, it is possible that their results may be too pessimistic,[6] and this issue is bound to be of central interest to CEBAF for some time yet. While elastic form factors are of interest, the real issue is whether or not exclusive processes in the deep inelastic region can be understood perturbatively. Examples of perturbative calculations of single and double π production are shown in Fig. 4. Note that these diagrams cannot be calculated

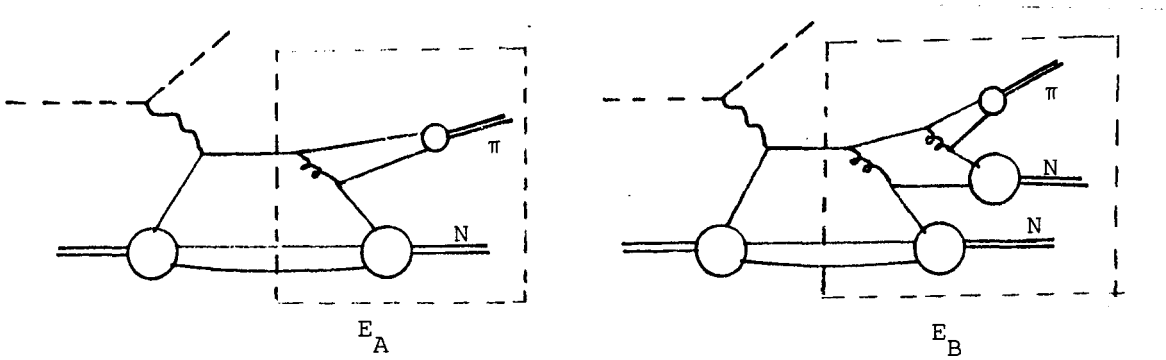

Fig. 4. Illustrated perturbative QCD diagrams for single and double π electroproduction.

without knowing the quark wave functions of the nucleon and pion, and hence the real issue is whether or not reasonable wave functions can be found which give good results. The success of perturbative QCD for

the inclusive cross section insures us that some sum rule exists:

$$\int \left\{ |E_A|^2 + |E_B|^2 + \ldots \right\} = 1 \qquad (7)$$

which may be helpful resolving these issues.

Models of Hadronization - This brings us directly to the more general question of how high energy quarks turn into nucleons and mesons. The diagrams shown in Fig. 4 are examples of the hadronization process in which it has been assumed that the non-perturbative aspects of the problem can be incorporated into hadronic wave functions. Particle theorists are using a variety of techniques to study this problem;[7] progress in this area may eventually suggest new experiments, or new ways to analyze old experiments done at CEBAF.

Lattice Gauge Calculations - Progress on fundamental non-pertubative QCD calculations could impact significantly on theoretical work of relevance at CEBAF, where physics is being studied in the transition region where the strong force is strong and non-perturbative aspects of QCD are important. Lattice gauge calculations, where QCD is solved on a space-time lattice, are one of the most promising techniques.

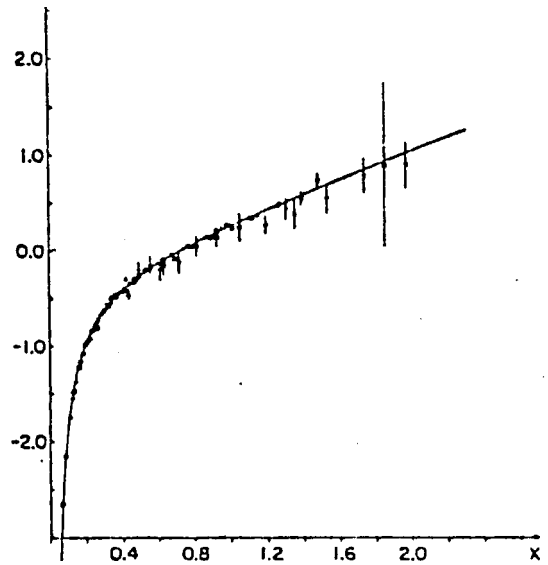

Fig. 5. Linear + coulomb fit to lattice calculation.

Fig. 5 shows a recent calculation[8] of the confining potential between two massive quarks. The numerical results are well fit by the linear plus coulomb form, providing an excellent justification for use of phenomenological linear confining potentials, and showing how useful such methods can be in providing quidance on how to model QCD.

2. Models of Hadrons

Since non-perturbative QCD is so hard to treat exactly, QCD inspired quark models of composite mesons and baryons are likely to continue to play a fundamental role in nuclear theory. One step in this program is to convert understanding of confinement as it is obtained from non-perturbative QCD into models which explain the spectrum, properties, and structure of all the observed baryons. Another step is to use these models to describe the nuclear force and the structure of nuclei.

Models of Single Baryons - Three different approaches to modeling confinement have been used. In one, confinement is achieved through a linear or quadradic potential which acts between all quark pairs.[9] In another, the chiral bag model,[10] the vacuum is divided into two regions separated by a sharp boundary. In the inner region ("inside" the bag) it is assumed that the physics is best described by quark-gluon degrees of freedom; quarks have nearly zero mass, perturbative QCD is a valid approximation, and collective degrees of freedom, such as the pion field, are excluded in some versions of this model ($M_\pi=\infty$). In the outer region it is assumed that the physics is best described by collective degrees of freedom; the pion has a small mass, and free quarks and gluons are forbidden ($M_q=\infty$).

Finally, non-topological soliton models[11] introduce a phenomenological field, often a scaler field (σ) which is regarded as a representation of possible low lying scaler glueball states, and solve the non linear equations of motion for the interaction of the field, treated classically, with the elementary quark fields. The quarks are confined in localized regions in space, where it is energetically favorable for them to burrow a hole in the vacuum state described by a non-zero sigma expectation value $\langle\sigma\rangle=\sigma_o$. Alternatively, it is possible to describe baryons as topological "knots", or skyrmions in which a non-linear concentration of meson fields has the properties of a baryon. These topological soliton models[12] are generalizations of an idea originally due to Skyrme;[13] the approach is also justified by the limit of QCD in which the number of colors (normally 3) is allowed to become very large.

Nuclear Potential Models from Quarks - Each of these models suggests a way to calculate the interaction between two nucleons. So far, the quark potential models have had the greatest application to study of the nuclear force.[14-15] Here it is assumed that the 6 quark wave function can be expressed in the following form

$$\psi(\xi_A, \xi_B, R_{AB}) = \mathcal{A}\{\phi_A(\xi_A)\phi_B(\xi_B)\chi(R_{AB})\} \tag{8}$$

where ξ_A and ξ_B are internal coordinates associated with two three quark clusters A and B, ϕ_A and ϕ_B are internal wave functions of the three quark clusters, R_{AB} is the distance between the two clusters and χ is the intercluster wave function. The operator $\mathcal{A}$ antisymmetrizes the quark coordinates, so that the RHS of (8) is actually a sum of terms with all possible choices of 6 quarks partitioned into antisymmetric 3 quark clusters. In applications, A and B range over a set of states with different internal symmetries, ϕ_A and ϕ_B are assumed to be known, and χ is found using the resonanting group method (RGM), or a variational principle. A complete sum over A and B will include clusters in which two SU(3) color octets are coupled to an overall color singlet. Such contributions will be called "color polarized" states, and one of the very interesting questions is how the presence of such virtual states will influence observable phenomena.

A common feature of recent calculations of this kind is that they are able to obtain the short range repulsive force. The calculation by Maltman and Isgur[15] is also able to obtain considerable intermediate range attraction from the excitation of virtual color polarized P state clusters. However, this force may be spurious since it arises from the same mechanism which also gives rise to a long range van-der-Waals force which is not seen in nature. The presence of such forces is a deficiency of all potential models.

In order to remove van-der-Waals forces from potential models, Hietarinta and Greenberg[16] introduced the idea of link operators (or strings) which connect the quarks together into geometrical configurations. States with different linkages are orthogonal. Examples of such linkages for $2(q\bar{q})$, 6q systems are shown in Fig. 6. By

channeling the forces through strings, or flux tubes, and requiring

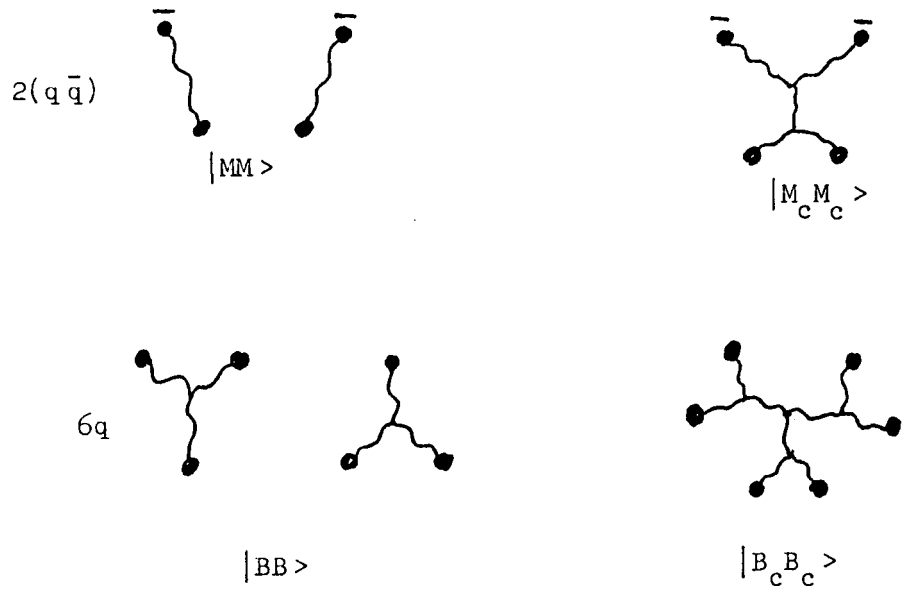

Fig. 6. Strings or links for various quark states.

that the potential increase linearly as the flux tube is stretched, all van-der-Waals forces are eliminated, because the long-range forces between clusters are either zero (as with the meson meson $|MM>$ and baryon-baryon $|BB>$ cases in Fig. 6) or grow linearly with the inter-cluster separation (as with the color polarized configurations $|M_c M_c>$ and $|B_c B_c>$). Of course the color polarized configurations are energetically favorable at short distances only; as they are pulled apart the stretching link grows in energy to the point where it is more favorable to create a $q\bar{q}$ pair from the vacuum, breaking the string and separating the state into two color singlet clusters. Applications of these ideas are being developed.[17]

Still another way of avoiding van-der-Waals forces, and a way which is considerably simpler that the link operator formalism, is the Hybrid model of Henley, Kisslinger and Miller,[18] or the 6 quark Compound State model of Kim and Orlowski.[19] Work by Lomon,[20] Simonov,[21] and Weber[22] also seems to fit into this general class of

approaches. Here the 6 quark wave function is treated as a nucleon-nucleon state when the intercluster separation r is greater than R_1, and as a pure 6 quark compound state when r is less than R_2 (R_1 does not necessarily equal R_2). In the language of Ref. 19, the wave function is

$$\psi_E(r) = \phi_n\phi_p\chi_E(r \geq R_1) + A(E)\phi_s(r \leq R_2) \qquad (9)$$

where E is the energy. The Loman-Feshbach boundary condition model, introduced long before quarks or confinement were known, seems to follow this general approach, and recent analysis by Lomon[20] is the most extensive and detailed applications of these ideas to the NN system.

4. Relativistic Few Body Problem

Meson theory, sometimes referred to as Quantum Hadrodynamics (QHD), is an effective field theory which treats certain quark clusters (such as N, Δ, π, ρ, ω and σ) as "elementary" particles, and constructs a relativistic theory of nuclear matter and of the few body system in terms of these degrees of freedom.) Such theories, while no longer fundamental, provide a calculable alternative with which to compare models which treat quark degrees of freedom explicitly. They complement the methods described in the previous sections by focusing on the long range part of the interaction; they treat the collective coordinates (the mesons and baryons) quite precisely, while handling the internal quark structure either not at all, or through the introduction of effective form factors and coupling constants which might be calculable from the underlying QCD. Should it turn out that the clustering of quarks into nucleons is quite pronounced, and that color polarized states play a minor role in nuclear structure, QHD could end up providing a very quantitative description of nuclei.

At the present time, quantitative applications of QHD to the few body system are quite advanced. A variety of relativistic two body equations exist, and good numerical fits to low energy deuteron properties and to NN phase shifts below 400 MeV have been found.[23] There seems to be no serious obstacles to extending these techniques to the three-body system, and work on this problem is underway.

Relativistic calculations of the deuteron form factor, using relativistic deuteron wave functions and including certain relativistic corrections to all orders in $(v/c)^2$ have been carried out.[24] These Calculations do not agree with the data at very high Q^2, suggesting that uncalculated isospin zero exchange currents are unexpectedly important, that a six quark core is being seen, or that the high Q^2 neutron electric form factor, unknown in this region, is larger than popularly assumed. Relativistic effects are believed to be important in ^3He, in electrodisintegration of the deuteron to the $^1S_0$ final state, and in photodisintegration of the deuteron at forward angles. A fully consistent relativistic treatment of electromagnetic interactions of few body systems including meson exchange currents, seem to be within our grasp and may give much insight in the next few years.

5. Nuclear Structure and the Nuclear Medium

Relativistic meson theory has been applied to both infinite nuclear matter and finite nuclei with considerable success. The original model of Walecka,[25] has been extended by Horowitz and Serot[26] to finite nuclei. The simplest version of these models includes only σ and ω fields, the σ providing attraction and the ω the repulsion which insures that nuclear matter will saturate. The effective mass of the nucleon is modified in the nuclear medium, and in finite nuclei it depends on the nuclear density.

Calculations of the charge density of large nuclei in the relativistic Hartree approximation have been quite successful, as illustrated in Fig. 7.

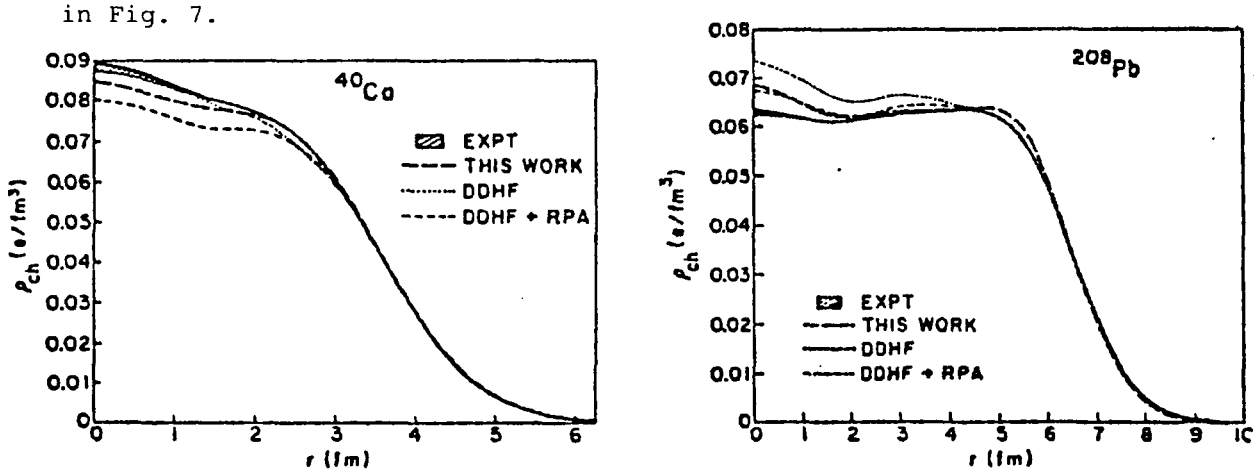

Fig. 7. Charge distributions for ^{40}Ca and ^{208}Pb. Relativistic Hartree results are indicated by the dashed line (Ref. 26). The solid curve and shaded region represent the fit to experimental (e,e') data.

With the recent success of the Dirac phenomenology in proton nucleus scattering,[27] there is the attractive possibility that the relativistic theory of finite nuclei may help in the calculations of final state interactions for the processes (e,e,'N) and (e,e'2N) which are expected to be an important part of the program at CEBAF.

6. Questions

With this background, I pose 4 specific questions for discussion by the Theory working group during the next week:

(i) In what region of the Q^2, ν plane can perturbative QCD be used to analyze exclusive electron scattering experiments?

(ii) How can the extra degrees of freedom due to the presence of quarks in nuclear matter be described and detected? Specifically, what are the experimental signatures of the color polarized states?

(iii) What new physics can be learned from coincidence experiments? Specifically, what extra information is contained in the new structure functions described by T. W. Donnelly (see his talk to this workshop), and how can the wave functions of nuclear ground states be separated from final state interactions and meson exchange currents?

(iv) What tests of QHD can be carried out at CEBAF? Specifically, how can the 3 nucleon system be studied, and how can relativistic meson theories of few body systems and many nucleon systems be tested?

These and other questions were discussed in over 6 hours of meetings during the week; a report of these discussions is included in this proceedings.

References

1. SURA Proposal for a Theory Group for the CEBAF, December 1983.
2. The Role of Electromagnetic Interactions in Nuclear Science, a NSAC report (P. D. Barnes, Chairman-1982).
3. S. J. Brodsky, Invited talk at the Conference on "New Horizons in Electromagnetic Physics", Charlottesville, VA 21-24 April 1982, P. 170.
4. G. P. LePage and S. J. Brodsky, Phys. Rev. D 22 (1980) 2157; S. J. Brodsky, C.-R. Ji, and G. P. Lepage, Phys. Rev. Lett. 51 (1983) 83.
5. N. Isgur and C. Llewellyn-Smith, Phys. Rev. Lett. 52 (1984) 1080.
6. C. Carlson, Invited talk to the BUTG workshop, July 23-24, MIT, to be published in the proceedings.
7. See for example, R. D. Field and S. Wolfram, Nucl. Phys. B213 (1983) 65; T. D. Gottschalk, Nucl. Phys. B214 (1983) 201.
8. J. D. Stack, Phys. Rev. D 27 (1983) 412.
9. N. Isgur and G. Karl, Phys. Lett. 72B (1977) 109; Phys. Rev. D 18 (1978) 4187; D 19 (1979) 2653; R. Koniuk and N. Isgur, Phys. Rev. D 21 (1980) 1868; Phys. Rev. Lett. 44 (1980) 845; C. P. Forsyth, Ph.D dissertation, Carnegie-Mellon University (1981) unpublished.
10. A. W. Thomas, CERN preprint TH-3368, submitted to Advances in Nuclear Physics; H. R. Fiebig and B. Schwesinger, Nucl. Phys. A393 (1983) 349; G. E. Brown and M. Rho, Phys. Lett. 82B (1979) 177; V. Vento, M. Rho, E. M. Nyman, J. H. Jun, and G. E. Brown, Nucl. Phys. A345 (1980) 413
11. R. Goldflam and L. Wilets, Phys. Rev. D 25 (1982) 1951; H. R. Fiebig and E. Hadjimichael, published in Phys. Rev., L. S. Celenza and C. M. Shakin, Brooklyn College preprints.
12. M. C. Birse and M. K. Banerjee, University of Maryland preprints; M. Rho, A. S. Goldhaber and G. E. Brown, Phys. Rev. Lett 51 (1983) 747.
13. T. H.R. Skyrme, Proc. Roy. Soc., London, 260 (1961) 127; Nucl. Phys. 31 (1962) 556.
14. M. Harvey, "Multi-Quark States and Potential Models," lectures given at the CAP summer school on "Progress in Nuclear Dynamics," Pearson College, Vancouver Island, 23 Aug.-3 Sept. 1982; D. Robson, Erice Summer School (1981), Progress in Particle and Nuclear Physics, Pergamon Press, ed. by D. H. Wilkinson; A. Fassler, et al. Nucl. Phys. A402 (1983) 555.
15. K. Maltman and N. Isgur, Phys. Rev. D 29 (1984) 952.
16. O. W. Greenberg and J. Hietarinta, Phys. Rev. D 22 (1980) 993.

17. D. Robson, Proceedings of the Indiana Workshop on Hadron Substructure in Nuclear Physics (1983), AIP #110, ed. W-Y, P. Hwang and M. H. Macfarlane, P 100; J. T. Londergan, ibid, P. 285; K. Yazaki, Nucl. Phys. A416 (1984) 87c.

18. E. M. Henley, L. S. Kisslinger and G. A. Miller, Phys. Rev. C 28 (1983) 1277.

19. Y. E. Kim and M. Orlowski, Proceedings of the Indiana Workshop on Hadron Substructure in Nuclear Physics (1983), AIP #110, ed. by W-Y. P. Hwang and M. H. Macfarlane, p. 271.

20. E. L. Lomon, Phys. Rev. D 26 (1982) 576.

21. Yu. A. Simonov, Phys. Lett. 107B (1981) 1; A. N. Safronov, ibid 124B (1983).

22 M. Bozoian and H. J. Weber, Phys. Rev. C 28 (1983) 811; H. J. Weber, ibid 26 (1982) 2333.

23. J. Fleischer and J. A. Tjon, Phys. Rev. D 21 (1980) 87; M. J. Zuilhof and J. A. Tjon, Phys. Rev. C 24 (1981) 736; F. Gross and K. Holinde, in preparation.

24. R. Arnold, C. Carlson, and F. Gross, Phys. Rev. C 21 (1980) 1426; M. J. Zuilhof and J. A. Tjon, Phys. Rev. C 22 (1980) 2369.

25. J. D. Walecka, Ann. Phys. (N.Y.) 83 (1974) 491.

26. C. J. Horowitz and B.D. Serot, Nucl. Phys. A368 (1981) 503.

27. See for example, B. C. Clark, S. Hama, and R. L. Mercer, in "The Interaction between Medium Energy Nucleons in Nuclei", proceedings of the IUCF workshop (1982), AIP conference proceedings #97 (edited by H. O. Meyer), p. 260.

Overview of the Facility

J. S. McCarthy
University of Virginia

Introduction

During the past year since the recommendation of the NSAC Panel on Electron Accelerator Facilities[1] was adopted, considerable progress has been made towards the establishment of the Continuous Electron Beam Accelerator Facility (CEBAF). Design improvements have been made, staff build up has begun, and research and development funds have been received from the DOE. Most significantly, the project has been recommended for inclusion in the FY 86 Congressional Budget.

General Facility Description

The concept of a linac-pulse stretcher accelerator is not new[2] and does not rely on the development of fundamentally new techniques. Rather, it represents a successful combination of well established linac and synchrotron technologies. A linac is used to efficiently accelerate high current pulses of electrons which are then injected into a pulse stretcher ring (PSR). These electrons are subsequently extracted from the PSR using the technique of slow extraction common to synchrotrons (Fig. 1). The present design was based originally on a suggestion by G. A. Loew.[3] The detailed parameters of the system are the result of an analysis of a broad variety of options.[4]

Figure 2 shows a layout of the proposed facility. The linac will produce a beam of 1.2 μs pulses at a variable repetition rate of up to 1 kHz. The beam energy will be variable between 0.5 and 4.8 GeV (maximum

unloaded beam energy) on a pulse to pulse basis. Pulsed elements in the beam switch yard (BSY) will permit successive pulses to be directed either to the PSR or to one of the end stations (A or C). Pulses directed to the PSR will be injected vertically during a single turn and then extracted during the period before the next pulse is injected. The extracted beam may be split if desired and all or part of it directed to each end station. Primary support facilities will be housed in three buildings. Two buildings already in existence will be renovated to provide office and shop space. The operations building, containing control and power distribution equipment, will be centrally located between the linac and PSR.

Linear Accelerator

The layout of the linear accelerator is shown in Figure 3 and the principal design parameters are listed in Table II. Electrons will be produced (polarized if necessary), bunched, and preaccelerated to 35 MeV in the injector region. They then will pass through a short, 5 section sector and the 3 major sectors (35 sections). For final energies below 2 GeV the electrons will be directed into the BSY. For energies above 2 GeV the beam will be recirculated through the 3 major sectors. Thus, 4 GeV electrons will be produced by acceleration through effectively a 75 section machine.

The accelerator will be composed of traveling wave, 2856 MHz disc loaded accelerating waveguides structurally similar to those in use at SLAC. Each 3 meter section will be powered by a 40 MW klystron/modulator transmitter. The transmitters in the injector region and in Sector 1 will require an rf pulse length of 2.0 μs while those in Sectors 2-4 will require an rf pulse length of 3.2 μs. Existing SLAC klystrons

plus development work in program at SLAC and KEK [6] form the basis for development of the required klystron. Both conventional (thyratron switched) and solid state modulator designs are under consideration.

The linac beam transport will consist of alternating quadrupole singlets with a center to center spacing of approximately 6.6 m. A computer simulation[7] of cumulative beam breakup phenomena (based on the use of the described focusing system and of two types of sections with their HEM_{11} mode frequencies shifted by 2 MHz relative to each other) was performed. Beam breakup thresholds of 720 mA and 420 mA for the unrecirculated and recirculated beams were calculated.

The recirculator chicane will consist of two 180° achromatic, isochronous arcs separated by a straight, achromatic phase matching region. Its length was selected such that the head of a pulse being recirculated will reenter Sector 2 immediately following the tail of the pulse. This "head-to-tail" recirculation will minimize the effects of transient beam loading and the potential for beam breakup.

An energy compression system[8] (ECS) will be located immediately following the linac. It will be used to reduce the energy spread of beams with energies less than 2 GeV if that attainable by selective timing of the linac klystrons is not adequate. The beam will enter and exit the ECS through the action of pulsed dipoles. Therefore, the use of the ECS for a particular energy will not preclude the availability of beams of other energies on a pulse to pulse basis.

Pulse Stretcher Ring

The pulse stretcher will consist of two 180° bend regions joined by straight, achromatic insertions. Each bend region will be composed of a 2I achromat [5] with a dispersion suppressing region at each end to match the optics of the bend region to those of the achromatic insertions. Both injection and extraction will take place in the same insertion. The PSR layout is shown in Figure 4 and the principal parameters are listed in Table III.

The beam from the linac will be injected vertically onto the PSR closed orbit during a single turn. The basic machine elements all will lie in a single plane; the vertical injection will be accomplished using an achromatic chicane to bring the beam up out of the common plane and then down into the PSR at an angle of 4° to the horizontal.

Beam will be extracted from the PSR using achromatic, half-integral extraction in the horizontal plane. Extraction will be initiated by a 1.6 m electrostatic septum located 1.5 cm from the closed orbit where the pitch of the extracted electron trajectories is about 6 mm. A magnetic septum will be used to complete the 4° horizontal extraction. The topology of the extraction phase space will be controlled by ramped quadrupole-octupole pairs in each insertion. A feedback system between the external beam monitoring devices and the ramped multipoles will be used to ensure the quality and stability of the extracted beam.

PSR rf power will be provided by two systems; one continuous and the other on only during the first several μs after injection. During and immediately after injection both systems will combine to produce an

overvoltage of about 6. Due to the momentum compaction of the lattice the stored beam distribution will rotate in longitudinal phase space; the initially small phase extent of the beam will increase and the energy spread correspondingly decrease. At this point the variable rf system will be turned off reducing the overvoltage to approximately 1.2 and confining the stored beam to a stable region in the longitudinal phase space having a much smaller energy spread. Simulations of this procedure predict a factor of four decrease in the PSR beam energy spread. A detailed account of this system is provided in ref. 9.

The primary potentially current limiting instabilities in the PSR were found to come from possible narrow band resonances in the rf cavities. However, the rf frequency of 714 MHz is sufficiently high that only a few impedance peaks will exist. It is felt that these can adequately be selectively damped. Nonetheless, as a precautionary measure present plans include the installation of a higher harmonic cavity to provide an additional damping mechanism.

Beam Switch Yard (BSY)

The BSY will provide transport of beams from the linac to the PSR or to the end stations and from the PSR to the end stations. Pulsed elements will be provided in the BSY to permit the variation of beam destination and energy on a pulse to pulse basis.

The beam extracted from the PSR can be split into three parts. High duty factor beams of differing intensity (high intensity to a primary beam experiment, low intensity to the tagged γ facility) can be

delivered simultaneously. It is anticipated that eventually many experiments will require a longitudinally polarized, high duty factor electron beam. Only vertical polarization will be maintainable in the PSR, so the beam line to each end station will contain space for the possible insertion of solenoids to form a dipole/solenoid chicane [10] capable of precessing the spin of the electrons from the vertical onto the horizontal axis with nearly 100% efficiency over the energy range from 0.5 GeV to 4.0 GeV.

Experimental Facilities

Primary experimental facilities will be housed in three end stations. Two of these (labeled A and C in Fig. 2) will be heavily shielded and capable of receiving full beam intensities. It is anticipated that each will house a pair of magnetic spectrometers. The third will be lightly shielded and, therefore, able to receive only low intensity (< 1μA) beams. It will house a locally shielded system for producing tagged photons and a large solid angle detector. The use of internal targets in storage rings has been receiving increased attention in recent years. [11] Facilities will be provided in the PSR to study their use.

Upgrade and Expansion

Flexibility for future upgrade and expansion has been built into the design from the beginning. In particular, the possibility of an increase in the beam energy has not been precluded. The linac energy could be increased easily by adding accelerating sections and klystrons to the straight section of the recirculation path and/or by moving the

injector upstream and adding them to the present Sector 1. The BSY and PSR elements could be modified to handle higher energies simply by increasing the electrical drive. The PSR would also require additional rf power, but the PSR is large enough to provide space for the added equipment.

Sith a linac in plase an obvious avenue of expansion is by the addition of other rings. A second pulse stretcher ring would permit the delivery of simultaneous high duty factor beams of different energies, and a ring dedicated to experiments with internal targets could be added. Provision has been made in the BSY for the addition of injection lines feeding such additional rings.

Staff Build up

One of the most important concerns of the project is the timely build up of the staff required to construct and commission the facility. During the past year several SURA institutions have hired faculty members whose interests and efforts will be directed towards the experimental program at CEBAF. The nine positions promised by the Commonwealth have been made available and a number of offers have been made. The filling of positions at these levels takes time, but progress is being made.

The shortage of accelerator specialists around the world has necessitated that we, to some extent, "grow our own". To this end we have established a cooperative program with SLAC whereby people, generally fresh physics and engineering Ph.D's, who are employed by CEBAF work with groups at SLAC for periods of up to one year. During this time they contribute to ongoing SLAC programs part-time and work on projects specific

to CEBAF part-time. In the process they gain valuable experience in accelerator related fields and are able to draw upon the considerable expertise available at SLAC in working on projects for CEBAF. We presently have three people in the program and expect to have ten by the end of the year. A parallel program at Fermilab is being discussed with senior officials of that lab.

On July 1, seventeen positions formerly connected to the Virginia Associated Research Campus will be transferred to the project. These positions include administrative, clerical, and technical personnel. Support for these positions comes and will continue to come from the Commonwealth of Virginia.

Funding

To date support for the project has come from non-federal resources. Primary sources have been the University of Virginia, the Commonwealth of Virginia, and other SURA institutions.

Anticipated funding for the next year include a combination of federal and other sources. The Commonwealth of Virginia has committed two million dollars, one for the year beginning July 1, 1984 and one for the year beginning July 1, 1985. These funds will be used for the support of CEBAF personnel here and at SLAC. One million dollars of federal (DOE) research and development funds will be made available from the FY 84 budget. These funds represent the first direct federal support of the CEBAF project. An additional $3.5 million has been included in the FY 85 Congressional Budget and, therefore, will be available late this year. These funds will be used to support intensified R & D

efforts and preliminary architectural and design work.

Research & Development

Plans for the research and development effort center on crucial technical components. In particular, bids from private companies will be solicited for the development of prototype klystro and modulators. These devices have long lead times (12-18 mo.) so a timely beginning is essential. Specialized devices such as the electrostatic septa and fast kicker magnets for the PSR will also be addressed early in the R & D effort.

References

1. "Report of the Panel on Electron Accelerator Facilities", D. A. Bromely (Chairman), DOE/ER-0164, April 1983.
2. R. A. Beck et al., "ALIS, An Electron Linac Beam Stretcher", Proc. of the 7th International Conference on High Energy Accelerators, Erevan, 1969.
3. G. A. Loew, "Properties of a Linac-Storage Ring Stretcher System", Proc. of Conf. on Future Possibilities for Electron Accelerators, Charlottesville, Virginia, January 1979.
4. R. C. York et al., "Multi-GeV Electron Linac-Pulse Stretcher Design Options", IEEE Trans. Nucl. Sci. NS-30, No. 4, August 1983.
5. Y. Kawazoc et al., "Tohoku University Report", TRKJ No. 3-E, October 1980.
6. R. Helm, private communication.
7. J. C. Sheppard et al., "Design of an Electron Beam Spectral Modification System", SLAC-PUB-2816, October 1981.

8. K. L. Brown, "A Second Order Optical Achromat", SLAC-PUB-2816, Feburary 1979.

9. B. E. Norum and R. C. York, "An Energy Independent Electron Spin Precessor", IEEE Trans, Nucl. Sci. NS-30, No. 4, August 1983.

10. R. P. Maloney et al., "Computer Modeling of Internal Targets in Electron Storage Rings", IEEE Trans. Nucl. Sci. NS-30, No. 4, August 1983.

---

*Work supported by the University of Virginia, the Southeastern Universities Research Association, and the U. S. Department of Energy.

Fig. 1. Linac-PSR Time Structure: (a) 200 mA, 1.2 μs linac beam pulses are injected into the PSR every 1.0 ms. (b) The average stored current in the ring is constant for approximately 20 μs after injection. (c) Current extracted from the ring rises to steady-state about 20 μs after injection, falling to zero about 10 μs before the next injection.

Fig. 2. Accelerator Facility Layout

Fig. 3. Linear Accelerator Layout

Fig. 4. Pulse Stretcher Ring Layout

Table I

Accelerator Design Requirements

Energy Range (@ 200 μA)	$0.5 \leq E_o \leq 4.0$ GeV
Energy Variability	Continuous from 0.5 GeV
Energy Spread	$\Delta E_o/E_o < 0.01\%$
Duty Factor	> 80%
Number of Beams	> 2 (1 to tagged γ facility)
Total Current	200 μA
Current per Beam	100 μA (standard end station)
	1 μA (tagged γ facility)
Transverse Emittance	0.2 π mm-mr in one plane
	0.4 π mm-mr in other

Table II

Linac Parameters

Energy Range (@ 200 μA)	$0.5 \leq E_o \leq 4.8$ GeV
Energy Variability	Continuous from 0.5 GeV
Energy Spread	$\Delta E_o/E_o < 0.2\%$
Pulse Repetition Rate	$\leq$ 1000 Hz (variable)
Accelerating Frequency	2856 MHZ
Bunch Frequency	714 MHz
Peak Current	> 200 mA
Transverse Emittance	20 (keV/c)-cm

Table III

Pulse Stretcher Ring Parameters

Circumference	362.773 m
Overall length	138.6 m
Overall width	76.2 m
Magnetic Radius	26.855 m
Packing Factor	46.5%
Harmonic Number	864
Momentum Compaction	0.022
Betatron Tunes	
Horizontal	8.5 (on resonance)
Vertical	8.8
Chromaticities	
Horizontal (Uncorrected/Corrected)	-10.4/0
Vertical (Uncorrected/Corrected)	-11.4/0
RF System	
Frequency	714 MHz
Peak Voltage (variable/continuous)	4.5/1.5 MV
Average Power (variable/contiuous)	5/350 kW

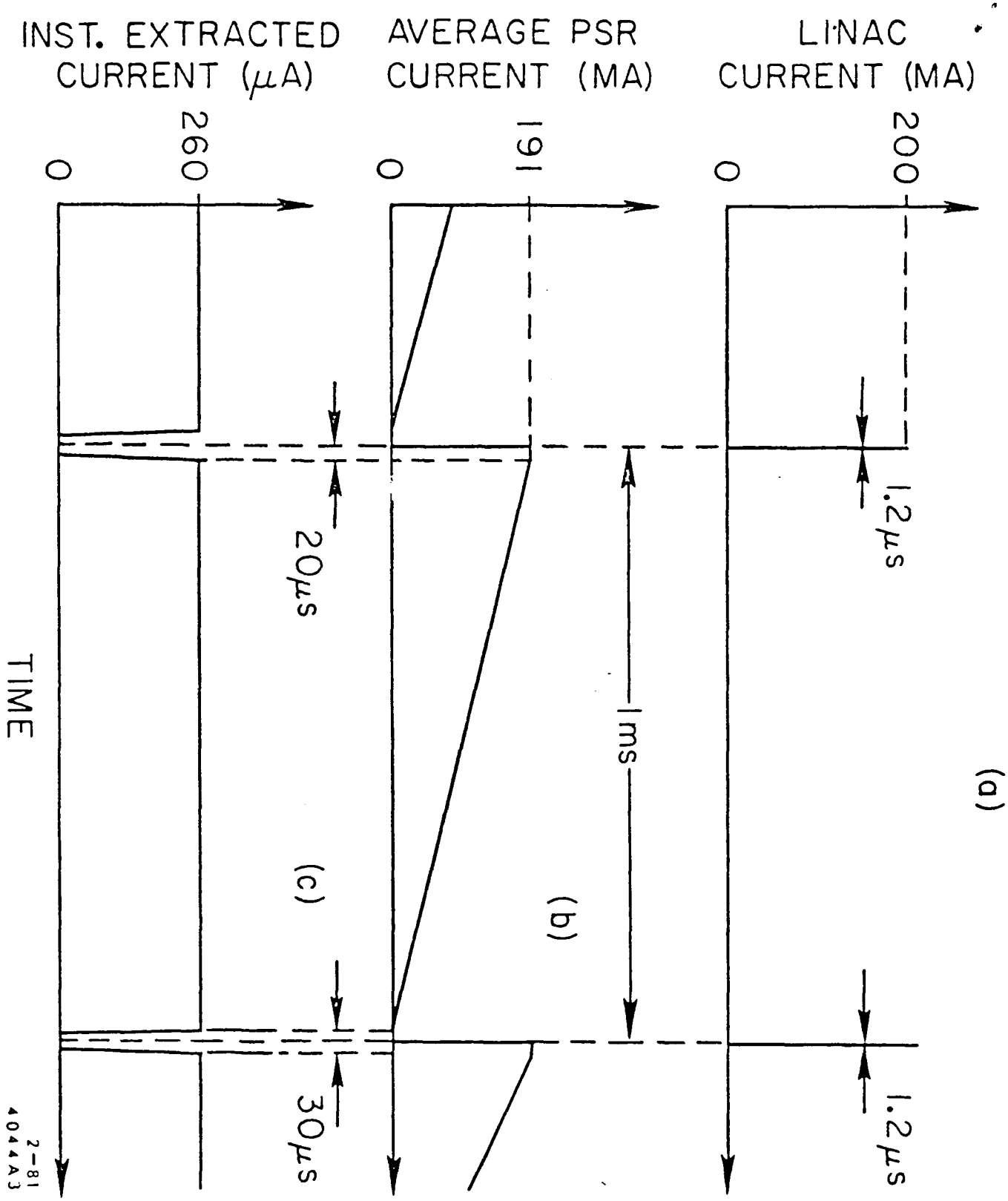
INST. EXTRACTED CURRENT (μA)
AVERAGE PSR CURRENT (MA)
LINAC CURRENT (MA)
0
260
0
191
0
200
20μs
1ms
1.2μs
(c)
(b)
(a)
30μs
1.2μs
TIME
2-81
4044A3

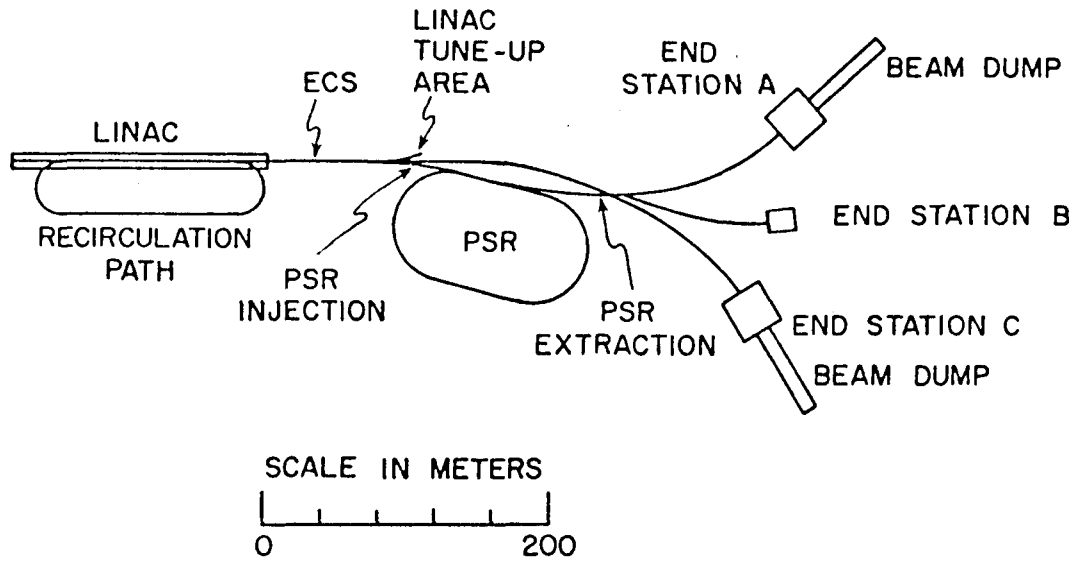
LINAC
TUNE-UP
AREA
ECS
END
STATION A
BEAM DUMP
LINAC
END STATION B
RECIRCULATION
PATH
PSR
PSR
INJECTION
PSR
EXTRACTION
END STATION C
BEAM DUMP
SCALE IN METERS
0
200

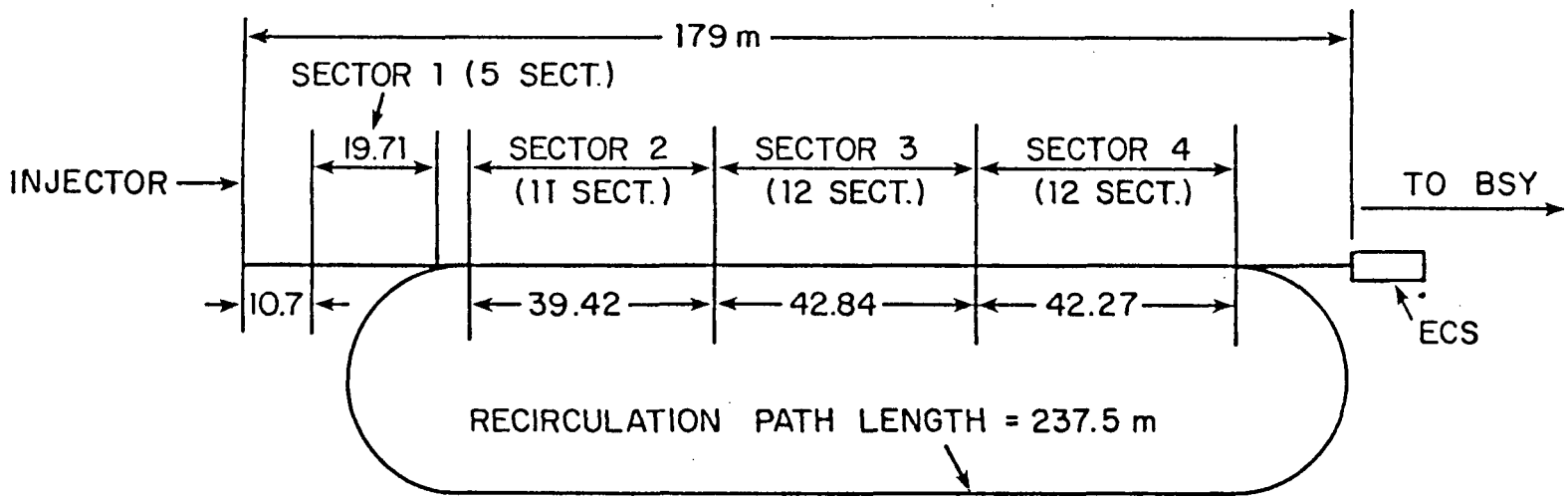
179 m
SECTOR 1 (5 SECT.)
19.71
SECTOR 2
(11 SECT.)
SECTOR 3
(12 SECT.)
SECTOR 4
(12 SECT.)
INJECTOR
TO BSY
10.7
39.42
42.84
42.27
ECS
RECIRCULATION PATH LENGTH = 237.5 m

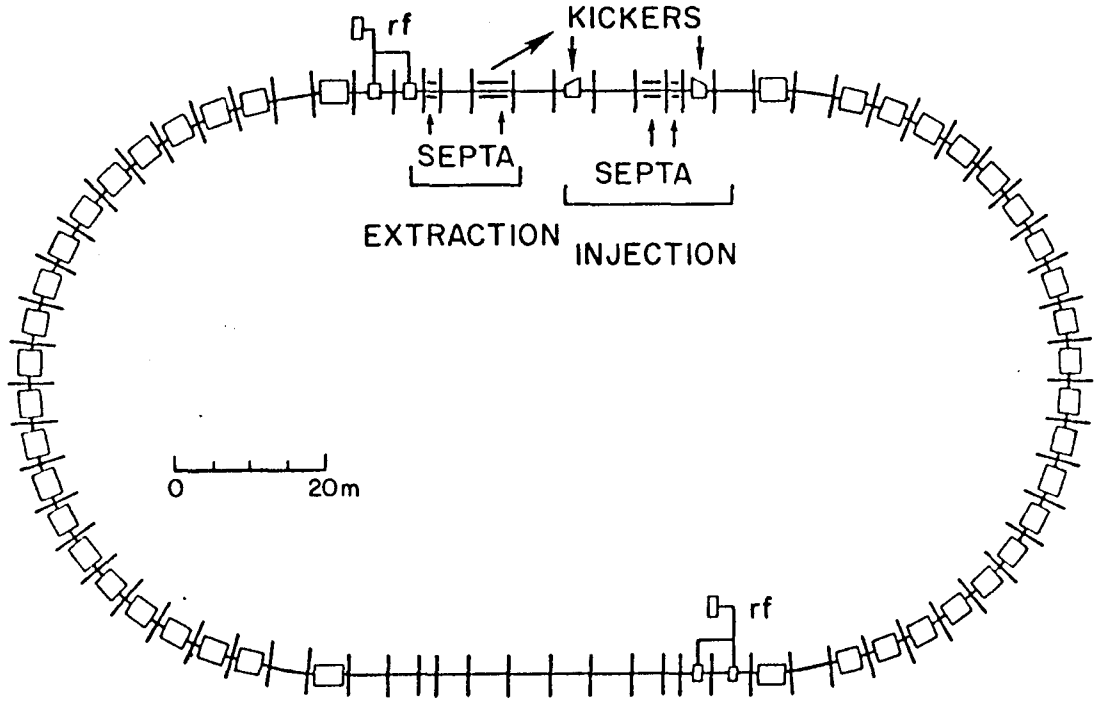
rf
KICKERS
SEPTA
SEPTA
EXTRACTION
INJECTION
0
20m
rf

Nucleon Physics with Chromodynamics: from high Q^2 to baryon spectroscopy to nuclear physics

Nathan Isgur
Department of Physics
University of Toronto
Toronto, Canada M5S 1A7

PREFACE

Quantum chromodynamics (QCD) is almost certainly the correct theory of the strong interactions, and although we are far from having rigorous solutions of the theory, models which incorporate some of the features of chromodynamics have had considerable success in explaining a wide variety of hadronic physics. These lectures concentrate on three areas where applications of such models may be of interest in nuclear physics.

This is not, however, a set of lectures designed to explore in a systematic way the application of quantum chromodynamics to nuclear physics. On the contrary, the three topics which I will discuss are almost as disjoint as they can be, beginning with the regime involving high Q^2 and thereby perturbative QCD where α_s is small, going through the moderate Q^2 relevant to baryon spectroscopy, and ending with the very low Q^2 relevant to nuclear binding. I cannot, however, even claim that these subjects were chosen to illustrate the range of possible applications of QCD to nuclear physics, though perhaps they do: they are just subjects in which I happened to be involved recently. Since their only real common thread is that they use models for hadrons based on chromodynamics, I will begin with an introduction to such models in section I. In the next three sections I will discuss in turn the "derivation" of nuclear physics from chromodynamics, the validity of the use of perturbative QCD to predict high Q^2 elastic electromagnetic form factors, and predictions (which test models for the nucleon) for a set of non-strange baryon resonances which have yet to be seen by conventional πN scattering but which should be produced by nucleon photoexcitation. I will close with some comments.

I. MODELS FOR HADRONS WITH CHROMODYNAMICS

Quantum chromodynamics (QCD) may be thought of as a generalization of quantum electrodynamics (QED), our most successful physical theory. Since the success of QED can be attributed to some extent to its possession of a very high level of symmetry through its gauge invariance, it was natural to concentrate on generalizing this symmetry; the nature of the resulting relationship is sketched in Table 1.

TABLE 1: QCD as a Generalization of QED

	QED	QCD
basic object	a one component (charged) fermion field ψ	a three component (coloured) fermion field ψ_α with α=R,B, or G
global symmetry	fermion Lagrangian invariant under global U(1):$\psi\rightarrow\exp(ie\chi)\psi$, χ a scalar	fermion Lagrangian invariant under global SU(3): $\psi\rightarrow\exp(ig\frac{1}{2}\lambda_i\theta_i)\psi$, θ_i an 8-vector, λ_i the Gell-Mann generators of SU(3)
local symmetry	demand invariance under local U(1): $\chi\rightarrow\chi(x)$	demand invariance under local SU(3): $\theta_i\rightarrow\theta_i(x)$
compensating gauge field	invariance implies a single compensating gauge field $A^\mu(x)$, the photon	invariance implies eight compensating gauge fields $G_i^\mu(x)$, the gluons
interacting fermions	minimal fermion coupling $\psi\gamma_\mu\psi A^\mu$	minimal fermion coupling $\psi\gamma_\mu\frac{1}{2}\lambda^i\psi G_i^\mu$
gauge field dynamics	Maxwell dynamics for A^μ via $F^{\mu\nu}=\partial^\mu A^\nu-\partial^\nu A^\mu$; no nonlinearities	non-Maxwellian dynamics for G_i^μ via $F_i^{\mu\nu}=\partial^\mu G_i^\nu-\partial^\nu G_i^\mu +gf_{ijk}G_j^\mu G_k^\nu$, with f_{ijk} the structure constants of SU(3); nonlinearities

Given that the only significant difference between the two theories is the non-linear gauge field term in the field strength $F_i^{\mu\nu}$ (which arises from the non-abelian character of SU(3)), it is astounding how different the two theories are. In QED the energy between fixed positive and negative charges separated by a distance r is associated with an approximately dipole electric field:

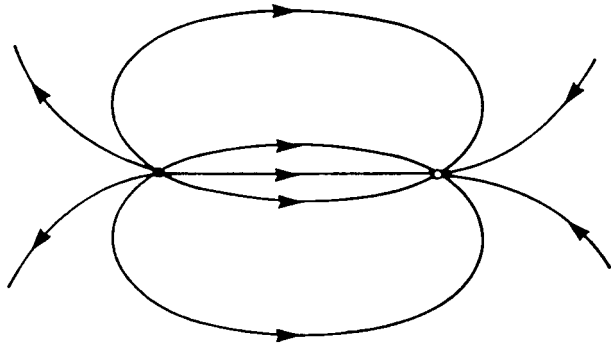

Fig. 1. The static electrodynamic field

In electrodynamics the precise field shape is influenced by a "vacuum polarization" due to quantum fluctuations of e^+e^- pairs, with the result that the charges are screened as in a dielectric. Thus while at large r the "effective coupling" $\alpha(r)$ goes to a constant, namely the fine structure constant α, for smaller r $\alpha(r)$ increases (by 10^{-18} meters, corresponding to the highest momentum transfers available today, it has increased by a few percent). In QCD the story is very different, because vacuum polarization occurs not only via virtual quark-antiquark pairs, but also via gluon pairs produced by the non-linear field term, and these extra effects (as it turns out) "antiscreen". The result is that for very small distances, where g is small so that all vacuum polarization effects are weak, QCD behaves much like QED with the "chromoelectric" fields between a fixed quark and antiquark approximately in a dipole shape with a field energy $-4\alpha_s(r)/3r$. However, $\alpha_s(r)$ <u>increases</u> with increasing r and it is now known from numerical studies of QCD on a lattice that for $r \gg 10^{-15}$ meters the chromoelectric flux has collapsed into a tube which produces a linear confining potential:

Fig. 2. The static chromodynamic field for large r

This change in the character of the interquark potential can be associated with a change from a weak coupling regime ($g<1$) to a strong coupling regime ($g>1$), and most hadronic models incorporate this two-component structure by assuming a simple sum of a spin-independent long range linear potential and one gluon exchange. The nature of the resulting relationship between quark models in QCD and atomic physics in QED is sketched in Table 2.

Unfortunately, QCD is <u>not</u> this simple. One of the things entirely omitted by this analogy is the fact that QCD will have quark bound states (called "hybrids") in which the gluonic field is not quiescent as in the preceding diagram , but in an excited state, and other states (called "glueballs") without any quarks at all. Associated with these extra degrees of freedom is that fact that while at short distance simple $\vec{\lambda}_i \cdot \vec{\lambda}_j$ potentials like that shown in Table 2 are correct, at large distances they can at best be a crude approximation to the complex structure of the theory. Nevertheless, $q\bar{q}$ and qqq models based on this analogy have worked very well. One example of this is illustrated in Figure 3; Figure 4 shows that the basic features of the models seem to persist even for light quarks. Indeed, while relativistic effects make the models less accurate for light quarks, they have been remarkable in their ability to explain not only the main spectroscopic features, but also detailed properties of hadrons made of u, d, and s quarks.

It will , of course , be some time before we are able to rigorously deduce the consequences of QCD in any but the simplest situations. In the meantime, it seems obvious that it is worthwhile applying the

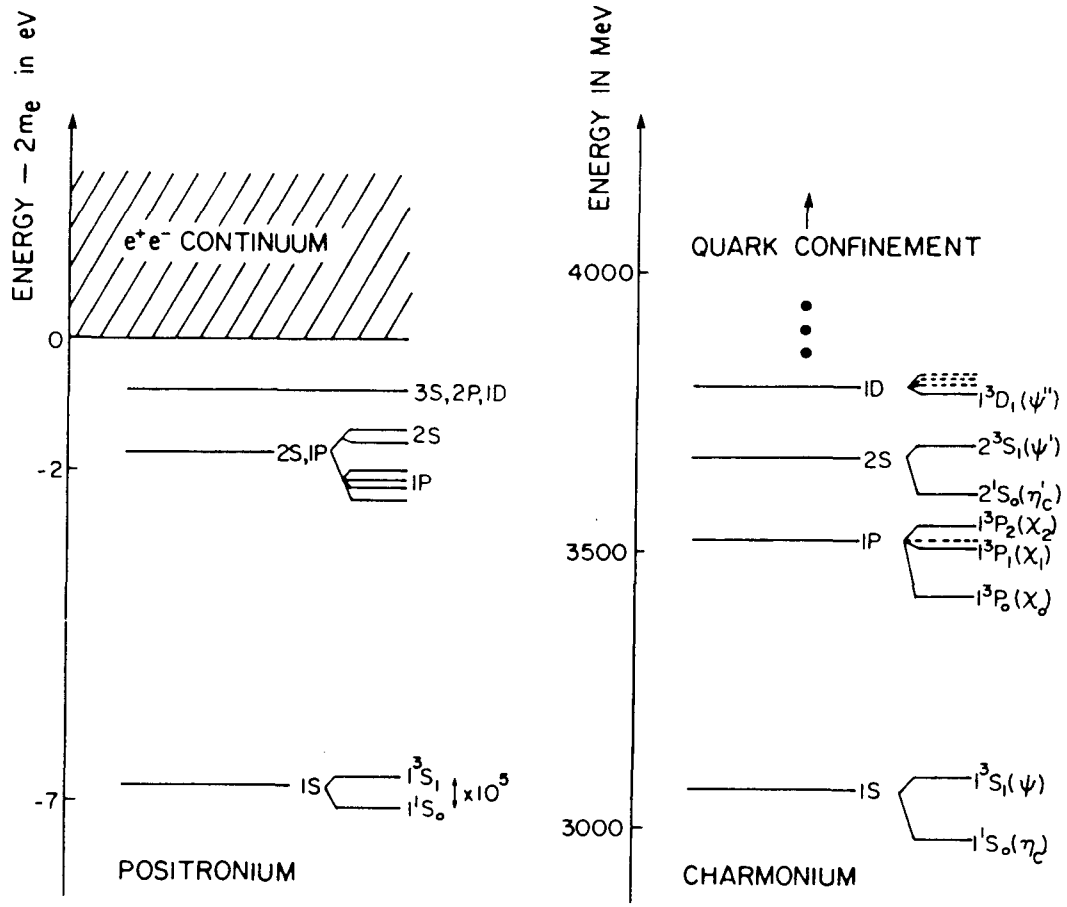

Fig. 3. The transition from positronium to charmonium: replacing m_e by m_c and $-\alpha/r$ by $\frac{4}{3}(-\alpha_s/r + c + br)$ leads from the spectrum on the left to that on the right.

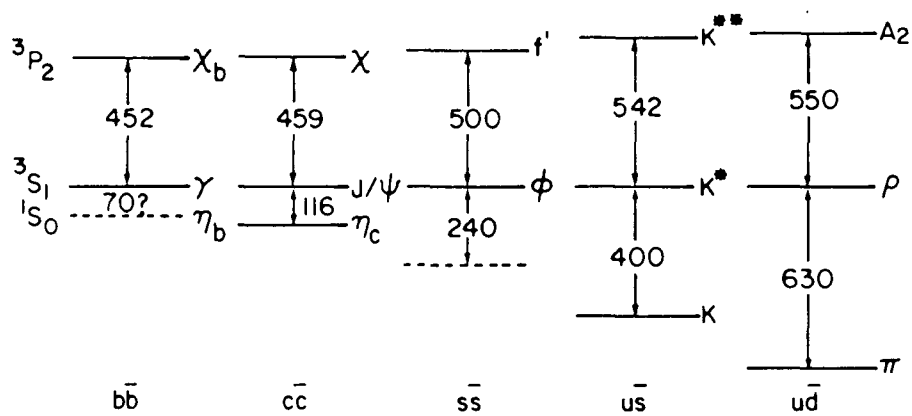

Fig. 4. The transition from heavy quarkonium to light quarkonium showing the apparent universality of the physics of all such systems.

TABLE 2: Quark Models in QCD versus Atomic Physics in QED

	QED	QCD
basic potential	$\frac{\alpha}{r}(\frac{e_1}{e})(\frac{e_2}{e})$	$(-\frac{\alpha_s}{r}+c+br)\frac{\lambda_1^i}{2}\frac{\lambda_2^i}{2}$
	electric	chromoelectric
spin-dependence	for example, $\frac{8\pi\alpha}{3m_1m_2}\vec{S}_1\cdot\vec{S}_2\delta^3(\vec{r})(\frac{e_1}{e})(\frac{e_2}{e})$	for example, $\frac{-8\pi\alpha_s}{3m_1m_2}\vec{S}_1\cdot\vec{S}_2\delta^3(\vec{r})\frac{\lambda_1^i}{2}\frac{\lambda_2^i}{2}$
	from magnetic moments	from chromomagnetic moments
typical "atom"	e^+e^-, positronium	$c\bar{c}$, charmonium; also non-abelian $q_Rq_Bq_G$ baryonic atoms
orbital excitations	for example, the Lyman series	for example, B(1235)-π(140) in $q\bar{q}$ and N(1520)-N(940) in qqq
spin splittings	for example, the 21 cm line of atomic hydrogen	for example, ρ(770)-π(140) in $q\bar{q}$ and Δ(1235)-N(940) in qqq
v/c	<<1 in hydrogen; ≈ 1 in uranium	<<1 in $b\bar{b}$, beautyonium; ≈ 1 in the nucleon

models we have to the more complex phenomena, like those of nuclear physics, in which we have a special interest.

II. DERIVING NUCLEAR PHYSICS: SIX QUARKS WITH CHROMODYNAMICS

Given the strong analogy of Table 2 between atomic physics and hadron physics, it is natural to try to extend the analogy to make a connection between molecular physics and nuclear physics. This analogy is sketched in Table 3 for the hydrogen molecule and the deuterium nucleus. Of course this basic analogy has some "technical" flaws, the most important being that in this case 6>>4. To see what I mean by this, note that in H_2 an adiabatic approximation (in which the electronic energy is calculated for fixed proton positions and then used as an interproton potential) works well since $m_p>>m_e$. Thus one really only needs to solve a Schrodinger problem for the spatial locations of two particles. In the case of ^2H, no adiabatic approximation is viable, and moreover the two quark spins and three colours play a crucial dynamical role.

There is one further analogy of another sort which I would like to stress. At this time it is safe to say that we understand the hydrogen molecule perfectly: enormous variational calculations have been able to reproduce its properties almost exactly. However, in some sense the very first calculation by Heitler and London in 1927

TABLE 3: The Hydrogen Molecule in QED versus Deuterium in QCD

	QED	QCD
symbol	H_2	^2H
"atomic" structure	$H_2 \leftrightarrow H + H$	$^2H \leftrightarrow p + n$
basic structure	$H_2 \leftrightarrow 2e^- + 2p$	$^2H \leftrightarrow 3u + 3d$
basic description	four body problem with Coulomb's law	six body problem with chromodynamics
"atomic" dissociation energy	4.48 eV	2.23 MeV
"atomic" separation	0.740 Å	3.9 fm
method of solution	variational	variational
"quasiparticle" description	H atoms in effective potential	nucleons in effective potential

was the most satisfying since on the basis of that calculation (which only reproduced the dissociation energy and equilibrium radius to about 50%) it was already possible to state the main physics conclusion (which had already been conjectured by Lewis in 1918): the chemical bond is a shared electron. A variational calculation for the six quark system with chromodynamics is technically of comparable complexity to the latest calculations for H_2, but it should be compared in spirit to the situation in 1927. The calculation is, relative to the complexity of the system, very crude, but if we are lucky we may still be able to answer some of the basic physics questions posed by the properties of nuclei.

The idea of such a calculation is an old one and I cannot possibly do justice to the history of the subject here. I would rather like to describe the particular approach which Kim Maltman and I took and our results.[1] Our calculation was very strongly based on the molecular analogy of Table 3 and the belief that some of the fundamental questions we wished to answer could only be addressed if we could calculate the six quark ground state wavefunction. We accordingly set out to do this instead of to study, for example, scattering via resonating group techniques. As already implied, the calculation was extremely arduous; it would have been even more difficult if we hadn't made use of a simple calculational trick. This was to concentrate on the 3u+3d quark sector (I_3=0 to particle physicists, T_3=0 to nuclear physicists) so that we could use $S_3^u \times S_3^d$ symmetry instead of S_6 symmetry (S_n is the permutation group on n

[1] K. Maltman and N. Isgur, Nuclear physics and the quark model: Six quarks with chromodynamics, Phys. Rev. D29, 952 (1984).

objects). This had the disadvantage that the calculation was not automatically diagonalized in isospin. However, the penalty for this was slight: the computer had to diagonalize some larger matrices than it would have otherwise. In exchange, it was possible to do the analytic calculations required in about a year instead of perhaps double that.

The calculation proceeded via a cluster expansion of the five relative coordinates. Two pairs of coordinates were expanded in a three quark harmonic oscillator basis; the fifth coordinate was described by an intercluster variational wavefunction. The cluster expansion was made in a basis space of 115 dimensions which included all possible colour, spin, flavour, and space combinations possible by allowing up to two units of intracluster spatial excitation; up to 15 parameters were used to expand the intercluster wavefunction which was allowed to be in an S, P, or D-wave. Our goal was to allow the six quark wavefunction to do anything it liked. For example, our wavefunction could certainly reach any reasonable "democratic", "spherical", six quark state clustered around the origin. I emphasize that although we used a cluster expansion, we did not put clustering in by hand.

For our Hamiltonian we used a model [2] of the type sketched in Table 1 which is known to provide a reasonably good description of baryon spectroscopy---clearly a minimal requirement if one is to believe the results of a "two nucleon" calculation. The model Hamiltonian is

$$H = \sum_i \left(m_i + \frac{p_i^2}{2m_i}\right) + \sum_{i<j} H^{ij}_{s.i.} + \sum_{i<j} H^{ij}_{s.d.} \qquad (1)$$

where the spin-independent interaction is

$$H^{ij}_{s.i.} = -\{e_o + \tfrac{1}{2}kr^2_{ij} + U(r_{ij})\}\ \tfrac{1}{2}\lambda^\alpha_i \tfrac{1}{2}\lambda^\alpha_j \qquad (2)$$

and the spin-dependent interaction is

$$H^{ij}_{s.d.} = -\frac{\alpha_s}{m_i m_j}\left\{\frac{8\pi}{3}\vec{S}_i\cdot\vec{S}_j\delta^3(\vec{r}_{ij}) + r^{-3}_{ij}S_{ij}\right\}\tfrac{1}{2}\lambda^\alpha_i\tfrac{1}{2}\lambda^\alpha_j \qquad (3)$$

with $\vec{r}_{ij} = \vec{r}_i - \vec{r}_j$, $\vec{S}_i$ the spins, and $S_{ij} = r^{-2}_{ij}(3\vec{S}_i\cdot\vec{r}_{ij}\vec{S}_j\cdot\vec{r}_{ij} - r^2_{ij}\vec{S}_i\cdot\vec{S}_j)$. The potential $U(r_{ij})$ appearing in (2) is introduced so that the three body problem can be solved analytically. One imagines that

$$U(r_{ij}) = -\{e_o + \tfrac{1}{2}kr^2_{ij}\} + \left\{-\frac{\alpha_s}{r_{ij}} + c + br_{ij}\right\} \qquad (4)$$

so that $H_{s.i.}$ is exactly the potential of Table 2 expected from QCD. The U=0 harmonic problem separates and can be solved exactly, so one proceeds by doing perturbation theory in the anharmonicity U about these solutions. Such a perturbative treatment is feasible because one is interested only in the low-lying levels of the system and for

[2] This model was first developed in some detail in N. Isgur and G. Karl, P-wave baryons in the quark model, Phys. Rev. D18, 4187 (1978). For a pedagogical overview see N. Isgur, Soft QCD, in The New Aspects of Subnuclear Physics, edited by A. Zichichi, Plenum, New York, 1980. See also the lectures by G. Karl in this volume.

such states one can choose e_o and k to minimize U. The mysterious absence of spin-orbit forces as an important feature of $H_{s.d.}$ will be discussed below.

I stress that this Hamiltonian is taken over completely from studies of baryon spectroscopy, so that our calculations for the six quark system are purely deductive with no free parameters whatsoever. In fact, the Hamiltonian was taken straight out of the lectures[2] "Soft QCD" I gave at Erice in 1978!

At the time we began our very lengthy calculations, the subject was in its infancy,[3] with early calculations based on an adiabatic approximation seeming to show a repulsive core. In later improved calculations, however, the core disappeared. Eventually it became understood via resonating group techniques that the adiabotic approximation was invalid, and the use of such methods seemed to strongly indicate that a repulsive core emerges naturally from the short distance dynamics. However, at least within the limited basis spaces possible for such techniques, there seemed to be no trace of nuclear binding! Our approach, while much less elegant than the resonating group methods, is considerably more powerful for studying the properties of the six quark ground states. As a measure of this one can compare our 115 term cluster expansion with the maximum of 6 terms employed in any resonating group calculation.

Our main results can be summarized as

1) We find that the 3u+3d quark ground state wave functions with I,J =0,1 and 1,0 show very strong clustering into two three quark systems with neutron and proton quantum numbers and properties. This shows that, within the context of our calculation, nuclear physics is really approximately the physics of nucleon quasiparticles. This is a nontrivial result, as evidenced by the fact that it is quantum number dependent: other six quark systems, when constrained to nuclear densities, do not exhibit such clustering.[4]
2) Given the strong clustering it is natural to project out of the full six quark wavefunction an n-p component. This component, which nearly saturates the full wavefunction, has an amplitude as a function of the n-p separation which we can then interpret as an effective internucleon wavefunction $\psi_{eff}(r)$. This $\psi_{eff}(r)$ can in turn be used to define a bound-state effective potential $V_{eff}(r)$, via the NN Schrodinger equation, which has the following very satisfactory properties:
a) it gives a strong repulsive core for r<1 fm,
b) it provides an intermediate range binding attractive region between 1 and 2 fm, and
c) the $^3S_1$ potential is less repulsive and more binding than the $^1S_0$ potential.

These features are illustrated in Fig. 5. We reemphasize that this potential is purely deductive: we have simply solved the six quark problem for a known Hamiltonian.

---

[3] A brief history with references can be found in Ref. 1.
[4] Private communication from Kim Maltman.

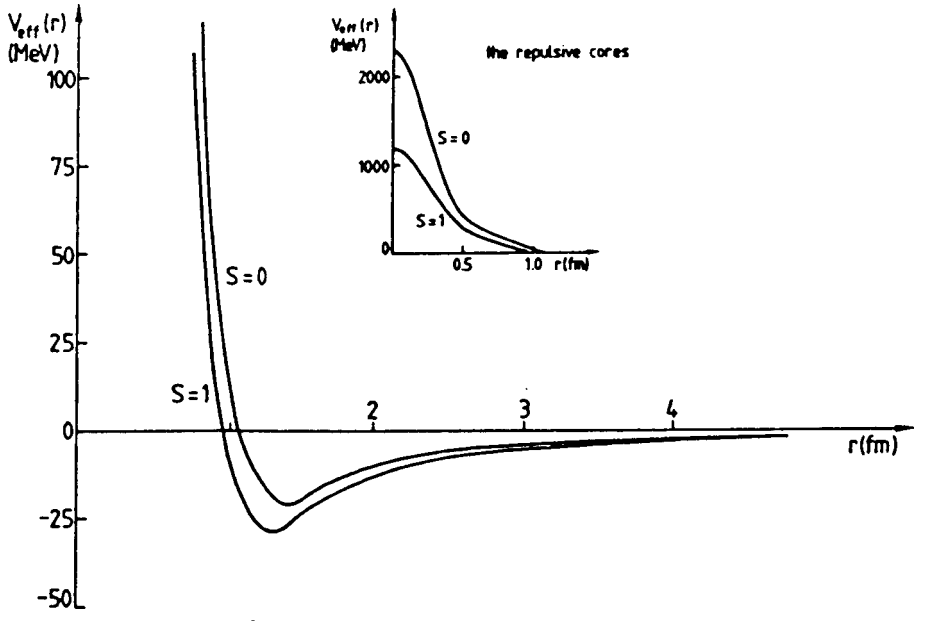

Fig. 5. The effective nucleon-nucleon potentials in the $^3S_1$ and $^1S_0$ channels arising from residual colour forces.

Let me immediately stress that I do not advocate this potential as a replacement for phenomenological nucleon-nucleon potentials. It is based on an approximate solution to a very rough model for the quark dynamics and so cannot be expected to be very accurate. What is relevant is that this calculation may point us in the direction of eventually replacing phenomenological potentials by derived ones, much as the original H_2 calculation of 1927, while quantitatively lacking, captured the basic physics of the situation and eventually led to today's more accurate understanding of the hydrogen molecule. In this spirit, let me attempt, on the basis of our calculation, to provide a picture of the nuclear force analogous to the molecular picture that "the chemical bond is a shared electron".

The attractive region of V_{eff} is the easiest to interpret: it is actually physically analogous in origin to the molecular case. Recall that, at least for separations larger than twice the Bohr radius, there is a van der Waals attraction between two hydrogen atoms which is a weak residue of the electrical forces producing the electrically neutral ep clusters. This weak attractive potential arises because the neutral atoms have a second order perturbation in their energy $-a^2/\Delta E$ from their amplitude a to temporarily excite each other via Coulomb's law into a virtual state with energy ΔE above their ground states (in which the atoms are in P-waves coupled to L=0). Semiclassically we would say that while the atoms are neutral, it is energetically favourable for them to develop small oppositely directed electric dipole moments. Two colour neutral

quark clusters can develop a weak (i.e., nuclear strength!) residual attraction by a closely related mechanism: they can temporarily excite each other (via the QCD version of Coulomb's law of Table 2) into a virtual state in which the clusters are in coloured P waves coupled to L=0 and to zero net colour. Semiclassically we would say that while the atoms are colour neutral, it is energetically favourable for them to develop small chromoelectric dipole moments correlated in their orientation in both space and in colour-space.

It is much more difficult to describe the physical origin of the repulsive core. Our calculations, first of all, confirmed the conclusion which had already been reached via resonating group techniques that the repulsive core is a non-adiabatic effect. This is not surprising: unlike the molecular case where the electron motion is fast relative to the motion of the protons, in the six quark problem there are no adiabatic coordinates once the two three quark clusters begin to overlap. As shown in the earliest calculations, a repulsive core does develop if the six quark system is arbitrarily constrained to remain in two purely nucleonic clusters (a consequence of the Pauli principle and the colour hyperfine interactions). The repulsive core apparently emerges from a complete calculation because the NN configuration does not have time to evolve into more energetically favourable configurations available to it: i.e., there is a dynamical constraint to the two nucleonic cluster sector. One may describe this constraint in other language by noting that there are kinetic energy terms associated with the mixing angles of non-NN configurations, and these kinetic energy terms create pseudoforces (analogous to centrifugal barrier effects) which produce the NN "constraint". This very dynamical origin for the repulsive core is consistent with its known complex dependence on the spin, orbital, and total angular momenta of the six quark system; note, for example, that the $\vec{S}_i \cdot \vec{S}_j$ dependence of the core has already emerged from our calculation.

There are many weaknesses of the calculation I have just described, and before going on it seems appropriate to mention some of them. This is not the place to discuss these issues fully, however, so I will just make an annotated list of some possible criticisms:

1) non-relativistic and other approximations: Since we were mainly concerned with the properties of the six quark system relative to two separated three quark clusters, many sources of error---including relativistic effects---tend to cancel.

2) the spin-orbit mystery: The baryon data enforce the near absence of spin-orbit effects, and spin-orbit effects of the strength allowed by the data would not significantly affect our results. However, until one understands the origin of their suppression, their possible importance cannot be ruled out.

3) the $\vec{\lambda}_i \cdot \vec{\lambda}_j$ confinement potential: The confinement potential of QCD is not as simple as the $\vec{\lambda}_i \cdot \vec{\lambda}_j$ potential of Table 2 and equation (2) suggests. More appropriate, for example, would be a description in terms of dynamical chromoelectric flux tubes [5] which can connect quarks and antiquarks in any way consistent with Gauss' law. The $\vec{\lambda} \cdot \vec{\lambda}$ potential nevertheless has many of the characteristics of the true potential: for example, it gives effective potentials between

5 Such a description can be found, for example, in N. Isgur and J. Paton, A flux tube model for hadrons, Phys. Lett. 124B, 247 (1983) in which the ideas used here are developed.

separated quark clusters which are identical to the lowest energy flux tube configurations. Equally important for applications is that it is much more practical to use than a full flux tube picture. There are, however, certainly some penalties to be paid for this simplification; the most widely discussed has been the existence in such a model of long range van der Waals- type potentials. The $\vec{\lambda}\cdot\vec{\lambda}$ potential produces mixing between flux configuration (or, equivalently, between quark internal colour configurations) which are power-law behaved for large separations. In reality this long-range mixing is cut off by two effects: for internuclear separations $r >> 1$ fm, flux tube configuration mixing will be suppressed by flux tube wavefunction effects, and also the naively constant interquark force will be screened by $q\bar{q}$ pair creation. Thus the long-range power law potentials arising from such interquark potentials are spurious and must be treated with care. I will describe their effects on our own calculation below.

4)the radial dependence of $H_{s.i.}$: In the actual calculations the anharmonic potential U was replaced by an attractive δ-function interaction. In baryon spectroscopy this replacement is known to be adequate for low-lying excitations. We have checked that, since it is averaged over clusters, it should also suffice for this problem, but this point deserves further study.

We have checked other possible weaknesses of our calculation and believe that it has no fundamental problems, even though our model for the Hamiltonian is very crude. The reason for this is that, if we are right, the basic features of nuclear physics are not very subtle consequences of QCD: they will emerge from any model which confines colour in a sensible way and which recognizes some of the basic phenomenological constraints from hadron spectroscopy (like the existence of important interquark spin-spin interactions).

Before finally applying our results to an actual nuclear system, we paused to ask ourselves if there were any regions in which our calculation would fail to take into account the dominant physics of the six quark system. We decided that there was one: when the system has segregated into two three quark clusters which are far apart, our infinitely stretchable flux tubes should be breaking to produce meson exchange rather than remaining intact to produce a long range power law tail. We further argued --- on both the most naive grounds represented by the cartoon of Figure 6 and on more rigorous grounds --- that only the region beyond about 2 fm should be affected. In this region only pion exchange is significant, so to proceed from the results of our calculation to a real nucleus we considered a "hybrid" model in which $V^{NN} = \hat{V}^{NN}_{eff} + \hat{V}^{ope}$. Here $\hat{V}^{NN}_{eff}$ is our derived NN potential cut off at some internuclear separation $r_c \sim 0(2fm)$ and $\hat{V}^{ope}$ is one pion exchange "cut in" at r_c. Our results for the properties of the simplest nucleus, deuterium, were not very sensitive to r_c : Table 4 compares our "hybrid" calculation with the data. The theory errors shown in the table reflect both sensitivity to r_c and also estimates of the errors arising in the various quantities from our basis truncation and our limited variational wave functions. The calculated deuterium wave functions are shown in Figure 7. The results are better than they deserve to be, given the quality of the model.

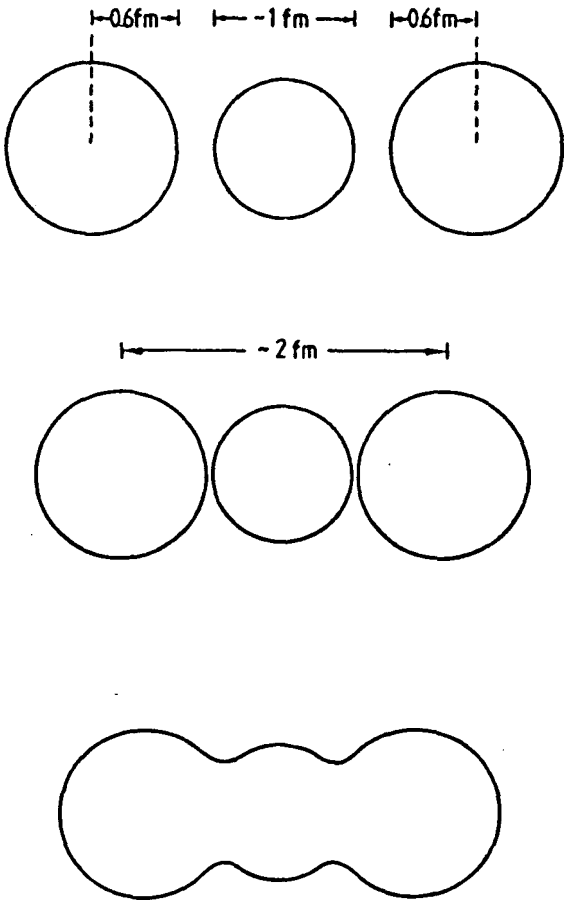

Fig. 6. A cartoon illustrating that for $r \gtrsim 2$ fm meson exchange is unlikely to be appropriate to the description of the inter-nucleon potential.

TABLE 4: Some Properties of the Six Quark Ground States

property	theoretical value	experimental value
E_d(MeV)	$-2.9\ ^{+0.8}_{-0.3}$	-2.23
$(r_d^2)^{\frac{1}{2}}$ (fm)	2.2 ± 0.5	1.95
Q_d (mb)	$+2.1 \pm 0.5$	+2.86
μ_d* (nuclear μ_N)	$+0.859 \pm .003$	+0.857
$E(^1S_0)$ (MeV)	$-0.4\ ^{+0.4}_{-0.1}$	unbound

*μ_d is calculated assuming that the departure from $\mu_p+\mu_n$ is due only to our 3.6% D-wave mixing

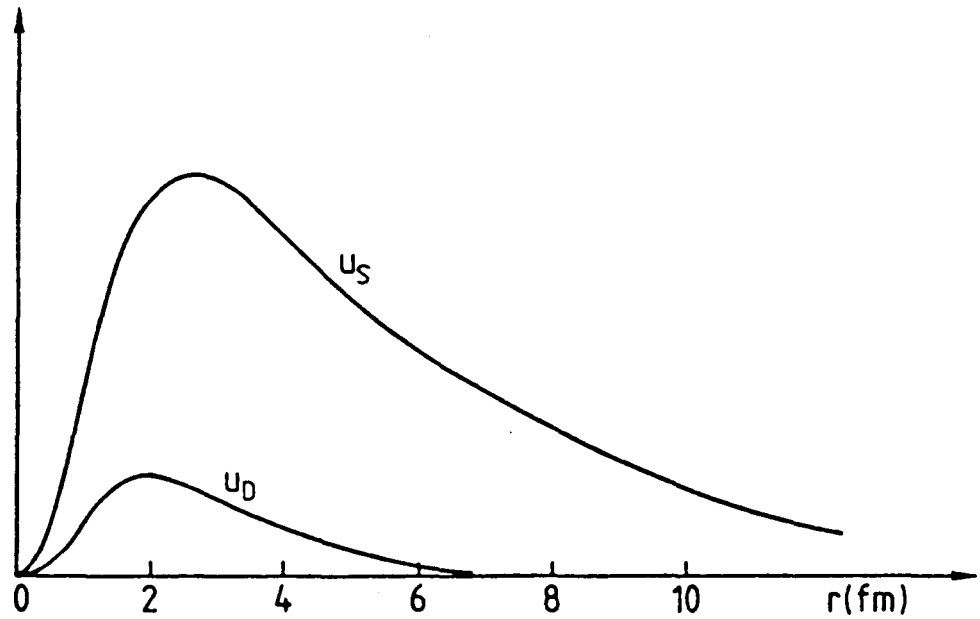

Fig. 7. The deuteron wavefunctions u_S and u_D shown with their correct relative normalization.

I would like to close this lecture by reemphasizing an earlier remark. The picture of nuclear physics which emerges from our calculation is, at best, at a very crude stage. It should not be expected that such calculations will rival in quantitative accuracy more phenomenological approaches for some time. On the other hand, I believe they do represent a useful and viable starting point from which to go beyond the "molecules are made of atoms" approximation to nuclear physics. This same advice was given long ago, appropriately enough, in Deuteronomy 1:6:

> "Ye have wandered long enough in the wilderness; turn you and go up into the high [energy] country."

III. EXCLUSIVE PROCESSES IN PERTURBATIVE QCD: ARE THEY CALCULABLE?

At short distances, QCD is a weakly coupled theory and, as discussed in section I, the usual perturbative techniques familiar from QED can be applied. It is a nontrivial matter, however, to decide whether a given process is ever a short distance process and, if so, in what range of kinematic variables perturbative QCD would apply. Inclusive lepton scattering (deep inelastic scattering) is a gold-plated example of a perturbative process: it can be proven to be short distance dominated for sufficiently large momentum ($\sqrt{Q^2}$) and energy (ν) transfers, and one can readily understand that asymptopia, the region where perturbative QCD applies, will be reached when both of these variables are large with respect to 1 GeV.

It has recently been vigorously argued that various measurable elastic scattering processes are calculable at high Q^2 in terms of perturbative QCD.[6] The argument is intuitively appealing. Consider elastic electron nucleon scattering as an example: at high Q^2 each of the three quarks in the nucleon must experience a large momentum transfer (of order Q). This must be accomplished via an electromagnetic interaction with one quark which by hard gluon exchange shares its momentum transfer with the other two quarks. Since each interquark interaction is a high Q^2 one for which $\alpha_s(Q^2)$ will be small, the process appears to be perturbative. It is, as one might imagine, a difficult task to turn these hand-waving arguments into proofs, but in the case of the pion elastic form factor this has been done, and in many other cases much progress has been made towards framing such a proof. At the same time, naturally, attempts have been made to relate the results of perturbative QCD for exclusive processes to data.[6] There has been a large body of applications, including calculations of F_π (the pion elastic electromagnetic form factor), $G^N_{M,E}$(the nucleon (N) magnetic (M) and electric (E) elastic electromagnetic form factors), elastic electromagnetic form factors of nuclei, elastic scattering amplitudes for AB→CD where A, B, C, and D are hadrons, $\psi \to H\bar{H}$ where H is a hadron, etcetera. Among the claims which have been made are that such processes provide the best testing ground for perturbative QCD and that existing data agree with the predictions of perturbative QCD. It has further been argued on the basis of these successes that measurements of nuclear form factors at moderate Q^2 values ($Q^2 \sim 0(10 GeV^2)$) would provide direct evidence for the quark degrees of freedom in nuclei.

To quote from our paper [7], Chris Llewellyn Smith and I would like to "sound a note of caution about attempts to explain existing exclusive data using perturbative QCD". Let me be clear that we have nothing new to add to the question of whether theorems on the applicability of perturbative QCD to such processes will eventually be proved. Our worry is that even if such theorems are true, they are irrelevant: we believe that there is a danger that perturbative QCD is only dominant in exclusive processes at Q^2 values which are not now and will probably never be available.

Our examination of this programme concentrated on the two showpieces F_π and G^N_M. Our main results are that

1) With reasonable guesses for the pion and nucleon wavefunctions, perturbative scattering like that of Figure 8 is <u>much</u>

---

[6] See for example, G.P. Lepage and S.J. Brodsky, Exclusive processes in perturbative quantum chromodynamics, <u>Phys.Rev. D22</u>, 2157 (1980); G.P. Lepage, S.J. Brodsky, T. Huang, and P.B. MacKenzie, Hadronic wave functions in QCD, in Particles and Fields 2, edited by A.Z. Capri and A.N. Kamal, Plenum, New York, 1983, p. 83; S.J. Brodsky, T. Huang, and G.P. Lepage, Hadronic wave functions and high momentum transfer interactions in quantum chromodynamics, <u>ibid.</u>, p. 143.

[7] N. Isgur and C.H. Llewellyn Smith, Asymptotic Q^2 for exclusive processes in quantum chromodynamics, <u>Phys.Rev.Lett. 52</u>, 1080 (1984).

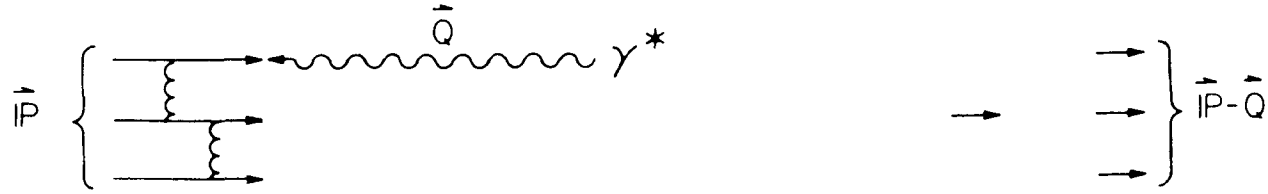

Fig. 8. A perturbative contribution to $G_M^N(Q^2)$.

less important than soft non-perturbative scattering like that of

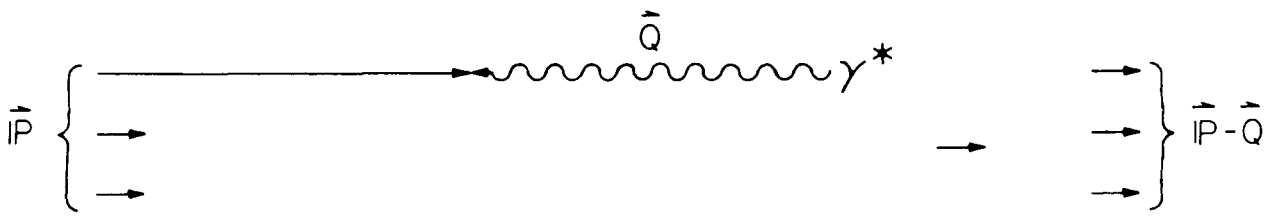

Fig. 9. A soft non-perturbative contribution to $G_M^N(Q^2)$.

Figure 9 which can easily explain the size of the data and
2) Unreasonable guesses do not help.

The problem is simply described. In deep inelastic scattering, perturbative QCD contributes in order $(\alpha_s/\pi)^0$ (since in zeroth order it is the parton model) while soft non-perturbative processes are guaranteed to go like m^2/Q^2 where m is some typical hadronic scale. We thus expect and see perturbative QCD in these processes for $Q^2 \gg m^2 \sim 1 GeV^2$. Consider, however, G_M^N which in perturbative QCD is predicted to behave asymptotically like $(\alpha_s/\pi)^2 Q^{-4}$. Assuming that perturbative QCD dominates asymptotically, the soft non-perturbative processes will now go like m^2/Q^6, but this means that we can only expect to see perturbative QCD for $Q^2 \gg m^2(\alpha_s/\pi)^{-2} \sim 100\ GeV^2$. The more quarks involved in a process, the worse things get: the perturbative process becomes suppressed by more powers of α_s/π but

the soft non-perturbative scattering, which is a strong interaction process from the region $\alpha_s/\pi \sim 1$, is not.

Of course these simple arguments might be misleading. As I will show below, however, they are easily substantiated by explicit calculation. I should emphasize that such explicit calculations must take one outside of the framework of perturbative QCD. Perturbative QCD only predicts the asymptotic Q^2 dependence of exclusive processes and not their normalization: to estimate the magnitude of such contributions to F_π and G_M^N we must have models for the pion and nucleon wavefunctions.

To make reasonable guesses for the infinite momentum frame (or, alternatively, light-cone) wavefunctions required to calculate scattering from, say, $+Q/2$ to $-Q/2$ as $Q \to \infty$, we relied on the quark model. Any hadron will have a decomposition into Fock space components which in general will involve not only the "valence" configurations $q\bar{q}$ and qqq, but also more complicated configurations with extra quark-antiquark pairs and gluons. The coefficients in such an expansion, it must be realized, depend not only on the dynamics of the system, but also on the choice of a field theory cutoff μ. Thus if one chooses $\mu \gg 1$ GeV one will be doing an expansion in "current quarks" in terms of which hadron spectroscopy would be very complicated. On the other hand, the success of the quark model argues that if one chooses $\mu \sim 0(1\ \text{GeV})$ one can make a simple expansion in "constituent quarks" in terms of which the valence components of Fock space dominate. This view is supported by the fact that when the evolution equations for the deep inelastic structure functions are run backwards, the $0(10\%)$ $q\bar{q}$ sea and $0(40\%)$ glue in the nucleon seen at $Q^2 \sim 0(10\text{GeV}^2)$ mostly disappears by $Q^2 \sim 0(1\ \text{GeV}^2)$. We accordingly assumed quark model rest frame wave functions for mesons and baryons respectively

$$\phi_M(\vec{p}) = \pi^{-3/4}\beta^{-3/2}\exp\{-(p_z^2+p_T^2)/2\beta^2\} \tag{5}$$

$$\phi_B(\vec{p}_\rho, \vec{p}_\lambda) = \pi^{-3/2}\alpha^{-3} \exp\{-(p_{\rho z}^2+p_{\lambda z}^2+p_{\rho T}^2+p_{\lambda T}^2)/2\alpha^2\} \tag{6}$$

where $\vec{p}=\vec{p}_q-\vec{p}_{\bar{q}}$, $\vec{p}_\rho=\sqrt{\frac{1}{2}}(\vec{p}_1-\vec{p}_2)$, and $\vec{p}_\lambda=\sqrt{1/6}(\vec{p}_1+\vec{p}_2-2\vec{p}_3)$. With $\beta=0.22$ GeV and $\alpha=0.32$ GeV these wavefunctions are known to give reasonable descriptions of the low energy properties of mesons and baryons.[2] We then took two prescriptions for the x-dependence (x is the usual quark momentum fraction) of the infinite momentum frame/light cone wave functions $\psi(x,\vec{p}_T)$ which control the asymptotic behaviour of F_π and G_M^N, keeping the same factorized p_T dependence as in (5) and (6):

I: We replaced p_{iz} in (5) and (6) by the weak binding form $m(x_i/\langle x_i\rangle - 1)$ where m is the usual constituent quark mass (330 MeV) and $\langle x_i\rangle = \frac{1}{2}(\frac{1}{3})$ for mesons (baryons).

II: We used $(x_1x_2)^\eta_M$ for mesons and $(x_1x_2x_3)^\eta_B$ for baryons for various η.

These guesses both give reasonable $Q^2 \sim 1$ GeV^2 structure functions, good descriptions of various static properties (for example, $f_\pi/f_\pi^{exp} = 1.4$ for case I and 1.2 for case II), and have mean

intrinsic p_T s of the expected magnitude.

The asymptotic forms of G_M^p given by these wavefunctions are shown in Figure 10: both cases I and II are more than two orders of

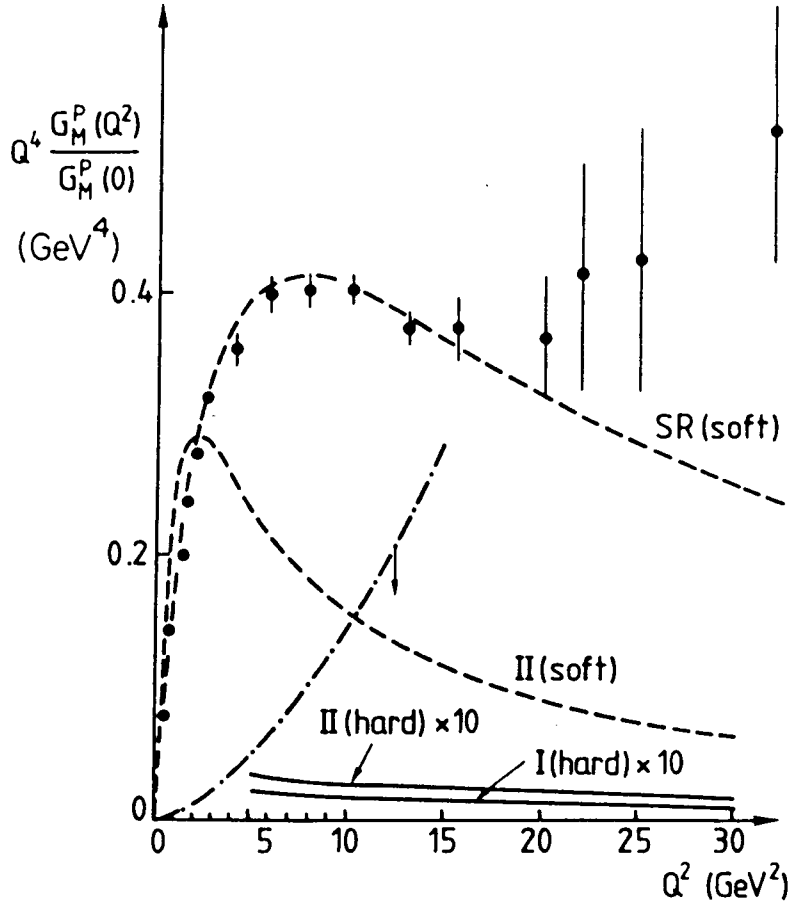

Fig. 10. Some contributions to $G_M^p(Q^2)$ compared to each other and to experiment: The solid "hard" curves show the leading asymptotic contributions calculated with Λ_{QCD}=150 MeV; note that these two curves have been multiplied by a factor of ten so that they can be seen. The dash-dotted curve is the bound on such contributions discussed in the text. The "soft" contribution II(soft) is given by the dashed curve; I(soft) is not shown since the case I wavefunction's x→0,1 behaviour, which controls the soft contribution, is unphysical. SR(soft) is the result of the third paper of Ref. 8. Note that contributions of order α_s/π , which might be important at intermediate Q^2, are not included.

magnitude below the data. On first obtaining this result we were perplexed since it seemed difficult to imagine that anything but hard scattering could be contributing to G_M^p at such high Q^2 relative to $\langle p_T^2 \rangle$. We nevertheless decided to examine soft scattering of the type shown in Figure 9. Unfortunately, it is impossible within this framework to make better than a rough estimate of the soft contribution to G_M^N. The main reason for this reflects a fundamental shortcoming of the use of infinite momentum frame or light cone wavefunctions in an unsolved theory: such wavefunctions cannot be kinematically constrained to be eigenstates of J^P. Thus although the "naive quark model" wave functions dominate F_π and G_M^N asymptotically, in general "Wigner rotated" pieces of the wavefunction play a role. In the case at hand the absence of good J^P quantum numbers means that our soft results depend on what frame we use and the component of the currents whose matrix elements we calculate. Nevertheless, we found that our wavefunctions always produced soft scattering which was much larger than hard scattering at $Q^2 = 10$ GeV^2 and comparable in magnitude to the data. The result for j^0+j^3 in a frame in which $q^0+q^3=0$ is also shown in Figure 10. Let me emphasize that the issue is not whether we can accurately calculate G_M^N; we can't. The main point is that with reasonable wavefunctions we can understand qualitatively the physics behind the observed strength of $Q^4 G_M^N$, and that these same wavefunctions strongly indicate that the perturbative contributions at available and at any foreseeable Q^2 are unimportant.

The analogous calculation of F_π serves as a check on our calculation: in the case of the pion we are singularly fortunate in being able to compare our calculated perturbative contribution with a rigorously known asymptotic result. The excellent agreement shown in Figure 11 indicates that it is unlikely that our nucleonic

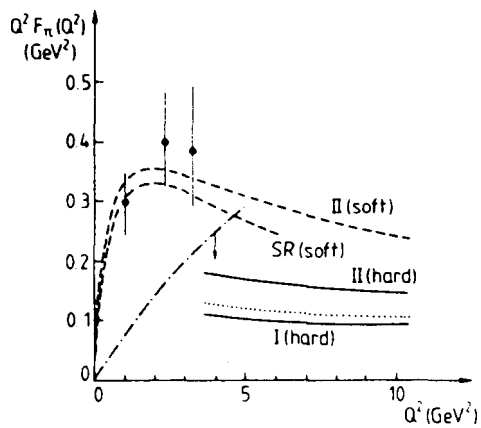

Fig. 11. Some contributions to $F_\pi(Q^2)$ compared to each other and to experiment: The solid "hard" curves show the leading asymptotic contributions calculated with Λ_{QCD}=150 MeV; the dotted curve between them is the rigorous result. The dash-dotted curve is the bound on such contributions discussed in the text. The "soft" contribution II(soft) is given by the dashed curve; I(soft) is not given since the case I wavefunction's $x \to 0,1$ behaviour, which controls the soft contribution, is unphysical. SR(soft) is the result of the second paper of Ref. 8.

calculation is far off the mark: we would certainly expect our simple quark model inspired wavefunctions to be more reliable for the nucleons than for the pions. Once again our soft calculation shows that wavefunctions with small $\langle p_T^2 \rangle$ are capable of generating contributions of the same magnitude as the data. Note that these observations regarding soft contributions alone should be sufficient to undermine confidence in these processes as tests of perturbative QCD at available Q^2's.

I would like to emphasize that the wavefunctions we used in our calculation were not in any way designed to produce the above results. They are actually ancient wavefunctions which can be found in my 1978 lectures at Erice on "Soft QCD" [2]. If we had allowed a rather small variation of α in (6) from its ancient value, we could in fact have made the soft contributions to G_M^p fit the data much better, but no choice of α could provide an explanation of the data as being due to hard scattering processes alone.

After completing these calculations, we learned of some work done by groups in the Soviet Union using totally different techniques based on the QCD sum rule phenomenology which seem to confirm our main conclusions. Their calculation of the soft contributions [8] shown in Figures 10 and 11, are actually much less problematic than ours as the sum rule method automatically produces frame independent results. Other calculations [9] agree with our estimate of the asymptotic normalization of G_M^N. We are therefore in a situation where two totally independent global studies of hadron physics, very distinct in approach and basic parameters, agree: these processes are dominated by soft, non-perturbative effects at available Q^2.

We did not like this conclusion since it would seem to wipe out a whole set of possible tests of perturbative QCD, so we spent some time looking for a way out. Unfortunately, the way seems completely blocked. For example, with larger $\langle p_T^2 \rangle$ hard scattering could fit the data for G_M^N, but this possibility runs into four difficulties:

1) The large intrinsic $\langle p_T^2 \rangle > 1$ GeV^2 required would be difficult, if not impossible, to reconcile with that required by other phenomenological studies.

2) Calculations with the large required $\langle p_T^2 \rangle$ would be inconsistent: the perturbative calculations are only valid for $Q^2 \gg 10 < p_T^2 > \simeq < p_T^2 > / < x^2 >$ since it is only under this condition that the form factor is controlled by the calculable perturbative tail of the wavefunction.

---

8 B.L. Ioffe and A.V. Smilga, Pion form factor at intermediate momentum transfer in QCD, Phys.Lett. 114B, 353 (1982); V.A. Nesterenko and A.V. Radyushkin, Sum rules and the pion form factor in QCD, Phys.Lett. 115B, 410 (1982); Local quark-hadron duality and nucleon form factors in QCD, Phys.Lett. 123B, 439 (1983).

9 V.M. Belyaev and B.L. Ioffe, Determination of baryon and baryon resonance masses from quantum chromodynamic sum rules. Nonstrange baryons, Sov.Phys. JETP 56, 493 (1982).

3) As one increases $\langle p_T^2 \rangle$ the soft contribution increases faster than the hard contribution. Thus if $\langle p_T^2 \rangle$ is adjusted to make hard scattering fit the data, then soft scattering would give a contribution roughly a thousand times larger than the data!

4) F_π is constrained by a rigorous asymptotic normalization so increasing $\langle p_T^2 \rangle$ cannot help this case.

One might, of course, also try other sorts of peculiar wavefunctions. For example, although the weak binding limit corresponds to $\eta \gg 1$ and both η_M and η_B evolve asymptotically to unity, one might consider using an $\eta < 1$ to fit F_π. However, this also runs into four difficulties:

1) A fit of the data with such a subasymptotic η_M would not be a test of QCD.

2) The use of $\eta_M < 1$ would lead to even larger soft contributions which would grow with Q^2.

3) The perturbative contributions calculated with $\eta_M < 1$ would be dubious. For example, with[10] $\eta_M = 1/4$, more than 50% of the "hard" scattering is due to the illegal end point region $x(1-x) < 0.05$.

4) The soft contributions to $F_\pi(Q^2)$ with $\eta_M < 1$ would lead to a nonanalytic dependence on Q^2 at $Q^2 = 0$.

Finally, we were able to show that even if one abandons all phenomonological constraints and ignores (for some reason) soft contributions entirely, it will be very difficult to provide a consistent picture of the data in terms of perturbative QCD alone. For factorizing ψ's with $\eta > 1$ one can show that

$$Q^2 F_\pi^{\text{pert}} \ll \{\alpha_s(Q^2)/\pi\} \frac{2Q^2}{3} \tag{7}$$

$$Q^4 G_M^{p\ \text{pert}} \ll \{\alpha_s(Q^2)/\pi\}^2 \frac{35Q^4}{54} \tag{8}$$

which are the bounds shown in Figures 10 and 11 on the maximum allowed perturbative contribution to the form factors at a given Q^2. These bounds result from a simple dilemma: if one tries to increase the hard scattering by, for example, increasing $\langle p_T^2 \rangle$, one always reduces the fraction of the wavefunction which can be used in the calculation of a perturbative high p_T tail to the wavefunction (since one is only allowed to integrate up to $p_T^2 \leq x_i^2 Q^2$ for scattering at Q^2). These bounds can only be saturated by allowing a behaviour for ψ which would in any event render perturbative QCD subdominant until much higher Q^2. Thus, although factorization is implausible and the bounds could be weakened somewhat by changing the argument of α_s, they clearly indicate further grave difficulties for interpretations of the data in terms of perturbative QCD.

Our results constitute a <u>prima facie</u> case that in other exclusive processes, such as electron-nucleus, πN, and pp elastic scattering, the calculable contributions due to n gluon exchange will not dominate until $Q^2 \gg (\alpha_s/\pi)^{-2} \text{GeV}^2$. If, as we suspect, this is so,

---

[10] As used in Fig. 12c of the first of Refs. 6

then it would appear to be impossible to ever test the many beautiful predictions of QCD for exclusive processes.

IV. RESONANCE PHOTOPRODUCTION AS A PROBE OF CHROMODYNAMICS

After drawing these pessimistic conclusions regarding certain tests of perturbative QCD with virtual photons, let me turn to one of the ways in which one can test the less precisely understood but perhaps more interesting non-perturbative features of QCD using real photons to explore the resonance region around 2 GeV. We should remember that QCD is still in its infancy so that although precise (and therefore very satisfying) results are at the moment only available in the perturbative regime $Q^2 \to \infty$, eventually we will extract non-perturbative results from this theory. Since these are the aspects of QCD that are new and interesting, corresponding to the regime in which the strong interactions are really strong, one could argue that in the long term experimental information on non-perturbative physics will prove to be more valuable than data relevant to perturbative QCD.

Unfortunately, at the moment our theoretical understanding of strong interactions is in a very rudimentary state. In particular, despite progress in numerical studies of QCD, for most purposes we must continue to rely on models of QCD for guidance. There are, in such circumstances, two key roles to be played by experimental strong interaction physics:

1) In spite of the rudimentary state of our understanding, there are some crucial known qualitative features of QCD which remain to be verified. These are: a) confirming the expected quantum numbers and rough level orderings of mesons and baryons, b) finding pure glue states, and c) finding hybrid mesons and baryons (in which both quark and gluonic degrees of freedom are in evidence).

2) Experiment must continue to check the quantitative predictions of models to produce progress in model building. This is valuable because a) even after precise numerical results are available, we will still want models to help us interpret them and b) successful models themselves suggest useful procedures to employ in numerical calculations (e.g., Zweig's rule suggests that the "quenched approximation" will be useful in lattice QCD studies).

The photoproduction of baryon resonances contains examples of both roles. Finding and cataloguing the baryons provides tests of both ordinary baryon spectroscopy and of the spectroscopy of baryon hybrids: their combined spectroscopy may be view as a qualitative test of the degrees of freedom of the three quark plus glue field system. Only somewhat more quantitative tests can distinguish between models for hybrid baryons. The bag model, for example, predicts that the first sets of nonstrange hybrids should appear in the 1.5-1.8 GeV range; this may be contrasted with some string model predictions which place the lowest such state at around 2.2 GeV. In addition, precise photoproduction measurements can be used as a fine probe of models for baryon structure.

In fact, we are faced at the moment with some interesting opportunities in baryon resonance physics. Of the 21 low-lying

(i.e., $2\hbar\omega$) positive parity N* and Δ* resonances predicted by the quark model, only about 10 have been found. The absence of the remaining states was initially interpreted by some as evidence that the naive quark model was miscounting degrees of freedom (e.g., that a baryon was "really" a diquark-quark system), but recent work indicates that the states are not absent from the spectrum, but rather just as yet undiscovered. More precisely, what Roman Koniuk and I showed [11] some time ago is that their absence could be explained in terms of mixings between and within SU(6) multiplets by the spin-dependent interactions (3) of QCD: unlike the pure SU(6) states, many of the mixed states tend to decouple from the πN channel. This means that they become almost impossible to see in $\pi N \to (N^*, \Delta^*) \to \pi N$ and very difficult to see in $\pi N \to (N^*, \Delta^*) \to XY$. The opportunity here for photoproduction is clear: γN is the only reasonable entrance channel for these resonances and $\gamma N \to (N^*, \Delta^*) \to XY$ where XY = πΔ, ρN, ωN, ΣK, ΛK, etc., completely avoids the suppressed πN coupling.

The search for such states needn't be carried out blindly. There is some evidence that the model Hamiltonian described in section II provides a good guide to the unknown terrain of these missing states. The most recent such evidence comes from the sighting of one such missing state, a $\Delta 5/2^+$ seen at around 1975 MeV, which had never been seen in πN elastic scattering but which was predicted to be observable in $\pi N \to \Delta^* \to \rho N$, where it has indeed just been found [12]. Table 5 lists some of the missing resonances which might be found in photoproduction; the predicted widths to various channels [11,13] are shown as a guide to those XY which are likely to prove the most fruitful.

These experiments will not be easy. But clearly the discovery of these resonances is an essential step in securing our understanding of baryon spectroscopy.

V. FINAL REMARKS

It now seems nearly certain that QCD is as fundamental to hadron and nuclear physics as QED is to atomic and molecular physics. Moreover, although the theory is very difficult to solve in the strong coupling regime, our understanding of the theory continues to improve. As it does we are able to produce more refined models for QCD which can act as interpolaters between the fundamental Hamiltonian and raw numerical solutions of the theory.

The lessons and opportunities in nucleon physics in this situation are manifold. In hadronic physics we can use QCD to understand more deeply the structure of the nucleon. With perturbative QCD we can

---

[11] R. Koniuk and N. Isgur, Baryon decays in a quark model with chromodynamics, Phys. Rev., 1868 (1980).

[12] D.M. Manley, Evidence for a second F_{35} pion-nucleon resonance near 2000 MeV, Phys. Rev. Lett. 52, 2122 (1984).

[13] R. Koniuk, Baryon-vector-meson couplings in a quark model with chromodynamics, Nucl. Phys. B195, 452 (1982).

TABLE 5: Some Missing Baryon Resonances (and Where to Find Them)

state	photoproduction amplitudes* $A^p_{3/2}$	$A^p_{1/2}$	$A^n_{3/2}$	$A^n_{1/2}$	strong coupling amplitudes** $N\pi$	$\Delta\pi$	$N\rho$	$N\omega$
$N\frac{5+}{2}(1955)$	+ 9	-67	-45	-22	0	- 7	- 8	+12
$N\frac{5+}{2}(2025)$	- 3	+ 2	+51	+15	1	- 7	+ 7	-11
$\Delta\frac{5+}{2}(1975)$	+76	+61			1	+ 6	-18	na
$N\frac{3+}{2}(1870)$	+ 6	-19	- 6	-21	3	- 4	+ 1	-10
$N\frac{3+}{2}(1955)$	+ 4	-16	-39	+ 6	1	- 9	+ 6	- 9
$N\frac{3+}{2}(1980)$	- 5	+19	+22	-20	1	+ 9	- 7	+ 3
$N\frac{3+}{2}(2060)$	0	- 1	-15	+ 2	1	+ 5	- 3	+ 9
$\Delta\frac{3+}{2}(1975)$	- 7	+18			0	- 8	+ 5	na
$N\frac{1+}{2}(1890)$		-20		- 1	4	+ 3	- 5	+ 6
$N\frac{1+}{2}(2055)$		+ 7		+ 3	1	+ 2	- 1	- 5

*the sign quoted here does not include the usual $A_{\frac{1}{2}}\pi N$ sign since it is irrelevant ; see Ref. 10 for details.

**when more than one LS state is possible, the largest is quoted; see Refs. 10 and 12 for details.

analyze the deep inelastic structure functions, Drell-Yan processes, high p_T jets, etcetera, but alas, probably not elastic form factors. With models for chromodynamics and numerical solutions of QCD on a lattice we can explore the static properties of the nucleons and their excitation spectra, including both ordinary baryons and hybrids. In nuclear physics it seems to me that we are in a position to begin making progress at the foundations of the subject: we can understand why nuclear physics is approximately the physics of nucleons and we can begin to understand the origins of nuclear forces. We can also begin to study quark and colour effects in nuclei, but with an appreciation of the fact that they will normally manifest themselves only as subtle departures from the multi-nucleon approximation.

ACKNOWLEDGEMENTS

The three vignettes described in these lectures were, as already mentioned, based on collaborations with Kim Maltman, Chris Llewellyn Smith, and Roman Koniuk. In addition to them I would like to

acknowledge conversations on these and related topics with many people, including Malcolm Harvey, Gabriel Karl, and Jack Paton. More adequate references to the topics discussed here can be found in the works cited. The research reported in these lectures was supported in part by a grant from the Natural Sciences and Engineering Research Council of Canada.

QUARK SIGNATURES IN NUCLEAR PHYSICS

C. E. Carlson
Physics Department
College of William and Mary
Williamsburg, VA 23185

Nuclear physicists are today interested in two theories of the fundamental degrees of freedom which can be used to describe nuclei or nuclear matter. One I shall call classical nuclear physics, and I am reminded that this might also be called quantum hadrodynamics. Classical nuclear physics is a phenomenological theory written in terms of nucleons bound together by a finite number of different types of mesons and it is expected to be valid within certain limits. The other theory is quantum chromodynamics[1] (QCD) and it is thought to be the fundamental theory of strong interactions. This theory should be correct in any situation. However, calculations using QCD are easy only when we can use perturbation theory and this is possible only at very short range or high momentum transfers and so we shall henceforth take "QCD" to mean "perturbative QCD."

It is important to contrast the consequences of QCD with those of classical nuclear physics. In certain situations, the qualitative high momentum transfer predictions of QCD and classical nuclear physics are the same. This is not the most interesting situation, although one experimenter happily pointed out the possibility of disproving both theories with one experiment. Still we should search for situations where QCD and classical nuclear physics do not give the same result and see for what parameter or what momentum transfers one theory begins to fail and the other theory to succeed.

In the bulk of this talk we will focus on high Q^2 elastic electron deuteron scattering. We will first point out a situation where classical nuclear physics and QCD give the same behavior, and afterwards show that with respect to the spin dependence of this process the two theories do not give the same result. Then we shall close with some remarks about when (i.e., at what momentum transfers) we might expect perturbative QCD to be valid.

The differential cross section for elastic electron-deuteron scattering is given by

$$d\sigma/d\Omega = d\sigma/d\Omega|_{NS} \ (A + B \tan^2 \theta/2), \qquad (1)$$

where θ is the electron's lab scattering angle, "NS" indicates a "no structure" differential cross section, and the functions A and B are given in terms of the charge, magnetic, and quadrupole form factors by

$$A(Q^2) = G_C^2 + \frac{2}{3}\eta G_M^2 + \frac{8}{9}\eta^2 G_Q^2 \tag{2}$$

$$B(Q^2) = \frac{4}{3}\eta(1+\eta)G_M^2 \tag{3}$$

with

$$\eta = Q^2/4M_d^2 \tag{4}$$

Let us determine the Q^2 dependence of the form factors at high Q^2. It suffices to consider the deuteron as a collection of parallel moving constituents, six quarks in QCD as in Fig. 1a.

Fig. 1a

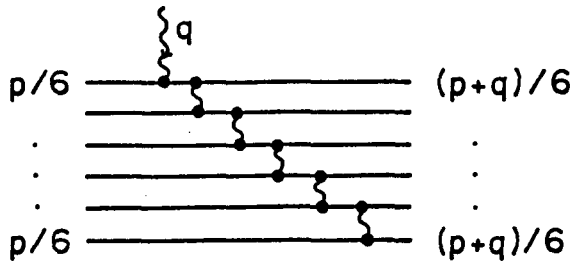

Fig. 1b

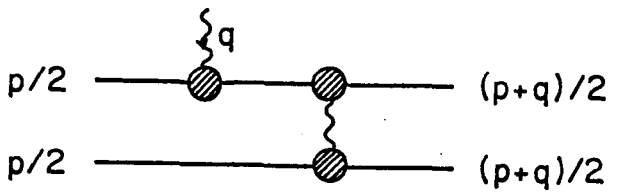

One of the quarks absorbs a virtual photon of momentum q, with $Q^2 = -q^2 > 0$. To rebind the deuteron the momentum must be shared about equally among the six quarks. We deal with a Q high enough to be much greater than the mean Fermi momentum of the quarks. The Fermi momentum distribution will determine how much deviation from equal sharing of momentum is allowed and so sets the scale of normalization but does not determine the asymtotic dependence of the amplitude on Q^2.

Analysis of Fig. 1a shows that we get a $1/Q^2$ from each far off shell quark propagator (there are 5 of these) and that other factors of Q from the numerators of the quark propagators, the

vertices, and the gluon propagators all cancel. The same result holds for any of the other diagrams that contribute to the deuteron form factor. This leads to a by now well known prediction[2,3]

$$[A(Q^2)]^{1/2} \sim 1/Q^{10}. \qquad (5)$$

One may however also do the same analysis using the "neutron-proton model" of the deuteron,[4] Fig. 1b. Now form factors should be inserted for the electromagnetic vertex and for the two meson-nucleon-nucleon vertices. As above, we get a $1/Q^2$ from the fermion propagator and factors of Q from the numerator of the fermion propagator, dirac matrices at the vertices, and meson propagator all cancel. Putting in standard dipole or monopole form factors at the vertices then leads to

$$[A(Q^2)]^{1/2} \sim (1/Q^4)(1/Q^2)^2(1/Q^2) = 1/Q^{10} \qquad (6)$$

This is the same as for QCD!

Perhaps we should take a pause in our presentation to see how well the data supports us so far. In Fig. 2a we show the data[5] for $A(Q^2)$ for Q^2 above .8 $(GeV)^2$ plotted versus Q^2. The falloff

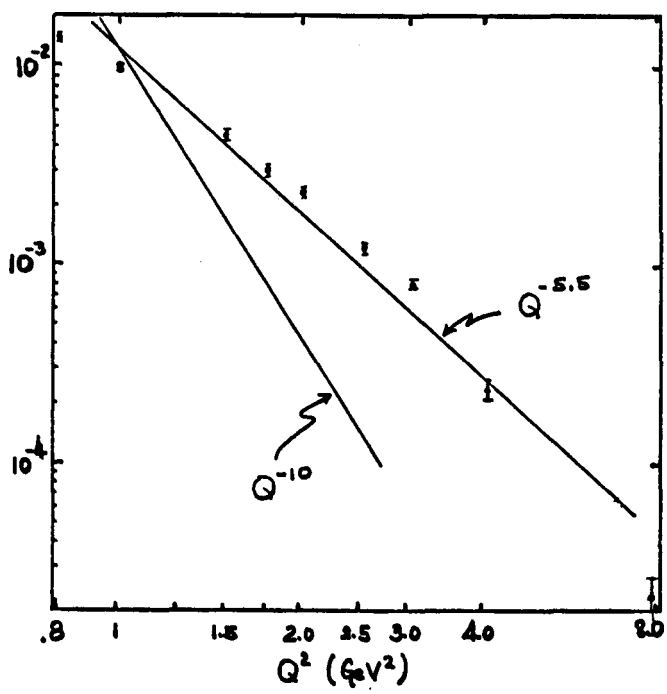

Fig. 2a. The deuteron form factor, $A^{1/2}$

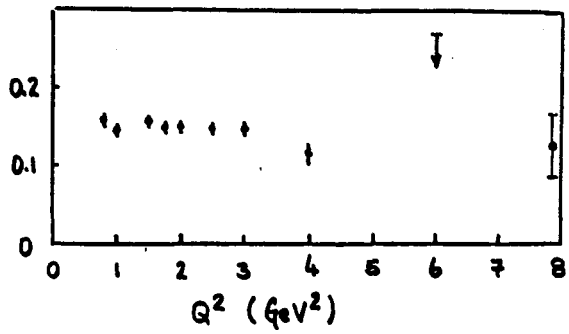

Fig. 2b. The reduced form factor $Q^2 f_d$

appears more like $Q^{-5.5}$ than like Q^{-10}, at least if we fit with a simple power. This could mean that the simplest result of perturbative QCD will not work until somewhat higher Q^2. However, it seems possible to guess the main corrections to the simple power law dependence. The lower three quarks in Fig. 1a absorb a massless vector boson with momentum q/2 and then share the momentum absorbed evenly among the three quarks, very much like an electromagnetic form factor. Similar things can be said about the top three quarks in the same figure. So we may conjecture that two factors of $1/Q^4$ in the $1/Q^{10}$ prediction have the same form as nucleon electromagnetic dipole form factors evaluated at $(Q/2)^2$. We define a "reduced form factor"

$$f_d(Q^2) = [A(Q^2)]^{1/2} / F_N^2(Q^2/4) \sim 1/Q^2 \qquad (7)$$

which should fall as $1/Q^2$, as indicated, and in Fig. 2b we show a plot of $Q^2 f_d(Q^2)$ versus Q^2. The flatness of the resulting curve suggests that we have made the perturbative QCD result work at a lower Q^2 by considering the reduced form factor and for the record we should state that the suggestion to use the reduced form factor preceeded rather than postdated the experimental data.

However for the spin independent data the basic QCD and classical nuclear physics results are the same and we shall proceed to the spin dependent cases[7] where the results are not similar. We can analyze[8] the spin dependence of a diagram like Fig. 1a with help from some simple rules. We shall give three, and they can easily be verified in the Breit frame. (Fig. 1a is just one of $O(10^6)$ diagrams that can be drawn in leading order for the deuteron form factor. A few more rules are needed to analyze all of them. The result is that they all behave the same way as Fig. 1a. Demonstrating this is easier than one might imagine without trying it, but will not be done here.)

The one gluon rule (Fig. 3a). This is part of the larger diagram. If the absorbed gluon is transverse (T), this piece is proportional to Q and conserves helicity; if the absorbed gluon is longitudinal (L), this piece is proportional to m (some mass scale) and flips quark helicity.

Fig. 3a.

Fig. 3b.

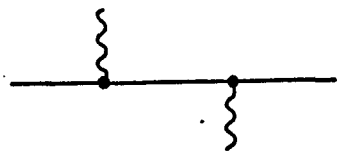

The two gluon (or gluon-photon) rule (Fig. 3b). Two gluons attach to a given quark line. If one gluon is T and the other L, the amplitude is constant in Q^2 (this includes the quark propagator but not the gluon propagators) and conserves helicity. This is the largest two-gluon amplitude. If both gluons are longitudinal the amplitude is O(m/Q) with quark helicity flipped and if both gluons are transverse the amplitude is zero.

The transverse gluon rule. Two quark lines connected by a transverse gluon have opposite helicity. There is no helicity correlation for two quarks connected by a longitudinal gluon.

The largest helicity amplitude for the deuteron form factor then falls like Q^{-10} compared to the leading amplitude for a single pointlike particle and is a helicity $0 \to 0$ transition. To get the largest amplitude for Fig. 1a the bottom gluon must be T and then L and T must alternate. Three pairs of quarks are connected by T gluons and so must have pairwise opposite helicities, and the total helicity of both the initial and final state is zero. Amplitudes with other initial and final helicities may be considered and are suppressed by powers of m/Q that can be determined using the above rules.

To express the results more formally we define the matrix elements of the electromagnetic current J,

$$G_{I,\lambda\lambda'} = \langle d',\lambda' | \varepsilon_I \cdot J | d,\lambda \rangle \qquad (8)$$

where ε_I, I = T or L, is the polarization vector of the photon and d and λ are the momentum and helicity of the incoming

deuteron. There are three independent G_I (not counting amplitudes related by parity or time reversal to the ones to be given) and they are, in the Breit frame,

$$-(1/Q)G_{L,00} = G_C + \frac{4}{3}\eta G_Q = \text{const} \cdot Q^{-10} \tag{9}$$

$$(1/Q)G_{L,+-} = G_C - \frac{2}{3}\eta G_Q = \text{const} \cdot Q^{-12} \tag{10}$$

$$-(1/Q)G_{T,+0} = \sqrt{\eta}\, G_M = \text{const} \cdot Q^{-11} \tag{11}$$

where the middle relation in each case comes from looking up the definitions[9] of the charge, magnetic, and quadrupole form factors from the electromagnetic current matrix elements and the last relation is the result of our QCD analysis.

From the above we see that G_C falls like Q^{-10}, G_M and G_Q both fall like Q^{-12}, and the leading order cancellation in $G_{L,+-}$ leads to the main result[8]

$$G_C = \frac{2}{3}\eta G_Q \tag{12}$$

at high Q^2.

We have already seen using Fig. 1b how classical nuclear physics can give the same result as QCD if the spin dependence is not examined. However in classical nuclear physics the exchanged particles could be scalar and pseudoscalar mesons and these exchanges flip the fermion helicities to leading order in (m/Q) so the spin predictions are not the same. A way to "fake" the QCD results is to allow, at high Q^2, only vector meson exchanges with only γ_μ couplings, but this is not a traditional procedure. In general, the helicity amplitude $G_{L,+-}$ will not be suppressed but will be dominated by scalar, pseudoscalar, and tensor coupled vector meson exchange at high Q^2, and the ratio G_C/G_Q will not be given by eqn. (12) but will depend on the relative size of the various coupling constants and the meson-N-N form factors. Some results for specific classical nuclear physics models will appear below.

We shall recall, now as a QCD test, one of the methods that has been suggested[10] for separating G_C and G_Q, namely measuring the polarization ratio p_x/p_{xz}. The vector polarization of the outgoing deuteron need not be zero if the initial electron is polarized, and p_{xz} is a tensor polarization. Since we will take ratios of form factors, if the causes of the non-leading corrections are similar in all cases, they may be expected to cancel out. We have

$$I_o p_x = -\frac{4}{3}\left[\eta(1+\eta)\right]^{1/2} G_M(G_C+\eta G_Q/3)\tan\theta/2 \qquad (13)$$

$$I_o p_{xz} = -2\eta\left[\eta+\eta^2\sin^2\theta/2\right]^{1/2} G_M G_Q \sec\theta/2 \qquad (14)$$

where $I_o = A + B\tan^2\theta/2$. Thus for high Q^2

$$p_x/p_{xz} = \frac{2}{3}(G_C+\eta G_Q/3)/\eta G_Q = \frac{2}{3} \qquad (15)$$

where the last equality used eqn. (12).

A plot of this polarization ratio for several classical nuclear physics models of the deuteron wave function is shown in Fig. 4. The Q's on this plot are not "asymtotic", but are in the range where agreement with QCD may work[3,6] for $A(Q^2)$. The classical nuclear physics predictions differ in both sign and magnitude from the asymtotic QCD prediction. If we suppose that the form factors G_C and G_Q have their asymtotic ratio but take account of the kinematic factors given in eqn. (12), the predictions from QCD are reduced for $\theta < 180^o$ (to the curve labelled "QCD" in Fig. 4 -- the line is not quite horizontal) but the difference from classical nuclear physics is still dramatic.

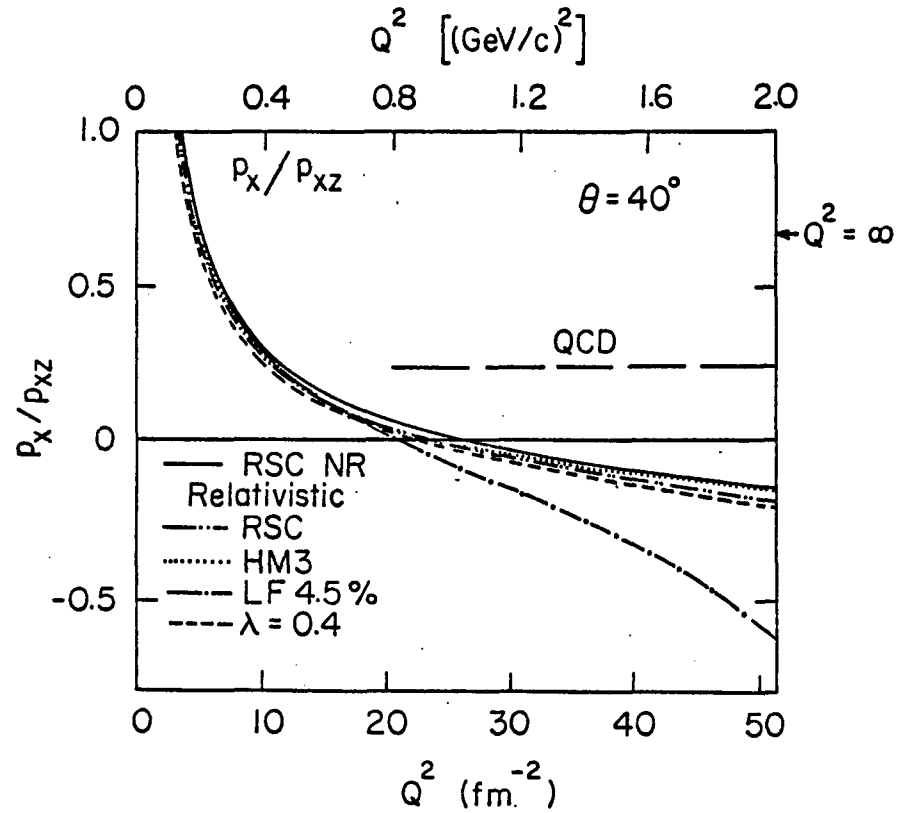

Fig. 4.

The contrast is also dramatic for the p_{zz} (also called T_{20}) as may be seen in a figure presented by Roy Holt in his talk at this conference.

A few comments may be made, inspired by experimental data, regarding what Q^2 is sufficient for perturbative QCD to work. We shall compare data to perturbative QCD predictions at the level of seeing if the correct power law falloff is observed. For example, we have the prediction for hadron form factors that they fall like $(1/Q^2)^{n-1}$ where n is the number of constituent quarks. This may or may not be working for the deuteron, but for the proton $Q^4 G_{Mp}(Q^2)$ is fairly constant[11] for Q^2 greater than 5 $(GeV)^2$.

(We should remember that there is a distinction between "power law asymtopia" and "logarithmic asymptopia". One is where the leading power of Q^2 as predicted by QCD is dominating the $O(m^2/Q^2)$ corrections. This can happen at a relatively modest Q^2. The data however will still show $\log(Q^2/\Lambda^2)$ deviations from the pure power law and the magnitude of these deviations cannot at present be predicted until we reach extremely extremely high momentum transfers.)

Other exclusive processes also have QCD predictions for their high momentum transfer behavior. If we have a two body to two body scattering

$$A + B \rightarrow C + D \qquad (16)$$

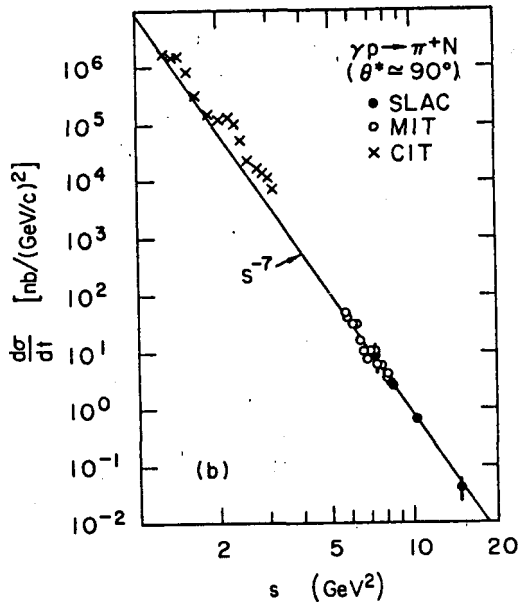

Fig. 5

then according to QCD scattering at fixed angle in the c. m. will fall with s, the c. m. energy squared, like[2,12]

$$d\sigma/dt \sim s^{2-N_A-N_B-N_C-N_D} \qquad (17)$$

where N_A is the number of quarks (or elementary fields) in A, etc. We shall show one example of this,[12] perhaps the best working of the lot, namely $\Upsilon + p \rightarrow \pi^+ + n$. Here the above rule claims $d\sigma/dt \sim s^{-7}$. The data is shown for c. m. scattering angle fixed at 90^0 in Fig. 5. It appears that

the QCD prediction works for Q^2 above 2 $(GeV)^2$. Other examples may be found in Ref. 12. There have been criticisms of applying perturbative QCD at momentum transfers as low as a few GeV,[13,14] but at least some of these criticisms apply more to "logarithmic asymtopia" than "power law asymtopia" and must at least be balanced against data which rather often picks out the power law behavior suggested by QCD.

We close by summarizing our main point that while overall results from QCD and classical nuclear physics can be rather similar, individual helicity amplitudes can be quite different. We have given one example of this as a prediction of a defintie ratio for two of the deuteron's electromagnetic form factors. The predictions from classical nuclear physics are quite different from QCD for momentum transfers greater than 1 $(GeV)^2$. Measurements of the relevant polarization may be quite feasible, and if not done before the forcoming SURA machine is ready will add greatly to that facility's interest.

REFERENCES

1. Reviewed by W. Marciano and H. Pagels, Physics Reports 36,137 (1978).
2. S. J. Brodsky and G. R. Farrar, Phys. Rev. Lett. 31,1153 (1973) and Phys. Rev. D 11, 1309 (1975); V. A. Matveev, R. M. Muradyan, and A. N. Tavkhelidze, Lett. Nuovo Cimento 7, 719 (1973).
3. S. J. Brodsky and B. T. Chertok, Phys. Rev. Lett. 37, 269 (1976) and Phys. Rev. D 14, 3003 (1976).
4. R. Woloshin, Phys. Rev. Lett. 36, 220 (1976); M. Gari and J. Hyuga, Nucl. Phys. A264, 409 (1976).
5. R. G. Arnold et al, Phys. Rev. Lett. 35, 776 (1975).
6. S. J. Brodsky, C.-R. Ji, and G. P. Lepage, Phys. Rev. Lett. 51, 83 (1983).
7. A. I. Vainshtein and V. I. Zakharov, Phys. Lett. 72B, 368 (1978).
8. C. E. Carlson and F. Gross, Phys. Rev. Lett. 53, 127 (1984).
9. See for example R. G. Arnold, C. E. Carlson, and F. Gross, Phys. Rev. C 21, 1426 (1980).
10. R. G. Arnold, C. E. Carlson, and F. Gross, Phys. Rev. C 23, 363 (1981).
11. See for example Fig. 14a of G. P. Lepage and S. J. Brodsky, Phys. Rev. D 22, 2157 (1980) or Fig. 2 of Ref. 13.
12. D. Sivers, S. Brodsky, and R. Blanckenbecler, Physics Reports 23, 1 (1976).
13. N. Isgur and C. H. Llewellyn Smith, Phys. Rev. Lett. 52, 1080 (1984).
14. V. A. Nesterenko and A. V. Radyushkin, "Quark-hadron duality and nucleon form factors in QCD," JINR preprint E2-83-464 (Dubna 1983).

What can we learn about the

Three-Nucleon Wave Functions

from

High Energy Electrons

Christian Hajduk
Physics Department
SUNY at Stony Brook, NY 11794

Abstract The theoretical interpretation of elastic and quasielastic electron scattering experiments on the three-nucleon ground states is reviewed. Additional experimental information is called for and the need for improved calculations within traditional nuclear physics is emphasized.

1. Introduction

When preparing this talk I wondered, what was I expected to speak about as a theorist at the site of a future important experimental facility? So I tried to figure out, what kind of experimental results are esteemed highest in the physics community. I came up with the following ranking:

1. The totally unexpected.
2. Refutation of a well established theory.
3. Confirmation of a new theory.
4. Rejection of a new theory.
5. Confirmation of an already well established theory.

Clearly by definition one can never preclude possibility 1. but by the same definition there is nothing I could do about it. My subject, classical theoretical nuclear physics (in this context classical means nuclear physics disregarding quark degrees of freedom) certainly qualifies as well established — it has been with us for forty years now. This eliminates numbers 3 and 4. So in an ideal world I were to review the available theoretical calculations and state results like: "If you don't find a diffraction minimum in the triton charge form factor at $4.0 \pm 0.2 fm^{-1}$, we have to abandon the theory." You then had to decide, if you wanted to run against the odds of measuring it at $3.9 fm^{-1}$ and consequently boring every audience. And maybe you became famous by not.

Unfortunately, in real nuclear physics it is virtually impossible to find rock solid predictions of that kind. It is far more probable, that *after the fact* half a dozen theorists will show up claiming they can explain your measurements. Three of them

will use the standard theory fiddling around with approximations and parameters, while the other three will make *ad hoc* assumptions how to patch the classical model up. The reason is, I have to admit, that nuclear theory does not live up to its promise of performing rigorous calculations or at least giving bounds on the errors caused by the approximations introduced along the way. I hope to illustrate this point while proceeding.

After these preliminaries I now ought to address the proper subject of my talk: Doubtlessly electron scattering is a venerable tool of proven usefulness in nuclear physics. However you don't want to employ a high energy continuous wave electron accelerator to measure bulk properties of nuclear wave functions, such as the electromagnetic radii or the width of the momentum distribution of nucleons inside a nucleus. Instead the emphasis has shifted to the experimental investigation of more intricate details:

— high momentum components in the wave function as finger prints of short range correlations and the nucleon-nucleon interaction.

— exotic components in the wave function like excited nucleons: Δ isobars, roper resonances etc.

— more complicated interactions of the electromagnetic probe with the nucleus like many body or meson exchange currents (MEC).

I will discuss, how these show up in electron scattering off ^{3}He and ^{3}H, the only nuclei, I know anything appreciable about.

However already at this stage I want to make an important reservation: All of the above effects exist, but it is impossible to disentangle them completely from each other. Take for instance the high momentum components on one hand and MEC on the other: The occurrence of a high momentum nucleon results from the exchange of a meson.

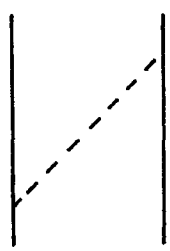

Figure 1.1 Exchange of a meson between two nucleons in time-ordered perturbation theory.

Hook a photon onto one of the nucleons.

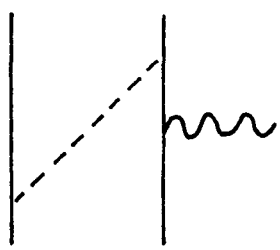

Figure 1.2 Exchange of a meson between two nucleons and simultaneous coupling to an external photon in time-ordered perturbation theory.

It is now a complete matter of taste, to attribute the effect of this diagram either to the nuclear wave function or to the current operator or to use any mixture.
The situation is similar for isobar admixtures to the wave function. The diagram

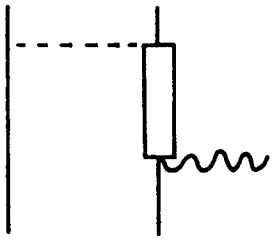

Figure 1.3 Interaction of two nucleons with an external photon via an intermediate Δ isobar.

can either be interpreted as a manifestation of virtual Δ isobars or, as is common practice, treated as just another meson exchange current.

In the first half of my talk I want to address elastic electron scattering off ^{3}He and ^{3}H, while the second half will be dedicated to quasielastic scattering and coincidence experiments.

2. Elastic Scattering

Elastic scattering off the trinucleon ground states may be not too challenging for experimentalists. However it has the advantage, that it is best understood theoretically: Within the Schrödinger theory and for given potentials initial and final states are calculable to known precision. This statement, however, does not apply to relativistic effects and mesonic degrees of freedom. I want to demonstrate a few principles for the relatively simple case of elastic scattering before proceeding to inelastic processes.

The cross section for elastic electron scattering from a spin-$\frac{1}{2}$ object is characterized by two amplitudes A and B

$$\frac{d\sigma}{d\Omega} = \frac{d\sigma}{d\Omega}_{Mott} Z^2 \left(A(Q^2) + \tan^2 \Theta/2 \, B(Q^2) \right) \tag{2.1}$$

where

$$\frac{d\sigma}{d\Omega}_{Mott} = \frac{\alpha^2}{4E_e^2} \frac{\cos^2 \Theta/2}{\sin^4 \Theta/2} \quad . \tag{2.2}$$

A and B can in principle be separated in a Rosenbluth plot. B is given by the transverse magnetic matrix element

$$B(Q^2) = \frac{2}{Z^2} \left(\frac{Q}{2m} \right)^2 \left(1 + \left(\frac{Q}{2M_A} \right)^2 \right) |F_{mag}(Q^2)|^2 \tag{2.3}$$

and A is an incoherent superposition of coulomb and transverse magnetic matrix elements

$$A(Q^2) = |F_{ch}(Q^2)|^2 + \frac{1}{2} B(Q^2) \quad . \tag{2.4}$$

Experimentally, for ^{3}He targets A is known up to momentum transfers of $Q = 10fm^{-1}$ [1], while B has been recently measured in Saclay [2] for $Q < 6fm^{-1}$. Very little information [3] is available about the corresponding amplitudes for ^{3}H. The two theoretically relevant objects are the charge and magnetic form factors F_{ch} and F_{mag}.

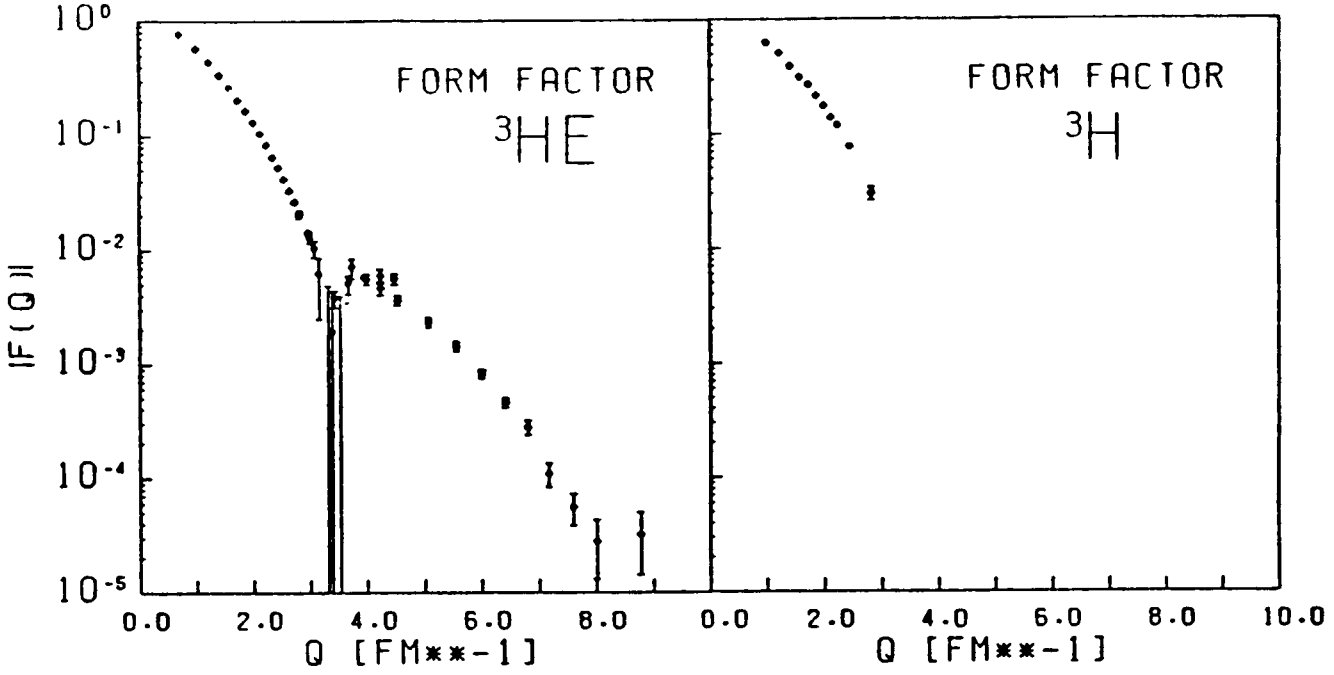

Figure 2.1 Compilation of the available experimental information [1] [3]on the charge form factors of ^{3}He and ^{3}H.

Let us first look at the charge form factor F_{ch}. As far as the amplitude B is measured, F_{ch} can be extracted from A. For higher momentum transfers it is assumed, that the contributions to A arising from magnetic scattering are small. Figure 2.1 shows the existing experimental information on both nuclei ^{3}He and ^{3}H.

I am going to compare these data to calculations [4] based on wave functions obtained by solving the nonrelativistic Faddeev equations using the Paris potential [5]. about the best calculation one can do today. The charge form factor calculation contains only contributions from the impulse approximation (IA), i.e. only the free currents of single nucleons are accounted for. Charge conservation guarantees that MEC corrections are zero at momentum transfer $Q = 0$. Let us assume for the moment, that this persists up to higher momentum transfers.

Comparing calculation and experiment for ^{3}He in figure 2.2 (the data for ^{3}H are completely inconclusive) one notes a factor 1/3 between theory and experiment in the secondary maximum, that is already at relatively moderate momentum transfers of $Q \approx 4fm^{-1}$. Since the charge form factor is essentially a convolution integral

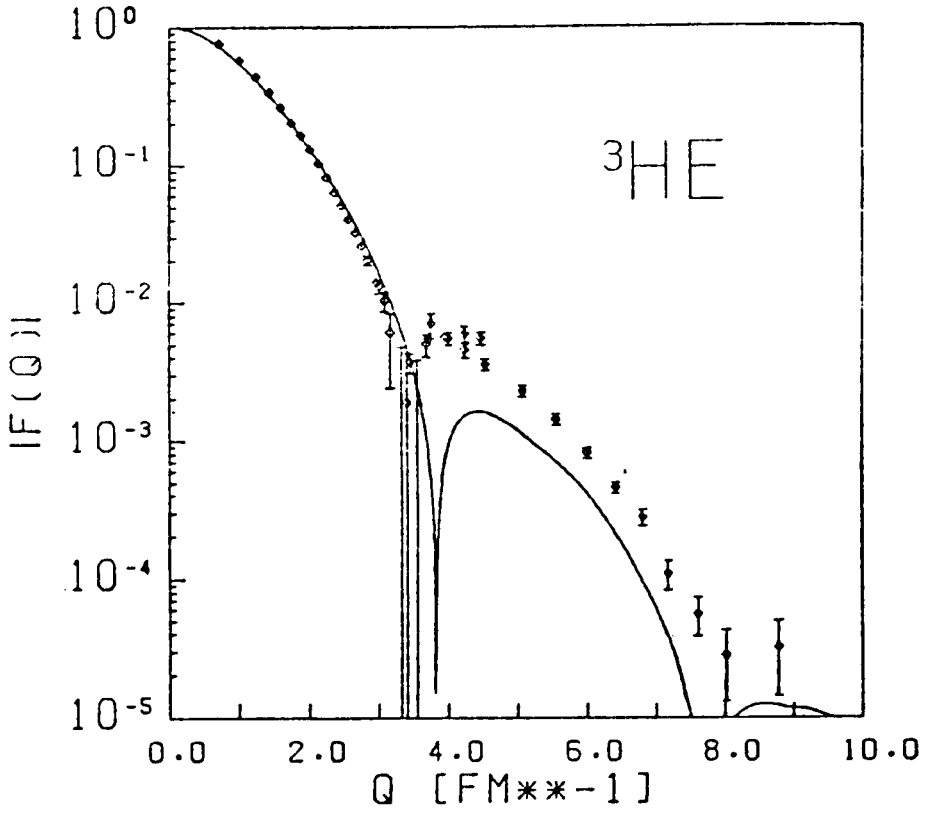

Figure 2.2 The ^{3}He charge form factor calculated [4] in impulse approximation from a wave function obtained using the Paris potential.

over the momentum space wave function

$$F_{ch}(Q^2) \propto \int d^2\hat{Q} \int d^3p\, d^3q\, \Psi_3(\vec{p},\vec{q})\Psi_3(\vec{p},\vec{q}+\tfrac{2}{3}\vec{Q}) \tag{2.5}$$

one is lead to the conclusion, that the theoretical wave function lacks high momentum components [6]. Note in passing, that the components we are talking about are a tiny detail indeed: their norm integral accounts for less than .5% of the total.

One may look at the same facts in a slightly different way, introduced by I. Sick [7], by Fourier transforming the charge form factor into a proton density. Then — see figure 2.3 — one observes a pronounced central depression in the quasiexperimental density which does not at all show up in the theoretical one. This has lead various groups [8] [9] into speculations about three-body forces favoring the triangular configuration in figure 2.4 over the collinear one.*

* In fact, the Δ mediated two-pion exchange three-body force does show this kind of geometrical behaviour [10], however the effect on the wave function turns out to be far too small to explain figure 2.3.

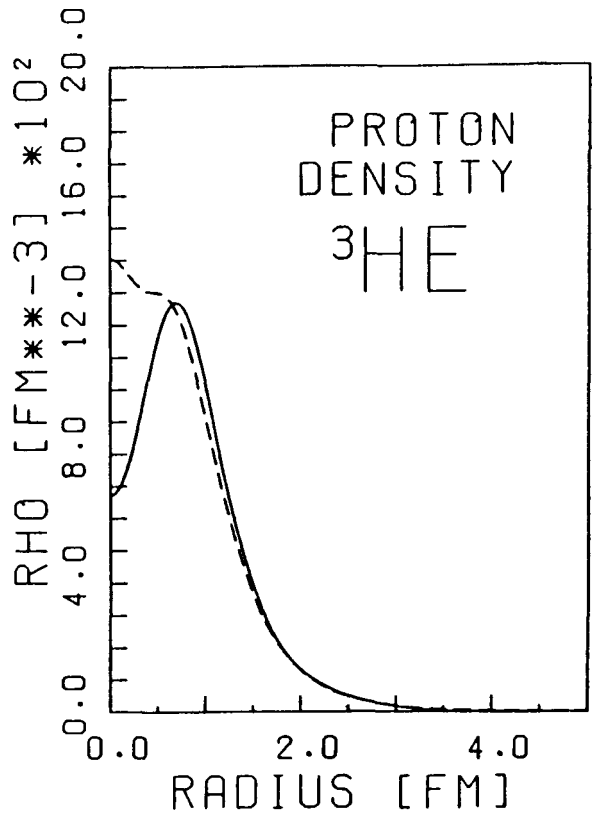

Figure 2.3 Comparison between the quasiexperimental (solid) [7] and the theoretical (dashed) [4] point proton density in ^{3}He.

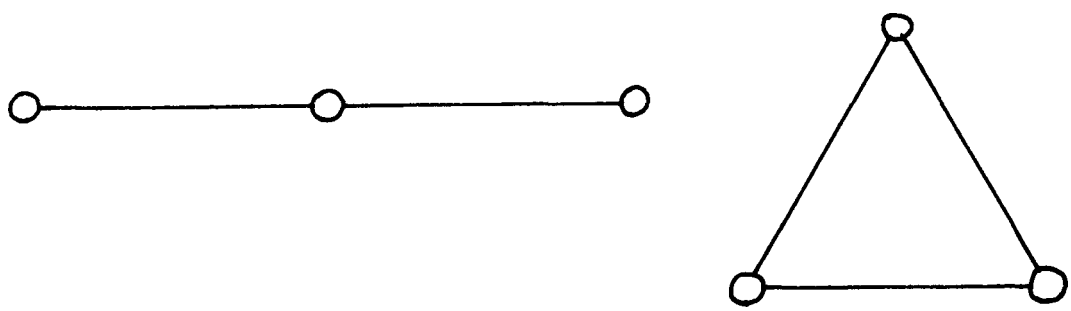

Figure 2.4 The density at $r = 0$ corresponds to a collinear configuration (a) of the three nucleons, while the maximum in fig. 2.3 occurs roughly at a triangular configuration (b), when two nucleons are at their equilibrium separation.

Thus it looks like the charge form factor could teach us quite interesting details about the ^{3}He wave function. Note however, that the whole discussion is based on a highly model dependent analysis of experimental data. If it turns out, that processes other than the currents of single nucleons become important, the whole argument collapses. I will return to the question of possible MEC contributions to

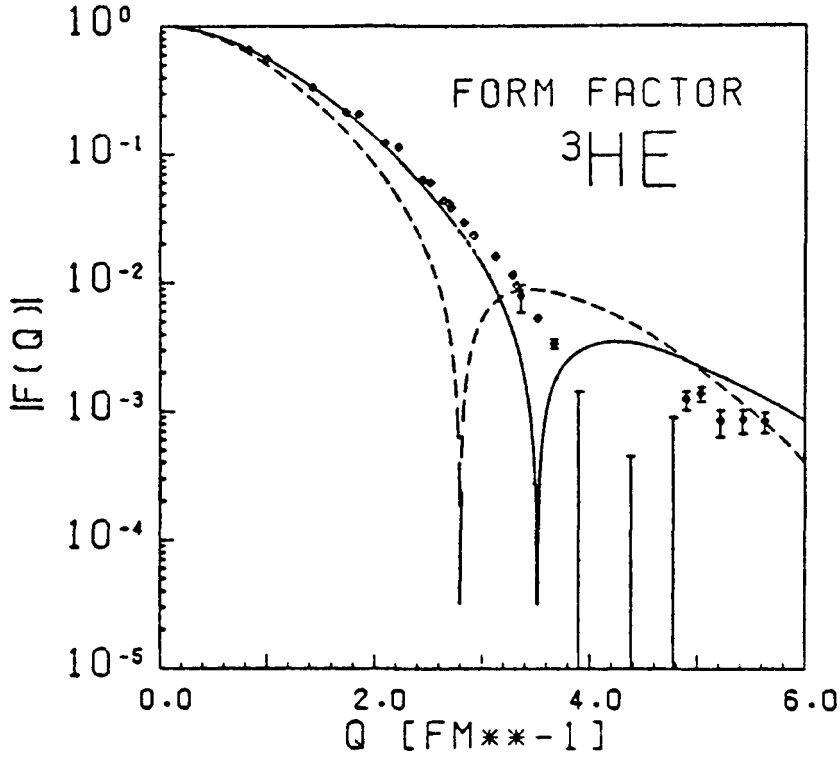

Figure 2.5 The ^{3}He magnetic form factor, impulse approximation (dashed) and calculation including MEC of $O(1/M)$ (solid) [20].

the charge form factor in a moment.

Consider next the magnetic form factor. There the impulse approximation fails dramatically, see figure 2.5. MEC corrections are important already for $Q = 0$, as has been noted by Villars [11] and Sachs[12] more than 35 years ago. In fact, according to the classification scheme developed by J. Friar [13], impulse approximation and meson exchange currents for transverse magnetic matrix elements are of the same order in $\frac{1}{M}$ in an expansion around the nonrelativistic limit.

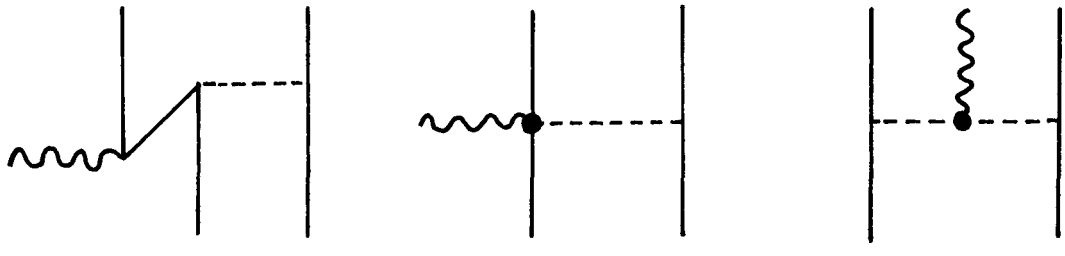

Figure 2.6 Meson exchange current diagrams: pair current (a) and contact term (b) are equivalent in lowest order $1/M$, mesonic current (c).

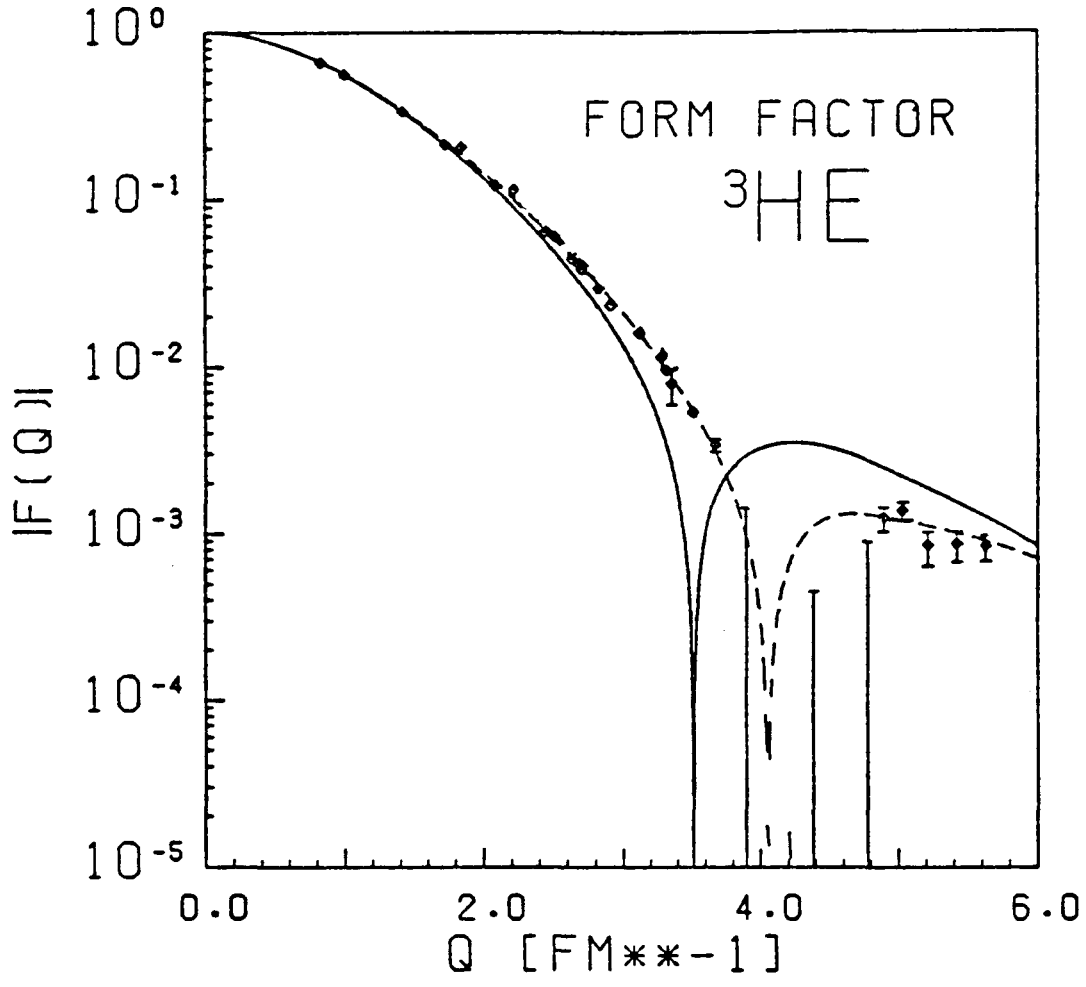

Figure 2.7 Difference in the ^{3}He magnetic form factor arising from use of F_1^v (dashed) or G_E^v (solid) as a form factor [20].

The dominant isovector MEC operators are well defined and generally agreed upon [14] [15]. The calculation of expectation values for these operators in the three-nucleon groundstates too is slowly converging [16] [17] [18]. Differences still arise about the question, what prescription to choose for regularizing the vertices in the considered diagrams. I present here the calculation by W. Strüve [18] [19] [20] based on the same wave function [4] as the one for F_{ch}. One realizes an agreement between theory and experiment now comparable to the one achieved for the charge form factor. The two latest competing calculations give a slightly better fit to the data for two different reasons. First they overestimate the Δ MEC of figure 1.3 because of unjustified approximations in their perturbative treatment [21]. Second and more important, they use F_1^v instead of G_E^v as a form factor at the electromagnetic vertices. As advocated by Arenhövel [22] the use of G_E^v is dictated by current conservation. On the other hand Riska and Mathiot [23] have argued, that for purely

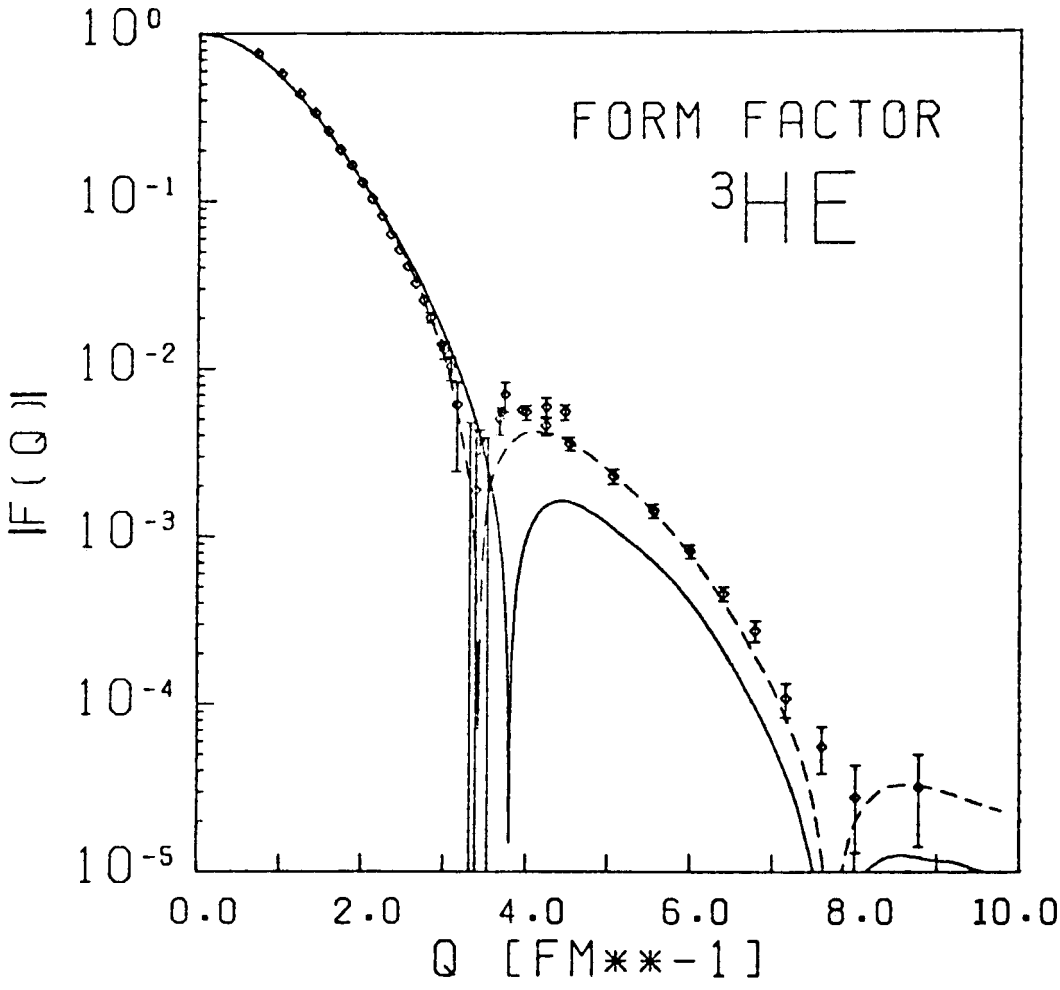

Figure 2.8 Calculation [20] of the ^{3}He charge form factor including pair current and NΔ transition current contributions (dashed) and IA as in fig. 2.2 (solid).

transverse observables like the magnetic form factor the use of F_1^v is adequate.

I take the following view on that subject: in leading nonrelativistic order we obtain comparable fits of F_{mag} and F_{ch}. If there are significant corrections of higher relativistic order — and the effect of the difference between F_1^v and G_E^v is $O(1/M^3)$ — we see the need for treating this order systematically. Unless that is done we can not decide what prescription represents the better theory: agreement with a single experiment can not be the sole criterion for a good theory!

For the charge form factor too, some relativistic corrections have been calculated: here MEC correctons are of order $O(1/M^2)$ while the IA is $O(1)$. Including the pair current (figure 2.6a) and the Δ transition current (figure 1.3) in fact improves the agreement between theory and experiment dramatically [19] [16], as proven by figure 2.8. However again this is no systematic treatment and the same

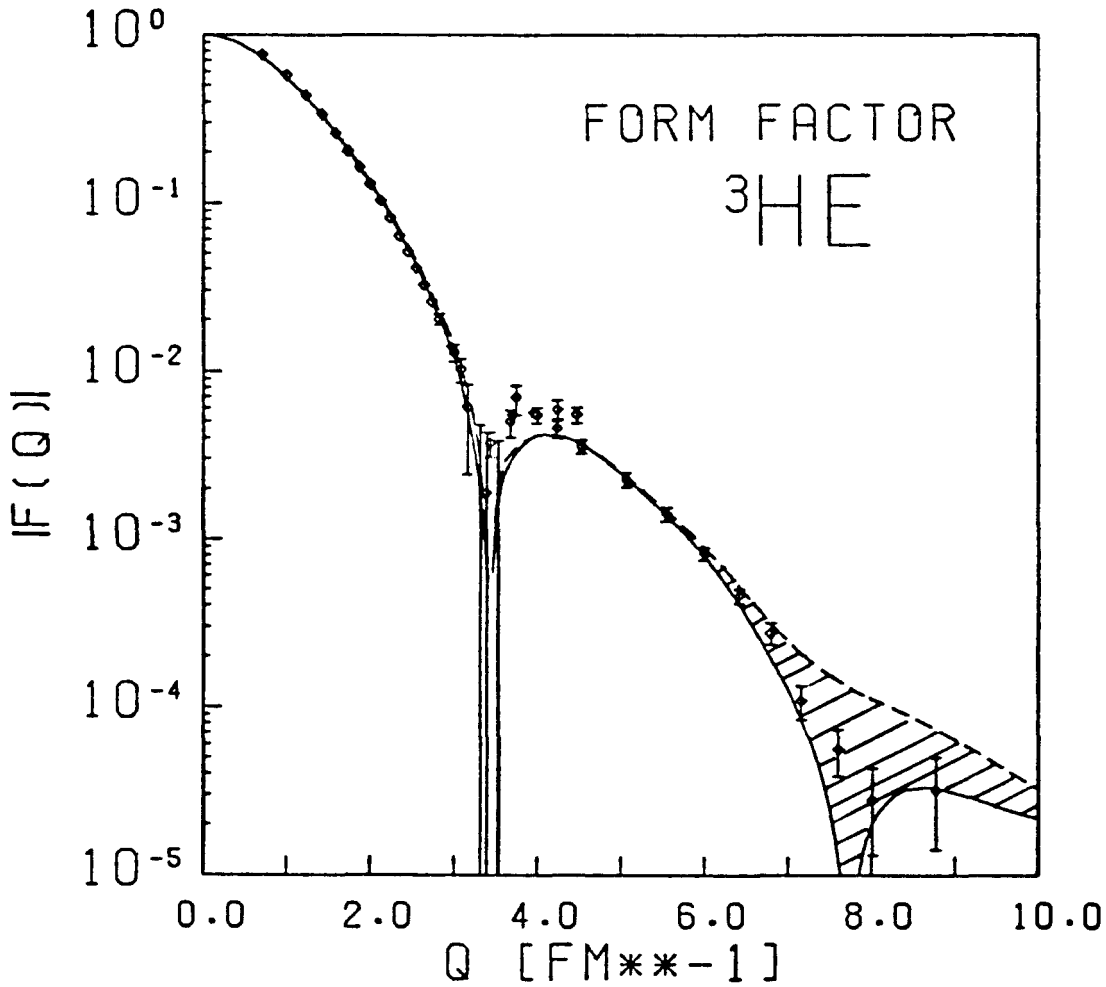

Figure 2.9 Comparison of F_{ch} (solid) and $A^{1/2}$ (dashed) using theoretical values [20] for F_{mag} and F_{ch}.

reservations as above apply here. As J. Friar [13] keeps on emphasizing: the higher order meson exchange currents are not even properly defined, unless one constructs the wave functions consistently to the same relativistic order. Furthermore one is *free* to perform unitary transformations, thereby shoveling contributions to matrix elements back and forth between IA and MEC. The MEC contribution to the secondary maximum in F_{ch} and the D-state percentage in ^{3}He are *not observables* but crutches used by theoreticians to organize their calculations.

What experiments remain to be done in elastic scattering off the trinucleons? On one hand theorists would like to know $B(Q^2)$ up to the same momentum transfers as $A(Q^2)$. That made a complete separation of F_{ch} and F_{mag} possible. Figure 2.9 gives an estimate based on a theoretical calculation, what contributions to $A(Q^2)$

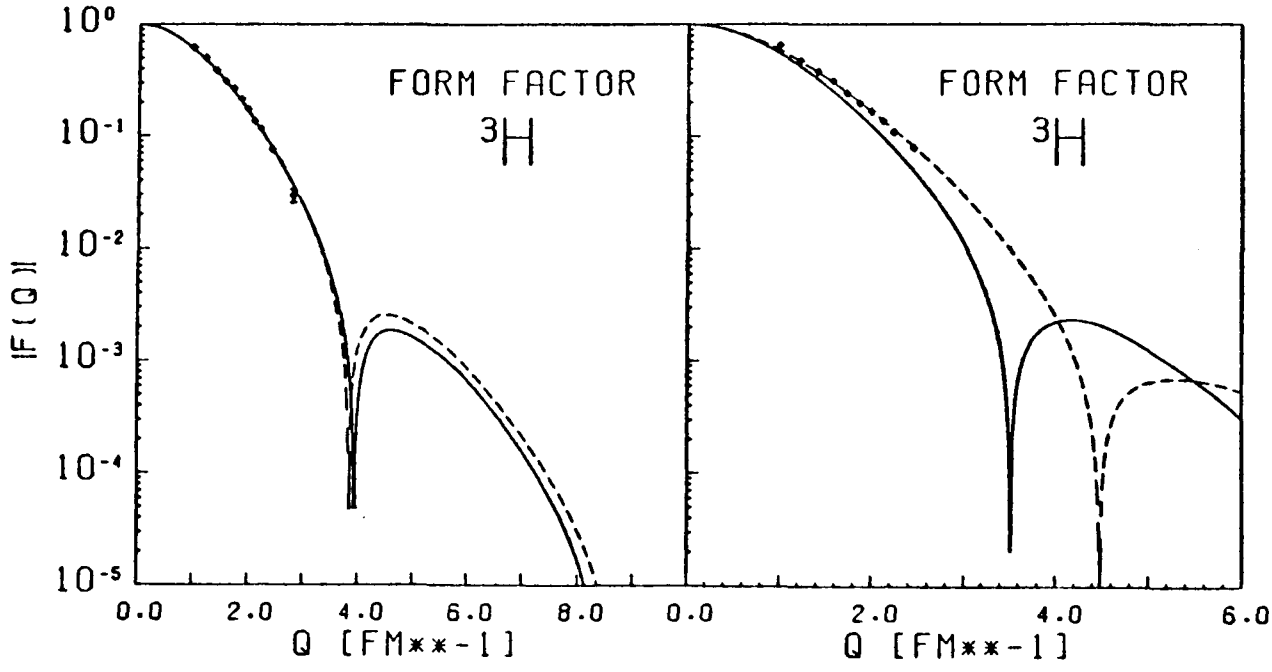

Figure 2.10 Predictions [20] for charge and magnetic form factors of ^{3}H: Impulse approximation (solid) and calculations including MEC (dashed) as in fig. 2.8 and 2.7 (using F_1^v) respectively.

can be expected from magnetic scattering [20]. Above $Q \approx 7fm^{-1}$ F_{mag} seems to dominate A. However, the theory for F_{mag} that far out may well be off reality by an order of magnitude in either direction.

The other long outstanding experiment is the measurement of the triton form factors. Especially the magnetic form factor is interesting. The meson exchange currents which have proven to be important for ^{3}He are purely isovector operators, therefore each calculation of the ^{3}He magnetic form factor implies a unique prediction of the one for ^{3}H. If experiments show, that the triton magnetic form factor is described significantly worse, the present theory is in trouble. For the charge form factor, a verification, that the difference between experiment and impulse approximation is an isovector, were a hint, that the selected processes of higher relativistic order considered so far (see above) are indeed important. A set of predictions and the currently available data are shown in fig. 2.10.

Before I leave the topic of elastic scattering, I want to state what I call:

The Law of Maximum Obstruction. *Whenever you think to enjoy a glimpse upon your favorite fine details of a wave function, watch out for a concurrent process involving the dominant amplitudes in the wave function to obscur your view.*

E. g., looking at the impulse approximation for F_{mag} — figure 2.5 — we observe that the position of the diffraction minimum depends sensitively upon the S-D transition matrix elements of the current operator. So it could be used to learn something

about the D-admixture in three-body wave functions. Were it not for meson exchange currents! Once considered they turn out to dominate the corresponding range of momentum transfers. Furthermore, because in MEC processes the momentum of the external photon is distributed among two nucleons, these are far less sensitive to the details of the wave function. Or take the charge form factor: The height of the secondary maximum seems to tell of missing high momenta — parts again might come from the D-state. However, if MEC are important, you see once more low momentum nucleons via a more complicated mechanism.

3. Inelastic Scattering and Coincidence Experiments

Now we proceed to the potentially most interesting topic of my talk: Since all inelastic processes in the trinucleons invariably lead into the continuum, kinematically complete experiments require the detection of at least one hadron in coincidence with the scattered electron. With the advent of 100% duty cycle high energy electron accelerators the whole field of coincidence experiments on nuclei becomes accessible for the first time.

Theoretically, while form factor calculations involve the matrix element of the current operator between the ground state wave functions

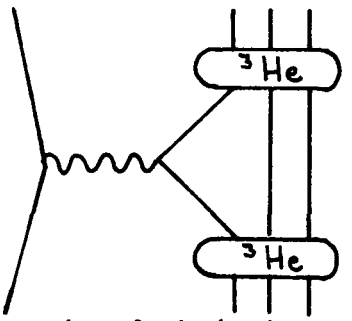

Figure 3.1 Schematic diagram for elastic electron scattering.

cross sections for inelastic scattering require the current to be sandwiched between the ground state and a three-body scattering state — an enormous complication of matters!

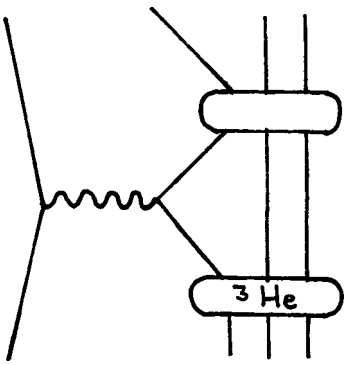

Figure 3.2 Schematic diagram for inelastic electron scattering.

However, the theoretical analysis of inelastic scattering experiments simplifies drastically, if one assumes a quasifree mechanism, also called plane wave impulse approximation (PWIA).

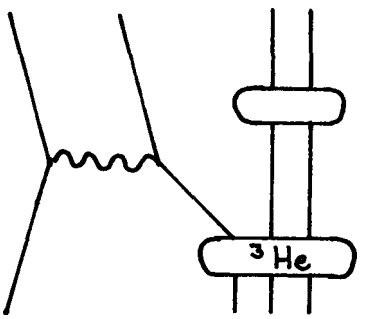

Figure 3.3 Schematic diagram for quasielastic electron scattering.

Then the cross section is essentially given by the ^{3}He-pd or ^{3}He-p(np) vertex function, embellished by the electromagnetic form factor of a single nucleon. While the charge form factor still is a convolution integral, see eq. 2.5, this seems like the most direct way to measure the ^{3}He wave function .

A full blown calculation of the three-body scattering state with realistic interactions is completely out of reach for the near future. Therefore most theoretical analysises [24] [25] have concentrated on the quasifree process. Only a pioneering calculation by Lehman and co-workers [26] tried to keep track of the final state interactions using separable potentials.

As advertised above, in quasifree scattering the sixfold differential cross section for detection of scattered electron and knocked out proton in coincidence is a product of the elementary cross section and the so called spectral function.

$$\frac{d^6\sigma}{d\Omega_e dE'_e d\Omega_p dp} = \frac{d\sigma}{d\Omega_e}\Big|_{ep} \int dE\, \delta(\omega - \frac{\hbar^2}{4m}(\vec{p}-\vec{Q})^2 - \frac{\hbar^2}{2m}\vec{p}^2 - E)\, S(\vec{p}-\vec{Q},E) \quad (3.1)$$

The spectral function $S(\vec{k},E)$ contains all the nuclear structure information and gives the probability to find a proton with given momentum $\vec{k}$ and separation energy E inside the target nucleus.

$$S(\vec{k},E) = \sum_f \left| \langle \psi^f_{23}(E+E_3); \vec{k} | \Psi_3(E_3) \rangle \right|^2 \quad (3.2)$$

Here the sum over f includes all (unobserved) final states of the remaining two-nucleon system.

The wealth of experimental data about inelastic electron scattering still comes from single arm experiments ^{3}He(e,é)X where all the nuclear final states go unobserved. Therefore, the proton momentum and direction in equ. (3.1) have to be integrated over

$$\frac{d^3\sigma}{d\Omega_e dE'_e} = \int d^3p\, \frac{d\sigma}{d\Omega_e}\Big|_{ep} \int dE\, \delta(\omega - \frac{\hbar^2}{4m}(\vec{p}-\vec{Q})^2 - \frac{\hbar^2}{2m}\vec{p}^2 - E)\, S(\vec{p}-\vec{Q},E) \quad (3.3)$$

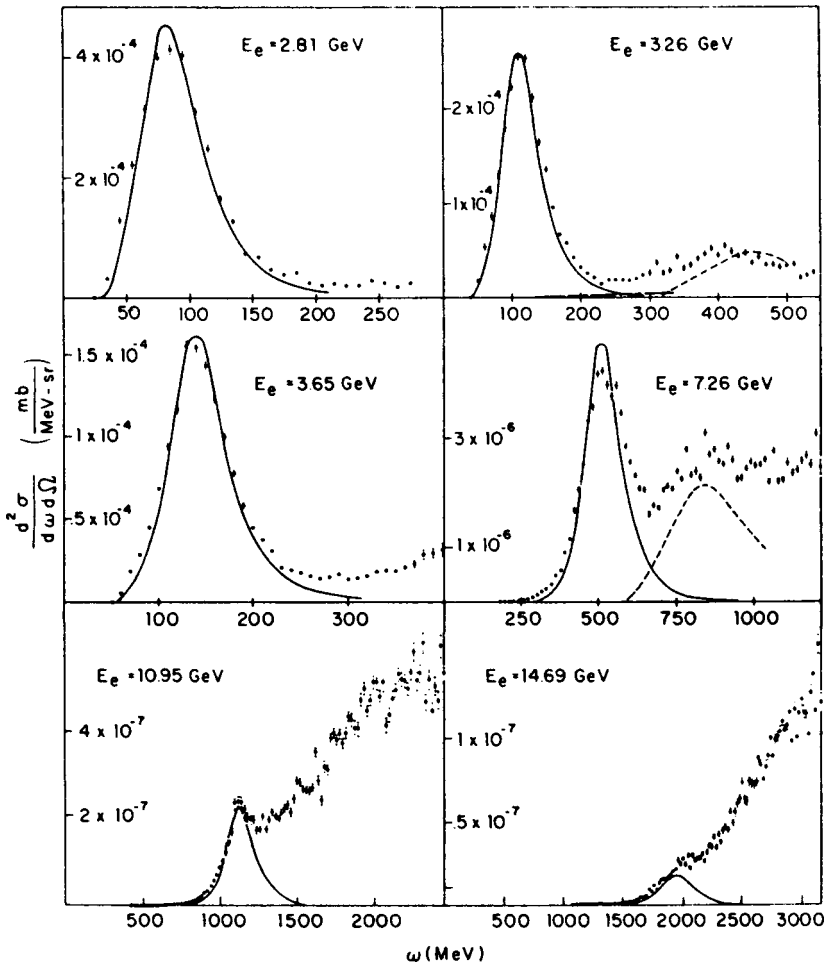

Figure 3.4 Triple differential cross sections for inclusive electron scattering experiments [27] as a function of energy transfer ω. Incident beam energy and scattering angle are held fixed.

Fig. 3.4 shows representative examples of the triple differential cross section as a function of the energy transfer ω. One clearly recognizes a dominant quasielastic peak, corresponding to $\omega = \frac{\hbar^2}{2m}Q^2$, that is a situation, where all the energy and momentum are transfered onto a single nucleon previously at rest. We conclude, that the quasifree mechanism is indeed an important process. However, the peak itself does not teach us much about ^{3}He, except, that there are protons inside. In fact the integral of the cross section under the peak is related to the number of protons via the Koltun [28] sum rule.

$$\int dE \int d^3k \, S(\vec{k}, E) = Z \tag{3.4}$$

Even the width of the peak — equivalently the first moment of the spectral function — is not terribly interesting. It gives a measure of the average momentum of the

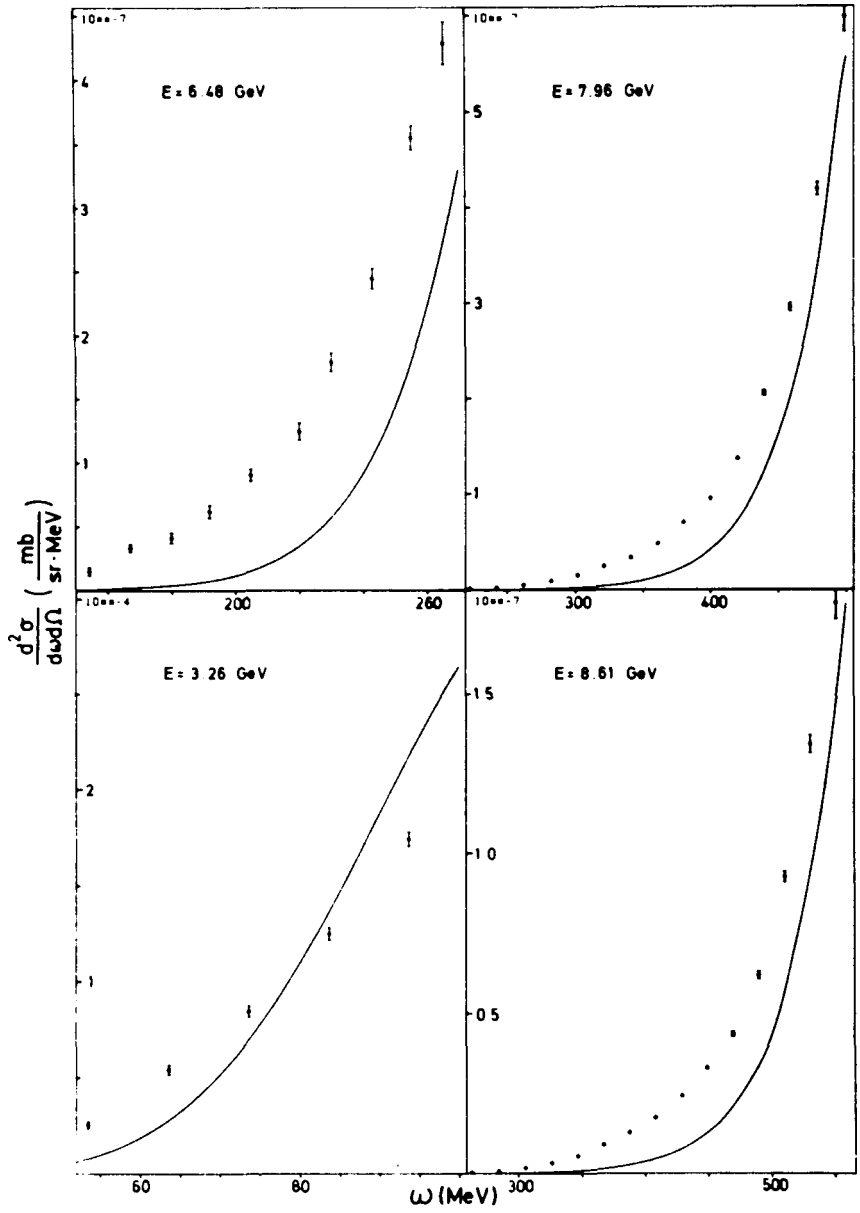

Figure 3.5 Low energy loss tail of the quasielastic peak (from ref. 25]).

nucleons smearing out the peak.

$$\int dE \int d^3k \, E \, S(\vec{k}, E) = \tfrac{1}{2} E_{kin} \tag{3.5}$$

If we want to see high momentum components, we have to go to either very large or very small energy losses, corresponding to a fast proton ($|\vec{k}| \approx |\vec{Q}|$) in the initial state with its momentum parallel or antiparallel to $\vec{Q}$ respectively. On the high ω end of the spectrum physics gets obscured by other inelastic processes like π production, so let us concentrate on the low energy loss end. See figure 3.5.

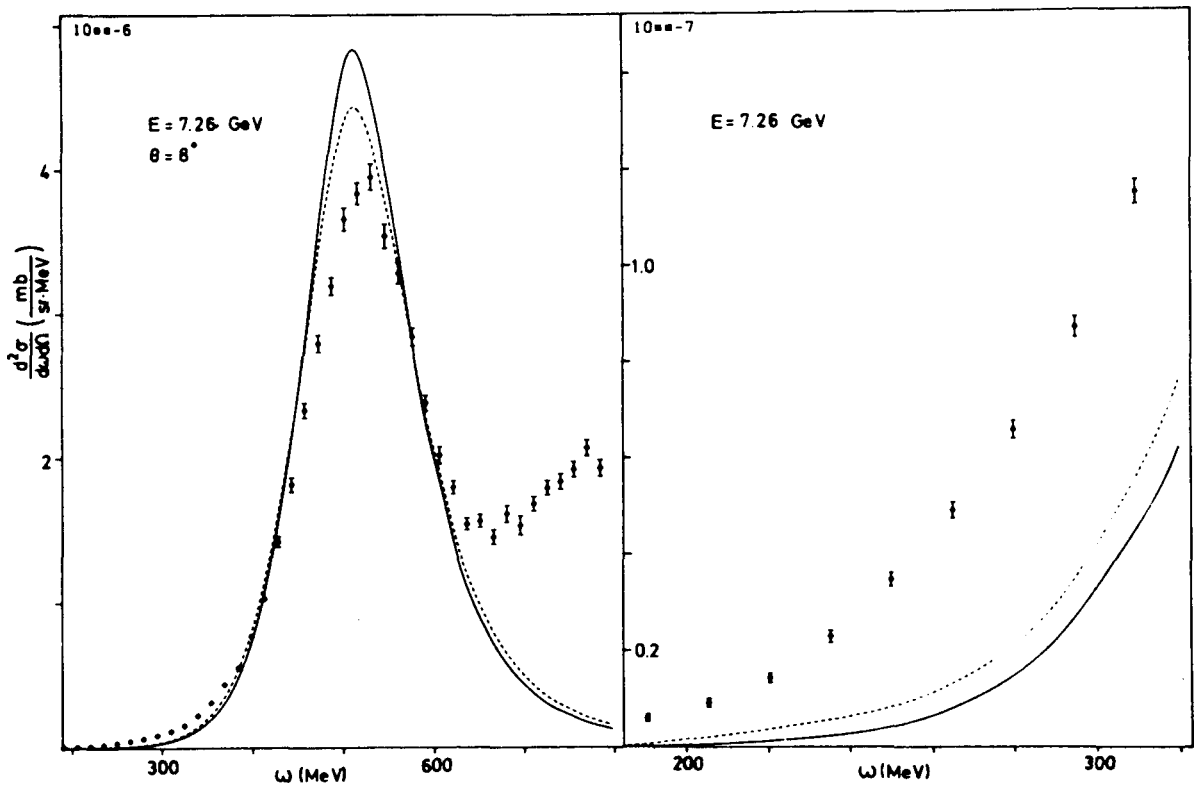

Figure 3.6 Cross sections at 7.26 GeV for the wave function obtained from the Paris potential (solid) and for the one adjusted to reproduce F_{ch} (dotted) [25].

Aha, again we are confronted with the fact, that the theoretical calculation [25] grossly underestimates the experiment. This has been interpreted as confirming evidence for a lack of high momentum components in the three-body wave functions [6] [29]. However, I want to challenge this interpretation and argue, that it probably is an effect of final state interactions:

1. If one modifies the ^{3}He wave function phenomenologically in order to accomodate the secondary maximum in the charge form factor, one gets improvement for the inelastic data too, but there still remains a dramatic discrepancy [25], see fig. 3.6. There seems to be *no common cure* for the two diseases!

2. The presently available coincidence experiments from Saclay [30] and Kharkov [31] are restricted to kinematics near the quasielastic peak in order to achieve acceptable counting rates. The Saclay data have been analyzed assuming PWIA to be valid, and the resulting momentum distributions — see fig. 3.7 — are in reasonably good agreement with theoretical predictions [25]. Laget applied his rescattering formalism [32] to the three-nucleon final states of this experiment. Preliminary results [33] indicate, that he can explain the remaining discrepancies satisfactorily. In this kinematic situation the effect is small, but the relative importance of FSI contributions to the cross section can be expected to increase, as one moves away from the peak towards lower energy transfers and finally to elastic scattering. After

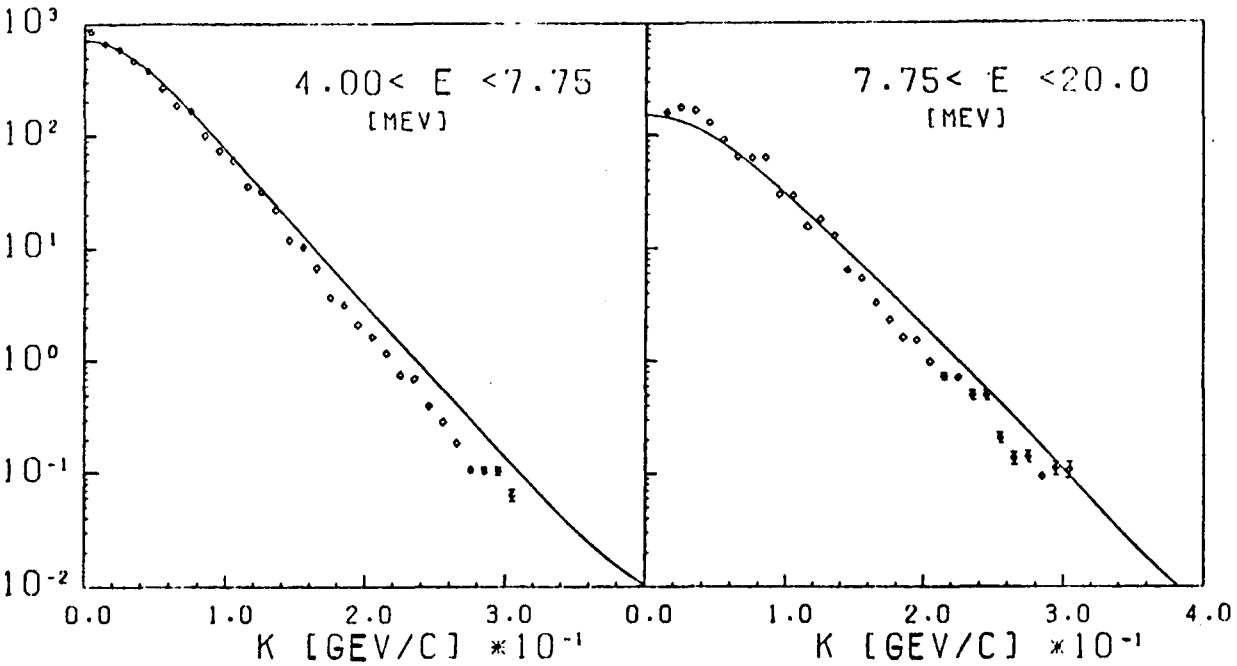

Figure 3.7 Momentum distributions extracted from coincidence experiments assuming PWIA [30] and the corresponding theoretical ones [25].

all, elastic scattering is made possible only by final state interactions!

3. The y-scaling [34] behaviour of the experimental cross sections has been used as an argument, that one sees indeed a one-nucleon process in the inclusive experiments [29]. The theoretical cross sections calculated in PWIA scale too. However the scaling function $f_{PWIA}(y)$ does coincide neither with the experimental one $f_{ex}(y)$ (as expected it lies below) nor with $f_{th}(y)$ as predicted in ref. [34], see figure 3.8. Since the derivation [34] implicitly takes care of all the final state interactions [35], the difference between the two scaling functions f_{th} and f_{PWIA} may be a measure of the importance of FSI effects.

4. There exists a calculation by Bidasaria [36] of what the author calls meson exchange effects. But what he in fact computes are parts of the correlations in the initial state — which calculations based on realistic wave functions contain automatically — and parts of the final state interactions due to the one-boson exchange potential. He claims to improve significantly upon the low energy tail of the coincidence cross sections. Although this is no definite evidence it is another hint.

Thus I suspect, that *the law of maximum obstruction* strikes again here: Low momentum nucleons in the initial state knocked out by a more complicated mechanism may wipe out the hoped for trace of high momenta in the ^{3}He wave function. And I urge, that the aspect of the reaction mechanism be thoroughly investigated,

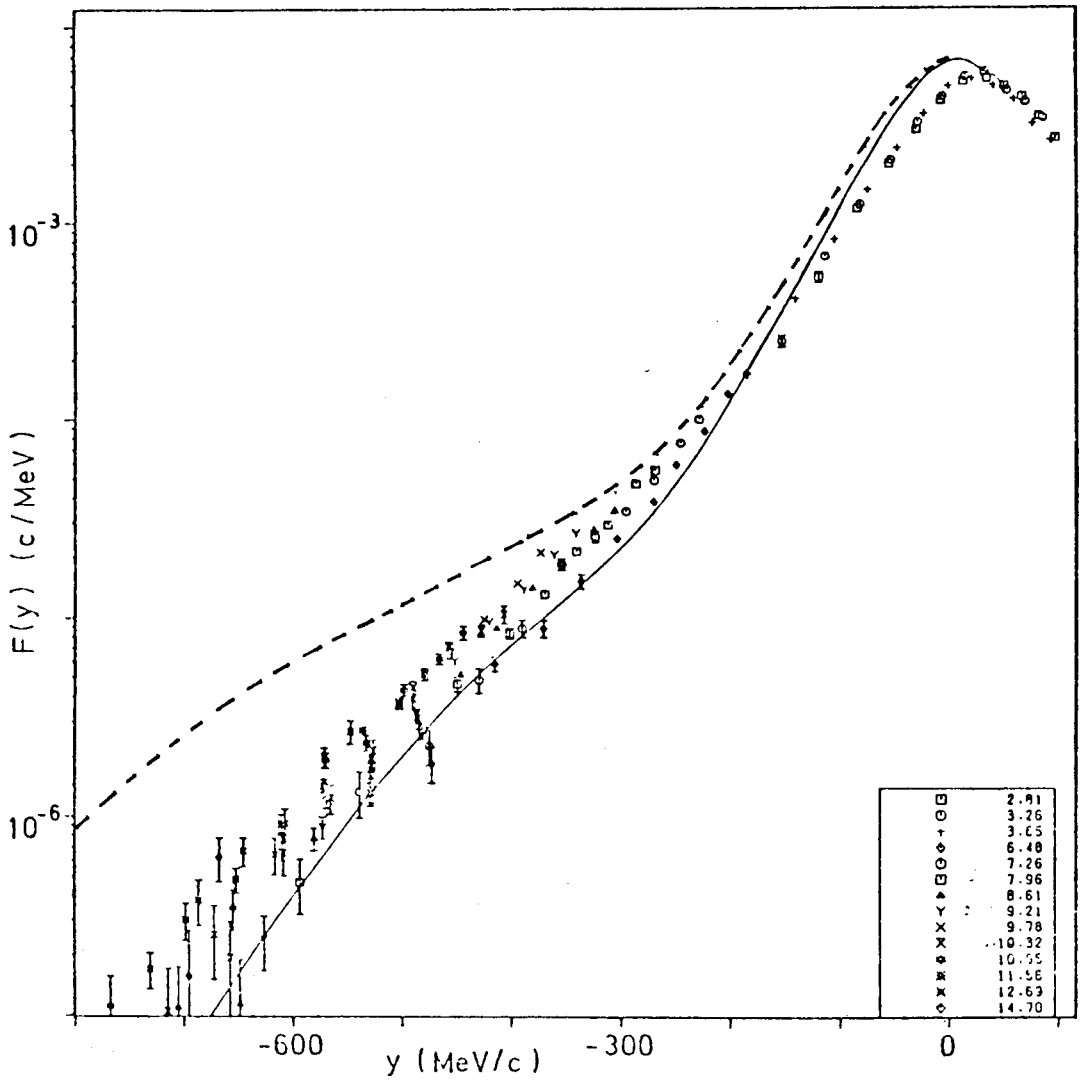

Figure 3.8 y-scaling of the experimental inclusive cross sections and the scaling functions f_{PWIA} (solid) and f_{th} (dashed).

before any conclusions about the underlying physics are drawn. Especially it seems premature to me, to take fig. 3.5 as proof that one sees quark degrees of freedom in nuclei [37].

As a test, of how well the reaction mechanism is theoretically understood, coincidence experiments in the far tail of the quasielastic peak would be very valuable. In order to calculate inclusive cross sections going beyond PWIA, toilfully computed theoretical information has to be integrated over.

Before I come to my final conclusions, I would like to spent a moment on experiments for the far future. There exists a proposal by Blankleider and Woloshyn

[38] to measure the quasifree scattering of longitudinally polarized electrons off polarized ^{3}He targets. The asymmetries should be sensitive to the poorly known neutron form factors. By the same token, one could think of using ^{3}H as a target to measure the form factors of a bound (off shell!) proton and compare it to those of a free one. However, an important caveat applies here too: all this rests on the assumption that MEC effects can safely be neglected.

4. Conclusions

Probably you are going to forget the details of my talk by next week, but maybe it pays to keep the morals in mind:

1. Go ahead and measure anyway, whatever theorists say. You will come up with details never seen before in nuclear physics.
2. However, the interpretation of the results will be difficult.
   (a) For principal reasons the explanations will never be completely model independent. Instead they will vary according to the language one chooses to adopt.
   (b) Before one ever can decide, whether classical nuclear physics breaks down, extremely hard theoretical homework remains to be done. There is no reason to expect, that an experiment, which took you years to plan, set up, calibrate, carry out and analyze, can be explained by a calculation on the back of an envelope. Specifically, I think, in the long run there is no way around a consistent relativistic treatment of three-body wave functions and meson exchange currents or around a serious attack on the three-body scattering problem.
3. Mind the law of maximum obstruction.

A theorist is a person
who believes
at most a single theory*
but every experiment.

Max Dresden [39]

Now guess how to define an experimentalist. It was not my job to change the first part of that definition — I hope I did achieve something on the latter one.

* depending on his/her honesty

Bibliography

[1] J. S. McCarthy, I. Sick and R. R. Whitney, Phys. Rev. **C15** (1977) 1396
M. Szalata et al., Phys. Rev. **C15** (1977) 1200
M. Bernheim et al., Nouv. Cim. Lett. **5** (1972) 431

[2] J. M. Cavedon et al., Phys. Rev. Lett. **49** (1982) 986
P. C. Dunn et al., Phys. Rev. **C27** (1983) 71

[3] H. Collard et al., Phys. Rev. **138** (1965) B57

[4] Ch. Hajduk and P. U. Sauer, Nucl. Phys. **A369** (1981) 321
Ch. Hajduk and P. U. Sauer, Nucl. Phys. **A405** (1983) 581

[5] M. Lacombe, B. Loiseau, J. M. Richard and R. Vinh Mau, Phys. Rev. **C21** (1980) 861

[6] C. Ciofi degli Atti, E. Pace and G. Salmè, in H. Arenhövel and A. M. Saruis (eds.): "From Collective States to Quarks in Nuclei", Lecture Notes in Physics **137**, Springer 1980

[7] I. Sick in C. Ciofi degli Atti and E. Sanctis (eds.): "Few Body Systems and Electromagnetic Interactions", Lecture Notes in Physics **86**, Springer 1978

[8] M. Fabre de la Ripelle, C. R. Hebd. Seances Acad. Sci. Ser. B **288** (1979) 325

[9] J. Carlson and V. R. Pandharipande, Nucl. Phys. **A371** (1981) 301

[10] W. Glöckle and R. A. Brandenburg, Phys. Rev. **C27** (1983) 83

[11] F. Villars, Phys. Rev. **72** (1947) 257

[12] R. G. Sachs, Phys. Rev. **74** (1948) 433

[13] J. Friar, in H. Arenhövel and D. Drechsel (eds.): "Nuclear Physics with Electromagnetic Interactions". Lecture Notes in Physics **108**, Springer 1979

[14] D. O. Riska, Nucl. Phys. **A350** (1980) 227

[15] M. Gari and H. Hyuga, Nucl. Phys. **A278** (1977) 372

[16] E. Hadjimichael, R. Bornais and B. Goulard, Phys. Rev. **C27** (1983) 831

[17] M. A. Maize and Y. E. Kim, Purdue University Preprint PNT6-83-14

[18] W. Strüve, Ch. Hajduk and P. U. Sauer, Nucl. Phys. **A405** (1983) 620

[19] W. Strüve, Ch. Hajduk and P. U. Sauer, in B. Zeitnitz (ed.): "Proceedings of the 10th International Conference on Few Body Problems in Physics", Karlsruhe 1983

[20] W. Strüve, private communication

[21] Ch. Hajduk, S. N. Yang and P. U. Sauer, Nucl. Phys. **A405** (1983) 605

[22] W. Leidemann and H. Arenhövel, Nucl. Phys. **A393** (1983) 385

[23] J. F. Mathiot and D. O. Riska, Phys. Lett. **133B** (1983) 23

[24] C. Ciofi degli Atti. E. Pace and G. Salmè, Nucl. Phys. **A358** (1981) 183; see also ref. [6]

[25] H. Meier-Hajduk, Ch. Hajduk and P. U. Sauer, Nucl. Phys. **A395** (1983) 332
[26] C. R. Heimbach, D. R. Lehman and J. S. O'Connell, Phys. Rev. **C16** (1977) 2135
[27] D. Day et al., Phys. Rev. Lett. **43** (1979) 1143
[28] D. S. Koltun, Phys. Rev. Lett. **28** (1972) 182
[29] I. Sick et al., Phys. Rev. Lett. **45** (1980) 871
[30] E. Jans et al., Phys. Rev. Lett. **49** (1983) 974
[31] V. A. Goldstein, Nucl. Phys. **A392** (1983) 974
[32] J. M. Laget, Nucl. Phys. **A296** (1978) 388
[33] E. Jans, doctoral thesis, Amsterdam 1982
[34] G. West, Phys. Rep. **18C** (1975) 263
[35] credit goes to S. Wallace for drawing my attention to this point.
[36] H. B. Bidasaria, Nucl. Phys. **A399** (1983) 563
[37] J. P. Vary, in W.-Y. P. Hwang and M. H. Macfarlane (eds.): "Hadron Substructure in Nuclear Physics", AIP Conference Proceedings **110** (1984) 171; and references therein
[38] B. Blankleider and R. M. Woloshyn, Phys. Rev. **C29** (1984) 538
[39] M. Dresden, in class, spring 1984

This contribution was typeset using TEX

COINCIDENCE AND POLARIZATION MEASUREMENTS WITH HIGH-ENERGY ELECTRONS*

T. W. Donnelly

Center for Theoretical Physics
Laboratory for Nuclear Science and Department of Physics
Massachusetts Institute of Technology
Cambridge, MA 02139

The material summarized here addresses the subject of coincidence and polarization measurements using high-energy electrons and amounts to a condensation of more extensive treatments presented in several recent workshops or schools (Donnelly, 1983; Donnelly, 1984; Donnelly, 1984a). In particular, in (Donnelly, 1983; Donnelly, 1984a) inclusion of polarization degrees of freedom into the formalism of electron scattering was focussed upon and several specific examples were given to illustrate the basic ideas involved. This material forms part of the broader view taken in (Donnelly, 1984), which serves as an introduction to electromagnetic response functions in general; more briefly this may be referred to as electromagnetic "super-Rosenbluth" physics.

This work is organized in a way which proceeds from familiar inclusive electron scattering involving unpolarized targets, to exclusive scattering involving one, two, or more particles detected in coincidence with the scattered electron (all without nuclear polarizations, but including both polarized and unpolarized electrons) and finally to inclusive scattering again, but now with nuclear polarizations specified in the initial or final state. An essential unity of form for the electron scattering cross sections emerges from these developments and gives rise to the general super-Rosenbluth formula.

In Fig. 1 we show electron-nucleus scattering in the lowest order (one-photon-exchange) approximation. Here an electron with 4-momentum K^μ is scattered to K'^μ, in the process exchanging a photon having

*This work is supported through funds provided by the U.S. Department of Energy (DOE) under contract DE-AC02-76ER03069.

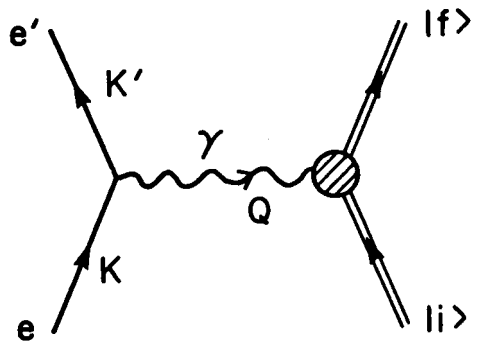

Fig. 1. Electron scattering in the one-photon-exchange approximation.

4-momentum $Q^\mu = K^\mu - K'^\mu$ with the nucleus (see the Appendix for a summary of the nomenclature and conventions used here). The energy transfer is usually denoted $\omega \equiv K^0 - K'^0$; the magnitude of the 3-momentum transfer is denoted $q \equiv |\vec{K} - \vec{K}'|$. For this process the momentum transfer is space-like, with $Q^2 = Q_\mu Q^\mu = \omega^2 - q^2 \leq 0$, that is, with $q \geq \omega$. The three electron kinematic variables may be taken to be the incident energy ε, the scattered electron energy ε' and the electron scattering angle θ. Alternatively, we may use q, ω and θ. For fixed scattering angle θ, it is possible to adjust the electron energies so that a given amount of energy ω is transferred to the nucleus. Thus, using the third degree of freedom, all values $q \geq \omega$ may be probed; for example, for a given nuclear transition the electron scattering form factors may be mapped out, yielding information on the spatial distribution of charges and current.

The electromagnetic interaction in lowest order (Fig. 1) factorizes into a leptonic electromagnetic current, a virtual photon propagator and a hadronic (nuclear) electromagnetic current. The propagator leads to an overall $1/Q^4$ behavior in the electron scattering cross section (this is just the $1/\sin^4 \theta/2$ dependence of the Rutherford or Mott cross sections). The remaining two factors lead to our characterization of the process as a semi-leptonic current-current interaction. Thus, the differential cross section may be written as the contraction of a leptonic tensor, $\eta_{\mu\nu}$ with a hadronic or nuclear tensor $W^{\mu\nu}$:

$$d\sigma \sim \eta_{\mu\nu} W^{\mu\nu} \quad . \tag{1}$$

We may wish to discuss unpolarized electron scattering, where an average over initial spins and a sum over final spins occur for the electron and for the nuclear states involved. On the other hand, we may be interested in studies with polarized targets, with polarizations measured in the final nuclear state, or both, either with or without polarized electrons. In each situation the electron tensor $\eta_{\mu\nu}$ and the nuclear tensor $W^{\mu\nu}$ take on specific general forms. We shall return below to discuss these in more detail.

Another characterization of the process of interest is according to how many particles (if any) are presumed to be detected in coincidence with the scattered electron. If only the scattered electron is detected we speak of inclusive electron scattering; if some particle is detected in coincidence with the electron, we speak generally of exclusive scattering. Let us introduce the nomenclature exclusive-1, exclusive-2, ..., if we have 1, 2, ... particles in coincidence with the electron (so then inclusive $\equiv$ exclusive-0). That is, we have

$$\begin{aligned} &(e,e') \quad \leftrightarrow \text{inclusive} \\ &(e,e'x) \quad \leftrightarrow \text{exclusive-1} \\ &(e,e'xy) \leftrightarrow \text{exclusive-2} \\ &\quad\vdots \qquad\qquad\quad \vdots \end{aligned}$$

Alternatively, the exclusive processes are referred to as double-, triple-, etc. coincidence reactions respectively. In each case the nuclear response function has a certain general kinematical form.

Naturally, these ideas are not specific to electromagnetic interactions, but may be extended to encompass general semi-leptonic electroweak studies. This wider scope forms part of the discussion in (Donnelly, 1984; see also earlier references contained therein) and lies beyond the narrower view taken here.

Let us begin by examining the basic leptonic vertex shown in Fig. 2 for the case of electromagnetic electron scattering when the current has the familiar form

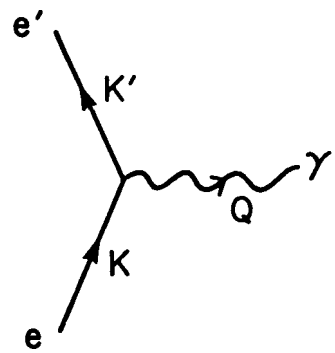

Fig. 2. Leptonic vertex for (electromagnetic) electron scattering.

$$j_e(K',\lambda';K,\lambda)_\mu \sim \bar{u}_e(K',\lambda')\gamma_\mu u_e(K,\lambda) \ . \tag{2}$$

Here the electrons are labelled with 4-momentum and helicity quantum numbers K,λ and K',λ' and the polar-vector (V) character of the electromagnetic current is apparent in that only spinor matrix elements of γ_μ occur. Analogous expressions can be written for the leptonic currents which occur when the weak interaction is considered. On the hadronic side (which is discussed in detail below) we have the electromagnetic current matrix elements J^μ_{fi}; that is, we have matrix elements of the electromagnetic current operator $\hat{J}^\mu$ taken between initial and final nuclear states. Matrix elements of the interaction hamiltonian then have the current × current character,

$$H'_{fi} \sim j_\mu J^\mu_{fi} \ , \tag{3}$$

and, in first-order perturbation theory (using Fermi's Golden Rule), lead to differential cross sections of the form

$$d\sigma \sim |H'_{fi}|^2 \sim |j_\mu J^\mu_{fi}|^2 \tag{4a}$$

$$\sim (j^*_\mu j_\nu)(J^\mu_{fi} {}^* J^\nu_{fi}) . \tag{4b}$$

Upon performing the appropriate averages over initial states and sums over final states (indicated by $\bar{\Sigma}$) and obtaining the tensors

$$\eta_{\mu\nu} \sim \bar{\Sigma}_{\text{leptons}} j^*_\mu j_\nu \tag{5a}$$

$$W^{\mu\nu} \sim \bar{\Sigma}_{\substack{\text{if} \\ \text{hadrons}}} J^\mu_{fi} {}^* J^\nu_{fi}, \tag{5b}$$

we then have the differential cross section written as the contraction of these leptonic and hadronic tensors:

$$d\sigma \sim \eta_{\mu\nu} W^{\mu\nu} . \tag{6}$$

For the electron (leptonic) tensor we have, using Eq.(2) for the electromagnetic current,

$$\eta_{\mu\nu} \sim \bar{\Sigma}\{\bar{u}_e(K',\lambda')\gamma_\mu u_e(K,\lambda)\}^*\{\bar{u}_e(K',\lambda')\gamma_\nu u_e(K,\lambda)\} . \tag{7}$$

If we are interested in unpolarized electron scattering we have

$$\bar{\Sigma} \to \frac{1}{2} \Sigma_{\lambda\lambda'}$$

and the appropriate tensor is (Donnelly, 1983a)

$$\eta_{\mu\nu}\Big|_{\substack{\text{unpol.} \\ (e,e')}} \sim K_\mu K'_\nu + K'_\mu K_\nu - g_{\mu\nu}(K\cdot K' - m_e{}^2) . \tag{8}$$

Note that this is symmetric under the interchange $\mu \leftrightarrow \nu$ and manifestly satisfies the current conservation condition (coming from $Q^\mu j_\mu = 0$, the continuity equation), $Q^\mu \eta_{\mu\nu}\big|_{\text{unpol.}(e,e')} = 0$. Of course this is more generally true of the electromagnetic tensor $\eta_{\mu\nu}$, regardless of the state of polarization or the nature of the specific process:

$$Q^\mu \eta_{\mu\nu} = 0. \tag{9}$$

We shall usually be interested in the extreme relativistic limit (ERL) for electron scattering where $\gamma = \varepsilon/m_e >> 1$ and so the term involving $m_e{}^2$ in Eq.(8) can usually be ignored and we have $k = |\vec{K}| \approx \varepsilon$, $k' = |\vec{K}'| \approx \varepsilon'$. For electron scattering with longitudinally polarized incident electrons and no scattered electron polarization measured we have (Donnelly and Raskin, 1984)

$$\bar{\Sigma} \to \Sigma_{\lambda'}$$

with the corresponding tensor

$$\eta_{\mu\nu}\Big|^{\text{ERL}}_{\substack{\text{pol.}\\(\vec{e},e')}} \sim \{K_\mu K'_\nu + K'_\mu K_\nu - g_{\mu\nu} K\cdot K'\} + ih\varepsilon_{\mu\nu\alpha\beta}K^\alpha K'^\beta, \tag{10}$$

where for simplicity we have assumed the extreme relativistic limit here. The first main term is just the ERL limit of Eq.(8), whereas the second contains the explicit dependence on the incident electron helicity $h=\pm 1$. Note that this new term is antisymmetric under the interchange $\mu\leftrightarrow\nu$ and manifestly satisfies the current conservation condition, $Q^\mu\varepsilon_{\mu\nu\alpha\beta}K^\alpha K'^\beta=0$, since $Q^\mu=K^\mu-K'^\mu$.

Next we turn to the hadronic (nuclear) tensor defined generally in Eq.(5b). As for the leptonic tensor discussed above, we can decompose this into pieces which are symmetric or antisymmetric under the interchange $\mu\leftrightarrow\nu$:

$$W^{\mu\nu} = W^{\mu\nu}_s + W^{\mu\nu}_a \ . \tag{11}$$

The differential cross section in Eq.(6) then becomes a sum of two contributions.

$$d\sigma \sim \eta_{\mu\nu}W^{\mu\nu} = \eta^s_{\mu\nu}W^{\mu\nu}_s + \eta^a_{\mu\nu}W^{\mu\nu}_a \ . \tag{12}$$

Let us now proceed to build these hadronic tensors from the available 4-momenta in the problem. We begin with simple familiar cases and progress towards the general "super Rosenbluth" forms.

(I) Inclusive electron scattering, no nuclear polarizations. In this situation we are now interested in the nuclear vertex shown in Fig. 3. Here the virtual photon from the electron scattering (Fig. 2) brings in 4-momentum Q and causes the nucleus to go from state $|i\rangle$ to state $|f\rangle$. These hadronic states have 4-momenta P_i and P_f, respectively, as shown in the figure. Thus we must build the hadronic tensors from the

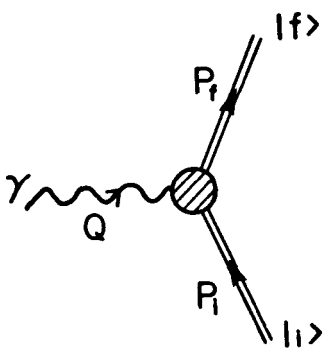

Fig. 3. Hadronic (nuclear) vertex for inclusive electron scattering.

4-momenta Q, P_i and P_f. In fact we can use momentum conservation to eliminate one, say $P_f=P_i+Q$, leaving two independent 4-momenta: $\{Q,P_i\}$. The possible Lorentz scalars in the problem are Q^2, P_i^2 and $Q\cdot P_i$. Since we presumably know what the target is and since $P_i^2=M_i^2$, we are left with two independent scalars to vary: $\{Q^2,Q\cdot P_i\}$. Moreover, since $Q^2=\omega^2-q^2$ and $Q\cdot P_i=\omega M_i$ in the laboratory system, we can regard our hadronic tensors to be functions of $\{Q^2,Q\cdot P_i\}$ or of $\{q,\omega\}$.

Now we wish to write $W_s^{\mu\nu}$ and $W_a^{\mu\nu}$ in terms of the two independent 4-vectors Q^μ and P_i^μ. Alternatively, instead of P_i it turns out to be useful to employ the 4-vector

$$V_i^\mu \equiv \frac{1}{M_i}\{P_i^\mu - (\frac{Q\cdot P_i}{Q^2})\,Q^\mu\}\ , \tag{13}$$

This is especially convenient because $Q\cdot V_i=0$, by construction. Thus, we shall use Q^μ and V_i^μ to build the hadronic tensors.

To begin with, $W^{\mu\nu}$ must be a second-rank Lorentz tensor and so we can write the following general expansions:

$$W_s^{\mu\nu} = X_1 g^{\mu\nu} + X_2 Q^\mu Q^\nu + X_3 V_i^\mu V_i^\nu + X_4(Q^\mu V_i^\nu + V_i^\mu Q^\nu) \tag{14a}$$

$$W_a^{\mu\nu} = Y_1(Q^\mu V_i^\nu - V_i^\mu Q^\nu) + iY_2\varepsilon^{\mu\nu\alpha\beta}Q_\alpha V_{i\beta}\ , \tag{14b}$$

where the scalar response functions (the X's and Y's) depend on the scalars discussed above:

$$X_i = X_i(Q^2, Q\cdot P_i) \ , \qquad i=1,\ldots,4$$
$$Y_i = Y_i(Q^2, Q\cdot P_i) \ , \qquad i=1,2 \ .$$

Next we note that, in the absence of parity violating effects from the weak interaction, the hadronic electromagnetic current matrix elements are polar vectors and so the tensors here must have specific properties under spatial inversion. In particular, the ε-terms in Eq.(14b) have the wrong behavior and so Y_2 must vanish.

Finally we must make use of the fact that $W^{\mu\nu}$ was constructed from currents in Eq.(5b) and that these electromagnetic currents are conserved quantities, $Q_\mu J^\mu_{fi}=0$. Hence we must impose the constraints

$$Q_\mu W_s^{\mu\nu} = 0 \tag{15a}$$

$$Q_\mu W_a^{\mu\nu} = 0 \tag{15b}$$

on the expansions in Eqs.(14). This leads us to the expressions (recall that $Q\cdot V_i=0$)

$$Q_\mu W_s^{\mu\nu} = 0 = (X_1 + X_2 Q^2)Q^\nu + (X_4 Q^2)V_i{}^\nu \tag{16a}$$

$$Q_\mu W_a^{\mu\nu} = 0 = (Y_1 Q^2)V_i{}^\nu \tag{16b}$$

and so $X_1+X_2Q^2=0$, $X_4=0$ and $Y_1=0$, using the linear independence of Q^ν and $V_i{}^\nu$. Defining $W_1 \equiv -X_1$ and $W_2 \equiv X_3$, to use more common nomenclature, we have then rederived the familiar results

$$W_s^{\mu\nu} = -W_1(g^{\mu\nu} - \frac{Q^\mu Q^\nu}{Q^2}) + W_2 V_i^\mu V_i^\nu \tag{17a}$$

$$W_a^{\mu\nu} = 0 \ . \tag{17b}$$

Contracting the hadronic tensor with the previous results obtained for the electron (Eqs.(8) or (10)) leads to the well-known form for inclusive unpolarized electron scattering (Von Gehlen, 1960; Gourdin, 1961; Bjorken, 1960):

$$\eta_{\mu\nu}W^{\mu\nu} = \eta^s_{\mu\nu}W_s^{\mu\nu} \sim W_2 + 2W_1 \tan^2\frac{\theta}{2} \ , \tag{18}$$

with only two independent response functions, W_1 and W_2, which may be separated by fixing q and ω (and hence the scalar variables Q^2 and $Q\cdot P_i$) and varying the electron scattering angle θ to make a Rosenbluth decomposition. Alternatively, it is useful to speak of contributions which are transverse (T) or longitudinal (L) with respect to the direction $\vec{Q}$ and to write the inclusive cross section in the form†

$$\frac{d\sigma}{d\Omega_e d\omega}\Big|^{\text{lab,ERL,no nuclear polarizations}}_{(e,e')} = \frac{1}{M_i}\sigma_M f_{rec}^{-1}\{v_L W_L^{(0)} + v_T W_T^{(0)}\}. \quad (19)$$

Here we have the Mott cross section

$$\sigma_M = \left(\frac{\alpha\cos\theta/2}{2\varepsilon\sin^2\theta/2}\right)^2$$

with recoil correction,

$$f_{rec} = 1 + 2\varepsilon\sin^2\frac{\theta}{2}/M_i \ . \quad (20b)$$

The electron kinematical factors are given by

$$v_L = (Q^2/q^2)^2 \quad (21a)$$

$$v_T = -\frac{1}{2}(Q^2/q^2) + \tan^2\frac{\theta}{2} \ . \quad (21b)$$

The longitudinal and transverse response functions are then related to the quantities introduced above by

$$W_L^{(0)} = (q^2/Q^2)W_1 + (q^2/Q^2)^2 W_2 \quad (22a)$$

$$W_T^{(0)} = 2W_1 \ . \quad (22b)$$

In the context of the discussions to follow we use the notation "0" to indicate that inclusive scattering is being considered here.

(II) Exclusive-1 electron scattering, no nuclear polarizations. Next we consider (e,e'x) reactions where a particle with 4-momentum P_1 is

†For the sake of clarity we shall often neglect recoil corrections in the present work; see (deForest and Walecka, 1966) for further discussions.

detected in coincidence with the scattered electron. Let us again assume that the total final nuclear state has 4-momentum P_f, so that all but the particle in coincidence (i.e., the unobserved particles) has 4-momentum P_0 (see Fig. 4). Momentum conservation allows us to eliminate these two ($P_f=P_i+Q$ and $P_0=P_f-P_1$), so that we are left with three independent 4-momenta from which to build the hadronic tensor: $\{Q,P_i,P_1\}$. The possible Lorentz scalars in the problem are Q^2,P_i^2, P_1^2, $Q\cdot P_i$, $P_1\cdot P_i$ and $Q\cdot P_1$. Again, we know the target mass, M_i and the mass of the detected particle, M_1, and so, since $P_i^2=M_i^2$ and $P_1^2=M_1^2$ are fixed, we are left with four

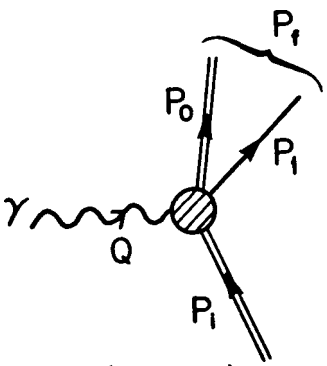

Fig. 4. Hadronic (nuclear) vertex for exclusive-1 electron scattering.

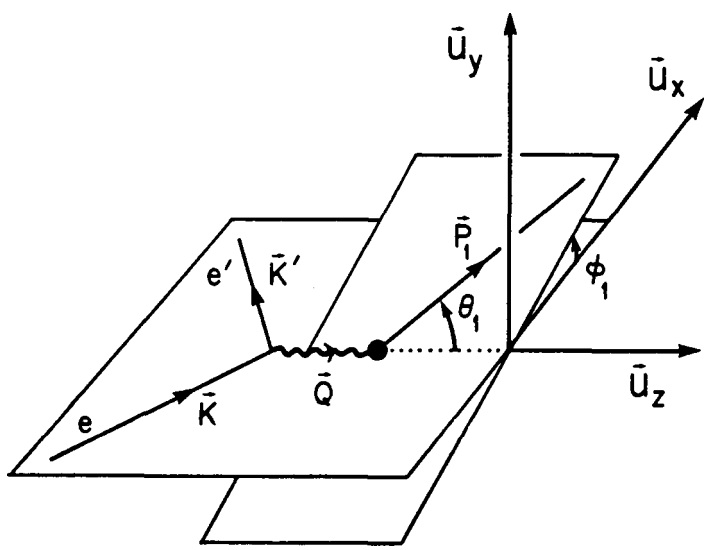

Fig. 5. Exclusive-1 electron scattering. Here the z-axis is chosen to be along $\vec{Q}$ and the electron scattering occurs in the xz-plane so that the y-axis is defined by $\vec{u}_y\equiv\vec{K}\times\vec{K}'/|\vec{K}\times\vec{K}'|$. The particle detected in coincidence with the electron has momentum $\vec{P}_1$, whose direction is given by angles (θ_1,ϕ_1) in this coordinate system.

independent scalars to vary: $\{Q^2, Q\cdot P_i, P_1\cdot P_i, Q\cdot P_1\}$. It is useful to express the kinematical dependence in the response functions in terms of laboratory system variables. We shall use the coordinate system shown in Fig. 5 to describe exclusive-1 electron scattering in which the detected particle has 3-momentum $p_1 = |\vec{P}_1|$ and is detected at angles (θ_1, ϕ_1) with respect to the chosen basis. The four scalar variables may be reexpressed in this laboratory system:

$$\begin{aligned} Q^2 &= \omega^2 - q^2 \\ Q\cdot P_i &= \omega M_i \\ P_1\cdot P_i &= E_1 M_i \\ Q\cdot P_1 &= \omega E_1 - q p_1 \cos\theta_1 \quad , \end{aligned} \tag{23}$$

where $E_1 = (p_1^2 + M_1^2)^{1/2}$ is the total energy of the detected particle. Note that the azimuthal angle ϕ_1 does not occur here; that is, the internal functional dependence involves θ_1, but not ϕ_1. The relevance of this will shortly be apparent. Thus the hadronic tensors for double coincidence reactions can be regarded to be functions of the scalar varaibles $\{Q^2, Q\cdot P_i, P_1\cdot P_i, Q\cdot P_1\}$ or of the laboratory quantities $\{q, \omega, E_1, \theta_1\}$.

Now, as in the case of inclusive scattering, we wish to write $W_s^{\mu\nu}$ and $W_a^{\mu\nu}$ in terms of the independent 4-momenta in the problem. Instead of $\{Q^\mu, P_i^\mu, P_1^\mu\}$ we use the equivalent set $\{Q^\mu, V_i^\mu, V_1^\mu\}$, where

$$V_i^\mu \equiv \frac{1}{M_i}\left\{P_i^\mu - \left(\frac{Q\cdot P_i}{Q^2}\right) Q^\mu\right\} \tag{24a}$$

$$V_1^\mu \equiv P_1^\mu - \left(\frac{Q\cdot P_1}{Q^2}\right) Q^\mu \quad , \tag{24b}$$

and have the convenient properties, $Q\cdot V_i = Q\cdot V_1 = 0$.

Since $W^{\mu\nu}$ must be a second-rank Lorentz tensor, we have the following expansions:

$$W_s^{\mu\nu} = X_1 g^{\mu\nu} + X_2 Q^\mu Q^\nu + X_3 V_i^\mu V_i^\nu + X_4 V_1^\mu V_1^\nu$$
$$+ X_5(Q^\mu V_i^\nu + V_i^\mu Q^\nu) + X_6(Q^\mu V_1^\nu + V_1^\mu Q^\nu)$$
$$+ X_7(V_i^\mu V_1^\nu + V_1^\mu V_i^\nu) \qquad (25a)$$

$$W_a^{\mu\nu} = Y_1(Q^\mu V_i^\nu - V_i^\mu Q^\nu) + Y_2(Q^\mu V_1^\nu - V_1^\mu Q^\nu)$$
$$+ Y_3(V_i^\mu V_1^\nu - V_1^\mu V_i^\nu) \quad , \qquad (25b)$$

where we have not written any ε-terms (cf. Eq.(14b)) using the parity properties of the electromagnetic tensor (∿VV). The scalar response functions depend on the scalars discussed above:

$$X_i = X_i(Q^2, Q\cdot P_i, P_1\cdot P_i, Q\cdot P_1) \quad , \quad i=1, \cdots, 7$$

$$Y_i = Y_i(Q^2, Q\cdot P_i, P_1\cdot P_i, Q\cdot P_1) \quad , \quad i=1, \cdots, 3 \quad .$$

Finally, we use the current conservation conditions (Eqs.(15)) to obtain the constraints

$$Q_\mu W_s^{\mu\nu} = 0 = (X_1 + X_2 Q^2)Q^\nu + (X_5 Q^2)V_i^\nu + (X_6 Q^2)V_1^\nu \qquad (26a)$$

$$Q_\mu W_a^{\mu\nu} = 0 = (Q^2 Y_1)V_i^\nu + (Q^2 Y_2)V_1^\nu \quad , \qquad (26b)$$

and so $X_1 + X_2 Q^2 = 0$, $X_5 = 0$, $X_6 = 0$ and $Y_1 = 0$, $Y_2 = 0$, using the linear dependence of Q^ν, P_i^ν and P_1^ν. For the symmetric hadronic tensor we obtain

$$W_s^{\mu\nu} = X_1\left(g^{\mu\nu} - \frac{Q^\mu Q^\nu}{Q^2}\right) + X_3 V_i^\mu V_i^\nu$$
$$+ X_4 V_1^\mu V_1^\nu + X_7(V_i^\mu V_1^\nu + V_1^\mu V_i^\nu), \qquad (27a)$$

in which there are four independent response functions, to be compared with inclusive scattering (Eq.(17a)) in which only two appeared. For the antisymmetric tensor we obtain

$$W_a^{\mu\nu} = Y_3(V_i^\mu V_1^\nu - V_1^\mu V_i^\nu) \quad , \qquad (27b)$$

in which a fifth response function appears, in contrast to inclusive scattering (Eq.(17b)) where the antisymmetric tensor vanishes.

When these hadronic tensors are contracted with the previous results given in Eq.(10) for the electron scattering leptonic tensor (we assume the ERL here for simplicity), we obtain

$$\eta_{\mu\nu}W^{\mu\nu} = \eta^{s}_{\mu\nu}W^{\mu\nu}_{s} + \eta^{a}_{\mu\nu}W^{\mu\nu}_{a} \quad , \tag{28}$$

where for the symmetric contributions we have

$$\eta_{\mu\nu}W^{\mu\nu}_{s} \sim v_{L}W^{(1)}_{L} + v_{T}W^{(1)}_{T} + v_{TT}W^{(1)}_{TT}\cos 2\phi_{1} + v_{TL}W^{(1)}_{TL}\cos\phi_{1} \quad . \tag{29}$$

Now, in addition to longitudinal (L) and transverse (T) pieces (cf. Eq.(19)), we also have a transverse-transverse interference (TT) and a transverse-longitudinal interference (TL). Of course the four response functions here are linear combinations of X_1, X_3, X_4 and X_7, and depend on the four scalar quantities discussed above. The v's are electron kinematical factors, where v_L and v_T are as defined above for inclusive electron scattering (Eqs.(21)) and where in addition we now have

$$v_{TT} = \frac{1}{2}(Q^2/q^2) \tag{30a}$$

$$v_{TL} = \frac{1}{\sqrt{2}}(Q^2/q^2)\sqrt{-(Q^2/q^2) + \tan^2\frac{\theta}{2}} \quad . \tag{30b}$$

We use the notation "1" to indicate that exclusive-1, (e,e'x) scattering is being considered here. For the antisymmetric contribution we have

$$\eta^{a}_{\mu\nu}W^{\mu\nu}_{a} \sim h v_{TL'}W^{(1)}_{TL'}\sin\phi_{1} \quad , \tag{31}$$

which is directly proportional to Y_3. This term now brings in still another electron kinematical factor

$$v_{TL'} = \frac{1}{\sqrt{2}}(Q^2/q^2)\tan\frac{\theta}{2} \quad . \tag{32}$$

The antisymmetric piece is also proportional to the electron helicity $h=\pm 1$, whereas the terms in Eq.(29) are independent of h. Thus the symmetric and antisymmetric contributions in electron scattering can be separated from one another by forming the sums and differences of the cross sections with specific electron polarizations, $d\sigma(h=+1) \pm d\sigma(h=-1)$. Note that the difference (electron-helicity-difference) cross section is in general not zero for exclusive (coincidence) electron scattering. This is to be contrasted with inclusive scattering where such terms vanish. Consequently measurements of such difference cross sections in the latter case are sensitive to parity-violating effects involving the weak interaction. The arguments which led to the usual inclusive electron scattering cross section (Eq.(19)) assumed only the presence of the parity-conserving electromagnetic interaction; when both electromagnetic and weak interactions are taken into account, the ε-terms in Eq.(14b) do not in general vanish, leading to antisymmetric response functions and non-zero helicity-difference cross sections. While such effects should also occur for exclusive scattering, they will generally be overwhelmed by the non-zero helicity dependence that occurs even when parity is conserved.

Putting all of this together we have a multiple-differential cross section of the form given in Eq.(19)(although now also differential in the momentum of the particle detected in coincidence with the electron). This involves the five independent response functions $W_L^{(1)}$, $W_T^{(1)}$, $W_{TT}^{(1)}$, $W_{TL}^{(1)}$ and $W_{TL'}^{(1)}$. The last, $W_{TL'}^{(1)}$, can be separated from the other four using the helicity dependence in the cross section as discussed above. Next, we can imagine using the explicit ϕ_1-dependence written in Eqs.(29) and (31) (recall that the scalar variables upon which the response functions depend do not contain any ϕ_1-dependence -- see Eqs.(23)). By varying ϕ_1 it is possible to separate $W_{TL}^{(1)}$, $W_{TT}^{(1)}$ and the combination $v_L W_L^{(1)} + v_T W_T^{(1)}$. Finally, by varying the electron scattering angle and making a familiar Rosenbluth plot, it is possible to separate $W_L^{(1)}$ and $W_T^{(1)}$, and so have independently determined the complete set of five response functions.

To obtain the inclusive cross section from these results we must integrate over the angle dependence (θ_1,ϕ_1) and sum over all open

channels. Indeed, as is apparent from Eqs.(29) and (31), integrating over the explicit ϕ_1-dependence immediately causes the TT, TL and TL' contributions to vanish, leaving only the L and T pieces as expected (see Eq.(19)).

Before going on to more complicated situations, let us look at the polarization cross section in a little more detail. As mentioned above, we can always form an electron-spin-averaged cross section

$$d\Sigma \sim \frac{1}{2}\{d\sigma(h=+1)+d\sigma(h=-1)\} \tag{33a}$$

and an electron polarization cross section

$$d\Delta \sim \frac{1}{2}\{d\sigma(h=+1)-d\sigma(h=-1)\} \ . \tag{33b}$$

The polarization asymmetry is then given by $d\Delta/d\Sigma$. Now, as we have just shown for exclusive-1 electron scattering (without nuclear polarizations) we have

$$d\Delta \sim v_{TL'}W^{(1)}_{TL'}\sin\phi_1 \ . \tag{34a}$$

In contrast, the TL part of the electron-spin-averaged cross section may be isolated using its unique dependence on $\cos\phi_1$; we have

$$(d\Sigma)_{TL} \sim v_{TL}W^{(1)}_{TL}\cos\phi_1 \ . \tag{34b}$$

It is easy to see (cf. Donnelly, 1983; Donnelly and Raskin, 1984) that the TL and TL' contributions come from calculating

$$2\sqrt{2}\mathrm{Re}W^{01} \sim \mathrm{Re}(T^*L)\cos\phi_1 \tag{35a}$$

$$-2\sqrt{2}\mathrm{Im}W^{02} \sim -\mathrm{Im}(T^*L)\sin\phi_1, \tag{35b}$$

respectively, and so the former involves the real part of an interference between transverse and longitudinal (charge) components of the currents, whereas the latter involves the imaginary part of the same interference; that is to say, $W^{(1)}_{TL}\sim\mathrm{Re}(T^*L)$, while $W^{(1)}_{TL'}\sim\mathrm{Im}(T^*L)$. Now, if the (e,e'x) reaction proceeds through a channel in which a single phase dominates for all projections of the current ($T\sim|T|e^{i\delta}$, $L\sim|L|e^{i\delta}$, with the same δ), then T^*L is real and $W^{(1)}_{TL}$ may be non-zero while $W^{(1)}_{TL'}$ vanishes.

Moreover, it happens that $W_{TL'}^{(1)}$ also vanishes in the absence of final-state interactions. Therefore, if $W_{TL'}^{(1)} \neq 0$, then interesting effects must be coming into play. For example, in the Δ-region, coincidence electron scattering will be driven to a large extent by the 33-amplitude (i.e., with one phase, δ_{33}) and, while $W_L^{(1)}$, $W_T^{(1)}$, $W_{TT}^{(1)}$ and $W_{TL}^{(1)}$ may all be non-zero, $W_{TL'}^{(1)}$ may be expected to vanish. To the extent that it does not vanish, one will be measuring the interferences of the 33-amplitude with amplitudes for some other channels and thus addressing interesting physics questions. Similar arguments will apply to the giant resonance region in nuclei where the electron polarization cross section will permit the interference of a given giant resonance say with the direct background to be studied with increased sensitivity. Presently work is in progress on calculations for (e,e'p) and $(\vec{e},e'p)$ reactions in the quasi-elastic region which already indicate that significant polarization cross sections are to be found even in this energy region and that interesting levels of sensitivity to the nature of the final-state interaction are to be found (Kleppinger, 1984; Van Orden, 1984).

(III) Exclusive-2 electron scattering, no nuclear polarizations. Now that the procedures are clear, let us proceed more rapidly to discussions which extend beyond familiar (e,e') and (e,e'x) analyses given above. Next we consider triple-coincidence, (e,e'xy) reactions, where two particles having 4-momenta P_1 and P_2 are detected in coincidence with the scattered electron. As before P_0 will stand for the 4-momentum in the final state except for P_1 and P_2 (see Fig. 6). Using momentum

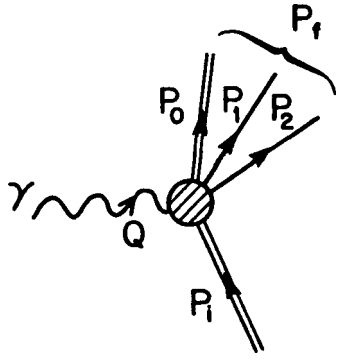

Fig. 6. Hadronic (nuclear) vertex for exclusive-2 electron scattering.

conservation we can eliminate the total final-state momentum, $P_f=P_i+Q$ and the unobserved particles' momentum $P_0=P_f-(P_1+P_2)$. This leaves four independent 4-momenta from which to build the hadronic tensor: $\{Q,P_i,P_1,P_2\}$. Assuming we know the target mass, M_i and the masses of particles 1 and 2, M_1 and M_2 respectively, we have three conditions, $P_i^2=M_i^2$, $P_1^2=M_1^2$ and $P_2^2=M_2^2$, leaving seven independent scalar quantities upon which the response functions depend: $\{Q^2,Q\cdot P_i,P_1\cdot P_i,P_2\cdot P_i,Q\cdot P_1,$ $Q\cdot P_2,P_1\cdot P_2\}$. Once again it is useful to employ laboratory variables as indicated in Fig. 7. Now there are two pairs of angles (θ_1,ϕ_1) and (θ_2,ϕ_2), for the two particles detected in coincidence with the scattered electron. These particles have 3-momenta $p_1 = |\vec{P}_1|$ and $p_2 = |\vec{P}_2|$ with energies $E_1 = \sqrt{p_1^2 + M_1^2}$ and $E_2 = \sqrt{p_2^2 + M_2^2}$ respectively. The seven scalar variables may then be re-expressed as

$$
\begin{aligned}
Q^2 &= \omega^2 - q^2 \\
Q\cdot P_i &= \omega M_i \\
P_1\cdot P_i &= E_1 M_i \\
P_2\cdot P_i &= E_2 M_i \\
Q\cdot P_1 &= E_1 - qp_1\cos\theta_1 \\
Q\cdot P_2 &= E_2 - qp_2\cos\theta_2 \\
P_1\cdot P_2 &= E_1E_2 - p_1p_2\{\cos\theta_1\cos\theta_2 + \sin\theta_1\sin\theta_2\cos(\phi_1-\phi_2)\}.
\end{aligned}
\tag{36}
$$

Note that now the azimuthal angles ϕ_1 and ϕ_2 occur as part of the scalar functional dependence of the reponse functions. In fact it is useful to define

$$\textbf{Exclusive-2:}\quad \Delta\phi_{12} \equiv \phi_1 - \phi_2 \tag{37a}$$

$$\Phi \equiv \frac{1}{2}(\phi_1 + \phi_2)\ , \tag{37b}$$

and then equivalently the response functions depend on the set $\{q,\omega,E_1,$ $E_2,\theta_1,\theta_2,\Delta\phi_{12}\}$, but not on the average azimuthal angle Φ.

As before, when building the hadronic tensor, it is useful to replace the set of 4-vectors $\{Q^\mu,P_i^\mu,P_1^\mu,P_2^\mu\}$ with the projected set $\{Q^\mu,V_i^\mu,$ $V_1^\mu,V_2^\mu\}$, where

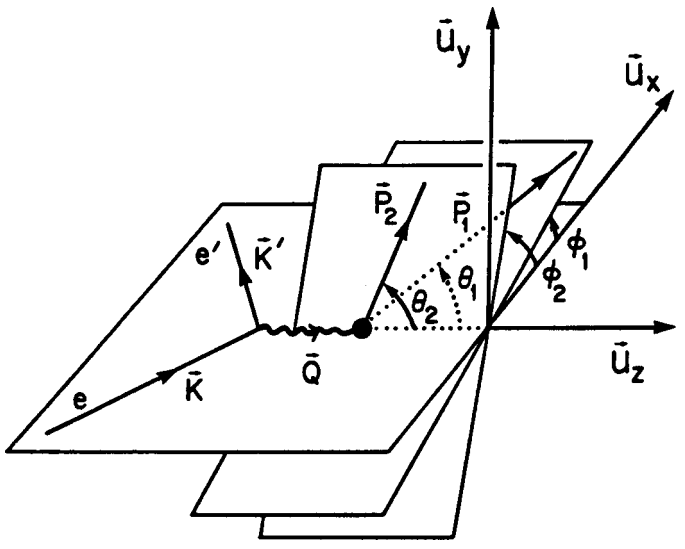

Fig. 7. Exclusive-2 electron scattering. The labelling is the same as in Fig. 5 except now with two particles detected in coincidence with the scattered electron.

$$V_i^\mu \equiv \frac{1}{M_i}\{P_i^\mu - (\frac{Q\cdot P_i}{Q^2})Q^\mu\} \tag{38a}$$

$$V_k^\mu \equiv P_k^\mu - (\frac{Q\cdot P_k}{Q^2})Q^\mu, \quad k=1,2\ , \tag{38b}$$

and where $Q\cdot V_i = Q\cdot V_1 = Q\cdot V_2 = 0$. Using the previous arguments we may write

$$W_s^{\mu\nu} = X_1 g^{\mu\nu} + \cdots + X_{11}(V_1^\mu V_2^\nu + V_2^\mu V_1^\nu) \tag{39a}$$

$$W_a^{\mu\nu} = Y_1(Q^\mu V_i^\nu - V_i^\mu Q^\nu) + \cdots + Y_6(V_1^\mu V_2^\nu - V_2^\mu V_1^\nu)\ , \tag{39b}$$

where no ε-terms are allowed using the parity properties of the tensors and where all 17 response functions depend on the seven scalar quantities discussed above. Finally, imposing the current conservation conditions on these general forms and contracted the results with the electron scattering leptonic tensor given in Eq.(10), we are led to the following results:

$$\eta^{s}_{\mu\nu} W^{\mu\nu}_{s} \sim v_L W^{(2)}_L + v_T W^{(2)}_T + v_{TT}(W^{(2)}_{TT}\cos 2\Phi + \tilde{W}^{(2)}_{TT}\sin 2\Phi)$$
$$+ v_{TL}(W^{(2)}_{TL}\cos\Phi + \tilde{W}^{(2)}_{TL}\sin\Phi) \qquad (40a)$$

$$\eta^{a}_{\mu\nu} W^{\mu\nu}_{a} \sim v_{T'} W^{(2)}_{T'} + v_{TL'}(W^{(2)}_{TL'}\sin\Phi + \tilde{W}^{(2)}_{TL'}\cos\Phi) \quad , \qquad (40b)$$

where we now have a final sixth electron kinematical factor

$$v_{T'} = \sqrt{-(Q^2/q^2) + \tan^2\frac{\theta}{2}} \cdot \tan\frac{\theta}{2} \qquad (41)$$

in addition to the other five defined in Eqs.(21,30,32). Clearly the notation follows the previous scheme with "2" standing for exclusive-2 (e,e'xy) reactions. Before discussing the structure of Eqs.(40), let us first consider exclusive-n reactions with $n \geq 3$.

(IV) Exclusive-3, -4, ... electron scattering, no nuclear polarizations. If we try to generalize the above ideas to situations with three or more particles detected in coincidence with the scattered electron, we find that the problem does not continue to get more and more complicated in form. For example, consider exclusive-3 scattering as indicated in Fig. 8. Now we must work with the 4-vectors $\{Q^\mu, P^\mu_i, P^\mu_1, P^\mu_2, P^\mu_3\}$. From these we can form 10 independent dynamical scalars (i.e., using the known masses M_i, M_1, M_2 and M_3 to eliminate four possibilities as before). In the general case of exclusive-n electron scattering there are $3n+1+\delta_{n0}$ such independent scalar quantities; equivalently the following set of

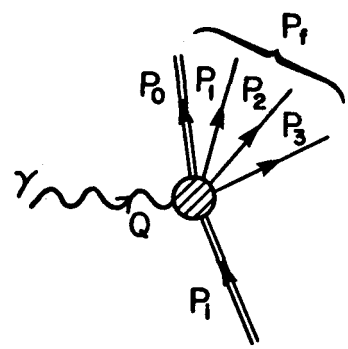

Fig. 8. Hadronic (nuclear) vertex for exclusive-3 electron scattering.

laboratory variables may be used:

$$\{q,\omega\} \quad , \quad n\geq 0$$

$$\{E_k,\theta_k,\ k=1,\ \ldots,\ n\} \quad , \quad n\geq 1$$

$$\{\Delta\phi_{12},\Delta\phi_{23},\ \ldots,\ \Delta\phi_{n-1n}\} \qquad n\geq 2,$$

where $\Delta\phi_{kk'} \equiv \phi_k - \phi_{k'}$. Only the azimuthal angle differences occur as dependencies contained within the response functions. This leaves the average azimuthal angle

$$\Phi \equiv \frac{1}{n}\,(\phi_1 + \ldots + \phi_n) \quad , \quad n\geq 1 \tag{42}$$

as the one kinematical aspect of the detected particles' momenta which does not occur as an argument in the response functions, but appears explicitly in the cross section. The case of n=3 is illustrated in Fig. 9.

If we continue with exclusive-3 scattering and try to build the tensor $W^{\mu\nu}$ from the momenta $\{Q^\mu,P_i^\mu,P_1^\mu,P_2^\mu,P_3^\mu\}$ we immediately observe that a certain saturation has occurred. At the level of exclusive-2 scattering we had four independent 4-momenta; now for $n\geq 3$ we are trying to use five or more independent vectors in a 4-dimensional space. We cannot do so, since the space is spanned by only four. In the case of n=3, for example, we can write

$$P_3^\mu = aQ^\mu + bP_i^\mu + cP_1^\mu + dP_2^\mu \quad , \tag{43}$$

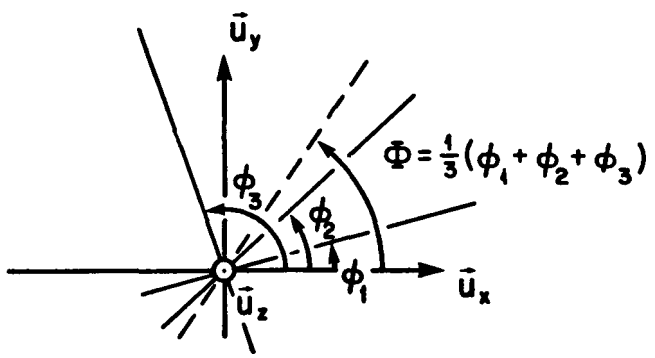

Fig. 9. Azimuthal angles entering in exclusive-3 electron scattering.

where a, b, c and d are scalar quantities. Thus we are back to having only the four momenta that were used for the n=2 case. Indeed, this is true for all $n \geq 3$. The general result for the scattering of electrons (polarized or not) where no nuclear polarizations are specified is then similar in form to Eqs.(40). The "super Rosenbluth" formula is

$$\frac{d\sigma}{d\omega d\Omega_e d\Omega_1 \cdots} = \frac{\sigma_M}{M_i}\Big\{[v_L W_L^{(n)} + v_T W_T^{(n)} + v_{TT}(W_{TT}^{(n)}\cos 2\Phi + \tilde{W}_{TT}^{(n)}\sin 2\Phi) + v_{TL}(W_{TL}^{(n)}\cos\Phi + \tilde{W}_{TL}^{(n)}\sin\Phi)] + h\,[v_{T'}W_{T'}^{(n)} + v_{TL'}(W_{TL'}^{(n)}\sin\Phi + \tilde{W}_{TL'}^{(n)}\cos\Phi)]\Big\}, \tag{44}$$

where Φ is given by Eq.(42) and the electron kinematical factors are given by Eqs.(21,30,32,41). For convenience we list them here again:

$$\begin{aligned}
v_L &= (Q^2/q^2)^2 \\
v_T &= -\frac{1}{2}(Q^2/q^2) + \tan^2\frac{\theta}{2} \\
v_{TT} &= \frac{1}{2}(Q^2/q^2) \\
v_{TL} &= \frac{1}{\sqrt{2}}(Q^2/q^2)\sqrt{-(Q^2/q^2) + \tan^2\frac{\theta}{2}} \\
v_{T'} &= \sqrt{-(Q^2/q^2) + \tan^2\frac{\theta}{2}}\,\cdot\,\tan\frac{\theta}{2} \\
v_{TL'} &= \frac{1}{\sqrt{2}}(Q^2/q^2)\,\cdot\,\tan\frac{\theta}{2}
\end{aligned}, \tag{45}$$

where as usual $0 \leq \{-Q^2/q^2 = 1 - (\omega/q)^2\} \leq 1$. In Eq.(44) for inclusive scattering (n=0) only the L and T terms contribute (see Eq.(19)). For exclusive-1 scattering, $\Phi=\phi_1$ and the response functions $W_{T'}^{(1)}$, $\tilde{W}_{TT}^{(1)}$, $\hat{W}_{TL}^{(1)}$ and $\tilde{W}_{TL'}^{(1)}$ are all absent (see Eqs.(29) and (31)). As before, in considering exclusive-n scattering, if we integrate over the angle dependence (θ_n,ϕ_n) and sum over open channels insofar as particle n is concerned, then we shall recover the exclusive-(n-1) results.

In the general case we may imagine using the helicity dependence to separate the T' and TL' from the L, T, TT and TL terms. After this the Φ-dependence may be used to separate $v_L W_L^{(n)}+v_T W_T^{(n)}$, $W_{TT}^{(n)}$, $\tilde{W}_{TT}^{(n)}$, $W_{TL}^{(n)}$ and $\tilde{W}_{TL}^{(n)}$ and to separate $W_{T'}^{(n)}$, $W_{TL'}^{(n)}$, $\tilde{W}_{TL'}^{(n)}$. Finally the θ-dependence in v_T may be used in making a Rosenbluth decomposition of $W_L^{(n)}$ and $W_T^{(n)}$. Thus all nine response functions are in principle experimentally accessible. Note that the original tensor $W^{\mu\nu}$ was constructed from bilinear products of the electromagnetic current matrix elements (Eq.(5b)). In turn the currents are 4-vectors which satisfy the continuity equation, $Q_\mu J^\mu_{fi}=0$; this implies[†] that $\omega J^0_{fi}=qJ^3_{fi}$, so that only three components of J^μ_{fi} are independent (say J^1_{fi}, J^2_{fi} and J^3_{fi}, with $J^0_{fi}=(q/\omega)J^3_{fi}$). Thus, there should be 3 x 3 independent terms in the cross section, and that agrees with the structure seen in Eq.(44).

(V) Inclusive electron scattering from polarized targets. Let us conclude our discussion of electron scattering with a brief look at the differences which occur when nuclear polarizations are considered. This subject is entered into in more depth elsewhere (Donnelly, 1983; Donnelly 1984a; Donnelly and Raskin, 1984; Donnelly and Sick, 1984), and so in the present context we show only how these ideas fit into the general "super Rosenbluth" schemes. Let us consider discrete nuclear states labelled $J_i^{\pi_i}$ and $J_f^{\pi_f}$. The inclusive electron scattering cross section for specific incident electron helicity h = $\pm$1 can be written

$$\left(\frac{d\sigma}{d\Omega}\right)^h_{fi} = \Sigma_{fi} + h\Delta_{fi} \ , \tag{46}$$

where the electron-spin-averaged cross section is given by

$$\Sigma_{fi} = \frac{1}{2}\left\{\left(\frac{d\sigma}{d\Omega}\right)^{+1}_{fi} + \left(\frac{d\sigma}{d\Omega}\right)^{-1}_{fi}\right\} \tag{47a}$$

and the electron polarization cross section is given by

[†]In fact, the nomenclature "longitudinal" used above is really not accurate: both longitudinal (μ=3) and "time" (charge, μ=0) components enter and are related by this current conservation identity.

$$\Delta_{fi} = \frac{1}{2}\{(\frac{d\sigma}{d\Omega})^{+1}_{fi} - (\frac{d\sigma}{d\Omega})^{-1}_{fi}\} \quad . \tag{47b}$$

The former is what is measured without having polarized electrons; the latter requires that the electrons be polarized. For longitudinally polarized electrons in the extreme relativistic limit it may be shown (Donnelly and Raskin, 1984) that

$$\Sigma_{fi} = \sigma_M f_{rec}^{-1}\{v_L R^L_{fi} + v_T R^T_{fi} + v_{TT} R^{TT}_{fi} + v_{TL} R^{TL}_{fi}\} \tag{48a}$$

$$\Delta_{fi} = \sigma_M f_{rec}^{-1}\{v_{T'} R^{T'}_{fi} + v_{TL'} R^{TL'}_{fi}\} \quad , \tag{48b}$$

where the electron kinematical dependence is contained in the Mott cross section, the recoil factor and precisely the same factors v_L, v_T, v_{TT}, v_{TL}, $v_{T'}$, and $v_{TL'}$, summarized in Eqs.(45). We shall consider two situations: (1) the target may be polarized, but no nuclear polarizations are known in the final state - this will be indicated fi; (2) the initial state is unpolarized, but polarizations may be measured in the final state (say by a second analyzing reaction) - this will be indicated fi. The response functions above are related in the two cases:

$$R^K_{fi} = \pm \frac{2J_f + 1}{2J_i + 1} R^K_{if} \quad , \tag{49}$$

where the plus sign occurs for K=L, T, TT and TL' and the minus sign for K=TL and T' (the nomenclature is similar to that used above for coincidence reactions). More complicated situations can also be studied, but this is sufficient for our present purposes.

Let us consider only polarized targets, since the recoil polarization formalism is immediately recovered using Eq.(49). The target polarization is specified by giving the M_J-substate population probabilities, $p_{(i)}(M_{J_i})$, referred to some axis of polarization. As indicated in Fig. 10 we shall choose this axis to point in the general direction (θ^*,ϕ^*). It is then possible to show that the response functions in Eqs.(48) have explicit dependences on the azimuthal angle ϕ^*:

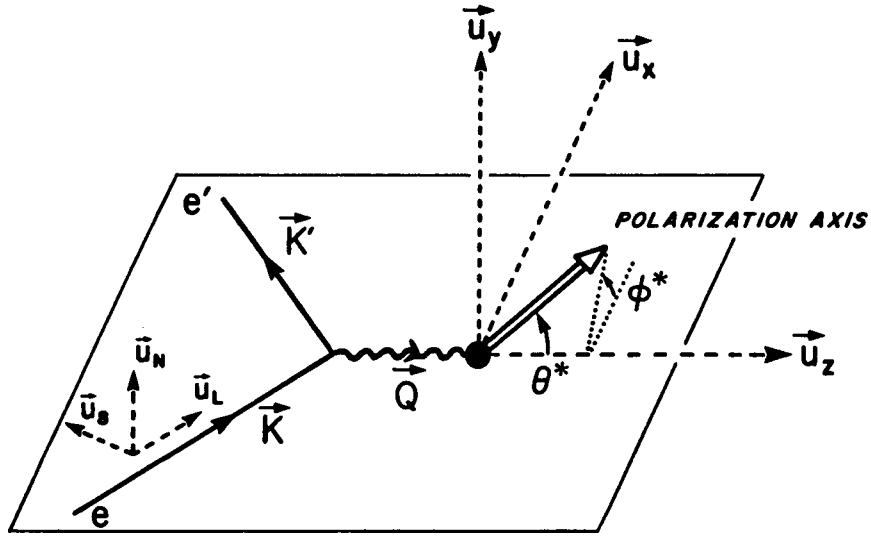

Fig. 10. Electron scattering from polarized targets. The polarization axis is specified by the angles (θ^*,ϕ^*) in the same coordinate system used for Figs. 5 and 7.

$$
\begin{aligned}
R_{fi}^{L} &= W_{fi}^{L} \\
R_{fi}^{T} &= W_{fi}^{T} \\
R_{fi}^{TT} &= W_{fi}^{TT} \cos 2\phi^* \\
R_{fi}^{TL} &= W_{fi}^{TL} \cos \phi^* \\
R_{fi}^{T'} &= W_{fi}^{T'} \\
R_{fi}^{TL'} &= W_{fi}^{TL'} \cos \phi^* \quad ,
\end{aligned}
\tag{50}
$$

where the W's are functions of q, ω and θ^*. The behavior here is reminiscent of the general structure seen above for exclusive electron scattering without nuclear polarizations. Using the electron helicity dependence to separate Σ_{fi} and Δ_{fi}, the ϕ^*-dependence to separate all but $v_L W_{fi}^{L} + v_T W_{fi}^{T}$, and finally the θ-dependence in v_T to separate these as well, all six of the response functions W_{fi}^{K}, K=L,T,TT,TL,T' and TL' are experimentally accessible.

Upon examining the response functions in more detail and proceeding through the angular momentum analysis that this entails, it proves to be

useful to employ Fano tensors (Donnelly and Raskin, 1984):

$$f_{\mathcal{J}}^{(i)} \equiv \sum_{M_{J_i}} (-)^{J_i - M_{J_i}} \langle J_i M_{J_i} J_i - M_{J_i} | \mathcal{J} 0 \rangle p_{(i)}(M_{J_i}), \tag{51}$$

where angular momentum conservation requires that $0 \leq \mathcal{J} \leq 2J_i$. For $\mathcal{J}=0$ we always obtain

$$f_0^{(i)} = 1/\sqrt{2J_i+1} \tag{52}$$

regardless of the state of polarization. For unpolarized targets where $p_{(i)}(M_{J_i})=(2J_i+1)^{-1}$ we have

$$\text{Unpolarized:} \quad f_{\mathcal{J}}^{(i)} = \delta_{\mathcal{J}0}/\sqrt{2J_i+1} \tag{53}$$

For situations where $p_{(i)}(M_{J_i}=+J_i)=1$, which we shall call 100% polarization, we have

$$\textbf{100\% Polarization:} \quad f_{\mathcal{J}}^{(i)} = \frac{(2J_i)!\sqrt{2\mathcal{J}+1}}{\sqrt{(2J_i+1+\mathcal{J})!(2J_i-\mathcal{J})!}} \tag{54}$$

When the target is aligned, that is, when $p_{(i)}(+M_{J_i})=p_{(i)}(-M_{J_i})$, then it is easy to show that all odd Fano tensors vanish:

$$\textbf{Aligned:} \quad f_{\mathcal{J}}^{(i)} = 0 \text{ for } \mathcal{J}=\text{odd}. \tag{55}$$

The Fano tensors are written out explicitly for the cases $J_i=0,1/2,1$ and 3/2 in (Donnelly, 1984a).

It may be shown that for the fi problem the nuclear response functions may be expressed in the following Legendre decompositions:

$$\begin{aligned} W_{fi}^{L} &= 4\pi \sum_{\substack{\mathcal{J} \geq 0 \\ \text{even}}} f_{\mathcal{J}}^{(i)} P_{\mathcal{J}}(\cos\theta^*) W_{\mathcal{J}}^{L}(q)_{fi} \\ W_{fi}^{T} &= 4\pi \sum_{\substack{\mathcal{J} \geq 0 \\ \text{even}}} f_{\mathcal{J}}^{(i)} P_{\mathcal{J}}(\cos\theta^*) W_{\mathcal{J}}^{T}(q)_{fi} \end{aligned} \tag{56}$$

$$W^{TT}_{fi} = 4\pi \sum_{\substack{J \geq 2 \\ \text{even}}} f^{(i)}_J P^2_J(\cos\theta^*)\, W^{TT}_J(q)_{fi}$$

$$W^{TL}_{fi} = 4\pi \sum_{\substack{J \geq 2 \\ \text{even}}} f^{(i)}_J P^1_J(\cos\theta^*)\, W^{TL}_J(q)_{fi}$$

where only tensors of even rank occur in the terms which contribute to Σ_{fi}, and

$$W^{T'}_{fi} = 4\pi \sum_{\substack{J \geq 1 \\ \text{odd}}} f^{(i)}_J P_J(\cos\theta^*) W^{T'}_J(q)_{fi}$$

$$W^{TL'}_{fi} = 4\pi \sum_{\substack{J \geq 1 \\ \text{odd}}} f^{(i)}_J P^1_J(\cos\theta^*) W^{TL'}_J(q)_{fi}, \tag{57}$$

where only odd-rank tensors contribute to Δ_{fi}. In making these decompositions, we have defined reduced response functions W^K_J, K=L,T,TT,TL,T' and TL', which do not depend on the polarization angles θ^* and ϕ^*.

The W's contain the nuclear structure information in the form of bilinear products of the Coulomb and transverse electric and magnetic multipole matrix elements for the transition i→f:

$$\begin{aligned} F_{CJ}(q) &\equiv \langle J_f || \hat{M}^{Coul}_J(q) || J_i \rangle / \sqrt{2J_i+1} \\ F_{EJ}(q) &\equiv \langle J_f || \hat{T}^{el}_J(q) || J_i \rangle / \sqrt{2J_i+1} \\ F_{MJ}(q) &\equiv \langle J_f || i\hat{T}^{mag}_J(q) || J_i \rangle / \sqrt{2J_i+1} \ . \end{aligned} \tag{58}$$

The CJ, J=0,1,2,... and EJ, J=1,2,... multipoles have natural parity ($\pi=(-)^J$), whereas the MJ, J=1,2,... multipoles have non-natural parity ($\pi=(-)^{J+1}$). In the case of elastic scattering parity and time-reversal conservation permit only even-J Coulomb and odd-J magnetic multipoles to be non-zero. The longitudinal (L) response functions contain only Coulomb multipoles, including interference terms CJ/CJ'; the T, TT and T' pieces contain only transverse multipoles with EJ/EJ', MJ/MJ', and EJ/MJ' interferences in general; the TL and TL' pieces contain Coulomb-transverse interferences CJ/EJ' and CJ/MJ'. In the explicit expressions for the response functions (Donnelly and Raskin, 1984) the

angular momentum conservation is always contained in a specific 6-j symbol. For example,

$$W^L_{\mathcal{J}}(q)_{fi} = (-)^{J_i+J_f}(2J_i+1) \times \sum_{JJ'\geq 0} (-)^{\frac{1}{2}(J-J')} \sqrt{(2\mathcal{J}+1)(2J+1)(2J'+1)} \begin{pmatrix} J & J' & \mathcal{J} \\ 0 & 0 & 0 \end{pmatrix} \begin{Bmatrix} J & J' & \mathcal{J} \\ J_i & J_i & J_f \end{Bmatrix} F_{CJ}(q) F_{CJ'}(q) \tag{59}$$

Thus, in addition to the condition $0 \leq \mathcal{J} \leq 2J_i$, we also have the vector addition requirements, $\Delta(JJ'\mathcal{J})$, $\Delta(J_i J_f J)$ and $\Delta(J_i J_f J')$. It is then straightforward to enumerate the various multipole matrix elements which occur once $J_i{}^{\pi_i}$ and $J_f{}^{\pi_f}$ are specified and to compare with the number of independent reduced response functions which are in principle experimentally accessible.

For instance, consider the case $J_i{}^{\pi_i}=3/2^+$ and $J_f{}^{\pi_f}=5/2^-$ where C1/E1, M2, C3/E3 and M4 multipoles can occur. Since $J_i = 3/2$ we may have $\mathcal{J}=0$ and 2 in Σ_{fi} and $\mathcal{J}=1$ and 3 in Δ_{fi}. Thus the possible reduced response functions are W_0^L, W_2^L, W_0^T, W_2^T, W_2^{TT}, W_2^{TL} (for six terms in Σ_{fi}) and $W_1^{T'}$, $W_3^{T'}$, $W_1^{TL'}$, $W_3^{TL'}$ (for four terms in Δ_{fi}). Returning to Eq.(59) for a moment, we see that W_0^L has only terms with $J'=J$; in fact it is proportional to the unpolarized longitudinal cross section and contains only the combination $F_{C1}^2+F_{C3}^2$. W_2^L, on the other hand, may have $J'\neq J$ so that a cross term of the form $F_{C1}F_{C3}$ may occur. Similar interference effects are seen in the other reduced response functions.

Before turning to specific examples of these ideas let us rewrite the five combinations of response functions which may be separated using the h and ϕ^* dependencies in the cross section in terms of the following tensor polarizations:

$$\begin{aligned}
\mathcal{J} = \text{even:}\quad & R^0_{\mathcal{J}}(q,\theta)_{fi} \equiv f^{(i)}_{\mathcal{J}}(v_L W^L_{\mathcal{J}}(q)_{fi} + v_T W^T_{\mathcal{J}}(q)_{fi})/F^2(q,\theta)^{fi} \\
& R^1_{\mathcal{J}}(q,\theta)_{fi} \equiv f^{(i)}_{\mathcal{J}} v_{TL} W^{TL}_{\mathcal{J}}(q)_{fi}/F^2(q,\theta)^{fi} \\
& R^2_{\mathcal{J}}(q,\theta)_{fi} \equiv f^{(i)}_{\mathcal{J}} v_{TT} W^{TT}_{\mathcal{J}}(q)_{fi}/F^2(q,\theta)^{fi} \\
\mathcal{J} = \text{odd:}\quad & R^0_{\mathcal{J}}(q,\theta)_{fi} \equiv f^{(i)}_{\mathcal{J}} v'_T W^{T'}_{\mathcal{J}}(q)_{fi}/F^2(q,\theta)^{fi} \\
& R^1_{\mathcal{J}}(q,\theta)_{fi} \equiv f^{(i)}_{\mathcal{J}} v'_{TL} W^{TL'}_{\mathcal{J}}(q)_{fi}/F^2(q,\theta)^{fi},
\end{aligned} \tag{60}$$

where the usual (unpolarized) form factors are given by

$$F^2(q,\theta)^{fi} = v_L F_L^2(q)^{fi} + v_T F_T^2(q)^{fi} \tag{61}$$

with longitudinal and transverse contributions. The unpolarized (e,e') cross section is then given by

$$\Sigma_0^{fi} \equiv 4\pi\sigma_M f_{rec}^{-1} F^2(q,\theta)^{fi}. \tag{62}$$

We may then display the complete (θ^*,ϕ^*) dependence of the cross sections separately from the (q,θ) dependence as contained in the tensor polarizations:

$$\Sigma_{fi} \equiv \Sigma_0^{fi}[1 + \sum_{\substack{J\geq 2 \\ \text{even}}} (P_J(\cos\theta^*)R_J^0(q,\theta)_{fi} + P_J^1(\cos\theta^*)\cos\phi^* R_J^1(q,\theta)_{fi} + P_J^2(\cos\theta^*)\cos 2\phi^* R_J^2(q,\theta)_{fi})] \tag{63}$$

$$\Delta_{fi} \equiv \Sigma_0^{fi}[\sum_{\substack{J\geq 1 \\ \text{odd}}} (P_J(\cos\theta^*)R_J^0(q,\theta)_{fi} + P_J^1(\cos\theta^*)\cos\phi^* R_J^1(q,\theta)_{fi})]. \tag{64}$$

In writing things this way we have used the special results

$$f_0^{(i)} W_0^L(q)_{fi} = F_L^2(q)^{fi} = \sum_{J\geq 0} F_{CJ}^2(q) \tag{65}$$

$$f_0^{(i)} W_0^T(q)_{fi} = F_T^2(q)^{fi} = \sum_{J\geq 1} \left\{ F_{EJ}^2(q) + F_{MJ}^2(q) \right\}, \tag{66}$$

so that

$$R_0^0(q,\theta)_{fi} = 1. \tag{67}$$

We shall return to these tensor polarizations in the next section and relate them to the more familiar t_{JM} polarizations used in discussing elastic scattering. Before turning to that discussion let us note two special circumstances. First, for $J_i=0$ or 1/2 we have

$$\Sigma_{fi} = \Sigma_0^{fi} \qquad (J_i=0,1/2), \tag{68}$$

that is, just the usual unpolarized (e,e') cross section. New information in Σ_{fi} is obtained only when $J_i \geq 1$. Secondly, for $J_i=0$ we have

$$\Delta_{fi} = 0 \qquad (J_i=0) \tag{69}$$

whereas for $J_i=1/2$ we obtain

$$\Delta_{fi} = \Sigma_0^{fi}(\cos\theta^* R_1^0(q,\theta)_{fi} + \sin\theta^*\cos\phi^* R_1^1(q,\theta)_{fi}), \quad (J_i=1/2) \tag{70}$$

with new information (i.e. beyond the usual unpolarized cross section) contained in Δ_{fi}.

Elastic Scattering

For elastic scattering the possible multipoles are

$$F_J(q) \equiv \begin{cases} F_{CJ}(q) & J=\text{even} \\ F_{MJ}(q) & J=\text{odd} \end{cases}, \tag{71}$$

where $0 \leq J \leq 2J_0$ with $J_i=J_f\equiv J_0$. The elastic reduced response functions may be written (Donnelly and Sick, 1984; Donnelly and Raskin, 1984):

$$W_\gamma^K(q)_{fi} = \sum_{J'J} A^K_{J'J;\gamma}(J_0) F_{J'}(q) F_J(q) , \tag{72}$$

where, of course, only the appropriate even- or odd-J multipole form factors occur:

$$\begin{aligned} &K = L && : J' = \text{even}, \quad J = \text{even} \\ &K = T, TT, T' && : J' = \text{odd}, \quad J = \text{odd} \\ &K = TL, TL' && : J' = \text{even}, \quad J = \text{odd} . \end{aligned}$$

The expansion coefficients may be expressed in the form

$$A^{K}_{J'J;\ell}(J_0) = X_{J'J\ell}(J_0) \times \begin{cases} \alpha_{J'J;\ell} & , \ K = L \\ \beta^{0}_{J'J;\ell} & , \ K = T, T' \\ \dfrac{2\sqrt{2}}{\sqrt{\ell(\ell+1)}}\,\beta^{1}_{J'J;\ell} & , \ K = TL, TL' \\ \dfrac{1}{\sqrt{(\ell-1)\ell(\ell+1)(\ell+2)}}\,\beta^{2}_{J'J;\ell} & , \ K = TT, \end{cases} \tag{73}$$

where we have defined functions

$$X_{J'J\ell}(J_0) \equiv (-)^{2J_0}[J_0]^2[J'][J][\ell] \begin{Bmatrix} J' & J & \ell \\ J_0 & J_0 & J_0 \end{Bmatrix} \tag{74}$$

$$\alpha_{J'J;\ell} \equiv (-)^{\frac{1}{2}(J'+J)} \begin{pmatrix} J & J' & \ell \\ 0 & 0 & 0 \end{pmatrix} \tag{75}$$

and

$$\beta^{\mathcal{M}}_{J'J;\ell} \equiv (-)^{\frac{1}{2}(J'+J-\mathcal{M})} \begin{pmatrix} J & J' & \ell \\ 1 & \mathcal{M}-1 & -\mathcal{M} \end{pmatrix}, \tag{76}$$

$$\mathcal{M} = 0,1,2 \text{ and } \ell \geq \mathcal{M} \text{ only,}$$

with $[x] \equiv \sqrt{2x+1}$. From these definitions we see that X-coefficients are completely symmetrical under permutations of J', J and ℓ and that $\alpha_{J'J;\ell}$, $\beta^{0}_{J'J;\ell}$ and $\beta^{2}_{J'J;\ell}$ are symmetrical under interchange of J' and J (since only J'=odd, J=odd, ℓ=even enters for the TT term which $\mathcal{M}$=2). Thus the summation in Eq.(72) may be written

$$\sum_{J'J}(\cdots) = \sum_{J'=J}(\cdots) + 2\sum_{J'<J}(\cdots) \tag{77}$$

for the L, T, TT and T' cases.

The above equations apply for the case where the target is polarized and the recoil nucleus polarization summed over. Of interest also is the case where the target is unpolarized, but the recoil nucleus polarization measured. Equation (49) then allows us to write

$$R^K_{ff} = \pm R^K_{fi} \quad \text{(elastic electron scattering)} \tag{78}$$

with similar relationships for the W's, where the plus sign occurs for K=L,T,TT and TL' and the minus sign for K=TL and T'. Thus, all of the above analysis applies (up to a sign) whenever either initial or final nuclear polarizations are specified. In the situation when the final-state recoil polarization is measured, it is convenient to express the cross section in terms of analyzing powers and polarization tensors. The latter are given in terms of the quantities discussed in the present work by

$$t_{j\mathcal{M}}(J_0) = \frac{(-)^{\mathcal{M}} R^{\mathcal{M}}_j(q,\theta)_{ff}}{[J_0]\, f^{(f)}_j} \times \begin{cases} 1 & \mathcal{M}=0,\ 0 \le j \le 2J_0 \\ \frac{1}{2}\sqrt{j(j+1)} & \mathcal{M}=1,\ 1 \le j \le 2J_0 \\ \frac{1}{2}\sqrt{(j-1)\,j\,(j+1)(j+2)} & \mathcal{M}=2,\ 2 \le j \le 2J_0 \end{cases} \tag{79}$$

We shall return below to an example where these are used (viz. for the deuteron).

Let us now turn from the general to the specific and look at a few illustrative examples. In all cases we shall assume that the target is 100% polarized and so use Eq.(54) for the Fano tensors.

(i) $J_0=0$

We recover only the usual unpolarized cross section

$$\Sigma_{fi} = \Sigma_0 \ , \ \Delta_{fi} = 0 \ . \tag{80}$$

(ii) $J_0=1/2$

Only C0 and M1 multipoles can occur and we have

$$\begin{aligned} \Sigma_{fi} &= \Sigma_0 \\ \Delta_{fi} &= \Sigma_0\{\cos\theta^* R^0_1(q,\theta)_{fi} + \sin\theta^* \cos\phi^*\, R^1_1(q,\theta)_{fi}\} \ , \end{aligned} \tag{81}$$

where we obtain from Eqs.(72-76)

$$R_1^0(q,\theta)_{fi} = -v'_T\, F_1^2(q) \;/\; F^2(q,\theta)$$

$$R_1^1(q,\theta)_{fi} = -v'_{TL}\, 2F_0(q)F_1(q) \;/\; F^2(q,\theta)\ , \tag{82}$$

with the usual form factor given in this case by

$$F^2(q,\theta) = v_L F_0^2(q) + v_T F_1^2(q)\quad . \tag{83}$$

With a polarized target and yet no electron polarization one does not learn anything beyond the usual unpolarized (e,e') cross section. In cases where $|F_0(q)| << |F_1(q)|$ or $|F_0(q)| >> |F_1(q)|$ the small form factor is hard to separate from the large one using the usual Rosenbluth separation method (i.e., varying v_T for fixed q to separate $F_0^2(q)$ and $F_1^2(q)$ in Eq.(83)), as they occur as their squares. On the other hand for polarized targets and polarized electrons one may determine Δ_{fi} which involves the interference $F_0(q)\ F_1(q)$ and hence is a much more sensitive probe of the small piece. A special fundamental example of this sort is provided by the nucleon itself, where at high q the transverse form factor dominates over the longitudinal one (Arnold and Gross, 1981; Arnold, Carlson and Gross, 1981). Measurements on ^{2}H or ^{3}He with polarized electrons and polarized targets (Cheung and Woloshyn, 1983; Blankleider and Woloshyn, 1984) would improve our knowledge of G_{En} which is presently very limited except at very low momentum transfer.

(iii) J_0=1

The possible multipoles are now C0, M1 and C2 and we have for the usual unpolarized form factors

$$\begin{aligned} F^2(q,\theta) &= v_L F_L^2(q) + v_T F_T^2(q) \\ F_L^2(q) &= F_0^2(q) + F_2^2(q) \\ F_T^2(q) &= F_1^2(q) \end{aligned} \tag{84}$$

Thus, with unpolarized scattering only the sum of the squares of the C0 and C2 contributions may be determined, not the C0 and C2 pieces separately.

With polarized targets, however, we have

$$\Sigma_{fi} = \Sigma_0\{1 + (P_2(\cos\theta^*)\ R_2^0(q,\theta)_{fi} + P_2^1(\cos\theta^*)\cos\phi^*\ R_2^1(q,\theta)_{fi} + P_2^2(\cos\theta^*)\cos 2\phi^*\ R_2^2(q,\theta)_{fi})\} \tag{85}$$

$$\Delta_{fi} = \Sigma_0\{P_1(\cos\theta^*)\ R_1^0(q,\theta)_{fi} + P_1^1(\cos\theta^*)\cos\phi^*\ R_1^1(q,\theta)_{fi}\}\ , \tag{86}$$

where

$$R_2^0(q,\theta)_{fi} = -\{v_L[\sqrt{2}\ F_2(F_0 + \frac{1}{2\sqrt{2}}\ F_2)] + v_T[\frac{1}{4}\ F_1^2]\}\ /\ F^2(q,\theta)$$

$$R_2^1(q,\theta)_{fi} = v_{TL}[\frac{\sqrt{3}}{2}\ F_1F_2]\ /\ F^2(q,\theta)$$

$$R_2^2(q,\theta)_{fi} = v_{TT}[\frac{1}{8}\ F_1^2]\ /\ F^2(q,\theta)$$

$$R_1^0(q,\theta)_{fi} = -v_T'[\frac{3}{4}\ F_1^2]\ /\ F^2(q,\theta)$$

$$R_1^1(q,\theta)_{fi} = -v_{TL}'[\sqrt{6}\ F_1(F_0 + \frac{1}{2\sqrt{2}}\ F_2)]\ /\ F^2(q,\theta)\ . \tag{87}$$

Thus, for example a measurement of R_2^0, either as here with polarized targets or by measuring the recoil polarization, together with the unpolarized longitudinal and transverse form factors allows a determination of the C0 and C2 contributions separately. Note that these tensor moments may be separated by using the (θ^*,ϕ^*) dependence above. In particular Σ_{fi} and Δ_{fi} may be separated using the dependence on the electron helicity h=±1. Then, R_1^0 and R_1^1 may be separated using either the θ^*-dependence or the ϕ^*-dependence or both. Likewise, R_2^0 and R_2^1 and R_2^2 may be separated from each other and from the unpolarized cross section. For completeness, let us use Eq.(78) to convert these expressions to the forms appropriate for measurements of the recoil polarization (R_2^1 and R_1^0 change sign) and use Eq.(79) to obtain the polarization tensors for spin 1:

$$
\begin{aligned}
t_{00}(1) &= R_0^0 = 1 \\
t_{10}(1) &= \sqrt{\tfrac{2}{3}}\, R_1^0 \\
t_{11}(1) &= -\sqrt{\tfrac{1}{3}}\, R_1^1 \\
t_{20}(1) &= \sqrt{2}\, R_2^0 \\
t_{21}(1) &= -\sqrt{3}\, R_2^1 \\
t_{22}(1) &= 2\sqrt{3}\, R_2^2
\end{aligned}
\tag{88}
$$

Upon employing the following relationships between the F's as used here and the G's as used elsewhere,

$$
\begin{aligned}
\sqrt{4\pi}\, F_0 &= (1+\tau) G_C \\
\sqrt{4\pi}\, F_1 &= -\frac{2}{\sqrt{3}} \sqrt{\tau(1+\tau)}\, G_M \\
\sqrt{4\pi}\, F_2 &= \frac{2\sqrt{2}}{3} \tau(1+\tau)\, G_Q \quad ,
\end{aligned}
\tag{89}
$$

where $\tau \equiv -Q_\mu Q^\mu / 4M_d^2$, we obtain the usual expressions for the polarization tensors as applied to the case of elastic scattering from deuterium.

(iv) $J_0 \geq 3/2$

The analysis presented here can straightforwardly be applied to higher-spin cases as well. Rather than repeating the formulas for such cases (Donnelly, 1983; Donnelly and Raskin, 1984; Donnelly and Sick, 1984), let us instead consider some "typical" results of calculations for specific nuclei. As a first example, let us consider the $\frac{3}{2}^-$ ground state of ^{7}Li using form factors calculated with Cohen and Kurath wave functions (Dubach, 1983). In fact an alkali is known to provide a practical polarizable target. We show in Fig. 11 results for unpolarized electrons of 500 MeV incident on polarized ^{7}Li nuclei. We assume that

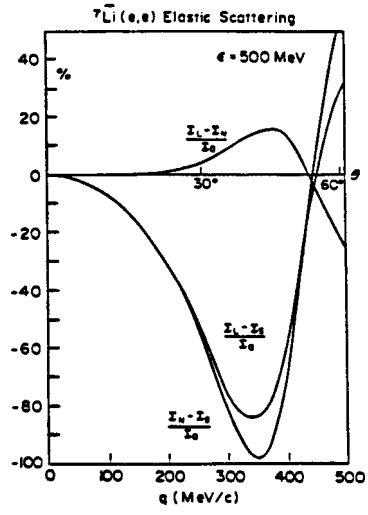

Fig. 11. Unpolarized elastic electron scattering from polarized ^{7}Li at 500 MeV incident electron energy. Cross sections in the L, N and S directions (see Fig. 10) are used to construct various asymmetries. Here Σ_0 is the unpolarized cross section.

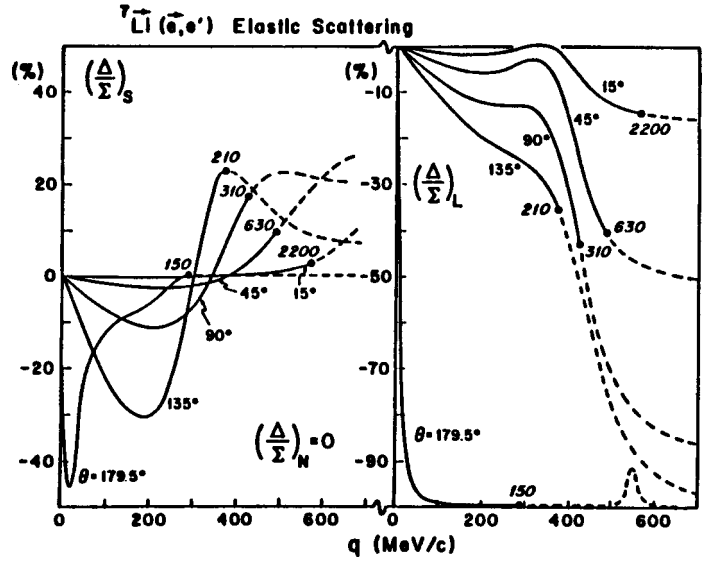

Fig. 12. Scattering of polarized electrons from polarized ^{7}Li. The polarization ratios Δ/Σ are shown for the S and L directions (see Fig. 10). The curves are labelled with the electron scattering angle θ and have dots on the curves to denote the places at which the cross section drops to 10^{-33} cm^2 sr^{-1}; solid lines correspond to larger cross sections and dashed curves to smaller cross sections. The numbers beside the dots give the electron energies ε corresponding to these conditions.

the target nuclei are 100% polarized in the L, N and S directions in Fig. 10, that is, along the incident beam direction, normal to the electron scattering plane and "sideways", respectively. Of course, as the electron kinematics change, the direction $\vec{Q}$ changes and so the angles (θ^*,ϕ^*) must change to keep the polarization axis fixed in the laboratory coordinate system. In Fig. 11 three different asymmetries are shown as functions of q or θ. Taking this new information together with the familiar unpolarized form factors F_L^2 and F_T^2 allows a complete separation of the four multipoles which occur. Drawing upon discussions of luminosities, etc. with polarized targets internal to a stretcher ring we estimate that, for target thicknesses on the order of 10^{15} atoms/cm^2, the practical minimum cross section is about 10^{-33} cm^2/sr. With ε=500 MeV this implies that momentum transfers out to beyond q 400-500 MeV/c should be accessible for this example. Using polarized electrons and polarized targets would permit Δ_{fi} to be determined in addition to Σ_{fi}. In Fig. 12 we show results for the polarization ratio Δ/Σ as a function of q for different scattering angles θ (and hence different incident electron energies ε). Solid curves correspond to cross sections above 10^{-33} cm^2/sr; dashed curves involve cross sections below this number. The dots mark the transition point (10^{-33} cm^2/sr) and occur at the electron energies indicated by the numbers near the dots. Clearly the polarization ratios are large for large scattering angles and intermediate energies, but become smaller at small $\theta \leftrightarrow$ large ε. This reflects the explicit tan $\theta/2$ in the electron kinematic factors v_T' and v_{TL}' (see Eqs.(45)).

Another spin-3/2 case is provided by the $3/2^+$ ground state of ^{39}K. The unpolarized elastic magnetic form factor is shown in Fig. 13 (see Donnelly and Sick, 1984). Here the dashed curve is a pure $1d_{3/2}$ proton form factor, the dotted curves show results when core polarization (CP) effects are included and the solid curve shows results when meson-exchange currents (MEC) are added as well (Suzuki, 1983). In fact, it appears that CP and MEC effects are rather different for the M1 and M3 form factors that together constitute F_T^2. The problem is that with unpolarized scattering we cannot separate the different multipoles. On the other hand with a polarized ^{39}K target it is possible to separate the M1 from the M3 and so gain finer information on the effects of interest.

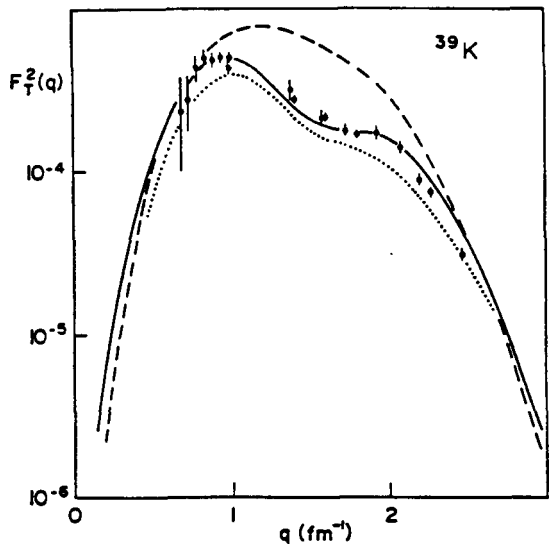

Fig. 13. Unpolarized elastic magnetic form factor for ^{39}K. The dashed curve represents the single-particle result; the dotted curve includes core polarization (CP); the solid curve includes meson-exchange current (MEC) effects in addition (Suzuki, (1983). The data are discussed in more detail in (Donnelly and Sick, 1984).

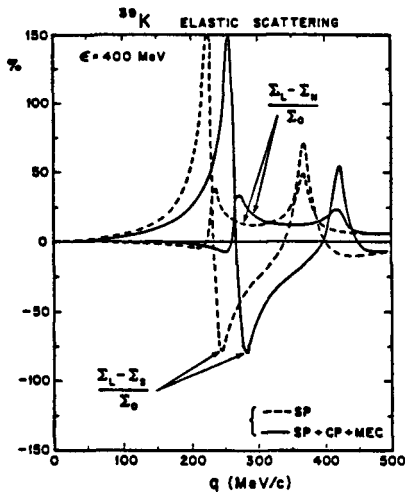

Fig. 14. Unpolarized elastic electron scattering from polarized ^{39}K at 400 MeV incident electron energy (labelling as in Fig. 11). The dashed and solid curves correspond to those in Fig. 13.

In Fig. 14 we show asymmetries of the type discussed above for ^{7}Li, indicating the pronounced shifts which occur when the CP and MEC effects are included. Clearly such new polarization information would have a

significant impact on electron scattering studies of nuclear structure.

Inelastic Scattering

The generalization of the formulas presented above for elastic scattering now to include inelastic scattering goes beyond the scope of this brief overview of the problem. They will be discussed in detail in (Donnelly and Raskin, 1984). For the present purposes let us consider only two illustrative examples.

(i) $J_i=1/2,\ J_f=3/2,\ \pi_f=\pi_i$

In this case we may have M1, C2 and E2 multipoles and the unpolarized form factors become

$$\begin{aligned} F^2(q,\theta) &= v_L F_L^2(q) + v_T F_T^2(q) \\ F_L^2(q) &= F_0^2(q) + F_2^2(q) \\ F_T^2(q) &= F_1^2(q) + F_3^2(q) \end{aligned} \tag{90}$$

A Rosenbluth separation will permit a determination of F_{C2}^2 and $F_{M1}^2+F_{E2}^2$, but not of the complete set of separated multipoles. With polarized targets, but without polarized electrons we obtain nothing new (this is the special spin-1/2 ground-state case):

$$\Sigma_{fi} = \Sigma_0^{fi} \tag{91}$$

On the other hand with polarized electrons and targets we may study

$$\Delta_{fi} = \Sigma_0^{fi}[P_1(\cos\theta^*)R_1^0(q,\theta)_{fi} + P_1^1(\cos\theta^*)\cos\phi^* R_1^1(q,\theta)_{fi}]. \tag{92}$$

where

$$\begin{aligned} R_1^0(q,\theta)_{fi} &= v_T'[\tfrac{1}{2}(F_{M1}^2 - F_{E2}^2 - 2\sqrt{3}\,F_{M1}F_{E2})] \,/\, F^2(q,\theta)^{fi} \\ R_1^1(q,\theta)_{fi} &= -v_{TL}'[F_{C2}(F_{M1} + \sqrt{3}\,F_{E2})] \,/\, F^2(q,\theta)^{fi} \quad . \end{aligned} \tag{93}$$

A specific fundamental case of this type is the $N(\frac{1}{2}\,\frac{1}{2},\ 938)\rightarrow\Delta(\frac{3}{2}\,\frac{3}{2},\ 1232)$ transition. In the most naive model both the nucleon and delta are com-

posed of three 1s quarks and the transition is a pure M1 spin-isospin flip. However, if orbital configurations are admixed by the color hyperfine interaction between quarks (e.g., L=2 with L=0 -- this is analogous to the D- and S-state admixing which occurs in the deuteron ground state because of the presence of a tensor part in the NN interaction), then C2/E2 multipoles will also be present. One can try to extract the longitudinal and transverse form factors in a usual Rosenbluth separation; however, the fact that only the squares of the individual multipoles occur in Eqs.(90) makes it difficult to see the small Coulomb contribution. On the other hand, with polarized electrons and protons it is now possible to measure R_1^0 and R_1^1 in Eq.(93). By working near $\phi^*=0°$ or 180° (i.e., in the electron scattering plane for the axis of polarization), the magnitude of the $\cos\phi^*$ term in Eq.(92) is maximized. Furthermore, by working near $\theta^*=90°$, the $P_1(\cos\theta^*)=\cos\theta^*$ factor can be made close to zero and the $P_1^1(\cos\theta^*)=\sin\theta^*$ factor can be made close to unity. With this as the polarization axis the R_1^0 term can be minimized and the R_1^1 contributions maximized. Importantly the latter contains the small C2 and large M1 contributions as an interference.

(ii) $J_i=3/2$, $J_f=1/2$, $\pi_f=\pi_i$

As in the case above we have M1, C2 and E2 multipoles with the same expressions for the unpolarized form factors (Eqs.(90)). However, now the initial state, which is presumed to be polarized, has spin-3/2 and it is the final nuclear state, whose polarization is summed over, which has spin-1/2. The situation is more akin to the example of elastic scattering from spin-3/2 polarized targets discussed in the previous section. Once again we shall not go into the detailed form of the cross section when polarizations are present (see Donnelly, 1983; Donnelly, 1984a; Donnelly and Raskin, 1984). Let us instead conclude by looking at results for a "typical" case.

As a specific example we consider the transition from the $3/2^-$ ground state of ^{7}Li to its $1/2^-$ (0.478 MeV) first excited state. Once again Cohen and Kurath wave functions were employed (Dubach, 1983). Beginning first with the situation where the ground state of ^{7}Li is polarized as in the elastic scattering case above, but where the incident electron is

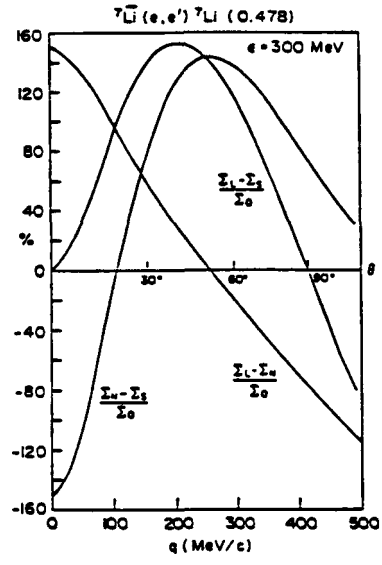

Fig. 15. Inelastic scattering of unpolarized electrons from polarized ^{7}Li at 300 MeV incident electron energy. The nomenclature is the same as in Fig. 11.

not polarized, we have the results shown in Fig. 15. The cross sections remain above the 10^{-33} cm^2sr^{-1} level out to beyond 400 MeV/c momentum transfer for this case where ε=300 MeV. In contrast to the elastic scattering situation where the asymmetries became small at low q (cf. Fig. 11), here they may remain large down to the lowest momentum transfers. The reason is that in the elastic case the low-q behavior is dominated by the elastic monopole charge form factor, F^2_{CO}, and at low-q this piece has no interesting polarization dependence by itself and so diminishes the overall effect at low momentum transfer. In Fig. 16 we show a more complete representation of the cross section Σ as a function of θ^* and ϕ^* for fixed electron kinematics (ε=300 MeV, θ=60°). The curve labelled ϕ^*=0° corresponds to sweeping the ^{7}Li polarization around from the direction of $\vec{Q}$ (θ^*=0°) to the direction opposite to $\vec{Q}$ (θ^*=180°) in the electron scattering plane. In the process one encounters the direction of the incident electron (labelled L) and the sideways direction (labelled S) as shown in Fig. 10. A similar sweep, but reflected in the plane defined by the normal direction and the direction $\vec{Q}$ is obtained when ϕ^*=180°. The remaining curve has ϕ^*=90° and so sweeps out the directions in polarization space from $\vec{Q}$ up through the normal

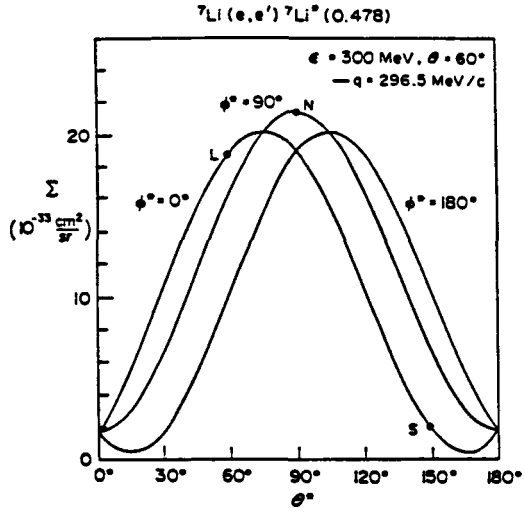

Fig. 16. Inelastic scattering of unpolarized electrons from polarized ^{7}Li at ε=300 MeV and θ=60°. Results are given as functions of the target polarization direction specified by (θ^*,ϕ^*). The special directions corresponding to L, N and S (see Fig. 10) are indicated.

direction (labelled N) and back to $-\vec{Q}$. Clearly these cross sections are large enough to make such experiments interesting (using our criterion of 10^{-33} cm^{2}sr^{-1} the units used here).

SUMMARY

Unpolarized Electrons:

When the helicity of the electron is not known we can only obtain the information contained in the electron-spin-averaged cross section $d\Sigma$. We have various levels of exclusivity:

(1) Inclusive, no nuclear polarizations — only two quantities are accessible, $W_L^{(0)}$ and $W_T^{(0)}$, the longitudinal and transverse response functions. They may be separated using the familiar Rosenbluth analysis. The former contains an incoherent sum of the squares of the Coulomb matrix elements; the latter contains an incoherent sum of the squares of the transverse electric and magnetic matrix elements.

(2) Exclusive, no nuclear polarizations — now more response functions enter, including ones containing transverse-transverse and transverse-longitudinal interferences; a generalized "super-Rosenbluth" formula comes into play. For exclusive-1 or (e,e'x) reactions there are four response functions. For exclusive-n, with $n \geq 2$, we have the maximal number of electron-spin-averaged response functions, namely, six. By using the azimuthal angle dependence coming from having a particle or particles detected in coincidence with the electron, along with the electron scattering angle dependence in the super-Rosenbluth formula, it is possible to separate all response functions from one another (see Eq.(44)).

(3) Inclusive, with nuclear polarizations — with polarized targets or with recoil polarizations measured (say in a second analyzing scattering experiment) new information is available. By varying the direction of polarization it is possible to separate four classes of response functions from one another (i.e., L, T, TT and TL contributions) and for each one of these to extract Legendre expansions involving the polar angle of polarization, θ^*. Each term in such decompositions contains specific interferences between the multipole matrix elements permitted by conservation of angular momentum, parity and invariance under time reversal. Thus, in a mixed-multipole situation, in general we have much more information than is contained in the unpolarized inclusive problem discussed above (case (1)). An important example is provided by elastic scattering from $^2\overleftrightarrow{H}$, where we desire to separate the C0 and C2 contributions and cannot do so without knowledge of the deuteron's (tensor) polarization. One special aspect of not having polarized electrons available is that for polarized spin-1/2 targets we recover only the unpolarized (e,e') cross section and so learn nothing new; to obtain new information in this case we need to have polarized electrons as well (see below).

Polarized Electrons:

When the helicity of the electron is known we can obtain not only the information discussed above, but also the new physics contained in the polarization cross section $d\Delta$. Again we have the various levels of exclusivity:

(1) Inclusive, no nuclear polarizations — this should vanish if parity is conserved. Of course, the interest in this special case is to measure the polarization cross section, $d\Delta = \frac{1}{2}(d\sigma(h=+1)-d\sigma(h=-1))$ and so study the effects of parity violation which in fact must be present at the level of the weak interaction.

(2) Exclusive, no nuclear polarizations — now non-zero response functions may enter even if parity conservation is assumed. In general a new transverse-transverse interference and new transverse-longitudinal interferences may occur (i.e., in addition to the ones discussed above). For exclusive-1 reactions only one more, a TL interference (requiring detection of particle x out of the electron scattering plane, see Eq.(44)), occurs and appears even at this early stage of the analysis to contain interesting sensitivities to, for example, final-state interaction effects. For exclusive-n, with $n \geq 2$, we have the maximal number of polarization response functions, namely, three. Again these may be separated by using the azumithal angle dependence coming from having a particle or particles detected in coincidence with the electron. Using the entire super-Rosenbluth formula in Eq.(44) a total of nine independent nuclear response functions in the general case can be obtained by using the θ, Φ and h degrees of freedom.

(3) Inclusive, with nuclear polarizations — as above (case (3), unpolarized electrons), there is new information available when nuclear polarizations are known. In fact two more classes of response functions beyond the L, T, TT and TL contributions occur, namely, the T' and TL' pieces (see Eq.

(48)). Again these may be separated using the ϕ^* dependence (see Eqs.(50)) and then decomposed into interfering multipole forms by making Legendre expansions in $\cos\theta^*$ (see Eqs.(56) and (57)). Importantly now, with polarized spin-1/2 targets together with polarized electrons, new information beyond the usual unpolarized inclusive cross section becomes available. A specific fundamental case of interest involves scattering from the nucleon itself (perhaps imbedded in a light nucleus) where we wish to separate the G_E and G_M form factors, especially for the neutron. This is difficult to do at high $|Q^2|$ with unpolarized electron scattering, since the magnetic form factor is dominant and the two terms in the usual Rosenbluth formula enter as their squares. However, with polarizations specified it is possible to focus on their interference, $G_E G_M$ and so enhance the sensitivity to the small (interesting) contribution. Another case is provided by the $N \to \Delta$ transition where the polarization response functions contain a similar TL interference (this time a C2/M1 interference) which reflects complexity beyond the level of a pure M1 spin-isospin-flip excitation, perhaps relating to deformations in the Δ.

Of course, the examples highlighted here are special fundamental few-body cases with high intrinsic interest. Beyond these lie many examples of transitions in complex nuclei where the entire spectrum of nuclear structure and nuclear reaction mechanism studies will be opened up when coincidence and polarization measurements with electrons become fully realized.

APPENDIX

We use the nomenclature and conventions introduced in (Donnelly, 1983) where 4-vectors are denoted by capital letters, $A^\mu=(A^0,\vec{A})$, $B^\mu=(B^0,\vec{B})$, etc., with Greek letters $\mu=0,1,2,3$. For 3-vectors we write $\vec{A}$, $\vec{B}$, etc. or, when referring to their components, A^i, B^i, etc., with Latin letters $i=1,2,3$. We use the metric (and all other conventions on γ-matrices, etc.) of Bjorken and Drell (1964), where $g_{\mu\nu}=g^{\mu\nu}=(+1$ for $\mu=\nu=0$, -1 for $\mu=\nu=1$,

2 or 3 and 0 otherwise) is the metric raising or lowering operator. Thus we have $A_\mu = g_{\mu\nu} A^\nu$, etc., where the summation convention is used. Four-vector scalar products are written $A_\mu B^\mu \equiv A \cdot B = A^0 B^0 - \vec{A} \cdot \vec{B}$. Furthermore, lower case letters are used to denote the magnitudes of 3-vectors: $a \equiv |\vec{A}|$, $b \equiv |\vec{B}|$, etc. In fact several special cases occur frequently and it is useful to introduce a common notation for them:

Q^μ, photons: $\omega \equiv Q^0$, $q = |\vec{Q}|$.

For real photons we have $Q^2 = \omega^2 - q^2 = 0$; for virtual photons in electron scattering, $Q^2 < 0$ (space-like).

P_i^μ, P_f^μ, P^μ, etc., hadronic states: $E_i \equiv P_i^0$, $p_i = |\vec{P}_i|$

$E_f \equiv P_f^0$, $p_f = |\vec{P}_f|$

$E \equiv P^0$, $p = |\vec{P}|$

etc.

where we have $P_i^2 = E_i^2 - p_i^2 = M_i^2$, etc.

Throughout the text we use $\hbar = c = 1$ and adopt the convention where a caret over a symbol "$\hat{J}$" is used to denote an operator in second quantization (in the nuclear Hilbert space).

REFERENCES

Arnold, R. G. and F. Gross (1981), in Future Directions in Electromagnetic Nuclear Physics, p. 141.

Arnold, R. G., C. E. Carlson and F. Gross (1981), Phys. Rev. C23, 363.

Bjorken, J. D. (1960) unpublished.

Bjorken, J. D., and S. D. Drell (1964), Relativistic Quantum Mechanics McGraw-Hill.

Blankleider, B. and R. M. Woloshyn (1984), Phys. Rev. C29, 538.

Cheung, C. Y. and R. M. Woloshyn (1983), Phys. Lett. 127B, 147.

deForest, T. and J. D. Walecka (1966), Adv. in Phys. 15, 1.

Donnelly, T. W. (1983), in Perspectives in Nuclear Physics at Intermediate Energies (ed. S. Boffi, C. Ciofi degli Atti and M. M. Giannini, World Scientific; Trieste, Italy 1983 - published 1984), p. 244.

Donnelly, T. W. (1983a), in Symmetries in Nuclear Structure (ed. K. Abrahams, K. Allaart and A. E. L. Dieperink, Plenum), p. 1.

Donnelly, T. W. (1984), Erice Lectures Electron Scattering and Neutrino Reactions in Nuclei, in the International School of Nuclear Physics "Nuclear and Subnuclear Degrees of Freedom and Lepton Scattering" (April, 1984)(to be published in Progress in Particle and Nuclear Physics).

Donnelly, T. W. (1984a), in Workshop on Polarized Targets in Storage Rings, Argonne National Laboratory (to be published).

Donnelly, T. W., and A. S. Raskin (1984), (to be published).

Donnelly, T. W., and I. Sick (1984), (to be published in Rev.Mod.Phys.).

Dubach, J. (1983)(private communication).

Gourdin, M. (1961), Nuov. Cim. 21, 1094.

Kleppinger, W. (1984) (private communication).

Suzuki, T. (1983), Phys. Lett. 120B, 27.

Van Orden, J. W. (1984) (private communication).

von Gehlen, R. (1960), Phys. Rev. 118, 1455.

NPAS - A Program of Nuclear Physics at SLAC

R. G. ARNOLD

The American University
Washington D. C. 20016

and

Stanford Linear Accelerator Center
Stanford, CA 94305

(September 1984)

1. Introduction

NPAS is a program of Nuclear Physics At SLAC[1] based upon a new injector on the SLAC linac that will produce a high intensity electron beam in the energy range 0.5 to 6 GeV. The new injector is under construction and will produce its first beam in the Fall of 1984. The new beam will primarily be used for electron scattering and electroproduction experiments in SLAC End Station A. NPAS is a national nuclear physics program open for competative proposals that will be operated within the SLAC high energy physics program. The program decisions are guided by a Nuclear Program Advisory Committee. The first round of approved experiments are now in progress and the first data will be taken in the 1984-1985 run cycle.

SLAC is presently the only place in the world where a high intensity, but low duty factor, electron beam in the GeV energy range is available for nuclear structure measurements. There are many experiments in this energy range waiting to be done. They will help stimulate interest and shape ideas for the next generation of experiments in the GeV energy range at high duty factor.

Talk presented at the CEBAF Summer Physics/Spectrometer Workshop, Newport News, Virginia, June 25-29, 1984.

2. The New Injector

The new injector (See Figure 1.), called the Nuclear Physics Injector (NPI)[2], is nearly a carbon copy of the main SLAC injector that has been operating for almost 20 years. The NPI is located at a point 1/5 of the length of the 2 mile long linac from the output end. Electrons entering at that location can be accelerated in the last 6 sectors of the 30 sector linac. The beam is generated in a pulsed 80 kV electron gun off the axis of the accelerator, and is deflected onto the accelerator axis by a small bend magnet. The beam is then bunched in special prebuncher and buncher sections before entering the main injector accelerator section where it is accelerated to approximately 35 MeV. Solenoid focussing coils are wrapped around the buncher and the injector accelerator sections and a series of special over-the-accelerator quadrupoles in Sector 25 are used to match the injector beam into the focussing system on the rest of the linac. The gun pulser can operate in either a standard mode with a pulse length variable up to 1.6 μs, normally used for End Station A experiments, or in a short pulse mode with a 2 ns pulse length used for filling the SPEAR storage ring with electrons. The entire injector complex is integrated into the SLAC computer control system, and it can be operated either by itself or interleaved on a pulse-to-pulse basis with other beams from the full linac.

The maximum beam energy from the NPI (See Figure 2.) depends upon the beam current, due to beam loading, and upon the status of the klystrons in the last six sectors. The maximum beam current is determined by the onset of beam breakup, and that depends upon the beam energy and on the amount of focussing on the linac. With the present klystrons, the energy gain is roughly 700 MeV per sector at low current, giving a maximum energy of 4.2 GeV. The maximum beam current will be 80 mA peak pulse current, and at that current the maximum energy will be loaded down to 3.5 GeV. Within the next two years all the klystrons on the linac will be changed to higher powered (50 mW) klystrons for the Stanford Linear Collider project, and more focussing will be installed on

the linac. When that is done the maximum energy from the last 6 sectors will be aproximately 6 GeV at a maximum current of 80 to 100 mA peak current. When the linac is operating at 180 pulses per second with a pulse width of 1.6 μs, the duty factor is 2.9×10^{-4} and the average current is 25 μA.

The maximum intensity from the NPI and the 6 sector linac is a factor of 10 to 50 times higher than can be obtained from the full SLAC linac when operated in the energy range below 6 GeV. This large increase in current is due to the decreased effects of beam breakup phenomena in the shorter linac.

3. The Experimental Facilities

The high powered NPI beam will make possible many experiments on electron scattering and electroproduction from nuclear targets in the kinematic range where electron scattering cross sections are low and pion production is large. The facilities of SLAC End Station A are ideal for such experiments. The high powered beam (25 μA at 6 GeV is 150 kW in the beam) can be delivered through the energy defining bend and slits system of A Bend into the well shielded experimental hall and deposited in a high powered beam dump outside the hall. End Station A is a large concrete hall containing three spectrometers on a common pivot, a large free floor space, overhead crane, utilities, and a complex of signal, high voltage, and low voltage cabling to a large data assembly area, called the Counting House. There are available general purpose target and spectrometer facilities that can be used without major modification, as well as a large inventory of magnets, shielding blocks, beam pipes, and other equipment that can be fashioned into building-block setups for one-time experiments.

The primary spectrometers that will be the work horses in the NPAS program are the 1.6 GeV/c and the 8 GeV/c spectrometers. (See Figures 3 and 4.) These instruments have modest resolution (aproximately ± 0.05 % in momentum and ± 0.2 mr in production angle) matched to the characteristics of the incident beam. The solid angles are 3 msr and 0.8 msr respectively. The detectors can

be arranged to suit the needs of particular experiments. For the 8 GeV/c spectrometer there is now available a modern set of multiwire proportional chambers for track measurements, and a gas Čherenkov counter and a lead glass total absorption shower counter for electron identification. The detectors in the 1.6 GeV/c spectrometer have not been modernized in 10 years. Two of the recently approved NPAS experiments NE1 and NE5 will use the 1.6 GeV/c spectrometer, and for that a new detector package for electron detection, including wire chambers for track measurements and a gas Čherenkov counter and a lead glass shower counter for electron identification, will be built.

There exists at SLAC a cryogenic target group with much experience in building liquid hydrogen, high pressure gaseous helium, and various solid targets capable of withstanding high beam power (as much as 100 Watts deposited in the target at 21° K). The End Station A Counting House contains electronics and controls for monitoring the beam, the spectrometers, the targets, and detectors. There is a VAX 11-780 computer for online and offline analysis. A large body of software for general purpose End Station A functions exists, and experimenters can build software systems for partucular experiments by adapting material from a large library of routines from previous experiments.

4. The NPAS Program

The NPAS program will be carried out entirely within the organizational structure of the SLAC high energy physics program and in much the same style. The SLAC Associate Director for the Research Division, currently R. Taylor, acts as the NPAS Director. He is assisted in the day-to-day operation of the program by the NPAS Coordinator, R. Arnold. The funding for the NPAS program is from the DoE nuclear physics budgets and is distinct from the high energy physics budgets at SLAC. The nuclear physics program will be carried out within the constraints of the annual NPAS budget, and within the limitations on the availability of accelerator time and other resources set by the demands of

the SLAC high energy program. Physics program decisions will be made by the Associate Director, in consultation with a Nuclear Program Advisory Committee. The present NPAC membership is listed in Table I. The NPAC will meet several times per year to monitor progress in the approved program and advise on proposals for new experiments. The NPAS budget for FY 1985 is slighly larger than one million dollars, which will allow setup and operation of two experiments with a total beam time of aproximately 6 weeks.

The running time for NPAS esperiments will normally be scheduled during periods in the year when the SLAC high energy physics program is not in operation, usually the month of January and the months of June through September. This will allow the NPAS program to take advantage of minimal electrical power costs, and the NPI can be operated without constraints on the linac operating parameters from the high energy physics users. The NPI will be used in other programs at SLAC in addition to the nuclear physics program. Electrons from the NPI will be used in the SLAC test beam program for the very important job of testing new detectors under development. The NPI will extend the energy range of the monochromatic gamma ray beam produced by back scattering from a laser beam down to the tens of MeV range necesary for calibration of NaI photon detectors. The NPI will also be used to fill the SPEAR storage ring with electrons for use in the sychrotron radiation research at the Stanford Sychrotron Radiation Laboratory. These other operations of the NPI will generally go on at low pulse rate concurrently with high rate nuclear physics experiments.

5. Current NPAS Experiments

At its meeting in May 1984, the NPAC recommended and the Associate Director approved four experiments (See Table II) out of the six proposals submitted. Experiment NE3 will use the 8 GeV/c spectrometer essentially as it is to measure inelastic electron scattering from a number of nuclei in the energy loss region forbidden for scattering from free nucleons between the quasielastic and the nuclear elastic peaks. This region where the Feynman scaling variable $x = Q^2/2m_p\nu$ is larger than one, or alternatively where the nuclear scaling variable y has large negative values, is where the inclusive electron cross section is sensitive to the high momentum components of the ground state nuclear wave functions. Previous experiments at SLAC on deuterium and helium targets[3] have probed the region extending to $y = -800$ MeV/c and out to momentum transfer Q^2 of 4 to 6 $(\mathrm{GeV/c})^2$. That data has stimulated much interest in the physics of nuclear structure at high internal momentum. The traditional nuclear models tend to underestimate the cross sections at large negative y, which leads to speculations about other non traditional scattering mechanisms, such as scattering from quark subclusters in the nucleons.[4] NE3 will extend the data in this kinematic region to nuclei heavier than helium. Data taking should occur in January 1985.

Experiment NE4 will measure electron scattering from deuterium at scattering angles around 180° to determine the elastic and inelastic structure functions $B(Q^2)$ and $W_1(\nu, Q^2)$ out to Q^2 perhaps as large as 5 $(\mathrm{GeV/c})^2$. A special double arm spectrometer capable of detecting electrons scattered around 180° in coincidence with the elastically recoiling nuclei is being constructed on the floor of End Station A. NE4 will begin testing components of the spectrometer, detectors, and shielding in the Fall of 1984. The major checkout run at low pulse rate is scheduled for May 1985, to be followed by a month of data taking at high rate.

The major aim of this experiment is to extend the data on the elastic magnetic form factor $B(Q^2)$ out to the largest attainable Q^2. Several possible scenarios for

$B(Q^2)$ are shown in Fig. 5. This experiment will measure over the Q^2 range where either there is a diffraction feature, as predicted by the impulse approximation models, or the diffraction feature is shifted or obliterated by scatering from meson exchange currents or by the onset of power low behavior of the form factor from scattering on the quark constituents of the nucleons. This measurement will yield important new knowledge about the nucleon-nucleon interaction at short distance and help to discriminate among the highly conflicting predictions.

Experiments NE1 and NE5 will measure inelastic electron scattering from selected nuclear targets in the energy loss region spanning the quasielastic peak and the excitation of the nucleon delta resonance. Measurements will be taken using the 1.6 GeV/c and 8 GeV/c spectrometers up to a momentum transfer of about 1.0 $(GeV/c)^2$. The aim of these experiments is to study the excitation and propogation of the of the delta resonance in nuclei. Information will be extracted from the width and position of the delta peak. A separation of the longitudinal and transverse response funtions will be made in the delta region and in the dip region between the delta and the quasielastic peaks. Previous experiments at lower energy have revealed a larger cross section in the dip region than can be easily understood in present models. A longitudinal-transverse separation may give some clues as to the source of the excess cross section in that area.

The collaborators for NE1 and NE5 have proposed to build a complete new detector package for the 1.6 GeV/c spectrometer. A design has been prepared and a proposal for funding has been submitted. Experiments NE1 and NE5 are not approved for data taking until after NE3 and NE4 are completed. The earliest time when they could receive beam would be in FY 1986.

6. Possible Future Program

There has never been available anywhere before an electron beam in the GeV energy range with intensity as high as that from the NPI, and many experiments are waiting to be done. The primary experiments for which the injector was proposed were elastic and inelastic electron scattering at large Q^2 from the light nuclei, and Experiment NE4 is the first part of that program. Work has begun on plans to secure approval for a ^3H target at SLAC. Assuming that a safe target able to withstand the high beam power can be designed, and that all the necessary approvals by safety review comitttees and the SLAC management can be obtained, the plan is to build a ^3H target for use in a complete set of measurements of elastic and inelastic structure functions. Also comparison would be made of deep inelastic scattering from ^3H, ^3He and d to get information about the inealstic structure functions of the neutron and about the isotopic dependence of the recently discovered EMC effect. Measurement of the elastic charge and magnetic form factors of ^3H out to large Q^2 and extension of the ^3He magnetic form factor to large Q^2 will provide unique information about the short range nucleon interaction and about the structure of the 3-body ground states.

In addition to electron scattering experiments at large Q^2 on the light nuclei, the energy and intensity from this new beam makes possible many other experiments on electro- and photoexcitation of nuclei. A major area for possible expansion in the future is to add a polarized electron source to the NPI. That would allow development of experiments to measure nucleon and deuteron charge form factors using the spin transfer method[5] and it would make possible more measurements of weak and electromagnetic interference in nuclear scattering.

References

1. More details about the NPAS program, the electron beam characteristics, and experimental facilities are availble in the NPAS Users Guide, SLAC-Report-269 (1984).

2. R. F. Koontz, Contribution to the 1984 Linear Accelerator Conference, Seeheim/Darmstadt, Germany, May 1984, SLAC Pub 3329 (1984).

3. P. Bosted, et al, Phys. Rev. Lett **49**, 1380 (1982).

4. H. J. Pirner and J. P. Vary, Phys Rev Lett. **46**, 1376 (1981).

5. R. Arnold, C. Carlson, F. Gross, Phys. Rev. **C23**, 363 (1981).

Table I
Nuclear Program Advisory Committee

Erich Vogt, Chairman	TRIUMF		
Joseph Cerny	LBL	Hobey DeStaebler	SLAC
Roy Holt	Argonne	James McCarthy	U. of Virginia
William Turchinetz	MIT	Dirk Walecka	Stanford

Table II
Approved NPAS Experiments

NE1, "Electroproduction of the Delta Isobar in Nuclei," Argonne National Laboratory: D. F. Geesaman, M. C. Green, R. J. Holt, H. E. Jackson (Spokesman), W. E. Kleppinger, R. S. Kowalczyk, T. S. H. Lee, J. P. Schiffer, B. Zeidman.

NE3, "Inclusive Electron Scattering from Nuclei," University of Virginia: R. Altemus, D. Day (Spokesman), J. S. McCarthy, R. Minehart, B. Norum, R. York; University of Basel: I Sick.

NE4, "Electron Scattering from Deuterium at Large Momentum Transfer at 180°," The American University: R. G. Arnold, P. E. Bosted, J. Gomez, A. T. Katramatou, G. G. Petratos, S. E. Rock, A. F. Sill, Z. M. Szalata; SLAC: R. A. Gearhart; University of Massachusetts: B. Debebe, R. S. Hicks, G. A. Peterson.

NE5, 'Electroproduction of Δ in Nuclei," University of Virginia: R. Altemus (Spokesman), D. Day, J. S. McCarthy, R. Minehart, B. Norum, S. Thornton, R. York; Florida State University: L. Dennis, K. W. Kemper.

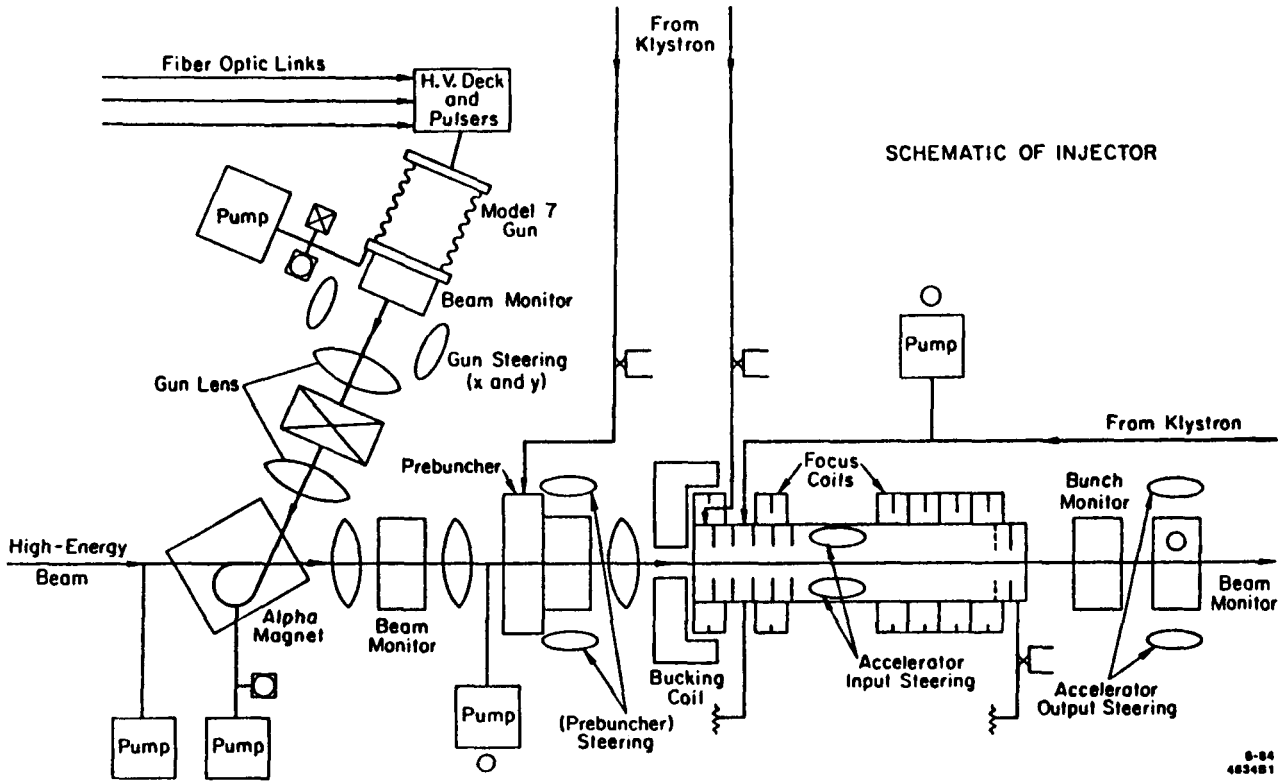

Fig. 1. A schematic of the Nuclear Physics Injector (NPI) located at the beginning of sector 25 in the 30 sector SLAC linac.

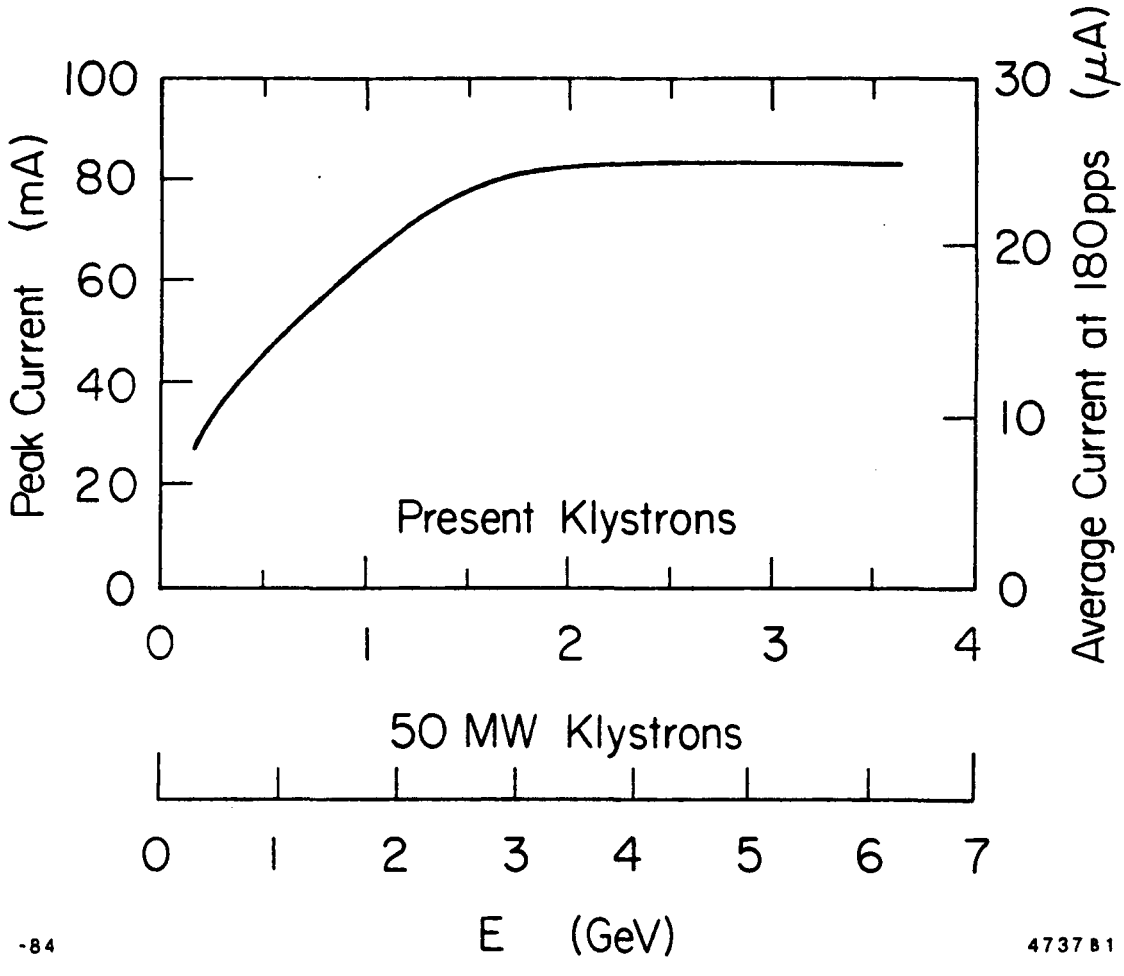

Fig. 2. Maximum beam current as a function of beam energy expected from the Nuclear Physics Injector and the last 6 sectors of the SLAC linac. The curve shown was extrapolated from measurements made of the maximum current obtainable in the first 5 sectors. The maximum beam energy will increase approximately as indicated by the lower energy scale when the SLC klystrons are operational. A useful rule of thumb is that the current for the standard SLAC pulse length of 1.6 μs corresponds to 10^{10} electrons/pulse per mA peak current.

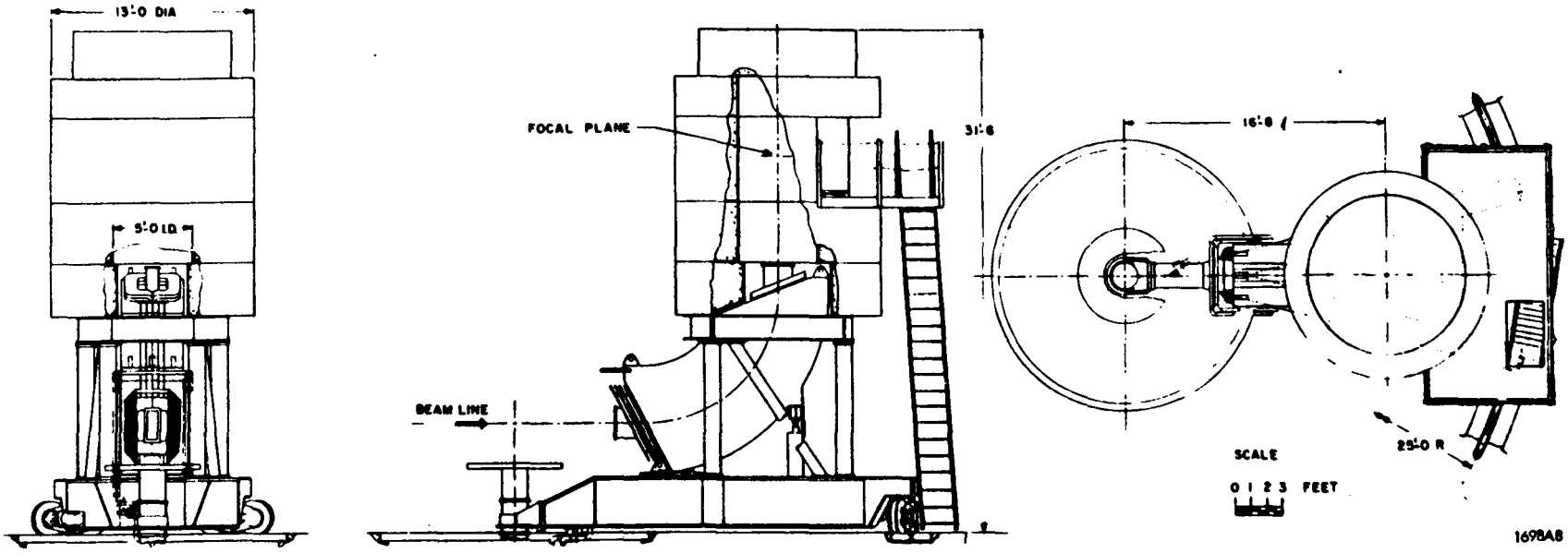

Fig. 3. 1.6 GeV spectrometer assembly.

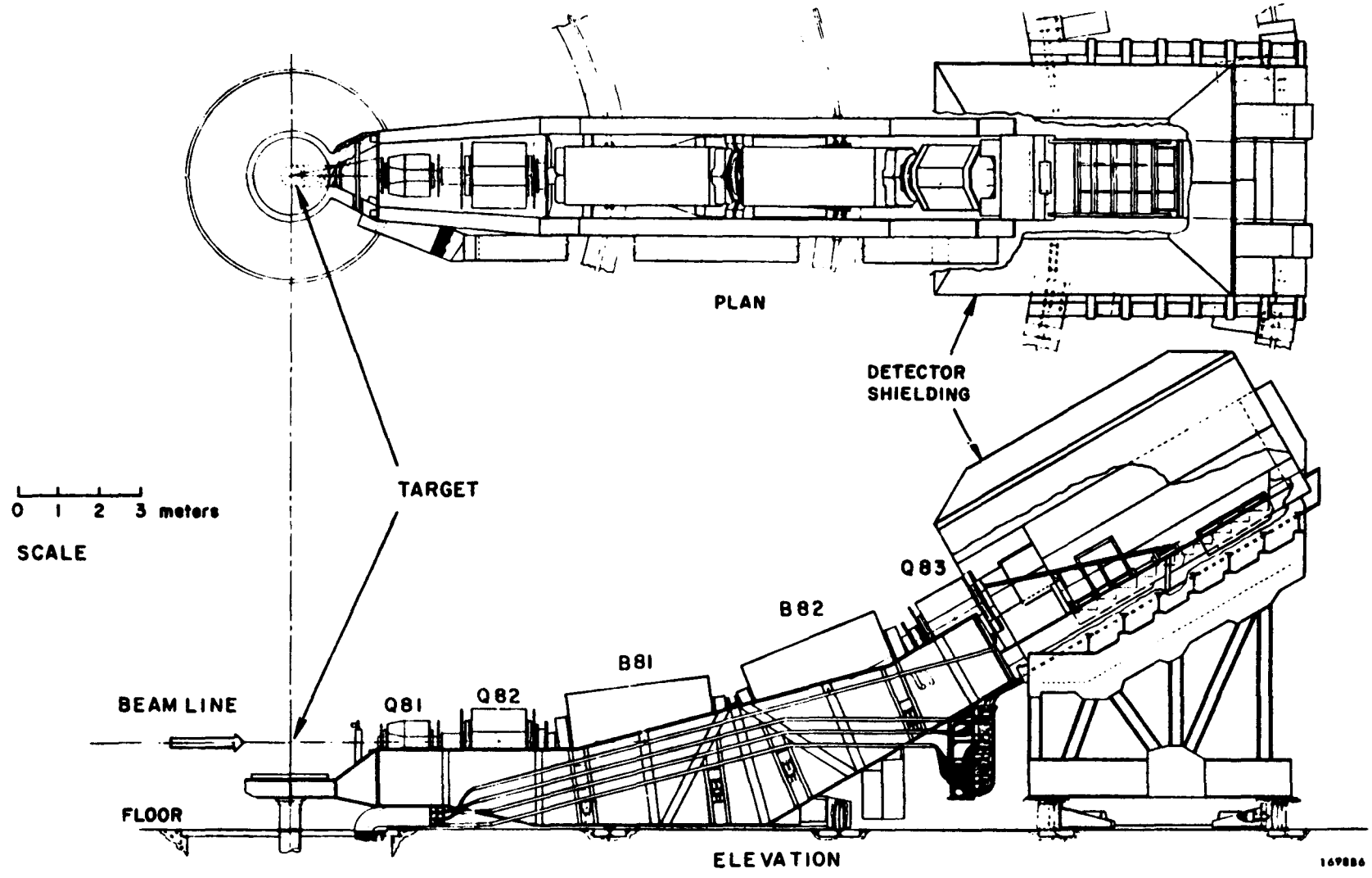

Fig. 4. 8 GeV spectrometer assembly.

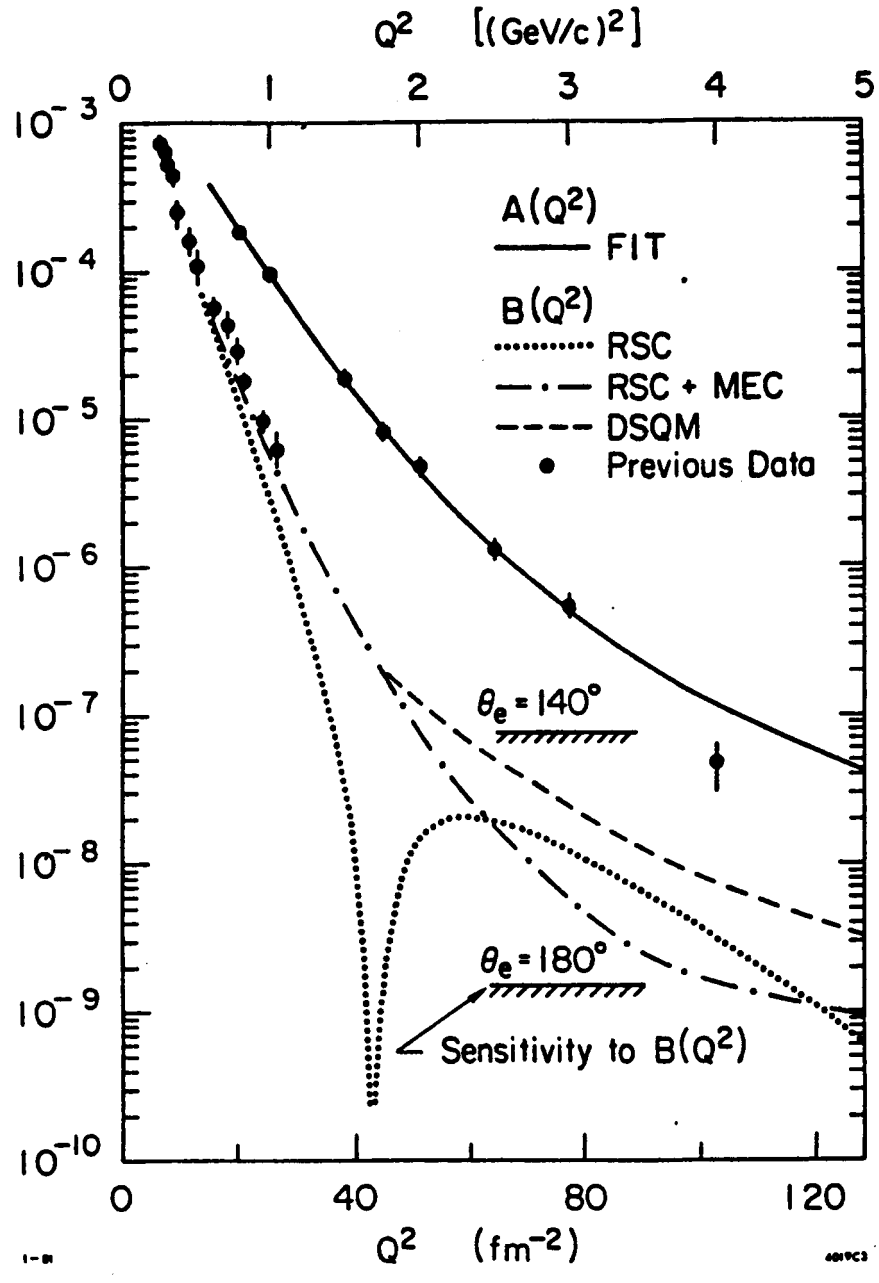

Fig. 5. Sensitivity of the proposed experiment to $B(Q^2)$ compared to previous data. The predictions for $B(Q^2)$ are: (1) RSC - impulse approximation using Reid soft core wave functions; (2) RCS+MEC - Reid wave functions and meson exchange currents; (3) DSQM - dimensional scaling quark model with the ratio $B(Q^2)/A(Q^2)$ arbitrarily normalized at $Q^2 = 1.75$ (GeV/c)^2.

SPECTROMETERS

Karl L. Brown
Stanford Linear Accelerator Center
Stanford, CA 94305*

Most of the important background information for this paper comes from the published reports SLAC 75, SLAC-PUB 3381, and CERN 80-04.

SLAC 75 is the publication where I first derived the basic second order optics theory and several of the first order optics theorems that I used in this paper.**

SLAC-PUB 3381 is a more recent paper which ties together optics from two points of view; the traditional 'ray optics' that has been used in the past for spectrometer design calculations and the 'phase ellipse optics' first inroduced by Courant and Snyder in their development of Alternating Gradient (AGS) theory in the early 1950's. I used the contents of this report to derive the spectrometer phase space acceptance equations that follow.**

The CERN 80-04 report is one of many versions of the TRANSPORT manual. However, it is the only one, presently available, that includes the original TRANSPORT APPENDIX containing a number of selected topics in charged particle optics. Among them is a paper that I presented at the 1970 Hamburg International Magnet Conference specifically aimed at the design of magnetic spectrometers for nuclear physics purposes. In addition the appendix provides an introduction to matrix optics that some people find useful when they are first trying to use the TRANSPORT program to design optical systems.

From these reports I derived the following design equations that I thought might be useful to members of the CEBAF conference who are interested in spectrometer design.

1) The first order resolving power of a magnetic spectrometer. This derivation first appeared in SLAC 75 and later in the Hamburg paper.

2) An equation relating the basic magnetic tolerances needed in a spectrometer to its resolving power.

3) An equation for the minimum magnetic air gap needed in a spectrometer as a function of the transverse emittance of the scattered beam from the target.

4) The maximum solid angle that can be expected from an array of magnetic quadrupoles.

5) The momentum acceptance of a spectrometer, as a function of the resolving power and pole width, at the exit of the spectrometer.

6) A statement of the empirically determined 'useful gap' of a dipole magnet.

---

*Address 1984/85: CERN, European Organization for Nuclear Research, 1211 Geneva 23, Switzerland.

The following figure represents the magnetic optical configuration of a typical spectrometer. The primary purpose of this figure is to define the parameters used in subsequentequations and to provide a representative model of a spectrometer as a guide for the calculations.

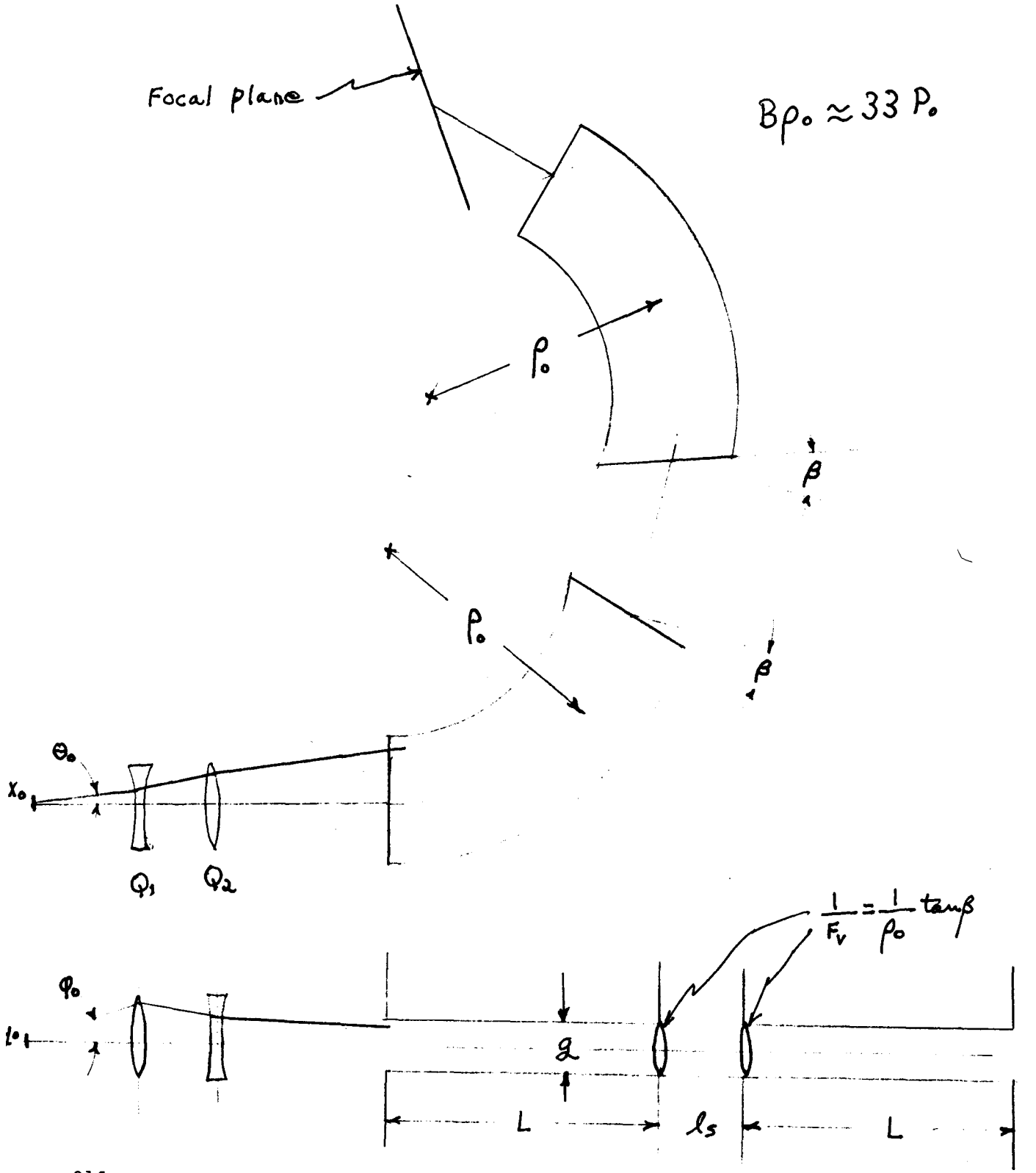

This particular model assumes a quadrupole doublet followed by two dipoles as an optical configuration that might typically be used for a focusing spectrometer. To further simplify the calculations, I assume the two dipoles to have the same central bending radius and the same deflection angle (length). The primary purpose of the quadrupole doublet is to provide phase space matching from the target to the dipoles so as to minimize the cost of the system. They provide the proper boundary conditions at the entrance of the first dipole so that the size of the beam envelope as it traverses the dipoles is minimized. Specifically the model assumes that the quadrupole phase space matching creates a beam envelope waist half way through each dipole and minimizes the maximum size of the beam at the entrance and exit of each dipole.

At the same time the quadrupoles are used to optimize the magnetic flux integral through the dipoles so as to optimize the resolving power.

The combination of these two factors can have a significant influence on minimizing the total cost of the system.

The equations for the resolving power of a magnetic spectrometer have been derived in SLAC 75 and also in the appendix of CERN 80-04. They are listed below in various forms for the benefit of the reader of this report. The parameters used in the equations are defined in the references cited but should also be apparent from the equations.

1) The differential equations of motion are :

$s'' + k^2 s = 0$

$c'' + k^2 c = 0$ monoenergetic equations

$d_x'' + k^2 d_x = 1/\rho$ dispersion equation

2) The solutions in matrix form are :

$x_i = \sum R_{ij} x_j$ where $x^1=x$, $x^2=x'$, $x^3=y$, $x^4=y'$, $x^5=\Delta\ell$, $x_6=(\Delta p/p)=\delta$

$$R_x = \begin{bmatrix} c_x & s_x & d_x \\ c_x' & s_x' & d_x' \\ 0 & 0 & 1 \end{bmatrix} \qquad R_y = \begin{bmatrix} c_y & s_y \\ c_y' & s_y' \end{bmatrix}$$

3) $$d_x = \int_0^S G(\tau,s)\,\frac{d\tau}{\rho} = \int_0^S G(\tau,s)\,d\alpha = M_x \int_0^S s_x\,d\alpha \quad \text{for point to point imaging}$$

4) Resolving power (1st order) $$R_1 = \left(\frac{p}{\Delta p}\right) = \frac{d_x}{2M_x x_0} = \frac{1}{2x_0}\int_0^S s_x\,d\alpha \qquad s_x = \frac{x(\tau)}{\theta_0}$$

or

$$R_1 = \left(\frac{1}{2x_0\theta_0}\right)\left(\frac{1}{B\rho}\right) \int B \cdot dA$$

The basic magnetic tolerance needed for a spectrometer having a resolving power of R = p/dp is derived below using the formalism of SLAC 75. I express this tolerance as the error in bending angle that is permitted for any trajectory normalized to the total bending angle of the spectrometer. It is not surprising to discover that the allowed error is inversely proportional to the desired resolving power, R, of the spectrometer.

The displacement of a ray at the focal plane of a spectrometer at positi s as a result of an angular error ($\Delta\alpha$) at an arbitrary position τ is given by

$$\Delta x(s) = G_x(\tau,s)\Delta\alpha = M_x s_x(\tau) \cdot \Delta\alpha \qquad \text{(for point to point imaging)}$$

where $G_x(\tau,s)$ is the Greens function between position τ and position s.

Equate $x(s) = M_x x_0$ (the image size at focal point) to $\Delta x(s)$ and use

$$2x_0 R_1 = \int_0^S s_x d\alpha \approx s_x \alpha_T$$

If we assume that $s_x \approx s_x$, the allowed error is :

$$\left(\frac{\Delta\alpha}{\alpha_T}\right) \approx \frac{1}{2R_1}$$

The value of the dipole magnet gap, g, required to accept a transverse emittance of epsilon (y) may be derived using the 'phase ellipse' formalism discussed in SLAC-PUB 3381. The result is given as a function of the length of each dipole magnet, L, the longitudinal separation of the dipole magnets and the focusing strength of the edge focusing at the end of the first dipole and the beginning of the second dipole. The approximation used in this derivation turns out to be a very good one for most applications. As a consequence this equation is a good guide line for making cost estimates. One must, of course, allow adequate space for the vacuum chambers in addition to the value of g calculated here.

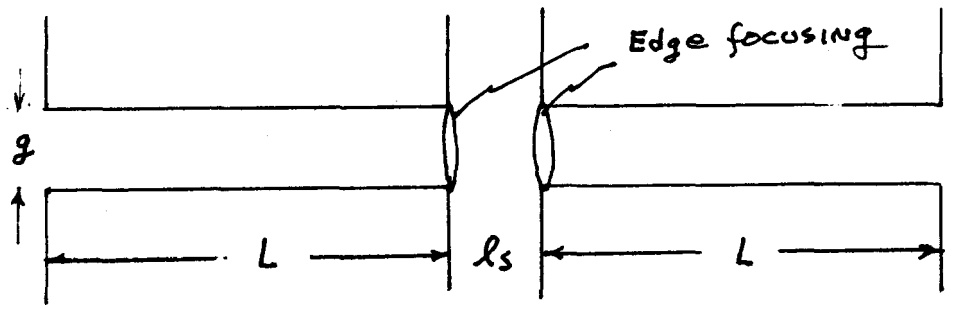

$$R_y = \begin{bmatrix} 1 & 0 \\ -1/F & 1 \end{bmatrix} \begin{bmatrix} 1 & \ell_s \\ 0 & 1 \end{bmatrix} \begin{bmatrix} 1 & 0 \\ -1/F & 1 \end{bmatrix} \begin{bmatrix} 1 & L \\ 0 & 1 \end{bmatrix} = \begin{bmatrix} & \beta\sin\phi \\ & \end{bmatrix}$$

If we assume $\sin\phi \approx 1$, which turns out to be a good approximation, we obtain :

$$R_{12} = L + \ell_s - L\ell_s/F \approx \beta$$

Then $$g/2 = (\beta\varepsilon_y)^{1/2} = \left[L\left(1+\ell_s\left(\frac{1}{L} - \frac{1}{F}\right)\right)\varepsilon_y\right]^{1/2} \approx (L\varepsilon_y)^{1/2} ,$$

where $\varepsilon_y = y_0\Phi_0$ is the emittance of the scattered beam in the transverse plane.

The maximum solid angle that can be accepted by a quadrupole doublet is a good representation of the best that one can expect to do with any quadrupole array. If one assumes that both quadrupoles in the doublet have the same available aperture, then the result is a very simple one. The maximum solid angle is just 1/3 that of a simple optical lens if it were located at the center of the first quadrupole. This means that the ratio of the acceptance angles in the two transverse planes will be 3/1 when the solid angle has been optimized.

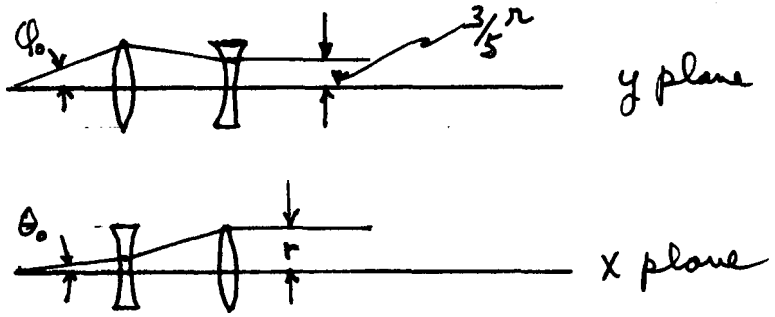

$\Omega_{max} = \pi/3 \left(\frac{r}{\ell_1}\right)^2 = 1/3$ that of a simple optical lens located at the center of F_1,

or $\Omega_{max} = \frac{\pi}{6.75} \left(\frac{r}{F_1}\right)^2 \approx 1/2 \left(\frac{B_0 L}{B\rho}\right)^2$ evaluated for the first lens.

Then $\left(\frac{\Phi_0}{\theta_0}\right) = 3/1$, $\ell_1 = 3/2\ F_1$, and $\ell_2 = 0.8\ \ell_1$.

The momentum bandwidth (range) accepted by a spectrometer may also be expressed as a function of the resolving power R. The momentum range is proportional to the width of the exit pole of the last dipole of the spectrometer and inversely proportional to the resolving power R. Another factor that enters is the optical magnification M. The result is approximate in that it assumes the dispersion at the end of the last magnet to be the same as it is at the focal plane. Therefore the equation for the momentum range is a lower limit and the actual range is somewhat larger depending on the exact design. But this equation at least shows the order of magnitude of the momentum range to be expected.

Let W_E = width of pole at the end of system,

$$d_x \leq M_x \int s_x d\alpha = M_x(2Rx_0),$$

but $d_x \cdot (\Delta p/p)_{range} = M_x(2Rx_0) \cdot (\Delta p/p) = W_E$,

or $(\Delta p/p)_{range} = W_E/M_x(2Rx_0)$.

Example : suppose $W_E = 2g \approx 400$ mm,

$M_x = 1$,

$(2Rx_0) = 10^4$ mm,

then $(\Delta p/p)_{range} \approx 4$ percent.

The useful width of a dipole magnet gap is determined by the extent of the fringing fields. Two basic solutions have been traditionally used in spectrometer designs in recent years. For uniform field magnets, where one desires to use the maximum possible field value, the edges of the poles are rounded off so as to provide a uniform magnetic saturation property. In this case the 'useful' pole width is approximately equal to (w-4g), where 2 is the iron pole width and g is the full value of the magnet gap.

Another typical solution is to provide pole face corrections to the magnet so as to maximize the useful pole width. This can be done but with some sacrifice in the maximum pole field that may be used. In this case the useful pole width may be as great as (w-3g/2). But in this case the useful field is usually limited to about 13 kg.

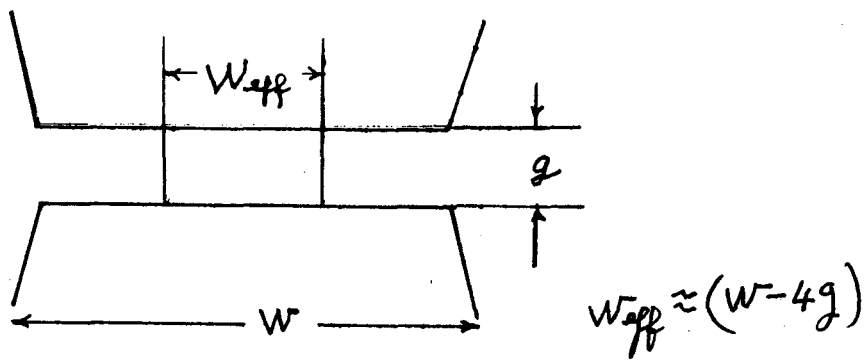

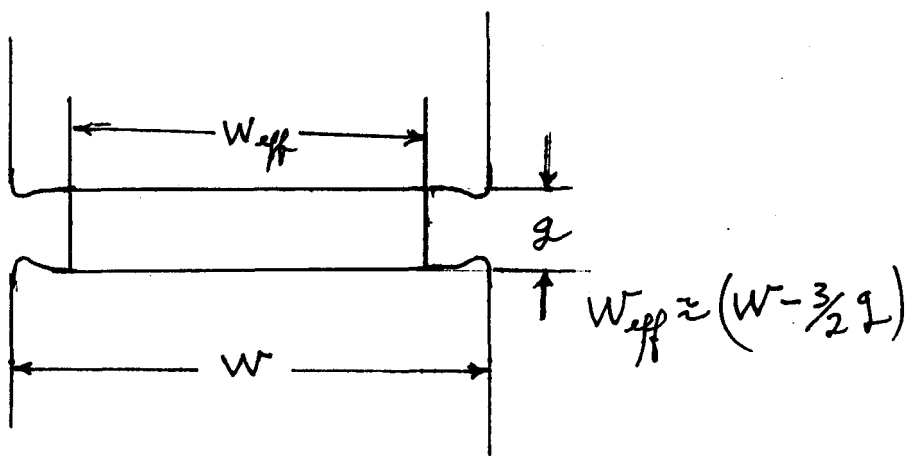

**Brown, K.L. A first- and second-order matrix theory for the design of beam transport systems and charged particle spectrometers. SLAC report no. 75.
**Brown, K.L. and R. V. Servranckx. First- and second-order charged particle optics. SLAC Pub. 3381, July 1984.

[Pgs. 322-332 contain copies of transparencies used by K.L. Brown during his talk on Spectrometers at the CEBAF 1984 Summer Workshop. --ed.]

SOLUTIONS OF DIFFERENTIAL EQUATIONS

- Assume Taylor Expansion

$$X_i = \Sigma R_{ij} X_j + \Sigma T_{ijk} X_j X_k + \ldots$$

$$X_1 = X \quad X_2 = X' \quad X_3 = y \quad X_4 = y' \quad X_5 = \ell \quad X_6 = \frac{\Delta p}{p}$$

$$R_s = \begin{bmatrix} C_x & S_x & d_x \\ C_x' & S_x' & d_x' \\ 0 & 0 & 1 \end{bmatrix} \quad ; \quad R_y = \begin{bmatrix} C_y & S_y \\ C_y' & S_y' \end{bmatrix}$$

$$|R| = 1$$

- $C'' + k^2 C = 0$
  $S'' + k^2 S = 0$ } MONOENERGETIC

  $d'' + k^2 d = h(s)$ -- DISPERSION

$$T_{ijk}'' + k^2 T_{ijk} + f_{ijk}\left(\frac{n, \beta, h}{B(x,y,s)}, \frac{c, s, d}{R_{ij}}\right)$$

Second Order ← First Order Solutions

f_{ijk} = DRIVING TERMS

GREEN'S FUNCTION SOLUTIONS

$$T_{ijk}(s) = \int_0^s F(\tau)\, G(\tau,s)\, d\tau$$

$$G(\tau,s) = S(s)C(\tau) - S(\tau)C(s)$$

$$T_{ijk}(s) = S(s) \int_0^s f(\tau)C(\tau)d\tau \; - C(s) \int_0^s F(\tau)S(\tau)d\tau$$

$$T'_{ijk}(s) = S'(s) \int_0^s f(\tau)C(\tau)d\tau \; - C'(s) \int_0^s f(\tau)s(\tau)d\tau$$

$$R_{x,y}(s) = \begin{bmatrix} R_{11}(s) & R_{12}(s) \\ R_{12}(s) & R_{22}(s) \end{bmatrix}_{x,y} = \begin{bmatrix} C(s) & S(s) \\ C'(s) & S'(s) \end{bmatrix}_{x,y}$$

WHAT ARE THE GREEN'S FUNCTIONS?

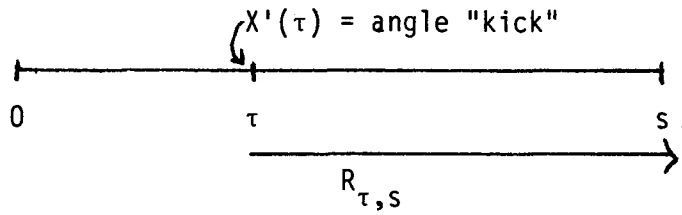

$$\begin{pmatrix} X(s) \\ X'(s) \end{pmatrix} = \begin{pmatrix} R_{11} & R_{1w} \\ R_{21} & R_{22} \end{pmatrix}_{\tau,s} \begin{pmatrix} X(\tau) \\ X'(\tau) \end{pmatrix}$$

R_{12} = GREEN'S FUNCTION FOR X(s)

R_{22} = GREEN'S FUNCTION FOR X'(s)

FIRST ORDER DISPERSION AND RESOLUTION

$$d_x'' + k_x^2 d_x = h = \frac{1}{\rho_0} \qquad h = f = \text{driving term}$$

$$d_x(s) = \int_0^s G(\tau,s)\,\frac{d\tau}{\rho_0} = \int_0^s G(\tau,s)\,d\alpha$$

$$d_x(s) = s_x(s)\int_0^s C_x d\alpha - C_x(s)\int_0^s S_x d\alpha$$

FOR POINT TO POINT IMAGE

$$S_x(s) = 0$$

$$d_x = -C_x(s)\int_0^s S_x d\alpha = M_x \int_0^s S_x d\alpha$$

$$R_1 = \frac{p}{\Delta p} = \frac{dx}{2M_x X_0} = \frac{1}{2X_0}\int_0^s S_x d\alpha$$

FIRST ORDER RESOLUTION

$$2X_0R = \int S_x d\alpha \simeq \bar{S}_x \alpha_\tau$$

$$S_x = \frac{X(s)}{\theta_0}$$

OR

$$R(2X_0\theta_0) = \int \frac{BX(s)ds}{B\rho_0}$$

OR

$$R = \left(\frac{1}{2X_0\theta_0}\right)\left(\frac{1}{B\rho}\right)\left(\int BdA\right)$$

AND

$$R = \frac{1}{2X_0\theta_0}\left(\ell_\theta - \ell_0\right)$$

TOLERANCES

$$G_x(\tau,s) = S_x(s)C_x(\tau) - S_x(\tau)C_x(s) = M_x S_x(\tau)$$

$$X(s) = G_x \Delta\alpha = M_x S_x(\tau)\ \Delta\alpha$$

EQUATE $X(s) = M_x X_0$

USE $2X_0 R \simeq \overline{S}_x\ \alpha_\tau$

ASSUME $\overline{S}_x \simeq S_x(\tau)$

THEN

$$\left(\frac{\Delta\alpha}{\alpha_\tau}\right) \approx \frac{1}{2R} = \frac{1}{2}\ \frac{\Delta p}{p}$$

SIZE OF GAP IN DIPOLES

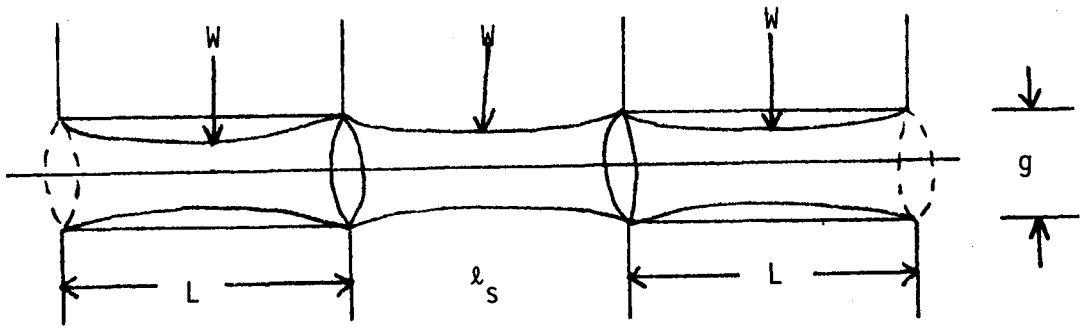

$$R_y = \begin{bmatrix} 1 & 0 \\ -\frac{1}{F} & 1 \end{bmatrix} \begin{bmatrix} 1 & \ell_s \\ 0 & 1 \end{bmatrix} \begin{bmatrix} 1 & 0 \\ -\frac{1}{F} & 1 \end{bmatrix} \begin{bmatrix} 1 & L \\ 0 & 1 \end{bmatrix}$$

$$R_y = \left[\begin{array}{c|c} C + \alpha s & \beta S \\ \hline & C-\alpha s \end{array}\right] = \left[\begin{array}{c|c} \left(1 - \frac{\ell s}{F}\right) & L + \ell_s - L\ell_s \\ \hline -\frac{2}{F} + \frac{\ell s}{F^2} & \left(1-\frac{\ell s}{F}\right)\left(1-\frac{L}{F}\right) - \frac{L}{F} \end{array}\right]$$

$$\beta S = \beta \sin\psi \qquad 2\cos\omega = \text{Trace} = \left(1-\frac{\ell s}{F}\right)\left(2-\frac{L}{F}\right) - \frac{L}{F}$$

$$g/2_{\,min} = \sqrt{\beta\varepsilon_y} \qquad \text{assume, i.e., } \sin\psi \tilde{=} 1 \text{ (good approximation)}$$

$$g/2 \tilde{=} \sqrt{L\left[1 + \ell_s\left(\frac{1}{L} - \frac{1}{F}\right)\right]\varepsilon_y} = \sqrt{K_y L \varepsilon_y}$$

$$\varepsilon_y = \gamma_o \psi_o \qquad K_y \lesssim 1.5$$

$$\begin{bmatrix} 1 & 0 \\ -\frac{1}{F} & 1 \end{bmatrix} \begin{bmatrix} 1 & \ell_s \\ 0 & 1 \end{bmatrix} \begin{bmatrix} 1 & 0 \\ -\frac{1}{F} & 1 \end{bmatrix} \begin{bmatrix} 1 & L \\ 0 & 1 \end{bmatrix}$$

$$\left[\begin{array}{c|c} 1 & \ell_s \\ \hline -\frac{1}{F} & \left(1-\frac{\ell s}{F}\right) \end{array}\right] \quad \left[\begin{array}{c|c} 1 & L \\ \hline -\frac{1}{F} & 1-\left(\frac{L}{F}\right) \end{array}\right]$$

$$\left[\begin{array}{c|c} \left[1-\left(\frac{\ell_s}{F}\right)\right] & L+\ell_s-\frac{L\ell_s}{F} \\ \hline -\frac{2}{F}+\frac{\ell_s}{F^2} & 1\frac{L}{F}+\left(1-\frac{\ell_s}{F}\right)\left(1-\frac{L}{F}\right) \end{array}\right]$$

$$2\cos\omega = \text{Trace} = \left(1-\frac{\ell_s}{F}\right)+\left(1-\frac{\ell_s}{F}\right)\left(1-\frac{L}{F}\right)-\left(\frac{L}{F}\right)$$

$$=\left(1-\frac{\ell_s}{F}\right)\left(2-\frac{L}{F}\right)-\left(\frac{L}{F}\right)$$

assume $\left(\frac{\ell_s}{F}\right) << 1$

Then $2\cos\omega \simeq 2-2\left(\frac{L}{F}\right) = 2\left(1-\frac{L}{F}\right)$

$$\boxed{\cos\omega \simeq \left(1-\frac{L}{F}\right)} \qquad \text{so if } \left(\frac{L}{F}\right)=1 \qquad \omega = 90°$$

what is a typical value of $\left(\frac{L}{F}\right) = \frac{1}{\rho} \tan\beta \simeq \alpha \tan\beta$ $\quad \alpha = 75°$ $\quad \beta = 30°$

so $\left(\frac{L}{F}\right) \simeq 3/4$

$\cos\omega \simeq \left(1-3/4\right) = 1/4 \qquad \omega \simeq 75° \qquad \sin\omega = 0.97 \simeq 1$ OK

Ω_{max} FOR QUAD DOUBLET

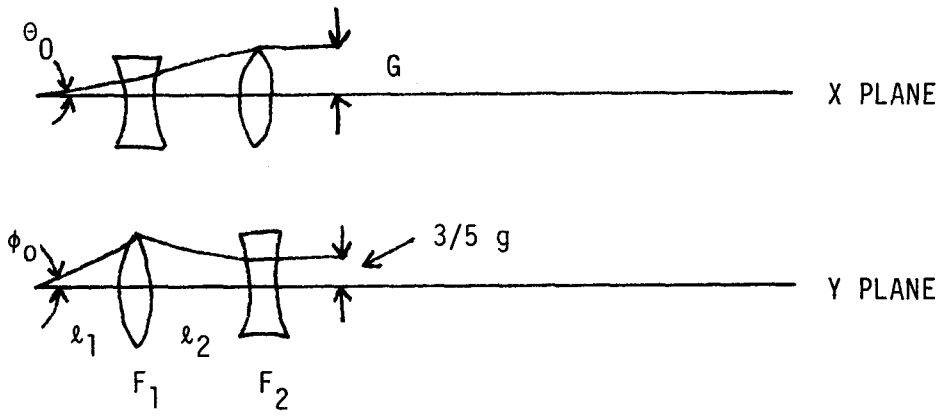

$$\Omega_{max} = \frac{\pi}{3}\left(\frac{g}{\ell_1}\right)^2 = 1/3 \text{ THAT OF A SIMPLE OPTICAL LENS}$$

OR

$$\Omega_{max} = \frac{\pi}{6.75}\left(\frac{g}{f_1}\right)^2 \simeq \frac{1}{2}\left(\frac{B_0 L}{B\rho_0}\right)^2$$

$$\left(\frac{\Theta_0}{\phi_0}\right) = 1/3$$

$$\ell_1 = 3/2\ f_1$$

$$\ell_2 = 0.8\ \ell_1$$

MOMENTUM RANGE

Let W_E = Width of POLE at END OF SYSTEM

$$d_x < M_x \int S_x d\alpha = M_x(2X_oR)$$

$$d_x\left(\frac{\Delta p}{p}\right) = M_x(2X_oR)\cdot\left(\frac{\Delta p}{p}\right) = W_E$$

$$\left(\frac{\Delta p}{p}\right) \tilde{=} \frac{W_E}{M_x(2X_oR)}$$

IF $W_E = 2$ g $\qquad M_x = 1 \quad (2X_oR) = 10^4$

$= 432$ mm

$$\left.\frac{\Delta p}{p}\right|_{range} \tilde{=} 4.3 \text{ percent}$$

USEFUL POLE WIDTH $

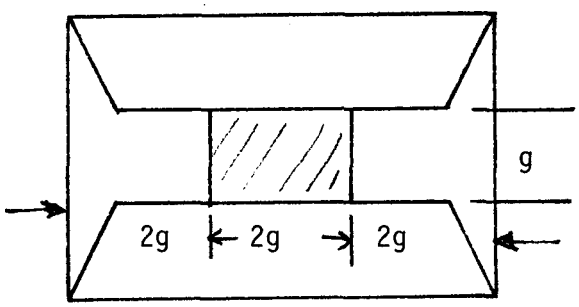

n = 0

$\rho_o \simeq 2 P_o$

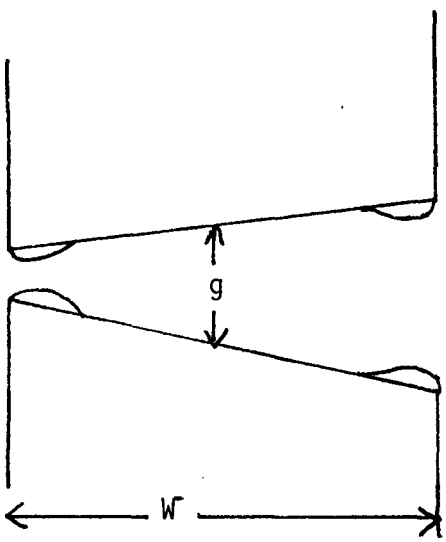

n = 1/2

B ≃ 13 Kg

$W_{eff} = W - 3/2\ g$

- MSU SUPERCONDUCTING SOLUTION (NOLEN)
- OTHERS

POLARIZED GAS TARGETS IN ELECTRON RINGS*

R. J. Holt

Argonne National Laboratory, Argonne, IL 60439

ABSTRACT

The feasibility of performing electron scattering experiments with polarized targets in electron storage rings is discussed. Three examples of the physics which would be accessible with this novel method are given. It is noted that this new method is compatible with recent proposals for linac-stretcher-ring accelerator designs. A new method for producing a polarized hydrogen or deuterium target is proposed and some preliminary results are described. A brief summary of laser-driven polarized targets as well as conventionally-produced polarized atomic beams is included.

INTRODUCTION

Although there is great interest in polarization phenomena in electromagnetic interactions with nuclei, this area remains essentially unexplored experimentally. The reasons for the interest are manifold, but fall primarily into three categories: (i) much greater sensitivities to small form factors, such as the electric form factor of the neutron, (ii) allow separation of elastic form factors for nuclei with spin ≥ 1, e.g., the deuteron, (iii) permit unravelling of multipole excitations of resonances in nuclei and isolation of structure functions.

Unfortunately, the experiments are extremely difficult, and in most cases, appear infeasible with present techniques. In this report we wish to discuss a novel method which should provide accessibility

*This work supported by the U. S. Department of Energy under contract No. 31-109-ENG-38.

POLARIZED GAS TARGETS IN ELECTRON RINGS*

R. J. Holt

Argonne National Laboratory, Argonne, IL 60439

ABSTRACT

The feasibility of performing electron scattering experiments with polarized targets in electron storage rings is discussed. Three examples of the physics which would be accessible with this novel method are given. It is noted that this new method is compatible with recent proposals for linac-stretcher-ring accelerator designs. A new method for producing a polarized hydrogen or deuterium target is proposed and some preliminary results are described. A brief summary of laser-driven polarized targets as well as conventionally-produced polarized atomic beams is included.

INTRODUCTION

Although there is great interest in polarization phenomena in electromagnetic interactions with nuclei, this area remains essentially unexplored experimentally. The reasons for the interest are manifold, but fall primarily into three categories: (i) much greater sensitivities to small form factors, such as the electric form factor of the neutron, (ii) allow separation of elastic form factors for nuclei with spin ≥ 1, e.g., the deuteron, (iii) permit unravelling of multipole excitations of resonances in nuclei and isolation of structure functions.

Unfortunately, the experiments are extremely difficult, and in most cases, appear infeasible with present techniques. In this report we wish to discuss a novel method which should provide accessibility

*This work supported by the U. S. Department of Energy under contract No. 31-109-ENG-38.

to polarization measurements in a broad range of interesting cases. Namely, we consider the situation where a thin polarized target is located inside an electron storage ring and the ring would be designed in such a manner as to provide longitudinally polarized electrons at the target position. There would be many advantages to this technique. First, one would make very efficient use of the electron beam, and thus, the demand on the electron injector is minimal. If the electron does not interact with the target, it merely would circulate in the ring until an interaction would occur; whereas, in the single-pass geometry the non-interacting electrons would pass directly to the beam dump. Another important advantage is the prospect of low background near a storage ring. At present, with storage rings which operate below a few GeV in energy there is essentially no background. This is due to the fact that only $\sim 10^{12}$ electrons are in the ring at any given moment and if all were lost simultaneously, the radiation dosage would be very small.

However, the primary advantage of the method is that with large circulating currents, one can consider much thinner targets than with the single-pass geometry. Thus, one can employ polarized atomic beams as targets. The advantages of polarized atomic beams over conventional polarized targets are, (i) the target material is pure or the contaminating host is small, (ii) the direction of the polarization axis can be changed readily with only a few gauss field, (iii) tensor as well as vector polarized targets are feasible, and (iv) the target polarization would not be compromised by beam heating or radiation damage as with the conventional targets.

In the remainder of this talk we shall focus on some of the physics problems which this method should render feasible, the counting rate advantages over external-beam geometries, and the feasibility of producing polarized targets. A new method for producing a polarized atomic beam will be discussed, along with a brief summary of the Workshop on Polarized Targets in Storage Rings, which was held at Argonne on May 17-18, 1984.

POLARIZATION IN ELECTRON SCATTERING

Three examples of physics measurements which could be performed as polarized internal target experiments are discussed below. These problems include the determination of the electric form factor of the neutron, the electric form factors of the deuteron, and the C2 transition in excitation of the free Δ.

A long-standing and most fundamental problem has been the uncertainty of the charge distribution of the neutron. The primary problem is that the electric form factor G_E of the neutron is small in comparison with the magnetic form factor G_M. Thus, a measurement of the cross section for quasi-free scattering from the neutron in deuterium has little sensitivity to G_E. Previous measurements of this kind are illustrated in Fig. 1. The curves in the figure represent predictions[1] based on the cloudy bag model. The quantity R is the bag radius in fm.

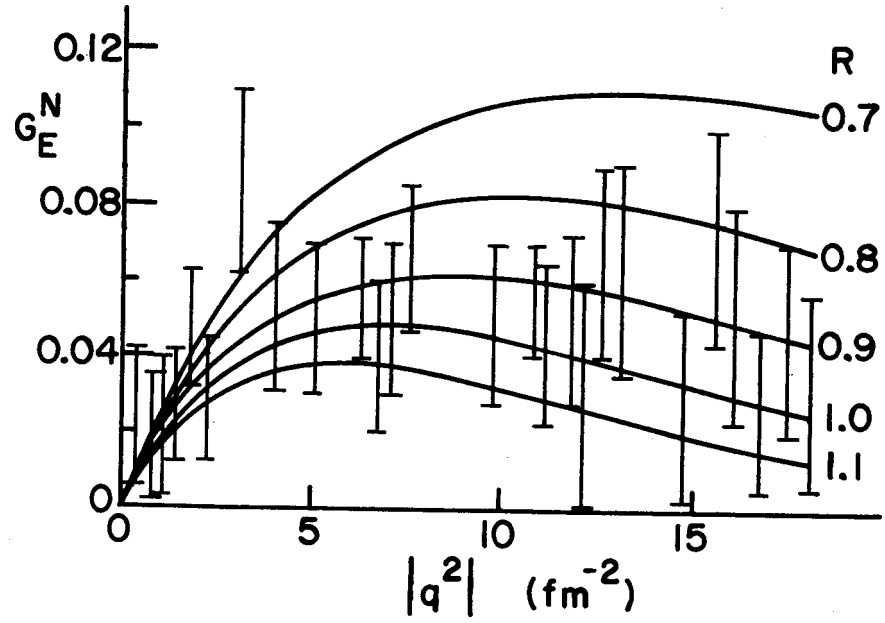

FIG. 1. Electric form factor of the neutron for various values of the bag radius (solid curves) and measured values (vertical lines).

On the other hand, a measurement of the analyzing power A_x from polarized electron scattering on a polarized deuterium target depends on the interference term between G_E and G_M according to the expression:

$$A_x = \frac{-2\sqrt{\eta(\eta+1)}\, G_E G_M \tan(\theta/2)}{G_E^2 + \eta G_M^2[1+2(\eta+1)\tan^2(\theta/2)]}$$

where $\eta=q^2/4M_d^2$, θ is the electron scattering angle and q is the four-momentum transfer. The quantity actually measured would be the asymmetry a_x from polarization transfer:

$$a_x = h\, p_T\, A_x$$

where h is the longitudinal polarization of the incident electron beam and p_T is the vector polarization of the neutron in the deuteron.

As an estimate of the feasibility of such an experiment, we will assume that a 1-GeV electron beam with h=0.4 and a circulating current of 40 mA will be available. (Such a facility has been proposed by the Massachusetts Institute of Technology for the Bates Linear Accelerator Center.) In addition, we assume a target with a thickness of 4×10^{15} atom/cm^2 and p_T=1 will be available. Cheung and Woloshyn[2] have calculated the cross section at q^2=10 fm^{-2} to be 10^{-2} μb/sr-MeV. With an electron spectrometer of $\Delta\Omega_e$=50 msr, the expected event rate is 130 events/hr. Thus, it should be possible to determine G_E to an accuracy of ± 10% over the momentum transfer region of $5 \leq q^2 \leq 15$ fm^{-2} (see Fig. 1) in approximately one month. An internal target facility at the Continuous Electron Beam Accelerator Facility (CEBAF) which has been proposed by the Southeastern Universities Research Association (SURA) should render experiments of this kind even more viable.

Another fundamental problem in nuclear physics is the fact that the electric form factors of the deuteron, charge F_C and quadrupole F_Q, have never been isolated in electron scattering studies. This problem can be seen from the form of the Rosenbluth formula for the

cross section:

$$\frac{d\sigma}{d\Omega} = \frac{d\sigma}{d\Omega_M} [A(q^2) + B(q^2) \tan^2(\frac{\theta}{2})]$$

where

$$A(q^2) = F_C^2 + \frac{8}{9} \eta^2 F_Q^2 + \frac{2}{3} \eta F_M^2, \qquad B(q^2) = \frac{4}{3} \eta(1+\eta) F_M^2 ,$$

and $\frac{d\sigma}{d\Omega_M}$ is the Mott cross section. Clearly, only A and B can be separated by cross section measurements, and thus, only F_M can be isolated. One important question in e-d scattering is concerned with the location of the first zero in the charge form factor of the deuteron. The exact location of the first zero, expected near $q \sim 4$ fm^{-1}, is sensitive to the deuteron model[3] as well as the isoscalar meson exchange currents.[4] Unfortunately, the quadrupole form factor masks the location of the zero in F_C, and thus, the location cannot be determined from a measurement of $A(q^2)$. However, a measurement of the tensor polarization in e-d scattering would permit one to isolate the charge and quadrupole form factors. The expression for t_{20} is given in terms of $X = \frac{2}{3} \eta F_Q/F_C$ and $Y = \frac{2}{3} \eta f(\theta) F_M^2/F_C^2$ below:

$$t_{20} = -(2)^{1/2} [X(X+2) + Y/2]/[1+2(X^2+Y)]$$

where the dominant contribution to t_{20} is from F_C and F_Q for $q < 8$ fm^{-1}, and $f(\theta) = \frac{1}{2} + (1+\eta) \tan^2(\theta/2)$.

If perturbative QCD is valid for e-d scattering for $q \gtrsim 5$ fm^{-1} as suggested by Brodsky and Chertok[5] and, more recently, by Carlson and Gross,[6] then $X \to 1$ as $q^2 \to \infty$, and thus, one might expect $t_{20} \to -(2)^{1/2}$ rather than a positive value as predicted by the conventional meson exchange model. Of course, the validity of perturbative QCD at such low values of momentum transfer is a matter of current debate.[7] Predictions for various models are shown in Fig. 2. The two data points in the figure were determined[8] with the use of a deuteron tensor polarimeter in which the polarization of recoil deuterons from e-d elastic scattering was measured.

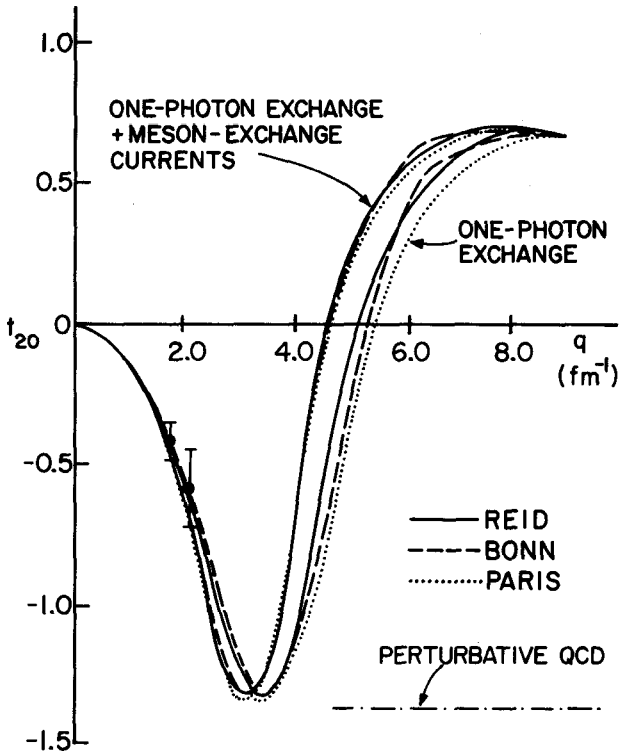

FIG. 2. The curves represent predictions of t_{20} in e-d elastic scattering for various deuteron wave functions. The presence of isoscalar meson-exchange currents produce a significant impact on t_{20} for $q \gtrsim 3$ fm^{-1}. The perturbative QCD limit illustrated here is discussed in the text. The data points are from ref. 8.

A comparison among the expected counting rates is illustrated in Fig. 3. The two points in this figure indicate the actual counting rates with a polarimeter. The curve labelled Aladdin arises from the assumption that one could employ the Aladdin synchrotron light source for these studies. Tests will be performed at Aladdin as soon as it comes into operation in order to determine the feasibility of performing an experiment in a synchrotron light-source ring. The assumptions that are involved in this estimate are that the circulating current would be 100 mA, a target thickness of 10^{14} atoms/cm^2, and a solid angle of 75 msr. The primary difficulty of a synchrotron light source is that the target thickness is limited to 10^{14} atoms/cm^2 by bremsstrahlung losses and the requirement of long storage times (~10 hrs.) The other curves in Fig. 3 denote the expected counting rates if an internal target station were commissioned at the proposed stretcher rings at MIT-Bates and CEBAF (SURA). Here a target thickness of 4×10^{15} atoms/cm^2 and currents of 40 mA and 100 mA, respectively, were assumed.

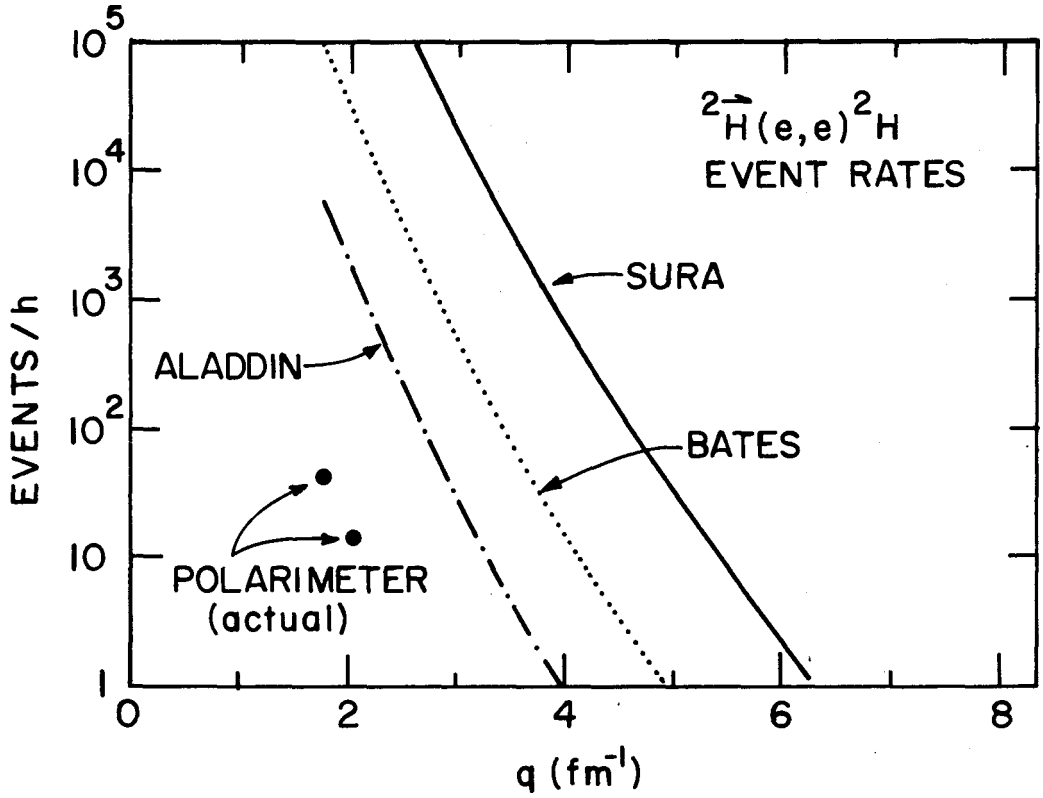

FIG. 3. Counting rates for measurments of t_{20} in e-d scattering as a function of momentum transfer. The points represent rates actually encountered in an experiment involving a polarimeter, Ref. 8. The three curves indicate expected rates for three types of electron rings.

The major advantage that this method holds over an experiment in which t_{20} of a recoil deuteron is measured with a polarimeter[8] lies not only in improved counting rates, but also in ultimate accuracy. Analyzing powers of polarimeters at higher energies, obtained by bootstrapping from "known" analyzing powers at lower energies as well as improvements in efficiency, would be expected to have greater uncertainties than the lower energy polarimeters. Presently, it would be difficult, if not impossible, to devise a high-energy deuteron tensor polarimeter in which the analyzing power is known to better than ± 0.1 and an efficiency of $\gtrsim 10^{-3}$. It is essential for $q \lesssim 4$ fm^{-1} to measure t_{20} with high accuracy in order to constrain the various

deuteron models. This accuracy could be achieved with a polarized internal target experiment in which the target polarization is monitored at low values of q where t_{20} is well known. For example, the exotic deuteron wave functions suggested by Coester and Ostebee[3] could be tested with an accuracy of ±0.03. Moreover, an accuracy of ±0.03 is necessary at 3 fm^{-1} to distinguish the presence of isoscalar meson exchange currents. An accuracy of ±0.01 would allow one to distinguish among present calculations[4] of t_{20} with the Paris, Bonn, Nijmegen and Reid wave functions in this momentum transfer region. This statistical accuracy (+0.01) could be achieved with only 300 hours of running time at the proposed ring at Bates at q = 3.0 fm^{-1} and with the assumption that the target would have a polarization of T_{20} = 0.3.

Note that it is expected that a spectrometer would not be necessary for this experiment provided that the beam strikes only the target in the target region. This condition certainly must be met at Aladdin and it would be expected to be met at the proposed Bates and SURA facilities. The electron and recoil deuteron would be detected in coincidence and the q-value would be determined by the incident electron energy and the electron scattering angle. A possible detector arrangement which is being proposed for the experiment at Aladdin is shown in Fig. 4. Background events from the target are expected to be negligible. The usual major source of background associated with the target is bremsstrahlung production in the target followed by photo-produced particles in the target. This process goes as the square of the target thickness and is negligible for the thin internal targets discussed here.

The longitudinal E2 transition (C2) between the free nucleon and the delta has received considerable attention in the past few years. Within the framework of the quark model this transition can correspond to an excitation of an s-wave quark in the nucleon to a d-wave quark in the delta, and thus, would be indicative of a deformed delta. Spherical bag models give rise only to M1 spin-flip amplitudes in the

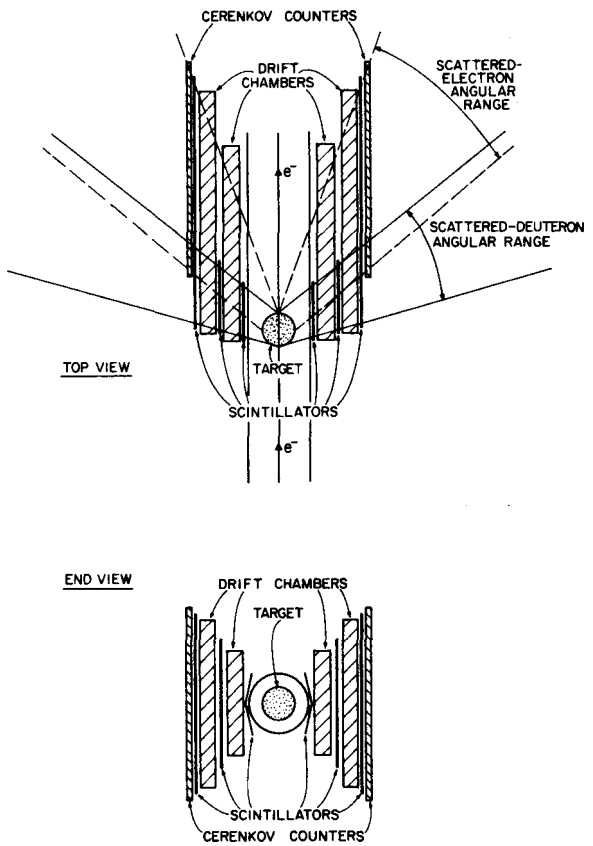

FIG. 4. Proposed detector arrangement for the $^2\vec{H}(e,e)^2H$ experiment at Aladdin.

nucleon to delta transition. Deformed nucleons can arise quite naturally from the chiral bag model, since the coupling $(\vec{\sigma} \cdot \vec{V}\phi_\pi)$ of the pion field to the quarks can be strongest along the spin axis of the nucleon. A "squashed" quark bag model[9] of the nucleon can explain the value of the axial vector coupling constant, the ratio of the $\pi N\Delta$ to the πNN coupling constants and the slope[10] of Regge trajectories. Perhaps more compelling evidence for this C2 transition is found from $H(e,e'p)\pi^0$ coincidence experiments[11] where a non-zero C2 coefficient was found. The deduced amplitudes from measurements[12] are shown in Fig. 5. Here, the M_{1+} notation refers to the M1 amplitude; whereas, E_{1+} and S_{1+} denote transverse E2 and longitudinal E2 amplitudes, respectively. Clearly, there appears to be a nonzero S_{1+} amplitude at low momentum transfer. Unfortunately, the coincidence experiments are

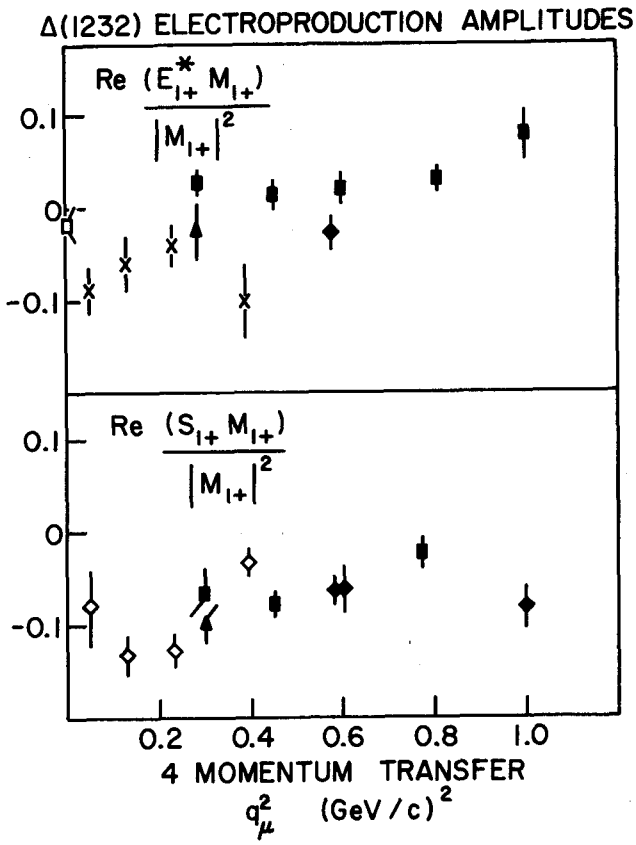

FIG. 5. The ratio $\mathrm{Re}(E^*_{1+}M_{1+})/|M_{1+}|^2$ and $\mathrm{Re}(S^*_{1+}M_{1+})/|M_{1+}|^2$ as a function of q^2_μ for π° electroproduction of the $\Delta(1232)$. This figure is adapted from reference 12. The open square represents the pion photoproduction results for E_{1+}.

extremely difficult and the ultimate accuracy of this technique is limited to the accuracy of the relative acceptance of the detectors for different scattering angles.

A far more sensitive determination of the C2 amplitude would be to measure the polarization transfer coefficient in the scattering of longitudinally polarized electrons from a polarized hydrogen target. The C2 amplitude can be measured with greater precision than the coincidence experiment since the detection system remains fixed and since the direction of the target polarization can be controlled

readily. Thus, this kind of measurement is well-suited to the polarized internal target method.

In order to further investigate the feasibility of performing this measurement, we now consider the problem in more detail. The expression[13] for the differential cross section is given by

$$\frac{d^2\sigma}{dE_e d\Omega_e} = \frac{d^2\Sigma}{dE_e d\Omega_e} + h \frac{d^2\Delta}{dE_e d\Omega_e}$$

where h is the degree of electron polarization and the Σ and Δ components of the cross section are given in terms of Donnelly's notation below:

$$\frac{d^2\Sigma}{dE_e d\Omega_e} = 4\pi\sigma_m f_{rec}^{-1} \{\left(\frac{q^2}{\vec{q}^2}\right)^2 F_{2C}^2 + \left[\frac{-q^2}{2\vec{q}^2} + \tan^2(\theta/2)^2\right](F_{2E}^2 + F_{1M}^2)\}$$

$$\frac{d^2\Delta}{dE_e d\Omega_e} = 4\pi\sigma_m f_{rec}^{-1} \{\tan(\theta/2)\left[\frac{-q^2}{2\vec{q}^2} + \tan^2(\theta/2)\right]^{1/2}\left(F_{1M}^2 - F_{2E}^2 - 2.3^{1/2} F_{1M}F_{2E}\right)\cos\theta^*$$
$$+ \sin\theta^* \cos\phi^* \frac{q^2}{(2\vec{q}^2)^{1/2}} \tan(\theta/2) F_{2C}(F_{1M} + 3^{1/2} F_{2E})\}$$

where σ_m is the mott cross section and f_{rec} is the nuclear (proton) recoil term. The starred angles refer to the orientation axis of the nuclear spin with respect to the momentum transfer direction and are illustrated schematically in Fig. 6. It is the second term in the cross section formula which gives rise to the improved sensitivity to the S_{1+} amplitude. In fact, S_{1+} is directly related to F_{2C} in the expression by

$$F_{2C}^2 = \frac{2W|q'|}{\pi^2 \alpha M_p} \left(\frac{\vec{q}}{q'}\right)^2 S_{1+}^2$$

where W is the delta mass, M_p is the proton mass and $|q'|^2 = (W^2 + M_p^2 - q^2)^2/4W^2 - M_p^2$. Clearly, the expression for $\frac{d^2\Delta}{dE_e d\Omega_e}$ gives rise to an interference between the amplitude of

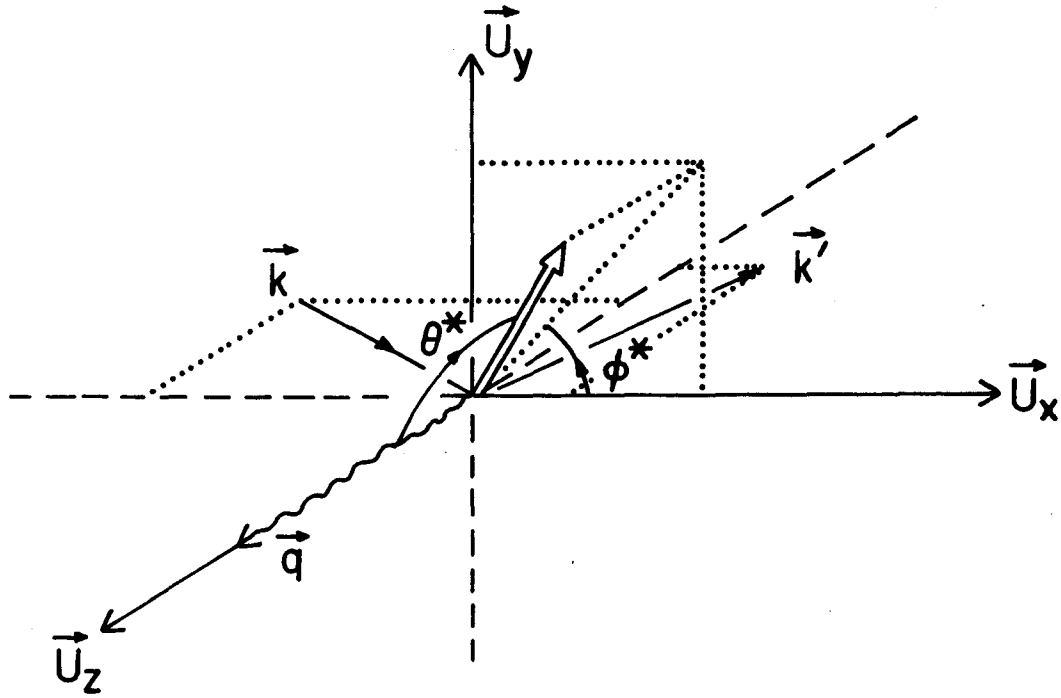

FIG. 6. Orientation of the target polarization axis.

interest F_{2C} and the dominant amplitude F_{1M}, the term arising from the M1 transition. The importance of controlling the orientation of the target polarization can be seen from this expression. The $\sin\theta^* \cos\phi^*$ term can be readily isolated from the $\cos\theta^*$ term and $F_{2C}F_{1M}$ interference term can be enhanced. For example, θ^* can be fixed at $\pi/2$ and ϕ^* can be rapidly changed between 0 and π to provide a high sensitivity measurement. With the same assumptions as in the previous cases, an estimate can be obtained for the time required for a measurement of S_1+/M_1+ with an accuracy of ± 0.01. An estimate of 15 days of running time would be required for a measurement of $q^2 = 0.05$ $(GeV/c)^2$ at the proposed stretcher ring for the MIT-Bates Linear Accelerator Laboratory.

REQUIREMENTS ON INTERNAL TARGET

Now that the prospective advantages of the internal target method have been discussed, we shall turn to a discussion of the limitations imposed on the target by the storage ring itself. Clearly, the synchrotron-light source rings impose the greatest constraints on the target, since the storage times are typically several hours. Bremsstrahlung production represents the largest loss mechanism for electrons in a storage ring. For the Aladdin storage ring the circulation time T_o is 0.32 μs and the storage time $T_{1/2}$ should be ~10 hrs. Thus, the maximum target thickness for deuterium in this ring is given by

$$n \leq 0.693 \frac{T_o}{\sigma_b T_{1/2}} = 10^{14} \text{ atoms/cm}^2$$

where σ_b is the bremsstrahlung cross section $\approx 0.06\ Z^2$ b. In a dedicated ring for internal target experiments, where the electron beam need only be stored for ~ 1000 turns, the target thickness limitation from bremsstrahlung losses would be ~ 10^{22} atoms/cm^2 for Z = 1. Thus, a dedicated electron ring for nuclear physics would be highly desirable.

Another consideration is the effect of multiple scattering on the electron beam. In the case of a synchrotron light source such as Aladdin, bramsstrahlung losses override the effect of multiple scattering. For the Aladdin ring and a target thickness of 10^{14} atoms/cm^2 of deuterium, the multiple scattering angle becomes only 5 μrad, and thus is negligible. The effect of multiple scattering is alleviated by synchrotron cooling of the beam. However, for a dedicated ring of, say, a storage time of 1000 turns and an angular acceptance of the ring of 1 mrad, the deuterium target thickness would be limited to 4×10^{18} atoms/cm^2. Thus, bremsstrahlung losses are the primary limitation for a synchrotron light source, while multiple scattering is a more important consideration for a dedicated ring.

A more stringent constraint on the target thickness would be due to ionization loss of the target polarization. In order to estimate the

polarization loss from ionization we will assume that if an atom is ionized then the polarization of the nucleus is lost. The ionization rate I_i is given by $I_i \leq \rho I_e E_i^{-1} dE/d\rho$, where ρ is the target density, $dE/d\rho$ is the energy loss in the target, I_e is the circulating electron current and E_i is the ionization energy of the target atom. With the choice of $dE/d\rho$ = 2 MeV-cm^2/g, E_i = 20 eV and $I_i \leq 0.1\ I_A^{\rightarrow}$, where $I_A^{\rightarrow}$ is the rate at which polarized atoms in the target can be replenished, the maximum luminosity $\mathscr{L}$ is given by $\mathscr{L} \leq 6 \times 10^{17} I_A^{\rightarrow}/A$ cm^{-1}s^{-1}. An atomic beam source which could provide 10^{17} polarized atoms/s would give a luminosity limit of 6×10^{34} A^{-1} cm^{-2} s^{-1}. It is expected that polarized atoms could be replenished at rates in excess of 10^{18} atoms/s with optical pumping techniques which will be described later. At present it would be difficult to fabricate a low-A target which could attain this luminosity limit, but it might very well represent the limitation on target thicknesses for $A \gtrsim 100$. Note, that the luminosities for experiments discussed in the previous section do not exceed 2.4×10^{33} cm^{-2} s^{-1}, and thus, ionization losses do not limit any of these experiments.

Apertures near the target region could interfere with the stored-electron beam. These apertures could either be in the form of orifices in a storage bottle to allow the electron beam to pass cleanly through or in the form of a nozzle and collector for a jet target geometry. In estimating the minimum size of an aperture, we will assume that electrons which strike the area around the orifice are lost. Clearly, the aperture size governs the storage time $T_{1/2}$ of the electron beam according to the expressions:

$$T_{1/2} = 0.693\ T_o/P$$

$$P = 1 - \frac{1}{\sqrt{2\pi}} \int_{-\infty}^{x} e^{-t^2/2}\, dt\ ,$$

where we have assumed that the electron-beam shape is a gaussian and x is the half-size of the aperture in standard deviations of the beam size. We find that $T_{1/2}$ is changing rapidly near x = 6 standard

deviations, i.e. for x = 5, $T_{1/2} \approx 10^{-4}$ hrs and for x = 7, $T_{1/2}$ = 20 hrs. Thus, the full aperture size should be >12 standard deviations. Since the storage time is so sensitive to the aperture size, the same rule approximately would apply to a target in a dedicated ring as well as a synchrotron light source. In the case of the Aladdin storage ring, σ_x is expected[14] to be 0.5 mm and σ_y, 0.08 mm. Thus, we have chosen a circular aperture of 7 mm in diameter for conceptual design purposes. Moreover, these apertures must move totally out of the beam during tuning and filling of the ring.

The final requirement on an internal target is that the ring vacuum, typically $\lesssim 10^{-9}$ torr, be restored in as short a distance as possible from the target position. This requires the target to be buffered from the ring by differentially-pumped vacuum systems. As part of the feasibility study, a system of this type was designed for the Aladdin storage ring and is shown in Fig. 7. Conventional and commercially-available vacuum pumps were used throughout the design. The pressure as a function of distance from the target is calculated and indicated in the figure. The pressure should be restored to the 10^{-9}-torr value in a distance of one meter from the target.

TARGET DESIGN CONSIDERATIONS

In the following conceptual design for an internal target, we shall consider a storage bottle which is replenished continuously with polarized atoms from an atomic beam source. In addition, we shall consider a tensor polarized deuterium target which could be employed in the Aladdin storage ring, i.e. a thickness of 10^{14} atoms/cm^2. Moreover, we will assume a spherical storage bottle of 10 cm diameter and two 7-mm orifices which permit the primary electron beam to enter and exit from the target chamber. The target density in the bottle would be 10^{13} atoms/cm^3. Then, the atoms would leak from the storage bottle at a rate of 4×10^{17} atoms/s at T=500°K or 8×10^{16} atoms/s at T=20°K. An atomic beam source must supply polarized atoms at this rate to the bottle. Unfortunately, a conventional atomic source operating at room

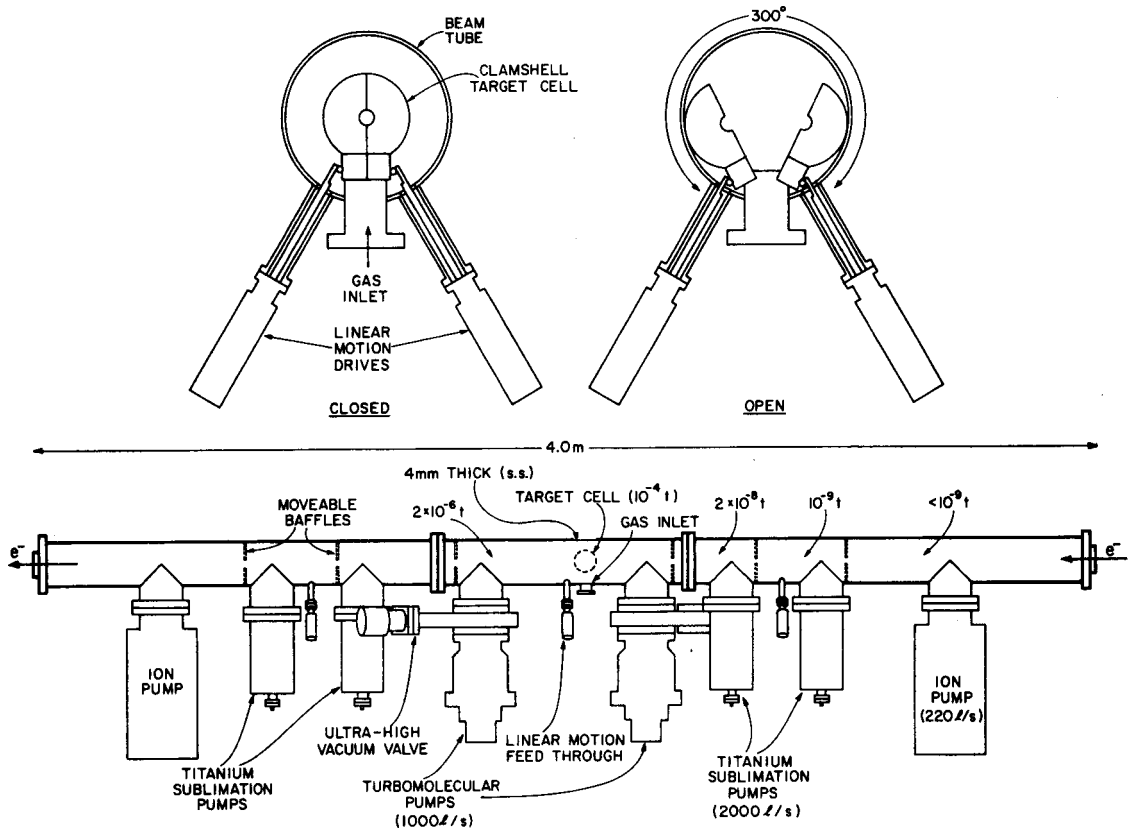

FIG. 7. Proposed vacuum system for an internal target in the Aladdin storage ring.

temperature could provide only 3×10^{16} atoms/s. It is expected that a low temperature atomic beam source would provide $\gtrsim 10^{17}$ atoms/s at T=20°K. Two groups[15,16] are attempting to provide polarized atomic beams of hydrogen from this kind of source. Another method which has the prospect of achieving 10^{17}-10^{19} polarized atoms/s is spin-exchange optical pumping. We shall consider the latter method in detail since it has implications not only for the Aladdin storage ring but also for a dedicated ring for nuclear physics.

Bhaskar et al.[17] recently demonstrated nuclear polarization through spin-exchange optical pumping by polarizing ^{129}Xe. In order to

understand how the nuclear polarization arises from spin-exchange collisions and how many polarized photons are necessary to produce a high degree of polarization, we shall consider the simplest case, i.e. $Na\uparrow + H\downarrow \rightarrow Na\downarrow + H\uparrow$ where the Na atom is polarized by optical pumping. The proton in hydrogen is polarized by successively polarizing the electron and allowing the hyperfine interaction to act between each collision. In the basis of the proton and electron spins $|m_p m_e\rangle$ the four states of the hydrogen atom are written as:

$$
\begin{array}{ll}
|++\rangle & a \\
\frac{1}{\sqrt{2}}\left(|-+\rangle + |+-\rangle\right) & b \\
|--\rangle & c \\
\frac{1}{\sqrt{2}}\left(|+-\rangle - |-+\rangle\right) & d
\end{array}
\qquad
\left.\begin{array}{l} P_{ba} = 1/2 \\ P_{cb} = 1/2 \\ P_{cd} = 1/2 \end{array}\right\} \quad P_{da} = 1/2
$$

with no external field. The spin-exchange collision changes only the electron spin and induces the transitions shown at the right. The hyperfine interaction then remixes states b and d. The populations of the four states can be written as recursion relations as a function of the number of spin-exchange collisions, n:

$$
\begin{aligned}
N_a(n) &= N_a(n-1) + P_{ba}\, N_b(n-1) + P_{da}\, N_d(n-1) \\
N_b(n) &= (1 - P_{ba})\, N_b(n-1) + P_{cb}\, N_c(n-1) \\
N_c(n) &= (1 - P_{cb} - P_{cd})\, N_c(n-1) \\
N_d(n) &= (1 - P_{da})\, N_d(n-1) + P_{cd}\, N_c(n-1)
\end{aligned}
$$

where P_{ij} are the probabilities of transition from state i to j during a spin-exchange collision. The proton polarization after n spin-exchange collisions and for $P_{ij} = 1/2$ is given by

$$
p(n) = \frac{N_+ - N_-}{N_+ + N_-}
$$

where $N_+(n) = N_a(n) + 1/2[N_b(n) + N_d(n)]$ and
$N_-(n) = N_c(n) + 1/2[N_b(n) + N_d(n)]$

The deduced proton polarization as a function of the number of spin-exchange collisions can be shown to be

$$p(n) = 1 - (1/2)^n.$$

This means that very few spin-exchange collisions, and consequently polarized photons, are necessary to polarize the proton.

When the same analysis is performed for deuterium the result is not easily reduced to a simple form, but it is straightforward to calculate the vector polarization $t_{10} = (3/2)^{1/2} (N_{+1} - N_{-1})$ and the tensor polarization $t_{20} = (1/2)^{1/2} (1 - 3 N_o)$ as a function of the number of spin-exchange scatterings. Here, the N's refer to the population of the three magnetic substates of the deuteron. The results for t_{10} and t_{20} are shown in Fig. 8. For a given Na atom polarization, only $\gtrsim 5$ scatterings are necessary to obtain essentially the maximum polarization of the deuteron.

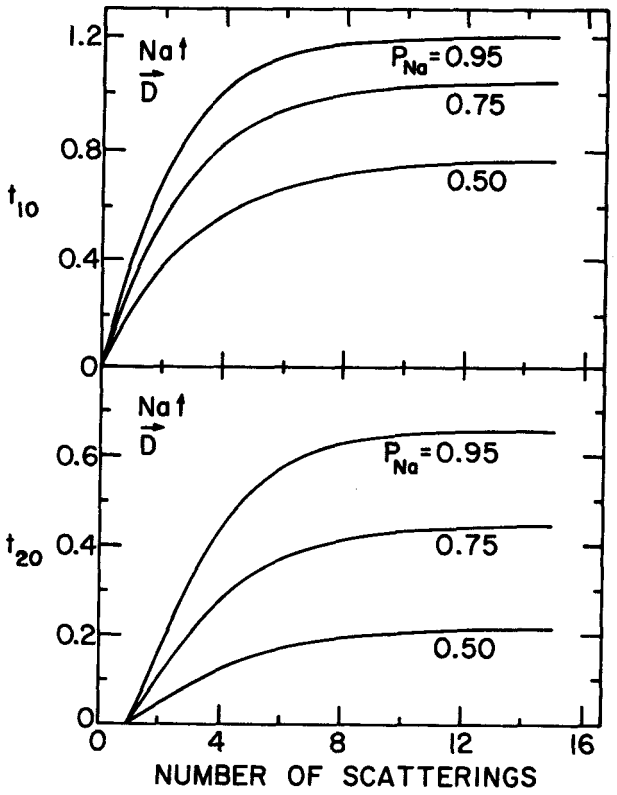

FIG. 8. Expected polarizations for the deuterium nuclei as a function of the number of atomic spin-exchange collisions.

With the assumption that 5 spin-exchange collisions are necessary to polarize deuterium one can determine that 2 watts of laser power at the Na D1-line is necessary to produce 4×10^{17} polarized atoms/s. This is a reasonable power output of a single CW dye laser. Furthermore, it is reasonable to expect that 20 watts of power could be employed to optically pump Na and one may achieve 4×10^{18} polarized atoms/s.

The density and thickness of alkali atoms that must be optically pumped can be estimated if we consider the process to take place in a tube of length ℓ, diameter 2a and one end open so that the polarized atoms can flow from the cell. The laser beam is directed toward the mixture of Na and D atoms in the cell from the direction of the opening in the tube. Then, the density n_{Na} of Na necessary to polarize the deuterium is given by

$$n_{Na} = \frac{N_{se}}{4\ell\sigma_{se}} \left(\frac{8a}{8a + 3\ell}\right)$$

where N_{se} is the average number of spin-exchange collisions that deuterium atoms undergo with Na atoms in the cell and σ_{se} is the Na-D spin-exchange cross section which is taken[18] to be 10^{-14} cm^2. If we take ℓ = 5 cm, a = 2.5 mm and N_{se} = 5, then the Na density is 2.9×10^{12} atoms/cm^3 and the thickness is 1.5×10^{13} atoms/cm^2. These values are consistent with Na densities and thicknesses that have been optically pumped[19] with high polarization and without a buffer gas or special wall coatings. An important consideration for the experiments considered here is the amount of contamination of the host Na atoms. The ratio of the Na density to that of deuterium is given by

$$\frac{n_{Na}}{n_D} = \frac{12\pi a^4 \bar{v}_D N_{se}^2}{\ell L \sigma_{se} (8a + 3\ell)^2}$$

where L is the intensity of the incident polarized photon beam (note that 1 watt corresponds to 3×10^{18} photons/s at the Na D1-line) and $\bar{v}_D$ is the mean speed of deuterium atoms in the laser cell. For the tube dimensions discussed above and a 2 watt laser beam, this ratio turns out to be 0.9%, a reasonably small value. A more detailed computer model of such a polarized source has been discussed[20] by M. Green.

An additional advantage of the spin-exchange method is that all dissociated deuterium atoms are used in the source. In the conventional atomic beam source most of the atoms are rejected by the small acceptance (~ 1-10 msr) of the hexapole. The novel atomic beam source requires a far less imposing vacuum system, an essential advantage for internal targets in storage rings, and a less elaborate rf dissociator system. However, since every atom passes through the source, one must maintain a high dissociation efficiency. A dissociation efficiency of 97% with an atomic beam rate of 10^{18} atoms/s has been achieved[21] routinely at the Los Alamos National Laboratory and represents an ideal development for the proposed atomic beam source.

Interactions with the walls represent a major concern for all schemes of polarized target development. With the geometry for a polarized target suggested here, the atoms have approximately 900 wall collisions before leaking out of the target cell. Although a depolarization probability of $<10^{-3}$ has been observed[22] for polarized hydrogen on teflon walls, nothing is known of the depolarization probability for other surfaces. With deuterium atoms, we are concerned not only with the depolarization probability, but also the recombination probability. Already, some information[23] is available for the recombination coefficient for hydrogen and deuterium atoms and is summarized in Fig. 9. A number of surfaces exhibit a minimum in the recombination probability near a temperature of 150° K. If the depolarization probability is also small at this temperature, then it might be the ideal temperature region to operate a storage bottle for polarized hydrogen targets. Unfortunately, the properties of teflon are not known as a function of temperature but, at present, teflon or teflon-like wall coatings hold the most promise for storage bottles.

POLARIZED TARGET DEVELOPMENT

A prototype of a polarized deuterium target which employs the spin-exchange method is being developed at Argonne and is illustrated in Fig. 10. In this scheme the target polarization can be detected by the

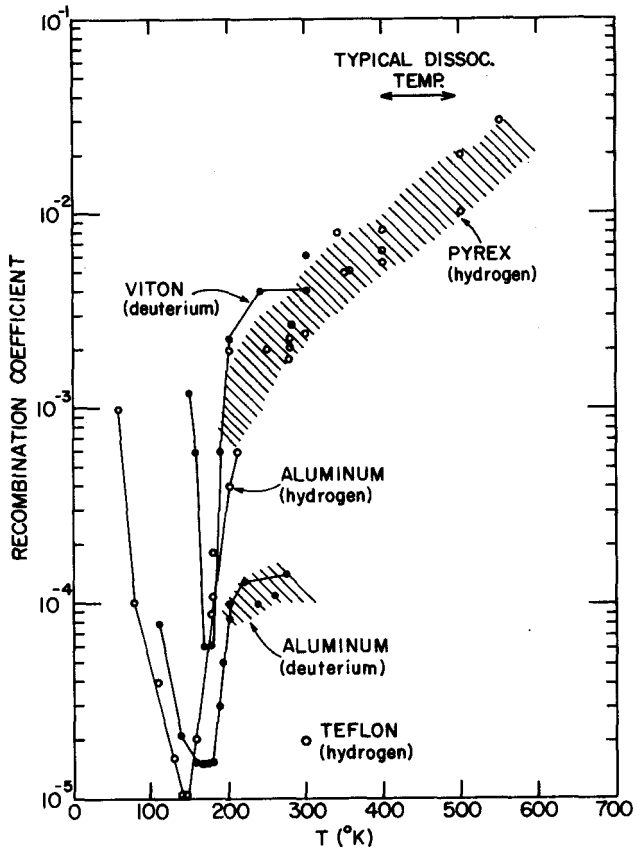

FIG. 9. Recombination coefficient of hydrogen and deuterium for various surfaces as a function of temperature.

$\vec{D}(^3He,p)^4He$ reaction. A 625-keV ^3He beam was incident upon the gas stream of deuterium atoms and the ~ 14-MeV protons were counted in Si surface-barrier detectors. At the $3/2^+$ resonance this reaction exhibits a 0.7-b cross section[24] and maximum analyzing power[25] for t_{20}, and thus, is ideal for the study of a thin tensor polarized deuterium target. The Helmholtz pair was used to maintain a field of ~4 gauss near the target, and consequently, to provide an orientation axis for the spin states of deuterium and Na. The laser cell was heated by forced air to ~500°K in order to vaporize the Na. In a preliminary test we have achieved a 2:1 signal-to-background ratio for observing the $D(^3He,p)^4He$ reaction and we have observed 10 mW of absorbed laser power which was driving the spin-exchange reaction of Na with D atoms. This corresponds to only 10^{15} polarized atoms/s flowing through the ^3He beam and would fall below our detection threshold. The major problem during this test was a poor dissociation efficiency, and presently, we are developing a reliable diagnostic for dissociation efficiency before resuming further studies.

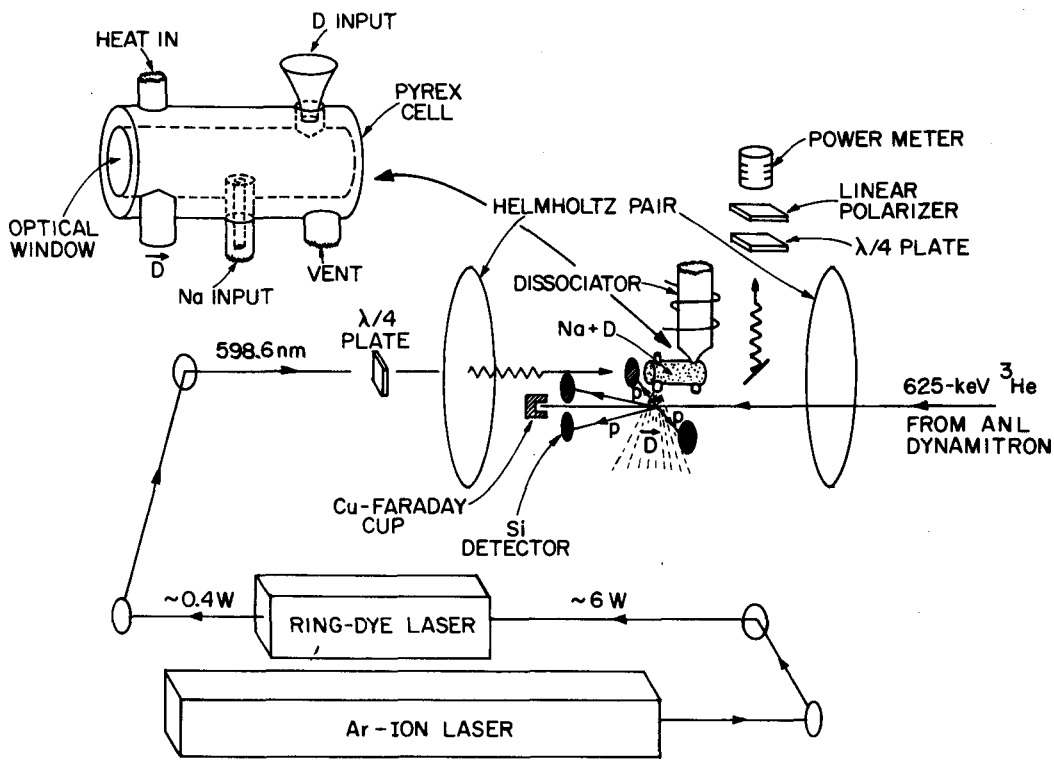

FIG. 10. Arrangement of a spin-exchange optically pumped polarized deuterium source and the method to detect the polarization.

SUMMARY OF OTHER TARGET DEVELOPMENTS

A brief summary of other target developments were reported[26] at the Workshop on Polarized Targets in Storage Rings, held at Argonne on May 17-18, 1984, is given in Table I. The first four entries in Table I are primarily concerned with producing polarized hydrogen or deuterium, using four different techniques. It appears quite likely that hydrogen or deuterium targets in the range of 10^{14} - 10^{15} atoms/cm^2 will be available in the near future. The last six entries in the table represent laser-driven polarized targets. The third and fourth entries also rely on spin-exchange as well as optical pumping; whereas, the last four targets are directly optically pumped. One can conclude from a

study of this table that the advent of lasers has had a substantial impact on the development of polarized targets.

Table I. Polarized Internal Targets in Development or Operation

Type of Target	Nuclei	Institution	Target Thickness Expected
Conventional atomic beam (cyogenically cooled)	H,D	CERN (SPS) ETH, Zurich	5×10^{12}-5×10^{13} atom/cm^2 (Objective)
Storage Cells	H,D	Wisconsin	10^{14}-10^{15} atom/cm^2 (Objective)
Low-temperature high-field storage cell	H,D	BNL-MIT (AGS)	10^{14} atom/cm^2 (Objective) (Pulsed)
Spin-exchange optical pumping	H,D.N,..etc.	ANL (Aladdin)	10^{14}-10^{15} atom/cm^2 (Objective)
Spin-exchange optical pumping	Noble Gases	Princeton	10^{19} atom/cm^2 (Lab Demonstration for X_e)
Optical pumping of alkali vapors	Li	Bell/MIT Rutgers	10^{15} atom/cm^2 (Operational target)
Optical pumping of alkali vapors	Cs	Princeton	10^{16} atom/cm^3 (Lab Demonstration)
Optical pumping of rare earth jets	Eu	ORNL	10^{15} atom/cm^2 (Objective)
Optical pumping	^{3}He	I.E.N.S. (Paris)	10^{18} atom/cm^3 (Lab Demonstration)

SUMMARY

We have demonstrated conceptually that polarized internal targets in storage rings should be a powerful method for the study of nucleons and nuclei. Furthermore, this method should be compatible with the recently-proposed linac-stretcher ring accelerator designs of MIT and SURA. It is clear that a wide variety of suitable polarized targets are technically feasible. At present, laser-driven polarized targets appear to be the most promising technology. Optical pumping combined with spin-exchange scattering provides an even larger array of polarized targets that will benefit from laser techniques.

ACKNOWLEDGMENTS

I wish to thank my collaborators who have contributed much toward the development of the polarized target: D. Geesaman, L. Goodman, M. Green, R. Kowalczyk, J. Napolitano, M. Peshkin, E. Ungricht, L. Young and B. Zeidman. In addition, I wish to thank H. Jackson for useful discussions of the electric form factor of the neutron and D. Geesaman for discussions of the question of the deformed nucleon. Finally, we thank H. G. Berry for the loan of the lasers.

REFERENCES

1. A. W. Thomas et al., Phys. Rev. D24, 216 (1981).
2. C. Y. Cheung and R. M. Woloshyn, Phys. Lett. 127B, 147 (1983).
3. F. Coester and A. Ostebee, Phys. Rev. C11, 1836 (1975).
4. M. I. Haftel et al., Phys. Rev. C22, 1285 (1980).
5. S. J. Brodsky and B. T. Chertok, Phys. Rev. Lett. 37, 169 (1976)
6. C. Carlson and F. Gross, preprint for Phys. Rev. Lett. (1984).
7. N. Isgur and C. H. Llewellyn Smith, Phys. Rev. Lett. 52, 1080 (1984).
8. M. E. Schulze et al., Phys. Rev. Lett. 52, 597 (1984).
9. V. Vento et al., Phys. Lett. 102B, 97 (1981).
10. K. Johnson and C. B. Thorn, Phys. Rev. D13, 1934 (1976).
11. R. Siddle et al., Nucl. Phys. B35, 93 (1971).
12. T. G. Trippe et al., Rev. Mod. Phys. 48, 51 (1976).
13. T. W. Donnelly, Workshop on Perspectives in Nuclear Physics at Intermediate Energies, Trieste, October 10-14, 1983.
14. E. Rowe et al., IEEE Trans. on Nucl. Sci. NS-28, 3145 (1981).
15. W. Grüebler in Proceedings of Workshop on Polarized Targets in Storage Rings, Argonne National Laboratory Report ANL-84-50, 1984.
16. L. Dick, private communication, 1983.
17. N. D. Bhaskar et al., Phys. Rev. Lett. 49, 25 (1982).
18. W. Happer, private communication, 1983.
19. Y. Mori et al., Nucl. Instrum. Meth. 220, 264 (1984).
20. M. C. Green in Proceedings of Workshop on Polarized Targets in Storage Rings, Argonne National Laboratory Report ANL-84-50, 1984.
21. R. G. H. Robertson, private communication, 1983.
22. M. D. Barker et al., Proceedings of the Fifth International Symposium on Polarization Phenomena in Nuclear Physics, AIP, 931 (1981).
23. R. G. H. Robertson et al., prepring, 1984; E. Ungricht and M. C. Green, private communication, 1984.
24. W. E. Kunz et al., Phys. Rev. 97, 456 (1955).
25. G. Ohlsen, Rep. Prog. Phys. 35, 717 (1972).
26. Proceedings of the Workshop on Polarized Targets in Storage Rings, Argonne National Laboratory Report ANL-84-50, 1984.

PHOTONUCLEAR EXPERIMENTS USING LARGE ACCEPTANCE DETECTORS

Bernhard A. Mecking *

Physikalisches Institut, Universität Bonn, W.-Germany

Experimental programs in photonuclear physics are discussed. The experiments concentrate on the combined use of low intensity (real and virtual) photon beams and large acceptance detectors for the detection of multiple particle final states. Count rate estimates and the consequences for the operation of a high intensity accelerator are given.

1. Introduction

Several electron accelerators in the GeV range with high duty-cycle ($d \geq 90\%$) are presently being proposed or already under construction. Most machines are designed to provide high intensity ($I \geq 100\mu A$) electron beams. This is indispensable for the exploration of processes with very small cross sections varying rapidly with the kinematical quantities. A typical experimental problem is the determination of the formfactor of light nuclei. A typical experimental setup consists of one (or two) small acceptance spectrometers with well shielded detectors; special target techniques have to be developed to cope with the high beam power.

In addition to these experiments there is a large class of problems that even give higher quality results if a low intensity beam is used. Typical experiments of this type require the coincident detection of several only loosely correlated particles in large acceptance detectors and/or the use of special targets, like e.g. polarized or track sensitive targets.

Some examples for these experiments will be given in the following report. Experiments with real photons will be discussed in chapter 2, a comment on virtual photons will be made in ch. 3. Typical experimental setups will be described in ch. 4; the consequences for the operation of a high power accelerator will be discussed in ch. 5.

* Heisenberg foundation fellow

2. Experiments Using Real Photons

2.1. Photoexcitation of baryon resonances

The analysis of elastic πN scattering data has given detailed information on the higher excitation modes of the nucleon. Mass, width, spin and parity for ≈30 objects with strangeness 0 have been determined. This experimental information has to be explained by microscopic models for the structure of 3-quark systems. The test of these models is not only relevant for particle but also for nuclear physics: a successful description of the properties of the nucleon and its excited partners can form the basis for a new understanding of the NN-force and the properties of nuclei.

In addition to the static properties, the quark models are also required to predict the decay modes. In contrast to hadronic decays, the electromagnetic decay $N^* \to N\gamma$ can easily be calculated once the wave functions of the quarks in the initial and the final state is given. Therefore, the measurement of the electromagnetic coupling at the γNN^* vertex for real and virtual photons provides the best way to test the dynamical features of microscopic quark models.

Most of the information on the electromagnetic properties of the nucleon resonances have been obtained by exciting a nucleon to a resonance N^* using real photons and observing the subsequent πN decay. By comparing the $\gamma N \to N^* \to \pi N$ process with $\pi N \to N^* \to \pi N$ one obtains the coupling constant at the γNN^* vertex. In practice the situation is complicated because

(1) the resonances are broad and overlapping (see fig. 1),
(2) there is background from nonresonant π-production,
(3) the experimental information on $\gamma N \to \pi N$ is far from being complete.

Despite of the unsatisfactory experimental situation the photocouplings of many nucleon resonances have been determined with some accuracy using the pion photoproduction data accumulated in the last two decades /KAJI81/. However, the couplings of those resonances that are only weakly excited in γN reactions could not be determined. This is essentially an experimental problem that can be solved by measuring accurate data sets for all necessary observables over the complete range of kinematical variables.

The $\gamma N \to \pi N$ reaction is described by 4 complex helicity amplitudes which are functions of two kinematical variables, e.g.: s (c.m.s. energy) and t (momentum transfer) or the photon energy k and the pion c.m.s. angle θ_π. The experimental determination requires seven different measurements to be made at each kinematical setting (one phase is arbitrary) /BARK75/. A possible combination of experiments involving single and double polarization experiments is shown in table 1. For most reaction channels, only single polarization data are presently available; some double polarization experiments have been performed at Daresbury and Kharhov.

To reduce the influence of experimental errors and to get rid of discrete ambiguities, it will be useful to complement these 7 measurements by additional double polarization experiments. Especially the combination of circularly polarized photons (from the bremsstrahlung of polarized electrons) and a polarized proton or deuterium target promises to give high quality results; no such measurements have been performed up to now.

To disentangle the isospin structure, these measurements have to be made for three of the four reaction channels: $\gamma p \to \pi^+ n$, $\gamma p \to \pi^0 p$, $\gamma n \to \pi^- p$ and $\gamma n \to \pi^0 n$. Usually, the last channel is avoided due to obvious technical difficulties.

Single pion photoproduction can serve as an example for a complete experimental program: the number of events necessary for a model-free experimental determination of all helicity amplitudes amounts to 10^9 (the subdivision is given in table 2). An event rate of ≈ 30/sec can be reached using $N_\gamma = 10^7$/sec and a large acceptance detector. The high rate can only be handled by excellent on-line and off-line computer capabilities. At this rate, the total running time for the complete program is roughly one year.

With increasing excitation energy the decay $N^* \to \pi N$ is suppressed in favor of decay modes like $N^* \to \pi \Delta$ or $N^* \to \varrho N$. Therefore, these resonances are only weakly excited in πN reactions and are very difficult to observe in elastic πN scattering. (This might explain that theoretical models predict far more resonances than have been observed in πN scattering.) On the other hand, the coupling to the γN channel can still be reasonably strong. This offers the unique possibility to search for these resonances in $\gamma N \to \pi\pi N$ reactions since γN is the only decay channel available in a formation experiment.

The background in the $N\pi\pi$ channel consists mainly of nonresonant double pion production and the production of vector mesons. Compared to single pion photoproduction the experimental information is very scarce. This is essentially due to the fact that in previous experiments the large acceptance apparatus necessary for the efficient detection of multiple particle final states was not available.

2.2. Vector meson production

The photoproduction of the light vector mesons off nucleons $\gamma N \to VN$ ($V = \varrho, \omega, \phi$) can be used to determine the hadronic content of the photon and the vector meson - nucleon coupling (this information is used e.g. in the analysis of the nucleon formfactors and in meson theories of the NN-interaction).

The spectroscopy of light excited vector mesons (for a review see /PAUL81/) will allow to develop and test models for the interaction of light $q\bar{q}$ pairs. The search for the radially excitated states is

especially important because this would allow (in combination with the excitation spectrum of the heavy $q\bar{q}$ states ψ and Υ) to get information on the radial dependence of the $q\bar{q}$ force as a function of the quark mass.

2.3. Photodisintegration of the deuteron

The photodisintegration of the deuteron is one of the most fundamental processes in photonuclear physics. Therefore, careful experimental investigations and a detailed theoretical understanding of the process are of great importance.

At photon energies well below the pion production threshold, where the diagram (a) plays a dominant role, the deuteron wave function and details of the NN-interaction can be studied. Above the pion threshold the cross section is enhanced by the production and reabsorption of nearly real pions (diagram (b)). In the region of the nucleon resonances, the interaction between a nucleon and its excited partner (diagram (c)) can be investigated.

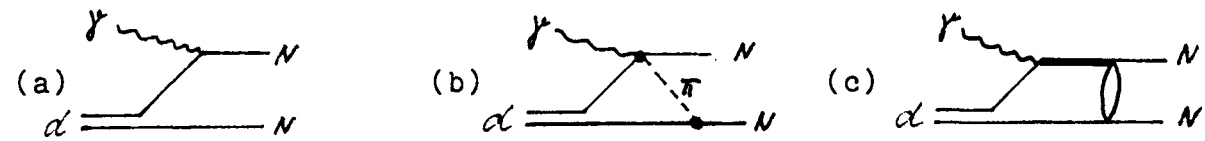

Despite of these interesting aspects, both the theoretical and the experimental situation in deuteron photodisintegration is unsatisfactory. The theoretical treatment of the process requires a good knowledge of the deuteron wave function (including the eventual admixture of nucleon resonances and 6-quark configurations) and a reliable description of nonresonant pion photoproduction and of the photoexcitation of the nucleon resonances and their interaction with nucleons (see e.g. /LAGE78/). In the framework of perturbative QCD, a prediction for the asymptotic behavior of the cross section has been made /BROD83/.

The experimental situation (for $k \gtrsim 100$ MeV) is characterized by large discrepancies between different data sets for the differential cross sections (see fig. 2). The data stop at $k \approx 800$ MeV. Only few experiments have been performed to investigate single polarization quantities like target asymmetry (using a vector polarized deuterium target), beam asymmetry (using a linearly polarized photon beam) and recoil nucleon polarization. No data exist for double polarization quantities.

Deuteron photodisintegration has a complicated spin structure. A completely model independent determination of the 12 complex helicity amplitudes will require 23 different observables to be measured as function of the photon energy and the proton c.m.s. angle. Most of the experiments require the combined use of a (linearly or circularly) polarized photon beam and a (vector or tensor) polarized deuterium target.

It is unlikely that this complete measurement will ever be made. Experimental techniques that will be available in the near future (e.g.: tagged polarized photons, vector polarized deuterium targets with high polarization) will allow to determine ≈10 observables in the range of the nucleon resonances (where the cross sections are reasonably high). At higher energies it will certainly be possible to measure differential cross sections; however, the measurement of polarization quantities will be difficult.

Due to the intimate connection between deuteron photodisintegration and the excitation of the nucleon resonances a detailed knowledge of the pion photoproduction off deuterons will also be required. Especially interesting are kinematical situations far away from the quasifree production region that can be reached by strong final state interactions only, e.g. $\gamma d \to \pi^0 d$ or $\gamma d \to \pi NN$ with either πN or NN very close to each other. These experiments will also shed light on the existence of resonant 6-quark states (dibaryon resonances).

2.4. Compton scattering

The elastic scattering of photons on protons is the most elementary process for the study of the photon-nucleon interaction (for a review see /BARA76/). The electric and magnetic polarizability of the proton (predicted by any microscopic model of the proton) can be determined from precise measurements below the pion threshold. In the region of the nucleon resonances, Compton scattering is very sensitive to the photocouplings of the nucleon resonances (the cross section is proportional to the fourth power of the coupling constant!).

Using the unitarity of the S-matrix the imaginary part of the scattering amplitude (at arbitrary angles) can be derived from the complete knowledge of the hadronic cross section (for the special case of the forward scattering amplitude this leads to the familiar optical theorem). In the region of the first nucleon resonance, only the well known single pion photoproduction has to be considered; at higher photon energies the situation becomes more uncertain due to contributions from $\pi\pi N$ final states. From the imaginary part alone, a lower limit for Compton scattering can be derived. Assuming the analyticity of the scattering amplitude the real part can be calculated from the imaginary part via dispersion relations.

The Compton process on the nucleon is described by six complex amplitudes. In the forward direction, only two nonvanishing amplitudes survive which can be separated by measuring the difference between the total hadronic cross sections for helicity 1/2 and 3/2 states (using circularly polarized photons on a longitudinally polarized proton target). No such measurements have been performed in the past; however, they will become feasible once polarized electron beams will be available.

The experimental information is very scarce because the cross sections are low and the dominating π^0-production process is difficult to reject. A clean identification of the Compton process is only achieved (for $k \gtrsim 200$ MeV) by detecting both proton and photon in the final state in coincidence. Even then, good energy and angular resolution for both particles is required to suppress $p\gamma$ coincidences from π^0-production (followed by an asymmetric decay of the π^0).

Most experiments concentrated on the measurement of differential cross sections. An example for $\theta_\gamma = 60^\circ$ is given in fig. 3. Also shown is the lower bound due to the imaginary part only (derived from all hadronic channels) /KOEL78/. Especially in the region of the first resonance, the lower bound comes close to the measured data and does not leave much room for the real part.

Considerable progress in the acuracy of the Compton scattering measurements can be reached by combining a monochromatic photon beam with a high quality large solid angle detector. Compared to previous experiments π^0-photoproduction can be further suppressed by using the second π^0 decay photon (which sometimes has to be detected close to the incident photon beam) as a veto. In addition, the knowledge of the primary photon energy will provide the complete kinematical overdetermination necessary for background rejection.

The counting rate for Compton scattering under realistic conditions (4π solid angle, tagged photon beam with $N_\gamma = 10^7$/sec, liquid hydrogen target with $1 g/cm^2$) will be 3/sec for a total cross section of $0.5\,\mu b$ (at $k \approx 1$GeV).

2.5. Nuclear Compton scattering and π^0-photoproduction

In the Δ-hole model (see e.g. /KOCH84/) there is an intimate connection between the Compton scattering amplitude (which also determines the total photoabsorption cross section), the coherent π^0-production and the elastic pion scattering since these processes result from different excitation or decay modes of a common intermediate Δ-hole state:

photon scattering π^0-production π elastic scattering

Once the parameters of the model are determined (usually from pion scattering), the cross sections for the other processes can be predicted without using any additional input.

Due to the nuclear formfactor both Compton scattering and π^0-photoproduction are peaked in the forward direction. There is not much experimental information available. Experiments to investigate π^0-

production are plagued by difficulties with the efficient detection of the π^0 decay photons and with problems to restrict the detected events to ground state transitions. In addition, Compton scattering suffers from the smallness of the cross section and from the high background due to π^0-production.

As in the case of Compton scattering on the proton, most of the experimental difficulties can be solved by using a 4π photon detector and a low intensity monochromatic photon beam.

The cross section for Compton scattering on ^{12}C has been calculated in the Δ-hole model /KOCH84/. At k=325 MeV a value of 30 μb/sr is predicted in the extreme forward direction, decreasing rapidly to 0.01 μb/sr at $\theta_\gamma = 90^\circ$. Measurements in the forward direction (which is, however, not too interesting because it is essentially constrained by the total cross section) do not seem to present unsurmountable difficulties, but the study of the differential cross sections at large angles (which contains the interesting information on Δ-propagation) is one of the most challenging experiments in photonuclear physics. The reason is not so much the low counting rate (for $N_\gamma = 10^7$/sec, ^{12}C target with 2g/cm^2, $\Delta\theta_\gamma = 10^\circ$ at $\theta_\gamma = 90^\circ$, $d\sigma/d\Omega = 0.01$ μb/sr one still obtains 0.01 event/sec) but the difficulty to suppress competing channels with much larger cross sections (like π^0-production) and the problem to obtain a good signature for a high energy photon to reject e.g. room background and cosmic radiation. An alternative way to the detection of the scattered photon in a crystal scintillator (like BGO or CsI) is the use of a converter followed by a 4π magnetic pair spectrometer. This would give a clean signature for photons but would also reduce the counting rate by approximately one order of magnitude.

For π^0-production the problems are easier to solve since the differential cross sections are larger and the two photon coincidence provides a better signature. For both Compton scattering and π^0-production, transitions to excited states of the final nucleus can be identified by detecting the deexcitation photon from the electromagnetic decay to the ground state in coincidence.

2.6. Photoproduction of hypernuclei

The differences between the structure of ordinary nuclei and hypernuclei (nuclei with a nucleon replaced by a hyperon, e.g. Λ or Σ) is due to the difference between NN and N-hyperon interaction. In the long run, these differences have to be explained in terms of the different quark structure of the nucleons and the hyperons.

Most of our knowledge on hypernuclei comes from the (K^-,π^-) exchange reaction. The main advantage of this process is the low momentum transfer to the final nucleus (reached at an appropriate K^--momentum) resulting in relatively large cross sections. The disadvantage is the distortion of the initial nucleus by the incoming K^-

and the strong final state interaction of the outgoing π^-. In contrast, in the $\gamma p \rightarrow K^+\Lambda$ reaction, only the relatively weak interaction of the outgoing K^+ has to be taken into account. This offers the opportunity to study low-lying Λ states even in heavy nuclei. However, the momentum transfer to the final nucleus is always high ($q \geq 200$ MeV/c), even in the extreme forward direction ($\Theta_{K^+} = 0^\circ$). The low cross section for the elementary process $\gamma p \rightarrow K^+\Lambda$ and the formfactor suppression results in very low cross sections for the production of hypernuclei (e.g.: 0.5 μb/sr for $^4He(\gamma, K^+)^4_\Lambda H$ at E_γ = 2 GeV and $\Theta_K = 0^\circ$, /BERN82/) that fall rapidly with increasing Θ_K.

The measurement of the excitation energy of the hypernucleus, using the incoming photon and the outgoing K^+ only, is very difficult because an overall energy resolution of $\approx$1 MeV is required. An alternative way to identify the hypernucleus is to observe its deexcitation photons in coincidence with the forward going K^+. The kaon would be analyzed in a relatively short magnetic spectrometer covering the forward cone with moderate resolution ($\Delta p/p \leq 0.1$ %); close to 4π coverage for the photons would be necessary. This method offers the additional advantage that the angular distribution of the photons can be used to analyze the polarization of the hypernucleus. If, in addition, hadrons from the decay of the hypernucleus can be detected it will also be possible to distinguish between the $\Lambda \rightarrow N\pi$ and the $\Lambda N \rightarrow NN$ decay modes. As has recently been demonstrated at Brookhaven /GRAC84/, the lifetime of hypernuclear levels ($\tau \approx 200$ psec) can be measured directly using precise timing for the decay products. This can give additional information on the ΛN interaction in the nuclear interior.

Count rate estimates show that under realistic conditions (10^7 tagged photons/sec, ^{12}C target with 2 g/cm^2, K^+-spectrometer with $\Delta\Omega$ = 50 msr, differential cross section for the production of one hypernuclear level 0.3 μb/sr, 60 % survival chance for the K^+) a counting rate of $\approx$300/day can be expected for each level.

The present knowledge of the elementary process $\gamma p \rightarrow K^+\Lambda$ is not sufficient. Therefore, a detailed study of the kaon photoproduction is a prerequisite for electromagnetic hypernuclear physics. This program would also contribute to the study of the higher nucleon resonances and their decay modes.

Some information on the hyperon interaction with nuclear matter can also be obtained from quasifree hyperon (Λ or Σ) production by observing the K^+ (to 'tag' the hyperon) and the hyperon decay or reaction products in coincidence. (The total cross section for quasifree Λ-production is roughly three orders of magnitude higher than the cross section for the production of Λ-hypernuclei!)

It has been pointed out before /BERT82, EPST79/ that the behavior of an excited hyperon in nuclei can be studied very similar to the $\Delta(1232)$-propagation. The narrow width of the hyperon (15.6 MeV for the $\Lambda(1520)$) will make it much easier to observe the effects of the surrounding nuclear medium. Again, the quasifree photoproduc-

tion of these resonances and the observation of the K^+ will give less distortion than the competing (K^-,π^-) reaction. Previous measurements /BARK80/ have shown that the total cross section for $\gamma p \rightarrow K^+\Lambda(1520)$ approaches 1 μb at k=2.5 GeV. For nuclear production a rate of $\approx$3/sec can be expected (^{12}C target with 1 g/cm^2, 4π solid angle, $N_\gamma = 10^7$/sec).

3. Comments on Experiments with Virtual Photons

The measurements with real photons ($q^2=0$) can be extended to space-like virtual photons ($q^2 < 0$) using electron scattering. This gives additional information on the dynamical structure of the process under investigation. In the case of the investigation of the nucleon resonances, the electromagnetic formfactors for the transition $N^* \rightarrow N\gamma$ can be determined (for a review see /FOST83/). In the limit $q^2 \rightarrow 0$ the formfactors turn into the photocouplings measured with real photons).

For electron scattering it is, however, much more difficult to obtain complete experimental data sets. Compared to real photons, all measurements have to be made as a function of the additional variable q^2 and for three photon helicity states.

In the case of simple final states (like in single pion electroproduction off nucleons: $eN \rightarrow e'N\pi$) the use of a high intensity electron beam and the coincident detection of the scattered electron and one of the final state hadrons in two small acceptance detectors gives sufficient count rate. For the detection of multiple particle final states (e.g. in the electroproduction of vector mesons or higher baryon resonances resulting in $\geq$3-body final states) a large solid angle ($\approx 4\pi$) detector will give higher count rate even if the electron beam intensity has to be reduced by several orders of magnitude.

The crucial question what maximum luminosity (target nuclei per cm^2 * incident electrons per sec) can be tolerated by a large acceptance detector. Only few electron scattering experiments using 4π detectors have been performed in the past. The LAME detector at the Cornell synchrotron /AHRE80/ was able to operate at an instantaneous electron beam intensity of 10^9 e^-/sec on a 0.5 g/cm^2 liquid hydrogen target, despite of unfavorable conditions (transverse magnetic field at the position of the target - large sensitivity to forward peaked electromagnetic processes, like bremsstrahlung and Møller scattering; the primary electron beam passed through the wire chambers).

From that experience it seems safe to assume that a 4π detector can tolerate a maximum luminosity of $3*10^{32}$ cm^{-2} *sec^{-1}. At this luminosity the hadronic interaction rate is roughly the same as in the case of a tagged photon beam. However, to make full use of the potential information in virtual photon experiments, the luminosity has to be

about two orders of magnitude higher. It is very unlikely that this can be achieved with a 4π detector optimized for tagged photon work (using accurate but slow components like drift chambers and scintillating crystals).

Many electron scattering experiments (especially in the realm of the baryon resonances or the vector mesons) will require the use of polarized proton or deuterium targets. In a typical polarized target (3 cm long NH_3) 10^9 e^-/sec will deposit $\approx$1 mW; at this power level, very low temperatures ($\leq$ 200 mK) can be maintained without difficulties. Also, at this low intensity the polarization will not be destroyed rapidly by radiation damage.

4. Experimental Setup

The bremsstrahlung of high energy electrons that are decelerated in the Coulomb field of a nucleus A ($eA \rightarrow e' A\gamma$) is the common source of photons for the investigation of photonuclear reactions. The main disadvantage is the continous energy spectrum (characterized by an energy flow that is nearly independent of the photon energy k : $k*N(k) \approx$ const for $k < E_0$, E_0 is the energy of the primary electron. The continous spectrum makes it

(1) necessary to determine the photon energy from an analysis of the photoproduced hadronic events,

(2) difficult to determine the photon flux with high precision.

Various monochromatization techniques have been applied to solve these problems (for a review see /BEIL80/). Given the present state of the art, the best choice for an electron accelerator with 100% duty-cycle is bremsstrahlung tagging. If in the future high energy lasers will become available, laser backscattering off relativistic electrons could become a superior method.

4.1. Tagged photon beam

Both photon energy determination and photon flux normalization can be achieved by detecting the final electron in coincidence with the hadronic event. The photon energy k is then determined by the energy difference between the initial and the final state electron: $k = E_0 - E'$ independent of the hadron detection. An appropriate scheme for 'tagging' the bremsstrahlung photons is shown in fig. 4 (details of bremsstrahlung tagging are described in /AREN82/ and /CARD83/). The decelerated electrons are magnetically analyzed and detected in a multi-channel hodoscope (tagging counters). The flux normalization of the hadronic cross section can now be obtained for each photon energy bin (corresponding to one electron detector) from

$$\sigma_{had} \sim \frac{\text{coincidence rate (hadron detector - electron detector)}}{\text{electron detector rate}}$$

The ratio is independent of the the absolute detection efficiency of the electron detectors. Therefore, the effective photon flux can be determined with high precision ($\leq 1\%$).

The maximum photon beam intensity that can be handled by a photon tagging system is limited by accidental coincidences between the hadron detector and the tagging counters. It is important to make a clear distinction between two different types of accidental coincidences:

(a) two tagging counters fire simultaneously (one real and one accidental hit within the resolving time of the coincidence τ). These events can easily be eliminated by rejecting double hits in the tagging counters (eventually already at the trigger level).

(b) the hadronic event is caused by the untagged part of the bremsstrahlung spectrum or by background. Ideally, there should be no hit at all in the tagging counters. Therefore, a single accidental hit has to be treated like a real event. The corresponding correction can only be made by measuring and subtracting delayed coincidences. This requires additional data to be taken and analyzed; it also reduces the statistical accuracy.

Accidental contributions of the type (b) should therefore be kept small. This can be achieved by using

(1) a high quality hadron detector that is not sensitive to background or the untagged part of the photon spectrum.

(2) a wide energy range tagging system that leaves only a small fraction of the photon energy spectrum uncovered.

The total correction factor f_{cor} for the accidental contributions from both (a) and (b) determines the maximum photon rate N_γ^{max}

$$N_\gamma^{max} = \frac{f_{cor} * \text{duty-cycle}}{\tau * (1 + \eta)}$$

where τ is the coincidence resolving time and η the ratio of the untagged hadronic rate to the hadron rate from the tagged part of the photon spectrum. Using τ = 1.4 nsec (in the case of stretcher rings, τ is usually limited by the bunch separation), a duty-cycle of 90%, a total correction factor f_{cor} = 5% and η = 2 yields $N_\gamma^{max} = 10^7$/sec. (This value should be regarded as a soft number since it depends on the details of the process under investigation

and on the size of the correction that the experimenter is willing to tolerate.) For the production of 10^7 photons/sec an electron current of $\approx$1 nA is sufficient (assuming a radiator thickness of 10^{-3} X_o).

The magnetic spectrometer for the analysis of the decelerated electrons should have the following properties:

(a) broad energy range. With a general purpose system it should be possible to cover the photon energy range $k \approx (0.2 - 0.95)*E_o$. This offers the following advantages:

(1) reduction of systematic errors and run time (if the whole range of interest can be covered simultaneously)

(2) reduction of the type (b) accidentals

(3) tagging of linearly polarized photons produced by coherent bremsstrahlung on a crystal radiator becomes possible (high photon polarization occurs only in the range $k \approx (.2-.5)*E_o$). The distribution of the counting rate in the tagging counters provides a high speed measurement of the photon spectrum that is used to derive the photon polarization.

(4) measurement of the polarization of incident electrons (needed for the production of circularly polarized photons). With a magnetized iron foil as a radiator the analyzing power of Møller scattering ($e^- e^- \rightarrow e^- e^-$) can be used. The two final state electrons (both with $E_o/2$) have to be detected in coincidence in the tagging spectrometer.

(b) point-to-point (between the radiator and the tagging counters) focussing in the deflecting plane. (This is necessary to achieve high photon energy resolution, independent of the angular divergence of the outgoing electrons.)

(c) solid angle acceptance matching the angular divergence of the outgoing electrons (the divergence increases roughly with 1/E)

(d) short overall distance between the radiator and the production target to keep the beam spot size on the target small

(e) deflection of the primary electron beam to avoid interference with both the hadron detector and the tagging counters.

A possible design for a tagging spectrometer is given in fig. 5. The magnetic field is produced by a single synchrotron type magnet with a strong radial gradient to provide focussing over an electron energy range $E' = (0.1\text{-}3.0)$ GeV. The primary beam with $E_o = 4$ GeV is deflected by 35°. The average dispersion in the detector plane is 2 mm/MeV.

4.2. Experimental setup for tagged photon beams

At a photon beam intensity of 10^7 photons/sec, the total hadronic interaction rate is of the order of 10^3/sec. This low rate makes large acceptance detectors both necessary and feasible. Detectors with close to 4π solid angle and a wide energy range have the additional advantage of a high detection efficiency for multiple particle final states. Also, the detection efficiency does not depend strongly on production angle, energy, decay mode and spin orientation of decaying particles like e.g. vector mesons.

The low intensity also offers interesting possibilities for the use of novel experimental techniques, e.g. the detection of low energy decay products of the final nucleus or the detection of heavy recoil nuclei in active targets (e.g. scintillating gases, high pressure drift chambers etc.).

Two examples for large acceptance detectors will be given: a simple scintillation counter arrangement and a sophisticated magnetic detector.

4.2.1. Scintillation counter detector for two-body final states

The detection efficiency for two-body reactions rises only linearly with the solid angle covered by the experimental setup. Therefore, for processes that have high enough cross section, a detector with a large solid angle (but still much smaller than 4π) provides an interesting alternative to a complex 4π detector. An example is given in fig. 6. The detector consists of two concentric rings of scintillation counters; thin counters close to the target provide a start signal (and distinguish between neutral and charged particles), thick scintillation counters in the rear (distance from the target $\triangleq$ 3m) give time-of-flight and (in combination with the deposited energy) some particle identification. The solid angle covered by the complete detector could reach 1/3 of 4π. The center of the detector is easily accessible, e.g. for the installation of a polarized target with arbitrary spin orientation. The detector is easy to build and operate. Due to the simple event structure, high data rates can be registered and analyzed off-line. The detector would be especially useful for measurements in $\gamma N \rightarrow \pi N$, $\gamma d \rightarrow pn$ etc. requiring polarized beams and targets.

Note that in all polarization experiments kinematical overdetermination is necessary to get rid of

(1) unwanted nuclear events (in the case of a polarized p (d) target using NH_3 (ND_3) or butanol)

or

(2) the high energy part of the bremsstrahlung spectrum (in the case of a polarized photon beam produced by coherent bremsstrahlung from a crystal radiator).

Overdetermination can be achieved by detecting both hadrons in the final state in coincidence and using their kinematical correlation.

4.2.2. Large acceptance magnetic detector

A detector with close to 4π solid angle and a wide energy acceptance is indispensable for the efficient detection of multiple particle final states. Magnetic analysis is necessary to determine the momentum of charged particles; low energy photons from the electromagnetic decays of nuclear levels as well as high energy photons from π^0 (η) decays or Compton scattering have to be detected with high accuracy.

A conceptual design for such a detector (which is always a compromise between conflicting requirements) is shown in fig. 7. The detector consists of a cylindrical drift chamber (the cylinder axis coincides with the photon beam) and scintillation trigger counters surrounded by a shell of photon detectors. The whole assembly is situated in a superconducting solenoid producing a $\approx$1.5 T magnetic field parallel to the incident photon beam. Higher fields (that would give better momentum resolution) are technically feasible; the disadvantage is that low momentum particles will no longer reach the tracking chamber.

The diameter and the length of the inner tracking chamber should be as large as possible. However, the price of a high quality photon detector (like CsI or BGO) will presumably restrict the tracking chamber to $\leq$ 1m diameter and $\leq$ 1m length. The expected momentum resolution (B = 1.5T, $\theta = 90°$, 8 points with $\Delta x = 80\,\mu$m (sigma) on the 35 cm long track) is shown in fig. 8a. At high momentum the behavior is dominated by the position resolution of the chamber, at low momentum by multiple scattering. The angular dependence of the momentum resolution is given in fig. 8b. Since the magnetic field is longitudinal (this has the advantage of keeping small angle e^+e^- pairs, which are copiously produced in the target, away from the detectors) the momentum resolution gets very bad at forward angles. For applications where this cannot be tolerated, e.g. production of hypernuclei via the (γ,K) reaction, a forward spectrometer has to be added (eventually with a toroidal field).

The combination of momentum and dE/dx measured in the tracking chamber and the energy deposited in the photon detector allows the identification of charged particles over a wide energy range. For many processes all particles in the final state can be detected; together with the knowledge of the primary photon energy this will additionally constrain the particle identification via 4-momentum conservation. It should be noted that similar detectors have already been operated (or are in the construction stage) at e^+e^- colliders (e.g.: a high resolution drift chamber surrounded by a BGO shell forms the central part of the L3 detector at LEP /L3TP83/, the CLEO II detector at CESR will use CsI crystals /CLEO84/). The

experience gained with these detectors will be very valuable for photonuclear detectors.

4.3. Advantages of combining a tagged photon beam and a large acceptance detector

The combination of a tagged photon beam and a large acceptance detector allows to cover a wide photon energy and angular range simultaneously. This is not only necessary to achieve high counting rates but it also reduces systematic errors: changes of the efficiency of the detector, of the target density, of beam and target polarization etc. effect all the data in the same way. Therefore, the combination is even superior to a truely monochromatic beam for the investigation of small effects like e.g. structures in the photon energy dependence of the cross sections or polarization observables. The price one has to pay is the increased complexity of the experimental apparatus. Also, to remeasure one data point takes as much running time as to cover the whole kinematical range.

5. The Operation of Large Acceptance Detectors at a High Power Accelerator

The beam currents that can be used in combination with a large acceptance detector are roughly four to five orders of magnitude below the primary beam current of a high power accelerator. To obtain complete data sets long running periods under constant conditions would be ideal. Clearly, the experiments have to be performed in a parasitic mode as far as beam power is concerned. However, splitting the primary high intensity beam has the important disadvantage that energy, intensity, time structure and polarization of the beam will be determined by the main user (and will possibly be changed often). This will make the parasite operation of a weak electron beam very difficult. The linac - stretcher ring combination offers a unique solution: a second stretcher ring (which is much less expensive than the linac itself) can be used to provide (completely independent of the first beam)

(1) a second high intensity beam for electron scattering

or

(2) a second low intensity electron beam for
  (a) the production of tagged bremsstrahlung photons
  (b) electron scattering with large acceptance detectors

or

(3) internal electron scattering using a (polarized) jet target

or

(4) backscattering of laser photons for the production of polarized monochromatic photons (usefulness will depend on laser development).

It is quite obvious that a second stretcher ring will make much better use of the installed experimental facilities. It will also make it easier to carry out a broad program in electromagnetic nuclear and particle physics.

6. Summary

Some examples have been given for experimental programs that require a low intensity high duty-cycle beam and a large acceptance detector. The experiments cover a wide range of problems in particle and nuclear physics with real and virtual photons. The full capability of a major laboratory is required to build and operate the complex detectors. Due to the low beam power the experiments can be carried out in a parasitic way. In the case of a (high power linac-stretcher ring)-combination, the ideal mode of operation would be to use a second stretcher ring to provide a fully independent second electron beam.

REFERENCES

/AHRE80/ L.A. Ahrens et al.:
A Large Aperture Spectrometer for Observation of Final States in Electroproduction,
Nucl. Instr. Meth. 173 (1980) 537

/AREN82/ J. Arends et al.:
The Tagged Photon Beam Facility at the Bonn 500 MeV Synchrotron, Nucl. Instr. Meth. 201 (1982) 361

/BARA76/ P.S. Baranov and L.V. Fil'kov:
Compton Scattering on the Proton at Low and Medium Energies, Sov. J. Part. Nucl. 7 (1976) 42

/BARB80/ D.P. Barber et al.:
Strangeness Exchange in the Photoproduction of $K^+\Lambda(1520)$ Between 2.8 and 4.8 GeV,
Z. Physik C - Particles and Fields 7 (1980) 17

/BARK75/ I.S. Barker et al.:
Complete Experiments in Pseudoscalar Photoproduction
Nucl. Phys. B95 (1975) 347

/BEIL80/ H. Beil and R. Bergère:
Monochromatic and Identifiable Photons Used in Photonuclear Research, Saclay report CEA-N-2144 (1980)

/BERN82/ A.M. Bernstein:
Electromagnetic Production of Hypernuclear States,
Proc. of the Int. Conf. on Hypernuclear and Kaon Physics, Heidelberg 1982, ed. by B. Povh, p. 409

/BERT82/ R. Bertini:
Hypernuclei and Baryon-Baryon Interaction,
Proc. of the Int. Conf. on Hypernuclear and Kaon Physics, Heidelberg 1982, ed. by B. Povh, p. 359

/BROD83/ S.J. Brodsky and J.R. Hiller:
Reduced Nuclear Amplitudes in Quantum Chromodynamics,
Phys. Rev. C 28 (1983) 475

/CARD83/ L.S. Cardman:
Photon Tagging (present practice and future prospects)
Proc. of the Magnetic Spectrometer Workshop, Williamsburg 1983 and Uni. of Illinois at Urbana-Champaign report P/83/12/168

/CLEO84/ The CLEO collaboration:
Cleo II. A proposal to upgrade the CLEO detector,
Cornell report CLNS 84/609 (1984)

/DURW80/ E.J. Durwen:
Differential Cross Sections for the Reaction $\gamma p \to \pi^+ n$ (in german), Bonn University, internal report BONN-IR-80-7 (1980)

/EPST79/ G.N. Epstein and E.J. Moniz:
Kaon-Nucleus Interactions in the $\Lambda(1520)$ Region
Proc. of the Kaon Factory Workshop, Vancouver 1979, ed. by M.K. Craddock, p.97

/FOST83/ F. Foster and G. Hughes:
Electroproduction of Nucleon Resonances,
Rep. Prog. Phys. 46 (1983) 1445

/GRAC84/ R. Grace et al.:
The Four-Fermion Weak Interaction and the Decay of $^{12}_{\Lambda}C$, paper M10, contributed to the Particles and Nuclei International Conference, Heidelberg 1984

/KAJI81/ R. Kajikawa:
Pion Photoproduction and Compton Scattering in the Resonance Region, Proc. of the 1981 Int. Symp. on Lepton and Photon Interactions at High Energies, Bonn, ed. by W. Pfeil, p. 352

/KOCH84/ J. Koch, E.J. Moniz and N. Ohtsuka:
Nuclear Photoabsorption and Compton Scattering at Intermediate Energy, Ann. of Phys. 154 (1984) 99

/KOEL78/ G. Kölbel:
Compton Scattering on the Proton in the Region of the First and Second Resonance (in german), Bonn University, internal report BONN-IR-78-16 (1978)

/LAGE78/ J.M. Laget:
Electromagnetic Properties of the πNN System (III). The $\gamma D \to pn$ reaction, Nucl. Phys. A312 (1978) 265

/L3TP83/ Technical proposal for L3, CERN report LEPC 83-5 (1983)

/PAUL81/ E. Paul:
Spectroscopy of the ρ, ω, ϕ Families (from Photoproduction and e^+e^- annihilation), Proc. of the 1981 Int. Symp. on Lepton and Photon Interactions at High Energies, Bonn, ed. by W. Pfeil, p.301

Table 1: Experiments in $\gamma N \to \pi N$ necessary for a complete determination of the helicity amplitudes

#	observable	photon polarization lin.	photon polarization circ.	target polarization	recoil nucleon polari.
1	$d\sigma/d\Omega$ diff. cross section				
2	T target asymmetry			**	
3	Σ beam asymmetry	**			
4	P recoil nucleon pol.				**
+	P recoil nucleon pol.	**		**	
5	G	**		**	
6	H	**		**	
7	T_x			**	**
8	E		**	**	
9	F		**	**	

etc.

+ Note that using polarized beam and target the recoil nucleon polarization can be determined without using a second scattering.

Table 2: Bin sizes and the number of data points for complete experiments in $\gamma N \to \pi N$

	range	bins	remarks
photon energy	150-2000 MeV	200	10 MeV bins
pion c.m.s. angle	10° - 170°	20	8° bins
observables		8	e.g. 1-8 of table 1
reaction type		3	all except $\gamma n \to \pi^\circ n$

$\approx 10^5$ data points $\longrightarrow$ with 10^4 events/data point a total of 10^9 events is necessary

FIGURE CAPTIONS

Fig. 1: Differential cross section for $\gamma p \to \pi^+ n$ at $\theta_\pi^{lab} = 65^\circ$. Experimental data from /DURW80/. Also indicated are the positions and the quantum numbers of the nucleon resonances known from πN scattering.

Fig. 2: Differential cross section for $\gamma d \to p\, n$ at $\theta_p = 90^\circ$. Theoretical curves from /LAGE78/.

Fig. 3: Differential cross section for $\gamma p \to \gamma p$ at $\theta_\gamma = 60^\circ$. The solid line is the unitarity bound derived by /KOEL78/.

Fig. 4: Schematic design of a facility for the tagging of bremsstrahlung photons.

Fig. 5: Design of a broad energy range tagging spectrometer with point-to-point focussing in the deflecting plane.

Fig. 6: Scintillation counter setup for two-body reactions

Fig. 7: Large acceptance magnetic detector to be used in combination with a weak photon (electron) beam.

Fig. 8: Momentum resolution of the magnetic detector shown in fig. 7
(a) for $\Theta = 90^\circ$ as a function of the momentum p
(b) for 1 GeV/c pions as a function of Θ

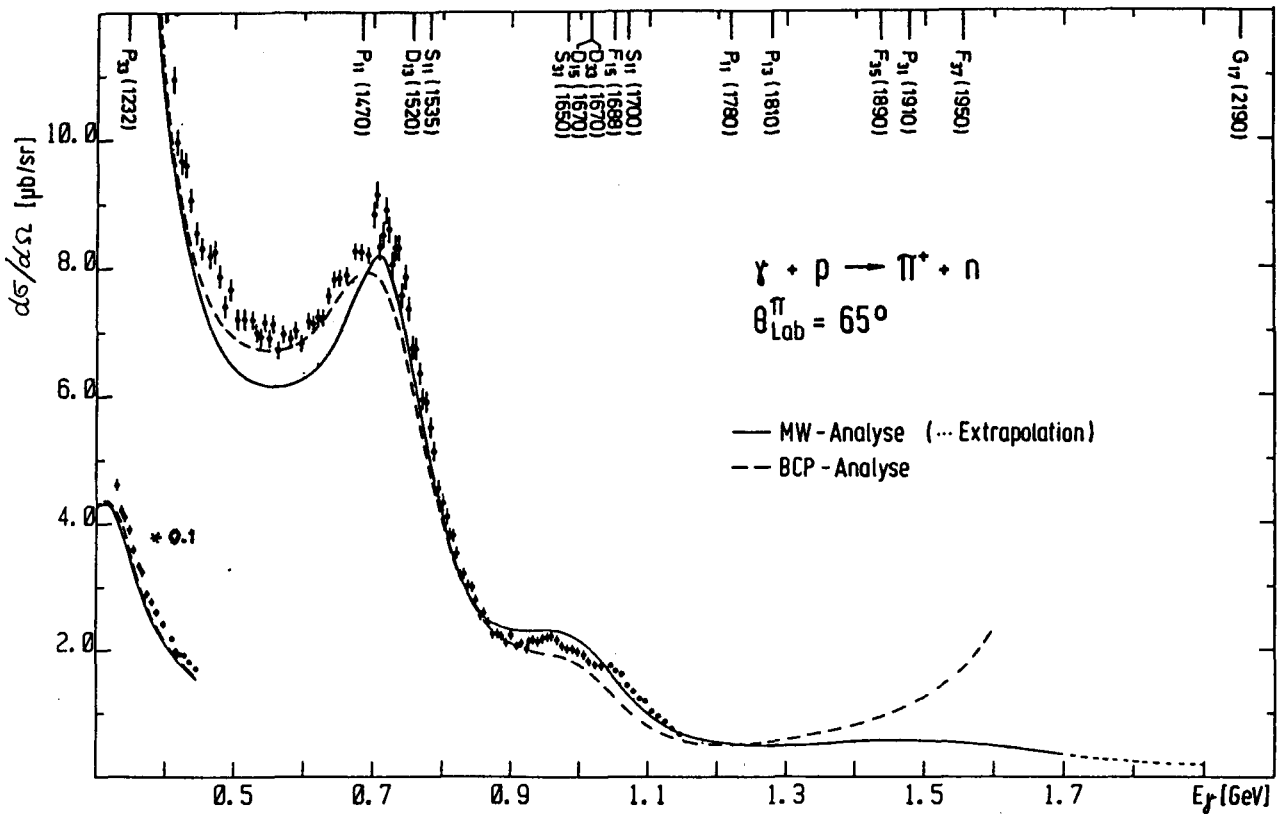
dσ/dΩ [μb/sr]
10.0
8.0
6.0
4.0
2.0
* 0.1
P33 (1232)
P11 (1470)
S11 (1535)
D13 (1520)
D15 (1670)
S11 (1650)
F15 (1688)
S11 (1700)
P11 (1780)
P13 (1810)
F35 (1905)
P31 (1910)
F37 (1950)
G17 (2190)
γ + p → π+ + n
θ_Lab^π = 65°
MW-Analyse (··· Extrapolation)
BCP-Analyse
0.5
0.7
0.9
1.1
1.3
1.5
1.7
Eγ [GeV]

Fig. 1

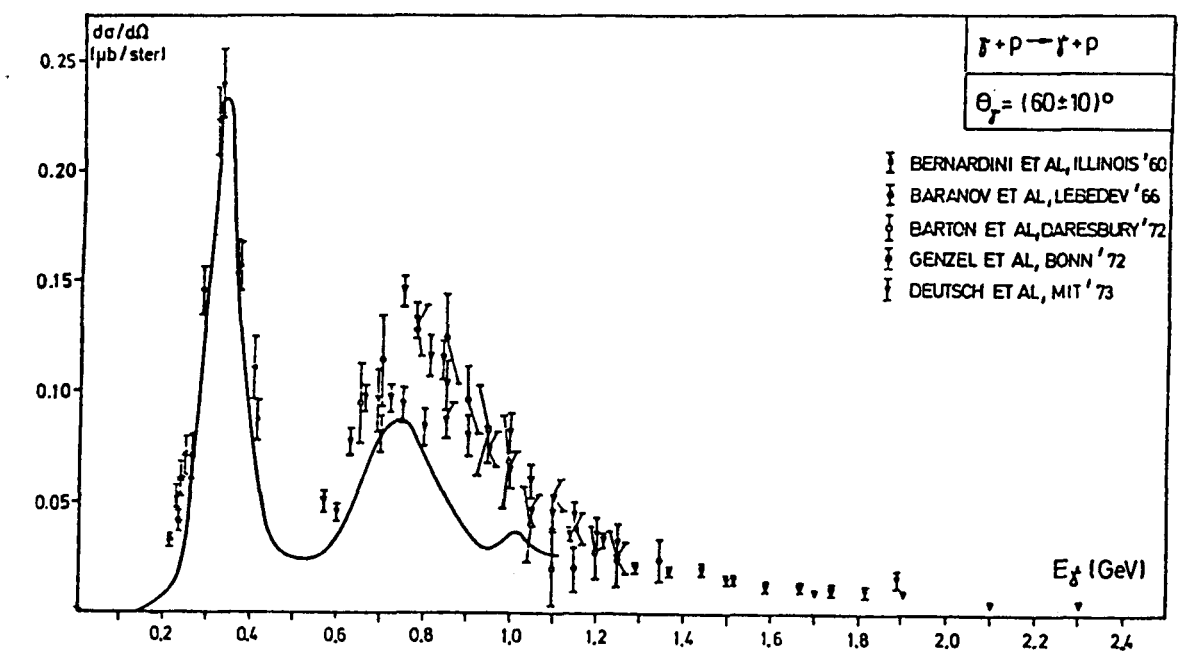
dσ/dΩ
(μb/ster)
0.25
0.20
0.15
0.10
0.05
γ+p→γ+p
θγ = (60±10)°
BERNARDINI ET AL, ILLINOIS '60
BARANOV ET AL, LEBEDEV '66
BARTON ET AL, CARESBURY '72
GENZEL ET AL, BONN '72
DEUTSCH ET AL, MIT '73
Eγ (GeV)
0.2
0.4
0.6
0.8
1.0
1.2
1.4
1.6
1.8
2.0
2.2
2.4

Fig. 3

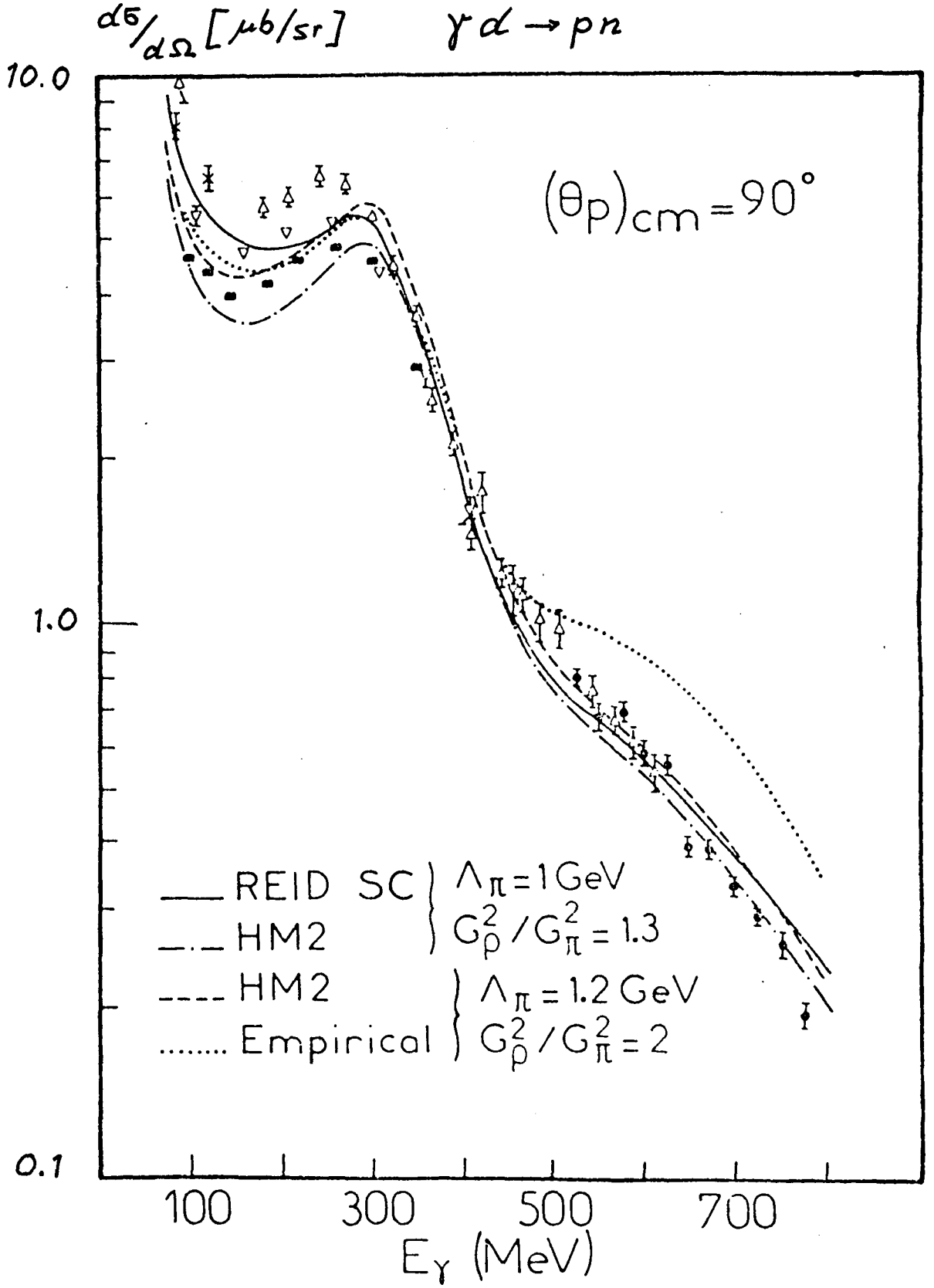
dσ/dΩ [μb/sr]
γd → pn
10.0
1.0
0.1
(θp)cm = 90°
REID SC
HM2
HM2
Empirical
Λπ = 1 GeV
G²ρ/G²π = 1.3
Λπ = 1.2 GeV
G²ρ/G²π = 2
100
300
500
700
Eγ (MeV)

Fig. 2

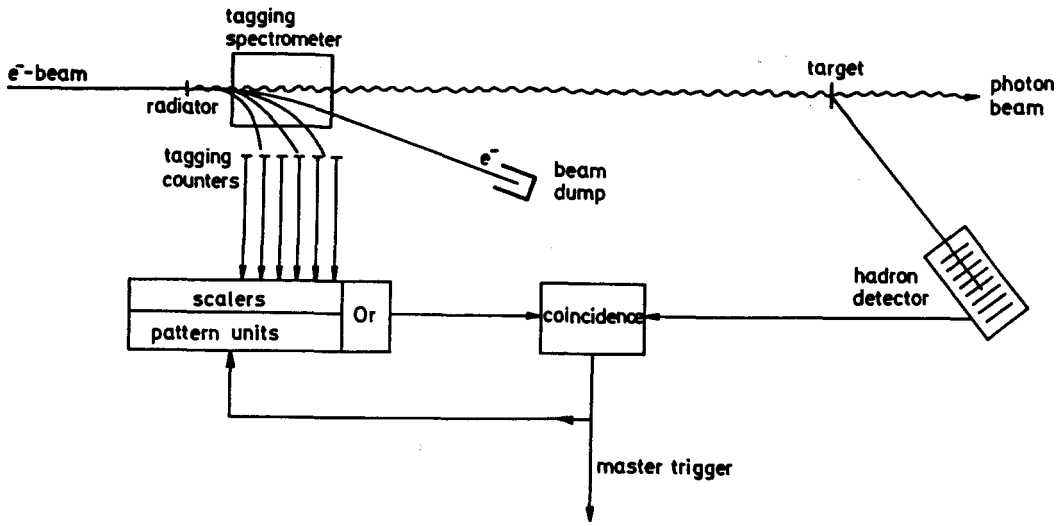
tagging
spectrometer
e⁻-beam
radiator
target
photon
beam
tagging
counters
e⁻
beam
dump
hadron
detector
scalers
pattern units
Or
coincidence
master trigger

Fig. 4

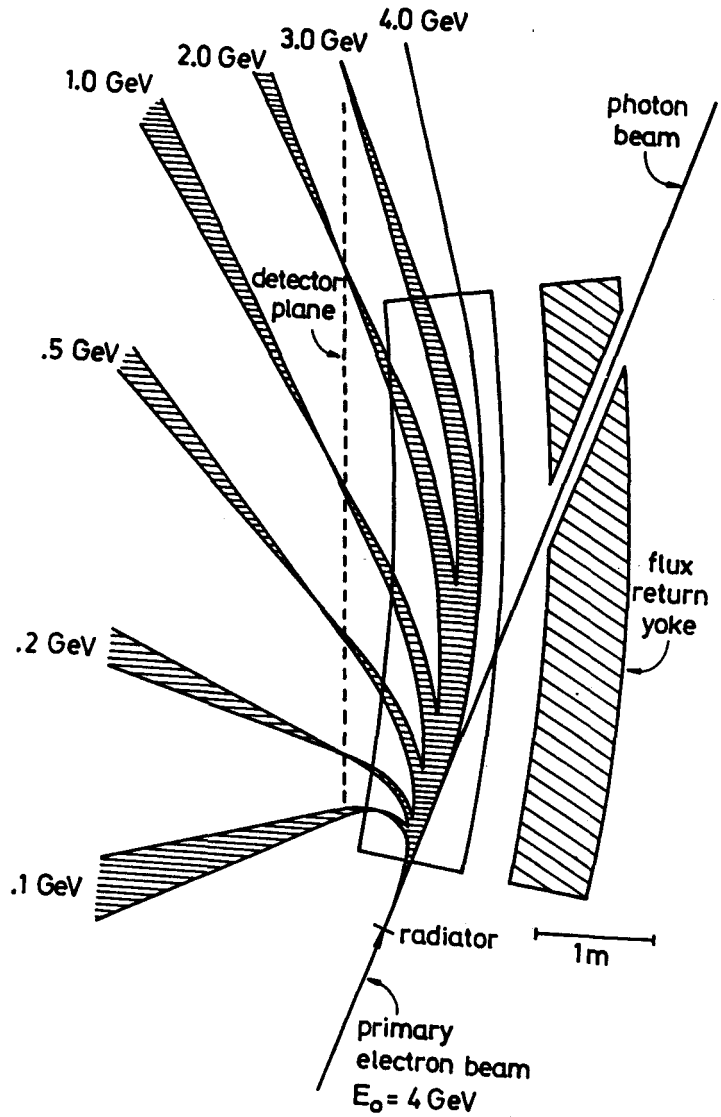
4.0 GeV
3.0 GeV
2.0 GeV
1.0 GeV
photon
beam
detector
plane
.5 GeV
flux
return
yoke
.2 GeV
.1 GeV
radiator
1m
primary
electron beam
E_o = 4 GeV

Fig. 5

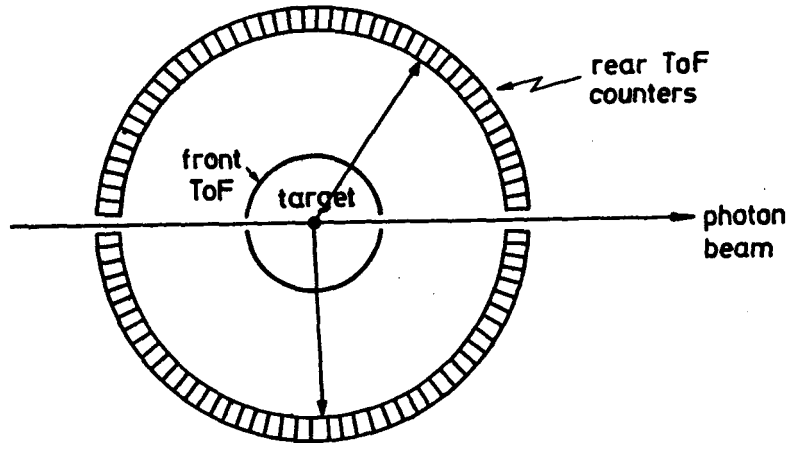
rear ToF
counters
front
ToF
target
photon
beam

Fig. 6

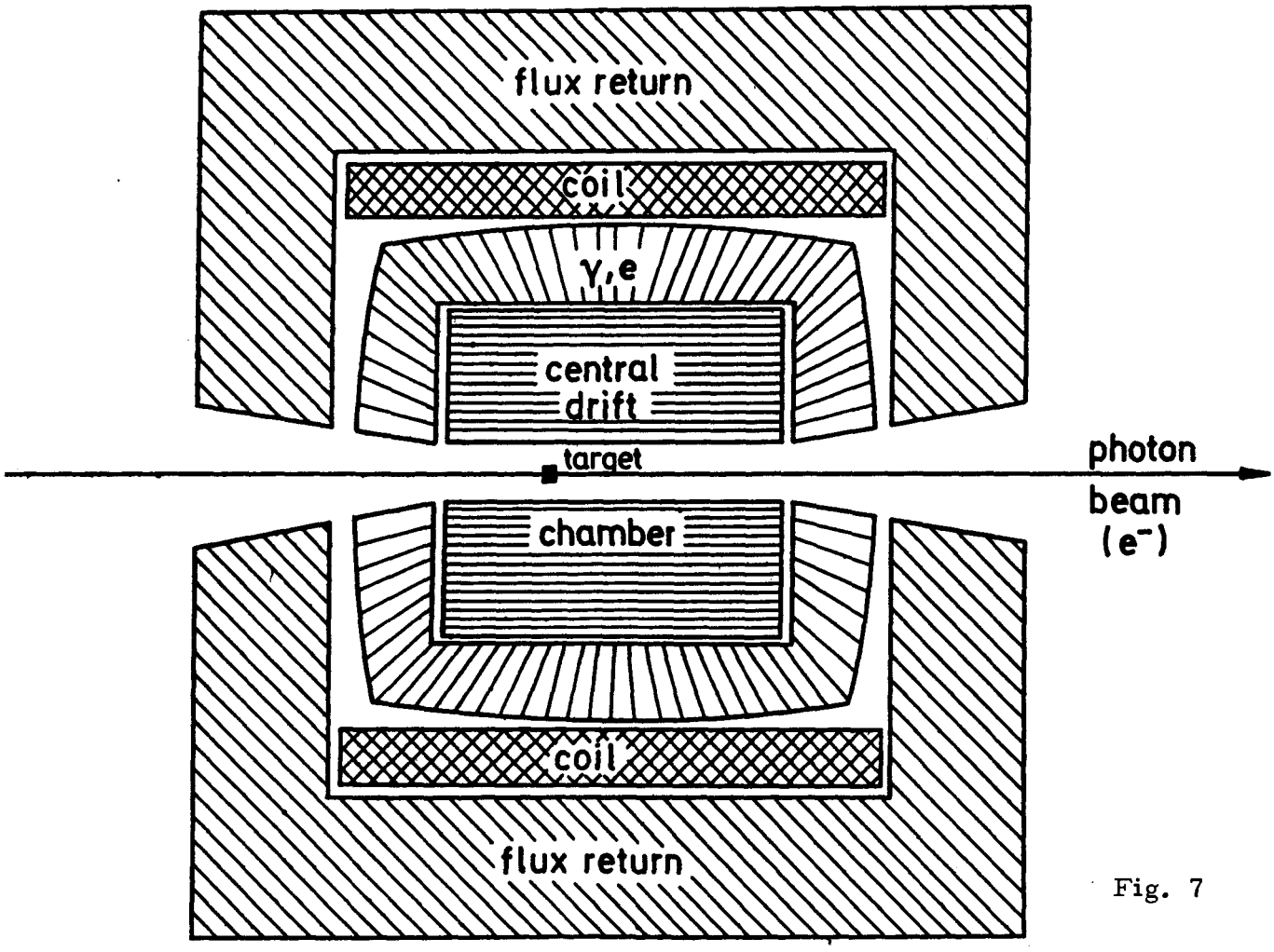
flux return
coil
γ,e
central
drift
target
photon
beam
(e⁻)
chamber
coil
flux return

Fig. 7

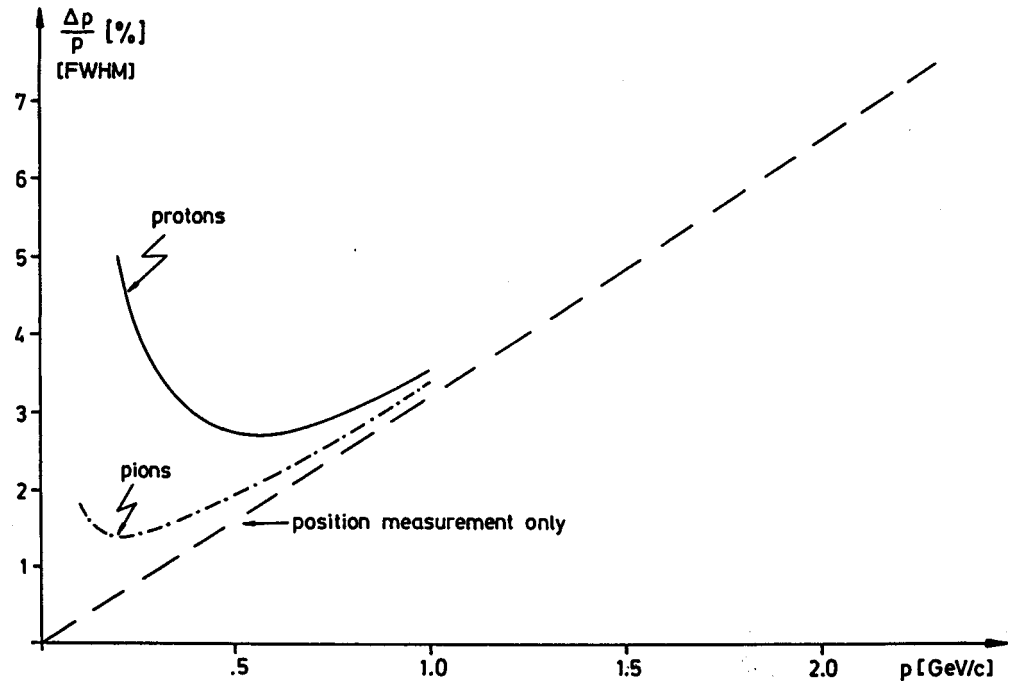
Δp/p [%]
(FWHM)
protons
pions
position measurement only
p [GeV/c]

Fig. 8a

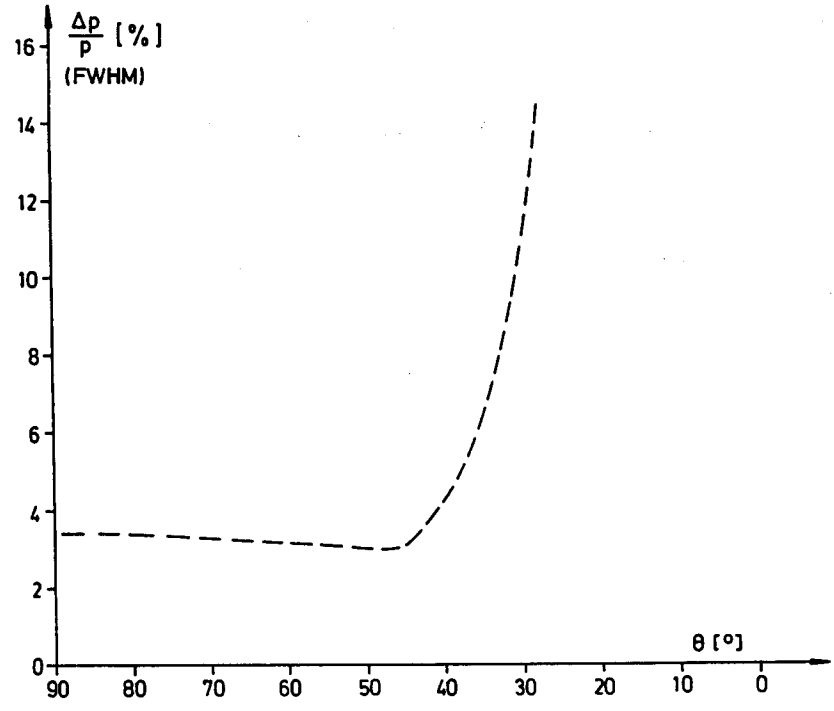
Δp/p [%]
(FWHM)
θ [°]

Fig. 8b

4π Detectors

Emery Nordberg
Cornell University
Ithaca, New York 14853

INTRODUCTION

For over a decade and into the foreseeable future large, general purpose, 4π detectors have been and will be in use at pp storage rings such as the ISR and SSC, e^+e^- storage rings such as DCI, SPEAR, DORIS, CESR, PEP, PETRA, TRISTAN, SLC and LEP, $p\bar{p}$ rings such as the CERN Collider and TEVATRON and ep rings such as HERA. The field's too large to cover systematically in my limited time at this workshop so I will pick and choose topics that I know about and think will be of interest to CEBAF. I will describe the features of 4π detectors at colliding beam faciliites and leave to the workshop working groups any adaptations to beam line physics. Many of the examples I will use will be from experience at CLEO and CLEO II. The CsI(Tl) crystal calorimeter proposed for CLEO II may be of special interest here.

Figure 1 illustrates a portion of a generic 4π detector viewed along the beam lines. It contains a magnetic field parallel to the beam line for charged particle momentum determination and so would be classed as a general purpose detector. An initial caution is that this barrel portion of the detector subtends about 95% of 4π for the inner elements and only about 75% of 4π for the outer elements. Detectors covering the ends of these cylindrical elements have special problems introduced by the geometry and by the fact that momentum analysis is very limited along the field lines. I will start with examples from the inside and work outward.

VERTEX DETECTORS

Vertex detectors in present colliding beam detectors are small cell drift chambers operated under conditions giving high spatial resolution. Their primary purpose is to locate the interaction point and secondary vertices from τ, B-meson or D-meson decays for example. They are operated at high gain so simultaneous measurements of dE/dx as in tracking chambers are not possible. Of course they also enhance the tracking and momentum resolution of the inner detector especially for low momentum, tightly curling tracks. Their other primary function is to trigger the experiment or gate TPC tracking chambers.

The Mark II vertex detector in operation for about two years and the CLEO vetex detector presently being installed have cells of a size approximately 4 mm from sense to field wires. The wires are located in the end plate to an accuracy about 20 μm. Mark II uses aluminum end plates and nylon bushings. CLEO uses insulating G-10 end plates and metal bushings. The Mark II detector has seven layers of sense wires at radii from 10.1 to 32.1 cm and CLEO has ten layers from 8.5 to 16.0 cm. In the $r\phi$ projection the uncertainty at the vertex from extrapolating the N measurements can be written:

$$\sigma^2_v = \frac{\sum_{i=1}^{N} (r_i/\sigma_i)^2}{\sum_{i\neq j}^{N} (r_i - r_j)^2/(\sigma_i\sigma_j)^2}$$

where σ_i is the $r\phi$ measurement error of the ith layer. Assuming that all the σ_i are the same and equal to 100 μm this expression yields $\sigma_v = 0.85\ \sigma_i = 85$ μm for Mark II and $\sigma_v = 1.6\ \sigma_i = 160$ μm for CLEO. In addition there is a contribution to the accuracy of locating the vertex from multiple scattering in the beam pipe and chamber material. This contribution can be written:

$$\sigma^2_{ms} = \left(\frac{.015}{p\beta}\right)^2 \sum_k R_k^2\ \Delta t_k$$

where Δt_k is the thickness in radiation lengths of material at radius R_k and p is the momentum in GeV/c. For CLEO most of the scattering material is contained in a carbon filament structural inner tube, a berylium beam pipe and a silver coating inside the beam pipe to supress synchrotron radiation. It all adds up to 0.9% of a radiation length. Therefore σ_{ms} = 95 μm/p for Mark II and σ_{ms} = 110 μm/p for CLEO. The contributions from measurement accuracy and multiple scattering must be added in quadrature to give the vertex location accuracy of a single track. The crossing point of two or more tracks is needed to reconstruct a primary or secondary vertex and so overall resolutions are greater than 200 μm. This is obtained only in the rφ projection. The z position accuracy when obtained by current division is two orders of magnitude poorer. The CLEO detector shown in Figure 2 has cathode strips near the innermost and outermost sense wires which will gain back some z-position accuracy.

The 100 μm resolution figure applies to operation at one atmosphere argon-hydrocarbon gas mixtures. This can be improved by operating at higher pressure. The improvement goes slightly slower than the square root of pressure. Pure hydrocarbons and the low drift velocity, low diffusion gas, dimethylether, have the potential for resolutions better than 30 μm but their survival is not ensured in a colliding beam environment. Drift chamber geometries such as the two stage time expansion chamber can also yield this improved resolution. Silicon strip detectors, CCD's or scintillating fibers are capable of better than 10 μm measurement resolutions but they suffer from large multiple scattering in the detector elements themselves as well as their cost and complexity. Silicon strip detectors or CCD's will be a useful part of the SLD detector with its very small diameter beam pipe.

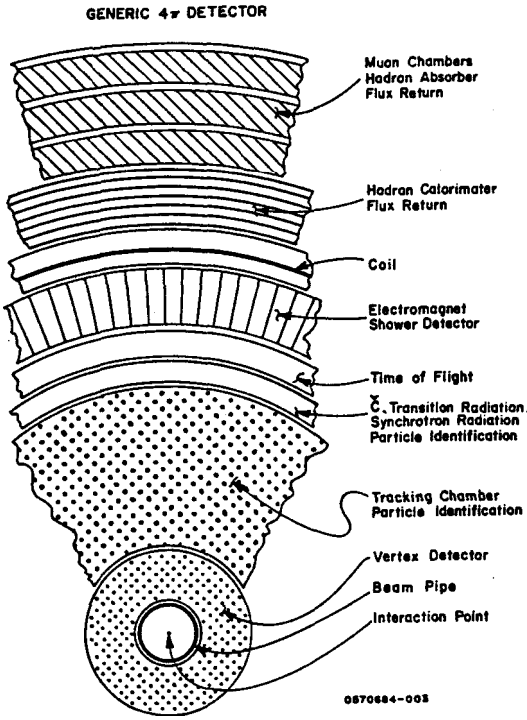

Fig. 1 Schematic view along the beam line of the elements of a general purpose 4π detector.

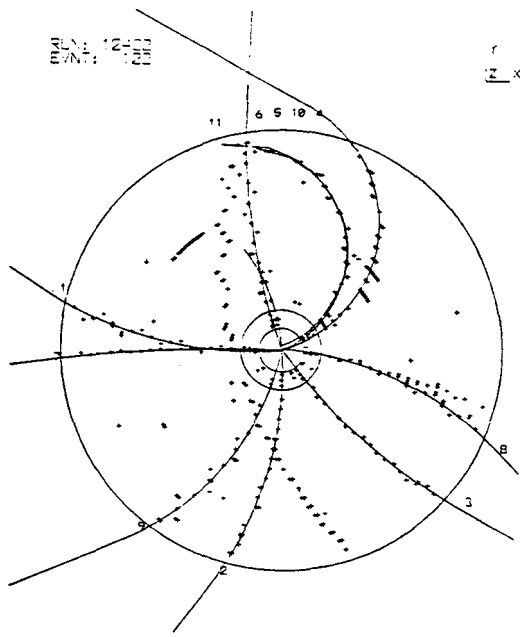

Fig. 3 An event in the CLEO drift chamber. The stagger in the hits along a track is caused by the stereo wire effect near the ends of the chamber.

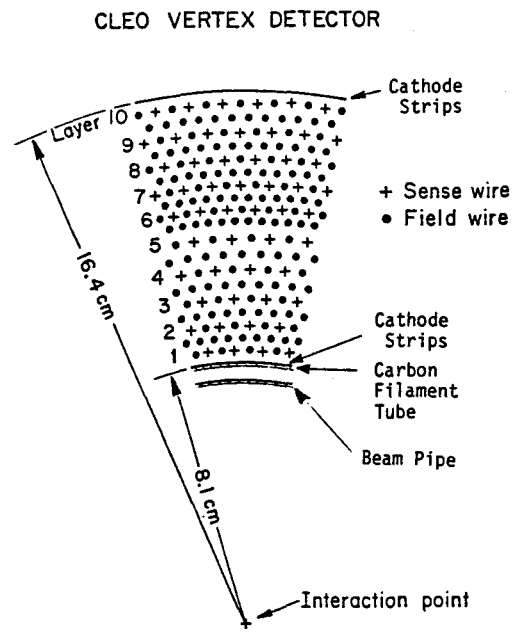

Fig. 2 A segment of the CLEO small cell drift chamber near the interaction point.

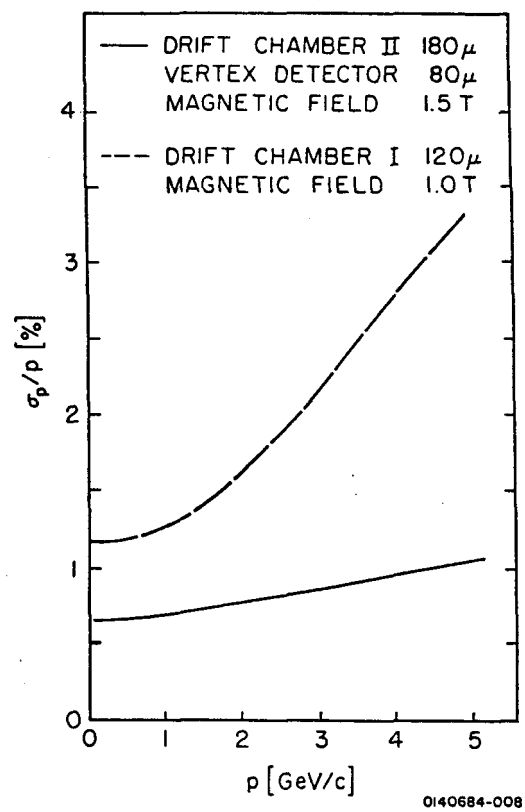

Fig. 4 Resolution versus momentum for the present CLEO 17-layer drift chamber and that projected for the CLEO II 51-layer chamber and new vertex detector.

TRACKING CHAMBERS

An essential element in a 4π detector is its tracking chamber which determines charged particle's momenta and directions. The chamber must be in a region of magnetic field. Tracking chambers are either time projection chambers or drift chambers of any one of several designs. The Mark II design with many rings of sense wires in small rectangular cells is in use in many detectors. The JADE jet chamber design has several sense wires on a radial line in a large pie shaped cell. The Mark III design has three sense wires on a staggered line in a smaller cell in order to locally resolve left right ambiguities. The best drift chamber position resolutions are obtainable at high gains ($>10^5$) where dE/dx ionization information is saturated. Resolutions of 150 - 250 μm are achieved. Most recent chambers also attempt to measure dE/dx and so operate at lower gain (few x 10^4) thus compromising spatial resolution to the region of 200 - 300 μm. TPC's determine the $r\phi$ coordinate by locating the centroid of cathode pad signals. Their inherent resolution in this corrdinate is poorer ($\sim$300 μm) but they obtain excellent dE/dx information.

Figure 3 shows an event in the CLEO tracking chamber and inner proportional chamber. Note that this inner chamber is not the vertex detector discussed above which is just being installed. The CLEO chamber has 17 layers of 11 mm cells; nine axial layers and eight layers of ±3° stereo angle. The 3° stereo layers allow a determination of track position in the direction along the beam line to a sigma 1/sin 3° $\simeq$ 20 times the $r\phi$ coordinate resolution (20 x 200 μm $\simeq$ 4 mm). Other chambers use current division on the signals of axial wires and can obtain a resolution about 1% x length $\simeq$ 2 cm. This technique has the advantage that a space point is determined for each hit and so track reconstruction is somewhat easier. Some drift chambers have cathode strips near some of the layers of sense wires. These cathode strips are capable of fractional mm resolutions like the cathode pads of a TPC. They must be fastened to very thin structural supports (usually foam cylinders) in order to keep multiple scattering low. A TPC has excellent tracking information in the direction along the beam line which is also the direction of the drift field.

The momentum resolution for the case of N equally spaced, equal accuracy measurements (N > 15) can be written:

$$\frac{dp_T}{p_T} \simeq \frac{P_T}{0.3} \frac{\sigma_{r\phi}}{(R_{max} - R_{min})^2 B} \left(\frac{720}{N + 4}\right)^{\frac{1}{2}}$$

where p_T is the momentum in the $r\phi$ projection (GeV/c), $\sigma_{r\phi}$ is the resolution of a single measurement in this projection (m), R_{max} and R_{min} are the radii (m) and, B is the magnetic field (Tesla). Increasing the magnetic field improves the resolution but there is a lower momentum cutoff where particles curl up in the field and never reach R_{max}. In addition there is a contribution to momentum resolution from multiple scattering within the chamber that must be added in quadrature. This term is approximately:

$$\frac{dp_T}{p_T} \simeq \frac{0.6\ t_{rl}^{\frac{1}{2}}}{(R_{max} - R_{min})\ B}$$

where t_{rl} is the thickness of the chamber in radiation lengths. Below about 1.5 GeV/c the multiple scattering dominates and above the measurement error dominates for chambers of one atmosphere. This behavior is calculated in Figure 4 for the CLEO II chamber of 51 layers, $\sigma_{r\phi}$ = 180 μm and t_{rl} = 0.60%. In this chamber 11 layers will be sereo layers and may also be operated at high gain and 40 layers are used for dE/dx measurements.

When information from the vertex detector is combined with the tracking chamber the situation is more complicated since the measurements are not equally spaced, they have varying accuracy and the material between the two also contributes to multiple scattering. Generally then a Monte Carlo program is used to calculate the momentum resolution.

Taking into account the polar angle the total momentum is $p = p_T/\sin\Theta$. The error in the total momentum is a combination of the perpendicular momentum error and the polar angle error. Momentum resolution becomes very poor as the polar angle goes to 0 or 2π.

PARTICLE IDENTIFICATION

Time of flight is a powerful technique in 4π detectors for determining the velocity of low momentum particles and thus their mass using the momentum information from the tracking chambers. There have been hopes for years that planar spark counters would develop sufficiently to be used in large systems and give their characteristic time resolution of 50 ps or so but so far they have not. All the large systems are fast plastic scintillator-photomultiplier combinations with the light brought out of the high magnetic field region via long light pipes. Characteristic time resolutions are in the range of 200 - 400 ps. If and when microchannel plate photomultipliers develop to the point they can be used in the magnetic field these resolution figures may be cut in half. To achieve these resolutions the photomultiplier must be sensitive to the first few photons reaching it. Often two discriminator-timing circuits are used and the time extrapolated to zero pulse height is determined. Figure 5 shows the momentum limit for particle identification as a function of the timing accuracy divided by the path-length of the time-of-flight counters. Typical values would be 0.4 ns for the 2σ timing accuracy and a 1 m flight path thus yielding π - k separation to about 0.8 GeV. The zero point of time is determined in colliding beam experiments by knowing when the beams intersect and so there is no need to fold in the accuracy of a second timing counter. These resolutions depend on knowing the location of the particle in the counter to a few cm from the tracking chamber or other detectors. Time-of-flight counters are usually located outside Cerenkov detectors in order not to degrade them. The choice of thickness of the time-of-flight scintillator is a compromise between improving the timing resolution and degrading the shower counter resolution located just outside. For optimum photon resolutions at low energies the pulse height of the time-of-flight counters should be added for those photons converting upstream of the shower counter.

The fast response of the timing counters makes them a convenient component of the trigger for the fast processors which determine if there are tracks in the track chambers. Cosmic ray rejection is also an important benefit.

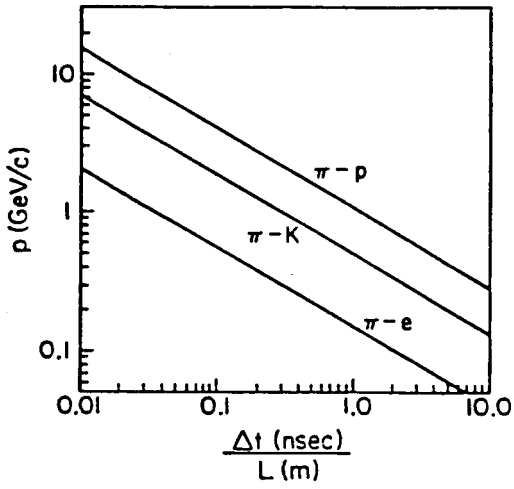

Fig. 5 Limiting momentum for distinguishing various particle types versus time-of-flight resolution divided by flight path length.

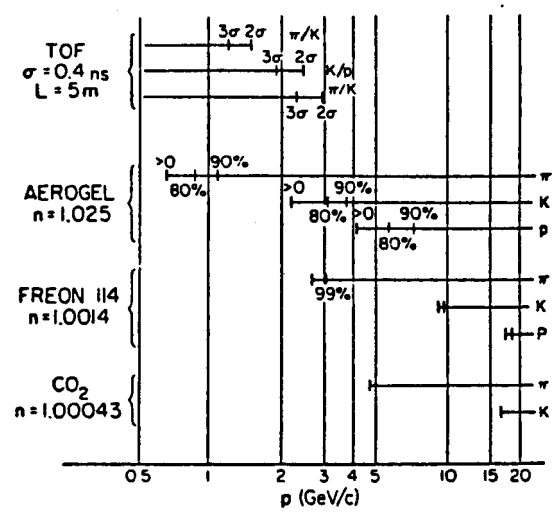

Fig. 6 TASSO time-of-flight and Cherenkov particle identification capabilities versus momentum.

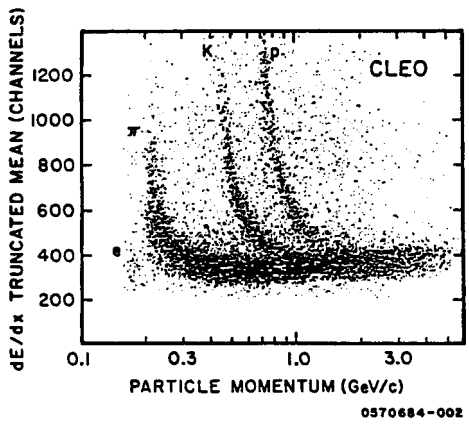

Fig. 7 Typical scatter plot of dE/dx truncated means measured in the outer proportional chambers versus momentum measured in the cylindrical drift chamber. Interactions in the solenoid coil between the drift chamber and the dE/dx chamber are the chief cause of the measurements which fall outside the bands for e, π, K and p.

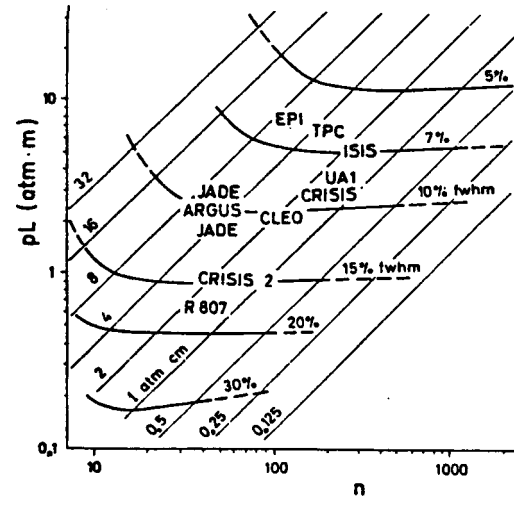

Fig. 8 Expected dE/dx resolution versus the parameters of detector length and number of samples. Various examples of the large systems are located on the plot.

Threshold Cherenkov detectors can also provide e - π - K - p separation. Initially the CLEO experiment used a one-atmosphere Freon gas Cherenkov detector to provide e - π separation until the dE/dx detectors were completed. Figure 6 shows the particle identification of the TASSO detector with time-of-flight, aerogel and gas Cherenkov detectors. This part of that detector only covers a fraction of 4π in the form of two opposing arms of the detector. As the momentum of a particle increases through the threshold region of a Cherenkov detector the amount of light, the number of photoelectrons, the pulse height and efficiency increase. Efficiencies are shown in Figure 6.

Ring imaging Cherenkov detectors are in use at the HRS detector at PEP and are proposed for DELPHI at LEP. In these systems the particles to be identified traverse a thin liquid radiator (eg. Freon 72, n = 1.278 for photons of 6.5 eV) and emit untraviolet radiation in Cherenkov cones. The radiation traverses a transparent region and enters drift chambers containing a photoionizable vapor (eg. 1% TMAE in methane). A suitable pattern recognition program will then find the rings of photoelectrons around the original track.

Transition radiation depends on the γ of the particle and so can be used to separate electrons from other particles. This has been done at the ISR with lithium foil radiators and xenon filled x-ray detectors.

Detection of synchrotron radiation is proposed for this purpose in the 3 Tesla AMY detector at TRISTAN. The synchrotron radiation is generated by tracks in the tracking chamber and detected just outside in xenon filled counters. This augments the π - e separation provided by the shower counters.

A very powerful and, by now, common method of particle identification is by measuring the ionization loss which is a function of velocity (and charge). At low energies dE/dx varies as $1/\beta$. At higher energies dE/dx comes to a minimum and rises again in the relativistic region before saturating at a constant value. In liquid or solid detectors this relativistic rise is negligible but they can be used in the low energy region. In gas detectors the relativistic rise is

a function of gas species and pressure. For atmospheric argon-methane (90% - 10%), for example, the rise is a factor of 1.4 and can be used for π - e separation above about 1.5 GeV. The ionization loss is a thin gas sample exhibits a Landau distribution with a high energy tail. In order to obtain good dE/dx resolution many thin samples must be measured. The usual technique is to average the lowest 40 - 70% of the samples and throw out the rest. Figure 7 shows this truncated mean for the CLEO detector. Clear bands for π, K and p can be seen. In this detector the dE/dx detector is outside the one radiation length of material in the coil and other portions of the detector. This causes the noticeable background confusion of particles multiple scattering or interacting so that their momentum or dE/dx is measured incorrently. Eliminating this source of confusion is a chief advantage of measuring dE/dx in the tracking chamber itself as is proposed for CLEO II to replace the CLEO dE/dx detectors.

Figure 8 illustrates the resolution in dE/dx truncated means as a function of number of samples and sample thickness. The curves are expected resolutions in argon and the position on the plot of various detectors is shown. The TPC at PEP has excellent resolution because it operates at high pressure and samples the ionization for every 4 mm track length. Figure 9 illustrates the relativistic rise region in the TPC at 4 atmospheres for cosmic ray muons. Note the large scale offset.

Fast sampling adc's allow improved resolution in the geometry of a time expansion chamber where the drift direction is in the direction of the track. Sub-millimeter track smaples are possible with $\sim$100 MHz sample rates and 1 cm/μsec drift velocities. Improvement of over a factor of two in the relativistic rise region is achieved. So far this technique has not been applied to 4π detectors.

CALORIMETERS

The most common type of electromagnetic calorimeter employed in 4π detectors is the sampling type with lead plates interspersed with scintillator, liquid argon, gas proportional chambers or gas chambers operated in a saturated mode. Some detectors (notably JADE and VENUS) employ lead glass blocks. Scintillating glass with approximately 5 times the light output of Cherenkov radiation has been used at Fermilab. So far the only large detectors employing NaI(Tl) crystals (Crystal Ball and CUSB) have been nonmagnetic. BGO crystals are proposed for LEP-3 and CsI(Tl) crystals for CLEO II, about which I will have more to say.

The energy deposited in a sampling calorimeter fluctuates statistically from event to event. The percentage energy resolution follows an $E^{-\frac{1}{2}}$ dependance and depends on sampling absorber (usually lead) thickness as $t^{\frac{1}{2}}$. A good approximation to the constant of proportionality is that a 1 GeV shower sampled with plates of 1 radiation length behaves as N = 53 uncorrelated tracks with its statistical fluctuations of $\sqrt{53}$. Then

$$\sigma_E/E = \sqrt{1/53}\ \sqrt{t/E} = 14\%\ \sqrt{t/E}$$

where E is measured in GeV and t in radiation lengths. For example the TASSO liquid argon calorimeter with 2 mm (0.36 r.l.) lead plates measures an energy resolution of $10\%/\sqrt{E}$ from 1 to 4 GeV.

In a calorimeter with gas as the sampling medium such as proportional chambers there are extra fluctuations associated with the Landau tail of δ-ray emmission and with the path length fluctuations of low energy electrons traveling at large angles. These additional contributions typically double the resolution over that observed in calorimeters using scintillators or liquid argon. For example the present CLEO lead-proportional tube shower chambers obtain $\sigma_E/E = 28\%\ \sqrt{t/E}$ for 5 GeV Bhabha electrons. Operating gas detectors in a saturated (limited streamer or Geiger) mode helps restore the resolution.

In a lead glass Cherenkov detector the light output is proportional

to the total track length of the shower electrons and positrons. This total track length, of course, undergoes intrinsic shower fluctuations and spatial nonuniformity of light attenuation also contributes to give the observed resolution of approximately

$$\sigma_E/E = 0.045/\sqrt{E}$$

This resolution is improved less than a factor of two by using scintillating glass even though its light output is five times as great.

In order to achieve better resolutions a crystal scintillating medium must be employed. For example the Crystal Ball, an array of 720 tapered triangular blocks of NaI(Tl), 16 radiation lengths long achieves a resolution given by the empirial expression: $\sigma_E/E = 0.01\ E^{\frac{1}{4}}$. This excellent response is non-gaussion with a tail on the low side so σ_E is usually determined from the FWHM. The observed slow resolution dependence on energy ($E^{-\frac{1}{4}}$) indicates that the limiting factors in such crystal calorimeters are not photoelectron statistics or shower fluctuations which vary as $E^{-\frac{1}{2}}$. In fact calibration errors, short term gain drifts and fluctuations in the leakage of the shower from the front, sides and rear of the crystal array all contribute to the resolution and lead to the observed slow energy variation.

Material in front of the crystals seriously degrades the resolution so in the case of a magnetic detector the crystals must be placed within the magnetic field. The one radiation length or so of the coil is tolerable in front of a sampling calorimeter but would make a crystal calorimeter not worth the effort. This leads to the choice of registering the scintillation light in recently available silicon photodiodes rather than magnetic-field-sensitive photomultipliers. Coupled to photodiodes the scintillator CsI(Tl) gives a bigger response than the traditional NaI(Tl) and it has other advantages as well. Table I compares the useful scintillators for electromagnetic calorimeters. BaF_2 with its very fast, ultraviolet emmission is a special case in which scintillating slabs are coupled to proportional chambers with a TMAE photocathode. CsI(Tl), besides emitting more light, is easier to handle than the brittle, hydroscopic NaI(Tl).

Table I

Comparison of Scintillators for Electromagnetic Shower Counters

	$CdWO_4$	$Bi_4Ge_3O_{12}$	CsI(Tl)	BaF_2 Fast	BaF_2 Slow	NaI(Tl)	Scint. Glass
Radiation Length (cm)	1.1	1.12	1.85	2.03		2.59	4.35
Density (gm/cm^3)	7.90	7.13	4.51	4.88		3.67	3.36
Photons/MeV	15000	5000	45000	2000	6500	40000	∿100
Decay constant (ns)	5000	300	980	0.8	620	250	80
Peak Emmission (nm)	540	480	565	225	310	415	430
Index of Refraction	2.3	2.15	1.80	1.57	1.50	1.85	1.60
Cleavage	<010>	none	none	<111>		<100>	none
Hardness (Mho)	4.3	5	2	3		2	
Hydroscopic	no	no	slight	no		very	no

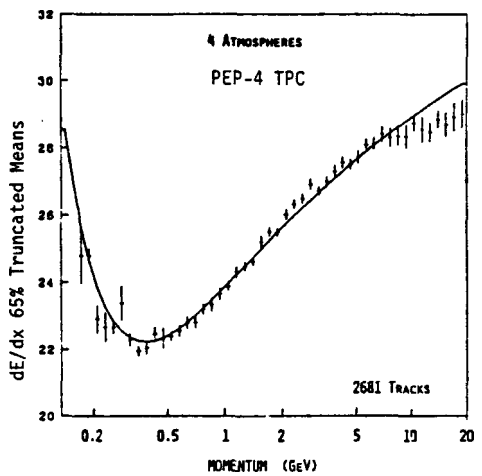

Fig. 9 Results from the PEP-4 TPC for the relativistic rise of muons, averaged over many tracks. A resolution for a single track of about 3% is obtained.

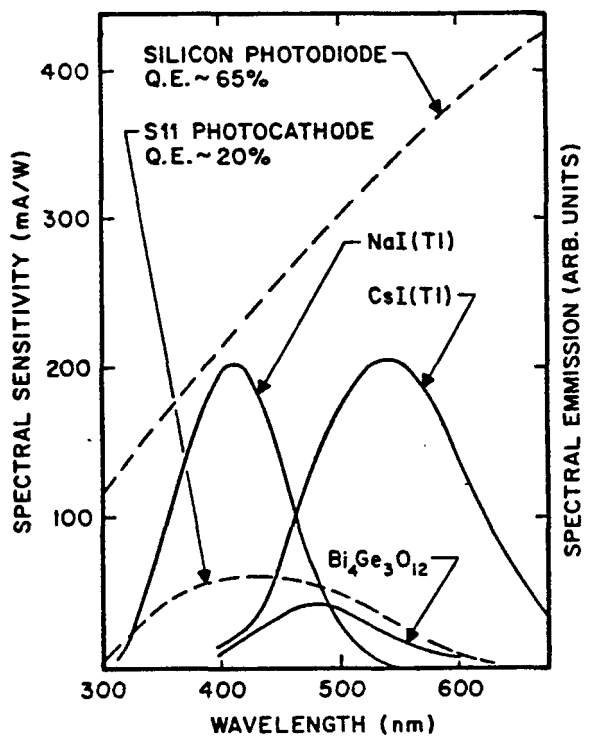

Fig. 10 Spectral emmission of CsI, NaI and BGO superimposed on the spectral sensitivity of a photomultiplier and photodiode. CsI is a particularly good match to photodiodes.

Figure 10 further illustrates the comparison of CsI(Tl), NaI(Tl) and BGO. The spectral emmission of CsI(Tl) is shifted toward the red where photodiodes are more sensitive. In the Harshaw catalog CsI(Tl) is labeled as having only 45% of the light output of NaI(Tl) but this is measured with an S-11 response photomultiplier which is insensitive to much of the light from CsI(Tl).

The factor of three increase in quantum efficiency of photodiodes over photomultipliers leads to better resolutions even with low energy sources where resolutions are limited by photoelectron statistics. This is shown in Figure 11 for small CsI(Tl) crystals coupled to photodiodes and to a red sensitive photomultiplier. The crossover where amplifier noise begins to dominate is below 1 MeV.

Our plans for CLEO II call for about 8000 CsI(Tl) crystal blocks. 6000 will be tapered in both directions with a front face about 5 x 5 cm^2, rear face about 6 x 6 cm^2 and 30 cm length (16 r.l.) for the barrel shower counter. 2000 will be 5 x 5 x 30 cm^3 for the pole tip counters. The layout is shown in Figure 12 in quarter section. We are working with four companies (BDH, England; Bicron, U.S.; Harshaw, U.S.; and Horiba, Japan) and expect a final production cost under $\$2/cm^3$. Four photodiodes (Hamamatsu, Japan) with separate preamplifiers will be attached to each crystal to provide reliability and stability.

The position of showers in a crystal calorimeter such as the Crystal Ball or CLEO II or a sampling calorimeter with tower construction is obtained to a fraction of a cell width by measuring the small energy spreading into adjacent cells. This can be done to better than 1 cm in the 5 cm blocks of CLEO II and is adequate for the physics at an e^+e^- storage ring. Two photon resolution is obtained down to about two block widths or 10 cm but the presence of two photons can be discerned below this though they cannot be resolved separately. Many sampling calorimeters are constructed with strips and can have slightly better position resolutions. Two photons far apart can hit the same strips in one view and confuse the resolutions in position and energy of both photons.

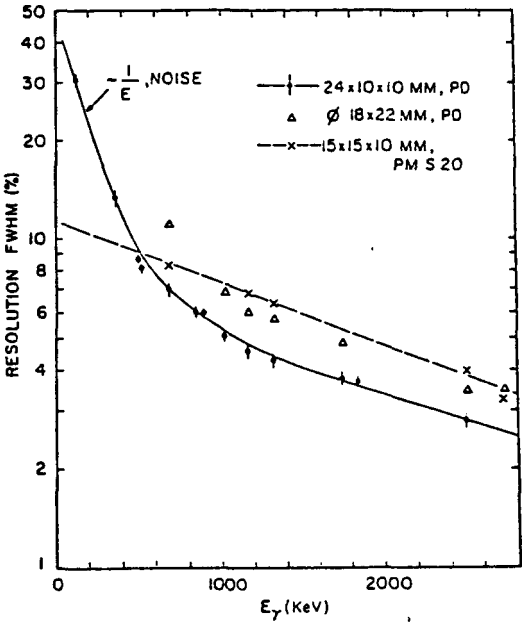

Fig. 11 Resolution of small CsI crystals with photomultiplier and photodiode readout for low energy photon sources.

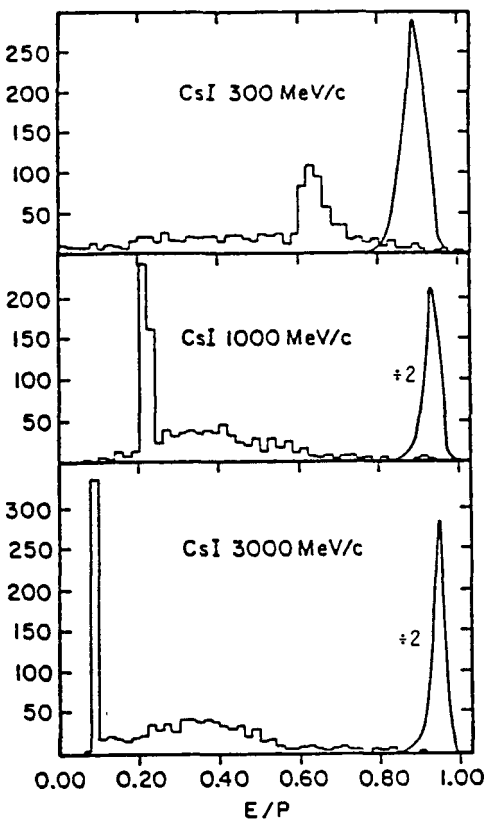

Fig. 13 Monte Carlo predictions of the distribution of energy divided by momentum for pions (histogram) and electrons (smooth curve).

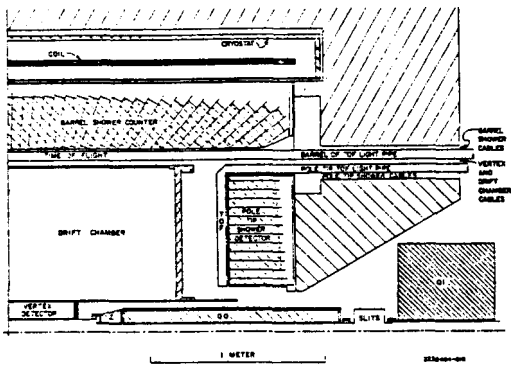

Fig. 12 CLEO II quarter section view perpendicular to the beam line. The plans call for about 6000 CsI tapered crystals in the barrel shower counter and about 1000 in each pole tip counter.

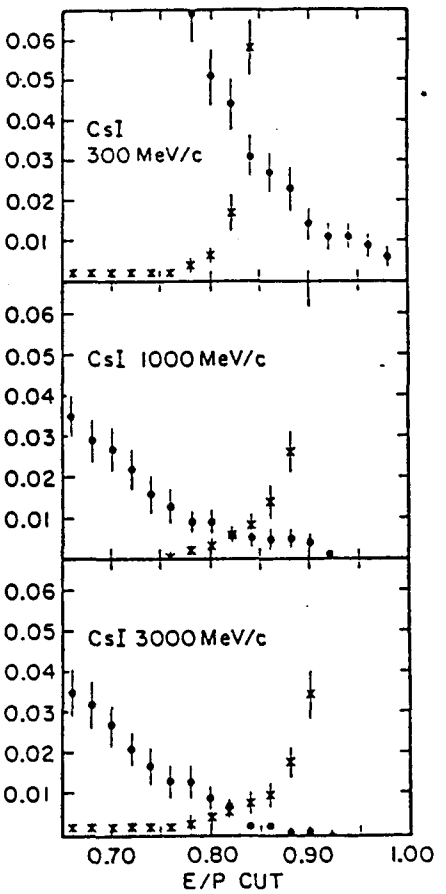

Fig. 14 Efficiency for detecting pions and inefficiency for detecting electrons as a function of the cut on E/P. The o's represent the fraction of pions passing the cut and the x's represent the fraction of electrons failing the cut.

Electron-pion separation improves for improved resolution of the shower chamber. For CsI(Tl) and momenta over 300 MeV/c the separation is very good as illustrated in Figures 13 and 14. These figures present calculations using the Oak Ridge high energy transport code for pions and the SLAC Electron-Gamma-Shower program for electrons. Pion rejections over 1000:1 can be obtained for momenta greater than 1 GeV/c using the shower chamber energy cut and dE/dx measurements or Cherenkov detectors.

I will not discuss hadron calorimeters as they are only useful at energies well above those of interest to this workshop.

SUPERCONDUCTING COILS

The present CLEO experiment has a superconducting coil inside the dE/dx detectors, time-of-flight counters and shower counters. It is of a type similar to the PEP-4 TPC coil with Nb-Ti-Cu superconducting wire wound on an aluminum bore tube to provide stability. It is about 0.7 r.l. thick. We are in the process of designing a larger coil to enclose the CsI(Tl) scintillation crystals. Our need is modest in comparison with coils for LEP now in the design stage. These coils and also the coils for TRISTAN experiments and for CDF all use superconducting wire stabilized with high purity aluminum which is about an order of magnitude more conducting than copper at liquid helium temperature. This allows such a coil to be indirectly cooled with a few tubes carrying liquid helium. We are also looking into a bath cooled design which would be cryostable. Table II lists the large superconducting solenoids for colliding beam experiments.

The iron yoke and pole pieces largely determine the magnetic field uniformity. For CLEO II we expect to obtain a uniformity of $\pm 0.5\%$ over the drift chamber volume. The main complexity comes in providing access to the ends of the drift chamber and cable and light pipe routes for all the detector elements. An iron yoke thickness of 60 cm would be adequate to carry the return flux but for muon detection an additional 60 cm will be added to filter out pions up to about 2 GeV. The iron will be interleaved with muon detecting chambers every 30 cm.

Table II

Properties of Present and Proposed Superconducting Detector Coils

Experiment/Location Design/Construction	Year B Field	Cryostat I.Dia. O. Dia.	Coil Dia. Length	Coil Thickness Stored Energy	Cooling System Current
HRS/PEP	1969	4.4m	5.0m	thick	Bath
Argonne	1.6T	5.6m	3.9m	60 MJ	2040A
PLUTO/PETRA	1972	1.4m	1.6m	thick	Bath
DESY	2.2T	2.0m	0.9m	4 MJ	1270A
ISR-I1	1976	1.4m		1.1Xo	Bath
CERN	1.5T		1.8m	3 MJ	2200A
CELLO/PETRA	1979	1.5m	1.7m	0.5Xo	Indirect
Saclay	1.3T	1.9m	3.4m	5 MJ	3000A
CLEO/CESR	1981	1.9m	2.0m	0.7Xo	Indirect
Cornell/AMI	1.0T	2.3m	3.2m	4 MJ	1600A
TPC/PEP	1984	2.0m	2.2m	0.7Xo	Indirect
Berkeley	1.5T	2.4m	3.3m	11 MJ	2225A
CDF/TEVATRON	1984	2.9m	3.0m	0.8Xo	Indirect
Fermilab-Tsukuba/Hitachi	1.5T	3.4m	4.8m	30 MJ	5000A
TOPAZ/TRISTAN	1984	2.7m	2.9m	0.8Xo	Indirect
KEK/Furukawa	1.2T	3.2m	5.1m	19 MJ	3560A
VENUS/TRISTAN	1984	3.4m	3.5m	0.6Xo	Indirect
KEK/Mitsubishi	0.5T	3.8m	5.2m	11 MJ	3333A
AMY/TRISTAN	1986	1.1m		thick	
Rochester-KEK/	3.0T		1.4m	30 MJ	
CLEOII/CESR	1986	2.9m	3.1m	thick	
Cornell/	1.5T	3.4m	3.3m	23 MJ	
ALEPH/LEP	1987	5.0m	5.3m	1.6Xo	Indirect
Saclay	1.5T	5.8m	6.4m	130 MJ	5000A
DELPHI/LEP	1987	5.2m	5.6m	4Xo	Indirect
Rutherford	1.2T	6.2m	6.8m	110 MJ	5000A

REFERENCES

General

BR81 Proceedings of the 1981 ISABELLE Summer Workshop, BNL 51443, Brookhaven (1981).

CL84 The CLEO Collaboration, Cornell Report CLNS 84/609 (1984), CLEO II, A Proposal

CO81 Detectors and Experiments for e^+e^- at 100 GeV, CLNS 81-490, Cornell (1981).

GI83 G. Gidal, et al., LBL-91 (1983) Major Detectors in Elementary Particle Physics.

HI80 D. Hitlin, AIP Conference Proceedings No. 62, High Energy e^+e^- Interactions, Vanderbilt (1980) 383, Some Topics in e^+e^- Instrumentation.

SL82 Proceedings of the International Conference on Instrumentation for Colliding Beam Physics, SLAC-250 (1982).

SN82 Proceedings of the 1982 DPF Summer Study on Elementary Particle Physics and Future Facilities, Snowmass (1982).

UP80 Proceedings from International Conference on Experiments at LEP, Uppsala (1980) Physica Scripta 23 (1981).

VI83 Nucl. Instr. and Methods, 217 (1983), Proceedings of the Wire Chamber Conference, Vienna (1983).

Vertex Detectors

CH84 G. Charpak and F. Sauli, CERN-EP/84-35 (1984), submitted to Annual Review of Nuclear Science, High Resolution Electronic Particle Detectors.

GE82 T. Gentile, et al., CLEO memo, unpublished (1982), Proposal to add a Vertex Detector to the CLEO Detector

JA82 J. Jaros, Proceedings of the International Conference on Instrumentation for Colliding Beam Physics, SLAC-250 (1982) 29, the Mark II Secondary Vertex Detector.

LI82 R. Lipton, Proceedings of the 1982 DPF Summer Study (1982) 371, Limits and Possibilities for Vertex Detectors.

RU82 R. Ruchti, Proceedings of the 1982 DPF Summer Study (1982) 54, Summary Report on Innovative Detector Ideas.

Vertex Detectors (cont)

RU84 D. Rust, SLAC-PUB-3311 to be published in the Proceedings of the 3rd International Conference on Instrumentation for Colliding Beam Physics, Novosibirsk (1984) Recent Developments in High Precision Vertex Chambers at SLAC.

SH81 K. Shinski, CLEO memo unpublished (1981), A High Resolution Vertex Detector for CLEO.

VI83 F. Villa, Nucl. Instr. and Mehtods 217 (1983) 273, Dimethylether: a Low Velocity, Low Diffusion Drift Chamber Gas.

Tracking Chambers

GL63 R. L. Gluckenstein, Nucl. Instr. and Methods 24 (1963) 381, Uncertainties in Track Momentum and Direction Due to Multiple Scattering and Measurement Errors.

HA82 D. Hartill, Proceedings of the Int. Conference on Instrumentation for Colliding Beam Physics SLAC-250 (1982) 106, Particle Identification and Tracking in Central Detectors.

Particle Identification

AG84 G. D. 'Agostini, et al., Nucl. Inst. and Methods 219 (1984) 495, Time-of-Flight Resolution for a long Scintillation Counter.

BE81 K. W. Bell et al., Nucl. Instr. and Mehtods 179 (1981) 27 A Large Scintillator Array for Particle Identification by Time-of-Flight.

BU83 A. Bungener, et al., Nucl. Inst. and Methods 214 (1983) 261, Electron Identification Beyond 1 GeV by Means of Transition Radiation.

GI83 R. Giles, CLEO Memo CBX 83-35 (1983), A Scintillator TOF System for CLEO II.

LY82 G. R. Lynch and N. J. Hadley, Proceedings of the Int. Conference on Instrumentation for Colliding Beam Physics SLAC-250 (1982) 85, Energy Loss Measurements in the PEP TPC.

OG84 A. Ogawa, et al., IEEE Trans. on Nucl. Science, NS-31 121, Large Area Spark Counters with Fine Time and Position Resolution.

WA81 A. H. Walenta, Physica Scripta 23 (1981) 354, Performance and Development of dE/dx Counters.

Calorimeters

BL83 P. Blum, et al., Nucl. Inst. and Methods, 213 (1983) 251, A Modular NaI(Tl) Detector for 20-1000 MeV Photons.

CO84 B. Cox, et al., Nucl. Inst. and Methods 219 (1984) 487, A Measurement of the Response of an SCGl-C Scintillation Glass Shower Detector to 2-17.5 GeV Positrons.

GR84a B. C. Grabmaier, IEEE Trans. on Nucl. Science NS31 (1984) 372, Crystal Scintillators

GR84b H. Grassmann, et al., submitted to Nucl. Instr. and Methods, Improvements in Photodiode Readout for Small CsI(Tl) Crystals.

IW80 S. Iwata, Report of the TRISTAN Working Group UTPN-165 (1980), Appendix 2, Calorimeters.

LA82 A. Ladage, Proceedings of the Int. Conference on Instrumentation for Colliding Beam Physics, SLAC-250 (1982) 180, The TASSO Liquid Argon Calorimeter.

LO84 E. A. Lorenz, IEEE Trans. on Nucl. Science NS31 (1984) 48, Scintillation Calorimetry and Readout Techniques.

MI84 N. Mistry, CLNS 84-613, to be published in the Proceedings of the 3rd International Conference on Instrumentation for Colliding Beam Physics, Novosibirsk (1984), A New Generation of Detectors for the e^+e^- Storage Ring, CESR.

TO84 W. Toki, et al., Nucl. Instr. and Methods, 219 (1984) 479, The Barrel Shower Counter for the Mark III Detector at SPEAR.

CEBAF 1984 SUMMER WORKSHOP
SUMMARY TALK

John Dirk Walecka
Institute of Theoretical Physics, Department of Physics
Stanford University, Stanford, California 94305

I would like to thank our hosts and the staff for this workshop. It is an interesting time to have such a workshop since there are so many opportunities ahead. I enjoyed it very much, and our hosts and the staff worked hard to make things run smoothly.

WHY NUCLEAR PHYSICS?

Let me start back at the beginning. Why is nuclear physics interesting? I do not know why we are always called upon to defend doing nuclear physics. In my opinion the frontiers in nuclear physics are, with the possible exception of some of the work going on at very high energy, as interesting, as challenging, and as basic as anything in physics.

The nucleus is a unique form of matter consisting of many baryons in close proximity. All of the forces of nature are present in the nucleus: strong, electromagnetic, weak, and gravitation, if we include neutron stars which are nothing more than enormous nuclei held together by the gravitational attraction. The current picture of the strong and electroweak interactions is formulated in terms of local gauge theories based on an underlying symmetry structure of $SU(3)_C \otimes SU(2)_W \otimes U(1)_W$. We shall see how the nucleus can be used as a unique microscopic laboratory to test this assumed structure of the fundamental interactions. The many nuclear levels and selection rules are invaluable tools in such studies. In addition, the nuclear many-body problem is of intrinsic intellectual interest. Furthermore, most of the mass and energy in the visible universe arises from nuclei and nuclear reactions. If the goal of physics is to understand nature, then we must surely understand the nucleus. Finally, in simplest terms, nuclear physics is the study of the structure of matter.

NUCLEAR PHYSICS

The traditional approach to nuclear physics starts with the assumption of structureless nucleons (n,p) interacting through static two-body potentials obtained from two-body scattering data. The non-relativistic many-particle Schrödinger equation is then solved in some approximation. The system can be probed and studied with electromagnetic and weak interactions, and in this

traditional approach, the currents for these interactions are constructed from the properties of free nucleons.

While this traditional approach to nuclear structure has had many striking successes, it is an oversimplification to treat the nucleus in this fashion. A more realistic approach starts with the observed hadrons, the baryons and mesons, as the basic set of underlying degrees of freedom. The theory must then incorporate general principles of physics such as special relativity and causality. The only consistent theoretical framework we have for describing such an interacting many-body system is relativistic quantum field theory. It should be renormalizable so that we have a theory that can be compared with experiment after the determination of a few phenomenological coupling constants and masses. I like to refer to relativistic quantum field theories of the nuclear many-body system based on the strongly interacting hadronic degrees of freedom, the baryons and mesons, as quantum hadrodynamics (QHD). More generally, one can take this as a description of the level of sophistication at which nuclear physics is currently being carried out. It will be a very long time indeed until lattice gauge theory calculations in quantum chromodynamics (QCD), which we shall subsequently discuss, will be able to do nuclear physics at anything approaching this level of sophistication.

WHY ELECTRONS?

Let me next briefly discuss why electrons provide such a powerful tool for studying nuclear structure [1]. First, the interaction of an electron with the hadronic target is known; it is given by quantum electrodynamics (QED), or more generally, by the standard model of the electroweak interactions. Second, the interaction is relatively weak, of order α the fine-structure constant. Thus one can make measurements without greatly disturbing the nuclear system. Third, one has kinematic flexibility with electrons as illustrated in Fig. 1. There are three lepton variables at our disposal: the Lorentz invariants q^2 and ν (the four-momentum transfer and energy loss in the laboratory respectively) and the scattering angle θ. Equivalently, one can choose q^2, $W^2=-(p-q)^2$, and θ where W is the mass of the final nuclear system. By varying θ at fixed q^2 and W^2 one can separate the longitudinal and transverse response functions for the target. By varying q^2 at fixed W^2 one can then essentially measure the Fourier transform of the transition charge and current densities. By inverting these Fourier transforms, one has a microscope for locating the spatial distributions of these quantities. It never ceases to amaze me that by carrying out macroscopic laboratory measurements, one can study

detailed spatial distributions of charges and currents in the nucleus on a distance scale of 10^(-13)cm and smaller. Finally, the electron provides an extremely versatile probe. Not only is there a Coulomb interaction with the charge density in the target, but also an interaction with the convection current and intrinsic magnetization distribution in the nucleus through the exchange of a transverse photon.

ACCOMPLISHMENTS

It serves us well to recall some of the accomplishments of electron scattering studies of nuclei (Arnold,Moniz).(*) Figure 2 illustrates the state of the art with respect to elastic charge scattering from spin-zero targets. The high q^2 data is from Saclay and the cross section has now been measured over 13 decades [2]. Figure 3 shows the charge distributions of three nuclei essentially obtained by taking the Fourier transform of the diffraction pattern illustrated in Fig.2. The shaded areas show the magnitude of the present experimental uncertainty in the charge distribution. The dashed curves show the present level of our theoretical understanding of these quantities [3], but I will not have time to go into detail on this topic. Our best knowledge of the charge distributions in nuclei, and hence of what the nucleus actually looks like, comes from electron scattering. Bob Hofstadter received the Nobel prize for his work in this area.

By looking at elastic magnetic scattering from nuclei with spin, one can similarly study the detailed spatial distribution of the magnetization density in the nucleus. This density comes predominantly from the last one or few valence nucleons, and both neutrons and protons contribute to it. Bill Donnelly and Ingo Sick have just completed a very nice review article on elastic magnetic scattering [4]. Excitation of nuclei through the Coulomb interaction allows one to study transition charge densities. The very lovely high resolution work from Bates on selected deformed nuclei has allowed one to determine the shape of the intrinsically deformed ground state whose rotations give rise to the low-lying excitation spectra. High-spin magnetic excitations in nuclei are induced systematically in electron scattering through the transverse electromagnetic interaction. Quasielastic electron scattering provides the most direct measure we have of the single-particle structure of nuclei.

One of the major advances in nuclear physics in the past few years has been the unambiguous identification of exhange currents in nuclei (Hajduk). These are additional

(*) Names in parentheses denote workshop speakers whose talks are relevant to the topic under discussion.

electromagnetic currents present in the many-body system due to the exchange of charged mesons. Figure 4 shows the elastic magnetic form factor for 3^He [5]. The dashed curve is based on the assumption of structureless nucleons, and it is obtained by solving the three-body Faddeev equations with two-body potentials. This calculation is simply inadequate to describe the data. The solid curves are obtained by including meson exchange currents [6,7]. The differences at large q^2 give you some feeling for the theoretical uncertainty in the calculations. The presence of these additional hadronic degrees of freedom in the nuclear system are clearly evidenced by these results. Furthermore, this figure clearly illustrates that it is crucial to get to high q^2 to obtain this striking and unambiguous information.(**)

Measurement of the process (e,e'p) in a coincidence experiment provides information on the single hole structure of nuclei. Measurement of the final e' and p energies determines that of the hole state in the residual nucleus. Variation of the momentum transferred to the nucleus then allows one to essentially measure the Fourier transform of the hole wave function. Such experiments have been carried out at Saclay, Bates, and NIKHEF. The current limitation in these experiments is duty factor. These experiments provide the best information we have on the single hole structure of nuclei. I expect that they will form the "bread and butter" of the next generation of high duty factor electron machines.

WHY QUARKS?

Particle physics has been revolutionized in the past decade and a half with the introduction of quarks. The evidence for quarks is <u>indirect</u> since we apparently do not observe free quarks in the laboratory. It is valuable, therefore, to summarize the evidence for quarks. It is particularly important to keep these things in mind when we talk about quark effects in nuclei. The evidence for quarks is basically threefold:

1) There are many observed hadrons, and they can be grouped into multiplets and supermultiplets. The regularities in hadronic spectra can be understood in terms of a simpler underlying set of degrees of freedom. With the assignment of the quantum numbers in Table I to the quarks, and the assumption that mesons are formed from ($\bar{q}q$) pairs and the baryons from (qqq) triplets, the spectra of observed hadrons can be readily understood. Furthermore, more detailed dynamical quark models of the internal structure of the hadrons can successfully correlate their observed properties.

(**) Recall 5fm^(-1) $\cong$ 1 GeV.

2) The structure of the electromagnetic and weak currents is marvelously simple and accurate when expressed in terms of the Dirac fields for the quarks. The electromagnetic current is simply

$$J_\mu^\gamma = i\left[\frac{2}{3}(\bar{u}\gamma_\mu u + \bar{c}\gamma_\mu c) - \frac{1}{3}(\bar{d}\gamma_\mu d + \bar{s}\gamma_\mu s)\right] \tag{1}$$

The charge-changing weak current is

$$\begin{aligned} J_\mu^{(+)} &= i\bar{u}\gamma_\mu(1+\gamma_5)(d\cos\theta_c + s\sin\theta_c) \\ &\quad + i\bar{c}\gamma_\mu(1+\gamma_5)(-d\sin\theta_c + s\cos\theta_c) \end{aligned} \tag{2}$$

where θ_c is the Cabibbo angle, and the weak neutral current in the standard model of Weinberg, Salam, Glashow and coworkers [8,9,10] is simply

$$\begin{aligned} J_\mu^{(0)} &= \frac{i}{2}\left[\bar{u}\gamma_\mu(1+\gamma_5)u + \bar{c}\gamma_\mu(1+\gamma_5)c - \bar{d}\gamma_\mu(1+\gamma_5)d\right. \\ &\quad \left. - \bar{s}\gamma_\mu(1+\gamma_5)s\right] - 2\sin^2\theta_W J_\mu^\gamma \end{aligned} \tag{3}$$

We recall that it was the goal to make the weak neutral current simple when expressed in terms of quark fields, i.e. to eliminate the strangeness changing weak neutral current terms $(\bar{s}d)$ and $(\bar{d}s)$, that led Glashow and coworkers to introduce charm and the c quark. These implications have been brilliantly verified experimentally. The quark model is truly predictive .

In the nuclear domain we confine ourselves to hadrons and nuclei formed from up (u) and down (d) quarks. In this case, the quark fields can be combined into a single two-component field ψ , and with the definitions

$$\begin{aligned} \psi &\doteq \begin{pmatrix} u \\ d \end{pmatrix} \\ G^\pm &\equiv G\cos\theta_c \end{aligned} \tag{4}$$

where G is the Fermi constant, the electromagnetic and weak currents of the standard model take the following form

$$\begin{aligned} J_\mu^\gamma &= i\left[\bar{\psi}\gamma_\mu\tfrac{1}{2}\tau_3\psi + \tfrac{1}{6}\bar{\psi}\gamma_\mu\psi\right] \\ J_\mu^\pm &= i\bar{\psi}\gamma_\mu(1+\gamma_5)\tau_\pm\psi \\ J_\mu^{(0)} &= i\bar{\psi}\gamma_\mu(1+\gamma_5)\tfrac{1}{2}\tau_3\psi - 2\sin^2\theta_W J_\mu^\gamma \end{aligned} \tag{5}$$

The field ψ is now an isospinor with respect to the strong interactions, and the isospin structure of the hadronic

electroweak currents is now transparent. We shall make use of these observations. It is important to note that the states may be very complicated in terms of quarks, for example they may contain any number of $(\bar{q}q)$ pairs, but the currents are simple, and are given by Eq.(5).

3) Dynamic evidence for quarks is obtained from deep inelastic electron scattering (e,e') from the nucleon [11]. The situation is illustrated in Fig.5. For elastic scattering (or inelastic scattering to one of the discrete nucleon levels) there is a form factor which falls with q^2. At large values of $1/x=2m\nu/q^2$ the cross section is independent of q^2, as illustrated in Fig.6, which indicates that one is scattering from point-like constituents [11]. The statement of Bjorken scaling is that the two-variable response surface becomes a function of a single variable

$$\nu W_2(\nu, q^2) \longrightarrow F_2(x) \qquad (6)$$

The experimental structure functions for the proton determined at SLAC are shown in Figs. 7-8. The quark-parton model of Feynman and Bjorken and Paschos allows one to calculate the asymptotic form of the structure functions [11]

$$F_2(x) = \sum_N P(N) \left\langle \sum_i Q_i^2 \right\rangle x f_N(x) \qquad (7)$$

Here P(N) is the probability that a very high momentum proton will have a structure consisting of N point-like constituents ("partons"). The second factor is the sum of the squares of the charges of the partons in this configuration, and $f_N(x)$ is the probability that a parton will carry a fraction x of the longitudinal momentum of the nucleon in this frame.

Also sketched in Fig.8 is the magnitude of the EMC effect [12]. Here the difference in the cross section/nucleon for deep inelastic muon scattering from 56^Fe and 2^H is measured and found to be different from 0. The EMC effect is a clear and unambiguous demonstration of the modification of the quark structure of nucleons in the nucleus .

QUANTUM CHROMODYNAMICS (QCD)

We consider next the theory of quantum chromodynamics (QCD) which is a lagrangian field theory of the strong interactions binding quarks into hadrons [13]. An extra intrinsic degree of freedom called color is introduced for the quarks. It can take three values (say red, green, blue). The quark field thus has the structure

$$\psi = \begin{pmatrix} u \\ d \\ s \\ c \end{pmatrix} \rightarrow \begin{pmatrix} u_R & u_G & u_B \\ d_R & d_G & d_B \\ \vdots & \vdots & \vdots \end{pmatrix} \equiv (\psi_R, \psi_G, \psi_B) \equiv \psi_i \quad ; i = R, G, B \tag{8}$$

The individual components of each colored field, u,d,s,c are now refered to as quark flavors. The weak and electromagnetic currents in this model are independent of color. They are written in terms of the three-component (actually multicomponent!) field $\underline{\psi} \equiv \begin{pmatrix} \psi_R \\ \psi_G \\ \psi_B \end{pmatrix}$ as follows

$$\bar{\underline{\psi}} \gamma_\mu \underline{\psi} \equiv \bar{\psi}_R \gamma_\mu \psi_R + \bar{\psi}_G \gamma_\mu \psi_G + \bar{\psi}_B \gamma_\mu \psi_B \tag{9}$$

Thus each color field has an identical coupling constant as indicated in Fig.9.

QCD is a local gauge theory built on the symmetry $SU(3)_c$. The lagrangian density of QCD is written as follows

$$\mathcal{L}_{QCD} = -\bar{\underline{\psi}} \gamma_\mu \left(\frac{\partial}{\partial x_\mu} - \frac{i}{2} g \underline{\underline{\lambda}}^a A^a_\mu(x) \right) \underline{\psi} - \frac{1}{4} \mathcal{F}^a_{\mu\nu} \mathcal{F}^a_{\mu\nu}$$

$$\mathcal{F}^a_{\mu\nu} = \frac{\partial}{\partial x_\mu} A^a_\nu - \frac{\partial}{\partial x_\nu} A^a_\mu + g f^{abc} A^b_\mu A^c_\nu \tag{10}$$

Here $A^a_\mu(x)$ with a=1,...,8 are gluon fields. They are massless and carry color. Since the lagrangian is written in terms of the fields $\underline{\psi}$, the color interactions are evidently independent of flavor, that is, each flavor of quark has the same coupling to the gluon field as is illustrated in Fig.10.(*)

The Feynman rules for QCD may now be derived. The components are illustrated in Fig.11. The ghost loops in the vector meson amplitudes are a technical complexity required in order to keep the theory unitary, covariant, and gauge invariant.

The truly remarkable feature of this theory is asymptotic freedom [13]. This means that when all the momenta in a process are very large, the renormalized coupling constant describing the process becomes very small. At very high momenta, or at very short distances, one can thus do perturbation theory.

It is also true that quarks and color must be confined since we apparently do not observe them in the laboratory. There are strong indications based on lattice gauge calculations that, due to the nonlinear nature of the couplings, QCD actually leads to the confinement of quarks and color. The nature of the confinement region, since

(*) A quark mass term of the form $\bar{\underline{\psi}} \underline{\underline{M}} \underline{\psi}$ where the mass matrix $\underline{\underline{M}}$ is diagonal in color can readily be included in Eq.(10).

there one is dealing with a strong coupling theory, is still an open question.

It is essential to note that in the standard model of the strong, electromagnetic, and weak interactions based on $SU(3)_c \otimes SU(2)_W \otimes U(1)_W$ the gluons have no weak or electromagnetic interactions .

ACCOMPLISHMENTS

We focus here on two of the accomplishments of the model of the fundamental interactions discussed above.
1) The phenomena of Bjorken scaling observed in deep inelastic electron scattering (e,e') indicates the existence of point-like constituents in the nucleon and provides dynamic evidence for quarks.
2) The parity violation observed in deep inelastic scattering (e,e') can be understood within this framework. Let us digress briefly to discuss this topic.

In addition to the electromagnetic interaction of the electron mediated by the exchange of a photon, there is in the standard model a weak neutral current interaction mediated by the exchange of a Z^0 as illustrated in Fig.12. Since the Z^0 is very heavy, this second term will always play a negligible role at low energies, of order of the weak interactions, unless one looks at a signal which is directly proportional to the presence of the weak interaction itself. Such a signal is provided by parity violation, which is forbidden to all orders in the electromagnetic interaction. The situation is illustrated in Fig.12 where the parity violating effect under consideration is the difference in cross section of right- and left-handed longitudinally polarized incident electrons. The general expression for the parity violating asymmetry within the framework of a V-A theory of the weak interaction is given by [1,14]

$$\left[\frac{d\sigma_\uparrow - d\sigma_\downarrow}{d\sigma_\uparrow + d\sigma_\downarrow}\right]\left[W_2^\gamma \cos^2\frac{\theta}{2} + 2W_1^\gamma \sin^2\frac{\theta}{2}\right] = \left\{b\left[W_2^{int}\cos^2\frac{\theta}{2} + 2W_1^{int}\sin^2\frac{\theta}{2}\right]\right.$$
$$\leftarrow A \rightarrow \quad \left. - a\left(\frac{2W_B^{int}}{M_T}\right)\sin\frac{\theta}{2}\left(q_0^2\cos^2\frac{\theta}{2} + q^2\sin^2\frac{\theta}{2}\right)^{1/2}\right\}\frac{G\,q^2}{4\pi\alpha\sqrt{2}} \qquad (11)$$

In the standard model we have

$$b = -1$$
$$a = -(1 - 4\sin^2\theta_W) \cong 0 \qquad (12)$$

Here b governs the axial-vector strength of the leptonic interaction and a the vector strength. Note that if $(\sin\theta_W)^2 = 1/4$, which is very close to the currently accepted value, then the parameter a vanishes.

The response surfaces appearing on the right-hand

side of Eq.(11) come from the analysis of the resonse tensors obtained from the following combinations of currents

$$W_{1,2}^{int} \text{ from } \left(J^{(0)}J^{\gamma}+J^{\gamma}J^{(0)}\right)$$
$$W_{3}^{int} \text{ from } \left(J_5^{(0)}J^{\gamma}+J^{\gamma}J_5^{(0)}\right) \tag{13}$$

The first involves the interference of the vector part of the weak neutral current and the electromagnetic current and the second the axial vector part. In this same notation, the double-differential cross section for electron scattering from a hadronic target, for example, takes the familiar form [1]

$$\left(\frac{d^2\sigma}{d\varepsilon_2 d\Omega_2}\right)_{ee'}^{ERL} = \frac{\alpha^2\cos^2\frac{\theta}{2}}{4\varepsilon_1^2\sin^4\frac{\theta}{2}}\frac{1}{M_T}\left[W_2^{\gamma}+2W_1^{\gamma}\tan^2\frac{\theta}{2}\right] \tag{14}$$

Let us combine the results of the previous discussion to obtain a simple expression for the parity violation observed in the SLAC experiment on deep inelastic scattering (e,e') from deuterium 2^H [15]. We take the model of the nucleon illustrated in Fig.13. We work in the nuclear domain and assume that the proton and neutron are each composed of three quarks, that is, p=(uuu) and n=(udd). In addition, we allow any number of gluons. We make use of the general expression for parity violation given in Eq.(11) and specialize to the case where $(\sin\theta_W)^2=1/4$ so that $\underline{a}=0$. We also specialize to the forward direction where the scattering angle $\theta \to 0$ as in the SLAC experiment. The use of the quark-parton model (Eq.(7)) then provides a very simple expression for the required ratio of response surfaces

$$\left(\frac{\nu W_2^{int}}{\nu W_2^{\gamma}}\right) = \frac{\left\langle 2\sum_i Q_i^{\gamma}Q_i^{0}\right\rangle_{3\text{-quark}}^{n} + (n\rightleftharpoons p)}{\left\langle \sum_i (Q_i^{\gamma})^2\right\rangle_{3\text{-quark}}^{n} + (n\rightleftharpoons p)} = \frac{4}{5} \tag{15}$$

The required charges are immediately obtained from Eq.(5) and Table I. and the result is just 4/5. Note that the neutron and proton response surfaces are added incoherently here since one is adding cross sections. The result is now the following very simple expression for the parity violation asymmetry

$$A_d = -\frac{Gq^2}{4\pi\alpha\sqrt{2}}\cdot\frac{4}{5} \tag{16}$$

It is compared with the SLAC data in Fig.14, and the agreement is all that one could ask.

We discuss one example of parity violation in electron scattering (e,e′) from a nuclear target. Consider elastic scattering from a 0+ nucleus. In this case the matrix element of the axial-vector current vanishes identically, and the parity violating asymmetry takes the following form

$$\mathcal{A} = \frac{G q^2}{2\pi\alpha\sqrt{2}}\, b \left[\mathrm{Re}\, \frac{F^{(0)}(q^2)}{F^{(\gamma)}(q^2)} \right] \tag{17}$$

This relation holds in any V-A theory of the weak neutral current interactions. Consider now the standard model in the nuclear domain where the currents have the detailed structure of Eqs.(5), and assume that the target nucleus has isotopic spin T=0. In this case, only the isoscalar parts of the currents can contribute and we have the effective relation

$$J_\mu^{(0)} \doteq -2\sin^2\theta_W\, J_\mu^{\gamma} \tag{18}$$

This implies a precise relation between the weak neutral current form factor and the electromagnetic form factor given by

$$F^{(0)}(q^2) = -2\sin^2\theta_W\, F^{(\gamma)}(q^2) \tag{19}$$

Thus, in the standard model we have

$$\mathcal{A} = \frac{G q^2}{\pi\alpha\sqrt{2}} \sin^2\theta_W \tag{20}$$

This result is originally due to Feinberg [16]. It is truly remarkable. It holds at all q^2, and is independent of the details of nuclear structure. Thus it holds at wavelengths where only the gross features of the nucleus are observed, to wavelengths where the nuclear structure can be described in terms of point nucleons, down to wavelengths where the baryon meson structure of the nucleus becomes important, and on to wavelengths where the structure of the system is to be described in terms of quarks and gluons. Moreover, whatever process one can think of that contributes to the electromagnetic form factor of the nucleus appearing on the right hand side of Eq.(19), there must be an <u>identical</u> process contributing to the weak neutral current form factor on the left hand side. A test of the strict linear dependence on q^2 in Eq.(20) thus provides a detailed test of the weak neutral current predictions of the standard model of the strong, electromagnetic, and weak interactions

in the entire regime of nuclear structure. An experiment to measure this parity violation with a ^{12}C target is under way at BATES (Moniz).

PICTURE OF THE NUCLEUS

On the basis of this discussion, we arrive at the picture of the nucleus illustrated in Fig.15.

We first observe that the structure of confinement in a many-baryon system is an unsolved problem. The theory of QCD is tractable at short distances or high momenta. It is complicated at large distances or at the boundary of the confinement regions. Progress here will be made both on the theoretical and on the experimental front.

As we have seen, the electroweak interaction in this picture couples to the quarks. These interactions see through the hadronic structure to the interior quark structure. The gluons providing the confinement are absolutely neutral to the electroweak interaction. Furthermore, the electroweak interactions are colorblind.

We can now understand the simplicity of the relations which we previously derived within the framework of the Standard Model. No matter how complicated the nuclear structure in terms of baryons or mesons ($(\bar{q}q)$ pairs) the electroweak interactions can see through this structure to the interior quark structure of the hadrons. The electroweak currents are simple in terms of quarks. The various semileptonic weak and electromagnetic processes then simply probe different components of these basic quark currents.

DISCUSSION

It is an interesting time for nuclear physics. In the first place, we have two different pictures of the nucleus based on different underlying degrees of freedom. Each picture has had striking successes in the appropriate region. Furthermore, we now have a very compelling theory of the underlying strong and electroweak interactions based on $SU(3)_C \otimes SU(2)_W \otimes U(1)_W$. Nuclei, where all of these interactions are present, provide unique microscopic laboratories for testing the assumed structure of the fundamental interactions.

It is instructive to compare QHD and QCD. QHD is a theory of nuclear structure based on baryons/mesons as the underlying degrees of freedom. The theory is simple at large distances, and is presumably correct there. For example, the Paris nucleon-nucleon potential clearly evidences the various meson exchanges at large internucleon separation. On the other hand, QHD is a complicated, strong-coupling theory at short distances.

In contrast, QCD is a theory of hadronic structure based on quarks/gluons as the underlying set of degrees of freedom. It is simple at short distances, where one has asymptotic freedom. It is complicated at large distances where one has a strong-coupling theory and confinement. Presumably QCD will encompass the results of QHD in this regime; indeed, it must do so if it is to be an acceptable underlying theory of nuclear structure.

QUESTIONS

Within this framework, we can pose many interesting questions for nuclear physics (Gross). Consider first the future directions of the QHD description of nuclear structure. Here we need more accurate calculations in the few-body systems, and more detailed experimental tests of this description of the nucleus. Reliable, relativistic QHD calculations of the few-body and many-body nuclear systems are also essential as we probe the nucleus to higher and higher q^2.

Consider next the QCD description of nuclei. Here a crucial problem is to find unique signatures of the different underlying degrees of freedom, the quarks and gluons, in the nuclear many-body system. We want to study the behavior of the multi-quark, many-baryon system which the nucleus provides. On a more fundamental basis, we can say that "Nuclear physics is the study of the strong-interaction aspects of the QCD lagrangian $\mathcal{L}_{QCD}$." (Isgur).

The EMC effect clearly demonstrates a modification of the quark structure functions of the nucleon in the nuclear environment. Can we understand the low x part of the EMC effect where there is currently a difference between the recent SLAC data (Arnold) and the original, much higher q^2 measurements of the EMC?

Another question is why do the simple quark scaling laws appear to work as well as they do? If we accept the fact that we are not yet in the asymptotic regime for exclusive hadronic processes where hadrons are formed and observed in the final state, and will not be there in the foreseeable future (Isgur), one still has to understand the phenomenological observation of simple scaling behavior in a wide variety of processes involving hadrons (Carlson).

The development of a unified theory of the electroweak interactions, and its striking successes, has to rank as one of the great intellectual achievements of our era. It is absolutely essential to continue to put the theory to tests of finer detail and higher precision.

A central question for nuclear physics is where do QHD and QCD, as currently formulated and carried out, give different results? It is very likely that important progress in our understanding of nuclear structure will come from this comparison. I have in mind here the situation with exchange currents. It was only after a long, thorough development based on structureless (n,p) as the underlying degrees of freedom with an interaction mediated by a static two-body potential, that the deficiencies in this description, and the effects of the additional hadronic degrees of freedom of QHD, could be unambiguously identified.

Another basic question is the underlying relationship between QHD and QCD (Carlson, Gross, Isgur). Here a variety of approaches are currently being pursued. One is to make a separation in coordinate space. A well-defined radius R is assumed, inside of which one can (hopefully!) use QCD and asymptotic freedom and outside of which one can have a description in terms of the hadronic degrees of freedom. A second approach (which is promising, but to my knowledge has not yet been fully developed) is to make the separation in momentum space using dispersion relations. The contributions of nearby singularities are given in terms of the observed hadronic degrees of freedom and the contributions of the far-away singularities can be calculated using asymptotic freedom. Still another approach is to assume that QHD provides the most direct description of the baryon/meson phase of nuclear matter, and QCD that of a quark/gluon phase. One can then study, and look for, a phase transition between them.#

WHY CEBAF?

CEBAF is an electron accelerator project for nuclear physics (McCarthy). The accelerator is designed to have the following characteristics:

1. I=240 μa This will provide high intensities for nuclear structure studies with electrons.
2. df=1 With a continuous beam, coincidence experiments will be possible.
3. $\Delta E/E \approx 10^{-4}$ High resolution in the machine will be well matched to the demands of nuclear physics.
4. E=4GeV This energy provides many advantages:
   - It provides a wide range of kinematic flexibility in terms of q^2, W, and Θ.
   - It will be possible to cover most of the interesting nucleon excitations under these kinematic conditions.
   - Improved parity experiments, where $A \propto q^2$, are made possible.
   - The few-baryon systems can be examined out to high q^2.
   - The reactions (e,e′N) and (e,e′2N) can be studied under extreme kinematic conditions.
   - One gets into the scaling region in inclusive (e,e′).
   - The reaction $(e,e'K^+)$, leading to a wide variety of residual hypernuclei, can be studied.
   - With the best available (energy-loss) spectrometers, one has $\Delta E/E \cong 10^{-5}$ and hence at E=4 GeV, ΔE≅40 KeV. This is comparable to the most conceivable demanding nuclear energy level separations. To my mind, this and the first point above are the most compelling arguments for setting 4 GeV as the initial target energy for the machine.

#See in this connection Ref. 17

In the end, what we are discussing here is an experimental tool for the 1990's. It will provide the most precise, accessible probe of matter. The interaction is known, and one knows what is being measured. It is a unique time for nuclear physics. What we are really discussing is a tool and a capability for the next generation of nuclear physicists.

SPECIFIC EXPERIMENTS

I would like to spend a little time discussing specific future experiments utilizing electron accelerators.

A. (e,e') Consider first singles experiments:

1. Parity (Moniz). I look forward to the parity experiment at Bates involving coherent, elastic scattering from ^{12}C. This is my own top priority in the field, for the reasons discussed previously. Precise measurements of the q^2 dependence of A would go far toward testing the picture of the nucleus illustrated in Fig. 15 and discussed in the text.
2. $^3H/^3He$ Comparison (Moniz, Hajduk). The three-body system is fundamental in nuclear physics. A comparison of elastic (and quasi-elastic) scattering from these two systems will allow a separation of the isovector exchange currents, which, at least at long-range, are calculable. Tritium experiments out to higher q^2 are currently underway at Bates and Saclay.
3. ^2H magnetic form factor $B(q^2)$ at high q^2 (Arnold). This experiment, given the top priority at the new NPAS program at SLAC, pushes our understanding of the nucleus to the extreme.
4. Discrete nuclear states at high q^2 (Moniz). One way to examine the short distance structure of nuclei is to look at the form factors for discrete nuclear transitions out to very high q^2 (Fig. 16). Systematic studies with a wide variety of levels are likely to teach us a great deal about the transition from traditional nuclear physics, to QHD (c.f. Fig. 4), to QCD descriptions of nuclei. Several exploratory experiments of this type are underway at Bates.
5. Further precise EMC studies (Arnold). The EMC effect provides a direct measurement of the modification of the quark structure function of the nucleon in the nucleus. As such, further precise studies are called for. This includes measurements of the A and q^2 dependences, and spin-dependent effects. Further theoretical development of the interpretation is also necessary. For example, what is the role of shadowing, and can it explain the difference in the low x results of EMC and SLAC?

B. (e,e'X) Consider next coincidence experiments (Moniz).

1. (e,e'N) The measurement of this process, under extreme kinematic conditions, promises to push our understanding of nuclear structure to the limit. This is just what we need in order to learn something new.
2. (e,e'2N) Again, measurement under extreme kinematic conditions will tax our understanding of the nucleus. Measurement of this process under the condition of large relative momentum of the

ejected pair may be the only way we can get unambiguous information on short-range nucleon-nucleon correlations in nuclei.

3. $(e,e'K^+)$ This experiment, done with high resolution, may in fact be the best way of studying hypernuclear physics (Donnelly, Hecking). If so, it opens a whole new dimension of nuclear structure.
4. $(e,e'\Delta)$ From this experiment we learn about the propagation of the final excited state of the nucleon in the nuclear medium (Arnold, Moniz).
5. $(e,e'\pi)$ The electromagnetic probe produces pions throughout the nuclear volume. In this way we can study the properties of this fundamental quantum of the nuclear force in nuclear matter. The reaction $(e,e'\pi^{\pm})$ will also excite collective nuclear oscillations. The process $(e,e'\pi^o)$ can take place coherently on the nucleus.
6. $(e,e'\gamma)$ Even though there is now substantial doubt that exclusive hadronic processes can be calculated with asymptotic QCD in the available range of q^2, perhaps this process can be (since it is still inclusive with respect to the quarks). Perhaps it can be used to examine the propagation of a "hot quark" in the nuclear medium.

C. (ee') + second scattering (Arnold, Gross, Holt).

These experiments may only be feasible with a df≅1 machine. The two highest priority experiments here are:

- Measurement of G_{En} for ^1n through polarization transfer. This experiment will teach us about the quark distributions in the neutron.
- Measurement of F_c for ^2H through the tensor polarization of the recoiling deuteron. This experiment will elucidate the short-distance behavior of the wave function, which is masked in the singles experiment (e,e') by the incoherent contribution of the quadrupole from factor F_Q.

D. Internal targets/nuclear polarization (Donnelly, Jenkins, Holt).

Experiments with either thin solid, or gas jet, internal targets and high-current electron beams in a stretcher ring promise to greatly extend the nuclear structure electron scattering capability, (e.g., to rare and unstable targets). Furthermore, such targets are readily polarized, and in such experiments one can unambiguously separate all the contributing electromagnetic multipole matrix elements, as we heard in the very nice talk from Bill Donnelly. Such a program, which forms a central part of the new Bates proposal (Moniz), has very exciting potential for a whole new era of nuclear structure studies.

SURPRISES?

In my opinion, there are at least two requirements for a project of this magnitude. First, there should be an anticipated "bread and butter" program of high-quality, important physics. Second, there should be a potential for some surprises, for some results that are of Nobel prize caliber. I believe that, given the present stage of nuclear physics, such surprises are quite possible. You can each make up your own list of important questions:

- Do high precision tests (and here I mean really high-quality, high-precision experiments) of electroweak theories show deviations from the standard model?
- Are there collective quark (or gluon) modes in nuclei with unique properties?
- Are there macroscopic color configurations which extend over the nuclear volume?
- Is there quark deconfinement in nuclei?
- Is there quark hopping between baryons?
- ???

COMMENTS

I would like to make a few personal observations on the current situation. We are discussing the construction of a nuclear physics capability for the 1990's. The goal is to provide the tools: The accelerator (McCarthy), spectrometers (Brown, Lightbody), and detectors (Nordberg, Whitney). In my opinion, it is crucial to build a significantly improved capability, unmatched anywhere in the world.

In moving toward this goal, one must be aware of what will get done in the 1980's at existing and upgraded, electron accelerators. For example, there are the following labs and experimental programs: Bates (parity, $^3He/^3H$), Saclay [$^3He/^3H$, (e,e'N)], NIKHEF (e,e'N), and SLAC [$B(q^2)$, EMC effect, $^3He/^3H$, G_E^n ?, parity?].

In my opinion, to make substantial progress in nuclear physics, we must push our picture of the nucleus to the extreme. This can involve

- High q^2, fixed W studies (involving definite final nuclear states).
- High q^2, high ν (or deep inelastic) studies.
- (e,e'N) and (e,e'2N) under extreme kinematic conditions.
- Further tests of y-scaling (Hajduk).
- Refined studies of electroweak interactions.

In discussing the role of quarks in nuclear physics, it is essential to keep in mind where we actually observe quark behavior in nuclei. We have seen that the electroweak interactions couple directly to the quarks (Fig. 15), and the EMC effect directly demonstrates the nuclear modification of the nucleon structure functions. The jury is still out on whether the observation of precocious scaling allows one to make a direct and simple connection with QCD through the invocation of asymptotic freedom and the use of perturbation theory, but there are now convincing theoretical arguments that asymptopia is still well over the horizon (Isgur). This in no way changes the fact,

however, that "nuclear physics is the study of the strong interaction aspects of $\mathcal{L}_{QCD}$." (Isgur).

CEBAF

Let me close with a few remarks on the CEBAF project. These are personal, gratuitous comments and should be taken as such. CEBAF has done well so far. However, it will be an uphill battle from now on. There are several reasons for this. The electromagnetic community is not large. Electron scattering experiments are tough, and it takes a lot of hard work and a lot of experience to get the physics out. It is a little like getting the meat out of a coconut. This is an area of physics where it is very difficult to come in, do a quick and important experiment, and get out again. Furthermore, at the present time, there is a very tough competition for national resources. The scientific community is advancing several major projects: e.g., SSC, CEBAF, LAMPF II, and RHIC. Finally, Congress has to deal with a staggering federal deficit.

It will take a lot of long, hard work on the part of a great many people to make CEBAF go.

It is crucial for CEBAF to get moving, to set directions, and to get staff. CEBAF must establish credibility in the community, and with the funding agencies, that it can carry through with a high-class effort, construct the proposed facilities, and build an absolutely first-rate laboratory.

I believe that ultimately the physics will justify the effort.

Thanks again for the workshop.

REFERENCES

1. J.D. Walecka, "Electron Scattering," ANL-83-50, Argonne National Laboratory (1984)
2. B. Frois et al., Lect. Notes in Phys. 108, Springer, Berlin (1979) p.52
3. C.J. Horowitz and B.D. Serot, Nucl. Phys. A368, 503 (1981)
4. T.W. Donnelly and I. Sick, "Elastic Magnetic Electron Scattering," Rev. Mod. Phys. (to be published)
5. J.M. Cavedon et al., Phys. Rev. Lett. 49, 986 (1982)
6. D. Riska, Nucl. Phys. A350, 227 (1980)
7. E. Hadjimichael, B. Goulard, and R. Bornais, Phys. Rev. C27, 831 (1983)
8. S. Weinberg, Phys. Rev. Lett. 19, 1264 (1967); Phys. Rev. D5, 1412 (1972)
9. A. Salam and J.C. Ward, Phys. Lett. 13, 168 (1964)
10. S.L. Glashow et al., Phys. Rev. D2, 1285 (1970)
11. J.I. Friedman and H.W. Kendall, Ann. Rev. Nucl. Sci. 22, 203 (1972)
12. R.L. Jaffe, Phys. Rev. Lett. 50, 228 (1983)
13. F. Wilczek, Ann. Rev. Nucl. Sci. 32, 177 (1982)

14. J. D. Walecka, "Electroweak Interactions with Nuclei," to be published in: Proc. Conf. on the Intersections Between Particle and Nuclear Physics (R.E. Mischke, ed.), Steamboat Springs, CO (1984).
15. C. Y. Prescott et al., Phys. Lett. 77B, 347 (1978); 84B, 524 (1979).
16. G. Feinberg, Phys. Rev. D12, 3575 (1975).
17. B. D. Serot and J.D. Walecka, "The Relativistic Nuclear Many-Body Problem," Advances in Nuclear Physics, eds. J. Negele and E. Vogt (to be published)

Table I Quark quantum numbers

Field/Particle	T	T_3	Q	B	S	C	Y=B+S+C
u	1/2	1/2	2/3	1/3	0	0	1/3
d	1/2	-1/2	-1/3	1/3	0	0	1/3
s	0	0	-1/3	1/3	-1	0	-2/3
c	0	0	2/3	1/3	0	1	4/3

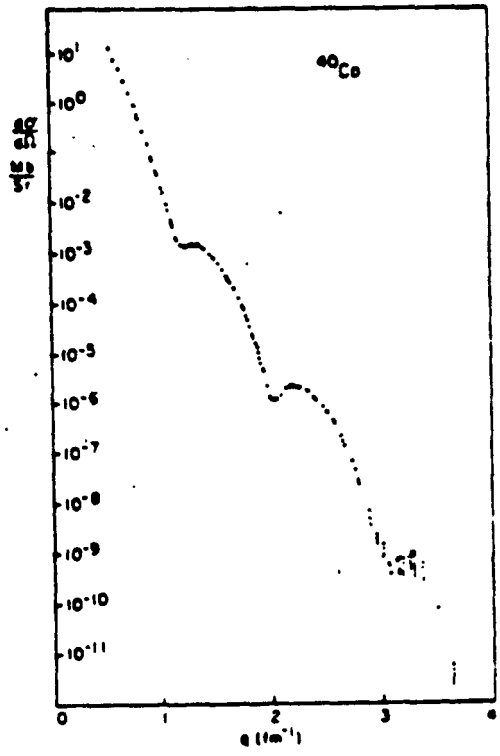

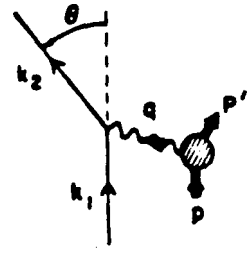

$q^2 = (k_2 - k_1)^2$

$\nu = p \cdot q / M_T$

θ

Fig.1. Kinematic situation for target response in semileptonic processes.

Fig.2. Elastic (e,e) cross section for 40Ca vs. momentum transfer [2]. The scattering here is from the charge distribution.

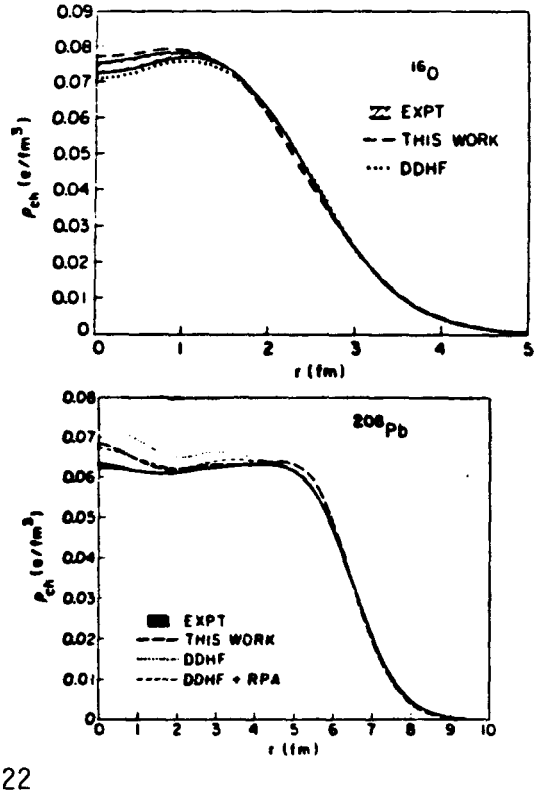

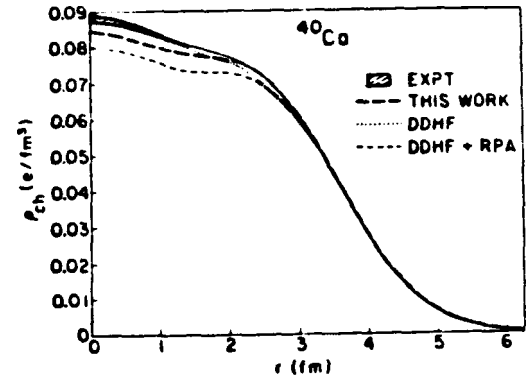

Fig.3. Experimental charge densities with estimated uncertainties from elastic electron scattering (solid lines and shaded areas) and relativistic Hartree calculations of these quantities within the framework of QHD (heavy dashed line). Taken from Ref. 3.

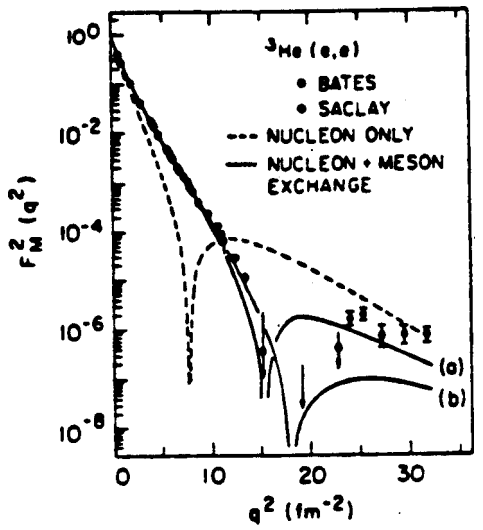

Fig. 4. Elastic magnetic form factor for 3^He(e,e) out to high q^2 [5]. Two exchange current theories are shown [6(b)] and [7(a)].

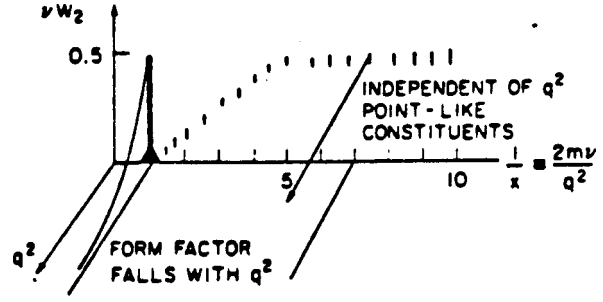

Fig. 5. Qualitative sketch of SLAC results on deep inelastic electron scattering (e,e') from the nucleon.

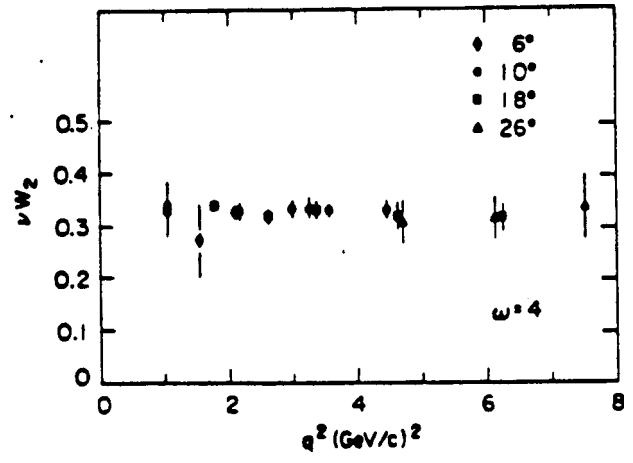

Fig. 6. Experimental demonstration that the response surface νW_2 for the proton is independent of q^2 at fixed $\omega = 1/x = 2m\nu/q^2$ in deep inelastic scattering. Taken from [11].

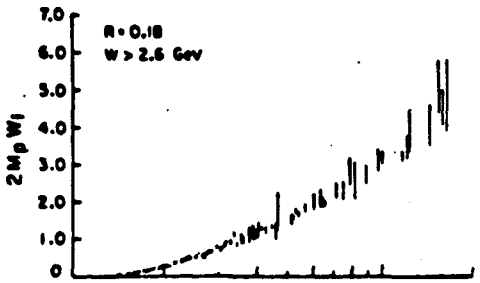

Fig. 7. Response surface $2mW_1$ for the proton as a function of the Bjorken scaling variable $\omega = 1/x$ [11].

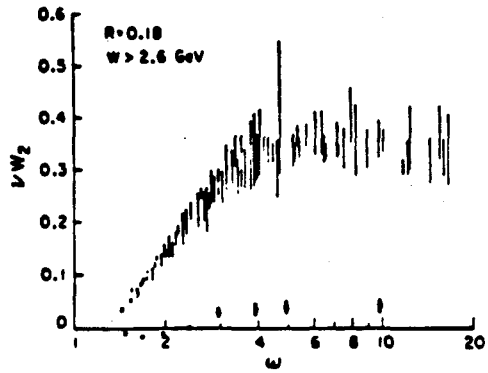

Fig. 8. Same as Fig. 7 for νW_2 [11]. (The modification of this function in 56^Fe observed by the EMC at CERN is shown at the bottom of this figure - see text.)

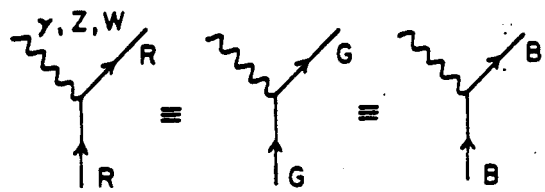

Fig. 9. Weak and electromagnetic quark couplings are independent of color.

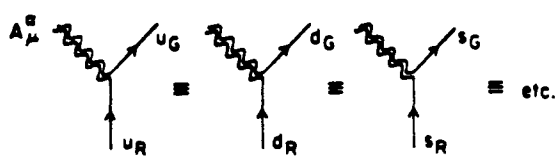

Fig. 10. Strong color interactions of the quarks are independent of flavor.

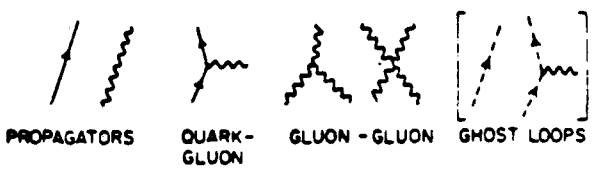

Fig. 11. Components of Feynman rules for QCD.

Fig.12. Parity violation in electron scattering (e,e').

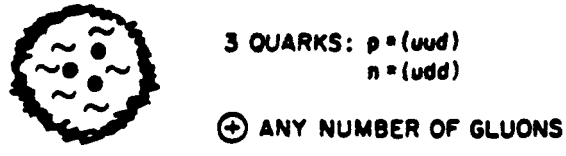

Fig.13. Model of the nucleon.

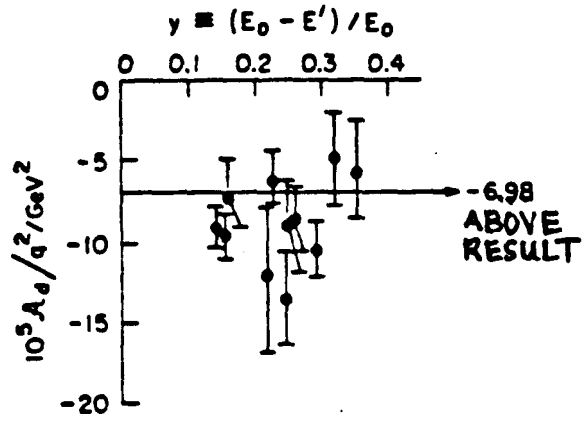

Fig.14. Result in Eq.(16) compared with SLAC data for parity-violation asymmetry in deep inelastic (e,e') from ^{2}H [15].

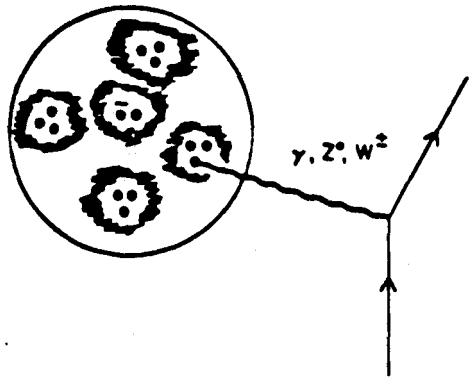

Fig.15. Picture of the nucleus in the Standard Model.

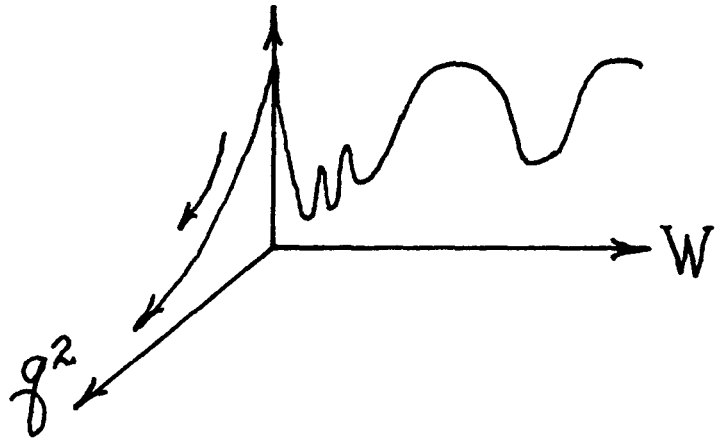

Fig.16. Form factor for discrete nuclear states out to high q^2.

Magnetic Spectrometer Working Group Report

CHAIRMAN: J. W. Lightbody, Jr.
National Bureau of Standards
Gaithersburg, MD 20899

Introduction

The physics program has been discussed a great deal up to this point - in the "Blue Book" and in the various accelerator facility proposals. The major core experiments using magnetic spectrometers that we have considered are shown in Fig. 1. Little new has been said regarding the importance of these experiments. The $(\vec{e},e'x)$ reaction relates to polarization transfer measurements; by measuring the recoil neutron polarization in the deuteron breakup, $d(\vec{e},e'n)$, the neutron charge form factor can be studied, and measurement of the recoil deuteron tensor polarization, $d(\vec{e},e'\vec{d})$, determines the deuteron quadrupole charge form factor. The (e,e'p) reaction in principle measures the one-body spectral function. A great deal of work remains to be done to understand distortion effects and to learn how to deal with off-shell effects in the fundamental electron-nucleon interaction. Hypernuclear studies of deep-hole states will be possible at CEBAF and will complement studies with hadronic probes. It will be possible to measure two-nucleon knockout reactions, (e,e'2N), wich may depend on the pair correlation function for nucleons within nuclear matter. As with other coincidence reactions [(e,e'p), e,e'πp), etc.] final state interactions must be dealt with carefully in order to make statements concerning the one- and two-body momentum distributions. Measure-ment of the pion and kaon form factors through (e,e'π) and (e, e'K) reactions

will also be possible at CEBAF. Electro production of delta resonances in nuclei via the (e,e'πN) reaction will permit measurement of details of the Δ-nucleon interaction. Clearly, many new and interesting physics problems will be accessible at CEBAF. A serious concern facing this working group is how to view the developments that will surely take place in the near term future (~ 6 years) before CEBAF comes on-line. A certain number of the important experiments listed above will be done. We must, therefore, look to new areas that may be opened by much higher resolution (ex. 10^{-5}). We certainly do not want to preclude such activities in the spectrometer design.

Discussion Points

Some of the questions that need to be answered are listed below. We used this list as a starting point.

(1)	How many spectrometers?	3
(2)	$\Delta\Omega$	large
(3)	Superconducting quads	breakeven at 1-1.5 GeV
(4)	Spot size	focus versus imaging
(5)	Dispersed beam	dispersion matching or not
(6)	Angular resolutions (inc. and scatt.)	multiple scattering limit
(7)	Phase ellipse rotation for x/θ correlation	
(8)	Out-of-plane	theory needed at high-q
(9)	What is θ_{min}	relation to quads, beam exit, bremsstrahlung heating
(10)	Spectrometer budget	18 M $(?)

We consider these briefly. The required number of spectrometers is generally

considered to be three, placed around a single pivot in the high current experimental area. Each of these spectrometers will have a large solid angle by present standards. It is clear that superconducting quadrupoles will be used in at least two of these spectrometers as the breakeven point between conventional and superconducting large bore quadrupoles occurs roughly at beam energies of 1-1.5 GeV. If the monoenergetic beam spot size is small enough the spectrometer can be a simple focusing device in the bend plane with the resolving power directly related to beam spot size. Otherwise the spectrometer may require an intermediate focus where a detector array can be used to separate the functions of momentum determination and source location, so that the resolving power does not depend on the monoenergetic beam spot size. With the rather wide energy spread in the primary electron beam, dispersion of the beam is essential. Dispersion matching of the spectrometer may, however, be an overly restrictive constraint. Angular resolution of both the incident and scattered particles is intimately connected to the question of energy resolution through kinematic broadening. Multiple scattering in the focal plane array and/or intermediate focus detectors may place limits on their resolution so care must be used in their application. Item (7) in the above list relates to a possible way to eliminate angle spread in the primary electron beam in favor of an extended horizontal beam spot. Item (8) is self-explanatory. The minimum scattering angle accessible to the spectrometer strongly affects the design of the first quadrupole. At small angles the primary beam must clear the quadrupole flux return yoke. Another question concerns the use of superconducting quads at such a far forward angle that bremsstrahlung from the target might represent a serious heating proglem. Finally, what is the CEBAF budget for spectrometers and what can be obtained with it?

Spectrometers

Figure 2 indicates our revised specifications for spectrometers. The main change is reduction in the 4 GeV spectrometer momentum acceptance to 10%. The 2 GeV spectrometer resolution requirement of 10^{-5} suggested by the hypernuclei experiment proponents seems unnecessarily high. The 10^{-4} figure listed is over the full acceptance of the spectrometer, however, and we expect that 10^{-5} could be approached at much reduced acceptance should future experiments require this. Some means of improving angular resolution will have to be devised before 10^{-5} energy resolution is achievable.

There are design alternatives to be considered. Should a spectrometer be dedicated in the sense of having fixed optics, or should we consider modular design. The modular concept would allow trade-offs in the product of resolving power (R), solid angle ($\Delta\Omega$), and momentum acceptance (ΔP). Other short term design goals are to achieve as near to an optimum design of a spectrometer as possible. With this as a benchmark we can then examine the R, ΔP, $\Delta\Omega$ trade-offs in light of various theorems K. Brown has suggested relating to maximum solid angle, optimum dipole gap size, and total cost. Also, we must consider spectrometers with large target capabilities.

Comments

Figure 3 indicates a few of the comments made during the workshop. Dispersion matching is a technique employed at Bates, NIKEF, and other labs for achieving high resolution data using an incident beam with a comparatively broad energy spread. The technique has been generalized to include double-arm measurements as well. Clearly, successful systems have operated in this fashion. It does, however, require all bend planes be in the plane of the beam dispersion. For out-of-plane measurements the resolution will be

worsened. As pointed out at the bottom of Fig. 3, the azimuthal and polar acceptances in the QQD type are not optimum. For vertical bend spectrometers the larger acceptance is in the scattering angle plane where cross section variations are the greater. Ideally, we would like a narrow θ-acceptance with broader ϕ-acceptance. Obviously, a horizontal bend plane would overcome this drawback. However, dispersion matching with, for example, one spectrometer bending horizontally and one vertically, is then precluded. Also, with one spectrometer in each plane there are possibly severe mechanical overlap problems. An alternative to dispersion matching is simply to disperse the beam in a well-defined way according to momentum and use software to compute the particle momentum and trajectory. This may require an intermediate focusing system as with EPICS, and as discussed in the Argonne GEM proposal. It is not clear yet how such a system would work in the environment of a 100 μA electron beam and must be looked at very carefully. It was pointed out that the cost of a spectrometer is tied strongly to its solid angle and resolving power and a good deal of effort should be put into looking at how well the beam spot can be defined. In the case of re-imaging techniques, we are probably limited to an order of 100 μ by detector resolution. This is, of course, a very small effective spot size. The question of whether a spectrometer of this design would work in the high background environment of an electron beam machine is important here as well. The alternative is to simply focus the beam as small as possible on target using quadrupoles. This, however, opens the question of beam heating. We need to seriously look at the question of what power densities on target can we reasonably expect to handle.

As a guide for the present design effort, EPICS was suggested as a close optimum spectrometer design for a cost scale. The EPICS specifications are also shown in Fig. 3, and its cost in 1974 was roughly 1.5 M$. If this cost can be scaled to present dollars and to the CEBAF energies, we see clearly that significant breakthroughs in design are called for if we are to fully equip the pivot post with three spectrometers.

K. Brown has suggested that for $(Q)^n$ $(D)^n$ type spectrometers the maximum solid angle places limits on the quadrupole pole tip fields and length as shown in item (4) of Fig. 3. For a 50 msr spectrometer operating at 4 GeV/c a 1 m. quadrupole will require a pole tip field of 4 T. This sets a scale for the R & D program on superconducting quads which we are recommending.

Figure 4 shows several ideas Blomqvist had for CEBAF spectrometers. The first of these is a QQDDQQ system suitable for long target applications. This is a symmetric system in the bend plane designed to have an essentially unit transfer matrix in coordinate space which means that the target image will be well defined and the detector can be so oriented to lay along that image or the software compensated to recognize this image. The design as given is for a 500 MeV/c system and permits use of a 6 cm target. Scaled to 2 GeV/c we can then tolerate a 24 cm long target. The design philosophy for any large target system is to not let the transverse magnification get too large. In the event that it does get too large, the dipole gaps grow so much as to make the system impractical.

Another example of Blomqvist's, one with a large solid angle ($\Delta\Omega$ = 70 msr), is shown at the bottom of Fig. 4. The acceptance aspect ratio ($\Delta\theta$:$\Delta\phi$) is 1:3, whereas we would prefer a ratio of 3:1 for a vertically bending system. In the conventional notation $\Delta\theta$ is in the bend plane, $\Delta\phi$ is in the

transverse plane. This design uses point-to-point focus in the bend plane, and parallel-to-point in the transverse plane for good scattering angle definition. A cross-over point in the transverse optics between the dipoles minimizes the dipole gaps. Blomqvist pointed out that if the system were to be operated with the bend plane horizontal, it would be desirable to have the (θ/δ) transfer matrix element close to zero in order to decouple the determination of scattering angle and particle momentum.

Figure 5 shows the relation between kinematic broadening and primary beam energy. We are used to operating in the regime of (E_1/M_T) below 0.1, where angular definition to 1 mradian induces at most 10^{-4} in momentum uncertainty. In the CEBAF region k_{max} can be near unity which translates an angle uncertainty of 1 mradian into an energy uncertainty of roughly 10^{-3}. This demonstrates rather sharply the need to consider systems with good angle definition.

Neuhausen of Mainz discussed a QDD spectrometer with p_{max} = 900 MeV/c, $\Delta\Omega$ = 30-35 msr and Δp = 20%. A schematic of this device is shown in Fig. 6. Maximal use of wire chambers and software connections is being made to hold down the cost of the spectrometer.

Recalling the previous discussions of optimum angular acceptance for electron scattering, narrow azimuthal acceptance is needed to limit the cross section variation across the acceptance, and to focus on the kinematics of interest. Because of the relative insensitivity of the scattering angle to polar angle variations, $\cos\theta_{sc} = \cos\theta_{azimuth} \cos\theta_{polar}$, the polar acceptance can and should be as large as possible to maximize the count rate. For a large azimuthal acceptance of $\pm$ 15° the detector system could easily be exposed to one or more orders of magnitude variation across the acceptance,

with events of interest confined to a few degrees at one extreme. In a similar vein we should carefully examine the need for large acceptance, large solid angle electron scattering spectrometers for knock-out reactions. Fig. 7 schematically indicates the knock-out reaction kinemat-ics. Operating at 4 GeV: $\theta_e = 45°$ with a 20-50 msr proton spectrometer centered on $\vec{q}$, the proton momentum distribution is probed out to roughly the Fermi momentum. If, in fact, we operate $\Delta\Omega_p$ far from quasi-free kinematics for probing high momentum components of the spectral function the cross section drops enormously, as much as an order of magnitude for every 100 MeV/c in nucleon momentum. Under such extreme variations in cross sections, it is not clear whether a large electron spectrometer acceptance is desirable. Obviously, we need not use all the available acceptance, but the cost of this large solid angle for a 4 GeV spectrometer is enormous. Details of kinematic and dynamical variations across the acceptance must be weighed carefully in designing the coincidence spectrometers.

Recommendations

Figure 8 summarizes our recommendations. First, we must proceed with trial designs for spectrometers to set a scale from which we can start realistic planning - budget, experimental hall, beam transport layouts, experimental trade-offs, etc. We expect superconducting technology will be an integral part of these designs. We do not know the limitations in this latter area and should address the subject at an early stage in the design.

The laboratory should provide two positions for the above effort. One position should be largely directed towards spectrometer design, the other towards cryogenic technology. We estimate that 250 K$ should be budgeted during the first year of CEBAF operation, to cover salaries, travel, consulting, and contractual arrangements.

We recommend that the management establish an external "core group" to meet every 3-4 months, and to work in conjunction with the CEBAF staff to optimize the spectrometer capability and review the designs. This format was successfully used in developing the HRS facility at LAMPF. Travel funds would be required for this purpose.

Finally, the CEBAF staff and "core group" should maintain strong contact and involvement with the larger body of experimental working groups: (e,e'p), ($\vec{e}$,e'x), hypernuclei, etc. It is expected that these latter groups will ultimately develop into major CEBAF user groups.

Figure 9 lists the attendant participants in the working group and their home institutions.

FIG. 1

PHYSICS PROGRAM

$(\vec{e},e'x)$ polarization transfer

(e,e'p) high and low resolution

hypernuclei $\Delta E \lesssim 100$ keV

(e,e'2N) correlations

π,κ form factors

(e,e'πN)

Serious Concern - We must look at the program and consider that some of these experiments will be done in ~ 6 yrs. We must, therefore, look to new areas that may be opened by much higher resolutions (ex 10^{-5}).

HOW?

FIG. 2

SPECTROMETERS

4 GeV	2 GeV	1 GeV
20 msr	20-50 msr	30-100 msr
10% $\frac{\Delta P}{P}$	20-30% $\frac{\Delta P}{P}$	20% $\frac{\Delta P}{P}$
2.10^{-4} $\frac{\delta P}{P}$	1.10^{-4} $\frac{\delta P}{P}$	1.10^{-3} $\frac{\delta P}{P}$
10-160°	10-160°	10-160°

Design alternatives

- Dedicated spectrometers
- Modular designs permitting

  $R \cdot \Delta\Omega \cdot \Delta P$ trade-offs

Other design goals

- Achieve "optimum" design
- Large target capability

FIG. 3

COMMENTS

(1) Dispersion matching

Pro - successful systems work reliably in single and double arm experiments

Con - dispersion matching unnecessary and expensive

(2) $ tied up in $\Delta\Omega$ and how well the spot size can be defined by magnet optics or imaging

(3) Cost scale for close to optimum spectrometer.

EPICS: $3 \cdot 10^{-4} \frac{\delta P}{P}$, $\Delta\Omega$ = 10 msr, $\frac{\Delta P}{P} \pm 10\%$

(1.5 M$ - 1974) P_{max} 700 MeV/c, wt. 130 ton

(4) Limits on Q-D type spectro $\Delta\Omega$

$\Omega_{max} = \frac{1}{2}\left(\frac{BoL}{B\rho}\right)^2$; $B\rho = 3.3\ P_o$ T-m

50 msr @ 4 GeV, B_o = 4T., L = 1 m.

(5) $\Delta\theta$-$\Delta\phi$ aspect ratio in QQD type systems wrong for cost optimum - (horizontal bends) vs (vertical bends)

FIG. 4

DISCUSSION

(1) Spectometer for long targets - Blomqvist

(sym)

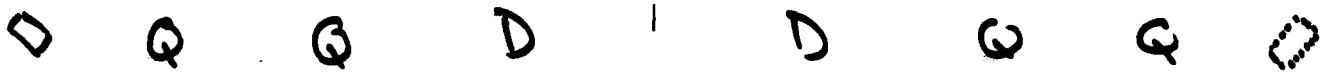

L = 0.3m L = 0.4m ρ = 1 m Δθ = ± 50 mr

φ = .24m φ = 0.30m α = 30° Δφ = ± 150 mr

B = 0.61T B = -.88T B = 1.67T ang. res. ~ 1 mr if angles are measured at end of system.

Scaled to 2 MeV O.K. for 24 cm target

Length = 24m for 2 GeV.

Design philosopy - do not let magnification $\langle y|y \rangle$ blow up

- want good depth of focus

$$\begin{bmatrix} -I & o & (x|\delta) \\ o & -I & o \end{bmatrix}$$

(2) Large solid angle (example)

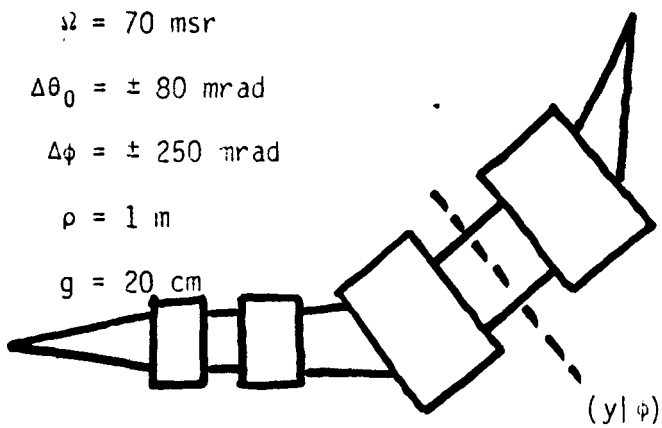

Ω = 70 msr

$\Delta\theta_0$ = ± 80 mrad

Δφ = ± 250 mrad

ρ = 1 m

g = 20 cm

$(x|\theta)$, $(y|y)$ = 0

In horizontal operation want $\theta/\delta = 0$ to decouple scatt & and momentum det.

$(y|\varphi) = 0$ (min. gaps)

Not suitable for despersion matching

FIG. 6

Mainz QQD Spectrometer - Neuhausen

P_{max} = 900 MeV/c , $\Delta\Omega$ = 30-35 msr

$\Delta P \simeq 20\%$

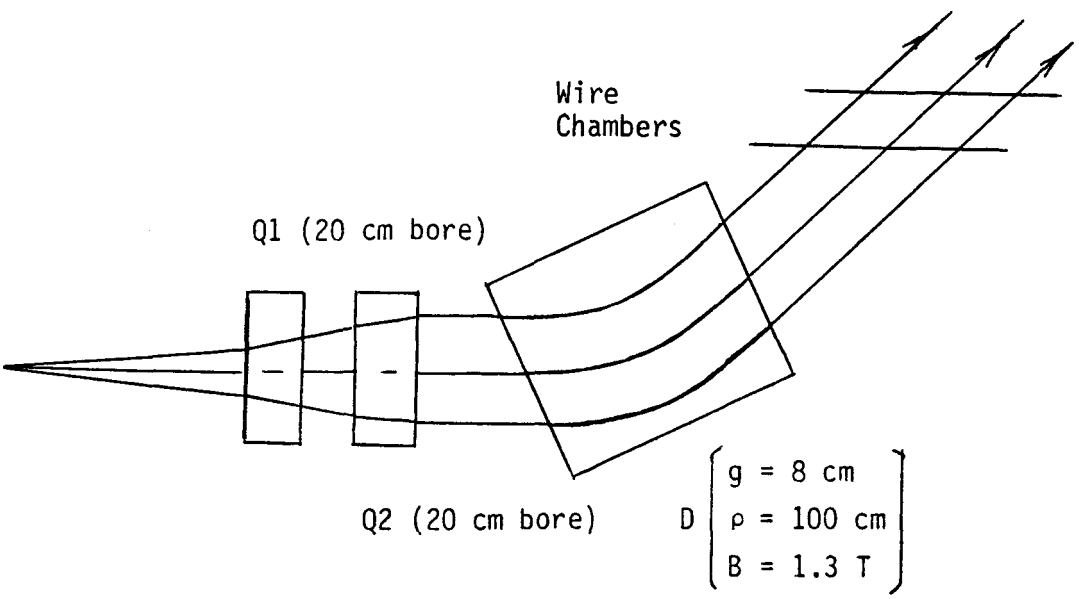

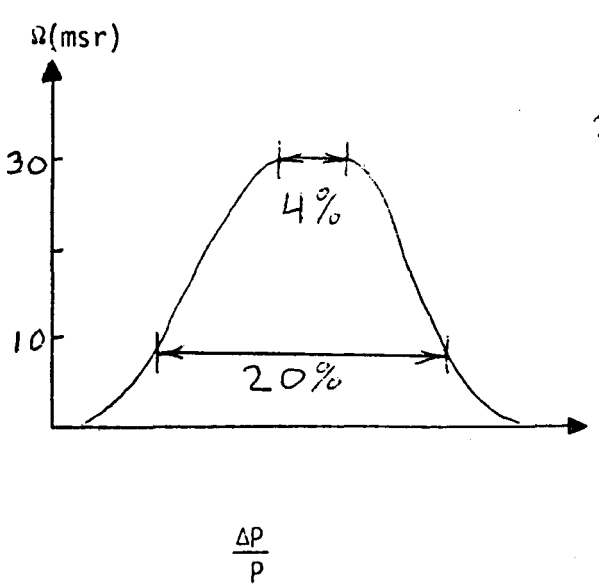

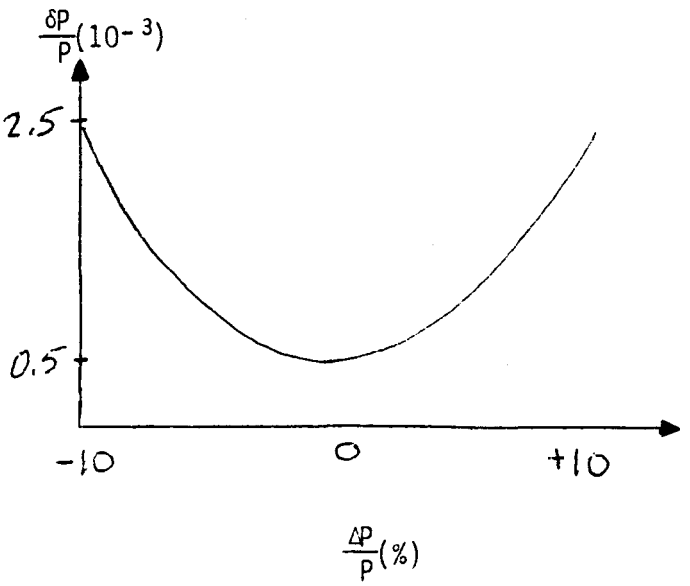

FIG. 7

DISCUSSION

(4) Large dynamical variations across spectrometer acceptance

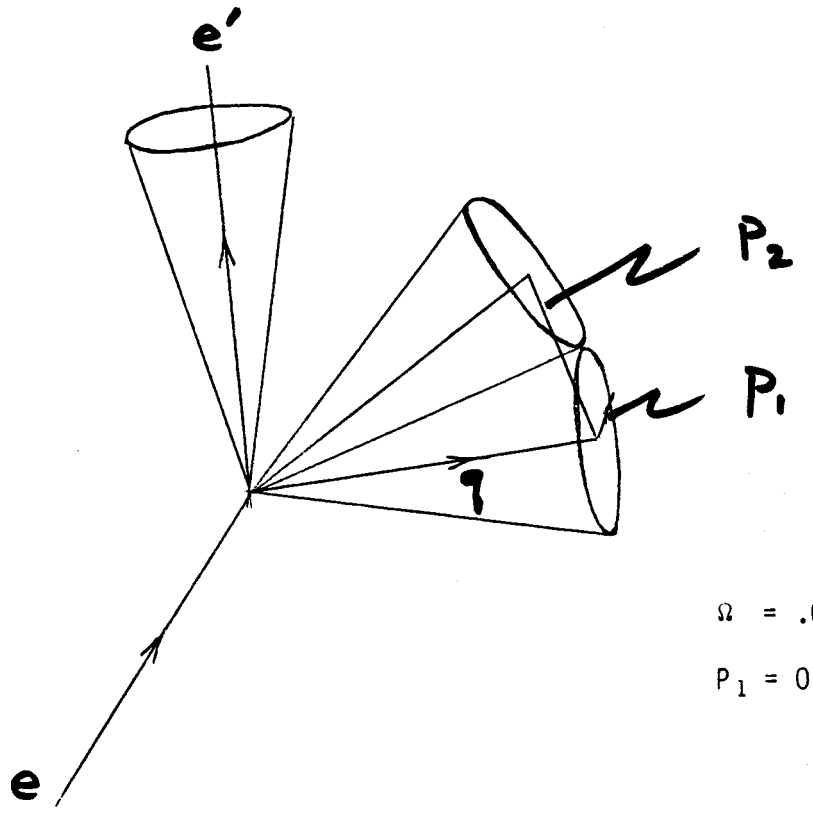

Ω = .02 - .05

P_1 = 0.2 - 0.3 GeV/c

Concern as with (e,e') case that detectors swamped by extraneous events.

FIG. 8

RECOMMENDATION

(1) Proceed with trial designs to establish a scale for realistic planning

- budget
- exp. hall/beam transport layout
- exp. trade offs

We expect superconducting technology will be integral to these designs.

(2) CEBAF should provide two positions for this effort - spectro design, cryogenics (Est. 250 k$ first year - salary, travel, consulting).

(3) Establish a "core group", meeting every 3-4 mos., which will work in conjunction with the CEBAF staff to optimize spectro (Travel funds req'd).

(4) The core group should maintain strong contact and involvement with the larger body of exp. working groups.

FIG. 9

Magnetic Spectrometer Working Group - Attendees

Ralph Minehart	Universiersity of Virginia
J. Michael Finn	Massachusetts Institute of Technology
Karl Brown	SLAC
E. Hayward	NBS
C. C. Chang	University of Maryland
John Winhold	RPI
Paul Stoler	RPI
Girard Audit	Saclay
Ross Hicks	University of Massachusetts
Reiner Neuhausen	University of Mainz
Edward E. Gross	ORNL
W. R. Dodge	NBS
K. I. Blomqvist	Massachusetts Institute of Technology
Carey Stronach	Virginia State University
H. Funsten	College of William & Mary
Ben Zeidman	Argonne
S. Thornton	University of Virginia
H. A. Thiessen	LANL
J. W. Lightbody	NBS

Workshop Report: Tagged Photons - Low Current Electron Beams and Large Acceptance -4π Detectors

R. Roy Whitney

INTRODUCTION

This working group focused on large acceptance detectors systems for both photon and electron beams. Because of the differences in the two beams it was the general opinion that the ideal detector to be used with a photon beam would be somewhat different than that used for an electron beam. The approach taken was to optimize the detector designs for each beam. If dual use appeared later, then this would be considered at that time.

TAGGED PHOTONS

The working group concurred that using a tagging counter and magnet system as presented in Figures 4 and 5 of B. Mecking's paper in this proceedings, a useful flux of 10^7 photons per second could be achieved. This photon beam would be useful for a variety of experiments involving nuclear resonances, mesons, few body systems, some nuclear structure, kaons - hypernuclei and fundamental properties of the photon and nucleon.

4π DETECTORS

To do these experiments a 4π detector system is required, because there are frequently many particles in the final states. Detection of scattered and produced photons is also a must so as to detect nuclear photon decays or neutral pion decays. Figure 7 of B. Mecking's paper shows a view of a possible 4π detector. A superconducting solenoid provides a uniform magnetic field over a volume two meters in diameter and two to three meters long. There is an iron flux return path. The central region is filled with drift chambers for the determination of the vertex and momentum of charged particles.

Between the central drift chamber region and the superconducting coil is a region of total absorption counters for photons and electrons. A detailed list of currently available materials along with their properties is given in E. Nordberg's paper in this proceedings. Because this detector needs to detect photons from a few MeV to multi GeV, CsI was felt to be the best choice of total absorption material. It is also the material that is most affordable.

FORWARD LOOKING MAGNETS

Because of the high forward momentum in the photon beam, many experiments will require a magnet separate from the super conducting solenoid. The group discussed three designs: 1) Simple Dipole, 2) Lampshade, and 3) Perfect 1/r. The simple dipole is easy to use but has the disadvantage of spreading out the electron-positron pairs that are produced at zero degrees. However, the rates for this process are manageable and, depending on availability, it was thought that a simple dipole should be considered as a definite possibility in planning the facilities.

The properties of the lampshade magnet are discussed in detail in the paper by J. Button-Shaffer in this proceedings. The difficulties of tracking particles, the fringe fields and the unusual azimuthal symmetry make the lampshade magnet difficult to use.

The Perfect 1/r magnet was considered to be interesting and worth more consideration. The development of this concept will be pursued during the coming year. Focal properties, etc. will be worked out.

LOW CURRENT ELECTRONS

Large acceptance detectors for low current beams received less attention by the group because the details of the physics have not evolved as far as has the situation with photons. One of the goals of the coming year is to delineate the physics and related experimental requirements.

For example, exclusive measurement of electroproduction of vector mesons and nuclear resonances was discussed. Knowledge of the form factors of the mesons and resonances can be used as a way of discriminating between the various theoretical models as to the constituents of the particle. Again a 4π detector is ideal, but use of CsI is not optimal because of its long decay time. Electron beams tend to produce large numbers of low energy photons.

Detector systems using TOF, lead glass, Cherenkov light, transition radiation, wire chambers and photo diodes were discussed. Some of these detector types are under rapid evolvement at this time.

The general feeling was that several of the experiments involving low current electon beams needed to be modeled. First the physics needed to be modeled and then optimal experimental detector systems considered. Several members of the group took this task on for the coming year. Several others took on the task of investigating those areas of detector technology which are rapidly evolving.

SUMMARY

The group has a fairly firm idea as to what they would like for a tagged photon beam and the 4π detector to go on that beam line. For the associated forward looking magnet there are two possibilities under conceptual development. Those members of the group most interested in the photons are working on details of appropriate components, overall layout and costing.

Those members of the group focusing on low current electron beams are developing the physics models of sample reactions and the experimental possibilities for their measurement.

The group will be meeting in January 1985 to discuss the progress and developments on the project.

SUMMARY OF INTERNAL TARGET WORKING GROUP* MEETING

R. J. Holt

Argonne National Laboratory

The objective of the internal polarized target method is to perform "super-Rosenbluth" separations so that small components of the nuclear electromagnetic currents become accessible, e.g., the electric form factor of the neutron. The method consists of placing a polarized gas target of thickness $\sim 10^{15}$ atoms/cm^2 inside a storage ring where circulating electron currents are typically 100 mA. This approach yields a reasonable luminosity ($\sim 10^{33}$ cm^{-2} s^{-1}) for many experiments. The primary advantages are: (i) an efficient use of electron beam so that there is only minimal demand for the injector, (ii) tensor polarized targets would be accessible for the first time, (iii) direction of the target polarization would be easily controlled with only a few-gauss field, and (iv) background should be minimal since secondary radiation from the target would be negligible. All of these points were covered in more detail in previous talks by T. W. Donnelly and R. J. Holt. Some of the physics which could be performed at an internal target station was discussed and it was decided that a few of the key experiments should set the scale of an internal target hall. Examples of the experiments discussed were measurements of (i) C2/M1 ratio in the N→Δ transition, (ii) electric form factor of the neutron with polarized deuterium and ^{3}He targets, (iii) t_{20} in e-d elastic scattering and (iv) extraction of multipole contributions in electro-excitation of nuclei.

The Argonne group agreed to look into requirements for experiments involving polarized H and D targets, while the Caltech group will look into an experiment involving polarized ^{3}He. A short summary of the experiments including requirements for experimental equipment will be prepared.

The feasibility of delivering longitudinally polarized electron beams to the internal target station in the CEBAF ring will be explored by B. Norum at the University of Virginia. The Argonne group will continue studies of the feasibility of internal polarized $\vec{H}$ and $\vec{D}$ targets. $\vec{H}$ and $\vec{D}$ sources also are being developed independently by groups at the ETH, CERN, U. of Wisconsin and BNL, and thus it is very likely that improved $\vec{H}$ and $\vec{D}$ sources will become available in the near future. The feasibility of a polarized ^3He target will be explored by the Caltech group.

The group recommended that CEBAF plan to include a polarized electron source as part of the project.

The next meeting of this group was set tentatively for January, 1985.

*Group members present at meeting: C. Barnes (Cal. Tech.), T. W. Donnelly, (MIT), B. Fillipone (Cal. Tech.), C. Guarldo (LNF-Frascati), M. Harvey (Old Dominion), R. Holt (ANL), K. Kemper (Florida State Univ.), J. Miller (Boston Univ.), R. Milner (Cal. Tech.), B. Norum (Univ. Virginia), J. Reidy (Univ. Miss.), J. Shafer (Univ. Mass.-Amherst), P. Souder (Syracuse Univ.).

Positron Beams at CEBAF

B. L. Berman
Lawrence Livermore National Laboratory
University of California
Livermore, California 94550

ABSTRACT

The results of the working group on positron beams at CEBAF are presented.

When it appeared that a considerable number of attendees at the CEBAF 1984 Summer Workshop were interested in participating in a working group on positron beams, one was organized. This group met twice (after an initial luncheon meeting) during the latter part of the week; some 26 persons took part in at least one of these meetings. Several questions were addressed during these meetings and although time considerations precluded detailed computations to be carried out, a number of interesting ideas emerged, a few of which were discussed at some length.

The first of these questions is: Why consider the construction of a positron-beam facility? A number of separate topics for study constitute the answer:

(a) Positron scattering from nuclei, in order to determine the dispersion corrections (the two-photon terms) to the electromagnetic interaction;

(b) Monochromatic photons, from (i) annihilation radiation, tagged or

off-angle, (ii) tagged positron bremsstrahlung, and (iii) channeling radiation, forward or back-scattered;

c)Weak-interaction studies, including (i) electroweak interference effects (which, however, require polarized positrons) and (ii) reactions of special interest, such as $d + e^+ \rightarrow p + p + \bar{\nu}$, the inverse of the p-p reaction in the sun;

(d) Solid-state studies of various kinds, particularly beam-solid interactions;

(e) Fundamental constants and symmetries measured with positrons; and

(f) Things we have not yet thought of.

How do we make a positron beam? We do so by conversion of the high-energy, high-current electron beam in a plate of high-Z material (perhaps W-Re), one to two radiation lengths thick. The energy loss in the converter is 25-50 MeV for electrons which do not radiate; the power dumped into the converter is $\lesssim$ 100 kW. The emergent electron beam may be useful for experiments or applications which require only poor beam quality or low currents.

Where would we make the positrons? After consideration of a number of possible sites, it appeared that the most favorable location was just prior to the second double-90° bend of the recirculator (see diagram). Some advantages of this location are that valuable equipment (downstream of the converter) would not be irradiated, electron beams (up to 2 GeV) could be used simultaneously (by pulse switching), and the facilities in all of the end stations could be used for positron beams (simultaneously if so desired).

How many positrons would we make? Extrapolating the conversion ratios and emittances from past experience with the positron-beam facilities at Livermore, Frascati, and Saclay, we estimate a useful flux of 1 to 4 μA of positrons at energies from about 750 to 3000 MeV, respectively. Even accounting for phase-space considerations, about one-third of this flux would

be accepted by the stretcher ring (for those experiments requiring 100% duty factor). In any case, these positron currents are enormous by present-day standards; we truly will have an "antimatter blowtorch."

How much would such a positron-beam facility cost? Our rough estimates were $\sim$ \$0.5 - 1.0 M for the converter facility and magnets, a like amount for water-cooled collimators, slits, and shielding, and another like amount for modifications to the beam-transport system, switching magnets, etc. The total cost would be of the order of 1% of that for CEBAF.

What is the bottom line? In view of the potential uses of a positron-beam facility, particularly those that we have not yet thought of, the relative ease of its installation and use if integrated into the facility at an early stage, and the low cost (the incremental cost per positron is about the same as the cost per electron), we conclude that we would be negligent indeed if we did not include a positron-beam facility as an integral part of CEBAF.

POSITRON BEAMS

Where?

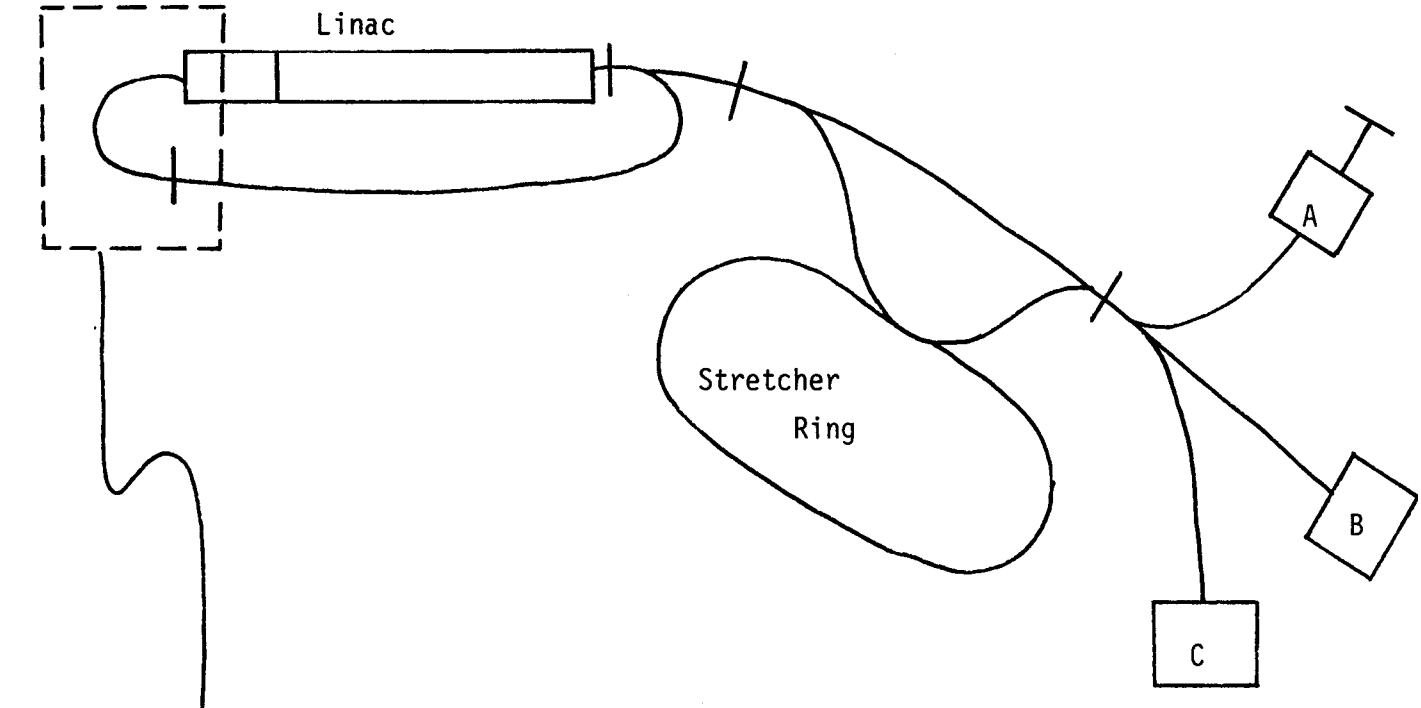

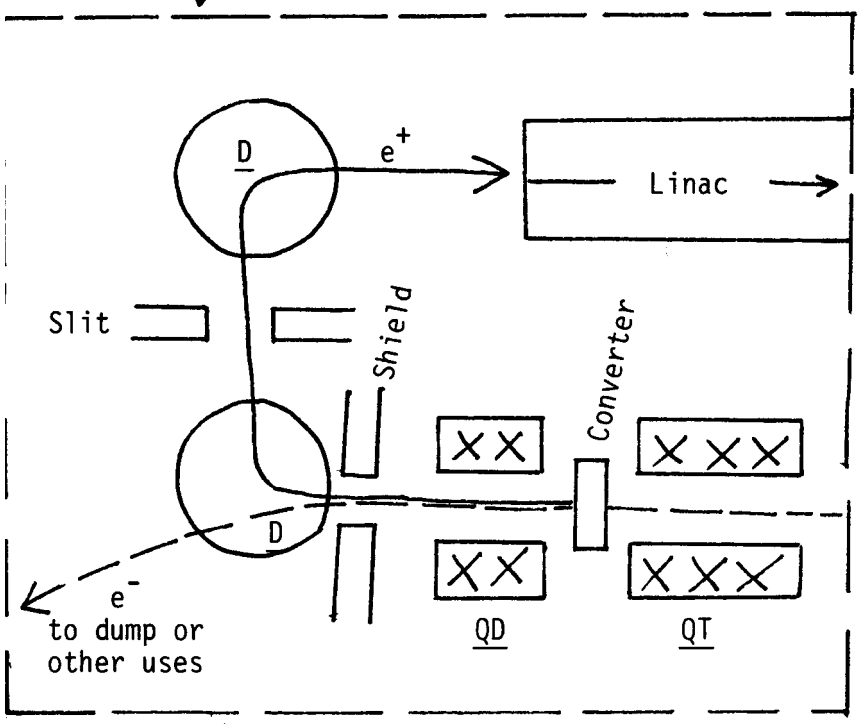

Advantages;

- Does not irradiate valuable equipment
- Simultaneous use of e^- possible (by pulse switching)
- Makes use of all facilities in end stations (all at once if desired)

REPORT OF THE THEORY WORKING GROUP

Franz Gross

Dept. of Physics, College of William and Mary

Williamsburg, VA 23185

The theory working group met four times during the week for a total of more than 6 hours of discussion. The topics discussed divide naturally into the five areas covered below. Over 30 physicists attended at least one of the sessions.

1. Validity of perturbative QCD calculations

The group discussed the issue of whether or not perturbative QCD could be used to understand exclusive processes at high momentum transfer. Nathan Isgur explained some of the details of his calculation of the asymptotic form factors of the pion and the magnetic form factor of the proton, done with Llewellyn-Smith[1] and reviewed in his contribution to this workshop.

The following issues arose from the discussion:

(i) While explanation of inclusive deep inelastic electron scattering is one of the triumphs of perturbative QCD, this success does not in itself quarantee that such techniques will work for the individual exclusive processes which make up the total cross section.

(ii) Calculation of the normalization of the Q^{-4} fall off of G_{MP} requires knowledge of the proton wave function at short distances, which cannot be obtained from perturbative arguments. How reliable are non-relativistic quark model wave functions for this purpose? Another ansatz for the proton wave function used by Brodsky and Lepage[2] and by Isgur and Llewellyn-Smith is $\psi_p \cong N(x_1x_2x_3)^\eta$ where x_i is the momentum fraction of the i^{th} quark. Calculations with this wave function show a very strong dependence on the parameter η, giving an answer about 100 times larger for $\eta \cong 0.6$ compared to $\eta \cong 1.4$. How reasonable is such a parameterization of the proton wave function, and how reliable is the overall calculation?

The normalization of G_{MP} may be more sensitive than other such calculations because the contribution of the leading logarithm is zero.

(iii) Isgur discussed his rigorous bound (see Ref. 1), which he explained was obtained by assuming the proton wave function could be factored into a product $f(x_i)\, g(p_{\perp i})$, where f and g are arbitrary functions.

2. Ideas for new experiments

In the second session, Joe Redish proposed four questions:

1. Do properties of the nucleon change in the nuclear medium (as a result of the nucleon's structure)?
2. Do the properties of a nucleon pair change in the nuclear medium (effective interactions-pair correlations-wave functions vs. six quark bags)?
3. If the structure of the nucleus is very different from a collection of nucleons (and mesons), how would this show up (percolation, quark band structure, delocalized color, etc.)?
4. Are their discrete phenomena associated with quark degrees of freedom that could be observed (six quark dibaryons, collective excitations, grant color resonances)?

Subsequent discussion eventually led to the following list of 9 ideas for experiments. The people listed after each idea agreed to consider the question further.

(i) $d(\gamma,\vec{p})X$ and $d(e,e'\vec{p})X$ - Kim

This would be an extension of the Kamae experiment[3] in which the polarization of outgoing protons from the photodisintegration of deuterons is measured as a function of proton angle. One would search for any unusual features, particularly in the region of 600 MeV photon energy, which might suggest the existance of dibaryons.

(ii) $A(e,e'x)Y$ - Kim

A general electroproduction search for dibaryons or other unusual "bumps".

(iii) $d(e,e'\vec{p})n$ near threshold in the final state - Koonin

This proposal would separate the charge monopole and quadrupole transition form factors describing electroproduction of the $^3S_1$ final state near threshold, hopefully by using the angular distribution and polarization of the outgoing proton to separate this state from the dominant $^1S_0$ transition. It is possible that such a measurement would be easier than separating the deuteron form factors G_C and G_Q, and would give similar information.

(iv) $d(\gamma,p)n$ at high energy - Hiller

Photoproduction of protons, at 90° has been proposed by Hiller and Brodsky as a test of the application of perturbative QCD to exclusive processes.

(v) $d(e,e'N_1^*)N_2^*$ and $p(e,e')N_1^*$ - Gross

Electroproduction of nucleon excited states from the deuteron may be a sensitive indicator of the presence of non-nucleonic degrees of freedom. The electroproduction of excited states from protons is interesting in its own right, but would also be needed for a comparison with the deuteron data.

(vi) $^3H(e,e'2n)p$ - Kim

Electroproduction of two neutrons from tritium may be a sensitive way to measure G_{en}.

(vii) $p(e,e'K)X$

It has long been suggested that the electroproduction of K's may be a way to measure the K meson form factor, similar to what is done with pions. However, because of the large K mass, it may be much more difficult to extract the K meson pole term (which gives the K form factor) from the background than in the analogous case of pion electroproduction. None of the theorists wanted to sign up to work on this problem!

(viii) $\vec{A}(\vec{e},e')X$ - Walecka

Study of inelastic scattering with polarized electrons and targets may teach us new information about quark distributions, similar to what has been learned in the EMC effect. If nuclei are chosen in which the polarization is due to a single nucleon, scattering from that

nucleon may be distinguishable from the other nucleons in the target. Possible nuclei with the desired properties which might be readily polarized are ^{7}Li(?), ^{23}Na(?), ^{39}K, ^{91}Ni, ^{153}Eu, ^{177}Hf, ^{205}Tl, and ^{209}Bi.

(ix) A(e,e'γ)X and p(e,e'γ)X
A(e,e'$\ell^+\ell^-$)X and p(e,e'$\ell^+\ell^-$)X - Walecka and Van Orden
These are Compton scattering processes in which either the initial, or both the initial and final photons are off shell. The ratio of such processes in nuclei to that from free protons might be interesting. Perhaps perturbative QCD would be successful with such comparatively simple exclusive processes.

In addition to these ideas for experiments, several people expressed interest in studying how exclusive channels accumulate to give the total inclusive cross section, particularly in the deep inelastic region. This issue is related to how quarks hadronize.

3. Physics to be learned from coincidence measurements

In the third session, the group discussed what could be learned from the new structure functions which can be measured in coincidence experiments (see Donnelly's talk elsewhere in this proceedings). In Donnelly's notation, the new functions are the transverse-transverse interference term W_{TT}, which accompanies a cos $2\phi_x$ dependence, where ϕ_x is the asymuthial angle of the detected hadron, and the transverse-longitudinal interference term W_{TL}, which accompanies a cosϕ_x dependence. If the detected hadron is in the electron scattering plane, $\phi_x = 0$ or π, so that W_{TL} will show up as an asymmetry in the distribution on either side of the direction of the momentum transferred by the electron.

W. Kleppinger and W. Van Orden reported on their first, preliminary calculations of these structure functions. Kleppinger found that the $p_{3/2}$ state in ^{16}O gives a large W_{TL}, while the same quantity is small for the $p_{1/2}$ state. W_{TT} is small in both cases. Van Orden found that the shapes of both W_{TL} and W_{TT} were sensitive to relativistic effects, and that W_{TT} was also small.

More calculations are eagerly awaited. It was suggested that these calculations may be relevant to the analysis of (e,e'2N) experiments, and that to facilitate comparison of experiments with theory, experimentalists

should be careful to extract each of the W structure functions from their data, whenever possible.

Donnelly has given the most general non-relativistic analysis of the coincident cross section; he finds that his analysis is identical to a relativistic treatment up to and including terms of order $(q/M^*)^2$, when q is the recoil momentum of the final state of mass M*. Hence, only for the lightest targets at the highest momentum transfer is a relativistic treatment necessary. The group thought that relativistic treatments of $\vec{d}(\vec{e},e'n)p$ and $d(\vec{e},e'\vec{n})p$ would be necessary to complete the analysis of the experiments which are designed to extract G_{en}, and that a relativistic treatment of electroproduction from the the three body system would be useful.

5. Work on the Three Body System

The final session of the working group was devoted to discussion of problems which must be solved before all the information contained in electron scattering data obtained from the three body systems can be extracted.

One outstanding problem is the calculation of final state interactions. Scattering wave functions for the three body system are difficult to obtain because the asymptotic conditions are hard to handle in the general case. B. Goulard described a method in which the current operating on the bound state wave function is taken as the source term in a Schrodinger equation for an outgoing wave. The scattering solution generated in this way is much easier to calculate because of the simpler boundary conditions and is precisely the scattering state needed for the final state interactions. This method was successfully used previously[4] to calculate final state effects in the process $\mu^- + {}^3H \rightarrow 3n + \nu$.

Finally, a relativistic treatment of the three body system, in which the current operator is obtained consistently from the dynamics is needed. Such a program has recently been initiated.[5]

REFERENCES

1. N. Isgur and C. H. Llewellyn-Smith, Phys. Rev. Lett. 52 (1984) 1080
2. G. P. Lepage and S. J. Brodsky, Phys. Rev. D22 (1980) 2157
3. T. Kamae, et al, Phys. Rev. Lett. 38 (1977) 468
4. J. Torre, and B. Goulard, Phys. Rev. Lett. 43 (1979) 1222
5. F. Gross, P. Sauer, A. Bulla and H. Henning.

LAMPSHADE MAGNET
for a
Large-Aperture Detector

J. Button-Shafer
University of Massachusetts

The possibility of using a "lampshade" (toroidal) magnet for forward-going particles (downstream from a solenoidal magnet enclosing the target) has been investigated for a trial design.[1] The parameters of the lampshade magnet studied are given in Fig. 1. (This figure shows two of the eight, or more, windings that are arranged symmetrically around the system center-line.)

The questions that were considered (as posed by Roy Whitney) were

1) What focussing properties, if any, would a lampshade magnet display?
2) What would be a reasonable magnet configuration for the expected range of momenta (1 to 4 GeV/c) and range of angles (3 to 25°)?

Useful references that were readily available included papers by D. Hendrie and P. Leconte.[2] (These dealt with design considerations.) Other material of interest was a design talk by B. Pope (on a costly lampshade magnet some five times larger than needed for CEBAF)[3] and a description of an actual toroidal magnet developed for the UA2 detector used to study high-energy $\bar{p}$-p collisions at CERN.[4] (For additional references, not so readily obtained, see the talk of Leconte.[2])

A computer program was written to calculate the components of the magnetic field at any position by combining the contributions from straight-line conductors of arbitrary length, orientation, and position. A second program tracked particles of any specified momentum and initial conditions, position and direction, through the field of the lampshade magnet (and an additional uniform field, if desired).

Fig. 2 shows the dependence of the azimuthal field component B_ϕ on radius, for eight coils spaced symmetrically in azimuth, in a ϕ cross-sectional plane midway through the magnet. (The coil member paralleling the axis is at r = 0.3 m; the outer, or return, coil member is at r = 1.8 m.) We note the approximate 1/r fall-

off of the field. Also, it can be shown that, for any appreciable deflection of particles at, say, $r > 0.8$ m, the maximum value of B_ϕ should be of the order of 2 Tesla; thus the number of Ampere-turns per coil with eight coils should be about 5×10^5 Amp/coil. (These program results are easily checked by using Ampere's Law.)

It was found that flux "leakage" for eight coils was not appreciable (though the use of twelve coils, with 30-degree azimuthal spacing, was also considered); only at positions closer to the windings than 0.1 m, radially or azimuthally, did the radial field component approach 20% of the maximum field (i.e., the B_ϕ value at $r \approx 0.4$ m).

Fig. 3 shows the radial positions at a fixed-z plane just downstream of the lampshade magnet, for rays leaving the target (4 m upstream of the magnet) at various angles and momenta. The most obvious features of these graphs are that there is almost no spatial dispersion, dr/dp, for large-angle emission (because of the weak field at appreciable distances from the axis); and at the lowest range of momenta, r vs. θ is double-valued, and the particle radius r varies only about 10% for the entire range of angles. (Note that the upstream solenoid is ignored for these calculations.)

As to resolution, the curves indicate that a $\Delta p/p$ of $\lesssim 0.2\%$ might be obtained for momenta up to 3.5 GeV/c and angles up to 15° for a maximum magnetic field of 2.0 T.

(During the workshop, the comment was made that the rapid fall-off of B_ϕ with radius could be somewhat diminished by staggering the inner portions of the windings, i.e., displacing radially some of the inner conductors, those paralleling the axis, within each coil package.[5])

A major consideration for the lampshade-magnet design is that the solenoid coils upstream will give particles emitted at non-zero production angles a significant transverse kick. At a modest angle of $\theta \approx 10^\circ$, the transverse (azimuthal) momentum change produced by a 1.0-Tesla solenoidal field extending two meters downstream from the target would be > 0.1 GeV/c; a 2-GeV/c particle would be displaced azimuthally some 15 cm by the time it enters the lampshade magnet (at a radius of 60 cm), for an azimuthal change of about 15°. Thus, a particle would not be in the azimuthal plane in which it started and might intersect a coil plane of the lampshade magnet as it passed through. See Fig. 4.

A final remark: It becomes apparent in looking at toroidal-magnet system designs (those intended for high-energy physics, at least), that detectors are distributed throughout the volume within the bounds of the toroidal magnet. Rather than use just the end points in some plane, physicists are likely to want to determine the trajectories of particles at several points (usually with

drift chambers). Illustrative of this is the lampshade design of B. Pope[3] and also the UA2 toroidal magnet.[4]

Discussion following the talk included, among other remarks, the interesting observation by Bernhard Mecking that any downstream (toroidal) magnet design would not have to keep the material for the inside windings minimal - and hence involve complex structural members to keep the coils from moving under the action of the very large forces they exert on each other. Since the target for the configuration considered would be some distance upstream of the lampshade magnet (within the solenoid that analyzes low-momentum particles), the forward particles would enter the lampshade magnet at radii larger than those of the inner coil members. There could even be a solid copper cylinder for the inside, with thin plates (or spokes?) at the ends of the magnet.

This work was supported by the Department of Energy through Contract No. DE-AC02-76ER03330.

FOOTNOTES

1. See the configuration suggested by Bernhard Mecking for a general-purpose magnetic detector in the October 1983 Mecking summary transmitted by David Jenkins in his January 12, 1984 memorandum to Internal Target and Tagged Photon Workshop members.
   Also see Roy Whitney's working report on "Very Large Aperture Detectors," March 24, 1984.

2. "Di-lepton spectrometer Based on the Lampshade Magnet," by David Hendrie; and "Very Large Solid Angle Spectrometers," by Philippe Leconte, in the "Proceedings of the Spectrometer Workshop," October 10-12, 1983, at Williamsburg, VA.

3. "A General Purpose Toroidal Detector," B. G. Pope, Proceedings of the 1981 Isabelle Summer Workshop, BNL-51443, p. 1072.

4. UA2 Collaboration (Bern-CERN-Copenhagen-Orsay-Pavia-Saclay), Proceedings of the International Conference on Instrumentation for Colliding Beam Physics, SLAC, 1982, p. 169; and CERN Courier, November, 1983, p. 373.

5. This was suggested by B. Mecking. While the peaking of the $B_\phi(r)$ curve can be suppressed by this technique, the small field values at larger radii will be unchanged unless the number of Ampere-turns is increased; and the radial component of field may become larger than desired at smaller radii. (Some staggering of inner conductors is necessary simply because of the limited space available at small radii.)

(assumed) DIMENSIONS:

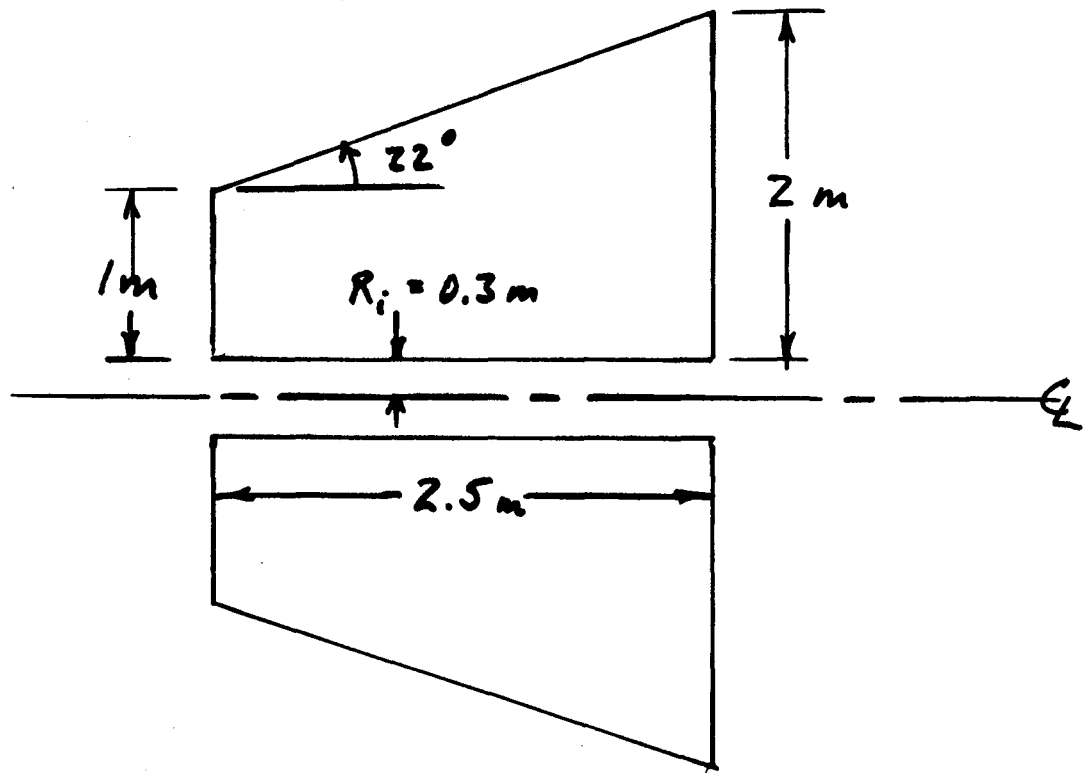

Figure 1.

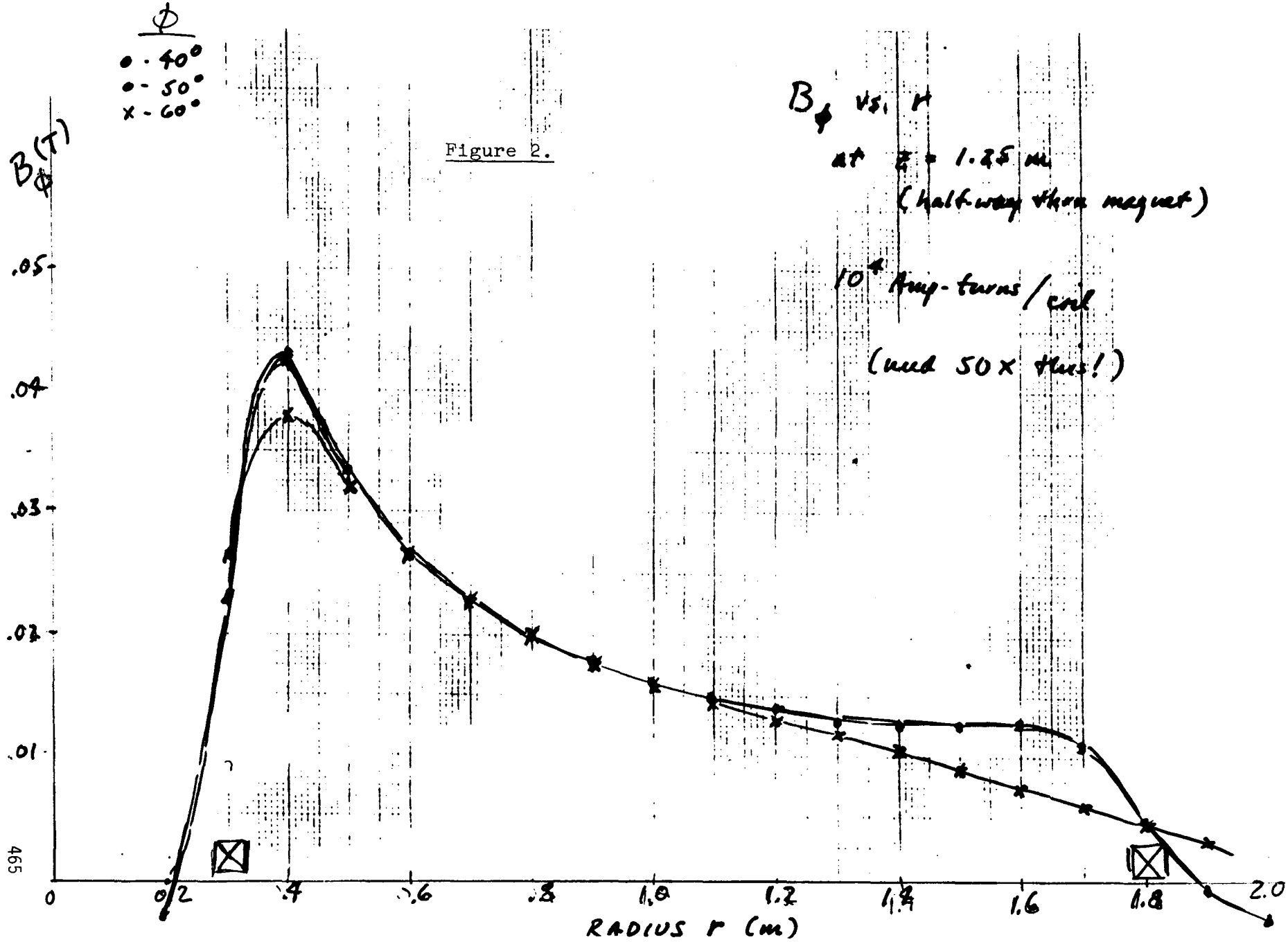
Φ
● - 40°
● - 50°
x - 60°
B_Φ vs. r
at z = 1.25 m
(halfway thru magnet)
10^4 Amp-turns / coil
(need 50× this!)
B_Φ (T)
.05
.04
.03
.02
.01
0
.2
.4
.6
.8
1.0
1.2
1.4
1.6
1.8
2.0
RADIUS r (m)

Figure 2.

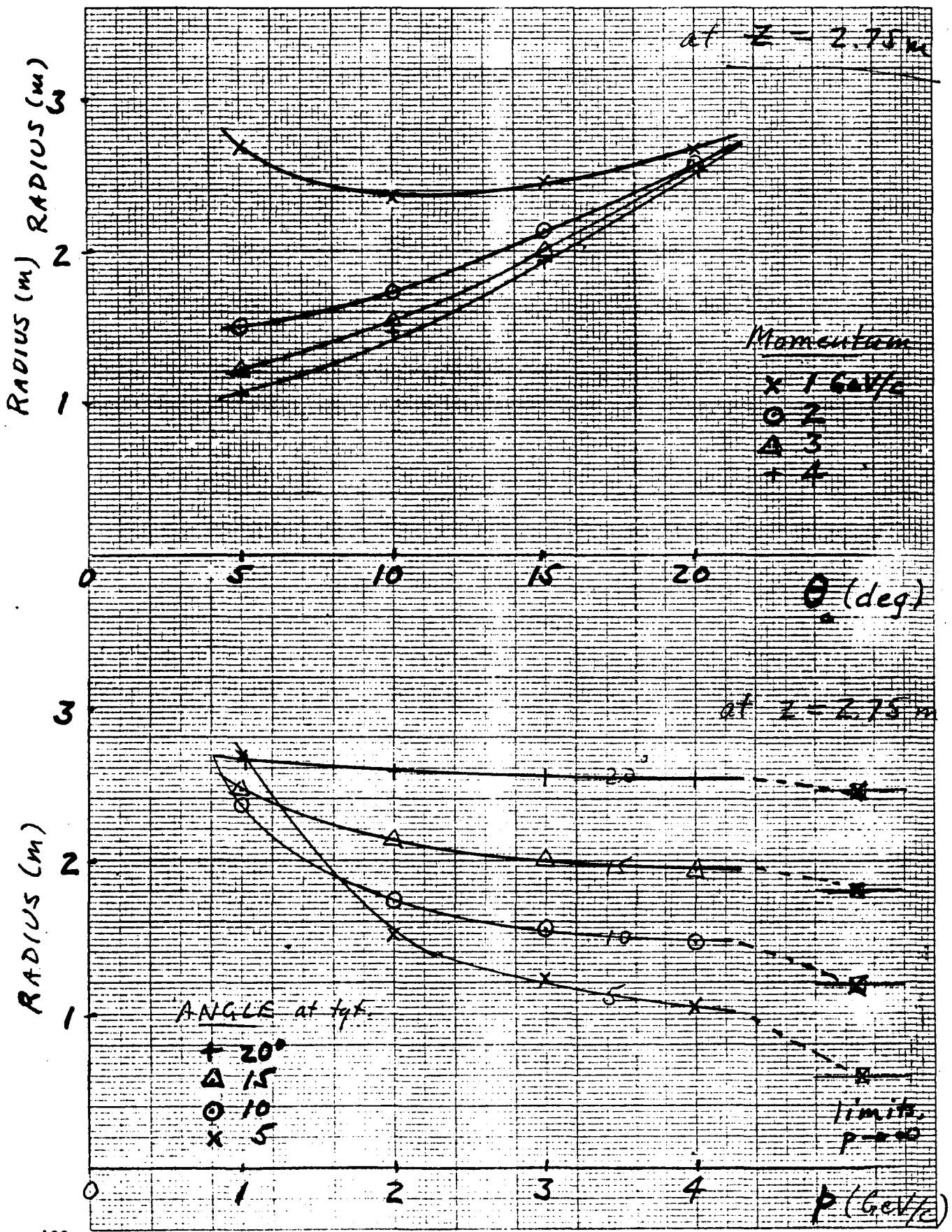
(NO UPSTR. SOLENOID)
at z = 2.75 m
RADIUS (m)
Momentum
× 1 GeV/c
○ 2
△ 3
+ 4
0
5
10
15
20
θ (deg)
at z = 2.75 m
RADIUS (m)
ANGLE at tgt.
+ 20°
△ 15
○ 10
× 5
limit, p → 0
1
2
3
4
p (GeV/c)

Figure 3.

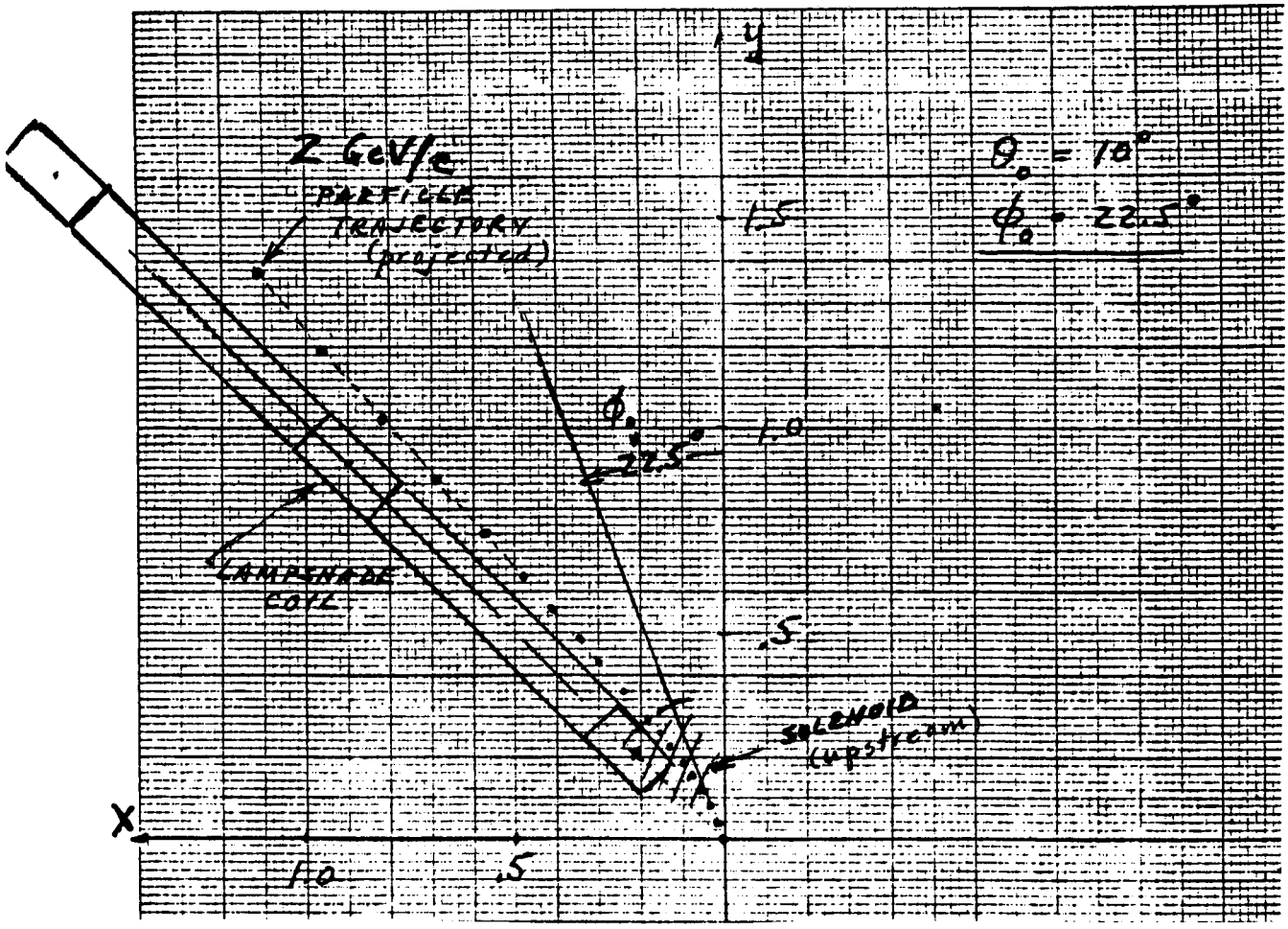
2 GeV/c
PARTICLE
TRAJECTORY
(projected)
$\theta_0 = 10°$
$\phi_0 = 22.5°$
1.5
1.0
.5
ϕ_0
22.5°
CAMPHASE
COIL
SOLENOID
(upstream)
y
x
1.0
.5

Figure 4.

Meson exchange in relativistic quark models*

John R. Hiller
Department of Physics, Purdue University
West Lafayette, IN 47907

Meson exchange is obtained as a long-distance approximation to baryon-baryon interactions in relativistic-quark models. The approach used may have other applications in nuclear and particle physics. The resonating group method[1] is applied to a light-cone Hamiltonian formulation[2] of the two-baryon eigenvalue problem. As an approximation to the full quark-gluon Fock state expansion,[2] a variational, relativistic, second quantized, cluster wave function is constructed from valence-quark states of hadrons. A mesonic contribution is explicitly included. For simplicity of discussion, niceties such as spin and isospin are mostly ignored; however, the method does in general include them.

The two-baryon system is described exactly by the appropriate solutions of the eigenvalue problem $H_{LC}\Psi = P^-\Psi$. Here H_{LC} is the light-cone Hamiltonian for quarks and gluons and P^- is the momentum component along the $\tau = t+z$ direction. It is convenient to write the Hamiltonian as the sum of three terms, $H_{LC} = K + V_o + V_1$, where K represents the kinetic energy contribution, V_o contains the terms of the potential that do not change particle (quark or gluon) number and V_1 consists of only those terms that do change particle number. The kinetic term can be given explicitly:[2]

$$K = \int \frac{dk^+ d^2k_\perp}{16\pi^3 k^+} [a^\dagger(\underline{k})a(\underline{k}) \frac{\vec{k}_\perp^2}{k^+} + b^\dagger(\underline{k})b(\underline{k}) \frac{\vec{k}_\perp^2 + m^2}{k^+} + d^\dagger(\underline{k})d(\underline{k}) \frac{\vec{k}_\perp^2 + m^2}{k^+}] \quad (1)$$

with $\underline{k} \equiv (k^+, \vec{k}_\perp)$, $k^\pm \equiv k^o \pm k^3$ and $\vec{k}_\perp \equiv (k^1, k^2)$ and where m is the quark mass, $a^\dagger$ is the gluon creation operator and $b^\dagger(d^\dagger)$ is the quark (antiquark) creation operator. Helicity and color indices are implicit. The potential terms can be obtained directly from the Lagrangian of Quantum Chromodynamics (QCD) if the gluon fields are treated in an essentially perturbative manner.[2] Such treatment is inappropriate for low-momentum interactions. Therefore, useful expressions for V_o and V_1 must come from a partial resummation of gluon effects in QCD or from relativistic quark models. One might even completely eliminate gluons in favor of some effective quark-quark interaction. In any case, the precise forms of V_o and V_1 will not be important.

Since the eigenstates of H_{LC} are unknown even for the simplest systems,[3] quark models usually deal with a simpler Hamiltonian that commutes with particle number operators. In the present context, such a Hamiltonian is $H_o \equiv K + V_o$. Some solutions of $H_o\Psi = P^-\Psi$ are created from the vacuum by operators[4] of the form[2]

$$M^\dagger(\underline{P}) = \int [dx]_2 [d^2t_\perp]_2 \psi_M(x, \vec{t}_\perp) b^\dagger(x_1P^+, x_1\vec{P}_\perp + \vec{t}_{\perp 1}) d^\dagger(x_2P^+, x_2\vec{P}_\perp + \vec{t}_{\perp 2}) \quad (2a)$$

*Work supported in part by the Department of Energy.

$$B^\dagger(\underline{P}) = \int [dy]_3 [d^2\vec{u}_\perp]_3 \psi_B(y,\vec{u}_\perp) \prod_{i=1}^{3} b^\dagger(y_i P^+, y_i \vec{P}_\perp + \vec{u}_{\perp i}) \qquad (2b)$$

where $\underline{t}_i$ and $\underline{u}_i$ are the momenta of the quarks relative to the hadronic momentum $\underline{P}$, $x_i \equiv t_i^+/P^+$, $y_i \equiv u_i^+/P^+$ and

$$[dx]_n \equiv \delta(1-\sum_{i=1}^{n} x_i) \prod_{i=1}^{n} dx_i, \quad [d^2t_\perp]_n \equiv 16\pi^3 \delta(\sum_{i=1}^{n} \vec{t}_{\perp i}) \prod_{i=1}^{n} \frac{d^2 t_{\perp i}}{16\pi^3}. \qquad (3)$$

Of course, (2a) and (2b) are to be identified with mesons and baryons, respectively.

With this machinery in place, an approximate, two-baryon solution to $H_{LC}\Psi = P^-\Psi$ can be written in the spirit of the resonating group method. The second quantized, trial wave function is

$$\Psi(\underline{P}) = \int [dz]_2 [d^2q_\perp]_2 \chi(z,\vec{q}_\perp) \prod_{i=1}^{2} B^\dagger(z_i P^+, z_i \vec{P}_\perp + \vec{q}_{\perp i}) |0\rangle$$

$$+ \int [dz]_3 [d^3q_\perp]_3 \chi_M(z,\vec{q}_\perp) \prod_{i=1}^{2} B^\dagger(z_i P^+, z_i \vec{P}_\perp + \vec{q}_{\perp i}) M^\dagger(z_3 P^+, z_3 \vec{P}_\perp + \vec{q}_{\perp 3}) |0\rangle. \qquad (4)$$

The number of terms in Ψ has been arbitrarily limited to two. The wave function χ is naturally identified with the ordinary baryon-baryon wave function and χ_M with an excitation of the two-baryon system. They are determined by the variational condition $\delta\langle\Psi|(H_{LC}-P^-)|\Psi\rangle=0$. Note that only H_o-P^- enters diagonal matrix elements and only V_1 can connect $B^\dagger B^\dagger|0\rangle$ and $B^\dagger B^\dagger M^\dagger|0\rangle$. The diagonal elements can be simplified with the use of the following relation (and the analogous one for $B^\dagger B^\dagger M^\dagger|0\rangle$):

$$(H_o - P^-) \prod_{i=1}^{2} B^\dagger(z_i P^+ z_i \vec{P}_\perp + \vec{q}_{\perp i})|0\rangle = [\sum_{i=1}^{2} (\frac{q_{\perp i}^2 + m_B^2}{z_i P^+}) - \frac{s}{P^+} + \tilde{V}_o] \prod_{i=1}^{2} B^\dagger(z_i P^+, z_i \vec{P}_\perp + \vec{q}_{\perp i})$$

$$|0\rangle, \qquad (5)$$

where m_B is the baryon mass, $s=P^2$ and the tilde restricts V_o to act only between quarks that are in different hadrons. Two coupled equations are then obtained

$$\int [dz]_2 [d^2q_\perp]_2 \langle 0| \prod_{i=1}^{2} B(w_i P^+, w_i \vec{P}_\perp + \vec{k}_{\perp i}) [\sum_{i=1}^{2} (\frac{q_{\perp i}^2 + m_B^2}{z_i P^+}) - \frac{s}{P^+} + \tilde{V}_o]$$

$$\times \prod_{i=1}^{2} B(z_i P^+, z_i \vec{P}_\perp + \vec{q}_{\perp i})|0\rangle \chi(z,q_\perp)$$

$$+ \int [dz]_3 [d^2q_\perp]_3 \langle 0| \prod_{i=1}^{2} B(w_i P^+, w_i \vec{P}_\perp + \vec{k}_{\perp i}) V_1$$

$$\times \prod_{i=1}^{2} B^\dagger(z_i P^+, z_i \vec{P}_\perp + \vec{q}_{\perp i}) M^\dagger(z_3 P^+, z_3 \vec{P}_\perp + \vec{q}_{\perp 3})|0\rangle \chi_M(z,q_\perp) = 0 \qquad (6a)$$

$$\int [dz]_3 [d^2q_\perp]_3 \langle 0|M(w_3\ldots) \prod_{i=1}^{2} B(w_i\ldots)\Big[\sum_{i=1}^{2} \frac{q_{\perp i}^2 + m_B^2}{z_i P^+} + \frac{q_{\perp 3}^2 + m_M^2}{z_3 P^+} - \frac{s}{P^+} + \tilde{V}_o \Big]$$

$$\times \prod_{i=1}^{2} B^\dagger(z_i\ldots) M^\dagger(z_3\ldots)|0\rangle \chi_M(z,q_\perp)$$

$$+ \int [dz]_2 [d^2q_\perp]_2 \langle 0|M(w_3\ldots) \prod_{i=1}^{2} B(w_i\ldots) V_1 \prod_{i=1}^{2} B^\dagger(z_i\ldots)|0\rangle \chi(z,q_\perp) = 0 \qquad (6b)$$

where m_M is the meson mass and an ellipsis in (6b) indicates an entry of the same form as those in (6a). A single equation for χ can be obtained from (6a) by substitution of a formal solution to (6b). This equation would then provide an approximate but fully relativistic description of the two-baryon system.

Careful examination of (6) gives insight into the structure of the resulting equation for χ. The matrix elements automatically include both "direct" contributions, where quark lines that leave one hadron all enter the same hadron, and "interchange" contributions, where at least one quark is interchanged between hadrons.[5] Those terms where a meson is present consist of self-energy effects, direct meson exchange and meson exchange combined with quark interchange. Contributions that include quark interchange fall off rapidly with increasing separation because of the behavior of the hadronic wave functions ψ_B and ψ_M, which decrease faster than a simple exponential. The direct terms associated with quark-quark interactions ($\tilde{V}_o$) are similarly damped. Therefore in the nonrelativistic limit $|\vec{k}_i - \vec{q}_i|$, $|\varepsilon| \ll m_B$, with $\varepsilon \equiv \sqrt{s} - 2m_B$, most terms do not contribute. One can then show that the equation for χ, without self-energy terms, becomes

$$[2m_B + \frac{\vec{k}_2^2}{2m_B}]\chi(\vec{k}_2) + \int d^3q_2 \frac{f(\vec{k}_2 - \vec{q}_2, \varepsilon)}{(\vec{k}_2 - \vec{q}_2)^2 + m_M^2} \chi(\vec{q}_2) = E\chi(\vec{k}_2) \qquad (7)$$

with $s = E^2$ and f a form factor that depends on direct terms in the matrix elements of V. Thus, the low-momentum behavior of χ is determined by the usual meson-exchange potential modified by a form factor that is, in principle, calculable.

References

1. For a review, see K. Wildermuth and W. McClure, Springer Tracts in Modern Physics 41 (1966).
2. For reviews, see S.J. Brodsky et al., SLAC-PUB-2868, published in Springer Tracts in Modern Phys. 100 (1982), and references therein.
3. Methods of solution are currently under investigation. S.J. Brodsky, private communication.
4. Nonrelativistic operators of this sort are discussed in, for example, M. Girardeau, Int. J. Quantum Chem. 17, 25 (1980).
5. This type of contribution is considered in the constituent interchange model. For a review, see D. Sivers et al., Phys. Rep. 23C, 1 (1976).

Electron Scattering from Discrete Low-Lying Levels of ^{13}C at High Momentum Transfer

R.L. Huffman, R.S. Hicks, J. Dubach, R.A. Lindgren,
G.A. Peterson, M.A. Plum and J. Shafer

The measurement of electron scattering cross sections at large momentum transfers has long been advocated as a means of studying not only the properties of the central region of the nucleus, but also of short-range processes such as meson exchange. Recent experiments on ^{13}C and other 1p-shell nuclei revealed unexpectedly large M1 cross sections above q = 2.5 fm^{-1}. These cross sections cannot be accounted for by reasonable p-shell models, even when one-pion exchange currents are included. Several calculations have predicted large core-polarization effects at these momentum transfers, however the results obtained are inconsistent: In some cases, e.g., ^{13}C, the agreement between experiment and theory is significantly improved; in other cases, e.g., ^{12}C, the comparison deteriorates. The fact that the excess M1 strength is concentrated at relatively high momentum transfers has led to alternative suggestions of possible contributions from mesonic interactions of shorter range than one-pion exchange.

Using the electron scattering facility at Bates, we have now extended data on the elastic M1 form factor of ^{13}C from q = 3.3 fm^{-1}, the limit of previous measurements, up to 4.6 fm^{-1} where the low cross section of 7×10^{-39} cm^2/sr was obtained. Above q = 3 fm^{-1} the elastic M1 form factor is observed to decrease monotonically with increasing momentum transfer. The results therefore lie in disagreement with theoretical calculations employing Woods-Saxon radial wave functions and one-pion exchange currents which predict a third diffraction maximum. High-momentum transfer data have also been obtained on other ^{13}C excitations, for example the pure E1 transition to the 3.088 MeV level, and the much-studied M4 transition to the $9/2^+$, T=1/2 level at 9.50 MeV.

The electron spectrum measured at 4.6 fm^{-1} shows an intrusive background level. About half this background can be attributed to cosmic rays entering the skyward-looking Bates detector system. The reduction of this background would permit the measurement of cross sections down to 10^{-39} cm^2/sr for 1p-shell nuclei. Future large-aperture spectrometers, such as those planned for CEBAF should enable cross sections of 10^{-40} cm^2/sr to be measured, i.e., cross sections approaching the level of neutrino interactions.

NN POTENTIAL WITH A SIX QUARK CORE FROM THE CONSTITUENT QUARK MODEL*

M. Beyer
Institut f. Kernphysik, Universität Mainz, West Germany

H. J. Weber
Dept. of Physics, University of Virginia, Charlottesville, VA 22901, USA.

Asymptotic freedom in terms of hadron mass splittings from the color hyperfine interaction in quark confinement models motivates building NN potentials from meson exchanges for NN distances $r > b$, and from gluon dynamics in a six quark core for $r \leq b$, with a suitable core radius b.

For $r > b$, we calculate a NN one-boson-exchange (OBE) interaction[1] from a quark-OBE potential using the bound quark wave functions of the constituent quark model (CQM). The two-body quark-OBE potential is required to have the QCD symmetries (including chiral invariance) of the lowest order, color singlet (u-channel gluon exchange) two-body, interaction at short distance, upon expressing it in terms of t-channel (effective $q\bar{q}$) exchanges which arise in the strong coupling phase for sufficiently low momentum transfer q_μ, where gluonic modes are frozen in. This assumption determines the quark-OBE up to an overall strength, $G/\sqrt{4\pi} = 0.8$, fixed from $g^2_{\pi NN}/4\pi = 14.4$. The successful predictions of the small δ, A_1, ω-tensor, and large ω-vector couplings at $|\vec{q}| = 0$ in Table 1 go beyond the broken SU(3) flavor symmetry with the F/D ratios of static SU(6) from the CQM, depend on relativistic quark wave functions and hold also for the MIT bag model.[2] An additional two-pion-exchange potential is approximated by effective scalar ($\sigma_{0,1}$) exchanges.

For $r \leq b$, the transition to the six quark core with its discrete energy spectrum E_ν is described by a simplified version of Simonov's optical model solution[3]

$$V_{hqh} = \sum_\nu V_{hq}|E_\nu\rangle(E_\nu - E)^{-1}\langle E_\nu|V_{qh} \qquad (1)$$

of the coupled six-quark-NN formalism with a sharp transition

$$\langle\vec{r}|V_{hq}|E_\nu\rangle = C_\nu\delta(r-b) + 0(E_\nu - E). \qquad (2)$$

Below the pion production threshold only the lowest level E_o is considered, and the delta function is spread by a Gaussian. Numerical results for $0.1 \leq b \leq 1.5$ fm for the $^1S_0$ and $^3S_1$ channels depend strongly on V_{hqh} for

lack of an angular momentum barrier; P waves are also sensitive to V_{hqh} if $b \geq 0.9$ fm, but less so. The residue C_0^2 in Eq. (2) and Table 2 controls the energy dependence of the phase shifts. The six quark core potential V_{hqh} consistently improves the results from the mesonic potential V_h. Fitting the core parameters and σ strengths allows reproducing the phase shifts for $T_{lab} \leq 300$ MeV, scattering lengths, effective ranges and deuteron properties to within a few per cent, except for the deuteron's quadrupole moment which is low by 12%. Our study indicates that NN potentials consistent with successful quark models may be used as tools to explore the six quark core phenomenology.

Table 1

Meson (Mass, MeV/c^2)	$g^2/4\pi$(f/g)^4 CQM	Bonn
ε(1200)	1.1	0
δ(960)	0.122	0.015
η(548.5)	5.183	4.274
π(138.5)	14.397	14.263
ω(782.3)	7.04(-0.39)	13.965(0)
ρ(763)	0.782(2.034)	0.253(6.61)
D(1285)	0.211	0
A_1(1100)	0.587	0
ϕ(1020)	0	1.265

Meson-nucleon couplings at q=0.

Table 2

$^1S_0$	E_0 = 277.5 MeV
	C_0^2 = 0.1184
	C = 0.1352
$^3S_1$	E_0 = 446.6 MeV
	C_0^2 = 0.2820
	C = 0.3636

Fitted core parameters for b = 0.9 fm.

*Work supported in part by the Deutsche Forschungsgemeinschaft (SFB201) and the U. S. National Science Foundation.

[1] M. Beyer and H. J. Weber, U. Mainz-Virginia preprint (1984); M. Bozoian and H. J. Weber, Phys. Rev. C28 (1983) 811.

[2] B.L.G. Bakker, M. Bozoian, J. Maslow, H. J. Weber, Phys. Rev. C25 (1982) 1134.

[3] Yu. A. Simonov, Phys. Lett. 107B (1981) 1, and in Proc. Xth Int. Conf. on Few Body Problems in Physics, Karlsruhe (1983).

[4] K. Erkelenz, Phys. Reports C13 (1974) 191; K. Holinde, ibid. C68 (1981) 121.

A Study of (e,e'N) Reactions From Nuclear Targets

W. E. Kleppinger
Argonne National Laboratory, Argonne, IL 60439

One of the primary goals of a high-energy, high duty-factor electron accelerator (CEBAF) will be to study coincidence reactions in the energy range 50 MeV $\lesssim \omega \lesssim$ 500 MeV, where ω is the energy transfer to the nuclear target. In this region, the predominant reaction mechanisms are the quasi-elastic knockout of nucleons and the electroproduction of pions. A key ingredient in obtaining a theoretical understanding of these processes will be the nucleon-nucleus and pion-nucleus optical potentials. In particular, in order to obtain a clear separation of the peaks corresponding to these two processes, one must be able to calculate the quasi-elastic tail adequately. In the present work, we shall focus on (e,e'N) reactions in the quasi-elastic region.

In general, a coincidence cross section can be decomposed into a sum of four structure functions W_i (i = L, T, CT, TT):[1]

$$\frac{d^5\sigma}{d\varepsilon_2 d\Omega_2 d\Omega_x} = \frac{1}{M_1}\,\sigma_{Mott}\,\{v_L W_L + v_T W_T + v_{CT} W_{CT}^{(+)}\,\sin\phi_x + v_{TT} W_{TT}\,\cos 2\phi_x\}\quad .$$

In the above expression, M_1 is the mass of the target, σ_{Mott} is the Mott cross section, and the v_i are leptonic kinematic factors. ϕ_x is the azimuthal angle of the outgoing coincidence particle. The structure functions can be expressed in terms of products of transition matrix elements of the electromagnetic current. Following the analysis in Ref. 1, the structure functions can ultimately be related to reduced matrix elements of the standard electromagnetic multipole operators.[2] In the quasi-elastic region, where the one-body piece of the current dominates, there are then two quantities needed to evaluate a cross section. The first of these are the single-particle matrix elements of the multipole operators O_{JK}

$$\langle \chi_{\underset{\sim}{q},\ell'j'} \| O_{JK} \| R_{n\ell j} \rangle \ ,$$

which depend on the nucleon-nucleus optical potential through the scattering wavefunction $\chi_{\underset{\sim}{q},\ell j}(\underset{\sim}{r})$. The second quantity required is a one-body density matrix element

$$\langle \psi_{A-1} \| \hat{b}_{n\ell j} \| \psi_A \rangle$$

for the transition.

We have evaluated (e,e'N) cross sections from ^{12}C and ^{40}Ca and can summarize our results as follows: First, since the target nuclei have J=0, the quantum numbers of the residual hole determine the shape of the nucleon angular distribution. The optical potential determines the overall magnitude of the cross section and has a small effect on the shape. Second, in the Coulomb-Transverse structure function $W_{CT}^{(+)}$, the contribution of the magnetization current averages to zero. This leaves only a Coulomb-convection current interference, which is approximately 10% of the total cross section. Finally, the Transverse-Transverse structure functions W_{TT} contributes approximately 1% of the total (see also Ref. 3 for a discussion of the second and third points above).

We have also considered (e,e'N) reactions where the incident electron is longitudinally polarized. One can then define an asymmetry parameter A as the difference in differential cross sections for right-handed and lefthanded polarizations of the incident electrons divided by the sum:

$$A \equiv \frac{d\sigma_{\uparrow} - d\sigma_{\downarrow}}{d\sigma_{\uparrow} + d\sigma_{\downarrow}} \ .$$

In an inclusive (e,e') experiment, it has been shown that the asymmetry A is due to an interference between the weak neutral and electromagnetic currents and also to parity admixtures in the nuclear wavefunctions.[4] While this is also true for (e,e'X) reactions with polarized electrons,[5] an additional contribution A_{FSI} exists which is due entirely to final-

state interactions

$$A_{FSI} = \frac{2v_{TT}\tan(\frac{1}{2}\theta_e)W_{CT}^{(-)}\cos\phi_x}{\{v_L W_L + v_T W_T + v_{CT} W_{CT}^{(+)}\sin\phi_x + v_{TT} W_{TT}\cos 2\phi_x\}} .$$

The new structure function $W_{CT}^{(-)}$ is due to an interference between the Coulomb and Transverse matrix elements and vanishes in the absence of final-state interactions. In the above expression, θ_e is the electron scattering angle in the laboratory frame. Our results indicate that the new structure function $W_{CT}^{(-)}$ is comparable in size to the structure function $W_{CT}^{(+)}$ which occurs in the unpolarized cross section. The asymmetry A_{FSI} may be sizeable at both forward and backward electron scattering angles (note that the relevant measure is the figure-of-merit $M \equiv A^2 d^5\sigma/d\varepsilon_2 d\Omega_2 d\Omega_x$). Since an electron beam generally has a residual polarization, this term may also "contaminate" the out-of-plane "unpolarized" coincidence cross section due to finite-detector-size effects.

This work supported by the U. S. Department of Energy under contract number W-31-109-ENG-38.

References

1. W. E. Kleppinger and J. D. Walecka, Ann. Phys. (NY) 146 (1983), 349.
2. T. de Forest, Jr. and J. D. Walecka, Advan. Phys. 15 (1966), 1.
3. J. S. O'Connell, Phys. Rev. C29 (1984), 1544.
4. G. Feinberg, Phys. Rev. D12(1975), 3575;
   J. D. Walecka, Nucl. Phys. A285 (1977), 349;
   M. Porrmann and M. Gari, Phys. Rev. Lett. 38 (1977), 947;
   B. D. Serot, Nucl. Phys. A322 (1979), 408.
5. W. E. Kleppinger, Nucl. Phys. A (1984).

STUDY OF COMPLEX NUCLEI USING INTERNAL TARGETS AT CEBAF

by

C. N. Papanicolas
Department of Physics and Nuclear Physics Laboratory
University of Illinois at Urbana-Champaign
Urbana, IL 61801

and

J. Calarco
Department of Physics
University of New Hampshire
Durham, NH 03824

Introduction

The availability of internal targets and intense circulating beams in electron rings which result in luminosities adequate for the performance of nuclear structure studies is today a reality. The pioneering experiments of the Novosibirsk group amply demonstrate the point.[1] Their success answers in a direct and dramatic way a number of questions regarding feasibility and backgrounds. Given, then, the demonstrated feasibility of nuclear structure studies using stored electron beams, what programs of study can we envision? More significantly, what new areas of study become accessible, and which experiments are best suited for internal targets? In what follows we shall attempt to formulate these questions more precisely, to give some tentative answers, and to raise more questions. Considering the occasion of this presentation I will assume that we will be dealing with a dedicated ring at CEBAF fed by the main LINAC whose parameters are given in the NEAL Proposal.

Categorization of the Physics

A classification chart of the physics of complex nuclei which we expect to encounter at CEBAF energies is offered in the idealized electron scattering spectrum shown in Figure 1. Two kinds of excitation can be identified readily: excitations characteristic of the nuclear system as a whole, such as the elastic peak, inelastic (bound) states and the giant resonances; and excitations characteristic of the nucleons themselves such as the quasi-free peak and the nucleonic resonances (Δ,N^*, etc.).

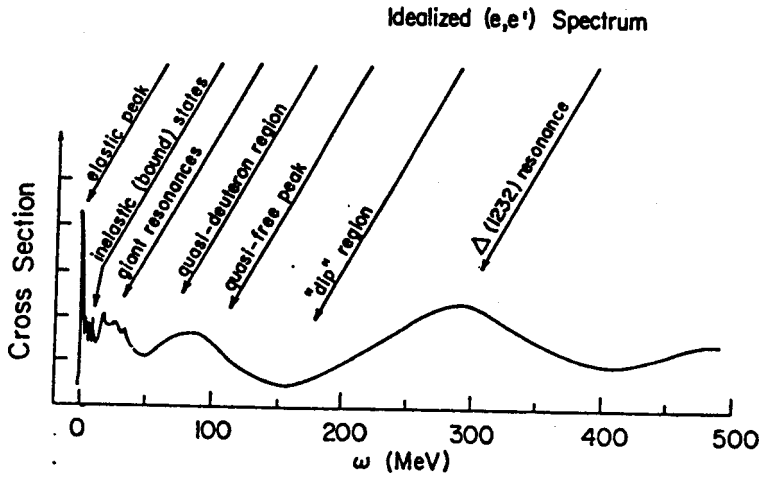

Fig. 1

We are clearly faced with a very broad and diverse range of phenomena. With the exception of elastic and inelastic scattering from discrete states in spin-zero nuclei, we have only begun to explore the phenomena displayed by the spectrum in Figure 1. In what follows we will examine several of the excitation regions shown in Figure 1 and we will try to identify areas where the use of internal targets offers significant advantages relative to the usual arrangement of extracted electron beams impinging on external targets. In order to facilitate a discussion of the relative merits of internal and external target experiments, we will examine the relevant technical aspects and parameters of both types of experiments.

Formalism

The general formalism for the electron scattering cross section including the detection of coincident particles has been given in the Plane Wave Born Approximation (PWBA) by deForest.[2] A form more specific to (e,e'x) reactions that proceed through definite intermediate states (e.g. giant resonances) has been described by Uberall and coworkers (Raphael and Uberall,[3] Drechsel and Uberall[4]), and by Kleppinger and Walecka.[5] However, in all this early work carried out in the framework of the Plane Wave Born Approximation it is assumed that the beam and target are both unpolarized. More recently Donnelly and coworkers[6] have begun to investigate the general form of the cross section including target and/or beam polarization.

In this presentation we will not attempt a comprehensive review of the theoretical framework of electron scattering. Rather, we will quote available results and summarize which observables are accessible to experiments under various conditions.

We begin by considering the simplest case, inclusive electron scattering. As is well known,[7] the cross section for inclusive electron scattering, in the absence of any observable polarizations, can be written as

$$\frac{d^2\sigma}{d\omega d\Omega} = \sigma_M \left[V_C|F_C|^2 + V_T|F_T|^2\right]$$

where σ_M is the Mott cross section, V_C and V_T are kinematic factors, and the F_C and F_T are the Coulomb and transverse nuclear form factors, or structure functions, which correspond to scattering induced by the transfer of longitudinally and transversely polarized virtual photons respectively. These

two structure functions are functions of the transferred momentum q and transferred energy ω. All nuclear structure information is contained in these structure functions which are proportional to the Hankel transforms of the nuclear transition densities and currents.[8] For the case of inclusive electron scattering with unpolarized beam and target, these two structure functions are the observable quantities, and q and ω are the variables at the experimenter's disposal. If more than one multipole can contribute to a process, the structure functions $|F_C|^2$ and $|F_T|^2$ are each an incoherent sum of contribtuions $F_C^2(L)$ and $F_T^2(L)$ for the allowed multipolarities, L.

If the electron beam is polarized but the target is not, then the scattering is modified by (1) parity violation effects, and (2) electromagnetic terms of order M_e/E. Since these terms are either extremely small or marginally relevant to a discussion of traditional nuclear structure physics, we shall not pursue them here. This is not to say that parity violation is not important, only that it is beyond the scope of a presentation on nuclear structure studies with internal targets.

If the target is polarized but the beam is not, then two new structure functions, W_{CT} and W_{TT}, are observable. The cross section is of the form:

$$\frac{d^3\sigma}{d\omega d\Omega d\Omega^*} = \sigma_M \left[W_C W_C + V_T W_T + V_{CT} W_{CT} + V_{TT} W_{TT}\right]$$

The first two terms in this expression are more general forms of the usual Coulomb and transverse structure functions (which must reduce to F_C^2 and F_T^2 when the target polarization is averaged to zero). The last two terms are due to a longitudinal transverse interference effect W_{CT} and a transverse photon polarization effect W_{TT}. Furthermore the structure functions W_C and W_T now depend upon θ^*, the angle of polarization of the target with respect to the direction of q. These structure functions can be expanded in Legendre polynomial series in θ^*, ie. $P_k(\theta^*)$. Then the coefficients of the polynomial with rank, k, of zero are the usual $|F_C|^2$ and $|F_T|^2$. The coefficients of the higher rank polynomials provide us with the possibility of observing terms such as $F_C^*(L)\ F_C(L')$ and $F_T^*(L)\ F_T(L')$, which are due to the interference between different allowed multipolarities, L and L'. The structure function W_{CT} is expandable as a series in associated Legendre polynomials of the first kind, $P_k^1(\theta^*)$. Again the coefficients contain terms such as $F_C^*(L)\ F_T(L')$ due to multipole interferences. In a similar fashion the term W_{TT} can be expanded

in a series in $P_k^2(\theta^*)$ with the coefficients depending upon $F_T^*(L)\ F_T(L')$. The latter two expansions (for W_{CT} and W_{TT}) contain terms of only even rank k. This means that interferences are observed only if L and L' can combine to give even values of k. Also J and J', the initial and final spin of the nucleus, must satisfy a similar restriction. This means that there is no new information from scattering elastically with unpolarized electrons from a spin 1/2 polarized target.

This restriction is lifted by measuring the scattering from a polarized target using a polarized electron beam. Two additional structure functions come in, these being the W_{CT} and W_{TT} terms again, but now contributing to expansions of Legendre polynomials in θ^* of only odd rank k.

We now turn to experiments in which an outgoing particle, x, is detected in coincidence with the inelastically scattered electron, ie <u>exclusive</u> (e,e'x) experiments. For the case where neither the beam nor the target is polarized the (e,e'x) cross section has the form

$$\frac{d^3\sigma}{d\omega d\Omega d\Omega_x} = \sigma_M \left[V_C W_C + V_T W_T + V_{CT} W_{CT} + V_{TT} W_{TT}\right].$$

This expansion is identical in form to that for inclusive scattering on a polarized target. The difference is that the structure functions now depend on θ_x instead of θ^*, and are expandable as a Legendre polynomial series in θ_x, where θ_x is the angle of the outgoing particle x with respect to the $\vec{q}$ direction. The reason for this similarity of form is that the θ_x correlation information provides the same definition of the final state polarization as that provided by θ^* for the initial state of a polarized target. In both cases the dependence of the reaction on the aximuthal angles ϕ_x (or ϕ^*) factors out of the structure functions into the kinematic factors. The information available from unpolarized (e,e'x) is essentially the same as that available from (e,e') on a polarized target.

If we perform a coincidence (e,e'x) experiment with a polarized electron beam (but with no target polarization), we observe a fifth structure function. This term is also due to an interference of longitudinal and transverse amplitudes, but with a different dependence on the reaction kinematics.

$$\left.\frac{d^3\sigma}{d\omega d\Omega d\Omega_x}\right|_{\substack{pol \\ \vec{e}}} = \sigma_M \left[V_C W_C + V_T W_T + V_{CT} W_{CT} + V_{TT} W_{TT} + V_{CT'} W_{CT'}\right]$$

The new structure function, W_{CT}', is sensitive to an interference between multipoles, and will vanish in the limit of an isolated resonance. In the region where the giant resonance and quasi-elastic processes both contribute, this new function should be sensitive to their interference and provide information that will assist in the multipole decomposition of the cross section.[6]

If the target is polarized but the beam is not, then coincidence experiments provide six observable structure functions, each of which is expandable in a double Legendre series, one in the correlation direction θ_x and the other in the polarization angle, θ^*.

The most complicated cases, those of coincident particle detection with both polarized beams and polarized targets, the measurement of the polarization of the outgoing particle, and cases in which more than one coincident particle is detected have not yet been completely analyzed. Donnelly[6] has recently shown, however, that the number of measurable structure functions cannot exceed nine even in the most complicated case. These will be interesting cases to investigate further as polarized target technology improves. Experiments with polarized beams and targets are clearly becoming feasible and preliminary estimates show that multi-particle coincidence experiments may in fact also be feasible (at least it can be shown that backgrounds in such cases are very low so that the true event rate, although low, is detectable above background).

We have not provided much detail on cases other than inclusive experiments on polarized targets and exclusive experiments on unpolarized targets, both with polarized beams. These are clearly experiments which are not feasible with present technology. In order to push into the next generation of experiments we must have polarized targets of thicknesses comparable to that presently available for unpolarized targets.

Beam Parameters

Extracted continuous electron beams of high quality are now available at Illinois and Mainz; numerous other labs are expected to acquire similar capability soon. In the comparison that follows we will therefore compare the high quality external beams racetrack microtrons are capable of producing to the internal beams expected in the CEBAF dedicated ring. In the few cases where the study of nuclear structure in complex nuclei requires energies

exceeding 1 GeV we assume the use of external beams from stretcher rings instead of microtrons. One very striking feature is evident in this comparison. Approximately the same luminosity is achieved in the two cases by very different combinations of target thicknesses and beam intensity. As we will see later all the experiments that can be best performed with internal targets in an electron ring derive from its unique ability to provide reasonable luminosities with ultra thin targets.

Feasibility: Experimental Considerations

For any feasibility estimate a crucial parameter is the maximum luminosity. The luminosity figures given in Table I can only serve as crude

Table I

Parameter	CEBAF Stretcher Ring[4]	Microtron
Operating Range	0.5-4.0 GeV	0.1-1.0 GeV
Energy Spread $E/\Delta E$	10^{-3}	$\sim 2 \times 10^{-4}$
Available Current	2×10^5 μA	100 μA
Maximum tolerable target thickness	$< 10^{-2}$ mg/cm^2	no limit 100 mg/cm^2(typ.)
Maximum atainable luminosity	$< 2 \times 10^3$	$\sim 10^4$

benchmarks. It is assumed that the maximum tolerable target thickness is available for the particular application we may be interested in (generally incorrect for the case of internal targets) and that it is desirable to make use of it (generally incorrect for external targets).

The count rate, N, in any experiment is given by the simple relation

$$N = L\sigma$$

where L is the luminosity, and σ is the reaction cross section of the process we are interested in. The luminosity is the product of target thickness, t, and the current intensity, I.

In Table II we tabulate a variety of typical inclusive and coincident measurements in order to set the scale on luminosities. The luminosity is

TABLE II

A. Inclusive

Experiment	Laboratory	$I(\mu A) \times t(mg/cm^2)$	$L(10^{-10} kgA/m^2)$
$(e,e')^{12}C$	Bates	50 x 200	1×10^4
$(e,e')^{208}Pb$	Saclay	20 x 100	2×10^3
$(e,e')^{140}Ce$	Bates	50 x 4.0	2×10^2

B. Coincident

$(e,e'p)^{12}C$	HEPL	25 x 5	125
$(e,e'n)^{208}Pb$	Illinois	0.2 x 40	8.0
$(e,e'\gamma)^{12}C$	Illinois	2.0 x 40	80
$(e,e'f)^{238}U$	Illinois	0.5 x 1.0	0.5
$(e,e'f)^{238}U$	HEPL	20 x 0.2	4.0
$(e,e'p)^{28}Si$	Mainz	30 x 5	150

given in units of $(10^{-10} kg\ A/m^2)$. We expect that the experiment using internal targets at the CEBAF ring to compare quite favorably with the luminosities given in Table II for external target measurements.

As shown in Table I the circulating current planned for the CEBAF dedicated ring is > 200 mA. The maximum thicknesses permissable for internal targets are not so well established especially for the case of polarized targets. A review of the different techniques that can be used to achieve maximum thicknesses for particular isotopes is beyond the scope of this presentation. An excellent review for unpolarized jet targets can be found in the proceedings of the Lund conference.[9] The proceedings of the Argonne workshop on polarized targets[10] will become available soon; it will provide an excellent reference to the densities and techniques available for producing polarized targets. For the purpose of this discussion we will assume:

$t \lesssim 10^{-3}$ mg/cm^2 for unpolarized jets

$t \lesssim 10^{-6}$ mg/cm^2 for polarized targets

which are rather conservative estimates for what is currently available. Actually far more favorable cases exist, especially for polarized targets (H^2, He^3, alkali and noble gases). For the above target thicknesses the resulting luminosities then are:

unpolarized targets: $(10^{-3}$ mg/cm$^2)$ x $(2 \cdot 10^5$ μA$)$ = 200 x 10^{-10} kg · A/m^2
polarized targets: $(10^{-6}$ mg/cm$^2)$ x $(2 \cdot 10^5$ μA$)$ = 0.2 x 10^{-10} kg · A/m^2

Comparing these numbers to the luminosities shown in Table II it immediately becomes obvious that experiments with unpolarized targets should present no count rate problems while the polarized target measurements are expected to be difficult.

The above luminosity argument does not set an absolute scale. It only tells us that if an experiment using a polarized target was to be performed with the same kinematical conditions as the coincidence measurements of Table II then it would be very difficult. Of course this is unrealistic. We need to examine more carefully the dependence on the kinematic variables such as incident beam energy, scttering angles and other relevant experimental parameters we have at our control.

Incident Beam Energy

The incident beam energy is perhaps the most important parameter at our control. In the study of complex nuclei we need to span as a wide range of momentum transfer as possible. We can achieve this by either varying the incident energy or by varying the scattering angle. Figure 2 shows the behavior of the various form factors which will dominate the 1 $\hbar\omega$ excitation spectrum in a heavy system like ^{208}Pb and a light system like ^{16}O. First we observe that, independent of the size of the system we want to study, momentum transfers of up to 3.0 fm^{-1} must be accessible to map out the behavior of 1 $\hbar\omega$ excitations. The same figure also shows (diagonal dotted lines) that these momentum transfers can be achieved by very different combinations of scattering angles and incident beam energies.

Figure 3 shows the dependence of the Mott cross section on the choice of the incident electron kinematics. Since Mott scattering modulates the response of any system to electron scattering, a substantial increase in the counting rate can be achieved by measuring at the smallest scattering angle possible. In practical terms this usually means 20° - 40° and as Figure 2 and 3 show the required energies lie comfortably within the operating range of the proposed ring.

establish, given the large uncertainties in beam profile and target thickness that are expected over the course of a measurement. One possible solution is to measure simultaneously the elastic scattering from the same target. Normalization considerations therefore imply the desirability of using electron scattering spectrometers having a large momentum acceptance.

A second area of concern is the energy definition of the incident beam. The energy spread $\Delta E/E = 10^{-3}$ of the injector linac proposed for CEBAF implies a resolution of 1 MeV at incident energy of 1 GeV. This resolution is unacceptable for the majority of nuclear structure studies. Except for the lightest nuclei the energy gap between the ground state and the first excited state is few hundred keV and quite often a few tens of keV. Two options seem to be available for rectifying this problem. Either the beam should be cooled in the ring to an acceptable beam spread or "energy loss" detection systems must always be employed. Both solutions are, in principle, technically feasible although both involve expensive and complicated equipment around the ring or the target area.

Finally, we note that the experience of facilities that already have internal target capabilities indicates[9] that the space around the target areas will be crowded with the elaborate vacuum systems associated with jet targets. The situation is even worse when polarized targets are used. This implies that 4π detection systems will be particularly hard to accommodate but large solid angle systems should still be feasible. It is worth observing that the detection systems associated with the coincidence experiments cataloged in Table II employ very modest solid angles (25-500 msr). Solid angles of this magnitude should be straightforward at internal target facilities. The above considerations let us to conclude the following on the feasibility of electron scattering experiments with stored electron beams:

a. Coincidence measurements with unpolarized targets should be easy.

b. Measurements with polarized targets are hard but feasible.

The preceeding discussion also led us to conclude that:

a. There is no obvious advantage in performing inclusive measurements with unpolarized internal targets.

b. An electron scattering program from polarized targets other than holmium will become feasible for the first time.

c. Cases in which particularly thin targets need to be used (for example if the recoiling nucleus needs to be detected in coincidence) will be ideally suited for internal targets.

We will proceed to examine the experimental possibilities, providing examples for some of the areas of study identified in our idealized spectrum of Figure 1.

The Physics

1. Elastic Scattering

This fundamental nuclear normal mode has been studied repeatedly since the development of the electron scattering probe. However, its power has been severely restricted to cases where there are only a few contributing multipoles. For elastic scattering this means nuclei with ground state spin of zero or half. In the case of zero spin, spin-parity selection rules allow only Coulomb monopole contributions. For spin half a magnetic dipole contribution is also allowed. For the case of elastic scattering time reversal disallows, however, transverse electric contributions. It is exactly for this reason that the Rosenbluth method allows the separation of the two allowed multipole excitations (CO/M1) in the case of spin half nuclei. It comes then as no surprise that the best studied ground change distributions are those of spin zero nuclei (see Figure 4).[12]

Actually the counter example of a high spin nucleus, such as ^{87}Sr (spin 9/2), demonstrates best the formidable problems facing the experimentalist trying to interpret ^{87}Sr elastic scattering. The magnetic scattering can been isolated from the coulomb scattering of ^{87}Sr by making use of the Rosenbluth method. Even so what is left (see Figure 5) is the sum of the five allowed multipoles, (M1, M3, M5, M7, M9) allowed by spin-parity selection rules. Further reduction of the experimental data to more fundamental quantities such as nuclear currents cannot be performed without isolating the contribution of each multipole. The case of ^{87}Sr (also ^{209}Bi) is actually very characteristic in another respect. For these nuclear systems, which are very important for our understanding of nuclear structure (due to their proximity to doubly closed shell nuclei) the precision and power of electron scattering cannot operate. The only possible solution is polarization of the target. With external beams this is not practical since the heating of the target by the beam destroys the polarization. Even in the most favorable case (Holmium) of a polarizable target the measurement is marginally feasible.

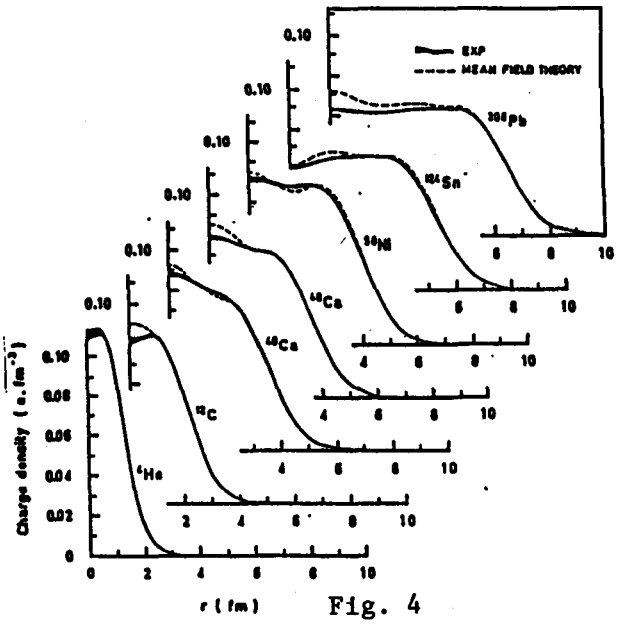

Fig. 4

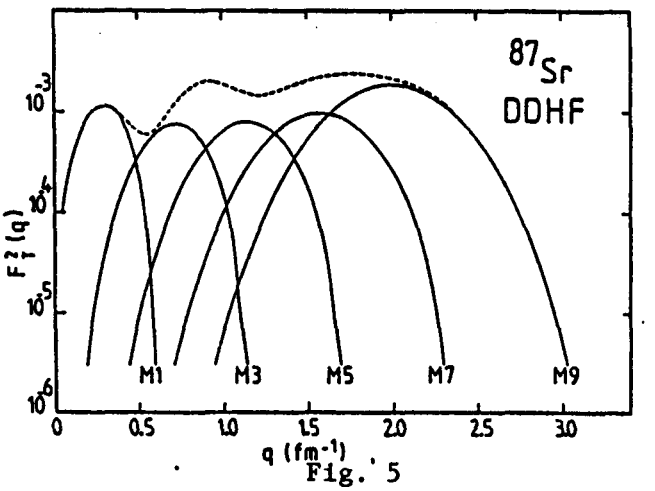

Fig. 5

The use of polarized jets as internal targets resolves the above difficulty. The very high degree of polarization achieved allows the experimenter to study each multipole independently by adjusting the polarization in order to select the appropriate Fano tensor. The heating of the target is rendered irrelevant in this situation since in effect the target is used only once.

In the case of elastic scattering the count rate is not a problem since the luminosities we have assumed assure us of reasonable counting rates in the range of 10^{-33} to 10^{-34} fm^{-2}. What is clearly a problem is first, the need to resolve the elastic from the first excited state already addressed, and second, the apparent inability to probe a substantial part of the lower multipoles if the incident energies at the CEBAF ring start at 0.5 GeV. We

clearly need (see Figure 3 and Figure 4) starting energies in the neighborhood 0.2 GeV.

In summary, we observe that the availability of internal targets a high degree of polarization will allow the study of the charge and magnetization distribution of odd/even nuclei with the same kind of precision which, up to now, was only possible for spin zero and spin 1/2 nuclei.

2. Inelastic scattering from discrete excited states

The detailed study of discrete excited states through inelastic scattering came of age in the early seventies. The new generation of accelerators of MIT/Bates, ALS-Saclay and Mainz with their intense beams and high resolution detection systems have provided us with precise data on hundreds of inelastic levels throughout the periodic table. The analysis techniques have been refined[8] so that the extraction of transition densities and currents with relatively small mode error is now routine. Indicative of the power and precision of this technique is the extracted transition density of the octupole excitation of ^{208}Pb at 2.615 MeV. The derived transition charge density shown in Figure 6 is characterized by a very small error band which excludes all theoretical calculations available today.

The ability to reconstruct transition charge densities and currents from inelastic electron scattering data is restricted to nuclei with zero spin ground state. The situation is slightly worse than the case of elastic scattering since the time reversal arguments, which prohibited transverse electric contributions in the elastic case are inapplicable. As a result the highly polished techniques of inelastic scattering analysis are only partially effective in the case of a spin half ground state. In such a case the Coulomb contribution involves a single multipole but the transverse structure function involves the incoherent sum of a magnetic and an electric multipole contribution. The 6.33 MeV transition[14] in ^{15}N, shown in Figure 7, is a typical example. The C2 contribution can be isolated using a the Rosenbluth separation but the E2 + M2 cannot be separated experimentally in an inclusive measurement. The situation becomes totally intractable for nuclei of spin greater than 1/2.

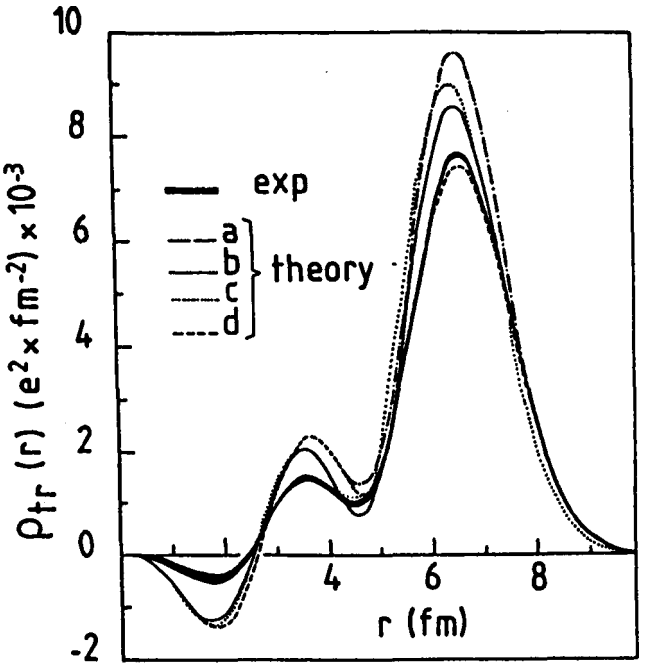

Fig. 6

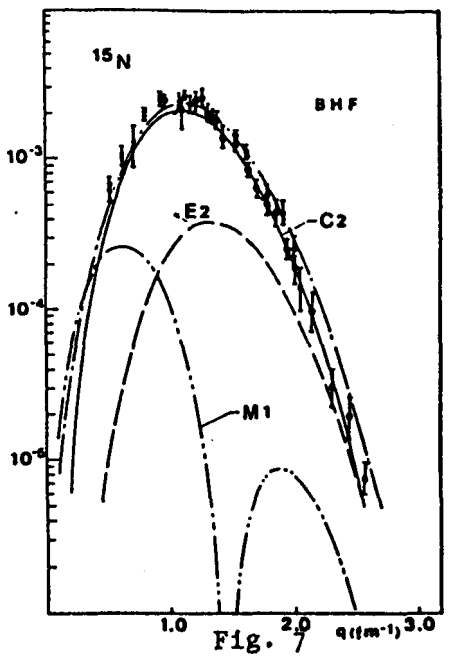

Fig. 7

The power of inelastic electron scattering can be brought to bear on all nuclei of the periodic table by exploiting two powerful and somewhat complementary methods: polarization of the target or coincidence measurement of inelastic electron scattering with the nuclear de-excitation product.

Inelastic electron scattering from polarized targets shares the same advantages and disadvantages as the corresponding elastic measurements. Actually the elastic and inelastic measurements will most probably end up being measured simultaneously in order to achieve reliable normalization for the inelastic cross section. As W. Donnelly demonstrates in his presentations, the experimental degrees of freedom allowed in such polarization measurements are in general adequate to allow the isolation of every contributing multipole regardless of the spin of the ground state. A very important exception

exists, that of spin 1/2 nuclei. For such important systems such as ^{15}N, ^{89}Y and ^{207}Pb to name a few, the polarization technique will not work.

In the section on formalism we have already extensively discussed the similarity between coincidence measurements of the (e,e'x) type and inelastic electron scattering from polarized targets. For the case of discrete bound levels (e,e'x) almost uniquely implies (e,e'γ). In special cases such as very low frequency excitations we expect the (e,e e_c) reaction[15], where e_c is a conversion electron, to supplement (e,e'γ). It is worth observing that the (e,e'γ) technique as potent in the case of a spin 1/2 ground state as for any other nucleus. In this regard (e,e'γ) will nicely complement the polarization measurements.

The feasibility of inelastic scattering from polarized targets will be of course limited by count rate much earlier that inclusive measurements allow today. Instead of the cross sections that are routinely reached today in single arm measurements ($\sim 10^{-38}$ cm^2) we will have to settle for cross sections of the order of 10^{-33} to 10^{-34} cm^2, unless a breakthrough in polarized internal target technology is achieved allowing thicker targets.

3. Giant Resonances

It has long been recognized that giant resonances are one of the most important phenomena in the field of nuclear structure physics. These resonances are characteristic of all but perhaps the very lightest nuclei. Furthermore for multipoles which have been adequately studied, it is known that they exhaust the appropriate sum rules. Giant Resonances thus correspond to highly collective normal modes of the nuclear system.

The coupling of the Giant Resonances to the other important normal mode of the nuclear system is of profound interest.[17] For instance, it is known, at least for the dipole case, that giant resonances couple strongly to simple one particle-one hole excitations. A better understanding of this mechanism will profoundly improve our understanding of core polarization, effective changes, and other related phenomena sensitive to the coupling of the various normal modes of the system. A related but poorly understood process is the dissipation of the energy of the giant resonance.[18] The process is very complex and involves a thorough understanding a nuclear dynamics. The detailed path to equilibrium, either by coupling to the continuum (escape with $\Gamma\uparrow$) or by gradual thermalization by coupling to more complex multiparticle-

multihole configurations (spreading with $\Gamma\uparrow$) is poorly understand and is at the limits of our current calculational ability. As pointed out by Broglia[19] the understanding of such processes is directly related to questions usually addressed in heavy ion reactions such as large amplitude collective nuclear motion and nuclear hydrodynamics.

Yet for all their importance in our understanding of nuclear structure, our present knowledge of giant resonances is quite primitive.[18] Photoreactions and capture studies have provided us with systematic information in the giant electric dipole resonance, and its ground state decay is known in a few selected cases, but a general study of the decay properties of the giant dipole resonance, ie how it couples to the continuum, still eludes us. Inclusive electron and hadron scattering studies have verified the existence of giant resonances for higher multipoles but systematic information only exists for L=2, and then only for medium to heavy nuclei.[17] More recently, studies of the coincident decay following electron and hadron scattering have been initiated.

These early coincidence experiments have also raised new questions $(\alpha,\alpha'p)$ and $(\alpha,\alpha'\alpha)$ studies[20] of the giant quadrupole resonance have demonstrated the large α decay width from the Giant Quadrupole Resonance (GQR), but in some cases there are serious disagreements with results in the same GQR obtained via α-capture. Recent hadron scattering studies have given clear evidence for the GQR in inclusive scattering, especially in heavy nuclei. However, coincidence experiments such as $(\alpha,\alpha'f)$ on uranium have lead to questions and discrepancies,[21] the most likely source of which is an incomplete knowledge of the hadron scattering mechanism.

Electron scattering, on the other hand, provides a known, weakly perturbative probe of nuclear structure. The one photon exchange is known to provide an accurate description of the scattering process. Thus the decay properties of the giant resonances can be studied without questions about the excitation mechanism. These in turn can be fed back into the analysis of the hadron scattering to provide a probe of the reaction mechanism.

An added advantage of electron scattering is that coincidence experiments remove most of the background (that due to the elastic radiative tail) at low q (see Figure 8).[22] In hadron scattering on the other hand the giant resonances sit on top of a near continuum background which is observed in coincidence and which is not fully understood.[23]

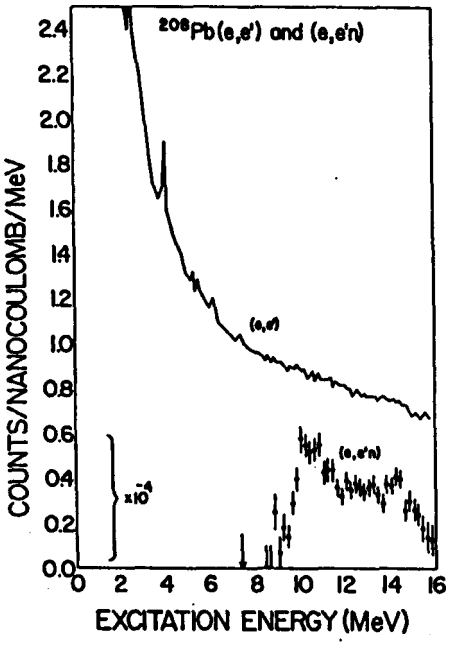

Fig. 8

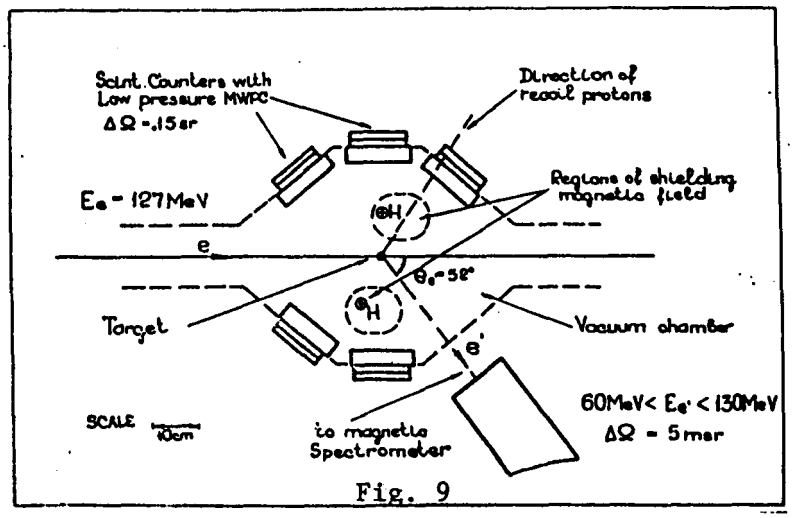

Fig. 9

Unpolarized coincidence experiments like those recently initiated at Illinois, Stanford, (see Table II) and, more recently, at Mainz, will provide detailed information on the decay branching ratios and angular correlations which in turn give information about the giant resonance's microscopic makeup. Complete measurements will also yield the W_{CT} structure function. This will allow a longitudinal-transverse decomposition of the coincidence cross section without having to go to back angles where count rates are going to be very low, (see discussion on experimental details).

All of these measurements can be performed with internal beams and targets. The luminosities are approximately the same in either case for most reactions of interest. The only exceptions are experiments for which certain complex decay particles are of interest requiring very thin targets, and experiments in which the target itself is either difficult to make or chemically unstable under bombardment. In these cases internal targets offer clear advantages.

The feasibility of using internal targets for giant resonance work has already been demonstrated by the Novosibirsk group.[1] The setup used in their study of ^{16}O giant resonances using the (e,e'p) and (e,e'α) channels is shown in Figure 9. The quality of their data, shown in Figure 10, is impressive

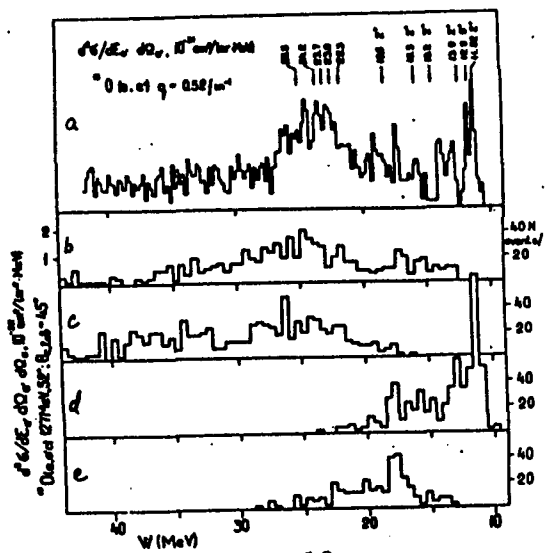

Fig. 10

indicating no background contaminations. These experiments are being carried out with circulating low energy electrons (more than a factor of ten lower than the ones contemplated for the CEBAF ring). This implies that counting rates (see Figure 3) and background problems should present absolutely no problem at CEBAF energies.

Use of internal targets in giant resonance research offers several advantages not offered by coincidence experiments using external beams. First is the already mentioned advantage of obtaining heavy decay fragments without straggling degredation. Several measurements will benefit from such development. The most obvious one is (e,e'f). Actually several options on this theme need further exploration. A very appealing possibilities the study of very deep inelastic scattering on fissioning nuclei. The removal of the elastic rotative tail from inelastic excitation spectrum can be achieved by requiring an anticoincidence between the inelastically scattered electron and recoiling nuclei of the same mass as the target. Except for the fission

studies on actinide nuclei, the electrofission of light nuclei is an area of research which has barely been touched. Sandorfi, et al.[24] in their pioneering experiments at Stanford on electrofission of light nuclei experiments at Stanford have witnessed the presence of low lying resonances (see Figure 11) which cannot be observed in the time reversed heavy ion reaction due to the Coulomb barrier. The nature of these resonances, presumed to be quite significant in nuclear dynamics is poorly understood. A measurement of their form factors will reveal their momentum content and one hopes, an understanding of their microscopic origin. In order to detect the very low energy fragments emerging from the target it is necessary to use target thicknesses of tens of $\mu g/cm^2$. This in turn reduces the coincident count rate substantially, actually to the point where only the electroproduction measurement is feasible with external beams. In the case of internal targets this limitation does not apply. The whole coincidence program would then actually be quite easy to implement.

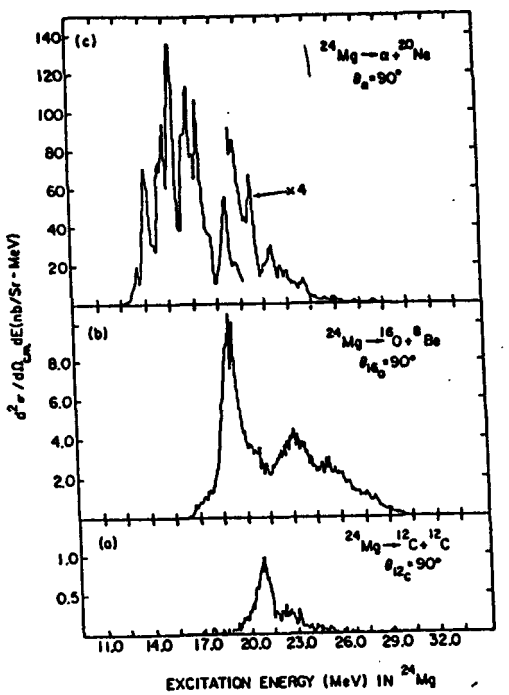

Fig. 11

Giant resonance studies on polarized targets clearly require internal targets. Polarized target experiments will certainly be feasible for inclusive scattering on giant resonances. Clearly no new information is available on the coupling of the giant resonances to the continuum. However, by measuring the cross section as a function of target polarization angle at fixed scattering angles, one obtains information which will, in principle, allow the total section be be decomposed into its multipole components, each separated into its longitudinal and transverse contribution. We have, however, to observe that in the case of giant resonance excitation such decomposition is by no means assured (as is the case for the discrete excitations). The reason is quite simple: giant resonances of different multipolarities overlap. It is this same difficulty actually that has prevented us for so from getting a better experimental handle on their properties. Certainly the extra "knobs" provided by polarization will greatly aid the experimentalist in disentangling them, but that in no way implies the same kind of flexibility and accuracy we expect to find in the case of discrete excited states.

Coincidence experiments on giant resonances using polarized targets would certainly give much new information on both the multipole decomposition and the coupling to the continuum. However, since state of the art polarized gas jet targets are presently thinner than unpolarized jets by a factor of ~ 1000, such experiments are only feasible with solid angles for the coincident particles approaching 4π. Such experiments as (e,e'f) are clearly feasible through this approach. Preliminary data from unpolarized (e,e'f) on ^{238}U have provided us with interesting results and left us with questions concerning the distribution of multipole strength in the fission channel.[21] In particular the angular correlation of fission fragments appears to be essentially isotropic except in the threshold region, so, except in that region, it offers no help in multipole decomposition. Since quadrupole and monopole strength functions an characterized by similar form factors, the only way of differentiating them is by using a polarized target. Furthermore since many of those targets with high fission probabilities also exhibit large ground state deformations, and it is known that the ground state deformation result in structure in the giant resonances (see Figure 12), polarizing the target will permit the individual components of the giant resonances to be

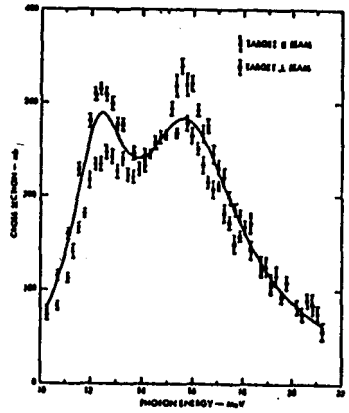

... The cross sections measured with the holmium target polarized parallel to the photon beam and perpendicular to the photon beam. The solid line is the two-component Lorentz curve fit to the unpolarized data.

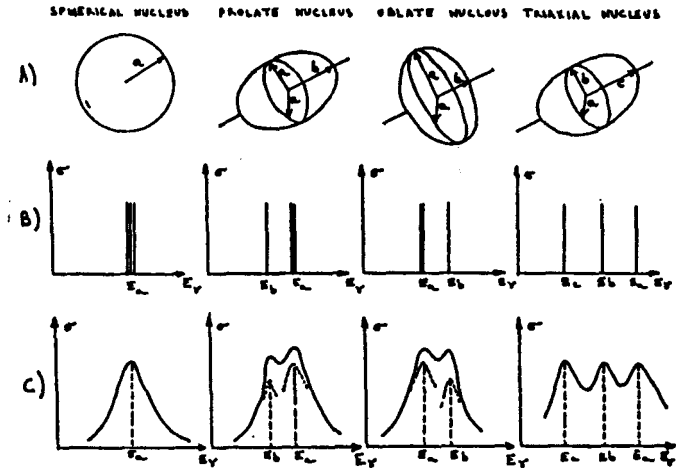

Fig. 12

studied.[25] For (e,e'x) experiments with polarized targets where x is a p, n, α, nγ, the problem with constructing a 4π coincidence array is formidable but perhaps not insurmountable. Crystal balls have been built and operate under

low luminosity conditions. These experiments are thus feasible if room background is small.

The energy scale for giant resonance experiments is typically be 0.1-1.0 GeV. Existing machines at Illinois and Mainz cover the 0.1-0.2 GeV region. However a complete study of the giant resonances requires q up to ~3 fm^{-1} (see Figure 3). We stress here that it is very important that all giant resonances in a particular well chosen target such as ^{16}O be studied in a self consistent way because the same basic particle-hole configurations are responsible for a wide spectrum of multipoles.[26] In order to effectively mount a program of GR studies up to q = 3 fm^{-1}, we have already pointed out that it is necessary to take data at as forward an electron scattering angle as possible.

Summary

The previous discussion indicates that the study of complex nuclei will greatly benefit by the introduction of electron scattering experiments from internal targets.

The availability of ultra thin targets and the feasibility of scattering from polarized targets are the two novel aspects of the proposed facility. In general, it appears feasible to perform:

Inclusive measurements from polarized targets

and

coincidence measurements from unpolarized jets.

These measurements nicely complement the coincidence measurements from external targets. It also appears that the study of non-zero spin nuclei will benefit most, at least in the case of elastic and inelastic scattering.

Finally it is our belief that the cases examined are broad and very important to our understanding of nuclear physics. Their investigation certainly warrants the expense required to establish such a facility.

Conclusion

As pointed out by R. Pollock[27] we are about to enter a new era. The era of internal target and polarization phenomena in which we are beginning to deviate from the targeting techniques pioneered by Rutherford and his students. Certainly the introduction of such techniques in electron scattering opens avenues of research presently inaccessible. We have barely

scratched the surface of a vast program that seems to lie ahead in nuclear structure studies. Other speakers have pointed out advantages that such a facility will bring to the few body problem[28] or the study of nucleonic resonances[24]. The prospects seem exciting to say the least.

The complexity of the experimental arrangement, especially if polarized targets are included,[10] will also dramatically increase. This will have a profound effect on the style with which nuclear physics will be practiced in the future.

It would hardly constitute an overstatement to say that this decade will be revolutionary for electromagnetic nuclear physics. Not only are continuous electron beams becoming widely available and coincidence measurements common, but another dimension has been added with the options allowed by internal targets.

Acknowledgements

It is a pleasure to acknowledge numerous discussions with many colleagues. In particular we would like to thank L. Cardman, W. Donnelly, D. G. Ravenhall, and S. E. Williamson for sharing their expertise and insights with us. This work was supported by the U.S. National Science Foundation under grant NSF PHY 83-11717 and the U.S. Department of Energy under grant DE-AC-79ER10338.

References

1. S.G. Popov in Proceedings of the Workshop on the Use of Electron Rings for Nuclear Physics Research in the Intermediate Energy Region", p. 150, J.O. Adler, Editor, Lund, Sweden (1983) see also Novosibirsk preprints 81-122 and 83-17.
2. T. deForest, Jr., Ann. Phys. (N.Y.) 45, 365 (1967).
3. R. Raphael and H. Uberall, Phys. Rev. 143, 671 (1966).
4. D. Drechsel and H. Uberall, Phys. Rev. 181, 1383 (1969).
5. Kleppinger and J.D. Walecka, Ann. of Phys. 146, 349 (1983).
6. See talk by W. Donnelly in this volume. Also W. Donnelly, Workshop on Perspectives in Nuclear Physics at Intermediate Energies, Trieste, Italy, October 1983, to be published.
7. T. deForest, Jr. and J. D. Walecka, Adv. in Physics 151, 1 (1966).
8. J. Heisenberg, Adv. in Nucl. Phys., 66, Vol. 12 (1981), W. Negele and E. Vogt, editors.
9. Proceedings of the Workshop on the Use of Electron Rings for Nuclear Physics Research in the Intermediate Energy Region, Volumes 1 and 2, J. O. Adler, editor, Lund, Sweden (1983). See articles by R.E. Pollock and especially J. Gspann.
10. Argonne Workshop on Polarized Targets in Storage Rings held in Argonne, May 17-18, R. Holt, editor, to be published.
11. C. N. Papanicolas, S. E. Williamson, H. Rothhaas, L. S. Cardman, G. Bolme, L. J. Koester, Jr., B. Miller, R. Miskimen, and P. Mueller, University of Illinois preprint.
12. J. M. Cavedon, Ph.D. thesis, Universite de Paris (1980) unpublished.
13. S. K. Platchkov, J. B. Bellicard, J. M. Cavedon, B. Frois, D. Goutte, M. Huet, P. Leconte, Phan Xuan Ho, P.K.A. deWitt Huberts, L. Lapikas and I. Sick. Phys. Rev. C25, 2318 (1982), and P.K.A. deWitt Huberts, in Proceedings of the conference "Modern Trends in Elastic Electron Scattering", Amsterdam (1978) C. deVries, editor.
14. Y. Horikawa et al., Nucl. Phys. A278, 297 (1977).
15. Nuclear Physics Laboratory March, 1983 Report "Nuclear Physics Research and High Duty Factor Electron Accelerators".
16. C. N. Papanicolas, et al., Proceedings of the International Conference on Nuclear Physics, V1, 323, Florence, Italy (1983). Ricci, editor.

17. Proceedings of Giant Resonance Topical Conference, Oak Ridge, F. E. Bertran, editor, Harwood Academic Publishers (1980).
18. L. S. Cardman, Nucl. Phys. A354, 173c (1981).
19. H. A. Broglia, Oak Ridge Conference op. cit.
H. A. Weidenmuller, Lecture Notes in Physics 108 (Springer-Verlag, Berlin, 1979).
20. K. T. Knopffe, Lecture Notes in Physics, Springer-Verlag, Vol. 108, 288 (1979).
21. H. Stroher et al., Phys. Rev. Lett. 47, 318 (1981) and references therein.
22. G. Bolme, Ph.D. thesis, University of Illinois (1983) unpublished.
23. F. Bertrand, Nucl. Phys. A354, 129c (1981).
24. A. Sandorfi, et al., Phys. Rev. Lett. 40, 1248 (1978).
25. R. Bergere, Lecture Notes in Physics, 61, 1, Springer-Verlag, Berlin (1977).
26. J. R. Calarco and S. S. Hanna in Future Directions in Electromagnetic Nuclear Physics, MIT (1981).
27. R.E. Pollock, Comments Nucl. Part. Phys. 12, 73 (1983).
28. See contribution by H. Jackson this volume.
29. See contribution by B. Mecking this volume.

THE KAON-NUCLEON INTERACTION IN A QUARK POTENTIAL MODEL*

R.K. CAMPBELL

Physics Department, Florida State University, Tallahassee, Florida 32306

The K^+-N system has several features which make it a good prototype for studying hadron-hadron interactions at the quark level.[1] There is no one pion exchange or tensor force and since the antiquark in the K^+ meson is strange it cannot annihilate with an up or down quark in the nucleon.

We have calculated the K^+-N interaction with a quark potential model using the resonating group method.[2] The quark potential and hadronic wavefunctions were taken from the work of Stanley and Robson.[3] The parameters of this model were fixed by fitting the meson spectrum using oscillator basis states. The baryon spectrum was then calculated using a set of three body oscillator basis states.[1]

By using a well determined model for mesons and baryons certain features of hadron-hadron interactions can be calculated in a self-consistent,parameter free fashion. For example, the inclusion of mixed orbital symmetry components of the internal nucleon wave functions has been shown to be important in calculating nucleon-nucleon quark exchange potentials and accounts for some intermediate range attraction in the singlet-even and triplet-even potentials.

The single channel resonating group equation is

$$[\, T_R+V_C(R)-E]F(\bar{R})-\int K_I(\bar{R},\bar{R}')F(\bar{R}')d\bar{R}'=0$$

where $K_I(\bar{R},\bar{R}')$ is the energy dependent interaction kernel.

*Supported in part by the U.S. Department of Energy.

The total isospin I=0 central K^+-N kernel is an order of magnitude weaker than the I=1 kernel. The S-wave phase shifts for the nonlocal interaction and an effective local potential[4] are given in figure 2.

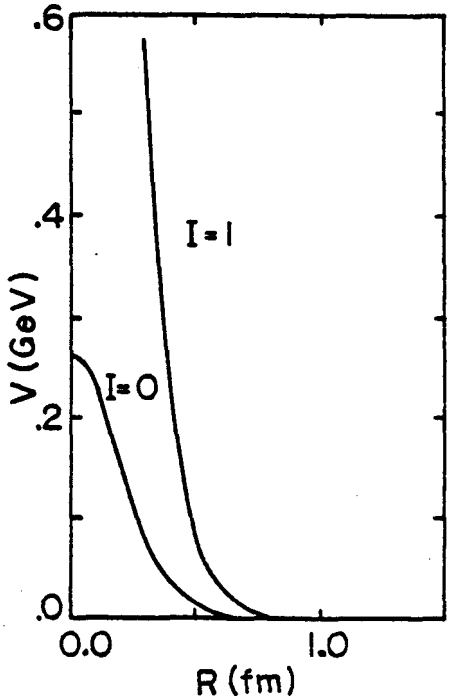

Fig.1 K^+-N effective local potential

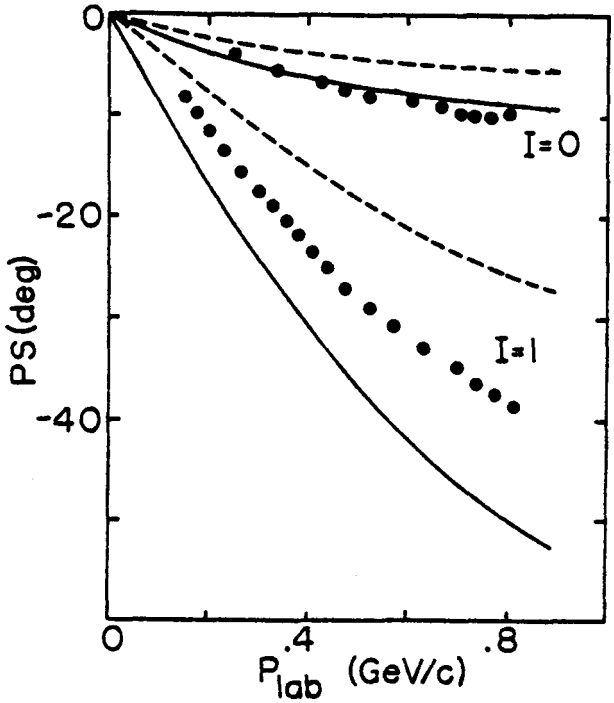

Fig.2 S-wave phase shifts
------ local
——— nonlocal
● ref. 5

References

1) D. Robson, Prog. in Part. and Nucl. Phys. 8, 257(1982).

2) Y.C. Tang et al, Phys. Rep. 47, 169(1978).

3) D.P. Stanley, D. Robson, Phys. Rev. D21, 3180(1980).

4) C.S. Warke, R. Shanker, Phys. Rev. C21, 2643(1980).

5) B.R. Martin, G.C. Oades, Proc. of the IVth International Conference on Baryon Resonances, ed. N. Isgur (1981).

CURRENT CONSERVATION AND MAGNETIC FORM FACTORS OF ^{3}He, ^{3}H*

M.A. Maize† and Y.E. Kim
Department of Physics, Purdue University, West Lafayette, IN 47907

We report the results of our recent calculation of the ^{3}He magnetic form factor, $F_M^{^3He}(Q^2)$, and the ^{3}H magnetic form factor, $F_M^{^3H}(Q^2)$, for the momentum transfer square, $Q^2<30fm^{-2}$, using the wave function obtained from a solution of the Faddeev equation with the Reid soft-core potential. For the electromagnetic currents, we use both the single-nucleon currents and the meson-exchange currents satisfying the requirement of current conservation consistent with the one-pion exchange interaction (OPEI) which includes the πNN vertex form factor, $F_{\pi NN}(k^2)$.

For the exchange currents, we consider both pion and ρ-meson exchanges as shown in fig. 1. The pionic, pair, and isobar currents (figs. 1a,1b, and 1c) will be denoted as $\underset{\sim}{j}^{(2)}_{\pi}$, $\underset{\sim}{j}^{(2)}_{\pi NN}$, and $\underset{\sim}{j}^{(2)}_{\pi N\Delta}$, respectively, and the corresponding ρ-meson exchange currents as $\underset{\sim}{j}^{(2)}_{\rho}$, $\underset{\sim}{j}^{(2)}_{\rho NN}$ and $\underset{\sim}{j}^{(2)}_{\rho N\Delta}$ (figs. 1a,1b, and 1c, respectively). Since $\underset{\sim}{j}^{(2)}_{\pi N\Delta}$ and $\underset{\sim}{j}^{(2)}_{\rho N\Delta}$ turn out to be transverse, they satisfy the current conservation automatically.

The explicit expressions of $\underset{\sim}{j}^{(2)}_{\pi}$ and $\underset{\sim}{j}^{(2)}_{\pi NN}$ used are

$$\underset{\sim}{j}^{(2)}_{\pi} = \frac{ig^2}{4M^2} F_\pi(Q^2)(\underset{\sim}{\tau}_1 x \underset{\sim}{\tau}_2)_z (\underset{\sim}{\sigma}_1\cdot\underset{\sim}{k}_1)(\underset{\sim}{\sigma}_2\cdot\underset{\sim}{k}_2)\frac{\underset{\sim}{k}_1 - \underset{\sim}{k}_2}{k_2^2 - k_1^2}\left[\frac{F_{\pi NN}(k_1^2)}{k_1^2+\mu^2} - \frac{F_{\pi NN}(k_2^2)}{k_2^2+\mu^2}\right] \tag{1}$$

and

$$\underset{\sim}{j}^{(2)}_{\pi NN} = \frac{ig^2}{4M^2} F_1^v(Q^2)(\underset{\sim}{\tau}_1 x \underset{\sim}{\tau}_2)_z \left[\frac{(\underset{\sim}{k}_1\cdot\underset{\sim}{\sigma}_1)\underset{\sim}{\sigma}_2}{k_1^2+\mu^2} F_{\pi NN}(k_1^2) - \frac{(\underset{\sim}{k}_2\cdot\underset{\sim}{\sigma}_2)\underset{\sim}{\sigma}_1}{k_2^2+\mu^2} F_{\pi NN}(k_2^2)\right] \tag{2}$$

where $(g^2/4\pi) = 14.5$, and M and μ are the nucleon and pion mass, respectively. $F_\pi(Q^2)$ is the $\gamma\pi$ vertex form factor (fig. 1a) and $F_1^v(Q^2)$ is the Dirac form factor for the $\gamma\pi N$ vertex in fig. 1b obtained with use of the pseudovector coupling for the photoproduction amplitude. The 3-momenta, $\underset{\sim}{k}_1$ and $\underset{\sim}{k}_2$, are given by $\underset{\sim}{k}_1 = \underset{\sim}{P}_1' - \underset{\sim}{P}_1$ and $\underset{\sim}{k}_2 = \underset{\sim}{P}_2' - \underset{\sim}{P}_2$ where $\underset{\sim}{P}_i$ and $\underset{\sim}{P}_i'$ are the initial and final momenta of the ith nucleon. Eq.(1) is not derived from Feynman diagram (fig. 1a) but is constructed so as to satisfy the current conservation,[1,2]

$$\underset{\sim}{Q}\cdot(\underset{\sim}{j}^{(2)}_{\pi} + \underset{\sim}{j}^{(2)}_{\pi NN}) = [V_{OPEI}, \rho(Q^2)] \tag{3}$$

with $F_1^v(Q^2) = F_\pi(Q^2) = G_E^v(Q^2)$[3,4] and $\rho(Q^2) = \sum_i \frac{1}{2}[G_E^s(Q^2) + (\tau_i)_z G_E^v(Q^2)]$ where $G_E^s(Q^2) = f_{ch}^p(Q^2) + f_{ch}^n(Q^2)$ and $G_E^v(Q^2) = f_{ch}^p(Q^2) - f_{ch}^n(Q^2)$ with normalizations $f_{ch}^p(0) = 1$ and $f_{ch}^n(0) = 0$, and $V_{OPEI} = V_{OPEP}F_{\pi NN}^2(k^2)$,

$k^2 = k_1^2 = k_2^2$. In the previous calculations,[5] the pionic current given by eq. (1) was not used.

We use a monopole form of $F_{\pi NN}(k^2)=(\Lambda^2-\mu^2)/(k^2+\Lambda^2)$ for the meson-exchange currents. For all pion-exchange currents, $\Lambda = 4\mu$ and 6μ are chosen to simulate the OPEI of the Reid soft-core potential. For all ρ-meson exchange currents, we use $\Lambda = 2.6\ m_\rho$ with $m_\rho = 773$ MeV. Our calculated results with $\underset{\sim}{j}_M^{(1)}$ (impulse approximation) and the total current, $\underset{\sim}{J} = \underset{\sim}{j}_M^{(1)} + \underset{\sim}{J}^{(2)}$ are plotted in figs. 2-5. $\underset{\sim}{j}_M^{(1)}$ is the spin (magnetic) current (we neglect a smaller convection current) and $\underset{\sim}{J}^{(2)}$ is the total mexon-exchange current, $\underset{\sim}{J}^{(2)} = \underset{\sim}{j}_\pi^{(2)} + \underset{\sim}{j}_{\pi NN}^{(2)} + \underset{\sim}{j}_{\pi N\Delta}^{(2)} + \underset{\sim}{j}_\rho^{(2)} + \underset{\sim}{j}_{\pi\overline{NN}}^{(2)} + \underset{\sim}{j}_{\pi N\Delta}^{(2)}$. Our previous result[3] for the case of $\Lambda = \infty$ is also shown for comparison. Fig. 2 shows comparison of the results for $|F_M^{^3He}(Q^2)|$ calculated with $\Lambda = 4\mu$ (..., $\Lambda_\rho = 2.6\ m_\rho$), $\Lambda = 4\mu$ (-·-·, $\Lambda_\rho = 2.6\ m_\rho$, $f_{ch}^n(Q^2) = 0$), $\Lambda = 6\mu$ (---, $\Lambda_\rho = 2.6\ m_\rho$) and $\Lambda = \infty$ (——, $\Lambda_\rho = \infty$), using the substitutions, $F_\pi(Q^2) \to G_E^v(Q^2)$ and $F_1^v(Q^2) \to G_E^v(Q^2)$. The experimental data are from references 6 (open circles) and 7 (dots). Fig. 3 gives comparison of the results for $|F_M^{^3H}(Q^2)|$ calculated with the same parameters used in fig. 2. The experimental data is from ref. 8 (open circles). Fig. 4 shows comparison of the results for $|F_M^{^3He}(Q^2)|$ calculated with $\Lambda = 4\mu$ (——, with $F_1^v(Q^2)$ instead of $G_E^v(Q^2)$ for $\underset{\sim}{j}_{\pi NN}^{(2)}$), $\Lambda = 4\mu$ (..., $F_1^v(Q^2)$ replaced by $G_E^v(Q^2)$), $\Lambda = 6\mu$ (-·-· with $F_1^v(Q^2)$ instead of $G_E^v(Q^2)$ for $\underset{\sim}{j}_{\pi NN}^{(2)}$), and $\Lambda = 6\mu$ (---, with $F_1^v(Q^2)$ instead of $G_E^v(Q^2)$ for $\underset{\sim}{j}_{\pi NN}^{(2)}$). In all cases of fig. 4, $\Lambda_\rho = 2.6\ m_\rho$. Finally, fig. 5 shows comparison of the results for $|F_M^{^3H}(Q^2)|$ calculated with the same parameters used in fig. 4. Our results indicate that we will need additional contributions such as those from multi-quark currents.

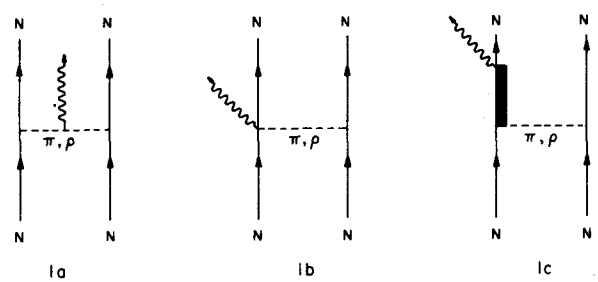

Fig. 1. Diagrams for exchange currents.

REFERENCES

1. M. Chemtob, in Mesons in Nuclei, M. Rho and D. Wilkinson (North Holland, Amsterdam, 1975) p. 495.
2. L.L. Foldy, J.A. Lock, in Mesons in Nuclei, M. Rho, D. Wilkinson (North Holland, Amsterdam, 1975) p. 465; Ann. of Phys. (NY) 93,276 (1975).
3. M.A. Maize, Y.E. Kim, "Meson-Exchange Currents and the ^{3}He Magnetic Form Factor", Nucl. Phys. A407, 507 (1983).

4. F.L. Friar, S. Fallieros, Phys. Rev. C13, 2571 (1976).
5. W. Strueve, Ch. Hajduk, P.U. Sauer, Nucl. Phys. A405, 620 (1983) and references therein.
6. P.C. Dunn, et al., Phys. Rev. C27, 71 (1983).
7. J.M. Cavedon et al., Phys. Rev. Lett. 49, 986 (1982).
8. H. Collard et al., Phys. Rev. B57, 138 (1965).
*Work supported in part by the U.S. National Science Foundation.
†Address after September 1, 1984: Dept. of Physics, Brown University.

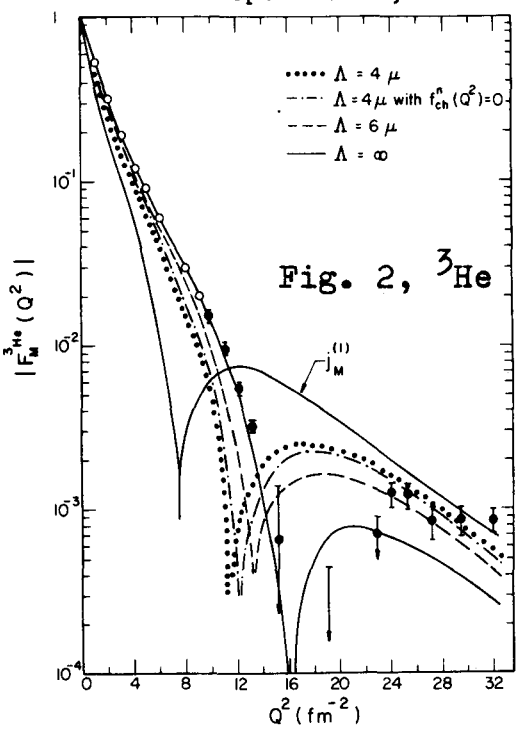

Fig. 2, ^{3}He

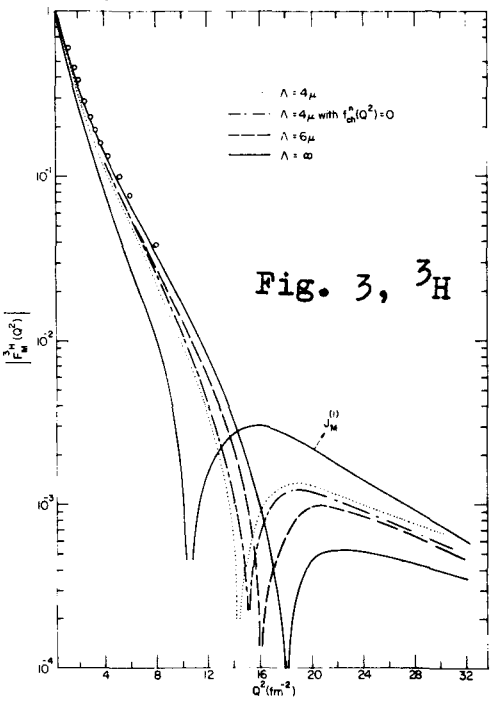

Fig. 3, ^{3}H

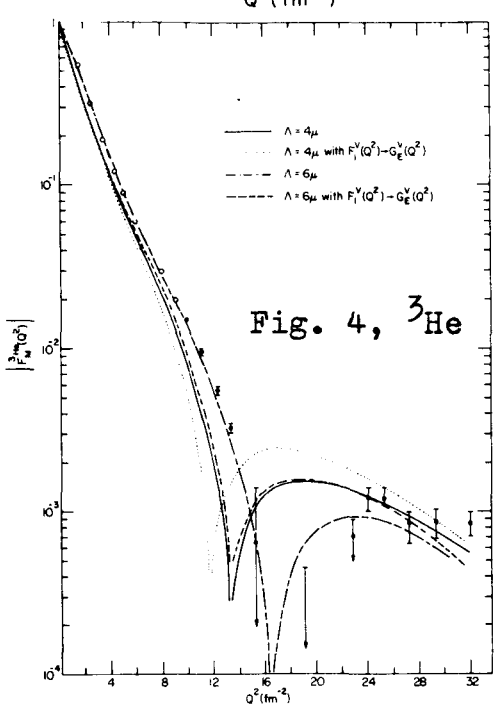

Fig. 4, ^{3}He

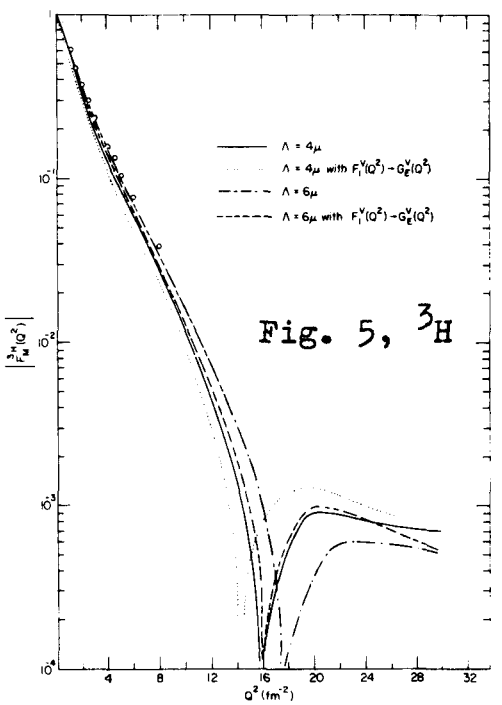

Fig. 5, ^{3}H

FINAL-STATE INTERACTIONS FOR ^{3}He, ^{3}H ELECTRO- AND PHOTO-DISINTEGRATIONS WITH SOLUTIONS OF THE FADDEEV EQUATION WITH REALISTIC TWO-NUCLEON POTENTIALS*

R. A. Brandenburg†, W. D. Braswell, K. T. Kim and Y. E. Kim

Department of Physics, Purdue University
West Lafayette, IN 47907

Since accurate experimental coincidence measurements of ^{3}He, ^{3}H electro- and photo-disintegrations are expected to be carried out at the Continuous Electron Beam Accelerator Facility (CEBAF), it is desirable to have accurate theoretical studies of the effects of the final-state interactions (FSI) for these processes at the CEBAF energies, using the realistic two-nucleon potentials and covering a complete final-state phase-space. Such theoretical studies of ^{3}He, ^{3}H electro- and photo-disintegrations are essential for testing the conventional potential-model description at lower and intermediate momentum transfers. They are also important for accurately determining the expected failure of the potential models at higher momentum transfers, before we speculate how significant the effect of the quark-degrees of freedom is for the three-nucleon systems at the CEBAF energies. Furthermore, these studies are useful for planning future experiments at the CEBAF involving ^{3}He and ^{3}H.

We have started to develop a set of computer programs for the Purdue Cyber 205 computer to calculate the coincidence cross-sections for (two- and three-body) electro- and photo-disintegrations of ^{3}He and ^{3}H, using the negative (bound state) and positive (continuum state) energy solutions of the Faddeev equation generated with the Reid soft-core[1] and Paris[2] potentials. The accurate negative energy solutions of the Faddeev equation with realistic two-nucleon potentials have been available since early 70's.[3] The accurate positive energy solutions of the Faddeev equation have not been achieved until now due to the complexity of the numerical problems involved. Most recently, one of us (R. A. Brandenburg) has developed an extensive computer code named "KASEY" for the Cyber 205 computer at Bochum and Purdue, which is capable of solving the Faddeev equation (with an expected accuracy

of better than 1%) for the positive energies (both below and above the break-up thresholds) using the Reid soft-core potential effective in the ^1S_o, $^3S_1 - {}^3D_1$, $^1P_1$, ^3P_o, $^3P_1$ partial wave states. The option of using other realistic two-nucleon potentials such as the Paris potential is now being incorporated in KASEY. The negative energy solutions can also be generated from a modified version of KASEY using the Reid soft-core and Paris potentials.

For both negative and positive energies, KASEY solves the Faddeev equation[4],

$$T = tP + tG_oPT \tag{1}$$

where t is the two-nucleon t-matrix, $P(= P_{123} + P_{132})$ is the sum of two permutation operators, and G_o is the free three-nucleon Green's function. The basic method of solution for eq. (1) used in KASEY is to iterate the integral equation (1) and then to sum the iterates using the Padé approximant techniques.[5] The scattering matrix M can be extracted from the T-matrix through $M = PV + PT = PG_o^{-1} + PT$ where M satisfies the AGS equation[6],

$$M = PG_o^{-1} + PtG_oM. \tag{2}$$

The positive energy scattering wave functions can also be extracted from the T-matrix. A series of papers describing the results of calculations for the n-d elastic and break-up cross-sections using KASEY will be published by one of us (R. A. Brandenburg).

We are now developing a set of computer codes for the Purdue Cyber 205 computer which will calculate the coincidence differential cross-sections for ^3H (and ^3He) electro- and photo-disintegrations (both two-body and three-body break-up) using the results generated by KASEY. Both the single-nucleon (impulse approximation) and two-nucleon (meson-exchange) currents will be included. We plan to investigate the effects of the final-state interaction for the following processes:

Electro-disintegrations of ^3H and ^3He

(1) Quasi-elastic electron scattering (spectral function,[7,8] Y-scaling[9], and nucleon-momentum distributions[8]).

(2) Deep inelastic electron scattering (the EMC[10] - SLAC[11] effect and ^{3}He, ^{3}H structure functions).
(3) Coincidence measurements of ^{3}H three-body disintegration (extraction of the neutron charge form factor[12]).
(4) Determination of the form factor for the neutral current[13] from the deep inelastic polarized electron scattering[14].

Photo-disintegrations and radiative capture

(5) Two-[15,16] and three-body[17] photo-disintegrations of ^{3}He and ^{3}H.
(6) Radiative capture, $p + d \rightarrow {}^3He + \gamma$[15].
(7) Weak nuclear forces (photon circular polarization and asymmetry in $n + d \rightarrow {}^3H + \gamma$).[18]

A brief discussion of each of the above processes will be given with emphasis on the physical significances as they relate to the possible future experiments at the CEBAF.

*Work supported in part by the U.S. National Science Foundation.
†Permanent address: Institute for Physics, University of Basel, 4056 Basel, Switzerland.

REFERENCES

1. R. V. Reid, Ann. of Phys. 50, 411 (1968).
2. M. Lacombe et al., Phys. Rev. C21, 861 (1980).
3. R. A. Brandenburg, Y. E. Kim and A. Tubis, Phys. Rev. C12, 1368 (1975) and references therein.
4. L. D. Faddeev, Soviet Phys. JETP 12, 1014 (1961); Mathematical Problems of the Quantum Theory of Scattering for a Three-Particle Systems, Davey and Co., New York (1965).
5. G. A. Baker, Jr.,Essentials of Padé Approximants, Academic Press, New York (1970).
6. E. O. Alt, P. Grassberger and W. Sandhas, Nucl. Phys. B2, 167 (1967).
7. A.E.L. Dieperink, T de Forest Jr., I. Sick and R. A. Brandenburg, Phys. Lett. 63B, 261 (1976).
8. E. Jans et al., Phys. Rev. Lett. 49, 974 (1982).
9. I. Sick, D. Day and J. S. McCarthy, Phys. Rev. Lett. 45, 871 (1980).
10. J. J. Aubert et al., Phys. Lett. 123B, 275 (1983).
11. A Bodek et al., Phys. Rev. Lett. 50, 1431 (1983).
12. B. A. Craver, Thesis, Purdue University (1976); Y.E. Kim, in Interaction Studies in Nuclei, edited by H. Jochim and B. Ziegler (North Holland, Amsterdam, 1975),p. 635; Y.E. Kim, in Lecture Notes in Physics, 86, 231 (1978).
13. S. Weinberg, Phys. Rev. Lett. 19 (1967) 1264; 27 (1971) 1688; A. Salam, in Elementary Particle Theory: Relativistic Groups and Analyticity (Nobel Symposium No. 8), ed. N. Svartholm (Almquist and Wiksell, Stockholm, 1968), p. 367.
14. C. Y. Prescott et al., Phys. Lett. 77B, 347 (1978); R. Conti et al., Phys. Rev. Lett. 42, 343 (1979).
15. B. A. Craver, Y. E. Kim and A. Tubis, Nucl. Phys. A276, 237 (1977) and references therein.
16. W. J. Brisco et al.,Phys. Rev. Lett. 49, 187 (1982).
17. D. D. Faul et al.,Phys. Rev. Lett. 44, 129 (1980).
18. E. Hadjimichael et al.,Phys. Rev. Lett. 27, 1322 (1971).

MULTI-QUARK COMPOUND RESONANCES IN NUCLEI AT THE CEBAF ENERGIES*

Y. E. Kim and M. Orlowski

Department of Physics, Purdue University
West Lafayette, IN 47907

Recently, we proposed a method of incorporating quark degrees of freedom in nuclei[1] based on the resonating group method.[2] One of the consequences of our theory for the resonating group quark-cluster model of nuclei is that the quark degrees of freedom in nuclei will manifest as the multi-quark compound resonances (MQCR) at higher excitation energies, which may be regarded as precursors to the formation of quark-gluon plasma states currently being speculated.

For the most simple case of isolated n-p system with only one open (s-wave elastic) channel, the scattering state, $\psi_E(r)$, can be written as[1,3]

$$\psi_E(r) = \phi_n\phi_p\chi_E(r \geq R_1) + A(E)\phi_s^1(r \leq R_2) \qquad (1)$$

where $\chi_E(r \geq R_1)$ is the exterior ($r \geq R_1$) wave function describing the relative motion between proton and neutron, ϕ_n and ϕ_p are the three-quark color-singlet nucleon bags, and $\phi_s^1(r \leq R_2)$ describes a interior ($r \leq R_2$) six-quark compound (SQC) state. The transition region between the SQC states and color-singlet two-nucleon states are restricted to the region between R_1 and R_2 with $R_2 > R_1$ and $(R_2 - R_1) \lesssim 0.6$ fm[4]. At the resonance energy, $E = E_r$, the amplitude $A(E)$ has a maximum and it's shape determines the width (or lifetime) of the SQC resonance. Therefore, near $E = E_r$, we have a quasi-confinement of six quarks or quark compound bag (QCB) which can be described as a quasi-bound state, $\psi_{E_r}(r) \simeq A(E_r)\phi_s(r \leq R_2)$ with $R_2 \simeq 1 \sim 2$ fm. At lower energies away from the resonance energy E_r, $A^2(E)$ diminishes and is estimated to be about 2 ~ 5% in the bound state deuteron wave function.[3] We note that the six-quark compound state may not exist as a separate physical object but may exist only in connection with hadronic bound or resonance states when hadronic clusters overlap strongly. ϕ_s ($r \leq R_2$) may be a predominantly hidden color state ψ_{cc} and be represented, for an example, by a linear combination[5]

$$\phi_s^1 = \sqrt{1/9}\,\psi_{NN} + \sqrt{4/45}\;\phi_{\Delta\Delta} + \sqrt{4/5}\;\phi_{cc} \qquad (2)$$

with

$$\psi_{cc} = |(uud)_8\,(ddu)_8\rangle + |(uuu)_8\,(ddd)_8\rangle \qquad (3)$$

Using the resonating group method[2], we solve dynamical model for the ansatz (1) in a restricted space given by the full variation in $\delta\chi$ and $\delta A(E)$. Setting $\langle\delta\psi|H(6q)-E|\psi\rangle \simeq 0$, we obtain

$$\langle\phi_n\phi_p\,\delta\chi|H(6q)-E|\phi_n\phi_p\chi\rangle + A(E)\,\langle\phi_n\phi_p\,\delta\chi|H(6q)-E|\phi_s^1\rangle = 0\,, \qquad (4)$$

and

$$\langle\phi_s^1|H(6q)-E|\phi_n\phi_p\chi\rangle + A(E)\,\langle\phi_s^1|H(6q)-E|\phi_s^1\rangle = 0. \qquad (5)$$

Applying the idea of the MQCR in nuclei, we have recently proposed a new consistent explanation of "anomalon"[11] as the effect of enhancement of nuclear cross-sections due to collective excitations of the multi-quark compound resonances (MQCR) in interacting nuclear systems.[12] Our predictions are consistent so far not only with the emulsion data[11] but also with the most recent results of plastic-counter measurements.[13] The new results of reference 14 strongly suggest that the anomalon effect should be investigated for the secondaries (and also primaries) with $4 < Z < 9$ before we can definitely rule out our model and the anomalon effect. Recently, Chemtob and Peschanski[15] have shown that the SQC cluster mechanism provides also a viable explanation of the EMC effect[16].

Ultimately, it would be desirable to do difficult counter (spectrometer) experiments for (both inclusive and exclusive) electron-nucleus, proton-nucleus and nucleus-nucleus scattering in the kinematic phase space where the energy tranfers to the target nuclei cover the MQCR excitations of ~ 0.5 GeV c.m. Some of the MQCR states in nuclei may turn out to be narrow (unlikely), but most of them may occur at the CEBAF energies as broad resonances. Thus the CEBAF can play an important and crucial role in probing the possible existence of the MQCR in nuclei, which may turn out to be precursors of the quark-gluon plasma states.

REFERENCES

1. Y. E. Kim and M. Orlowski, AIP Conference Proceedings, 110, 271 (1983).
2. J. A. Wheeler, Phys. Rev. 52, 1083 (1937); ibid., 1107 (1937); K. Wildermuth and Y. C. Yang, "A Unified Theory of the Nucleus", Academic Press, New York (1977).
3. Y. E. Kim and M. Orlowski, "Nuclear Chromodynamics and Six-Quark Compound Bag Component of Deuteron", to be published in Phys. Lett.
4. C. G. Callen et al., Phys. Rev. Lett. 45, 313 (1980).
5. M. Harvey, Nucl. Phys. A352, 301 and 326 (1981).
6. T. Kamae, Nucl. Phys. A374, 25C (1982).
7. T. Kamae et al., Phys. Rev. Lett. 38, 468 (1977); Nucl. Phys. B139, 394 (1978); W. Grein et al., Phys. Lett. 96B, 176 (1980).
8. Y. E. Kim and M. Orlowski, "Six-Quark Compound State in Deuteron", to be published in Phys. Rev. C.
9. C. K. Warke, R. Shanker, W. Greiner, J. Phys. G: Nucl. Phys. 7, L1 (1981).
10. A. DeRujula, H. Georgi, S. Glashow, Phys. Rev. D12, 147 (1975).
11. E. M. Friedlander, et al., Phys. Rev. C27, 1489 (1983) and references therein.
12. Y. E. Kim and M. Orlowski, LBL Report No. LBL-16281, p. 173 (1983).
13. J. D. Stevenson, J. A. Musser, and S. W. Barwick, Phys. Rev. Lett. 52, 515 (1984); W. Heinrich et al., Phys. Rev. Lett. 52, 515 (1984).
14. A. Z. M. Ismail et al., Phys. Rev. Lett. 52, 1280 (1984).
15. M. Chemtob and R. Peschanski, J. Phys. G: Nucl. Phys. 10, 599 (1984).
16. J. J. Aubert et al., Phys. Lett. 123B, 275 (1983).

*Work supported in part by the U.S. National Science Foundation.

The elimination of the six-quark interior state gives rise to an additional potential of a separable form with energy-dependent strength $\lambda(E) = (e^1 - e)^{-1}$. We obtain from eqs. (2) and (3) ($E^1 \simeq E_r$),

$$(T + V_{NN} - \frac{|\psi^1\rangle \langle\psi^1|}{e^1 - e} - e)\ \chi = 0 \quad . \tag{6}$$

Here T is the kinetic energy operator of the n-p system, V_{NN} is the NN potential with the boundary condition at r_o, e and e^1 are defined by $(E - e_n - e_p)$ and by $(E^1 - e_n - e_p)$, respectively, where $e_{n(p)}$ is the nucleon mass corresponding to a QCD solution of $H(3q)\phi_{n(p)} = e_{n(p)}\phi_{n(p)}$. The form factor ψ^1 is defined as

$$\psi^1(r) = \langle \phi_s^1 | H(6q) - E | \phi_n \phi_p \quad r \geq R_1 \rangle = c^1 \delta(r - r_o), \tag{7}$$

where the quantity c^1 depends weakly on energy and represents the effective coupling strength of H(6q) between the interior quark and the exterior nuclear phase of matter. From eqs. (6) and (7), we obtain the S-matrix element, S_ℓ, in a state of angular momentum ℓ as

$$S_\ell = \exp(2i\delta_\ell^{NN}(e)) \quad \frac{e^1 - e - \Delta(e) + \frac{1}{2} i\Gamma(e)}{e^1 - e - \Delta(e) - \frac{1}{2} i\Gamma(e)}. \tag{8}$$

The exponential function $\exp(2i\delta_\ell^{NN}(e))$ contains the background phase shift $\delta_\ell^{NN}(e)$, of the NN potential solutions, i.e., without the knowledge of the six-quark state excitation. $\Delta(e)$ is the energy pole shift due to the coupling of the resonance state to the open channel, and $\Gamma(e)$ is the resonance width. Eq. (8) reveals already the form of Breit-Wigner resonance formula for pure elastic scattering.

Evidences for isolated dibaryon or six-quark resonances have been rapidly accumulated in recent years.[6] One good candidate for the lowest SQC resonance state with the deuteron quantum number, $(I)J^\pi = (0)1^+$, is the dibaryon resonance recently observed by Kamae et al.[7] in the proton polarization measurement of the deuteron photodisintegration, which occurs at $E_r \simeq 2.36$ GeV with a total width of $\Gamma \simeq 0.34$ GeV. Unless we find new narrow dibaryon resonances near or below the Kamae resonance in the future experiments, it is most likely that our identification of ϕ_s^1 with the Kamae resonance is correct. The fact that the Kamae resonance is observed in the deuteron photodisintegration will then turn out to be an important consideration for the future experimental programs in probing the MQCR in nuclei at the CEBAF. Using our formulation, we have determined the probability of the six-quark compound state component of deuteron to be 2.2 - 5.5%[3] using the experimental np partial width of the dibaryon resonance of Kamae et al.[7] Our estimate of 2.2 - 5.5% is consistent with an estimate of 3-4% using the experimental data and quantum chromodynamics prediction for the deuteron form factor[8] and also with another estimate of 2.73% by Warke, Shank, and Greiner[9] from the DeRujula-Georgi-Glashow quark model.[10]

WORKSHOP PARTICIPANTS

Raymond G. Arnold
S.L.A.C
Stanford University
P.O. Box 4349
Stanford, CA 94305

G. Audit
Cen-Saclay BP No. 2
F-91190
Gif-sur-Yvette
France

Helmut Baer
MP 4, MS H-846
LAMPF
P.O. Box 1663
Los Alamos, NM 87545

Charles A. Barnes
Dept. of Physics
California Institute of Technology
Pasadena, CA 91125

Jacob Becher
Dept. of Physics
Old Dominion University
Norfolk, VA 23508

Barry L. Berman
Lawrence Livermore National Lab.
P.O. Box 808
Livermore, CA 94550

William Bertozzi
Dept. of Physics
MIT, Bldg. 26-441
Cambridge, MA 02139

K. Ingvar Blomqvist
Dept. of Physics
MIT, Bates
Cambridge, MA 02139

William Briscoe
Dept. of Physics
George Washington University
Washington, DC 20052

Nance Briscoe
National Bureau of Standards
Gaithersburg, MD 20899

Karl L. Brown
Stanford Linear Accelerator Center
P.O. Box 4349
Stanford, CA 94305

Warren W. Buck
Dept. of Physics
Hampton University
Hampton, VA 23668

David C. Buckle
CEBAF Site
12070 Jefferson Ave.
Newport News, VA 23606

Janice Button-Shafer
Dept. of Physics
GRC Tower C, University of Massachuse
Amherst, MA 01003

R. Campbell
Dept. of Physics
Florida State University
Tallahassee, FL 32306

Lawrence S. Cardman
Nuclear Physics Laboratory
University of Illinois
23 Stadium Drive
Champaign, IL 61820

Carl E. Carlson
Dept. of Physics
College of William and Mary
Williamsburg, VA 23185

Chia-Cheh Chang
Physics Program
University of Maryland
College Park, MD 20742

Hall L. Crannell
Intermediate Energy Physics
National Science Foundation
Washington, DC 20550

William R. Dodge
National Bureau of Standards
Gaithersburg, MD 20899

William T. Donnelly
Dept. of Physics
Massachusetts Institute of Technology
Cambridge, MA 02139

Brad Filippone
Dept. of Physics
California Institute of Technology
Pasadena, CA 91125

Michael Finn
Dept. of Physics
MIT, Bldg. 26-445
Cambridge, MA 02139

Jacob Flanz
Lab for Nuclear Science
MIT, Bates
Cambridge, MA 02139

Gregg Franklin
Dept. of Physics
Carnegie-Mellon University
Pittsburgh, PA 15213

H. Funsten
Physics Dept.
College of William & Mary
Williamsburg, VA 23185

Bernard Goulard
Dept. of Physics
University of Montreal
Montreal, H3C 3J7
Quebec, Canada

Franz L. Gross
Dept. of Physics
College of William and Mary
Williamsburg, VA 23185

Edward E. Gross
Oak Ridge National Laboratory
Oak Ridge, TN 37831

Carlo Guaraldo
Lab. Naz. Frascati (INEN)
Casella Postale 13
00044 Frascati, Italy

C. Hajduk
Dept. of Physics
SUNY at Stony Brook
Stony Brook, NY 11794

Heidegret Hajduk
SUNY Stony Brook
Dept. of Physics
Stony Brook, NY 11794

Tim Havens
Dept. of Physics
College of William and Mary
Williamsburg, VA 23185

Mark D. Havey
Dept. of Physics
Old Dominion University
Norfolk, VA 23508

R. L. Heath
EG/G Idaho, Inc., Physics Division
P.O. Box 1625
Idaho Falls, ID 83401

David L. Hendrie
Bldg. 70A
Lawrence Berkeley Laboratory
Berkeley, CA 94720

William P. Hesse
Dept. of Physics
Randolph-Macon College
Ashland, VA 23005

Ross S. Hicks
Dept. of Physics
University of Massachusetts
Amherst, MA 01003

John Hiller
Dept. of Physics
Purdue University
West Lafayette, IN 47907

Harry D. Holmgren
Physics Program
University of Maryland
College Park, MD 20742

Roy J. Holt
Argonne National Laboratory
9700 S. Cass Avenue
Argonne, IL 60439

Nathan Isgur
Dept. of Physics
University of Toronto
Toronto M5S 1A7
Ontario, Canada

David A. Jenkins
Dept. of Physics
Virginia Polytechnic Institute
and State University
Blacksburg, VA 24061

Donald Joyce
Dept. of Physics
College of William and Mary
Williamsburg, VA 23185

Kirby W. Kemper
Physics Department
Florida State University
Tallahassee, FL 32306

Yeong E. Kim
Dept. of Physics
Purdue University
West Lafayette, IN 47907

William Kleppinger
Physics Division
Argonne National Laboratory
Argonne, IL 60439

Steven Koonin
Division of Physics & Astronomy
California Institute of Technology
Pasadena, CA 91125

William J. Kossler
Dept. of Physics
College of William and Mary
Williamsburg, VA 23185

John W. Lightbody, Jr.
National Bureau of Standards
Gaithersburg, MD 20899

Marcos Martins
National Bureau of Standards
404 Girard St., #303
Gaithersburg, MD 20877

James S. McCarthy
Dept. of Physics
University of Virginia
Charlottesville, VA 22901

Bernard Mecking
Rheinische Friedrich-Wilhelms-Univ.,
Bonn
Physikalisches Institut
Nussallee 12
5300 Bonn 1, West Germany

James Miller
Dept. of Physice
Boston University
Boston, MA 02215

Richard Milner
Mailstop 106-38
California Institute of Technology
Pasadena, CA 91125

Ralph C. Minehart
Dept. of Physics
University of Virginia
Charlottesville, VA 22901

Ernest Moniz
Lab. for Nuclear Science
MIT, Bates
Cambridge, MA 02139

Reiner Neuhausen
Institut fuer Kernphysik
Univ. Mainz
Postfach 3980
D-6500 Mainz
West Germany

John Norbury
NASA
Mail Stop 160
Hampton, VA 23665

Emery Nordberg
Wilson Lab
Cornell University
Ithaca, NY 14853

Blaine E. Norum
Dept. of Physics
University of Virginia
Charlottesville, VA 22901

John Parmentola
Dept. of Physics & Astronomy
University of Pittsburgh
Pittsburgh, PA 15260

Charles Perdrisat
Physics Dept.
College of William and Mary
Williamsburg, VA 23185

Francisco Prats
Dept. of Physics
George Washinton University
Washington, DC 20052

James J. Reidy
Dept. of Physics
University of Mississippi
University, MS 38677

Robert T. Siegel
Dept. of Physics
College of William and Mary
Williamsburg, VA 23185

Stanley E. Sobottka
Dept. of Physics
University of Virginia
Charlottesville, VA 22901

Paul Stoler
Dept. of Physics
Rensselaer Polytechnic Institute
Troy, NY 12181

Gabriel Tamas
CEN Saclay
DPHN/HE Cen Saclay
91191 Gif-sur-Yvette Cedex
France

Larry Towsend
NASA Langley Research Center
Mailstop 160
Hampton, VA 23665

Wallace J. van Orden
Physics Program
University of Maryland
College Park, MD 20742

Roy R. Whitney
Dept. of Physics
University of Virginia
Charlottesville, VA 22901

Jennifer Poor
Dept. of Physics
College of William and Mary
Williamsburg, VA 23185

E. F. Redish
Dept. of Physics & Astronomy
University of Maryland
College Park, MD 20742

W. Sapp
Dept. of Physics
MIT, Bates
Cambridge, MA 02139

Daniel I. Sober
Dept. of Physics
Catholic University
Washington, DC 20064

Paul A. Souder
Dept. of Physics
Syracuse University
Syracuse, NY 13210

Carey E. Stronach
Dept. of Physics
Box 358
Virginia State University
Petersburg, VA 23803

Henry A. Thiessen
MP-14, MS-847
LAMPF
P.O. Box 1663
Los Alamos, NM 87545

Linda Vahala
Dept. of Physics
Old Dominion University
Norfolk, VA 23508

J. Dirk Walecka
Dept. of Physics
Stanford University
Stanford, CA 94305

E. John Winhold
Dept. of Physics
Rensselaer Polytechnic Institute
Troy, NY 12181

David Winn
HG Eng. Physics Lab.
Harvard University
42 Oxford Street
Cambridge, MA 02138

M. Yamazaki
Dept. of Physics
MIT, Bates
Cambridge, MA 02139

Benjamin Zeidman
Argonne National Laboratory
9700 S. Cass Avenue
Argonne, IL 60439

John L. Wood
School of Physics
Georgia Institute of Technology
Atlanta, GA 30332

Richard York
Dept. of Physics
University of Virginia
Charlottesville, VA 22901